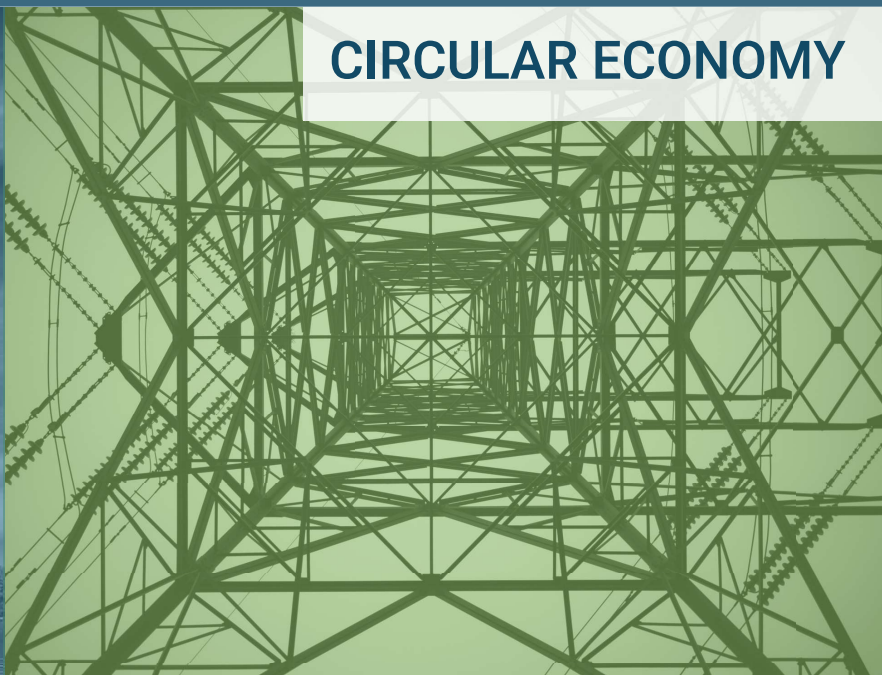EDITORS:
KRZYSZTOF PIKOŃ
MAGDALENA BOGACKA

CONTEMPORARY PROBLEMS OF POWER ENGINEERING AND ENVIRONMENTAL PROTECTION

CIRCULAR ECONOMY

eit InnoEnergy
Knowledge Innovation Community

Silesian University of Technology

Edited by Krzysztof Pikoń and Magdalena Bogacka

CONTEMPORARY PROBLEMS OF POWER ENGINEERINGS AND ENVIRONMENTAL PROTECTION 2018

Gliwice, 2019

Contemporary Problems of Energy and Environmental Protection

The exponential growth of industrialization and economic development increases the demand to energy. The amount of energy required is produced by various sources such as renewable, non-renewable and nuclear energy source, nevertheless, the difficulties caused by the former has great impact on the environment. To overcome this barrier, it is necessary to invest in research and development, which helps us to develop more innovative and greener projects that have minimal impact on environment and is sustainable based on the energetic, economic, and social needs. For the future it is important to analyse all the possible option to improve our technology in different sectors such as clean coal technology, energy storage, circular economy and alternative fuel technologies which helps us to barricade climate problems and air pollution problems.

The monograph "Contemporary Problems of Energy and Environmental Protection" is the sixth volume of the scientific edition. This monograph consist of manuscripts prepared by young scientists, mainly students as well as scholars from different research fields. Their research and inferences were presented during the VIth Conference on Energy and Environmental Protection, mainly focused on newly emerging technology – circular economy. The conference took place on 7th December, 2018 in Centre of New Technologies in Silesian University of Technology, Gliwice. The conference staged an excellent opportunity to share the knowledge and ideas of young scientists who wanted to make a difference and contribute to a better future, in harmony with the natural environment while securing energy needs of the society.

The event, as from the beginning, was organised entirely by the students of Silesian University of Technology as a part of project management course and as one of the essential elements of Pedagogical evolution department.

MSc Clean Fossil and Alternative Fuel Energy is fixated on establishing a future generation with innovative thinking and a unique blend, together with passion and constantly improvising educational methodologies. Moreover, the international environment with close industrial connections shed more light to the theory knowledge in the field of fuel and energy technology to the students. This conference is an excellent example of shaping business and soft skill in the program curriculum. Though it was time consuming, we believe this is a valuable experience for the students which will help them in the future.

We are proud of student's commitment, dedication and skills, toward the conference which made this a big success from the pasts and we are happy to see them getting themselves improved through each step of this event.

We would like to express our appreciation to InnoEnergy for supporting MSc Clean Fossil and Alternative Fuel Energy program and the VIth Conference on Energy and Environmental Protection.

Shemin Sagaria

Table of Contents

Forecast of emissions of gaseous air pollutants from power sector

Agata Sternal[1], Artur Wyrwa[2]

[1] *BSc – AGH University of Science and Technology, Faculty of Energy and Fuels, Al.Mickiewicza 30, 30-059 Kraków, Poland, e-mail: asternal2@gmail.com*

[2] *PhD – AGH University of Science and Technology, Faculty of Energy and Fuels, Al.Mickiewicza 30, 30-059 Kraków, Poland, e-mail: awyrwa@agh.edu.pl*

Abstract

Upcoming years are expected to be very important for Polish energy sector. A big share of power units require complex modernization of boilers and depollutioning systems to fulfill emission standards. Such strict EU environmental and climate policy will also lead to closing some of the units. In the paper calculations of emission levels based on the fuel parameters, specification of installed devices and energy production data were carried out taking into account also installed depollutioning systems. The bottom-up approach was used in which current and future SO_X and NO_X emission levels were estimated for each boiler installed in the centralized power and heat generation sector. The results show that substantial part of boilers was not properly prepared to implement IED emission standards in 2016. Furthermore, many of them are going to exceed new emission limits, namely those implemented with the new BAT conclusions that will enter into force in 2021. This situation would lead into difficult situation and may cause losing power and heat safety of the country.

Keywords: BAT conclusions, IED Directive, emissions, pollutants, power system, CHP, Poland

1.   Introduction

XXI century is a century of expanded societies, especially in Europe. This expansion causes conducting of many researches and publications. Scientific articles are later publicized in trade papers and also in the Internet. It means that people have unlimited access to them. This two cases influence awareness of communities. In one hand it is easy to break the news, in other some issues or just fudze can be introduced without any hitch.

One of the topics important for European societies nowadays is air pollution. However researches show that problem with air pollution exists from many years and the maximum value of pollution has been noticed in 1980 (regarding to sulphur dioxide) [1], it is well known that pollutants present in air harms human body and environment in general [2]. That is the main reason of the fact that either national, or EU rules and regulations came into being. Now those legal acts regulate pollution from different sectors – from energy production, through road transport to wastes utilization. It is apparent that air pollution standards are tightened up rapidly. Decreasing emission limits for large combustion plants force their adjustments, what is linked with modernization of exhaust gases purification systems. The most stringent document presently is Best Available Techniques conclusion (BREF). Keeping some BREF emission levels (i.e. NOx) in Polish energy sector would be impossible without the change of methods of flue gases treatment. Such replacement of older equipment is connected with huge costs. Because of that it is also important to point that in certain cases rapid changes of standards, especially in sectors which have domestic importance, except for advantages, may also appear contraindications. Considering operation of large power plants, changes mentioned above may for instance cause energy production discontinuity and damage of domestic economy. It means that power plants' modernization would influence costs of supplied energy and affect each and every of citizen.

Because of fast changes in European law, decluttering of all actual law regulations is needed both for power plant managers and society. Presence of historical emissions and also forecast for next years based on law regulations may help imagine how big are changes in the energy sector in the compartment of 20 years and average costs of modifications and environmental benefits calculations would be helpful for proponents who are going to procure for departure from BAT conclusions.

This study is a peculiar résumé which collects and summarizes all aspects of air pollution regulations as a forecast of gaseous pollutants emission.

2. Methodology

Data monitoring and analysis is an important tool to control and forecast performance of the process in either case. On the one hand, available databases are huge sources of information which can be used to check current and historical emission values or carry out many calculations. On the other, with the use of production data and/or fuel parameters one can estimate emissions. The goal of the research was to connect and compare emission of SOX and NOX obtained in a different ways. Fuel consumption was derived: (i) based on the energy production data and (ii) based on the E-PRTR database. The estimated fuel consumption was one of the major input to calculate SOX and NOX emissions.

2.1. SO$_X$ and NO$_X$ emissions determination

First step was determination of sulphur dioxide emission based on the fuel parameters and type of the purification systems.

At first fuel type was assigned to the boiler with the help of ARE catalogue (Catalogue of professional power plants and heat and power plants, 2015). It was assumed that sulphur content in ash equals 22%. Raw production of SO2 was calculated using the equation:

$$P_{SO_2} = \frac{2 \cdot S}{LHV}(1 - S_a)$$

where:

P_{SO2} — SO2 production [t/PJ]

LHV — lower heating value [PJ/t]

S — sulphur content in fuel [%]

S_a — sulphur content in ash expressed as total sulphur content [%]

Secondly, using the information about de-SOx methods, SO2 emission was calculated:

$$E_{SO_2} = P_{SO_2} \cdot (100 - \eta)$$

where:

E_{SO2} — SO$_2$ emission [t/PJ]

P_{SO2} — SO$_2$ production [t/PJ]

η — efficiency of SO$_2$ removal [%]

Unit conversion to [mg/Nm3] was done with the use of mean flue gases volume corresponding to fuel type which is presented in the Tab. 2.1.

Tab. 2.1. Mean exhaust gases volume

Mean exhaust gases volume	Hard coal	Lignite	Biomass	Liquid fuels	Natural gas and biogas
[m^3/MJ]	0.37	0.43	0.43	0.32	0.27

Calculation of NOx production differs from SOx methodology. Amount of NOx produced depends on the fuel type. This dependency is presented in the Tab. 2.2.

Tab. 2.2. NOx production factor [7]

NOx production factor	Hard coal	Lignite	Biomass	Liquid fuels	Natural gas and biogas
[t/PJ]	256	216	65	30	30

Knowing NOx production factor and denitrification efficiency, one can calculate NOx emission.

$$E_{NO_x} = W_{NO_X} \cdot (100 - \eta)$$

where:

E_{NOX} NO_X emission [t/PJ]

W_{NOX} NO_X emission indicator [t/PJ]

η efficiency of NO_X removal [%]

Obtained results were compared with the ones reported in the E-PRTR database. Emission values in E-PRTR are given in [kg], hence, to express them in per GJ or per m^3 units calculations of fuel consumption had to be carried out. Fuel consumption was calculated based on the CO_2 emissions using emission factors presented in the Tab. 2.3.

Tab. 2.3. CO2 emission factor [8]

2.2. Forecast preparation

Preparation of forecast requires strictly determined goal. One has to know what to show in this kind of data expression. In this paper emissions estimates for 2015 are presented and compared with current and future emission standards determined by law. Three different legal papers were taken into account:

- LCP – (Large Combustion Plants Directive) former legal paper, which was in force till the end of 2015

- IED – DIRECTIVE 2010/75/EU OF THE EUROPEAN PARLIAMENT AND OF THE COUNCIL of 24 November 2010 on industrial emissions (integrated pollution prevention and control). It is the most important legal document that is in force in European Union. IED Directive divides combustion plants into two groups, new units and existing units, with different emission limits. Term "new unit" refers to units that have been granted an operation permit before 7th January 2013. Such units shall meet emissions limit values presented in Part 1 of Annex V to the IED Directive. Term "existing unit" refers to any unit, which is not a "new unit". Emission limit values for such object are presented in Part 2 of Annex V. Both groups are further divided taking into account size of the boiler [4].

- BAT – COMMISSION IMPLEMENTING DECISION (EU) 2017/1442 of 31 July 2017 establishing best available techniques (BAT) conclusions, under Directive 2010/75/EU of the European Parliament and of the Council, for large combustion plants. This document is a reference when setting a permit for installation to which IED Directive is applied and concerns the same type of activities [5].

- Regulation of the Minister of Environment – Behind this term one should understand Regulation of the Minister of Environment from 1st March 2018 in the matter of emission standards for some installation types, fuels combustion sources and devices for wastes combustion or co-combustion. This legal document is a transposition of IED Directive into national law. The regulation contains also some important definitions which have to be determined. In most cases they are the same as in the IED Directive (for instance division into new and existing plants is the same), because the Regulation is a transposition of that legal document. However Regulation already defines medium combustion plants term (MCP) which are units with 1-50 [MW] of total rated thermal input, which are not included in the IED Directive. Those units will be divided into existing (before 2019) and new (after 2019) [6].

3. Results

Performed calculations lead up to obtain results which are presented in the form of graphs in this chapter.

3.1. Comparison of calculated SO$_X$ and NO$_X$ emissions with E-PRTR database

In the Fig. 3.1 amount of SO_X released by power plants is presented. 20 points form a linear dependence between calculated and reference values of the emission. The most of the power plants releases up to 15 [kt] of SO_X yearly, but the biggest emitter produces 30 [kt/year].

In the Fig. 3.2. SO_X emissions from CHP plants are presented. The number of CHPs taken into account in the research is higher than power plants (65 to 20), the accumulated emissions from CHPs are, however, smaller (76 [kt]) than in power plants (114 [kt]). It is connected with higher production ability of power plants.

The lowest values are recorded for the units that have small boilers installed, that are used only in case of peak demand, mostly gas turbines. In the same time, the highest values of emission one can observe from units that do not have de-SO_X installations.
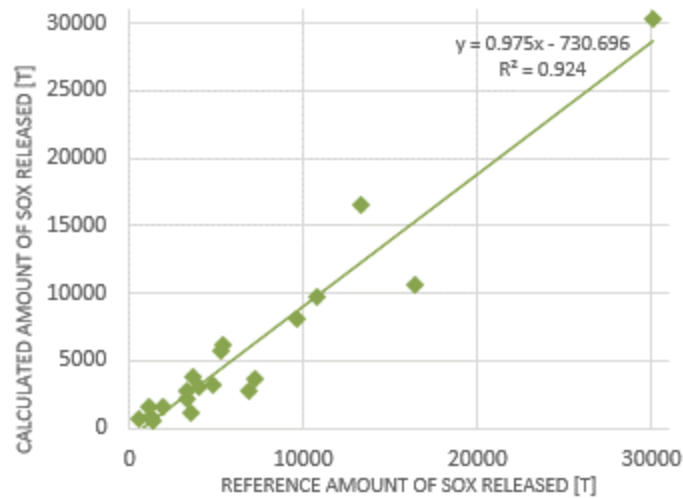
Fig. 3.1. Amount of SOx released by power plants
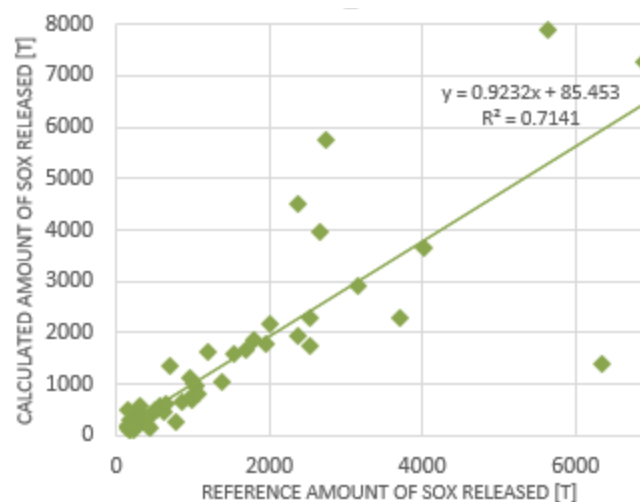
Fig. 3.2. Amount of SOx released by heat&power plants

In the Fig. 3.3. amount of NO_X released by power plants is presented. The most of the power units release up to 10 [kt] of NO_X yearly, but the biggest emitter produces about 40 [kt/year].

In the Fig. 3.4. NO_X emissions from CHP plants are presented. One can observe that emissions from CHPs are definitely lower (with maximum emission of about 4 [kt]) than in case of power plants. This is connected with lower energy production potential of CHP plants. In the graph one can observe that there are few outliers that may influence the reliability of collected data.

Similarly, the lowest values are recorded for the units that have small boilers installed, are used only in case of peak demand. In the same time, the highest values of emission one can observe from units that do not have appropriate denitrification installations.
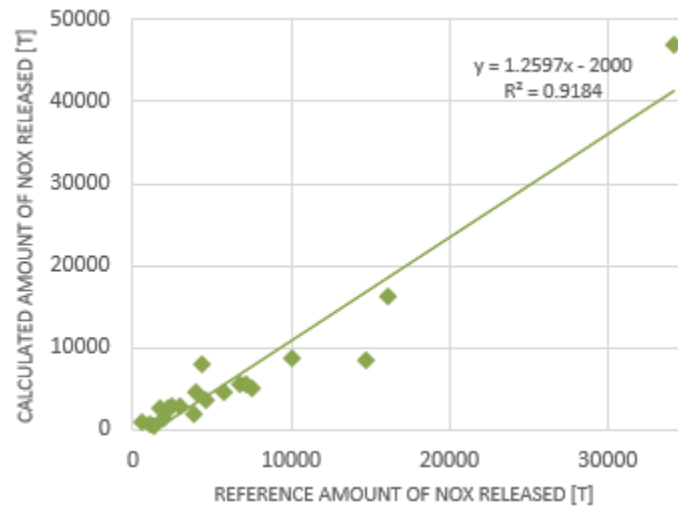
Fig. 3.3. Amount of NOx released by power plants
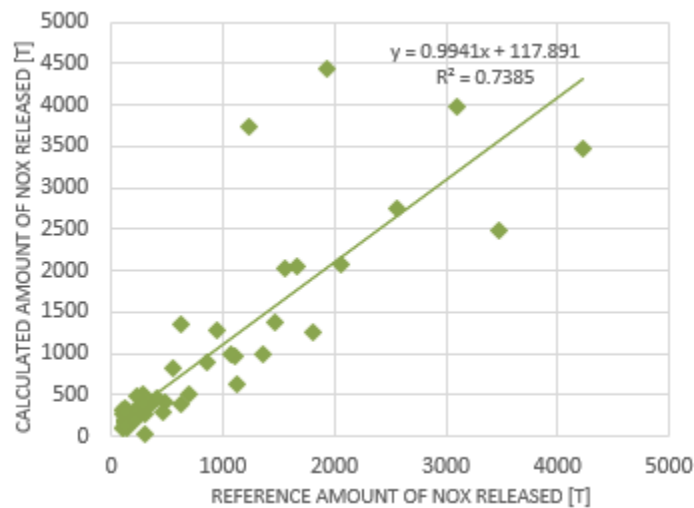
Fig. 3.4. Amount of NOx released by heat&power plants

3.2. Forecast chart

Next step in results analysis was preparation of forecast chart. Forecast graph includes pollutant emission level expressed in [mg/Nm^3], calculated with the use of data from 2015, as a function of boiler's total rated thermal input. Moreover standards constituted by law are presented. When analyzing, one has to know that LCP standard was in force till the end of 2015, IED norms have been in force since January 2016 and will be replaced by BAT standards in August 2021. The main goal of the forecast is to present emission level from 2015 and demonstrate how big is the share of units that are not prepared for the implementation of new standards because of insufficiently low emission values.

Fig. 3.5. shows unit SO$_X$ emission from Polish power plants expressed in [mg] of SO$_X$ emitted from power unit per one normal [m^3] of exhaust gases. Such presentation of records aims in formation of dependence between boiler size and emission, what informs which type of boiler is polluting the most. In presented Fig., one can observe that biggest unit emissions are recorded for boilers with total rated thermal input below 400 [MW]. A reason for that might be connected with the fact that this types of boilers have lower production ability, what makes them usually less feasible to invest in. Because of that such boilers have not that efficient desulphurization installation in comparison to those used in bigger boilers. As an effect of well-balanced solutions in bigger boilers, emission form them does not exceed 400 [mg/Nm^3] when in smaller one exceeds even 1500 [mg/Nm^3].
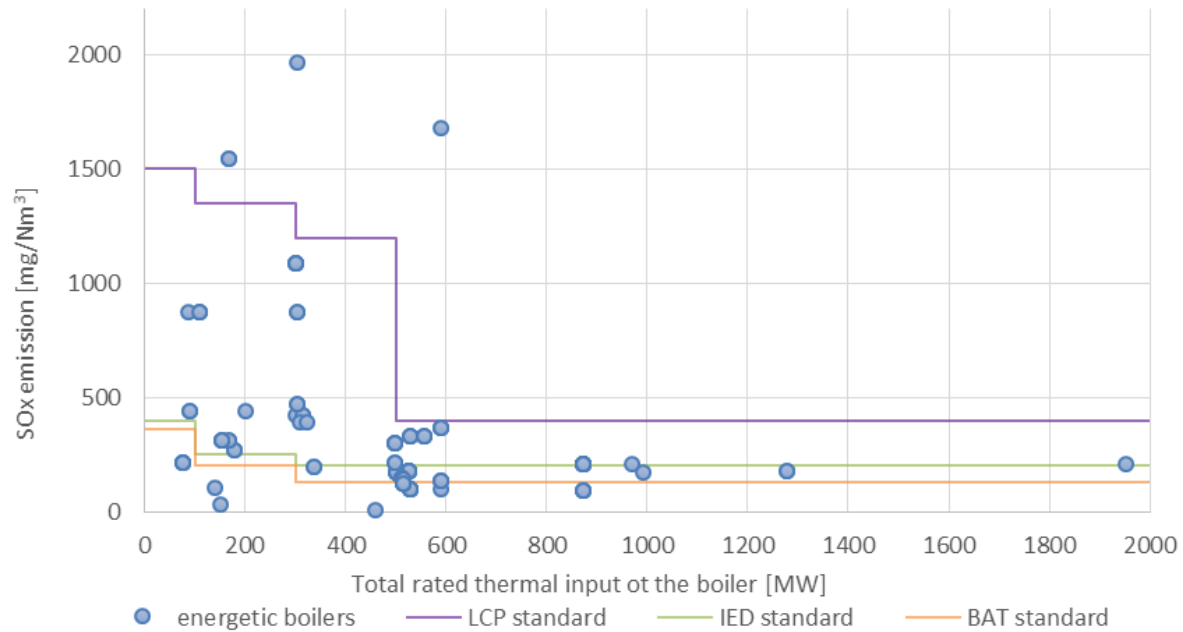
Fig. 3.5. SOx emission as a function of boiler size in power plants

Fig. 3.6. shows dependence between boiler size and unit SO_X emission from polish heat&power plants. The biggest heating boilers in Poland have total rated thermal input up to 150 [MW] (excluding one boiler, that was deconditioned from an energetic, into a heating one) and the biggest energetic boilers in heat&power plants reach up to 350 [MW]. As it could be noticed, the biggest share definitely constitute boilers with the size in ranges from 1 to 50 [MW]. It is connected with the fact that there are lots of small units producing heat and energy in Poland. Such a big fragmentation of production allows decreasing a complex heat transport process, but in the same time increase share of small boilers, in which money are not likely put into. Because of that such boilers are not equipped in efficient desulphurization installation what makes the pollution bigger. That is why in the Fig. 3.6., one can observe that biggest unit emissions are logged for boilers with total rated thermal input below 200 [MW]. As it could be seen, emission form some boilers installed in Polish heat&power plants exceeds even 1500 [mg/Nm^3].

In general one can see that bigger units emit less SO_X than smaller ones, but fortunately almost all boilers are working in compliance with LCP standards. However, assuming no changes in installations since 2015, almost 90% of all boilers in size ranges from 100 [MW] to 300 [MW] installed in polish heat&power plants exceed IED standard and are going to exceed BAT standard too. Situation looks also bad in case of bigger units. About 80% of the biggest units will overrun BAT emission standards when nothing is changed till 2021. Fortunately most of the biggest units (90% of units >500[MW]) were properly prepared to implement IED emission in 2015.
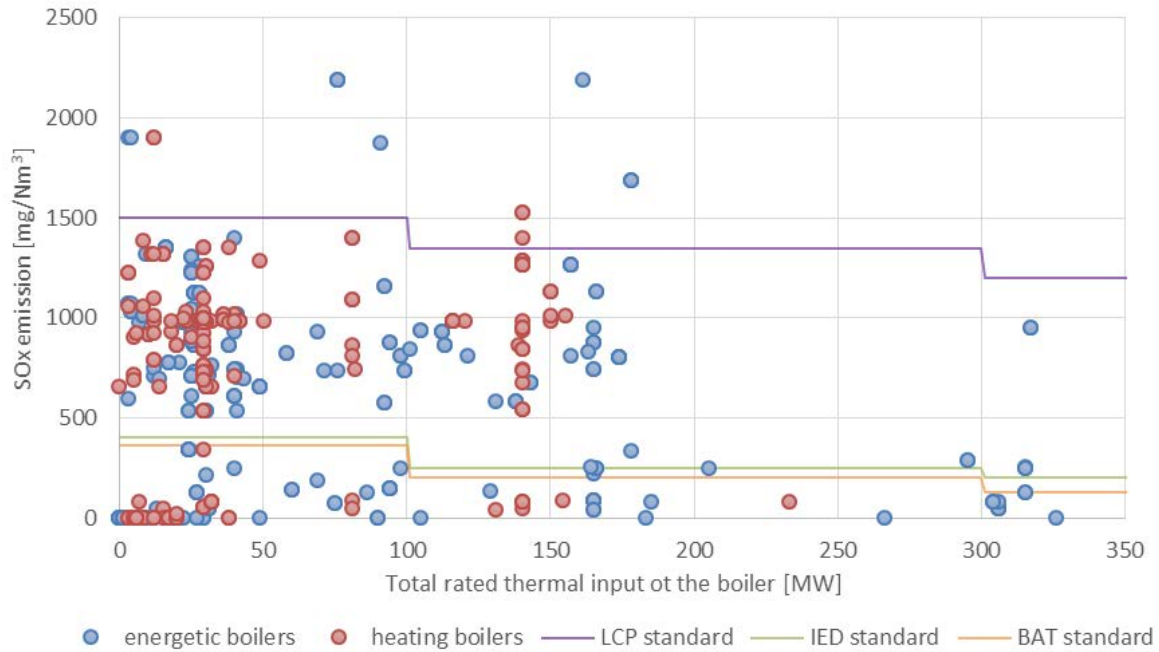
Fig. 3.6. SOx emission as a function of boiler size in heat&power plants

Fig. 3.7. shows unit NO_X emission from polish power plants expressed in [mg] of NO_X emitted from power unit per one normal [m^3] of exhaust gases produced. NO_X emissions are influenced by the parameters of combustion process, not by the composition of the fuel, as it was in case of sulphur. In general coals are expected to emit definitely more NO_X than, for instance, gas or oil. Because of the relations presented above, some boilers without de-NO_X systems have equal unit NO_X emissions what can be noticed in the Fig. 3.6. For instance lots of boilers are characterized by unit NO_X emission equal 490 [mg/Nm^3] and in some boilers emission does not exceed 5 [mg/Nm^3]. In contrast to SO_X, in case of NO_X one cannot determine visible dependence between boiler size and NO_X emission. Both big and small boilers emit bigger amounts of this pollutant into air. It is mostly connected with absence or poor denitrification installations. This aspect in Polish power units has been faintly developed yet. However one can observe that all of the boilers in Polish power plants were properly prepared to implement LCP standard and in 2015 there were no boilers that has exceeded that limit. Thing looks worse in case of IED standards which are not kept up in more than 75% of boilers in each size group. Moreover all of the boilers below 100 MW do not meet both IED and BAT standards. That makes implementation of the standards challenging. One can surmise that all of those objects have been asking for derogation or are prepared to be closed in next few years.
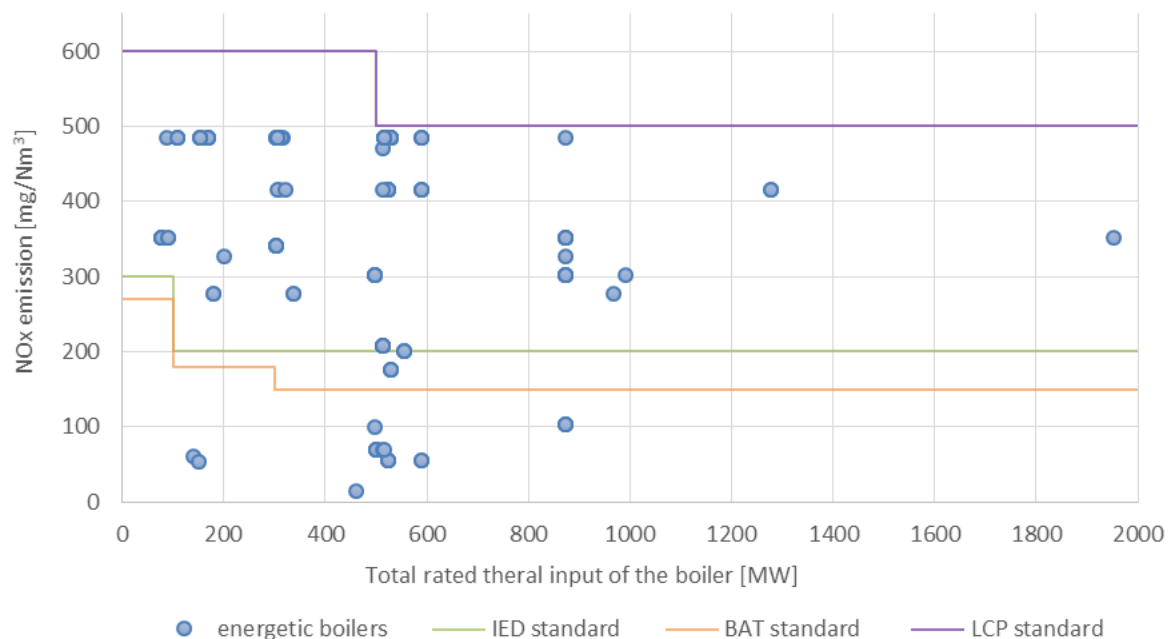
Fig. 3.7. NOx emission as a function of boiler size in power plants

In case of CHP plants, presented in the Fig. 3.8., the issue looks similar. There is no big correlation between boiler size and NO_X emission. One remark, one can observe is that boilers with total rated thermal input above about 170 [MW] produce up to about 500 [mg/Nm³] whilst smaller boilers can generate even 700 [mg/Nm³]. Emissions from CHPs look even worse than emission from power plants. There is a bunch of boilers, both heating and energetic, that are about 100 [mg/Nm³] above the LCP standard. Even more units is going to exceed LCP and BAT emission standards. What is interesting, bigger percent of energetic than heating boilers are exceeding allowable limits. In case of small unit below 100 MW it is 80% of energetic and 67% of heating boilers.
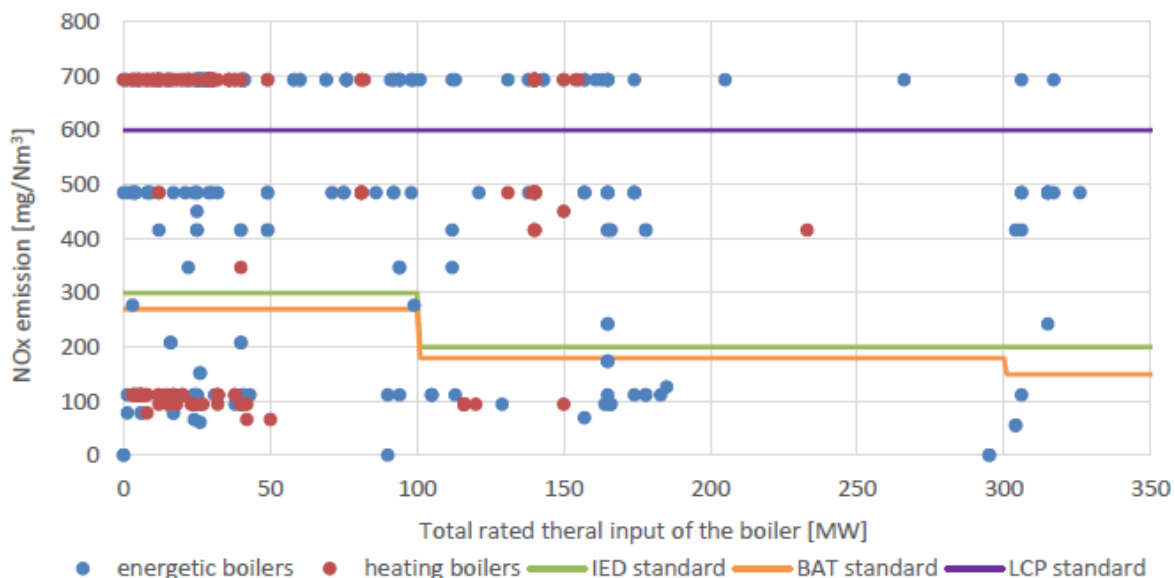
Fig. 3.8. NOx emission as a function of boiler size in heat&power plants

4.   Accuracy of estimation and sensitivity analysis

In the end, statistical parameters were calculated to check the reliability of presented data. A perfect data model would have FB and NMSE values equal to 0 and other parameters (MG, VG, R, FAC2) equal 1 [9]. Taking into

account whole statistical analysis, only one of all those indicators is out of the assumed range – MG in power plants (Fig. 3.1) that equals 1.30 what means that data are might be slightly overpredicted, however that value overrun the mean by 30% what is still accepTab. Such record may be caused by presence of quite high amount of low value records when few of them were visibly higher and MG (and VG) is strongly influenced by extremely low values. This relation could be warranted by low MG value for CHP plants in the Fig. 3.2. There are no huge differences between records, so even smaller values are not outliers anymore and the MG value is close to reference. Such statistical analysis allows one's to determine the reliability of presented data and in case of SO_X emissions presented in this paper one can say that all of he presented data are representative and proclaims that calculations that led to obtain Fig.s 3.1- 3.2. were carried out free from errors.

Tab. 4.1. Statistical parameters SO_X

Object type	FB	MG	NMSE	VG	R	FAC2*
Power plants (Fig. 3.1)	0.15	1.30	0.05	1.25	0.96	0.92
Heat & power plants (Fig. 3.2)	0.00	1.05	0.23	1.18	0.85	1.02

To sum up and check correctness of calculations concerning NOX emission, statistical parameters were calculated according to the scheme as in case of SOX. As it was already presented before, a perfect data model would have FB and NMSE values equal to 0 and other parameters equal 1. Observing the data, one can say that the data closer to the model are presented in the Fig. 3.3. At first, those data presents the most suiTab. values of FB, FAC2 and NMSE. Moreover in case of 3.3. MG is also in accepTab. range. The values of R are also close to the model values. The less satisfying is graph presenting emissions from CHP plants (Fig. 3.4.). Both low MB and positive NMSE proclaim that those data are underpredicted. Underprediction appears when there is more values which are below mean than above it. Taking into account remaining parameters one can observe VB and FAC2 above and R below the ideal values. However the 3.4. case is still in accepTab. range. Statistical analysis, which was carried out for dataset presented in the graphs 3.3. and 3.4., allows one's to determine the reliability of calculations. In case of NOX emissions presented in this paper one can say that all of presented data, even that which are more outlying from a model case like in Fig. 3.4., are representative and proclaim that calculations that led to obtain Fig.s 3.3. and 3.4. were carried out free from errors.

Tab. 4.2. Statistical parameters NO_X

Object type	FB	MG	NMSE	VG	R	FAC2*
Power plants (Fig. 3.3.)	-0.01	1.10	0.10	1.19	0.96	1.02
Heat & power plants (Fig. 3.4.)	-0.15	0.81	0.21	1.25	0.86	1.11

5. Conclusions

Environmental protection policy of European Union influence all sectors of Polish economy. In case of energy production the most important legal papers are now the IED Directive and BAT conclusions which determine emission standards for power units with total rated thermal input bigger than 50 MW. European controlling agencies strictly care about redeeming allowable emission limits in power plants. The major source of information for them is E-PRTR database established to give an access for detailed data for whole European community. In the paper the E-PRTR database constituted a reference to compare the results and checked their correctness. Taking into account both pollutants (SO_X and NO_X) calculated values were more close to the reference E-PRTR values in case of power plants. This is due to the more precise data delivered by power plants. Analysis that has been done in the paper shows that definitely bigger SO_X emissions in power plants arenoticed in units with relatively small thermal input installed. In case of CHP plants, however, this dependence is not as clearly visible as in case of power plants. That means that operators modernize firstly biggest units with higher production capacity and then smaller units. Things look different in case of NOX production, where emissions are similar through all boilers' sizes. In the same time forecast charts show that there might be a serious problem

with keeping emission on a level that does not exceed future emission standards. In case of SO_X released from power plants already about 75% of all boilers in size ranges from 100 to 300 MW were expected to exceed IED standards that came into force in 2016. This share is even higher in case of more strict BAT emission levels that are going to be in force since August 2021. It equals over 80%. Exactly the same share of boilers are over the standards in case of CHP plants with sizes from 100 to 300 MW. Taking into account NOX emissions, differences between share of units that will have exceeded IED and BAT conclusions is mostly the same. This is an effect of small difference between allowable NOX emission limits in those two legal documents. However, still share of boilers that is above allowable emission limits is huge. It equals about 80% in all categories mentioned for SO_X above. Forecast charts show that in best situation are units with big boilers that are mostly already modernized. Modernization of boilers and purification system is the only (but costly) solution to keep the units working. Moreover, modernization of units that ale old and are predicted to work only few more years is uneconomic and not practical. That all influences the fact that only about 15% of all boilers installed in power plants declare relevant upgrading in years 2016-2021 [10]. There are some boilers that are planned to be closed because of their economical unfeasibility of modernization. To guarantee constant supply of energy after decommissioning, other energy sources must be added and the efficiency of boilers should be increased [3]. In the face of insufficient alternative energy sources (no nuclear power plant, low share of RES) keeping the conventional power sources working is a priority in case of energy safety of the country.

References

[1] Klimont Z., Smith S. J., Cofala J.: The last decade of global anthropogenic sulfur dioxide: 2000–2011 emissions, Environmental Research Letters, 8 (2013). Access: 28.11.2017

[2] Kaufman D, Franz C.: Biosphere 2000: protecting our global environment, Kendall Hunt Pub Co, 2000.

[3] Rezaei F. and others: SOx/NOx Removal from Flue Gas Streams by Solid Adsorbents: A Review of Current Challenges and Future Directions, Energy Fuels, 2015, 29 (9), pp 5467–5486.

[4] DIRECTIVE 2010/75/EU OF THE EUROPEAN PARLIAMENT AND OF THE COUNCIL of 24 November 2010 on industrial emissions (integrated pollution prevention and control).

[5] COMMISSION IMPLEMENTING DECISION (EU) 2017/1442 of 31 July 2017 establishing best available techniques (BAT) conclusions, under Directive 2010/75/EU of the European Parliament and of the Council, for large combustion plants.

[6] Rozporządzenie Minstra Środowiska z dnia 1 marca 2018 r. w sprawie standardów emisyjnych dla niektórych rodzajów instalacji, źródeł spalania paliw oraz urządzeń spalania lub współspalania odpadów.

[7] Wyrwa A.: Integrated impact assessment of emissions from the Polish energy sector for determination of the optimal mix of energy generation and pollution control technologies, Kraków, 2009.

[8] KOBiZE: Wartości opałowe (WO) I wskaźniki emisji CO2 (WE) w roku 2015 do raportowania w ramach Systemu Handlu Uprawnieniami do Emisji za rok 2018, Warszawa, 2017.

[9] Patryl L. , Galeriu D.: Statistical Performances measures - models comparison, Commissariat `a l'Energie Atomique, DAM, DIF, F-91297 Arpajon (France), 2011.

[10] Agencja Rynku Energii: Katalog Elektrowni I Elektrociepłowni Zawodowych 2015 rok, Warszawa, kwiecień 2016.

Analysis of physical and chemical properties of solid product from biomass torrefaction

Hubert Put

AGH – University of Science and Technology/Faculty of Energy and Fuels, al. Adama Mickiewicza 30, paw. D-4, p. 17, technologia@weip.agh.edu.pl

Abstract

Biomass is becoming more and more widely-used source for energy production in Poland. Despite of many advantages, biomass is characterized by some disadvantages too such as high content of moisture, biodegradability and difficulty in milling, etc. Process that can improve these properties of biomass is torrefaction. It is a thermal pre-treatment process in oxygen free atmosphere holds at temperatures between 200-300°C. Torrefaction of Sidahermaphorodita,Piceaabiesand straw was studied at temperatures 230, 260,and 290°Cand residence times werespecified for 0,5, 1 and 1,5h. The torrefaction were conducted in an electric furnace, the chemical composition of raw and biochars were done by Elementary Analyser Leco628 while technical analyses were performed according to European Standards. The increase in carbon content was observed: c.a. 12% for Sidahermaphorodita, 13% for Piceaabies, and above 11% for straw. A decrease of hydrogen content in all of three analysed materials was also noticed. The results clearly show that torrefaction process improve properties of biomass, and make it more coal like.

Key words: biomass, torrefaction, analysis, chemical, properties, solid, products, sidahermaphorodita, piceaabies, straw, moisture, ash, volatile matter, van Krevelen

1. Introduction

1.1. Biomass in Poland and worldwide

Biomass in Poland becomes more and more popular source of Energy. Looking into the statistics, biomass

constituted 9,25% of the energy having been sourced then. However biomass gained even more popularity.

If youlook into the statistics, it had the biggest share among renewable energy sources if you consider sourced

energy,which was 62,5% in 2015.

Power installed in biomass power plants in Poland extoled to 1 362,03 MW in 2017. It is an 6.3% increase in comparison to year 2016 and a 66% increase in comparison to year 2012. [1]. There are 36 power plant blocks for biomass in Poland currently [2]. Biomass used for incineration or co-firing in power plants are, for instance, sawdust (as a scrap after machining process or milling wood in sawmills), woodchips, bark, straw, hay and plants specially designated for energetic purposes such as cane, sunchoke or smartweed or silvergrass [3]. Biomass, as a raw material used for burning and co-firing has many advantages. It is neutral if you consider carbon dioxide production – one can assume that biomass consumed carbon dioxide that was produced during its burning. It is also a good fuel considering sulphur emission. What is more, biomass can be sourced from many places, what, theoretically, lowers the problem connected with its transport. Despite those advantages biomass holds also variety of flaws such as: high reactivity, high moisture content, biodegradability, lowermelting point than coal (what can lead to parching of boiler's heating Surface), chlorium and potassium content (what increases a risk of creation of corrosion on metal elements of boilers). Biomass is also a complicatedsource of primary energy due to requirement of its' prior preparation, for instance, by drying. Different kinds of biomass may also have crop protection products leftovers as well, what is crucial when it comes to usage such plants for energetic purposes because of a threat of discharging such compounds as dioxines and furanes [4,5].

In connection with disadvantages of raw biomass usage for burning and co-firing purposes, there are a range of methods to facilitate aforementioned process and cause it to be less burdensome. Among methods of

refinement biomass used for energetic purposes one can enumerate pelletization, hydrothermal bituminization, gasification, pyrolysis and also torrefaction, which is a topic of this paper.

1.2. Biomass worldwide

The primary energy supply of forest biomass used worldwide is estimated at about 56 EJ, which means woody biomass is the source of over 10% of all energy supplied annually. Overall, woody biomass provides about 90% of the primary energy annually sourced from all forms of biomass. [6]

When one look at the statistics, leading countries using biomass as a source of energy for burning and co-firing in power plants are U.S.A. , China and Japan. World total capacity is estimated to be 122 GW.

1.3. Torrefaction process

Torrefaction is a process, which transforms biomass into a solid fuel with properties similar to coal. It is based on thermic processing of biomass in the temperature 200÷300°C under the pressure close to atmospheric, without oxygen access to the material. Biomass is subjected using many stages if one concerns torrefaction progress, what is presented at undermentioned graphic

Biomass →Drying process → Torrefaction →Cooling process → Biochar

The prcess should be led in a proper way to provide an appropriate grindability to a material after torrefactionprocess, simultaneouly obtaining low loss of energy, caused by loss of volatile matter. Relatively bigger lossof oxygen and hydrogen during the whole process in comparison to loss of carbon get the properties oftorrefaction product along to low-quality coal.Its calorific value is from 18 to 23 MJ/kg, it has from 1 to 6%of moisture content and is defined by low bulkdensity. The features of this material are as well: crispness,homogeneity and hydrophobic naature, whatcauses that it can be warehoused outside and will not biodegrade.

2.   Objective and extent of the paper.

Objective of this paper is comparative analysis of input biomass physicochemical properties and solid productscreated during its torrefaction. Research was conducted with regard to changes of technical and chemicalproperties.

Extent of paper included:

1)   Torrefaction in parameters mentioned below:

✓   Temperature: 230°C, 260°C i 290°C

✓   Conducting process time : 0,5h, 1h i 1,5h

2)   Technical analysis execution for input materials and obtained materials:

✓   Moisture content – 3 measurements

✓   Volatile matter content – 3 measurements

✓   Ash content – 3 measurements

✓   Loss of mass cused by torrefaction – 2 measurements for each material for every time assumed for a process and for every assumed temperature

Torrefaction times were 0,5h,15 and 1,5h, whereas torrefaction temperatures were 230°C, 260°C and 290°C which resulted in 18 measurements for every material.

3)   Chemical analysis for input materials and obtained biochars:

✓   C,H,N compounds analysis – 3 measurements

✓   Calculation of O compound, based on measurement of C,H and N compounds content.

3. Experimental part

3.1. Research material

While doing my research, three types of biomass were used:

a) Sidahermaphorodita – a plant which belongs to malvaceae family. Crops of this plant are superb for briquette and pellets fabrication. [7]

b) Piceaabiesis a plant that grows at northern side of Europe and in the mountains (the Carpathians, the Sudeten, the Alps) and in the Balkans. It can be also found in Northern America. [8]

c) Straw are ripe and parched aristas of grain plants and parched grain legumes, linen or rapeesed. It is primarily used as a pasture and bedding for breeding animals, only surplus iss used for energetic purposes. [9]

Sidahermaphoroditaused in a laboratory research was characterised by light brown colour and it has to beinitially prepared, by chopping and milling. This material came from polish cultivation. Straw was a mix ofdifferent aristas and was featured by light yellow to dark brown colour. It was also compulsory for this materialto chop and mill. Straw was provided by EKOPROD sp. z.o.o. Piceaabieswas characterised by light yellowcolour, needed to be milled and chopped and was provided by sklepdrewna.pl company.Sidahermaphoroditaand straw were delivered in a form of long stems and piceaabieswas delivered in theform of small chips, which were chopped and milled in a grinder LN-100 distributed by Testchem companywith 1,0 mm sifter, available in ASH UST Centrum Energetyki

3.2. The description of test stands

Test stand for torrefaction process included a 1,65kW furnace with torrefaction chamber having dimension10x10x20cm. Its outer dimensions were 29x29x34cm. The insulation of furnace was made of saphile, coil heaterwere made of chamotte moulding with thermos-resistant wire. Control was held using temperature regulator AR604/51/P with a transmitter that could be supplied with a current with 85 to 260V voltage. The furnace washeatedelectrically, it was equipped with one first-class coated thermocouple TP-202 type K (NiCR-NiAl). Argon wasalso infeeded into the chamber, as a gas to create a neutral atmosphere inside the furnace.

3.3. Methodology of performed researched

The research were fully made using experimental apparatus available in Department of Heat Techniques and Environmental Protection at Faculty of Metal Engineering and Industrial Computer Science

3.3.1.   Torrefaction calculation formula for loss of mass

$$m_{u,\%} = \left(\frac{m_1' + m_2' - m_3' + m_1'' + m_2'' - m_3''}{2} \right) \times 100 \qquad (1)$$

where,

$m_{u,\%}$ - percentage of the mass' loss due to torrefaction

m_1 – mass of an empty crucible

m_2 – mass of crucible with material before torrefaction

m_3 – mass of crucible with torrefied material

The results were rounded out to two decimal places.

Upper indexes relate to the number of sample put into the furnace (' – sample no.1, '' – sample no.2)

Technical analysis of researched biomass samples and created torrefied materials involved determining of moisture content, ash content and volatile matter content. All analysis were conducted in muffle furnace ofCzylok company, type FCF 22SHM with computer programmer with heating driver.

3.3.2. Moisture content analysis

Research conducted according to EN 14774-2:2009 (E) norm – Solid biofuels – Determination of moisture content – Oven dry methos – Part 2: Total moisture – Simplified method. Calculation pattern:

$$M_{ar} = \frac{(m_2 - m_3) + m_4}{(m_2 - m_1) + m_4} \times 100 \qquad (2)$$

Where,

M_{ar} – moisture content [%]

m_1 – empty crucible mass [g]

m_2 – mass of crucible with material before drying [g]

m_3 – mass of crucible with material after drying [g]

m_4 – moisture content connected with crucible, to which material was poured [%]

The result was rounded out to one decimal place. For each material three analysis were led.

3.3.3. Ash content analysis

Rresearch conducted according to EN 14775:2009 (E) – Solid biofuels – Determination of ash content.

Calculation pattern:

$$A_d = \frac{m_3 - m_1}{m_2 - m_1} \times 100 \times \frac{100}{100 - M_{ad}} \qquad (3)$$

Where,

A_d – ash content in a sample [%]

m_1 – empty crucible mass [g]

m_2 – mass of crucible with material before the research [g]

m_3 – mass of crucible with ash [g]

M_{ad} – moisture content of testes material used for calculation of moisture content [%]

The result was rounded out to one decimal place. For each material three analysis were led.

3.3.4. Volatile matter content analysis

Research conducted according to norm EN 15148:2009 (E) - Solid biofuels – Determination of content of volatile matter

   Calculation pattern:

$$V_d = \left[\frac{100(m_2 - m_3)}{m_2 - m_1} - M_{ad} \right] \times \left(\frac{100}{100 - M_{ad}} \right) \qquad (4)$$

Where,

V_d – volatile matter content in a sample [%]

m_1 – mass of empty crucible mass with lid [g]

m_2 – mass of crucible with lid and material before the research [g]

m_3 – mass of crucible with lid and leftover after the research [g]

M_{ad} – moisture content of test material determined by normy EN 14774-3 [%]

The result was rouned out to one decimal place. For each material three analysis were led.

After technical analysis, samples of biomass were proceeded to being torrefied.

4. Raw biomass' and torrefied biomass' physicochemical features analysis

Chemical analysis was conducted with usage of Truespect LECO CHN 628 analizer.

4.1. Presentation and discussion of results

The results of this paper are presented in the form of Fig.s.

4.1.1. Moisture content
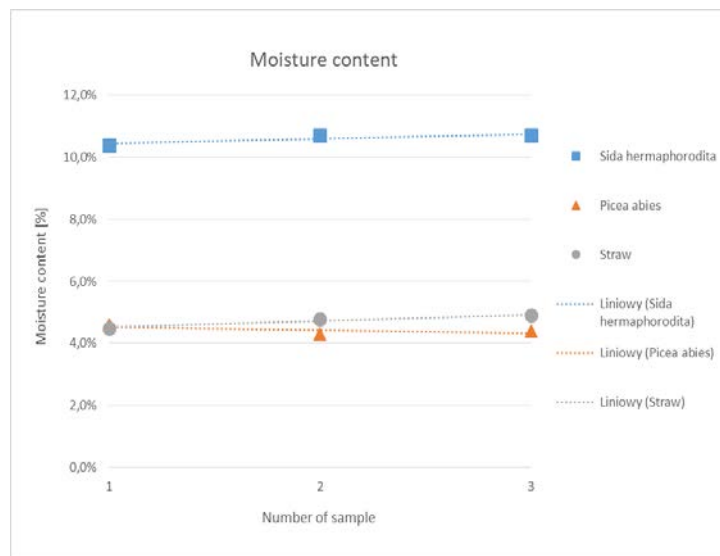
Fig. 1. Moisture content in examined samples

Piceaabies included over two times bigger amount of moisture than other kinds ofanalysed biomass.

Average moisture content in straw is 4,4%, in sidahermaphorodita it is 4.7%, however if we consider

Piceaabie

4.1.2. Ash content
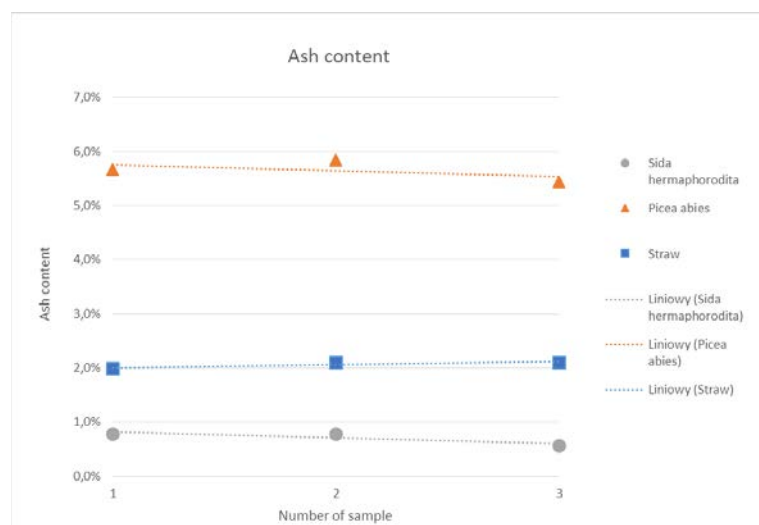
Fig. 2. Ash content in examined samples

The difference in ash content between different biomass materials are more clear. The lowest ash content is distinguishable in piceaabies, averagely 0.7%, a bit more of it is included in sidahermaphorodita, it is 2.1%. The biggest amount of ash is in straw – average for this biomass material is 5.6%.

4.1.3.   Volatile matter content
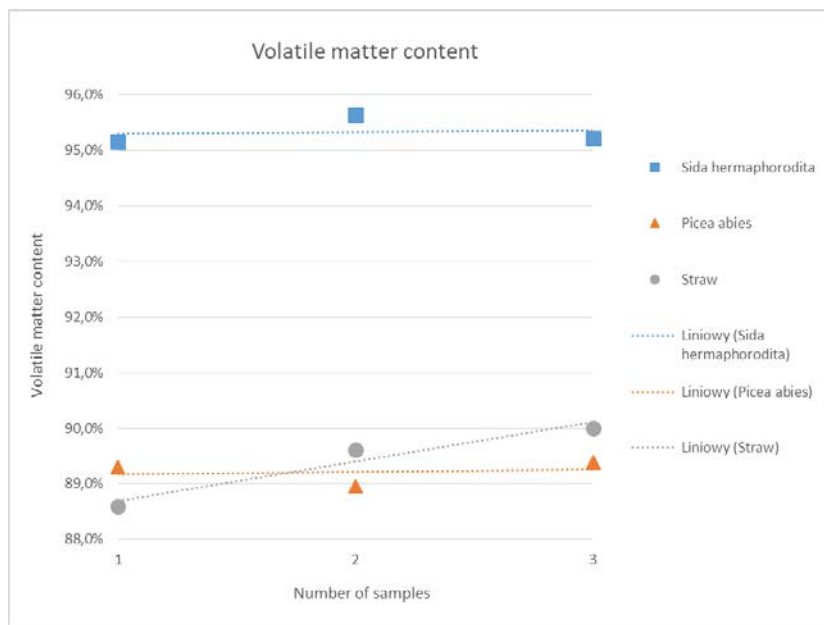
Fig. 3. Volatile matter content in examined samples

Volatile matter content was the greatest in sample with piceaabies, average is 95.3%. Pretty similar of its content was found in straw and sidahermaphorodita, it was slightly bigger than 89% for both biomass materials.

4.1.4.   Torrefaction of sidahermaphorodita
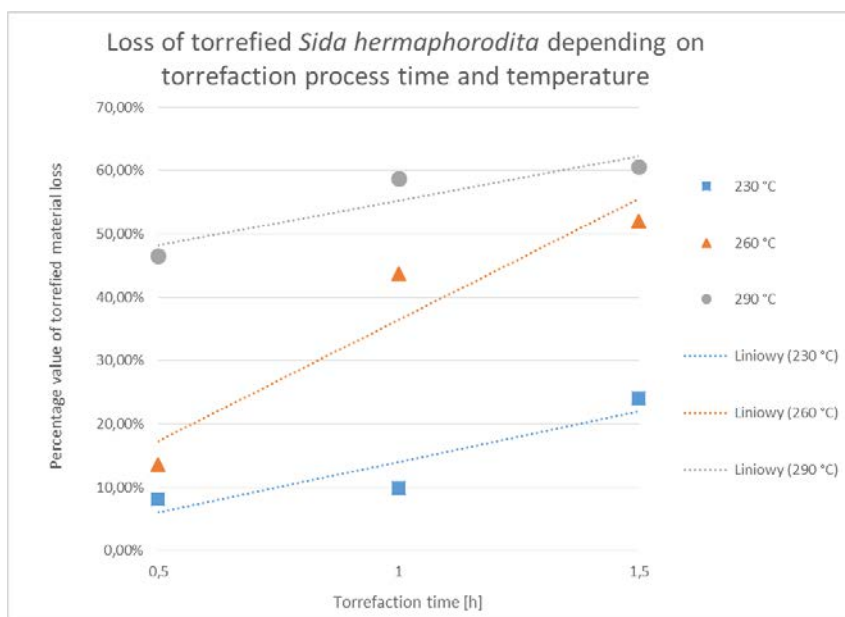
Fig.1. Loss of torrefiedsidahermaphorodita depending on torrefaction processtemperature and time

The biggest loss of material's mass in examined times and temperatures of torrefaction total over 60% of

initial material's mass. When temperature was 230°C and 290°C the increase of mass loss was slight, whereas for 260°C change in mass loss in comparison between 0,5h torrefaction and 1,5h torrefaction was almost 35%.

4.1.5.   Torrefaction of piceaabies
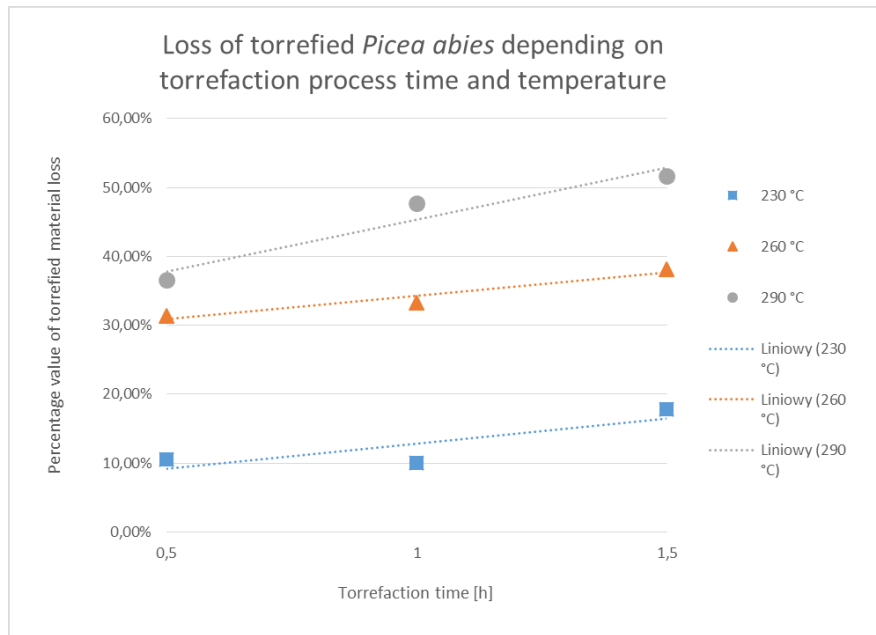
Fig.2. Loss of torrefiedPiceaabies depending on torrefaction processstemperature and time

For piceaabies the biggest mass loss total slightly over 50%. The difference in mass loss for the same temperatures were little, whereas what is noticeable is a far bigger difference in this parameter for 230°C and260°C, taking into account the same torrefaction time.

4.1.6.   Torrefaction of straw
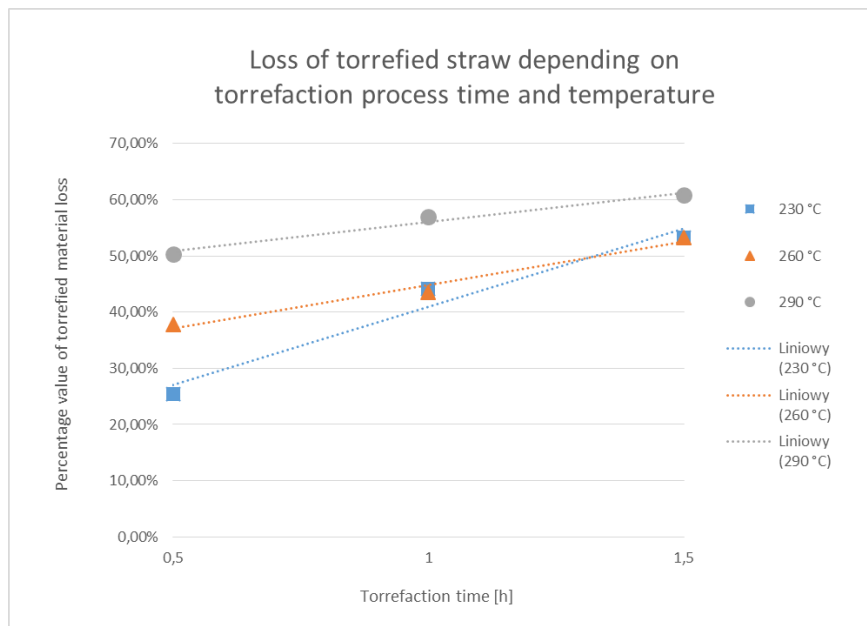
Fig.3. Loss of torrefied straw depending on torrefaction processstemperature and time

Maximal mass loss for straw was slightly over 60% for 290°C. Massive losses were indicated also for other temperatures, they were over 50%. What is worth indicating is that the results almost equalized for 230°C

and 260°C loss mass taking into account torrefaction time, consecutively, 1h and 1.5h.

4.1.7.   Chemical analysis of sidahermaphorodita

In raw state this material has almost 50% of carbon content. Maximal result that was achieved in examinedtemperatures and torrefaction times was over 60% of carbon content in the sample. The increase in carboncontent was from 4% to 12%. The biggest decrease in hydrogen content was 2.7%, however, in comparisonto raw state, the result was 6.4%. The nitrogen content in samples increased subtly during the process, thebiggest increase is 0.4%. What is worth indicating is the fact that nitrogen content decreased for 230°C,comparing raw state with 0,5h of torrefaction process.

Relationship between percentage carbon content from temperature and time of torrefaction for *Sida hermaphorodita*

Relationship between percentage hydrogen content from temperature and time of torrefaction for *Sida hermaphorodita*
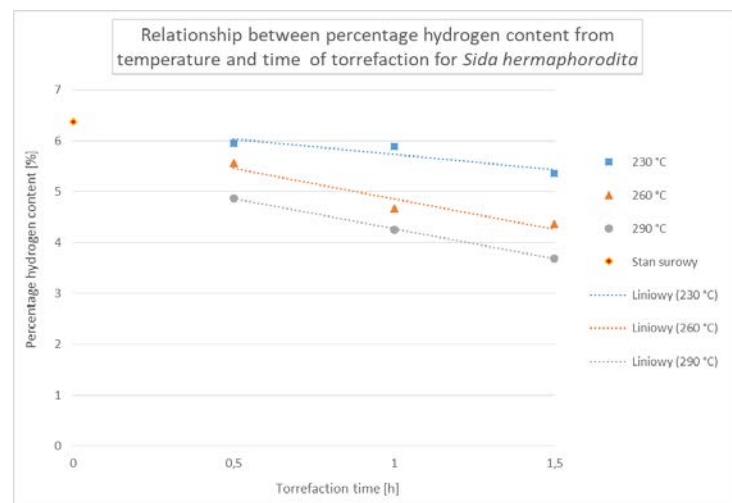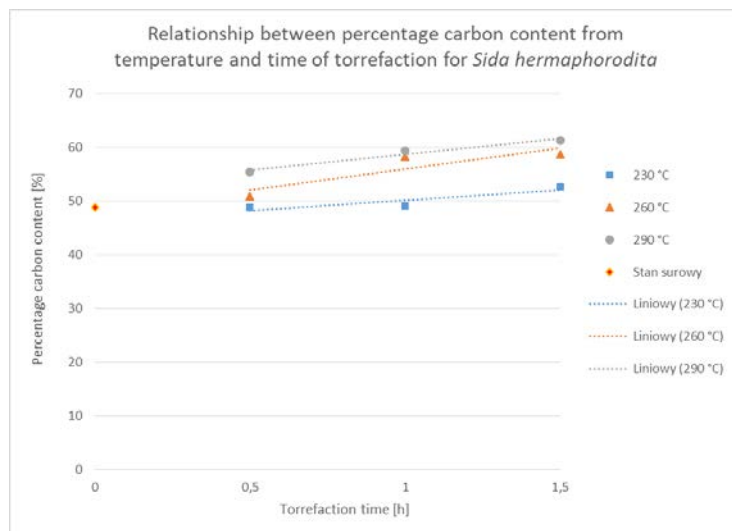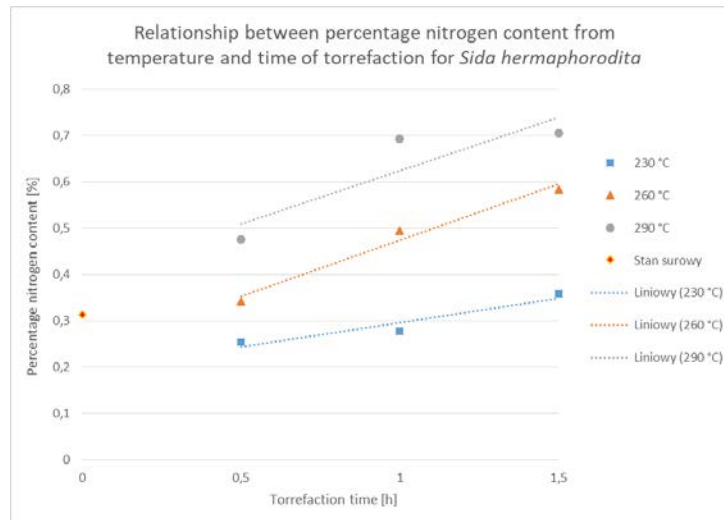
Fig.s 4,8,9. Relationships between percentage of compounds content from temperature and time for Sida hermaphorodita

4.1.8.   Chemical analysis of piceaabies

Carbon content in a sample increased by 13% as a consequence of torrefaction in comparison to raw state. For this process, carbon content is almost the same for 230°C and 260°C. Hydrogen content thanks to torrefaction decreased maximally of 1.57%. This decline was noticed for 290°C, for 1h measurement. Afterwards, piceaabies sample increased its hydrogen content. The loss of hydrogen content was approximately linear. The content of nitrogen was inappreciably small as counting 0.02%
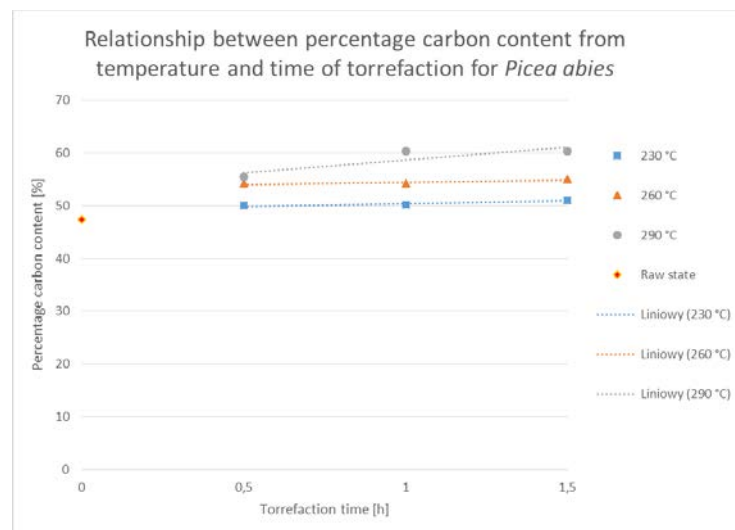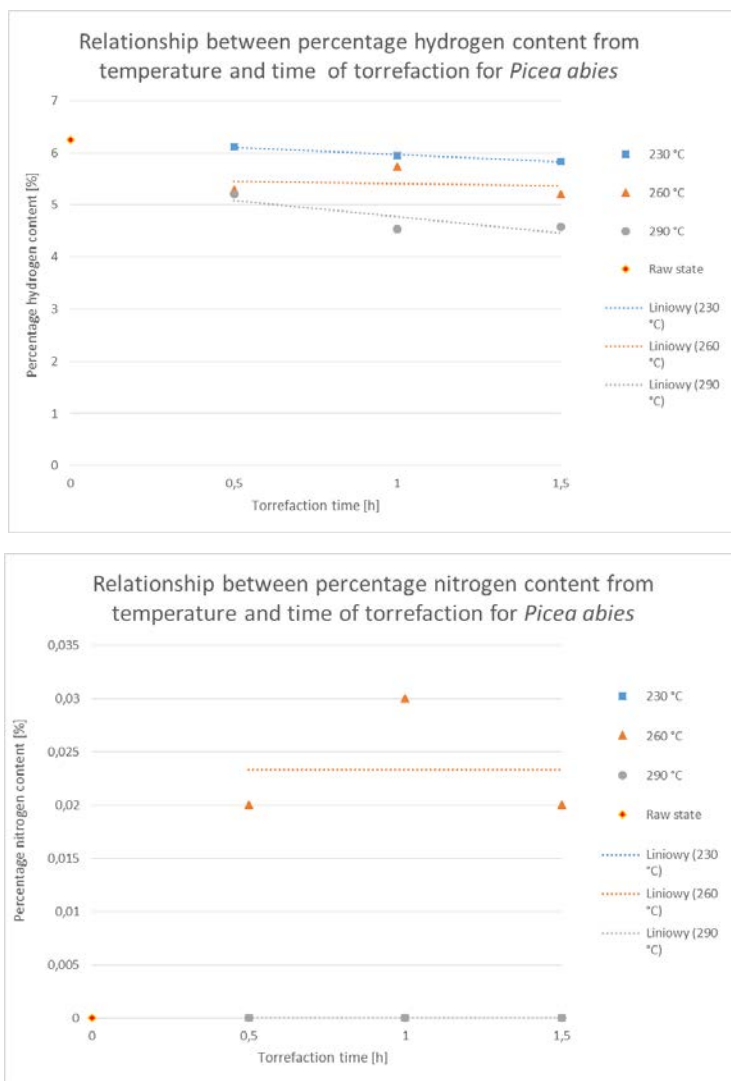
Fig.10,11,12. Relationship between percentage of nitrogen content from temperaturę and time for picea abies

4.1.9.   Chemical analysis of straw

Carbon content in straw thanks to torrefaction changed slightly for 260°C and 290°C. An 3% increase was noticed. Share of hydrogen in sample decreases maximally for 0.8%. The nitrogen content in any of the samples exceeded 1%.
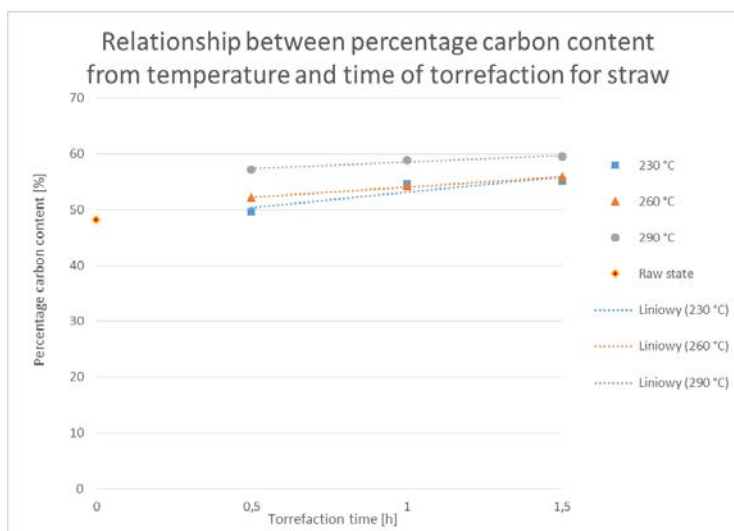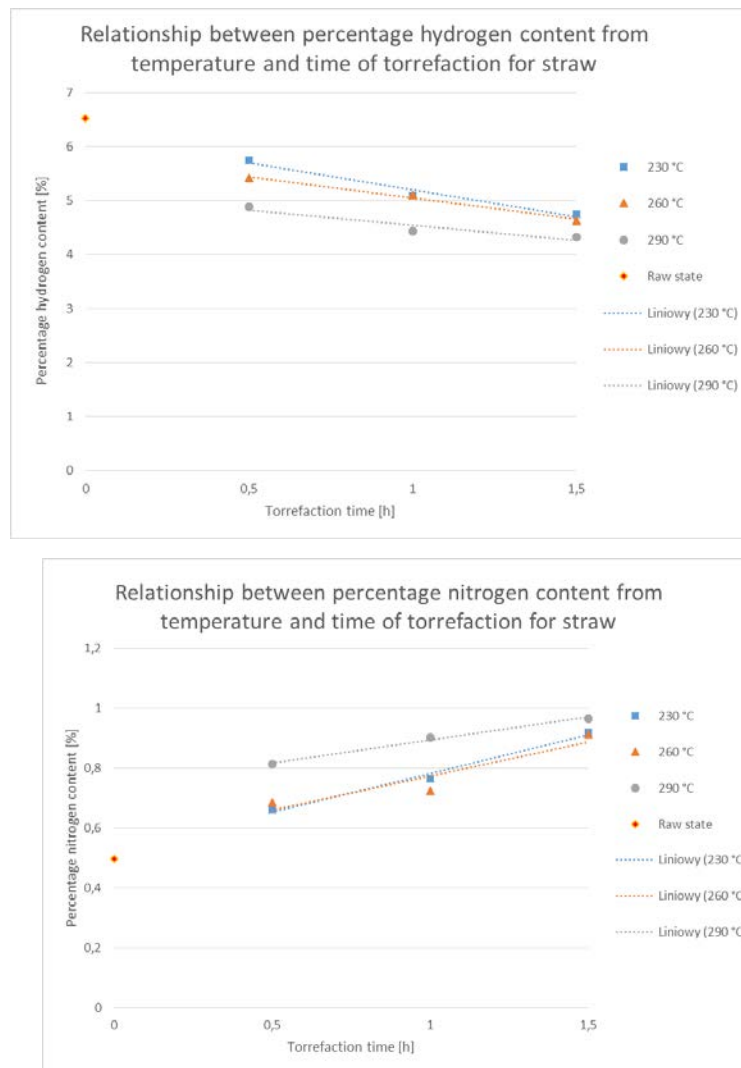
Fig. 13,14,15. Relationship between percentage of compounds content from temperaturę and time for straw

5.   Van Krevelen Fig.s for analysed materials.

Correlations between H/C and O/C molar ratio are presented on van Krevelen Fig..

Points on the Fig.s symbolize parameters of samples obtained due to torrefaction process.
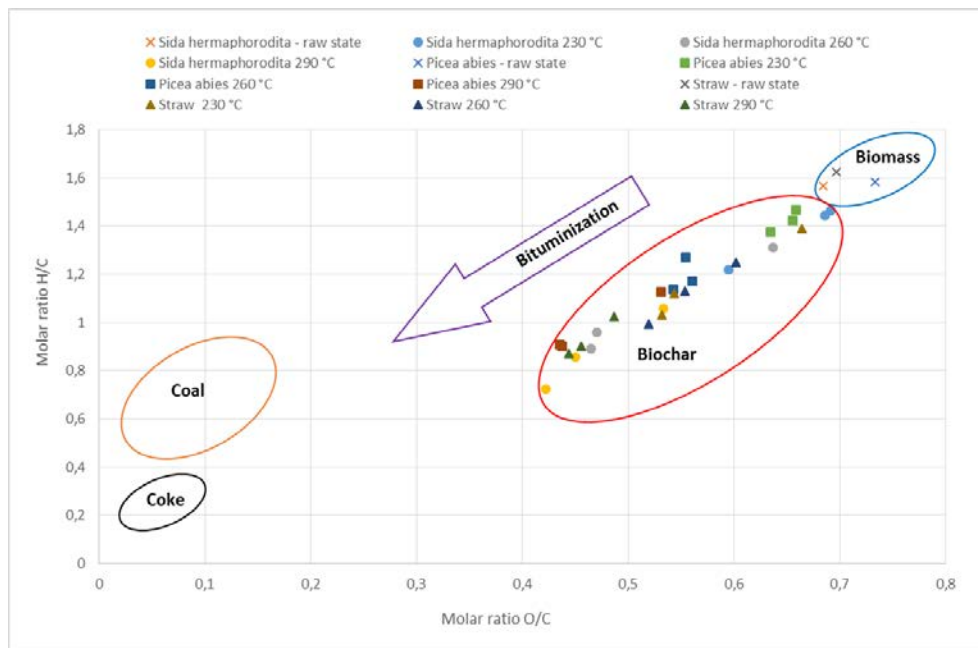
Fig. 16. Van Krevelen Fig. for all examined materials

Analysing results presented on van Krevelen Fig.s there is assumed that samples, which residued in the same temperature the longest inside the furnace move in the left-down side of the Fig.. Similar connection can be observed considering growth of temperature in the reactor: the higher temperature, the closer torrefied material is nestled to left-down verge of the Fig..

6. Conclusions

Conducted analysis and presented results allowed to formulate following conclusions:

a) Piceaabies has the biggest amount of moisture content – it is far unfavourable, due to lowering of the materials' calorific value and volatile matter content, what causes easier ignition and faster burning.

b) Straw has the biggest amount of ash, what can be one of the causes of creating a deposit covering heating surface of boilers, what is obviously a disadvantage for this fuel.

c) Sidahermaphorodita and straw lose majority of its mass (about 60%) during torrefaction process, whereas this factor is a bit more than 50% for piceaabies. It proofs that two aforementioned materials can be used more effectively in co-firing process. What is more, straw does not need to have temperature higher than 230°C to have acceptable results in mass loss.

d) All fuels reach similar results considering carbon content in boundary experiment conditions, which were 290°C and 1,5h, what is about 60%. The most effective in this case is straw – this material after an hour of torrefaction reaches the same results as for higher temperatures. Moreover, in this case, straw had similar results comparing to other fuels having more time for torrefaction and higher temperature, what could limit torrefaction time to obtain demanded results.

e) Hydrogen maintained the biggest level in piceaabies after torrefaction. There were values from 0.2% to 1.1% depending on the temperature. Hydrogen induces moisture creation after biomass burning, so it is definitely a flaw of using this biomass. Chosen plants are stable regarding changes in hydrogen content, which lowers from 0.1% to 1.4% between considered temperatures. Therefore, piceaabies in temperature 260°C (0.7% growth) and straw (1% growth) in temperature 230°C might be treated as exceptions.

f) As for the case of sidahermaphorodita and straw, nitrogen, due to torrefaction process, increases its share. Nevertheless, these are small values – in the first aforementioned material nitrogen content did not exceed 0.7%, whereas for straw the maximum value was no more than 1%. Piceaabieshas the

content of nitrogen of fractions of percent. Nitrogen is unfavourable for usage of torrefied material – while burning, it can cause creation of, dangerous for environment, nitric oxides.

To summarize, torrefaction has a real meaning as a process of biomass preparation for burning or co-firing. Research did prove that thanks to torrefaction, not only straw and piceaabies but sidahermaphorodita as well get closer with their features to coal considering carbon content, and molar ratio oxygen-to-coal and hydrogen-to-coal.

Word of thanks

I would like to give cordial acknowledgement to PhD MałgorzataWilk for guidance during the process of writing present paper, to prof. MaiuszFilipowicz for being a conference reviewer of this paper and to all workers of the department for kindness in whatever I did for this paper to develop.

References

[1] https://www.ure.gov.pl/pl/rynki-energii/energia-elektryczna/odnawialne-zrodla-ener/potencjal-krajowy-oze/5753,Moc-zainstalowana-MW.html, Moczainstalowana (MW) – stanna 30.09.2017, 18.12.2017, Strona 1

[2] http://www.biomasa.org.pl/aktualnosci/270-ciekawy-artykul-o-biomasie-w-biomasie.html, JolantaKamińska, „Biomasakrajowa w rękachkoncernów", MagazynBiomasa, Marzec 2015

[3] https://enerad.pl/oze/wykorzystanie-i-wytwarzanie/biogazownie/biomasa/, „Biomasa – Jakiesąrodzajebiomasy"

[4] https://www.odnawialne-firmy.pl/wiadomosci/pokaz/90,elektrownia-biomasowa-wady-i-zalety, „Elektrowniabiomasowa i współspalanie – wady i zalety", 2016 SzymonSzufa: "Biomasa i jejwykorzystanie w energetyce", KatedraTechnikiCieplnej i Chłodnictwa, WydziałMechaniczny, PolitechnikaŁódzka,

[5] https://www.statista.com/statistics/264637/world-biomass-energy-capacity/

[6] http://biomax.com.pl/slazowiec-pensylwanski, Krzysztof Olkowski, „Ślazowiecpensylwański"

[7] http://www.ekologia.pl/wiedza/ziola/swierk-pospolity/charakterystyka/, „Świerkpospolity"

[8] http://www.biomasa.org/index.php?d=artykul&kat=50&art=46, A. Grzybek, P. Gradziuk, K. Kowalczyk, „Rodzajebiomasy" napodstawieSłoma – energetycznepaliwo, Warszawa, 2001

Biodegradation as a solution for global problem of plastics contamination

Emilia Capała[1], Anna Kowalczyk[1],Marek Chyc[2], Dariusz Latowski[1]

[1]Department of Plant Physiology and Biochemistry, Faculty of Biochemistry, Biophysics and Biotechnology, Jagiellonian University, Gronostajowa 7, 30-387 Kraków, Poland,

emilia.capala@doctoral.uj.edu.pl; kowalczyk_anna@onet.eu;dariuszlatowski@gmail.com

[2]Department of Environmental Protection, State Higher Vocational School in Tarnów, Mickiewicza 8, 33-100 Tarnów, Poland, mrsch7@gmail.com

Abstract

Polylactide (PLA), due to its physicochemicalproperties, is a promising material for many applications. It can completely replace other polymers from the plastic material industry in the future. In this study, biodegradation of PLA modified and unmodified with starch was tested. The effectof two microorganisms, *Aspergillusniger* and *Penicillumminioluteum*, on the degradation of PLA was analyzed. Samples were incubated with molds for 3 months. The degree of PLA degradation was analyzed by massloss, changes in chemical and physical structure of samples before and after incubation with microorganisms. The chemical structure was determinedby Attenuated Total Reflection Fourier Transform Infrared Spectroscopy (ATR-FTIR) and the physical structure was detected by Scanning Electron Microscope (SEM). The greatest massloss was observed in samples incubated with *A. niger*. FTIR analysis showed significant changes in chemical structure of both foil components – polylactide and starch. Microscopic analysis confirmed residual degradation of foil.

Keywords: biodegradation, starch modified polylactide, *Aspergillusniger,* FTIR, SEM

1. Introduction

Plastic consists of one or many synthetic and semi-synthetic organic polymers [1]. The most important feature of this materialis plasticity, making it easy to process to the target shape. Another crucial matter is the cost of production. Due to favourable features the most common polymersare polyethylene, polyethylene terephthalate and polyvinyl chloride. The huge demand for cheap and easily processed materials, like packagings or disposable articles [2] caused constantly increasingplastic pollution around the world. One of the finest method to utilize these wastes is biodegradation. To improve the efficiency of this process it is crucialto develop biodegradable material and optimize conditions of biodegradation, for example temperature, humidity and the most important – microorganisms. Several biodegradable polymers has been already developed, i.e. cellulose, polyhydroxybutyrate. One of the biodegradable polymers, which is commonly used in many industries, is polylactide (PLA). Polylactide is the lactic acid polymerobtained from renewable resources. Lactic acid or lactide are used as monomers in polymerization reaction to produce PLA. The first discovered microorganism capable to degrade PLA was bacteria isolated from soil – *Amycolatopsis* species [3]. The enzymes which hydrolyze PLA were isolated from *Amycolatopsis* genus [4,5]. There are many modifications of PLA foil driven during the production of plastics. The first one is based on technology production when several ingredients like thermoplastic starch (TPS) are added to improve physicochemical properties of the polylactide material.

One of the most common molds occurring in the nature is *A.niger*[6]. Due to its properties, *A. niger* is widely used in various industries. The most common application is the production of citric acid [7, 8, 9]. *A. niger* also produce enzymes, like glucoamylase, which is used in food industry [10, 11]. *A. niger* occurs on the surface of plastic waste, which suggest that this mold potentially can derive energy from polymers and in that way degrade them. Another fungusspecies used in industry is *Penicilliumminiolteum*. This fungusis used in sugar industry because of its ability to produce enzyme, dextranase, which breaks α (1,6) glycosidic bonds[12, 13]. The main aim of this research was to study the biodegradation of polylactide foil by one of the most common fungi – *A.niger* and identify factors affecting this process.

2.   Material and Methods

1.2 Microorganisms

The strain of *A.niger* was isolated from soil, where plastic waste were deposited. Themold species was identified basing onmorphologic features in macro- and microscopic scale and then confirmed by genetic analysis.

During previous experiments, in control samples incubated in sterile medium, different myceliawere observed. The mold has gotcharacteristic colors of hyphae, yellow and green, which facilitate to identify the mold as *P.minioluteum*. The identification of the species was confirmed by genetic analysis [14].

Both fungi were cultivated on Potato Dextrose Agar (PDA) at 20±1°C in the dark.

2.2 Polylactide foil samples

Several types of polylactide foil were tested. The production technology of all tested foils was developed in Department of Organic Technologies of New Chemical Syntheses Institute in Puławy, Poland. Unmodified polylactide foil (PLAW) and modified with thermoplastic starch (TPS) were used. The content of starch was 20% (PLA20R) and 50% (PLA50R). To studythe production technology effecton biodegradation degree of PLA, two different types of PLA50 were used – PLA50R and PLA50W. Foil obtained by method R (blow method) was thin and flexible, whereas foil produced using W method (effusion method) have a thick and hard structure. Furthermore, four additional ingredients, which have not exceeded 0.75% of the PLA50R content were tested and markedas PLA50R1, PLA50R2, PLA50R3, PLA50R4.

Each type of foil was cut into 1 cm^2 pieces, disinfected by rinsing in 70% ethanol. Prepared samples of foil were treated with *A.niger* and *P.minioluteum*.

3.2 Incubation

The foil samples were incubated with microorganisms in liquid medium without carbon source: NH_4NO_3–1.0, KH_2PO_4–0.5, $MgSO_4$–0.5, $FeSO_4$–0.001, $ZnSO_4$–0.001 [g/L]. Each type of foil was treated with mono-culture of both species of molds and with dualculture as well. Control samples were incubated in sterile liquid medium for3 months with shaking 100 rpm at 20±1°C with light avoiding.

4.2 Analysis of the biodegradation

After the incubation, foil samples were disinfected by rinsing in 70% ethanol. The degree of biodegradation was determinedby massloss andchanges in the chemical and physical structure. The massloss was calculated as percentage mass reduction, the difference between the initial mass and the mass after incubation was divided by the initial mass of a given sample and converted into percentage value.The chemical structure before and after the incubation was analyzed with Fourier Transform Infrared Spectroscopy (FTIR) with Thermo Scientific Nicolet iS10 in the range from 600 to 4000 cm^{-1} and processed withOMNIC 9.2.86 software. The tested foil spectra were compared with thespectraof foiluntreated with microorganisms and medium. The physical structure of the foil surface was detected by Scanning Electron Microscope (SEM) with Carl Zeiss camera (EVO MA 15) electron microscope using 20 kV filament current and analysed with Carl Zeiss SmartSEM V05.04.00 software.

3.   Results and discussion

1.3 The effect of *Aspergillusniger* and *Penicilliumminioluteum* on polylactide foil biodegradation

The biodegradation of polylactide foil by mono- and dualcultures of *A.niger* and *P. minioluteum* was tested. To improve fungi grow sucrose was added to the medium (20 g/L). After the incubation in dual culture of fungi the fragmentation of PLA20R was observed (Fig. 3.1). This type of degradation was not observed after the incubation withmono-cultures or dual cultures in medium without carbon source. Fragmentation of only PLA20R samples treated with both fungi in medium with sucrose indicates that biodegradation of PLA20R is the most efficientwhen both species are applied and the sucrose is added. Probably sucrose as easily available source of carbon, caused significant increase in fungus biomassand thus concentration of enzymes, which can hydrolyzebonds in polymers. The fragmentation of PLA20R foil was very promising. This result inspires

to further research to confirm the hypothesis of production cooperating exoenzymes which hydrolyzepolymer's bonds. However, the conditions of fragmentation process were unfavourable financially, because of the sucrose addition. For this reason, an another way to improve biodegradation process was investigated.
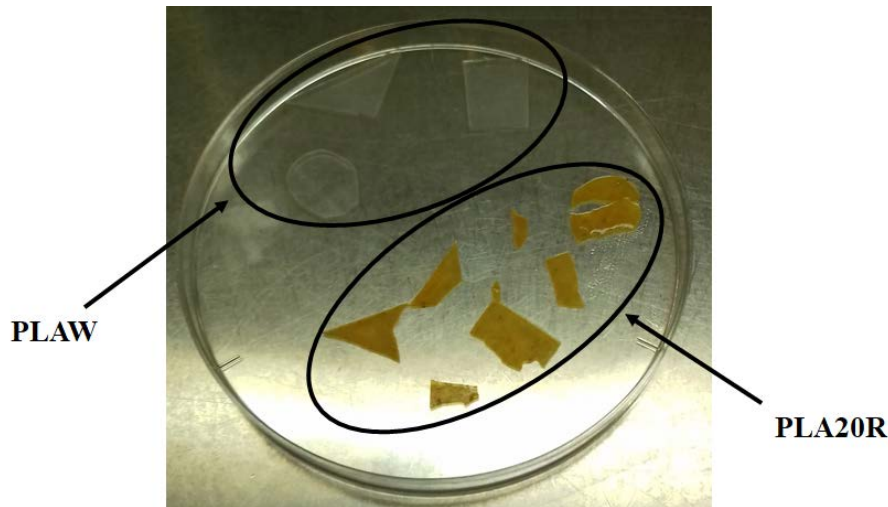
Fig. 3.1 PLAW and PLA20R samples after the incubation with *Aspergillusniger* and *Penicilliumminioluteum* in liquid medium with sucrose

2.3 The effect of starch addition on polylactide foil biodegradation

Two different contents of starch in polylactide foils were tested: 20% (PLA20R) and 50% (PLA50R). The samples properties were compared with unmodified polylactide foil. The mass reduction of PLA20R and PLA50R samples treated with *P. minioluteum*, both withmono-culture and dualculture with *A. niger*,waslower than weight loss of samples incubated with*A. niger* mono-culture.This data suggest that *P. minioluteum*has not a positive effect on polylactide biodegradation in liquid mineral medium. Therefore, samples treated with *P. minioluteum* had not been submitted further analysis of biodegradation rate.

There was no significant difference in weight loss between PLAW samples incubated in sterile medium and treated with microorganisms (Fig. 3.2). Notable difference in mass reduction between treated and untreated with microorganisms samples was observed in PLA50R (Fig. 3.2).The most degraded samples were PLA50R treated with *A. niger*, whichachieved 24.78±3.30% of weight loss (Fig. 3.2). These results indicate that the highercontent of starch in polylactide foil, the greaterbiodegradation by *A. niger*, but PLAW, PLA20R and PLA50R were produced by using different technology and it was difficult to compare biodegradation of these three types of foils. To study the impact of foil production technology on polylactide biodegradation process another study was performed.
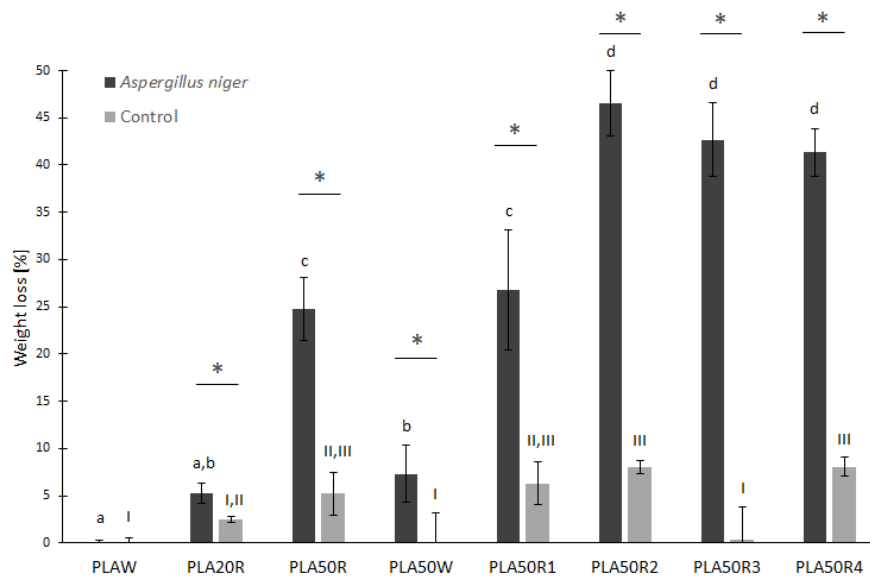
Fig. 3.2 Percentage mass reduction of foil samples after 3 months incubation with *A. niger* (*Aspergillusniger*) and in sterile liquid mineral medium (Control); * indicates difference between the control and the *A. niger* treated group; a–d indicates samples treated with *A.niger* with no significant difference; I–III indicates control samples with no significant difference; post-hoc ANOVA – Tukey's HSD test was used $p<0.05$, $n=6$

3.3 The impact of foil production technology on polylactide foil biodegradation

Two types of PLA50 foil were used, one of them was produced using R method (PLA50R) and the second by W method (PLA50W). Mono-culture of *P. minioluteum*and dual cultures of tested molds had inconsiderableimpact on foil mass. Significant changes in mass reduction of both foils were observed after the incubation with *A. niger* (Fig. 3.2). There are also significant differences between PLA50R and PLA50W (Fig. 3.2). In both types of incubation – with *A. niger* and in sterile medium, higher percentage massloss wasobserved in PLA50R samples. PLA50R samples incubated with *A. niger* degraded in 24.78±3.30%, whereas PLA50W only 7.31±3.00% (Fig. 3.2). These results suggest that production technology plays important role inpolylactide foil biodegradation.Method R occurred to bemore favourable for producing biodegradable material than method W. This could be one of the reasons why PLAW was not degraded as well as PLA20R and PLA50R.

4.3 The effect of trace amounts of foil additions on polylactide foil biodegradation

Several additional ingredients (1–4) were tested to investigate theireffect on PLA50R biodegradation. In all PLA50R foils a significant role of *A. niger* in biodegradation was observed (Fig. 3.2). Percentage mass reduction washigher after the incubation with *A. niger* than after the incubation in sterile medium (Fig. 3.2). There was no difference in weight loss of PLA50R1 and PLA50R, whatindicates that ingredient 1 in small amounts does not present positive influence on polylactide foil biodegradation by *A. niger*. Addition of ingredient 2, 3 and 4 increase weight loss of polylactide foil. PLA50R2, PLA50R3 and PLA50R4 was degraded in 46.55±3.45%, 42.68±3.91% and 41.34±2.52% respectively (Fig. 3.2), but there was no significant differences between them. Obtained results have shown that ingredients 2, 3 and 4 havea positive impact on PLA50R biodegradationby*A. niger*.

5.3 The effect of *Aspergillusniger* on chemical structure of polylactide foils

The massloss analysisdemonstrated notable degradation of polylactide foils by *A. niger*. To verify if this species affect the chemical structure of foil and which foil component was degraded, FTIR analysiswas applied. The spectra show the dependence of the absorbance towavenumber (cm⁻¹). The greatest changes in FTIR spectra after incubation with *A. niger*wereobserved forPLA50R2 samples (Fig. 3.5). There was a significant difference in absorbance in range 3600–3000 cm⁻¹ (Fig. 3.5). In this range OHgroups from starch absorb energy [15]. There is no signal in this range in PLA50R2 treated with *A. niger* spectrum, which indicates that starch was degraded partially by breaking –OH bonds. There are also differences in absorbance of 1750 cm⁻¹ maximum

(Fig. 3.5) where the C=O bond of carbonyl and carboxyl group absorbs the energy, but signal from carboxyl group is much more higher than signal from carbonyl group [16]. Carboxyl group occurs in the end of polylactide chain [17]. The greatest absorbance of 1750 cm^{-1} maximum was observed in spectrum of PLA50R2 samples treated with *A. niger*. Probably *A. niger*degraded polylactide causing depolymerization of polylactide and as a result realised carboxyl groups which increased the absorbance in 1750 cm^{-1}. In the range 1180–1080 cm^{-1} the greatest absorbance was observed in spectrum of PLA50R2 samples treated with *A. niger* (Fig. 3.5). In this range the energy is absorbed by C–O in glucose molecule [15]. Presumably starch was hydrolyzed to glucose. In addition there are significant differences in range 1016–600 cm^{-1}. Absorbance in this range illustrates vibrations of C–O and C–H bonds [16]. Both bonds occur in polylactide and starch molecule. Decreased absorbance in range1016–600 cm^{-1} after the incubation with *A. niger* suggest, that C–O and C–H bonds werepartially broken.

Comparison of FTIR spectra demonstrated biodegradation of both components of foil – polylactide and starch.
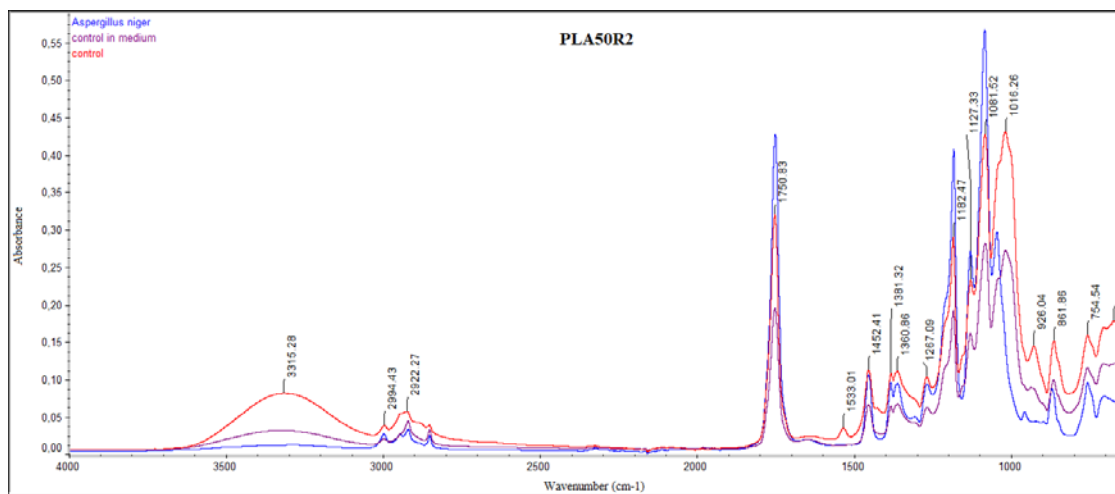
Fig. 3.5 The comparison of FTIR spectra PLA50R2 samples treated with *A. niger* (*Aspergillusniger*), incubated in sterile medium (control in medium) and untreated (control)

3.6 The effect of *Aspergillusniger* on physical structure of polylactide foils surface

As the greatest changes in mass reduction (Fig. 3.2) and chemical structure (Fig. 3.5) were caused by *A. niger*. To study the effect of incubation on physical structure of foils SEM was applied. There were significant differences between samples untreated and treated with *A. niger* (Fig. 3.6). The photograph B (Fig. 3.6) illustrate the damage of PLA50R2 samples, the surface is visibly ragged in opposite to smooth surface of foil which was not treated with fungi (Fig. 3.6A). This difference indicates that *A. niger*can degrade polylactide foil.
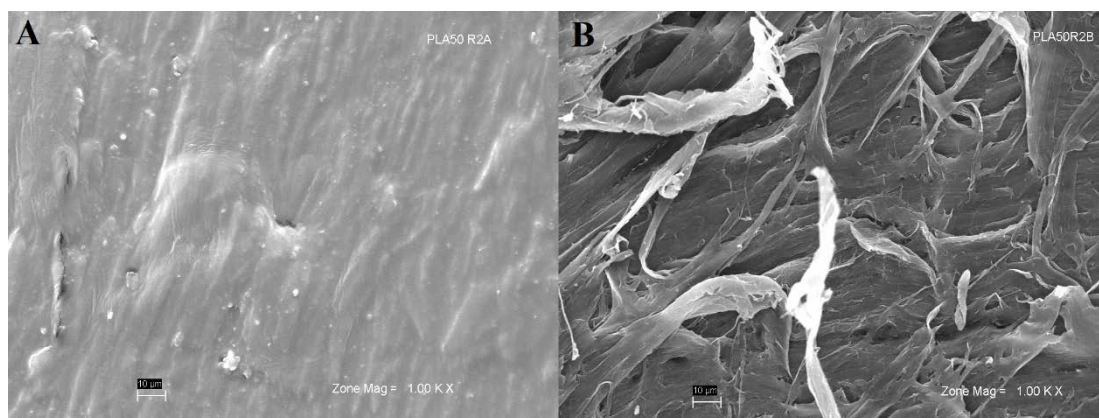
Fig. 3.6SEM photographs of polylactide foil containing 50% of starch and less than 0,75% of additional ingredient (PLA50R2) control samples (A) and treated with *A. niger* PLA50R2 samples (B); magnification 1000×

4. Conclusions

One of the most common occurring naturally fungus, *Aspergillusniger* has the ability to degrade polylactide-starch foil. The degree of biodegradation depends on content of starch, foil production technology and applied additives. Although *A. niger* was isolated together with *Penicilliumminioluteum* the properties of these two mold species appeared different. Monocultures of *A. niger* can biodegrade polylactide-starch foil better than mono-cultures of *P.minioluteum*. However it is worth to notice, that dual cultures of these species in environment containing easy accessible source of organic carbon,can fragment the foil. The greatest massloss reachedover 45% and FTIR analysesconfirmed degradation of both foil components– polylactide and starch, as well. Also, SEM photographs show significant changes in physical structure of foil surface after the incubation with *A.niger*. These results prove that *A. niger* can be applied in PLA biodegradation. Perspective studies include searching for PLA-degrading enzymes from *A. niger.*

Acknowledgment

References

[1] M. Vert,Y. Doi, K.-H. Hellwich, M. Hess, P. Hodge, P. Kubisa, M. Rinaudo, F. Schué, Terminology for biorelated polymers and applications (IUPAC Recommendations 2012), Pure ApplChem 84 (2): 377–410, 2012.

[2] G. Gourmelon, Z. Mármol, G. Páez, M. Rincón, K. Araujo, C. Aiello, Global Plastic Production Rises, Recycling Lags, Vital Signs, Worldwatch Inst., pp. 1–7, 2015.

[3] H. Pranamuda, Y. Tokiwa, H. Tanaka, Polylactide degradation by an Amycolatopsis sp.,Appl Environ Microbiol, vol. 63, no. 4, 637–1640, 1997.

[4] K. Nakamura, T. Tomito , N. Abe, Y. Kamio, Purification and characterization of an extracellular poly(L-lactic acid) depolymerase from a soil isolate, Amycolatopsis sp. strain K104-1, Appl Environ Microbiol,vol. 67, no. 1,345–353, 2001.

[5] F. Li, S. Wang, W. Liu, G. Chen, Purification and characterization of poly(L-lactic acid)-degrading enzymes from Amycolatopsisorientalisssp.orientalis, FEMS MicrobiolLett, 282:52–58, 2008.

[6] E. Schuster, N. Dunn-Coleman, J. Frisvad, P. Van Dijck, On the safety of Aspergillusniger– A review, Appl. Microbiol. Biotechnol., vol. 59, no. 4–5, pp. 426–435, 2002.

[7] L. Karaffa, C. P. Kubicek, Aspergillusniger citric acid accumulation: Do we understand this well working black box?, Appl. Microbiol. Biotechnol., vol. 61, no. 3, pp. 189–196, 2003.

[8] S. E. Baker, Aspergillusniger genomics: Past, present and into the future, Med. Mycol., vol. 44, pp. 17–21, Jan. 2006.

[9] M. Papagianni, Advances in citric acid fermentation by Aspergillusniger: Biochemical aspects, membrane transport and modeling, Biotechnol. Adv., vol. 25, no. 3, pp. 244–263, 2007.

[10] J. Verdoes, P. Punt, A. Stouthamer, C. van den Hondel, The effect of multiple copies of the upstream region on expression of the Aspergillusnigerglucoamylase-encoding gene observed, Gene, vol. 145, no. 2, pp. 179–187, 1994.

[11] B. Svensson, K. Larsen, A. Gunnarsson, Characterization of a glucoamylase G2 from Aspergillusniger, Eur. J. Biochem., vol. 154, no. 3, pp. 497–502, Feb. 1986.

[12] A. M. Larsson, R. Andersson, J. Ståhlberg, L. Kenne, T. A. Jones, Dextranase from Penicilliumminioluteum: reaction course, crystal structure, and product complex, Structure, vol. 11, no. 9, pp. 1111–21, Sep. 2003.

[13] E. R. Jiménez, Dextranase in sugar industry: A review, Sugar Tech, vol. 11, no. 2, pp. 124–134, Jun. 2009.

[14] A. Kowalczyk, E. Capała, M. Chyc, P. Tyński, W. Sadurski, T. Kowalski, D. Latowski,, Biodegradation of Polylactide Modified with Starch by Selected Species of Molds, Proc. 3rd World Congr. New Technol., vol. ICEPR114, 2017.

[15] T. H. Mu, M. Zhang, L. Raad, H. N. Sun, C. Wang, Effect of α-amylase degradation on physicochemical properties of pre-high hydrostatic pressure-treated potato starch, PLoS One, vol. 10, no. 12, pp. 1–15, 2015.

[16] R. M. Silverstein, F. X. Webster, D. J. Kiemle, Spektroskopowe metody identyfikacji związków organicznych., Wydawnictwo Naukowe PWN, 2007.

[17] M. Nampoothiri, Nair NR, John RP., An overview of the recent developments in polylactide (PLA) research, BioresourTechnol, vol. 101, no. 22,8493–501, 2010.

Gasification and pyrolysis process of alternative fuels

Izabella Maj[1], Piotr Ostrowski[1]

[1]*Silesian University of Technology,Institute of Power Engineering and Turbomachinery, e-mail: izabella.maj@polsl.pl*

Abstract

The paper presents results of research for biomass and waste gasification/pyrolysis process with use of flue gas as a converting agent. Syngas (process gas) as well as possible char being a result of the process are combustible and can be recirculated to the boiler's combustion chamber. Presented technology includes a rotary reactor that operates continuously and is integrated with a power boiler, for example WR-25 type grate boiler. The paper presents laboratory research of selected alternative fuels: Refuse derived fuel (RDF), wood chips, nut shells, sewage sludge, coal sludge, mixture of 50% coal sludge with 50% RDF. Basing on the laboratory research a computational model was developed to determine an industrial-size process parameters. The model allows to determinethe reactor's dimension: inner diameter D_{wr} and length L_r. as well as how much alternative fuel can be gasified/pyrolysed in this process.

Keywords: gasification, pyrolysis, biomass, waste

1. Introduction

In thermochemical conversion, the entire fuel is converted into gases or liquids, which are then synthesized into the desired chemicals or used directly for combustion or co-combustion. Gasification is a chemical process that converts carbonaceous materials into useful convenient gaseous fuels or chemical feedstock. Pyrolysis, partial oxidation, and hydrogenation are related processes. Gasification takes place in reducing (oxygen-deficient) atmosphere requiring heat. The purpose of gasification or pyrolysis is not just energy conversion but production of chemical feedstock as well.Pyrolysis takes place in the total absence of oxygen, except in cases where partial combustion is allowed to provide the thermal energy needed for this process. Pyrolysis is a thermal decomposition of the biomass into gas, liquid, and solid. There are three variations of pyrolysis: Torrefaction, or mild pyrolysis,slow pyrolysis,fast pyrolysis [1].

Under the current law regulations it is advisable to develop new technologies for biomass waste thermal conversion. Thermal conversion of waste lead to the following benefits: Conversion of waste chemical energy into heat and electricity, reduction of mass and volume of waste,reduction of landfills number, reduction of the sanitary and epidemiological danger,solid products of the process can be used for agricultural purposes.Pyrolysis or gasification processes allow to reach following benefits without problems connected to direct waste combustion and co-combustion. Feeding boiler's combustion chamber with syngas (process gas, which is a result of gasification/pyrolysis process) significantly reduces slagging, fouling and high temperature corrosion of heated surfaces of the boiler. Products of gasification and pyrolysis process can be accumulated and used at another time or purpose, what is an advantage of these processes comparing with direct combustion.Moreover according to actual Polish law [2] it is forbidden to store waste that can be characterized by:

a) Total organic carbon (TOC) content above 5% of dry matter,

b) loss on ignition (LOI) above 8% of dry matter,

c) lower calorific value above 6 MJ kg of dry matter.

Presented laboratory research and calculation procedure have been developed due to strong need for creating new technologies for waste and biomass thermal conversion. The aim of presented study is:

- To assess the possibility of using flue gas as a converting agent for thermal conversion of alternative fuels (waste and biomass) and to recognize the usage of selected alternative fuels for thermal conversion in low temperature gasification/pyrolysis process witch use of flue gas as a converting agent,

- To assess the influence of process temperature, fuel granulation and moisture content on syngas composition and the conversion rate of selected fuels,

- To determine construction parameters for the rotary gasification reactor assuming that gasification/pyrolysis process is performed continuously in an industrial scale.

2. Law principles of process gas combustion and co-combustion

The technology of indirect co-combustion of waste through the integration of a gasification reactor with a power boiler does not require the construction of a new thermal waste facility. It can be based on a local waste management facility, which ensures continuous supply of waste and local boiler house or energy company that provide the possibility of integrating the reactor with its boiler. The implementation of gasification technology is therefore cheaper than the construction of a new waste combustion facility. In addition, it is not associated with any objections from the local community [3].

The Industrial Emissions Directive of European Commission [4] distinguishes gasification and pyrolysis of waste from combustion. Article 42 of the Directive indicates that special requirements for thermal treatment of waste do not apply to gasification or pyrolysis installations. It provides that if the syngas from these thermal processes is purified such it does not cause emissions bigger than combustion of natural gas it is no longer threatened as waste combustion. This rule was implemented in September 2014 into Polish legislation [5]. According with the requirements of the Directive, combustion of syngas from gasification of waste should meet the emission requirements for natural gas. They are defined in the following standards: PN-C-04752: 2011 and PN-C-04753:2011. Meeting this requirements for syngas combustion allows to omit the technical requirements set by the Regulation of the Development Ministry ("waste regulation") [6] regarding the waste thermal treatment conditions:

• Flue gas temperature from higher than 850°C in no less than 2 seconds

and

• The total organic carbon content (TOC) in slags and ash less than 3% mass, or loss of ignition (LOI) for slags and lower than 5% on dry matter.

Moreover there is no need to apply emission standards provided for waste combustion and co-combustion. When purified syngas is combusted the power unit should comply with emission standards for natural gas combustion in energy facilities.

3. Laboratoryresearchresults

Experimental laboratory research was conducted to develop design requirements and to identify the usability of the selected alternative fuels (biomass and waste fuels) for indirect co-firing in power boilers. Tests were conducted for following fuel types: Refuse derived fuel (RDF), biomass - wood chips, food processing waste - nut shells, sewage sludge, coal sludge, mixture of coal sludge 50% witch RDF 50%.Tests were conducted in a laboratory gasification reactor designed and constructed specifically for this purpose. The experimental stand enables the weight loss of a sample and resulting gas composition to be recorded. The sample mass is approximately 3 g, which distinguishes the method from the classic TGA method, which is frequently used for fuel thermal conversion investigations. Presented experimental setup enables to investigate gasification, pyrolysis, torrefecation and combustion, depending on agent composition and temperature requested. Experimental equipment allows to measure and record following parameters: Initial mass of the fuel sample, syngas composition (O_2, CO_2, CO, CH_4, C_nH_m), process temperature and gas flow.Tests were conducted in the temperature range of 350-850°C and with the application of dry and wet converting agents and for fuel in two states: as received and ground. It allows to identify the impact of the process temperature, the type of gasification agent and fuel granulation on the resulting gas (syngas) composition. Results of experimental gasification/pyrolysis process of RDF fuel are presented in Fig.s3.1-3.4.
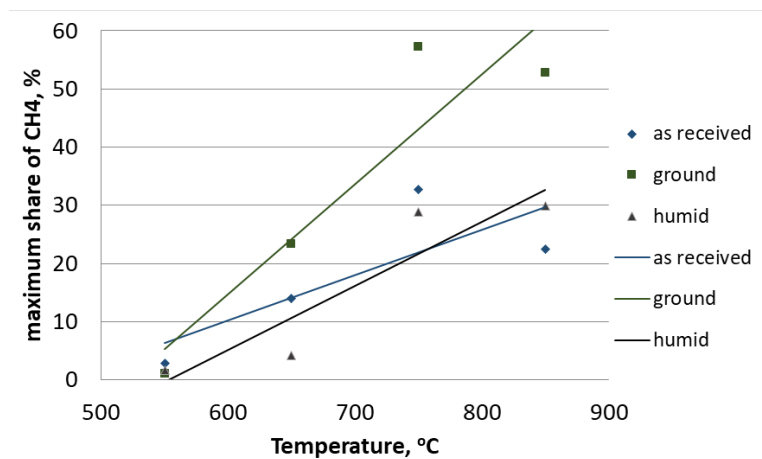
Fig. 3.1. Max CH$_4$concentration in syngas for RDF conversion process
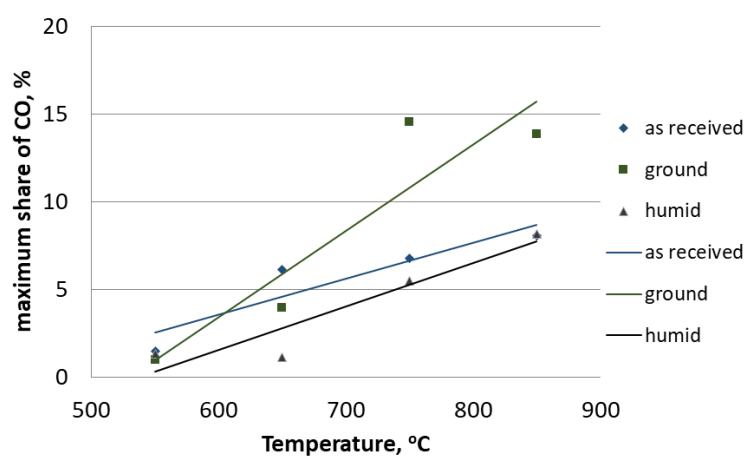
Fig. 3.2. Max CO concentration in syngas for RDF conversion process
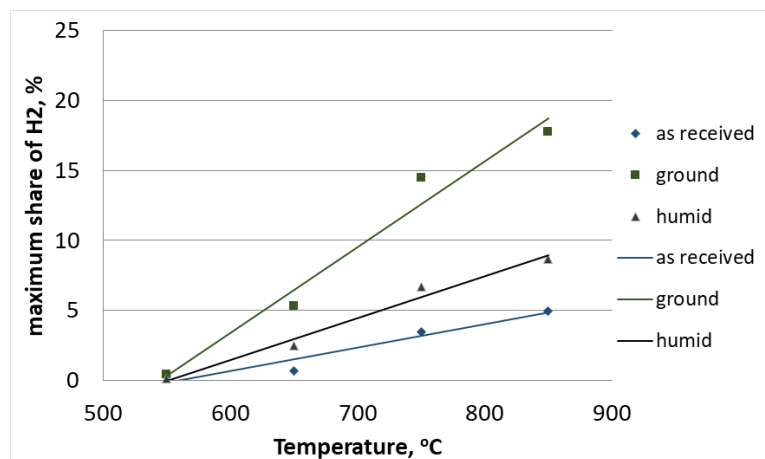
Fig. 3.3. Max H$_2$ concentration in syngas for RDF conversion process
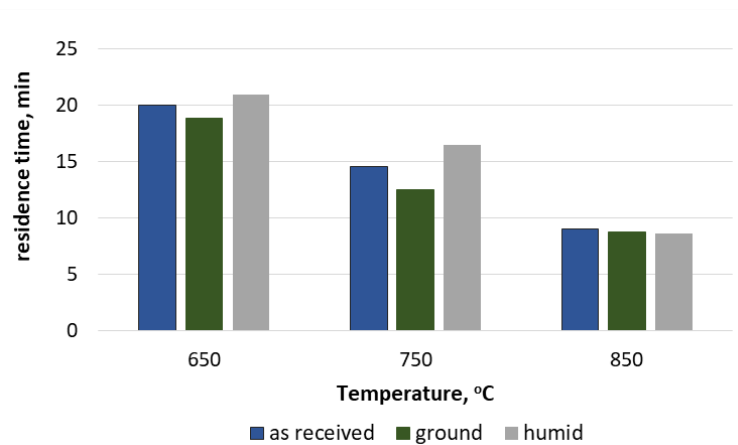
Fig. 3.4 Residence time for RDF

4. Industrial-scale gasification/pyrolysis process parameters

Basing on the laboratory research results a calculation procedure was developed. In allows to determine the syngas flow and composition as well as reactor's dimensions and operating parameters. Gasification/pyrolysis reactor is supposed to be integrated with a power boiler according to scheme on Fig. 4.1.
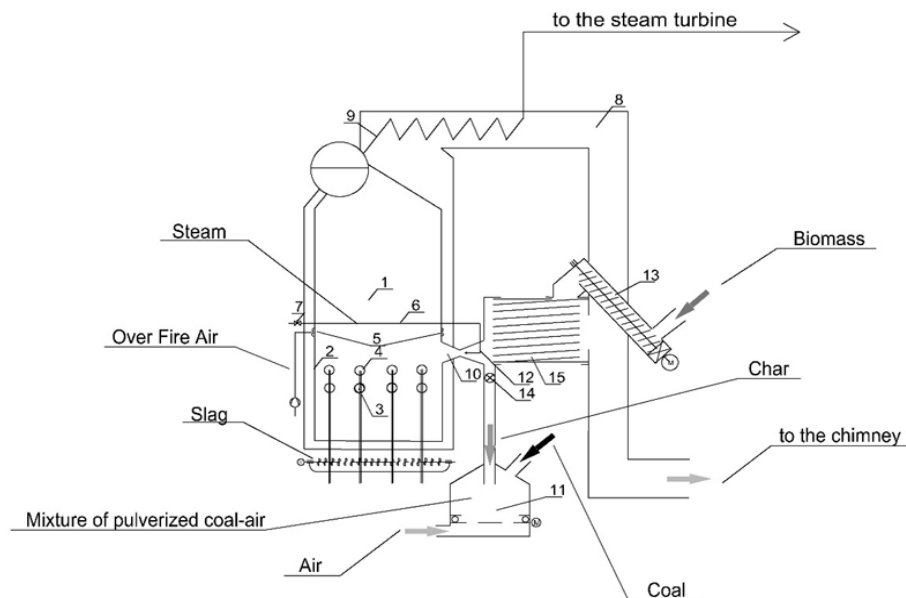
Fig. 4.1 Scheme of integration of power boiler with biomass and waste thermal treatment reactor

Research base on an idea of indirect co-combustion of waste and biomass in power boilers. The developed co-combustion technology was based on patent applications [7-10] and previous experience [11-18]. Flue gas flowing out from the combustion chamber – 1 goes through the heat exchanger – 9 and through the flue gas duct, from where it flows to the chimney. The installation for indirect co-firing of biomass consists of a reactor 15 supplied with a stream of shredded biomass in the feeder system – 13 and a stream of flue gas induced by the injector – 10. Flue gas is taken from the combustion air duct – 8 by the stream of a working agent (water steam, compressed flue gas) supplied to the nozzle – 12 by injector – 10. These flue gas enters the reactor – 15 where the thermal treatment of biomass is made. The output of the flue gas injector – 10 is adjusted to the process requirements by a control valve – 7 built in the propeller duct – 6 to the drive nozzle – 12. Flue gas flowing out from the reactor – 15 with flammable gas products of the degradation process feeds the burners – 3 and 4, and solid flammable and non-flammable products are transported through the lock – 14 and possibly returned to the process.

As an example of calculations for integrating the reactor with WR-25 boiler is presented in Tab. 4.1. Reactor under construction is presented in Fig. 4.2. Reactor's parameters are defined as:

L_w – Reactor's length

D_w – Reactor's inner diameter

β – angle of reactor's axis

n_{obr} – revolutions per minute

Fig. 4.2 Gasification/pyrolysis reactor under construction

Tab. 4.1 Process parameters and reactor's properties for integration of gasification/pyrolysis reactor with WR-25 boiler

Parameter	Symbol	Value	Unit
Fuel flow	$\dot{m}_{sub}$	397,9	kg/h
Residence time	τ_p	516	s
Reactor diameter	D_{wr}	1,424	m
Reactor lenght	L_r	4,807	m
L/D ratio	L_r/D_{wr}	3,376	-
Revolutions per minute	n_{obr}	1 (with regulation range 0,5-1,5)	rpm
Reactor's axis angle	β	16	°
Gas velocity (inside the reactor)	vg	0,5	m/s

Presented calculations assume 6% oxygen share in flue gas. It takes into account that 2,5% of flue gas from WR-25 boiler is provided to the gasification reactor. Enthalpy of flue gas allows thermal conversion of 397,9 kg/h (9,55 tones per day) of RDF fuel. Presented calculation was conducted for each of tested fuel having regard three

oxygen concentration levels: 6%, 8% and 10%, which are typical for grate boilers. Total oxygen in assumed to take part in partial combustion taking part in the reactor. Results summary are presented in Tab. 4.2.

Tab. 4.2 Gasification/pyrolysis process parameters (calculated) and reactor's dimensions

Fuel type	Concentration of O_2 in flue gas	Syngas composition (calculated)				Fuel stream	Reactors dimensions	
		[CH$_4$]	[CO]	[N$_2$]	[CH$_4$]	$\dot{m}_{sub}$	D$_{wr}$	L$_r$
		%	%	%	%	kg/h	m	m
RDF	6%	9,54	2,39	73,56	9,54	397,9	1,424	4,807
	8%	15,06	3,77	68,32	15,06	703,8	1,601	5,404
	10%	19,85	4,96	63,79	19,85	1142,0	1,821	6,145
Wood chips	6%	2,08	8,33	74,81	2,08	370,1	1,414	1,053
	8%	3,34	13,33	70,05	3,34	665,4	1,584	1,179
	10%	4,46	17,86	65,91	4,46	1078,5	1,796	1,337
Nut shells	6%	2,58	9,73	73,22	2,58	430,6	1,427	1,912
	8%	4,05	15,24	67,93	4,05	774,3	1,605	2,151
	10%	5,31	19,97	63,39	5,31	1256,5	1,826	2,447
Sewage sludge	6%	2,82	8,94	73,68	2,82	412,7	1,423	6,351
	8%	4,45	14,40	68,55	4,45	741,8	1,599	7,142
	10%	5,86	18,55	64,12	5,86	1203,0	1,817	8,115
Coal sludge	6%	10,16	1,26	73,96	10,16	295,5	1,397	9,311
	8%	15,94	1,97	69,09	15,94	502,6	1,594	10,618
	10%	21,37	2,63	64,47	21,37	812,2	1,813	12,077
Coal sludge 50% + RDF 50%	6%	13,83	0,21	71,77	13,83	318,3	1,440	2,143
	8%	21,90	0,33	65,45	21,90	565,4	1,631	2,429
	10%	28,63	0,44	60,18	28,63	912,2	1,867	2,780

5.   Conclusions

Gasification/pyrolysis processscan be a way of alternative fuels co-firing in industrial or power plant boilers. As a first step laboratory research was carried out to investigate usability of selected fuels for low-temperature gasification/pyrolysis. This process may take place in temperature ranging from 350°C. Laboratory research was conducted in a reactor designed and constructed fora thermal conversion of 1-3 g mass sample. The aim of the study was to use the flue gas-alike gas mixture as a gasifying agent. The result of presented laboratory research is the assessment of the usability of selected alternative fuels for indirect co-firing in power boilers and to build a knowledge base for industrial-size process. Investigated parameters were: gasification kinetics (recommended time for total gasification – residence time), fuel granulation, process temperature. Basing on laboratory results a computational model was developed to determine parameters for industrial-size process. It assumes a rotary reactor that operates continuously and is connected to a grate boiler WR-25. Presented method of in-direct co-combustion of waste and biomass can be a part of local waste management or an element of renewable energy sources system.

References

[1] BasuPrabir: Biomass Gasification and Pyrolysis Practical Design and Theory.

[2] Rozporządzenie Ministra Środowiska z dnia 9 grudnia 2014 r. w sprawie katalogu odpadów. Dziennik Ustaw Rzeczypospolitej Polskiej 2014 poz. 1923

[3] Nikodem W.: Zgazowanie odpadów komunalnych, Polityka energetyczna, tom 10, zeszyt specjalny 2, 2007

[4] Directive 2010/75/EU of the European Parliament and of the Council of 24 November 2010 on industrial emissions (integrated pollution prevention and control)

[5] Ustawa o odpadach z dnia 14 grudnia 2012 roku (tekst jednolity Dz.U. z 2016, poz. 1987

[6] Rozporządzenie Ministra Rozwoju z dnia 21 stycznia 2016 r. w sprawie wymagań dotyczących prowadzenia procesu termicznego przekształcania odpadów oraz sposobów postępowania z odpadami powstałymi w wyniku tego procesu. Dziennik Ustaw 2016 poz. 108.

[7] Ostrowski P., Pronobis M., Kalisz S., Gramatyka F., Wejkowski R., 2008. Patent PL212497 Method and installation of biomass pyrolysis prior to cofiring, in particular in power boilers (in Polish). WUP: 10/12.

[8] Ostrowski P., Pronobis M., Kalisz S., Gramatyka F., Wejkowski R., 2008. Patent PL212557 Method and installation of carbonisation and biomass gasification prior to cofiring, in particular in power boilers (in Polish). WUP: 10/12.

[9] Ostrowski P., Pronobis M., Kalisz S., Gramatyka F., Wejkowski R., 2008. Patent PL214645 Method and installation of biomass gasification prior to cofiring, in particular in power boilers (in Polish). WUP: 10/12.

[10] Ostrowski P., Pronobis M., Kalisz S., Wejkowski R., Remiorz L., 2013. Patent application P393836 Method of measuring and gas stream meter in short closed ducts of large cross-section area, in particular in air and flue gases boiler and ventilation circuits (in Polish). BUP 13.08.

[11] Ostrowski P., Maj I., Kalisz S., Polok M.: Biomass low-temperature gasification in a rotary reactor prior to cofiring of syngas in power boilers. Applied Thermal Engineering 2017 vol. 118, s. 785-795 ,DOI: 10.1016/j.applthermaleng.2017.02.120 [7] Ostrowski P., Kalisz S., Pronobis M., 2010. The concept of jet-ventilator assisted in-direct biomass cofiring in boilers (OTHERM). International Conference on Boiler Technology ICBT'2010, Szczyrk, Poland, 18-22 October 2010.

[12] Ostrowski P., 2013. Innovative measuring techniques and technologies in modernisation of energy and industrial installations and equipment (in Polish). Monograph of Silesian University of Technology, Nr/507.

[13] Litka R.. Kalisz S., 2012. Thermochemical analysis of a flue gas-driven biomass gasification. Chemical and Process Engineering, 33 (3), 487-503. DOI: 10.2478/v10176-012-0041-y.

[14] Ostrowski P., Remiorz L., 2012, Measurement of gas flow in short ducts, also rectangular, Elsevier Editorial System Flow Measurement and Instrumentation, 49 (2), 301-311

[15] Ostrowski P., Maj I., Kalisz S., Polok M: Testing of an innovative installation for alternative fuel low-temperature gasification prior to co-firing in power boilers. Procedia Engineering vol. 174 s. 1877-7058, DOI: 10.1016/j.proeng.2017.01.175

[16] Maj I, Kudlek E., Ostrowski P., Pronobis M: Investigation of sewage sludge gasification with use of flue gas as a gasifying agent. E3S Web of Conferences vol. 14 s. 2267-1242, DOI: 10.1051/e3sconf/20171402001

[17] Maj I.: Badanie kinetyki zgaozwania wybranych paliw alternatywnych oraz zalecenia dla eksploatacji przykotłowych instalacji zgazowania. Praca doktorska, Politechnika Śląska, Instytut Maszyn i Urządzeń Energetycznych, Gliwice 2018

Ecological Waste Heat Recovery for grate boilers

M.Eng. Jakub Sobieraj[1]

[1]Division of Boilers and Steam Generators, Faculty of Energy and Environmental Engineering, Silesian University of Technology, jakub.sobieraj@polsl.pl

Abstract

Paper presents the technology of Ecological Waste Heat Recovery (EWHR) which has been developed by the researchers from Division of Boilers and Steam Generators and implemented by spin-off of this Division – N-ERGIA sp. z.o.o. EWHR system is a hybrid system which allows to reduce emission of the pollutants contained in the flue gas (e.g. SO_2, PM) and increase the overall boiler efficiency at the same time. The paper presents description of the technology, economical calculation and results of the emission measurements. EWHR system is described as a solution for municipal and industrial grate boilers to the more restricted legislation.

Keywords: grate boiler, emission, flue gas treatment

1. Introduction

EWHR (Ecological Waste Heat Recovery) is a relative cheap solution for flue gas treatment system and at the same time it allows to increase the overall boiler efficiency decreasing the stack loss and recover latent heat from flue gas. The efficiency increase is a vital for all industrial subjects and the demanding's comes from legislation. Second problem which could be solved with EWHR technology is a limitation of the emission from combustion plants. The emission standards are very strict and could be a real problem especially for older industrial and municipal boilers. Emission standards from BAT conclusions according to the IED limit the emission of SO_2, NO_x, PM's (dust) and few other pollutants what makes the plants need to be modernized and adapted to the new legislation's rules. Tab. 1.1. pre

sents emission standards for existing combustion plants built before 29.03.1990.

Tab. 1.1. Current emission standards for boilers between 5..50MW put into use before 29.03.1990   with 6% O_2 concentration in flue gas

SO_2 , mg/m^{3}n	NO_X , mg/m^{3}n	PM, mg/m^{3}n
1500	400	100

What is more, currently legislation will be replaced by new one for MCP (Medium Combustion Plants – units >5MW) which is more restricted even in case of existing units. The emission standards are shown in Tab.1.2.

Tab.1.2. New emission standards for existing units >5MW since 2025

SO2 , mg/m3n	NOX , mg/m3n	PM , mg/m3n
200 (biomass), 400 (other solid fuels)	650	30

Since 2018 the new units with >5MW have to meet emission standards shown in Tab.1.3.

Tab. 1.3. Emission standards for new units >5MW since 2018

SO_2 , mg/m³n	NO_X , mg/m³n	PM , mg/m³n
200 (biomass), 400 (other solid fuels)	300	20

Regarding the data contained above it's obvious that the gas treatment systems have to be very efficient and reliable to meet new emission standards. Big advantage of the EWHR system is it could limit different pollutants within one system which is also heat recovery system in the same time. What is important, the EWHR system could be applied for different fuel types like a gaseous or solid fuel. The EWHR system was developed by the Division of Boilers and Steam Generators at the Faculty of Energy and Environmental Engineering and implemented by N-ERGIA Sp. z.o.o. Spin-off of the Silesian University of Technology.

2. EWHR implementation on the grate boiler

EWHR system was successfully implemented in the stocker boiler with heat output 2,32 MW and capacity 3 t/h. The new installation was projected in parallel with the existing old one to be able to use bypass. Installation consist of 2 heat exchangers: dry heat exchanger and wet heat exchanger (scrubber) connected in row. Dry heat exchanger is cooled by a condensate from a boiler and the excessive heat is used in primary air pre-heater. Scrubber is cooled with water with alkalines additive what allows to reduce SO2 emission, PM's emission, recovery heat and transfer it to the primary air, own needs heat and/or demineralized water. This condensate could be used also as a water to boiler (has to be prepared). Cooled and dried flue gas (with recovered latent heat) flows through the stack to the environment. Fig 2.1. Presents the scheme of the installation.
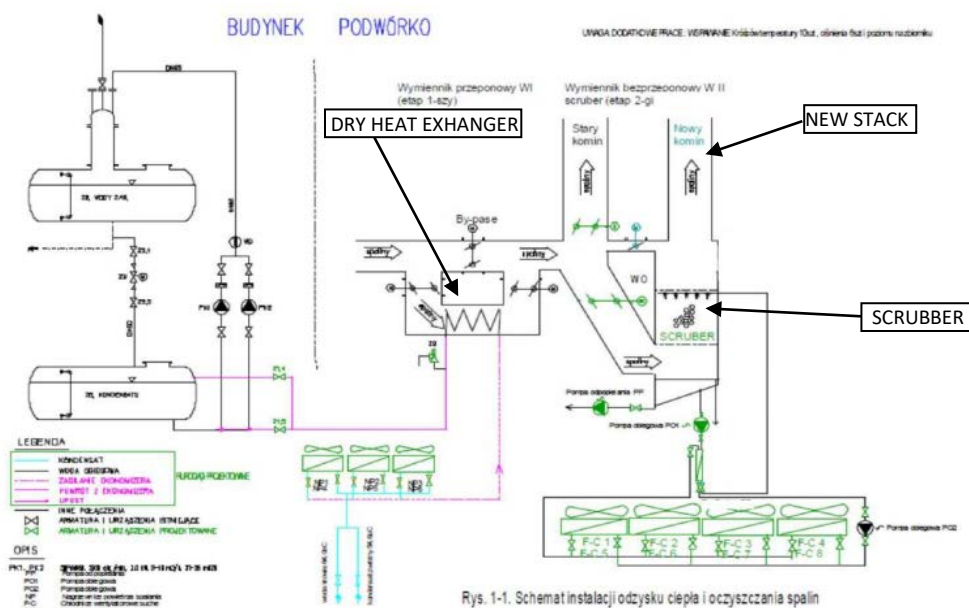
Fig. 2.1. Scheme of the EWHR system

3. Efficiency and savings

Efficiency is an indicator that shows the difference between the real and ideal processes. The definition of the efficiency could be different according to the process, device, medium or working principle. In the case of the industrial or municipal boilers the efficiency is calculated as a ratio of the heat transferred to the medium (steam or water depends on boiler type) to the chemical energy concluded in the fuel. This method is called direct method and requires the steam parameters, fuel properties and fuel mass flow to be known. Usually the efficiency of the boiler is calculated according to the LHV (Lower Heating Value) what could be inadequate in case of boilers in which flue gases are cooling down below dew point and condensation occurs. Direct method is

difficult to apply because of the fuel mass flow measurement especially in case of the solid fuel like a coal or biomass. Direct efficiency is quite simple to evaluate for the gas and oil fired boilers. Equation (3.1) presents the formula for direct efficiency calculations.

$$\eta = \frac{Q_{transferred\ to\ the\ medium}}{Q_{in\ fuel}} \qquad (3.1)$$

Second method for efficiency measurement is the indirect method which assume that the efficiency is equal to 1 and all the losses that appear in the processes occurring in the boiler decrease this value and should be subtracted. This method is presented in equation (3.2) Efficiency could be calculated indirectly also according to the equation (3.3), where heat fluxes are used. Generally losses in the boilers are: stack loss, enthalpy and unburned particle loss in the fly ash and incomplete combustion loss, heat loss to the environment (could be assumed as a constant for each type of the boiler), boiler house heating, desalination and blowdown loss.

$$\eta = 1 - \sum loss \qquad (3.2)$$

$$\eta = \frac{Q_{in\ fuel} - \sum Q_{loss}}{Q_{in\ fuel}} \qquad (3.3)$$

In this analysis the most important loss is the stack loss. The loss comes from the flue gas enthalpy what is strictly connected with its temperature. The higher the outlet temperature the higher the loss. Typically the flue gas outlet temperature is in between 130 – 240ºC in order to avoid sub-cooling to the acid dew point. This values limit the gaseous and oil boilers efficiency to 94%, pulverized coal boilers to 92% and grate boilers to 84% (76% in case of flue and smoke tube type boiler).

EWHR is a system which allows to reduce the outlet loss by decreasing temperature and recover the latent heat from condensation process. Latent heat is a difference between the specific enthalpy the saturated steam and specific enthalpy of the saturated water. The latent heat of the steam concluded in the flue gases is equal to 2258 kJ/kg with assumption that the flue gas pressure is equal to the atmospheric. Thanks to the efficiency increase and emission limitation power plants and municipal boilers combust less fuel to produce the same amount of the usable heat what makes that whole process is much cheaper. Savings which comes from the more efficient process could be assumed by efficiency calculations or by calculating the fuel saving. The difference between fuel usage before and after modernization multiplied by the fuel cost per unit (e.g. PLN/t) gives the potential profit that comes from the system implementation. Investment cost (CAPEX) has to be included as a cost which reduces profit. Economical analysis will be presented further.

4. Performance of the EWHR system

Once the EWHR system was implemented on the flue tests were conducted. The results of the operation tests of the boiler house equipped with flue and smoke tube type boilers with capacity of 2 x 3 t/h working with load of about 50% for roughly 8200 h/a are presented in the Tab.s below. Tab. 4.1. shows the results from two boilers working in the winter with total output heat equal to the 3006 kW.

Tab. 4.1. Heat recovered and transferred by the EWHR system

Boilers heat	3006 kW				
Heat recovered			Heat transferred		
Cooling			Heating		
Dry HX	Scrubber	Total	Dry HX	Scrubber	Total
166,6 kW	167,5 kW	334,1 kW	164,9 kW	165,8 kW	330,8 kW
		11,11%			11,00%

Tab.4.2. shows the calculation of PP (Payback period) rate. The PP rate shows how long it takes to return the investment. Calculations were conducted for the operation parameters from Tab. 4.1.

Tab.4.2. PP calculation

Boiler's heat generation	MW	3,006
Heat recovered	MW	0,1654
Number of boilers	pcs.	2
Working time annually	h	8200
Recovered energy annually	MWh	2712,6
Energy price per unit (steam)	PLN/MWh	95,00
Profits annually	PLN	257 693
Cost of investment	PLN	636 000
Payback period	years	**2,47**

Calclations shows that the paybac period is quite short and accepTab.. Short period of payback is very beneficial not only because of the profits but also decrease the risks which have to be included in the detailed analysis. Due to the fact that the economic and political environment causes dynamic changes in the legislation in this type of investment, a relatively quick recovery time is required.

5. Emissions

Data contained in the previous section show the economic justification for the use of the system EWHR. The Tab.s below show the emission data that was obtained after implementing the system under operating conditions. Few different configurations of the scrubber were tested to check the overall performance of each configuration and to examine the capabilities of the device.

Tab.5.1. Emission from the EWHR with half fluidized spray water and NaOH composition scrubber, 6% $[O_2]$ in the flue gas

	$[NO]$, mg/m^3_n	$[NO_2]$, mg/m^3_n	$[SO_2]$, mg/m^3_n	PM, mg/m^3_n
Before EWHR	261,8	401,4	1313,0	205,2
After EWHR	254,4	390,2	98,33	48
Emission reduction	Δ NO	Δ NO$_2$	Δ SO$_2$	Δ PM
	7,4	11,2	1214,7	157,2
	1,65%	2,79%	92,51%	76,67%

Tab.5.2. Emission from the EWHR with water spray scrubber, 6% $[O_2]$ in the flue gas

	$[NO]$, mg/m^3_n	$[NO_2]$, mg/m^3_n	$[SO_2]$, mg/m^3_n	PM, mg/m^3_n
Before EWHR	396,8	430,2	1149,2	164,85
After EWHR	391,4	400,0	911,9	63,54
Emission reduction	Δ NO	Δ NO$_2$	Δ SO$_2$	Δ PM
	5,4	30,2	237,3	131,31
	1,36%	7,02%	20,65%	79,65%

The results presented above confirm the effectiveness of the flue gas purification system and the potential of the system allows to guess that the emission can be reduced even more. There is one more configuration which allows to use NaClO to reduce NO_2 emission under the emission limit. What is interesting, the use of only water causes a significant reduction of PMs emissions to the environment and also has a certain effect on the reduction of sulfur dioxide.

6. Conclusions

The EWHR system implementation significantly increasing the efficiency of the boiler and allows to decrease the operational costs and emission of CO_2 by 11% in the winter. Reduced cost of the fuel is equal to 257 700 PLN/annually and what causes that payback period rate is equal to roughly 2,5 years. Emission control measurements confirm compliance with the requirements of emission standards what demonstrate that the unit is suiTab. for operation. The experience also allows to expect that the installation also reduces the emission of chlorine oxides. EWHR system is scalable and could be applied to the different boilers and different types of boilers. Pre-studies shows that the effect of implementation on different boiler could be even better than in the case described above.

Acknowledgment

References

[1] Szargut J., Termodynamika techniczna,, Wydanie Politechniki Śląskiej, Gliwice, 2000.

[2] Pronobis M., Modernizacja kotłów energetycznych,, WNT, Warszawa 2013.

[3] Prawo energetyczne DU RP z 06.02.2017 poz. 220 (jednolity tekst ustawy) Energy Law DU RP of 06.02.2017 item 220 (uniform text of the Act).

[4] Commission Implementing Decision (EU) 2017/1442 of 31 July 2017 establishing best available techniques (BAT) conclusions, under Directive 2010/75/EU of the European Parliament and of theCouncil, for large combustion plants (notified under document C(2017) 5225).

[5] Dyrektywa Parlamentu Europejskiego i Rady 2010/75/UE z dnia 24 listopada 2010 r. w sprawie emisji przemysłowych (zintegrowane zapobieganie zanieczyszczeniom i ich kontrola) (Dz. Urz. UE L 334 z 17.12.2010, str. 17, z późn. zm.) Directive 2010/75 / EU of the European Parliament and of the Council of 24 November 2010 on industrial emissions (integrated pollution prevention andcontrol) (Of. Journal of the European Union L 334, 17/12/2010, page 17, with late changes).

[6] Rozporządzenie MŚ. w sprawie standardów emisyjnych dla niektórych rodzajów instalacji, źródeł spalania paliw oraz urządzeń spalania lub współspalania odpadów. DU RP z 4.11.2014 poz.1546 Regulation of the Minister of the Environment regarding emission standards for certain types ofinstallations, fuel combustion sources and waste incineration or co-incineration devices. DU RPof 4 November 2014, item 1546.

[7] Dyrektywa Parlamentu Europejskiego i Rady (UE) 2015/2193 w sprawie ograniczenia niektórych zanieczyszczeń do powietrzaze średnich obiektów energetycznego spalania (MCP). Directive 2015/2193/EU of the European Parliament and of the Council on the certain pollutants emission limitation by medium combustion plants (MCP).

Combustion characteristic of halloysite doped biomass: impact on ash deposition tendency

Waldemar Gądek[1], Szymon Ciukaj[2], Sylwester Kalisz[3]

[1]*Division of Boilers and Steam Generators, Institute of Power Engineering and Turbomachinery, Silesian University of Technology, e-mail:waldemar.gadek@polsl.pl*

[2]*Division of Boilers and Steam Generators, Institute of Power Engineering and Turbomachinery, Silesian University of Technology, e-mail:sylwester.kalisz@polsl.pl*

[3]*Division of Boilers and Steam Generators, Institute of Power Engineering and Turbomachinery, Silesian University of Technology, e-mail:szymon.ciukaj@polsl.pl.*

Abstract

Deposit formation, erosion and corrosion are combustion problems which are related with the negative influence of fuel inorganic matterto the combustion system and hence decrease the thermal efficiency of the boiler. The uncontrolled deposit formationmight limit the flue gas flow in the boilerthus give mechanical restrictionswhich may stop theboiler operation. This paper presents the results from the investigation of the halloysite use as an additive for mitigating slagging and corrosive deposits formation, commonly found in boilers fired with the agricultural biomass with high alkali metals (K+Na) and chlorine content. In this study straw biomass samples were conditioned with thehalloysite in the order to decrease ash deposition tendency and compared to ash deposition tendency resultingform combustion of hard coal. The experiments were carried out on laboratory Pulverized Fuel Combustion Chamber (PFCC).

Keywords: halloysite , combustion, biomass

1. Introduction

Deposit formation, erosion and corrosion are combustion problems which are related with the negative influence of fuel inorganic matterto the combustion system and hence decrease the thermal efficiency of the boiler. The uncontrolled deposit formation might limit the flue gas flow in the boilerthus give mechanical restrictions which may stop the boiler operation. Generally, two types of deposit formation can be recognized in firing systems: slagging and fouling. In the high-temperature refractory sections of the boiler furnace and other surfaces in the radiant section of the boiler, slagging is prevailing. It appears as a result of radiative heat transfer, which is dominant there and causes the presence of molten ashes. Slagging decreases the heat absorption in the furnace resulting in the furnace exit gas temperature increase. Whereas, fouling takes place in the furnace outlet and convective heat transfer sections of the boiler. There are two types of fouling: the high-temperature fouling which is determined by the formation of semi-fused, sintered ash deposits which appear typically in the flue gas temperature range of 1300 ˚C - 900˚C and the low-temperature fouling which is related with the formation of the loose or slightly sintered deposits built-up in flue gas temperature range900 ˚C – 300 ˚C [1-5].

Utilization of biomass as carbon neutral fuel brings many benefits. However, combustion and co-combustion of biomass, especially agriculture residue biomass, is associated with many technical problems such as: bed agglomeration in CFB/BFB boilers, slagging and fouling, chlorine corrosion, decreased boiler efficiency which do not occur in conventional fossil fuel combustion. Those problems are associated with high alkali metal (K and Na) contents in the fuel, especially potassium as a deposit formation precursor. In the presence of sulphur, chlorine and silica, the alkali silicate would be formed which is characterized by low melting or softening point what may result in high deposit formation on boiler heat surfaces.

Biomass boilers generally suffer from serious problems with slagging and fouling of the superheaters [5-9]. These problems are primarily due to the large content of 'troublesome' elements such as potassium and chlorine which are contained in biomass. The release and transformation of these inorganic elements lead to different ash related problems during the combustion processes.

2. Methodology

2.1. Additive

Halloysite belongs to aluminosilicate additives used for biomass enhancement. It has a chemical formula desribedas Al2Si2(OH)5·nH2O. Halloysite is a unique 2-layer mineral with a large interplanetary space with high sorption capacity. Aluminium (Al) forms octalateral elements (octahedral), whereas silicon (Si) quadrilateral ones (tetrahedra). The content of inter-packet water (the number of crystal water particles n) depends on the elementary crystal structure and temperature. Halloysite is characterized by a large number of replacements of atoms for atoms Si and Al in crystal structures. It causes that halloysite has the capacity for forming various types of bonds with ions which are near to bases or lateral surfaces of crystals. In halloysite, the structure can be seen free spaces in booth layers, which are locations for various ions (especially K). Available space determines the type of adsorbed ions [10, 11].

Halloysite is characterized by a large surface area which is about 60÷80 m2/g and results from the tubular construction of crystals and has a small hardness grade (1÷2 in Mohs scale), which facilitate it for mechanical processing. Halloysiteis also characterized by its high-temperature resistance and high reactivity, which is the result of phase changes occurring in temperature range >550 °C significantly increasing the ability to form compounds with alkali metals with high sintering and melting temperatures.

The halloysiteadded to the fuel has the following physical and chemical parameters:

- Bulk density: 0.72 -0.85 g / cm3

- pH = 7

- Chemical composition:

- Al2O3 - 32-40%

- SiO2 - 33-44%

- Fe2O3 - 15-20%

- TiO2 - 1.5-4%

- CaO <0.8%

- K2O <0.1%

- Na2O <0.1%

- S <0.05%

- Moisture content: 2-4%

- Specific surface area: 60-70 m2 / g

- Hardgove index (HGI) ≥200

2.2. Investigated fuels

In this study a cereral straw DS0 and WS hard coal from polish mine KWK Sobieski were investigated. Raw biomass fuel was milled, mixed with halloysite and pelletized. Results of analysis are presented in Tab. 1. Analysis were carried out in certified laboratory using PN-ISO procedures. In contrast to typical ultimate analysis in Tab.2.1 content of potassium and sodium are presented as critical for deposition tendency. Total content of alkali metals (Na +K) are also included. Investigated biomass is characterized by considerable higher content of alkali metals 1,33% wt. compared to coal 0,65% wt. Moreover DS0 is described by low content of sulfur 0,11% wt. compared co coal 1,46% wt. The presence of sulfur in fuel effectively decrease deposition tendency of fuel. Fuels composition of DS0 (without halloysite) DS4 with additive dose 4% wt. of halloysite and coal WS is shown inTab.2. 1

Tab.. 2.1 Results of proximate and ultimate analysis of fuel

Proximate analysis wt% (as fired)			
No.	DS0	DS4*	WS
Moisture	11.7	11.7	3.9
Ash	9.13	13.13	13.8
Volatiles	61.11	58.03	34.37
Fixed Carbon	18.05	17.14	47.93
Ultimate analysis wt% (as fired)			
C	38.98	37.01	61.69
H	4.85	4.6	4.65
S	0.11	0.11	1.46
N	0.76	0.72	0.98
Cl	0.38	0.36	0.34
Na	0.071	0.068	0.34
K	1.26	1.210	0.31
O	32.76	31.08	12.53
LCV (MJ/kg)	14.37	13.64	23.77
(Na+K)	1.33	1.28	0.65

*Theoretical (calculated) fuel state are presented for 4% wt. dosage of halloysite.
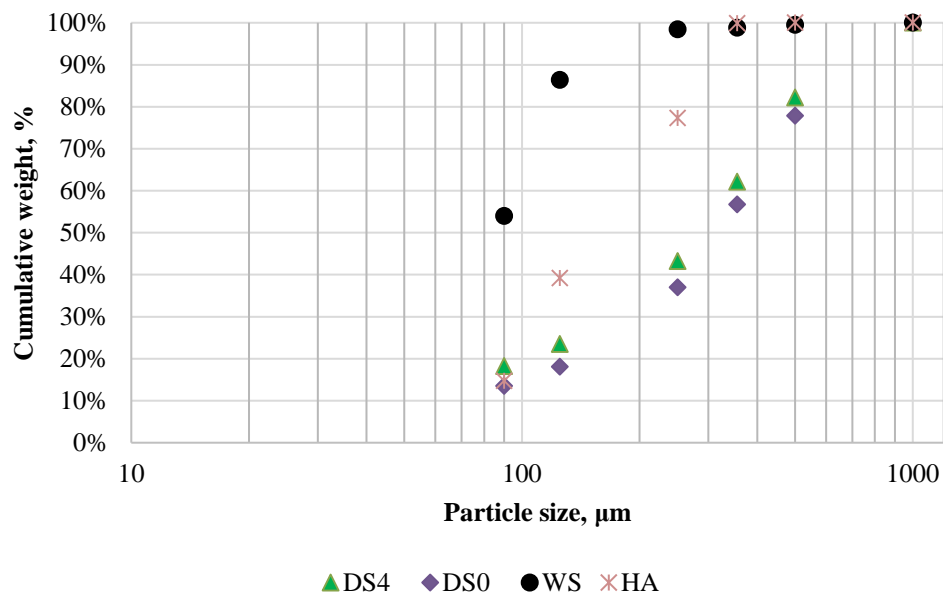
Fig. 2.1. Particle size distribution of investigated fuels.

Fuel particle size distribution (PSD)is one of the parameters determining sufficient burnout, flame properties and heat exchange in PF Boiler (Pulverized Fuel). In this study sieve analysis was performed in the order to determine size distribution. Analysis was carried out on vibrating module LPzE-2e MULTI SERW on mesh size: 1000, 500, 355, 250, 125, 90 μm. Biomasses are characterized by much less fragmentation compared to coal.

Particle size distribution are presented in Figure 1. In the case of coal WS less than 54,0 % particles are smaller than 90 μm and less than 86,4 % are smaller than 125 μm. Granulation of WS corresponds industrial milling installation. Biomasses are described by lower level fragmentation <90 μm DS0=13,4%; <125 μm DS0=18,1%; It is highly probablethat particles >500 μm can negatively increase share of unburnt carbon in resulting ash. Increased PSDof fuels conditioned with halloysite is associatedwith the particle size distribution of the hallositeadditive. The 77,2 % of additive particles (see symbol HA in Fig. 2.1) are smaller than 250 μm. Generally biomass particles are much coarserand longer compared to coal particles. The particle shape strongly impact on deposit formation in PF Boiler.

2.3. Experimental Facility

Pulverized Fuel Combustion Chamber (PFCC) is aespecially designed combustion reactor for advanced investigation of fuels properties. The Reactor is electrically heated (30 kWel) insulated 4 m long pipe made of acid-proof and heat-resistant steel. The inner diameter of reactor is 300 mm. The maximum operatedtemperature is 1050^0C. Reactor is equipped with pulverized fuel burner and high accuracy K-TRON feeder +/-0,001 kg/h. Scheme of laboratory facility is presented in Fig. 2.2. Reactor consist of 5 main parts:

- insulated vertical combustion chamber

- gas preheating section

- gas cooling and particle colleting section

- feeding system

- control system and data acquisition

For the ash depositionmeasurements a stainless steel deposition probe is used. The deposition probe metaltemperature is measured by K-type thermocouple and controlled by Valve Control Unit based on the Siemens Sinamics 7 controller. As probe cooling medium pressurized air is used. Outlet diameter of probe is 37 mm. Mass of deposits were scale in the order to determine ash deposition efficiency η_{os}. Qualitative analysis were carried out on the collected deposits samples including ash oxides analysis, ash fusibility experiments and SEM-EDS analysis. At the depositionport, the flue gas examination was performed with Siemens Ultramat 23including: NO as NO_2, CO, SO_2, O_2 using.

The deposition rate (deposit mass flow density) and the effectiveness of deposit forming were determined:

$$\eta_{os} = \frac{\dot{m}_{DC}}{\dot{m}_{Fash}} \cdot \frac{A_F}{A_{DC}}$$

(2.1)

where:

$\dot{m}_{DC}$ – deposit mass flow density (deposition rate[1]), g/m²h

$\dot{m}_{Fash}$ – mass flow density of the ash flowing along reactor cross-section, g/m²h

A_F – surface area of the reactor cross-section under analysis, m²

A_{DC} – the deposit probe inflow surface area, m².

---

[1] the total measured mass of the deposit collected from the probe surface for a specific measuring time
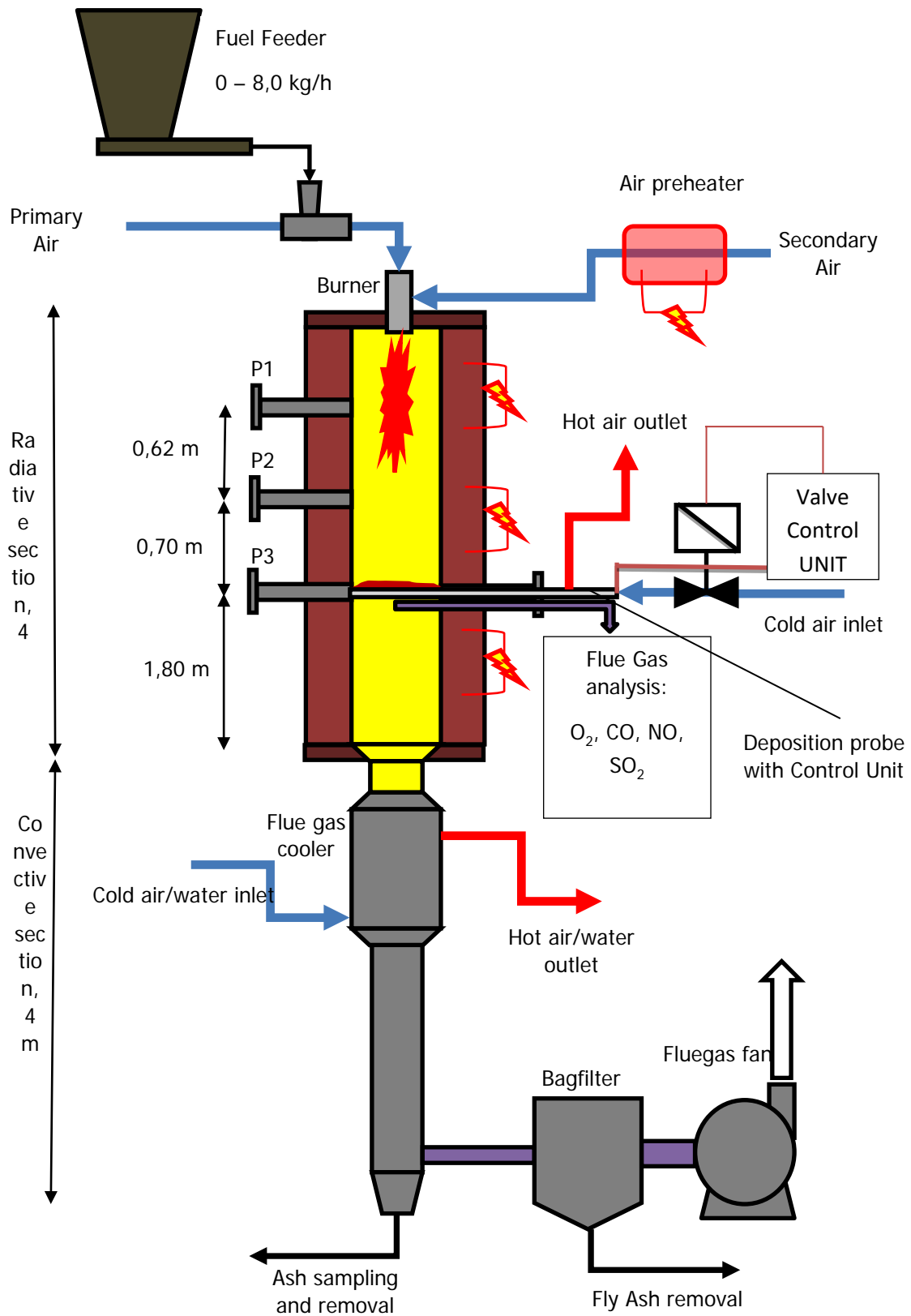
Fig. 2.2. Pulverized Fuel Combustion Chamber located in Institute of Power Engineering and Turbomachinery, Silesian University of Technology.

3. Results and discussion

The aim of this study was to determine the deposition efficiency for halloysite doped biomasses compared with raw biomasses and typical hard coal combustion. Constant fuel thermal input criterion was chosen [12-16]. The experiment reproduce the work of steam superheater in PF boilers.Experiments were carried out on fuel thermal input Q_{th}=7,0 kW at reactor wall temperature, 900^{0}C for DS0, DS4 and WS. Excess air ratio λ was maintained at constant level 1,20 +-/0,03 measured at port P3 (see Fig. 2.2). In all cases primary air flow consist 30-35% of total combustionair. Mass of collected deposits were scale in order to determine deposition rate and deposit effectiveness. In all cases τ time of deposit probe exposure is120 minutes. In Tab. 3.1 main parameters of reactor experiments conditions are shown. Increasing the temperature of combustion significantly increases the deposition rate. However, the increase of temperature contributes to decrease the unburnt carbon in ash. In the case of deposition experiments two parameters are particularly essential.

The first one is deposition rate which influences the sootblowers use in power boilers. This parameter is interesting from PF boiler service. Another parameter is deposition efficiency η_{os} considered as fly ash loadin flue gas stream. Deposition efficiency is a convenient indicatorto compare the deposition tendency of fuels with varyingash content and chemical ash composition. In reactor temperature900^{0}C for DS0 (raw fuel) deposits efficiency is changing from 7.33%, to 5.25% for DS4 (with halloysite) . Halloysiteadditiondecrease deposition rate and deposition efficiency. Deposition efficiency is approaching the level for coal ash characteristic WS (3.57%). It is concluded thathalloysite addition change physical and chemical structure of biomass deposits resulting in comparable to coal combustion deposits.

Considering deposits efficiency and thermal input of fuel η_{os}/Qth the fuels with halloysite dosage reach values close to coal (see Tab.3.1.) For 900^{0}C indicator are as follows: WS=0.51; DS0=1.41; DS4=0.75. Pictures of collected deposits are presented in Fig.3.1–3.5. Deposits with halloysite are more powdery which make it more easily to be removed by sootblowers. The resulting deposits are close to coal deposits properties (compareFig. 3.2 with Fig. 3.5). Moreover, deposits with halloysite change color in orange shade. Ash deposits without halloysite are highly sintered forming complex ash agglomerates. In the Fig.3.6 the photo of interior reactor of PFCC is presented after numbers of experiments. After number of deposits tests, thick ash deposits have been formed in upper part of reactor (in high temperature zone). The thickness of deposits can be around 50-100 mm which indicates a significant threat of deposits agglomeration in PF boiler during biomass combustion.

Fig.3.1. Ash deposit collected during DS4 900^{0}C tests. Part of the deposit has automatically dropped out.

Fig.3.2. Ash deposit collected during DS4 900^{0}C tests - close-up image, powdery deposit.

Fig.3.3. Ash deposit collected during DS0 900^{0}C tests.

Fig.3.4. Ash deposit collected during DS0 900^{0}C tests - close-up image, visible sintered ashes and agglomerates .
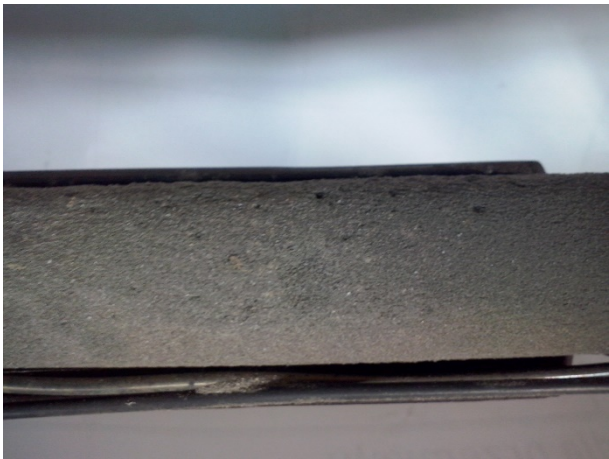
Fig.3.5. Ash deposit collected during WS 900^{0}C tests, no visible unburnt carbon in deposit.

Fig.3.6. Photo of reactor interior (inner diameter 300 mm) after biomass depositions experiments. Visible thick deposit coating in upper part of reactor, close to burner (deposit thickness can be around 50-100 mm).

Tab.. 3.1 Main parameters of reactor and results of investigation

Fuel	Symbol	DS0 900	DS4 900	WS 900	Unit
Lower Calorific Value	LCV^r	14.366	13.641	23.772	%
Ash content	A^r	10.78	13.94	10.47	%
Fuel input,	B	1.754	1.847	1.06	kg/h
Combustion air	Vp	8.53	8.73	9.15	Nm3/h
Fuel Thermal input	Qth	7.0	7.0	7.0	kW
Probe inflow surface area	A$_{DC}$	0.071	0.071	0.071	m2
Ash stream	m ash	0.189	0.257	0.111	kg/h
Ash mass flow density	m Fash	2675.0	3642.5	1570.1	g/m2h
Outer diameter of probe	φ	37	37	37	mm
Probe effective length	l	300	300	300	mm

Exposure time	τ	120	120	120	minutes
Deposition rate	m_{Fash}	41.42	30.02	8.81	g/m2h
Deposition effciency	η_{os}	9.86	5.25	3.57	%
Indicator	η_{os} /Qth	1.41	0.75	0.51	%/kW
Temperature of probe	t probe	480	480	480	^0C
Temperature of reactor	t react.	900	900	900	^0C
Excess Air Ratio	λ	1.19	1.22	1.21	-
CO	CO	35.2	29.5	76.1	mg/Nm3 @6% O_2
NO	NO	408.6	531.5	483.9	NO as NO_2 mg/Nm^3 @6% O_2
SO_2	SO_2	76.1	64.6	1914.1	mg/Nm^3 @ 6% O_2

3.1. AFT analysis of ash deposits

For the fusibility tests ash samples were formed into pyramids. Maximal temperature of experiments does not exceed 1500°C under reduction and oxidizing conditions. Initial Deformation Temperature (IDT), Softening Temperature (ST) Hemispherical temperature (HT), Fluid Temperature (FT) and its specific shapes were determined by camera and computer system according to procedure described in [17]. Results of ash fusibility experiments are shown in Tab. 3.2. Results of AFT test confirmedthat addition of halloysiteto biomass changes themelting behavior of biomass deposits comparable to coal deposits. In reducing conditionstheShrinkage Temperature change for biomass samples with addition of halloysite issignificant where DS4=1130^0C compared to unconditioned biomass DS0=870^0C.the same tendency is observed of other temperatures ST, HT, FT.

Tab. 3.2 Results of ash fusibility experiments of investigated deposits.

Temp. ^0C/ Fuel	Reduction Conditions			Oxidizing Conditions		
	WS	DS0	DS4	WS	DS0	DS4
IDT	1130	870	1130	1190	1030	1150
ST	1160	1040	1190	1290	1080	1190
HT	1190	1200	1260	1370	1180	1240
FT	1360	1330	1300	1420	1260	1290

4. Conclusions

In thisstudyseveralbiomasses, and coal were examined in order to determine ash deposition tendency in PFCC reactor. Phenomena of ash deposition tendency during combustion of biomasses affects negatively utilization of these fuels. The increasing accuracy of the ash deposition prediction methodology allows the proper selection of fuels that can be safely used in power boilers. Research conducted in this study categorize investigated agricultural biomasses as fuel with high potential of ash deposition tendency. Addition of halloysite as additiveeffectivelydecreasedeposition tendency. Chemical composition of additive doped biomass is comparable to coal deposit characteristics. However,mixingthe fuelwith additive and sTab. combustion process is crucial for economical boiler operation.

Acknowledgment

Centre for Research and Development in Poland and the Federal Ministry of Education and Research in Germany

References

[1] Teixeira P., Lopes H., Gulyurtl I., Lapa N., Abelha P., "Evaluation of slagging and fouling tendency during biomass co-firing with coal in a fluidized bed", Biomass Bioenergy, 39 (2012), pp. 192-203.

[2] Płaza P., "The Development of a Slagging and Fouling Predictive Methodology for Large ScalePulverised Boilers Fired with Coal/Biomass Blends", Cardiff University, 2013.

[3] Couch, G, "Understanding slagging and fouling in pf boilers", IEA-CCC Report, 1994.

[4] Frandsen, F, J, "Ash Formation, Deposition and Corrosion When Utilizing Straw for Heat and Power Production", Doctoral Thesis, Technical University of Denmark, 2011.

[5] Wang L. , . Hustad J.E, Skreiberg Ø. , SkjevrakG. , Grønli M., "A critical review on additives to reduce ash related operation problems in biomass combustion applications" Energy Procedia, 20 (2012), pp. 20-29.

[6] Bryers R.W., "Fireside slagging, fouling and high-temperature corrosion of heat transfer surface due to impurities in steam raising fuels", ProgEnerg Combust Sci, 22 (1996), pp. 29-120.

[7] Miles T.R., Miles Jr. T.R., Baxter L.L., Bryers R.W., Jenkins B.M., Oden L.L., "Alkali deposits found in biomass power plants, A preliminary investigation of their extent and nature", Summary report for National Renewable Energy Laboratory, 1617 Cole Boulevard, Golden, CO 80401-3393, NREL Subcontract TZ-2-11226-1, 1995.

[8] Jensen P. A., Stenholm M., Hald P., "Deposition investigation in straw fired boilers", Energy and Fuels 11_1997. 1048–1055.

[9] Michelsen H. P., Larsen O.H., Frandsen F.J., Dam-Johansen K., "Deposits and high temperature corrosion in a 10 MW straw fired boiler", Fuel Process. Technol. 54 _1998. 95–108.

[10] Kalisz S., Ciukaj Sz., Mroczek K. Kress T., Tymoszuk M., Wejkowski R., Pronobis M., Kubiczek H. Impact of halloysite fuel additive on 650 t/h PC boiler co-firing biomass. Part I - deposition characteristics. 12th International Conference on Boiler Technology 2014.

[11] Pronobis M., Sołtys J. Halloysite as an additive for thermal treatment of waste [Haloizytjakododatek do termicznegoprzetwarzaniaodpadów]. 2013.

[12] Weber R., Kupka T., Zając K.: Jet flames of refuse derived fuel. Combustion and Flame 156 (2009) 922 – 927.

[13] Ndibe C., Maier J., Scheffknecht G.: Combustion. cofiring and emissions characteristics of torrefied biomass in a drop tube reactor. Biomass & Bioenergy 79. (2015) 105 - 115.

[14] Pronobis M.: Modernizacja kotłów energetycznych. WNT. Warszawa 2002.

[15] Orłowski P., Dobrzański W., Szwarc E.: Kotły parowe: konstrukcja i obliczenia. Wyd. 3. WNT Warszawa 1979.

[16] Weber R., Y. Poyraz, A. M. Beckmann, S. Brinker.: Combustion of biomass in jet flames. Proceedings of the Combustion Institute 35. (2015) 2749 – 2758.

[17] PN-ISO 540:2001: Paliwa stałe - Oznaczanie topliwości popiołu w wysokiej temperaturze metodą rurową.

Study on the solar pyrolysis of waste biomass: a current status of the project

Szymon Sobek [1], Sebastian Werle [2];

[1] *Institute of Thermal Technology, Silesian University of Technology, Szymon.Sobek@polsl.pl*
[2] *Institute of Thermal Technology, Silesian University of Technology, Sebastian.Werle@polsl.pl*

Abstract

To follow European Union (EU) and national legislations in the renewable energy sector, biomass is continuously gaining in importance. Until 2020 EU Member States are obliged to increase the share of renewable energy to 20% in total EU energy consumption, along with a 20% decrease of greenhouse gas emissions and overall energy consumption. Thermal methods of biomass conversion are the most popular ways of utilizing its energy potential. Among these methods it can be specified: combustion and co-combustion, gasification and pyrolysis. The process that distinguishes itself by the highest rate of converting biomass energy is pyrolysis. Conventional implementation of mentioned earlier processes, based on the heat generated from the combustion of non-renewable fuels, results in significant emissions of greenhouse gases, which contradicts the concept of eco-friendly and green energy production. The idea of solar energy adaptation as a heat source for pyrolytic reactors opens up new opportunities for original and efficient energy production from biomass. In this paper popular science summary of 1-year work in "Study on the solar pyrolysis of waste biomass" project has been presented with emphasis on experimental part and kinetic analysis of pyrolysis process.

Key words: Pyrolysis, Biomass, Utilization, Solar-Thermal, Renewable Energy Sources (RES), Kinetics.

1. Introduction

In 2016 almost 80% of world's final energy consumption is still provided by fossil fuels , continuously diminished by rising growth rate of modern renewables. Increase trend in renewable energy deployment continued in 2017, especially in power sector, thanks to: (1) increasing access to finance, (2) global concerns about energy security, (3) human health and the environment, (4) growing energy demand in young and developing economies, (5) urgent need for emission-free electric energy and (6) clean cooking facilities and dedicated policy initiatives and support for ambitious targets [1]. Solar energy could be a promising option for the future biomass conversion support, because of several reasons: first, solar energy is the most abundant energy source of renewable energy and sun emits it at the rate of 3.8 x 10^{23} kW, out of which approximately 1.8 x 10^{14} kW is intercepted by the earth [2]. Second, solar energy is completely free and environmentally clean. Solar-driven thermochemical biomass conversion processes provide several ways of high-quality renewable fuels production and opens up original way of solar energy storage. Concentrated solar power (CSP) has been used as a heat source to perform thermochemical conversions such as gasification, combustion and pyrolysis [3]. In recent years solar gasification and pyrolysis has been a subject of numerous studies, where kinetic analysis, CFD modelling, temperature impact on products and different bed types has been investigated [3–11]. For scientific investigation of solar biomass pyrolysis, the construction of laboratory reactor is crucial. Solar biomass conversion reactors, are usually fluidized bed or fixed bed, where feedstock is heated directly with solar radiation or indirectly, through highly conductive reactor wall [3,7]. In general, solar-thermal biomass conversion units adapted technology from commercial solar collectors, comprising concentrating mirror with the reactor as a receiver [8–14]. For Researchers willing to study solar pyrolysis in regions that lacks of natural solar-thermal potential adapted artificial light sources as sunlight simulators [15–20]. Main reason for using artificial light source is independence from natural, adverse conditions which may occur during experiments with natural sunlight.

The goal of presented project is comprehensive investigation of solar pyrolysis of waste biomass. Three types of waste biomass will be examined in experiments: waste wood, straw and sewage sludge. Project connects interdisciplinary approach using experimental data in order to validate numerical model of pyrolysis. Three main scientific tasks are being realised:

1.   Multiparameter measurement of the waste biomass solar pyrolysis process,

2.   Physical - chemical analysis of the products obtained after the process,

3.   Construction of a mathematical model of the solar pyrolysis process.

In this paper 1-year work summary is presented, with emphasis on first task, being the subject of PhD work of the Author. Experimental investigation of solar pyrolysis task is divided into several work packages:

- Designing and construction of a laboratory measurement station (the reactor),

- Ultimate, proximate and chemical analysis of the biomass samples,

- Analysis of the influence of the temperature of the pyrolysis process on the individual share post-process factions,

- Thermogravimetric and calorimetric measurements of the solar pyrolysis reaction kinetics,

- Determination of the conversion rate of chemical energy of biomass in the chemical energy of useful pyrolysis products.

2. Laboratory reactor

In order to examine solar pyrolysis of waste biomass, proper reactor has to be constructed. In last year most of the effort was put on literature review and consultations with companies producing artificial light sources. As a result, the complete design of laboratory station has been accomplished. The heart of the station is artificial sun, being the high-power xenon arc lamp. The lamp produces 288 W_{th} in a form of concentrated radiation. Lamp radiation is directed onto reactor surface, where biomass samples are located. Reactor is a copper block with four ducted channels, with 169mm of total length. Due to expectation of high temperatures (300-600 °C), the reactor is insulated with industrial insulation mat. Volatiles released during pyrolysis are moved out from reaction zone with flow of inert gas (nitrogen) and directed to liquid fraction condenser. Series of water cooled Dreshl scrubbers are adapted as a condenser in order to provide clean pyrolysis gas for further analysis.
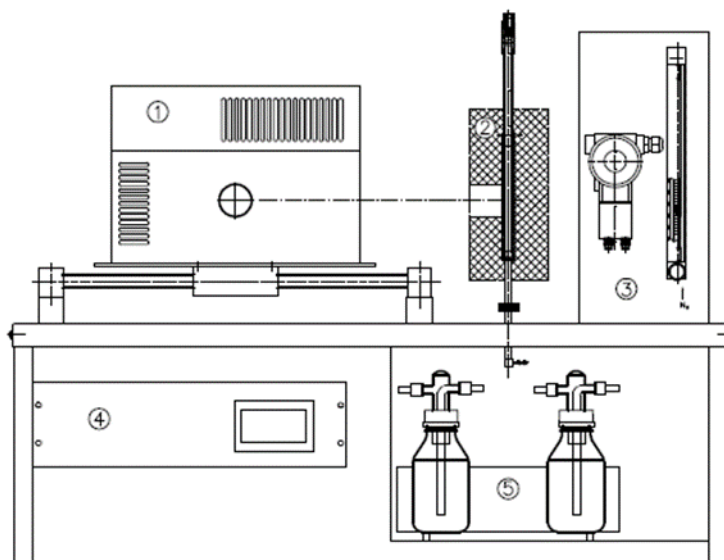
Fig. 2.1. Design of laboratory reactor (1-xenon arc lamp, 2-insulated copper reactor, 3- inert gas manometer and reactor pressure meter, 4- data activation system box, 5- liquid fraction condenser)

3. Ultimate, proximate and chemical analysis of wood samples

Ultimate and proximate analysis has been determined using plasma spectrometer Thermo iCAP 6500 Duo ICP according to Polish norms: PN-G-04528-02:1977, PN-EN 196-2:2013-11, PN-EN 15936:2013-02 and PN-EN 15936:2013-02. Chemical analysis has been carried out using extraction system Ankom A200 and FOSS Fibertec 2010 and 2011 according to application note FOSS 3434 – AOAC 2002:04/ISO 16472:2005.

Tab. 3.1. Ultimate, proximate and chemical analysis of investigated wood samples (sawdust).

Property	Method	Status	Unit	Value
Proximate analysis				
Moisture, total	PN-EN ISO 18134-2:2017-03	ar	%	9
Ash	IB_TL_31_03 from 01.12.2010	dry	%	0.75
Volatiles	PN-EN ISO 18123:2016-01	dry	%	83.3
Calorific values				
Higher heating value	PN-EN 14918:2010	ar	kJ/kg	18 760
Lower heating value	PN-EN 14918:2010	ar	kJ/kg	16 870
Ultimate analysis				
Carbon	PN-EN ISO 16948:2015-07	dry	%	49.61
Hydrogen	PN-EN ISO 16948:2015-07	dry	%	5.94
Nitrogen	PN-EN ISO 16948:2015-07	dry	%	0.06
Sulphur	PN-EN ISO 16994:2016-07	dry	%	0.02
Oxygen	As a difference	dry	%	44.359
Chemical analysis				
Lignin	FOSS AN 304	ar	%	27.9
Cellulose	FOSS AN 304	ar	%	54.8
Hemicellulose	FOSS AN 304	ar	%	11.8

In Tab. 3.1. results of ultimate, proximate and chemical analysis for investigated wood samples has been presented. Analysed wood samples in case of ultimate and proximate analysis presented typical properties for woody biomass. Chemical analysis revealed very high cellulose content above 50%, which allows to assign the tested wood to the sub-category of cellulose-derived (cellulosic) biomass [21,22].

4. Preliminary kinetic analysis

After construction of the research stand and analysis of the fuel, next step is kinetic analysis of solar pyrolysis of waste biomass. As far as pyrolysis goes, origin of the heat supply does not matter, thus kinetic analysis for solar and conventional pyrolysis is the same. In this paper preliminary kinetic analysis based on model-free approach is presented. Model-free (iso-conversion) kinetic analysis is free of any reaction model assumptions. In preliminary analysis the pyrolysis activation energy will be determined using both differentia[22]l (Friedman) and integral (Ozawa-Flynn-Wass, Kissinger-Akahira-Sunose) methods.

4.1. Experimental and methods

Model-free analysis was introduced using Netzsch Kinetics Neo (v.2.0.1) based on series of thermogravimetric (TGA) experiments in temperature range 25-800°C for 10 mg of wood samples in nitrogen atmosphere. Set of dynamic measurements were carried out on thermogravimeter with DSC sensor STARe System TGA / DSC3 HT 1600 with heating rates of 5,10 and 20 K·(min)$^{-1}$. Due to the fact that kinetic analysis is just preliminary, in other words, the aim is to get familiar with the software, the data from TGA experiments were adapted from other studies performed by Authors.
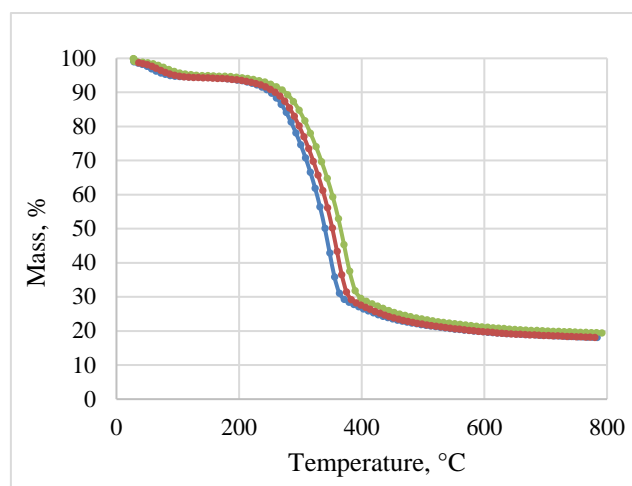
Fig. 4.1. Thermogravimetric data for 10 mg of wood samples carried out at heating rates of 5 (blue), 10 (red) and 20 (green) K·(min)$^{-1}$

Tab.. 4.1. Mass loss and TGA experiment time for wood samples at different heating rates

Heating rate, K·min^{-1}	Sample mass, mg	Time, min	Mass drop, %
5	10.1	152.0	80.5
5	10.1	156.8	80.9
10	10.3	74.4	80.5
20	10.8	36.8	79.4
20	10.8	43.2	80.9

4.2. Isoconversional method for the determination of the activation energy

The integral Kissinger-Akahira-Sunose, Ozawa-Flynn-Wall and the differential Friedman methods (Tab. 3.2.) were used to calculate the run of the Isoconversional activation energy E_a with increasing conversion [23]. Determination of activation energy is based on "Isoconversional principle", according to which the reaction rate at constant extent of conversion is only a function of temperature [24]. Dimensionless reaction extent, or conversion rate, α, is defined as a mass of volatiles present at any time related to total amount of volatiles released, or a current mass loss of the sample related to total amount of mass decomposed. In kinetic computations it means that for same conversion points from the TGA measurements at different heating rates, activation energy and other kinetic parameters, like pre-exponential factor or reaction model, can be decrypted from experimental data with mathematical transformations. Each presented method uses different graphic analysis of TGA data (Tab. 3.1.) where activation energy is found from the slopes and intersections of specific lines on the graphs.

Tab.. 4.2. Graphic analysis with pros and cons of investigated model-free methods

Method	Graphic analysis	Advantages	Disadvantages
Friedman	logarithm of conversion rate versus temperature inverse	• multiple-step reactions • each reaction point is evaluated • suiTab. for dynamic and isothermal measurements	• for parallel and independent reactions gives mean values of E_a

Kissinger-Akahira-Sunose	logarithm of heating rate over temperature versus temperature inverse	• suiTab. for multi-step reactions • each reaction point is evaluated	• for parallel and independent reactions gives mean values of E_a • only for set of dynamic measurements
Ozawa-Flynn-Wall	logarithm of heating rate versus temperature inverse	• multiple-step reactions • each reaction point is evaluated	• for parallel and independent reactions gives mean values of E_a

4.3. Kinetic analysis results
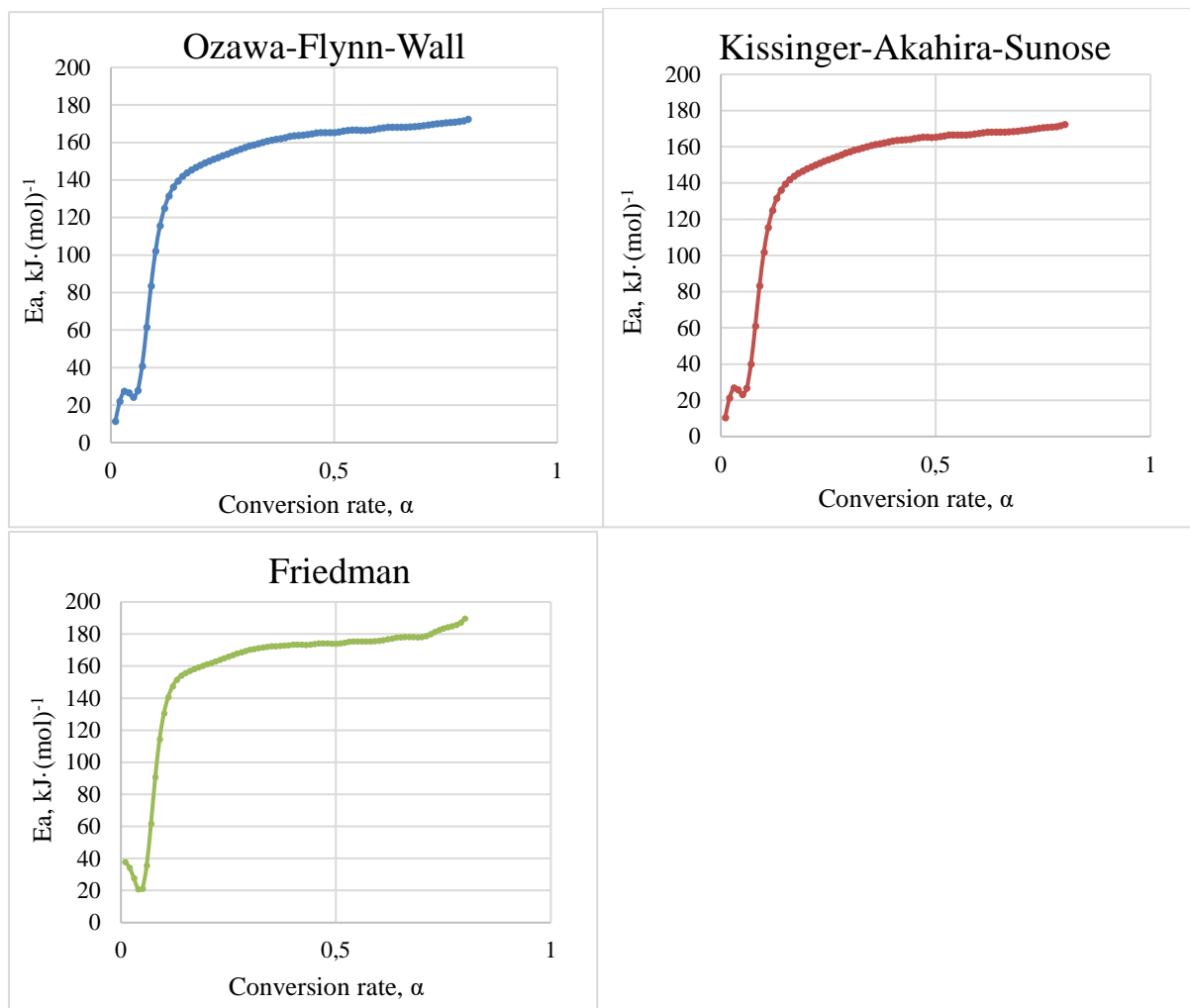
Fig. 4.2. Activation energies as a function of conversion extent, calculated for different Isoconversional methods

Presented on Fig. 3.2 activation energy graphs lead to a conclusion, that each of presented model-free method gives similar results. Understanding of activation energy in case of pyrolysis is crucial. As can be seen, in each case, process starts with obvious increase of endothermicity due to moisture evaporation. Next pyrolysis reaction occurs, resulting in quick activation energy increase up to plateau level, sTab. throughout the rest of the process. Such a complex reaction like pyrolysis should not be brought to one activation energy, like in global reaction models. Presented model-free methods gives conversion dependent mean activation energy, which S.Vyazovkin referred as effective activation energy [24]. Effective activation energy means that during the decomposition from

all the reactions occurring, one has the highest impact on whole process endothermicity. Significant activation energy peak occurs in each case at the end of reaction ($\alpha \sim 1$). This phenomenon is strictly connected to the computational errors of Isoconversional methods at conversion rates higher than 0.85 (Tab. 4.3.) [25]. Despite flat TGA curves at the end of conversion, Isoconversional methods results in significant peaks, which regarding to literature, are usually omitted from analysis .

Tab. 4.3. Effective activation energies with standard deviations calculated for three Isoconversional methods

Conversion, α	Ozawa-Flynn-Wall		Kissinger-Akahira-Sunose		Friedman	
	E_a, kJ mol^{-1}	SD, kJ mol^{-1}	E_a, kJ mol^{-1}	SD, kJ mol^{-1}	E_a, kJ mol^{-1}	SD, kJ mol^{-1}
0.1	102.072	21.176	101.802	22.829	130.561	14.972
0.2	147.948	4.752	147.81	5.041	161.165	6.019
0.3	157.434	3.441	157.302	3.648	170.256	4.835
0.4	163.258	3.649	163.129	3.870	173.492	3.452
0.5	165.382	4.495	165.251	4.774	174.014	2.092
0.6	167.542	5.301	167.411	5.626	175.949	1.621
0.7	169.016	5.939	168.884	6.308	178.226	1.812
0.8	172.471	7.501	172.342	7.964	189.805	7.933
0.9	**298.846**	**13.401**	**298.761**	**13.895**	**334.677**	**16.696**
0.95	**563.679**	**38.797**	**563.626**	**39.754**	**624.423**	**41.770**

Tab. 4.3. presents effective activation energies for wood samples calculated for three isoconversional methods. Regarding results and standard deviations, integral methods gave almost the same results, however differential Friedman method yielded slightly higher activation energies for the same extent of conversion. Activation energies after extent of conversion 0.8 were removed from the graphs on Fig. 4.2, assuming those results as faulty. Nevertheless acquired activation energies for wood pyrolysis in nitrogen atmosphere, presents satisfying fit with literature data, where activation energies for woody biomass are varying usually from 160 to 290 kJ·(mol)$^{-1}$, depending on sample size, mass, heating rate and wood components ratios [22,26–29]. What has to be mentioned, presented kinetic analysis should be treated optimistically. To estimate proper activation energy for investigated solar pyrolysis process, more effort should be put in obtaining computational-worthy data (TGA, DSC) in order to reflect investigated process properly in terms of heating rates, temperature programs and samples sizes.

5. Conclusions

In presented paper, the 1 year summary of work in the project "Study on the solar pyrolysis process of the waste biomass" has been presented. Complete design of laboratory station has been accomplished. Analysis of investigated biomass: ultimate, proximate and technical has been performed, in this paper results for wood samples was presented. Preliminary kinetic analysis yielded in activation energies estimated based on TGA experiments, which results had been adopted from another study. The aim of kinetic analysis was not only estimation of activation energy, yet to practice work with the Netzsch Kinetics Neo software. For the future 3 task are going to be executed: proper kinetic study of waste biomass pyrolysis, analysis of the influence of the temperature of the pyrolysis process on the individual share post-process factions and determination of the conversion rate of chemical energy of biomass into chemical energy of useful pyrolysis products. Proper kinetic analysis will include model-based and model-free analysis, which will result in estimation of proper kinetic triplet for solar pyrolysis: activation energy, pre-exponential factor and reaction model. The last two tasks in order to be performed need operational laboratory station, which start up is estimated at the beginning of 2019.

Acknowledgments

References

[1]. R. Adib REN, M. Folkecenter, A. Development Bank, M. Eckhart Mohamed El-Ashry David Hales Kirsty Hamilton Peter Rae, F. Bariloche, Renewables 2018 · Global Status Report, 2018. doi:978-3-9818911-3-3.

[2]. N. Kannan, D. Vakeesan, Solar energy for future world: - A review, Renew. Sustain. Energy Rev. 62 (2016) 1092–1105. doi:10.1016/j.rser.2016.05.022.

[3]. S. Bellan, N. Gokon, K. Matsubara, H.S. Cho, T. Kodama, Heat transfer analysis of 5kW th circulating fluidized bed reactor for solar gasification using concentrated Xe light radiation, Energy. 160 (2018). doi:10.1016/j.energy.2018.06.212.

[4]. B.J. Hathaway, J.H. Davidson, Demonstration of a prototype molten salt solar gasification reactor, Sol. Energy. 142 (2017) 224–230. doi:10.1016/j.solener.2016.12.032.

[5]. A.P. Muroyama, I. Guscetti, G.L. Schieber, S. Haussener, P.G. Loutzenhiser, Design and demonstration of a prototype 1.5 kWthhybrid solar/autothermal steam gasifier, Fuel. 211 (2018) 331–340. doi:10.1016/j.fuel.2017.09.059.

[6]. R. Li, K. Zeng, J. Soria, G. Mazza, D. Gauthier, R. Rodriguez, G. Flamant, Product distribution from solar pyrolysis of agricultural and forestry biomass residues, Renew. Energy. 89 (2016) 27–35. doi:10.1016/j.renene.2015.11.071.

[7]. P.G. Loutzenhiser, A.P. Muroyama, A review of the state-of-the-art in solar-driven gasification processes with carbonaceous materials, Sol. Energy. 156 (2017) 93–100. doi:10.1016/j.solener.2017.05.008.

[8]. H. Grassmann, M. Boaro, Solar Biomass Pyrolysis with the Linear Mirror II, Smart Grid, (2015) 179–186. http://search.proquest.com/openview/4a55bbabd411640d4f5c1e223d0b86c5/1?pq-origsite=gscholar.

[9]. M. Bashir, X. Yu, M. Hassan, Y. Makkawi, Modeling and Performance Analysis of Biomass Fast Pyrolysis in a Solar-Thermal Reactor, ACS Sustain. Chem. Eng. 5 (2017) 3795–3807. doi:10.1021/acssuschemeng.6b02806.

[10]. K. Zeng, D. Gauthier, D.P. Minh, E. Weiss-Hortala, A. Nzihou, G. Flamant, Characterization of solar fuels obtained from beech wood solar pyrolysis, Fuel. 188 (2017) 285–293. doi:10.1016/j.fuel.2016.10.036.

[11]. M. Sánchez, B. Clifford, J.D. Nixon, Modelling and evaluating a solar pyrolysis system, Renew. Energy. 116 (2018) 630–638. doi:10.1016/j.renene.2017.10.023.

[12]. S. Morales, R. Miranda, D. Bustos, T. Cazares, H. Tran, Solar biomass pyrolysis for the production of bio-fuels and chemical commodities, J. Anal. Appl. Pyrolysis. 109 (2014) 65–78. doi:10.1016/j.jaap.2014.07.012.

[13]. K. Zeng, D. Gauthier, J. Soria, G. Mazza, G. Flamant, Solar pyrolysis of carbonaceous feedstocks: A review, Sol. Energy. 156 (2017) 73–92. doi:10.1016/j.solener.2017.05.033.

[14]. K. Zeng, D. Gauthier, R. Li, G. Flamant, Solar pyrolysis of beech wood: Effects of pyrolysis parameters on the product distribution and gas product composition, Energy. 93 (2015) 1648–1657. doi:10.1016/j.energy.2015.10.008.

[15]. O. Boutin, M. Ferrer, J. Lédé, Flash pyrolysis of cellulose pellets submitted to a concentrated radiation: Experiments and modelling, Chem. Eng. Sci. 57 (2002) 15–25. doi:10.1016/S0009-2509(01)00360-8.

[16]. O. Boutin, M. Ferrer, J. Lédé, Radiant flash pyrolysis of cellulose - Evidence for the formation of short life time intermediate liquid species, J. Anal. Appl. Pyrolysis. 47 (1998) 13–31. doi:10.1016/S0165-2370(98)00088-6.

[17]. A.H. Rony, D. Mosiman, Z. Sun, D. Qin, Y. Zheng, J.H. Boman, M. Fan, A novel solar powered biomass

pyrolysis reactor for producing fuels and chemicals, J. Anal. Appl. Pyrolysis. 132 (2018) 19–32. doi:10.1016/j.jaap.2018.03.020.

[18].   M.G. Gronli, M.C. Melaaen, M. Grønli, M.C. Melaaen, Mathematical model for wood pyrolysis - Comparison of experimental measurements with model predictions, Energy & Fuels. 14 (2000) 791–800. doi:10.1021/ef990176q.

[19].   O. Authier, J. Lédé, The image furnace for studying thermal reactions involving solids. Application to wood pyrolysis and gasification, and vapours catalytic cracking, Fuel. 107 (2013) 555–569. doi:10.1016/j.fuel.2013.01.041.

[20].   V. Pozzobon, S. Salvador, J.J. Bézian, M. El-Hafi, Y. Le Maoult, G. Flamant, Radiative pyrolysis of wet wood under intermediate heat flux: Experiments and modelling, Fuel Process. Technol. 128 (2014) 319–330. doi:10.1016/j.fuproc.2014.07.007.

[21].   T. Kan, V. Strezov, T.J. Evans, Lignocellulosic biomass pyrolysis: A review of product properties and effects of pyrolysis parameters, Renew. Sustain. Energy Rev. 57 (2016). doi:10.1016/j.rser.2015.12.185.

[22].   S. Wang, G. Dai, H. Yang, Z. Luo, Lignocellulosic biomass pyrolysis mechanism: A state-of-the-art review, Prog. Energy Combust. Sci. 62 (2017) 33–86. doi:10.1016/j.pecs.2017.05.004.

[23].   G. Baldauf-Sommerbauer, S. Lux, J. Wagner, M. Siebenhofer, Determination of the kinetic triplet by an isoconversional and a regression method applied to the decomposition of mineral iron carbonate in nitrogen, Thermochim. Acta. 649 (2017) 1–12. doi:10.1016/j.tca.2017.01.001.

[24].   S. Vyazovkin, Isoconversional Kinetics of Thermally Stimulated Processes, Springer International Publishing Switzerland 2015, 2015.

[25].   X. Yao, Q. Yu, Z. Han, H. Xie, W. Duan, Q. Qin, Kinetic and experimental characterizations of biomass pyrolysis in granulated blast furnace slag, Int. J. Hydrogen Energy. 43 (2018) 9246–9253. doi:10.1016/j.ijhydene.2018.03.173.

[26].   C. Branca, C. Di Blasi, A summative model for the pyrolysis reaction heats of beech wood, Thermochim. Acta. 638 (2016) 10–16. doi:10.1016/j.tca.2016.06.006.

[27].   J.E. White, W.J. Catallo, B.L. Legendre, Biomass pyrolysis kinetics: A comparative critical review with relevant agricultural residue case studies, J. Anal. Appl. Pyrolysis. 91 (2011) 1–33. doi:10.1016/j.jaap.2011.01.004.

[28].   J. Cai, W. Wu, R. Liu, An overview of distributed activation energy model and its application in the pyrolysis of lignocellulosic biomass, Renew. Sustain. Energy Rev. 36 (2014) 236–246. doi:10.1016/j.rser.2014.04.052.

[29].   T. Sonobe, N. Worasuwannarak, Kinetic analyses of biomass pyrolysis using the distributed activation energy model, Fuel. 87 (2008) 414–421. doi:10.1016/j.fuel.2007.05.004.

Torrefaction process of acacia, pine and *Miscanthus giganteus*

Maciej Śliz[1]

[1]*Faculty of Metals Engineering and Industrial Computer Science, AGH University of Science and Technology, Al. Mickiewicza 30, 30-059 Kraków, Poland, e-mail: msliz@agh.edu.pl*

Abstract

Torrefaction process is one of pretreatment methods closely investigated in recent years in means to find the best process parameters for upgrading biomass properties. To determine most suiTab. parameters, temperature and residence time, a series of experiments were conducted. Three different materials: acacia, pine and *Miscanthus giganteus* were processed in torrefaction reactor under 230, 260 and 290°C for 0.5; 1 and 1.5 hours. Received biochars were analyzed in order to characterize the elemental composition. Moreover, higher heating value, molar ratios of H/C and O/C and energy efficiency of the process were determined. The most optimal operating conditions of torrefaction turned out to be the temperature 260°C and residence time 1.5 hours. Results showed that investigated biomass has only few percent of moisture, even less ashes and around 80% of volatile matters. Higher heating value before treatment was in range of 19-20.5 MJ/kg and after it reached a range of 22 to 23 MJ/kg with energy yield from 76 to 88%.

Keywords: torrefaction, acacia, pine, *Miscanthus giganteus*

1. Introduction

In these days more attention is brought to clean, renewable and environmentally friendly energy. Human impact on global warming is now commonly known threat to climate change. Lots of greenhouse gases are produced in conventional power plants. Combustion of coal is treated as one of the most polluting ways of generating electrical energy. In order to decrease negative influence of coal combustion, biomass co-combustionis being introduced [1]. Most commonly used biomass are wood chips and agricultural waste but energy crops are getting more and more popular. Unfortunately, biomass has a few drawbacks. High moisture content, biodegradability, hydrophilicity, low bulk density, high heating value lower than coal, and low grindability discourage power plants from co-combustion [2, 3]. There are pretreatment methods which can make biomass of different origin more attractive fuel. One of them is torrefaction. It is a process which takes place in specially designed reactor where samples are treated in temperatures in range of200 to 300°C and in an inert gas atmosphere to prevent combustion. Pressure is held around 1 atm.Residence time is also an important factor and usually fits in range offew minutes to a dozen hours [4-8]. In high temperature polymeric compounds such as hemicellulose, cellulose and lignin start to decompose. Mainly hydroxyl group is detached and H_2O molecules are removed [4]. After treatment all mentioned earlier disadvantages are irrelevant. Torrefied biomass has low moisture content, higher bulk density and high heating value, improved grindability and is more brittle. Moreover, all biodegradation processes are limited. That is why handling and transporting of torrefaction product becomes easier and cheaper [9].

Main goal of this paper is to determine optimal process parameters, temperature and residence time, for torrefaction of lignocellulosic biomass. In order to torrefy three types of biomass were selected: *Miscanthus giganteus* as an example of energy crop, acacia as an example of deciduous tree and pine as an example of coniferous tree. Three different temperatures were applied: 230, 260 and 290°C, and three different residence times were maintained: 0.5; 1 and 1.5 hours. To examine effects of torrefaction proximate and ultimate analyses were conducted prior and after process. The same procedure were used for high heating value determination.

2. Materials and metho

1.2 Materials

Biomass examined in this study was received from two sources. *Miscantheus giganteus* was supplied by ECOPROD Ltd from agricultural area of Silesia in Poland. It came in form of shredded straw and in order to ensure uniformity of sample it was chopped and grinded in a cutting mill. Afterwards it was sieved to receive particle size less than 1 mm. Acacia and pine was delivered as sawdust from carpentry enterprisein Ochotnica

Dolna, Poland.Diameter of less than 2 mm was sufficient for conducted experiments. Feedstock due to low moisture content was stored in open paper bags to protect it from biodegradation. Prepared samples are shown in Fig. 2.1.
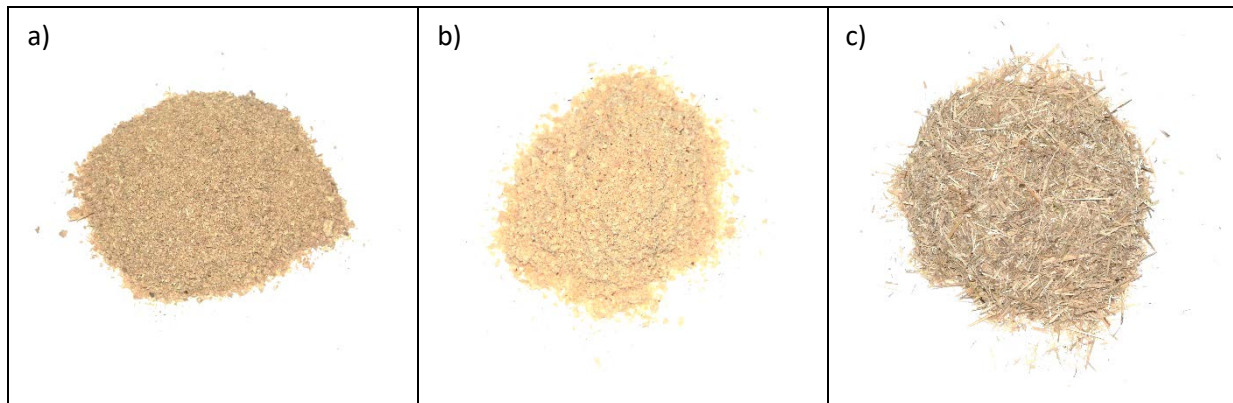
Fig. 2.1. Untreated biomass samples a) acacia, b) pine, c) *Miscanthus giganteus*

2.2 Torrefaction

A torrefaction was conducted in apparatus designed and assembled in the laboratory of the Department of Thermal Technology and Environmental Protection at the Faculty of Metal Engineering and Computer Science at AGH UST. The schematic diagram of laboratory set up is shown in Fig. 2.2. The most important elements of reactor are quartz tube with a diameter of 4 cm and a length of 50 cm placed in an electric furnace and insulated with a layer of ceramic fibre with a thickness of 3 cm. The temperature inside tube was measured by NiCr-NiAl thermocouple connected directly to the temperature control panel. Moreover, the rotameter provided a constant flow of inert gas through the reactor chamber, which in this case was argon. The volumetric gas flow was maintained at 5dm^3/h. The exhaust gases were treated in a scrubber and were not analyzed in this experiment.
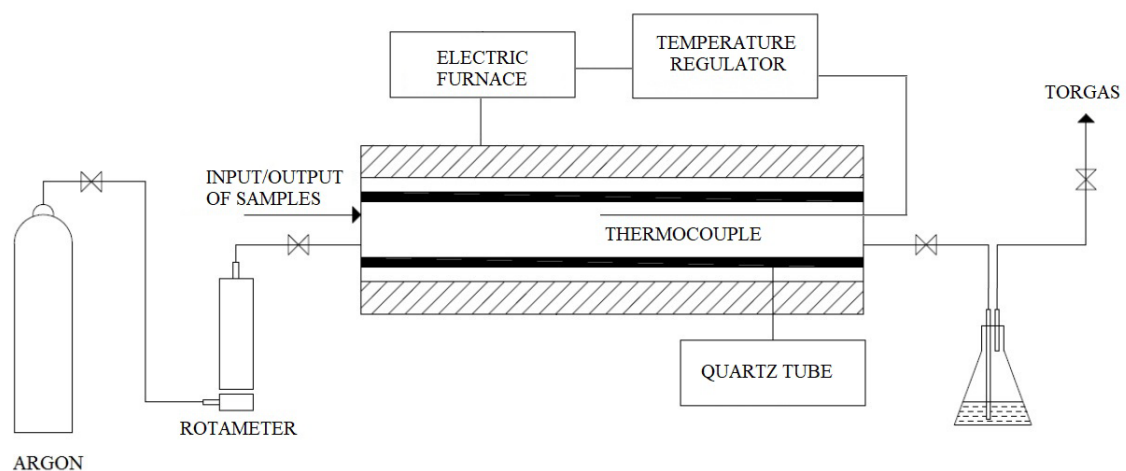
Fig. 2.2. Schematic diagram of torrefaction installation [7]

3.2 Analytical methods

Firstly, the proximate analysis was performed. Moisture, ash and volatile matter contents were determined according to European Standards. The moisture content was examined by maintaining 2g of the samples in the dryer at 105±2°C for at least 4h to achieve constant mass as is described in EN 14774-2. The ash content was measured by means of EN 14775: 2g of samples were heated for 30minutesin muffle furnace to 250°C and held for 1h than further heated for 30minutesto 550°C and held for another 2h. EN 15148 was used to determine volatile matter content. 1g of biomass was inserted to furnace at 900°C for 7 minutes [10-12].

Secondly, the ultimate analysis was conducted. Carbon, hydrogen and nitrogen content were measured by Elemental Analyser Truespec LECO CHN628. It is using high temperature combustion in oxygen and thanks to IR and thermal conductivity sensor is able to determine elements of interest.

Using received results allowed to estimate oxygen content

$$O = 100 - C - H - N - Ash - Moisture \tag{1}$$

where,

O   oxygen content, (%)

C   carbon content, (%)

H   hydrogen content, (%)

N   nitrogen content, (%)

The molar ratios of O/C and H/C were calculated in order to design van Krevelen's diagram

$$\frac{O}{C} = \frac{\frac{O}{16}}{\frac{C}{12}} \quad and \quad \frac{H}{C} = \frac{\frac{H}{1}}{\frac{C}{12}} \tag{2}$$

where,

O   oxygen content, (%)

C   carbon content, (%)

H   hydrogen content, (%)

High heating value (HHV) was determined using two different methods: computational and experimental. The equation used was given by A. Friedl [13]:

$$HHV = 3{,}55 \cdot C^2 - 232 \cdot C - 2230 \cdot H + 51{,}2 \cdot C \cdot H + 131 \cdot N + 20600 \tag{3}$$

where,

HHV   high heating value, (kJ/kg)

C   carbon content, (%)

H   hydrogen content, (%)

N   nitrogen content, (%)

In experimental method calorimeter LECO AC500 was usedto determine HHV. Samples were compressed into Tab.ts and placed into pressure vessel where dueto ignition wire combustion in oxygen was initiated. Pressure vessel is submerged into the water whose temperature is constantly monitored. Based on known parameters of water and changes in its temperature, software is capable of calculating high heating value with great precision.

Ultimate analysis and high heating value determination were conducted prior and after torrefaction in order to observe its effect on the examined samples.

3. Results

Proximate and ultimate analyses, molar ratios and HHV results for tested biomass feedstocks are shown in Tab. 3.1. All of them are very similar in terms of elementary composition. Carbon, hydrogen, nitrogen and oxygen contents are around 50%, 6%, 0.01% and 35%, respectively. Ultimate analyses revealed moisture content about 8%. Ash content for *Miscanthus giganteus* is 2.6% while acacia and pine have only c.a. 0.2%. Volatile matter level in all materials is above 80%. Difference in two determination methods of high heating value is around 6%. In this research more important is change in HHV after pretreatment method than its specific value. Therefore, in further analysis computational method was mainly used.

Tab.. 3.1. Results of analyses prior to torrefaction.

	Acacia	Pine	*Miscanthus giganteus*
C, %	49.1	51.2	48.1
H, %	6.4	6.77	6.33
N, %	0.12	0.03	0.08
O, %	35.99	33.74	35.74
M_{ar}, %	8.17	8.13	7.2
A_{ar}, %	0.22	0.13	2.55
VM_{ar}, %	82.26	86.71	81.37
H/C	1.564	1.587	1.579
O/C	0.678	0.615	0.709
HHV_c, kJ/kg	19 600	20 682	19 138
HHV_e, kJ/kg	-	-	17 872

Effect of torrefaction can be seen usinganalytical methods by comparing the physical and chemical properties of the samples prior and after pretreatment but also by visual effects. Samples were getting darker and they changed colour through light brown to black for the most rigid torrefaction conditions. Photographs of samples after torrefaction in different conditions are shown in Fig.3.1.

Fig. 3.1. Photographs of *Miscanthus giganteus* after torrefaction in different conditions.

Tab.. 3.2. Chemical and physical results and energy factors obtainedbefore and after torrefaction [14].

Biomass	Temp. °C	Time, hh:mm	N, %	C, %	H, %	O, %	HHV, kJ/kg	Energy yield, %	Molar ratio O/C	Molar ratio H/C
Acacia	As received		0.12	49.1	6.40	44.38	19600	100	0.678	1.564
	230	00:30	0.07	52.5	5.92	41.51	20926	95.85	0.593	1.353
		01:00	0.22	53.9	5.77	40.11	21493	93.49	0.558	1.285
		01:30	0.19	53.9	5.80	40.11	21506	93.55	0.558	1.291
	260	00:30	0.07	55.2	5.81	38.92	22084	90.76	0.529	1.263
		01:00	0.13	55.4	5.80	38.67	22178	88.74	0.523	1.256
		01:30	0.22	57.3	5.65	36.84	22966	87.65	0.482	1.183
	290	00:30	0.16	56.4	5.63	37.81	22531	82.68	0.503	1.198
		01:00	0.23	57.5	5.35	36.92	22847	77.08	0.482	1.117
		01:30	0.25	60.2	5.11	34.44	23886	65.05	0.429	1.019
Pine	As received		0.03	51.2	6.77	42.00	20682	100	0.615	1.587
	230	00:30	0.01	52.9	6.33	40.76	21292	98.08	0.578	1.436
		01:00	0.10	53.1	6.21	40.59	21339	97.37	0.573	1.403
		01:30	0.07	53.4	6.18	40.35	21459	96.21	0.567	1.389
	260	00:30	0.00	53.5	6.20	40.30	21506	93.03	0.565	1.391
		01:00	0.05	54.1	6.19	39.66	21787	90.11	0.550	1.373
		01:30	0.08	57.3	6.25	36.37	23372	88.40	0.476	1.309
	290	00:30	0.03	56.0	6.10	37.87	22632	84.05	0.507	1.307
		01:00	0.08	58.2	5.83	35.89	23505	78.12	0.462	1.202
		01:30	0.08	61.1	6.04	32.78	25114	67.89	0.402	1.186
Miscanthus Giganteus	As received		0.08	48.1	6.33	45.49	19138	100	0.709	1.579
	230	00:30	0.14	50.3	6.08	43.48	20030	94.51	0.648	1.450
		01:00	0.22	50.4	5.73	43.66	19961	91.56	0.650	1.364
		01:30	0.28	51.6	5.86	42.26	20531	87.08	0.614	1.363

260	00:30	0.09	51.8	5.90	42.21	20610	87.32	0.611	1.367
	01:00	0.13	52.9	5.89	41.08	21097	84.53	0.582	1.336
	01:30	0.26	55.9	5.62	38.22	22310	76.91	0.513	1.206
290	00:30	0.22	55.9	5.81	38.07	22425	76.50	0.511	1.247
	01:00	0.37	57.7	5.07	36.86	22753	61.22	0.479	1.054
	01:30	0.44	62.2	4.83	32.54	24572	58.04	0.392	0.932

In collected data a few trends can be found. The higher temperature and longerresidence time applied,the higher carbon content was achieved. This corresponds to the changes observed in colour of the samples and to theincrease of high heating value. In order to decide which conditions are the most suiTab. for torrefaction of lignocellulosic biomass energy yield was calculated by given equation [8]:

$$\eta_E = \frac{m_t}{m_b} \cdot \frac{HHV_t}{HHV_b} \cdot 100\%$$

(4)

where,

m_b mass of sample before torrefaction, (g)

m_t mass of sample after torrefaction, (g)

HHV_b high heating value before torrefaction, (kJ/kg)

HHV_t high heating value after torrefaction, (kJ/kg)

Moreover making use of molar ratios van Krevelen's diagram was created, shown in Fig.3.2.
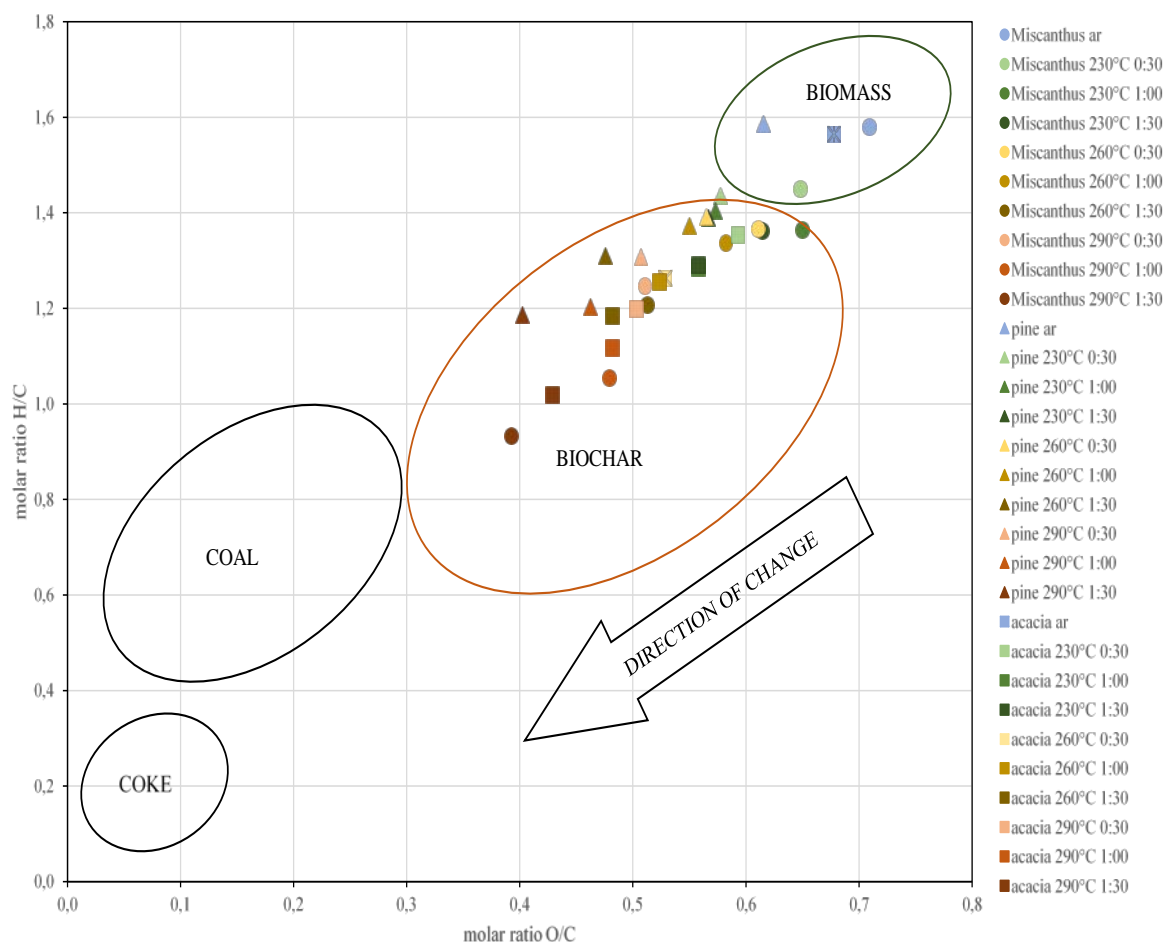
Fig. 3.2. Van Krevelen's diagram for all studied samples.

By observing trends in Fig. 3.2 it could be seen that the properties of the biochars obtained under longer residence time and higher temperatureprocessare movedcloser towards coal. Molecules of H_2O are emitted from polymeric chains in biomass structure which leads to decrease in hydrogen and oxygen contents giving an effect of increase in carbon content.
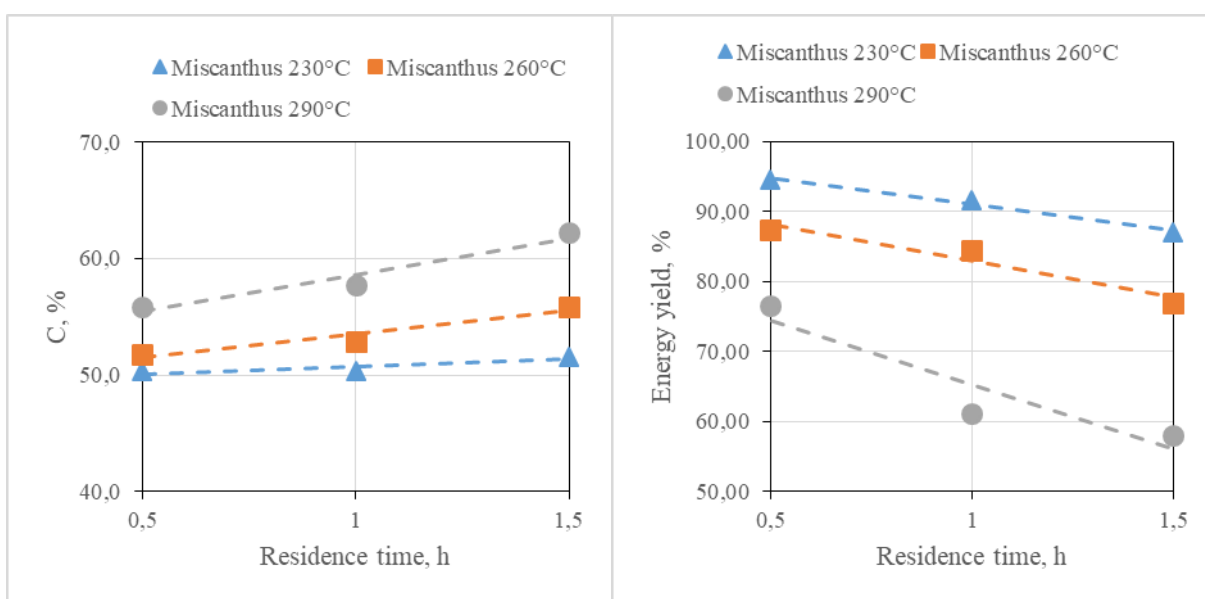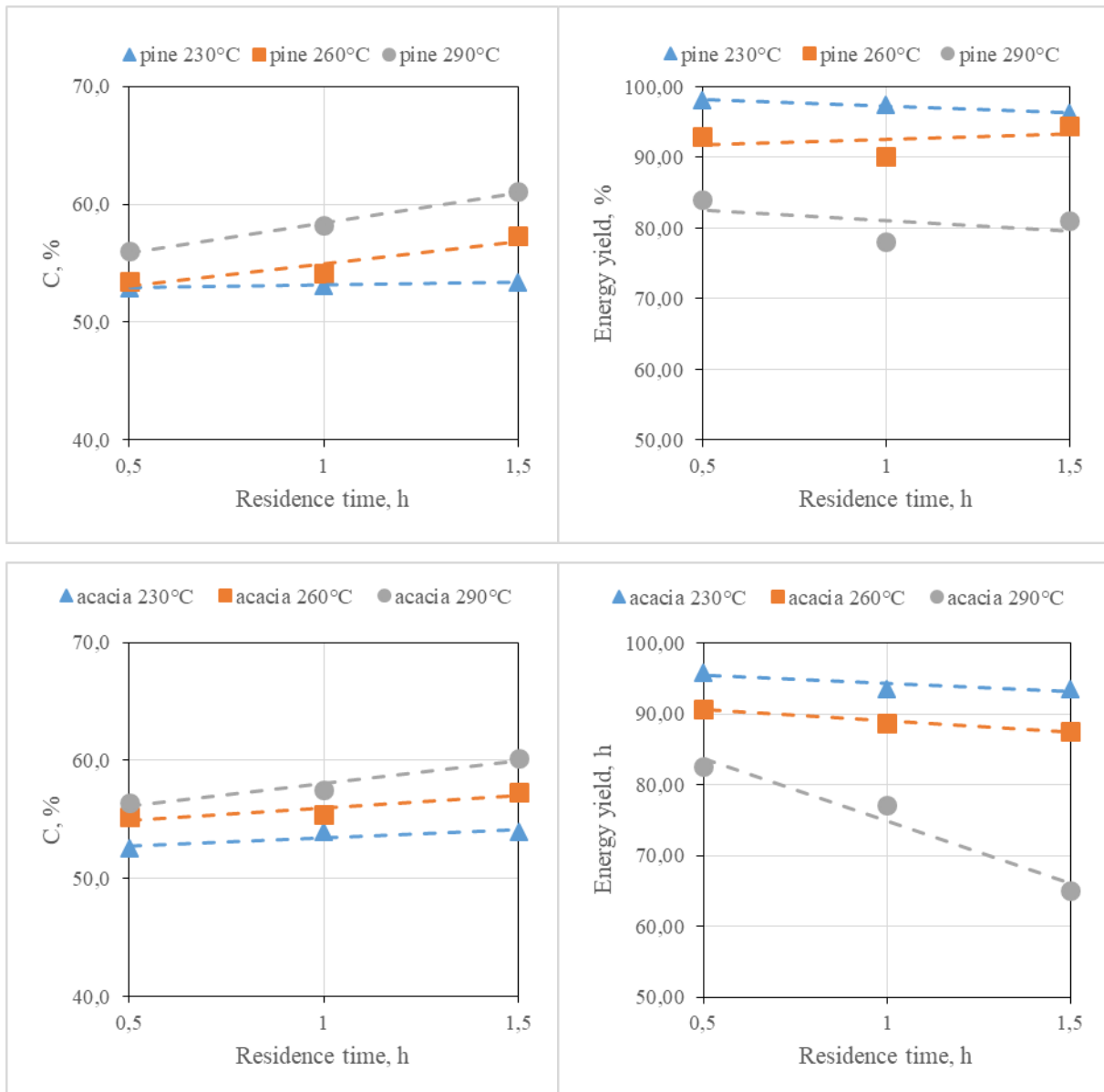
Fig. 3.3. Diagrams presenting carbon content and energy yield in torrefied samples.

In Fig. 3.3the carbon content and energy yield in torrefied samples are depicted. The following conclusion canbe made: more carbonaceous properties of biochars are obtained at higher temperature and the temperature impact is more visible than the influence of the residence time. It must be also pointed out that reaching higher temperature leads to bigger losses in energy yield due to change in mass of sample.

4. Conclusions

Torrefaction process was successfully conducted. Received biochars confirmed enhanced properties such as: lower moisture content, hydrophobicity, higher high heating value, brittleness, improved grindability and limited biodegradation.

From all examined conditionsof the process (residence times: 0.5; 1 or 1.5h and temperatures: 230, 260 and 290°C) the most optimalare 1.5 hour of residence time and 260°C. Moreover, it may be validated dueto calculated energy yields. In the case of the application of 290°C, iteffects in much higher efficiency losses which is unfavourable. Chosen conditions allow to obtain anincrease by 13-17% in high heating value and corresponding energy yield between 77-88% in torrefied samplescompared to raw biomass.

Acknowledgment

References

[1] B. Acharya, I. Sule, A. Dutta, *A review on advances of torrefaction technologies for biomass processing*, Biomass Conversion and Biorefinery 2 (2012)349-369.

[2] H. S. Kambo, A. Dutta,*Comparative evaluation of torrefaction and hydrothermal carbonization of lignocellulosic biomass for the production of solid biofuel*, Energy Conversion and Management 105 (2016) 746-755.

[3] H. S. Kambo, A. Dutta,*Strength, storage, and combustion characteristics of densified lignocellulosic biomass produced via torrefaction and hydrothermal carbonization*, Applied Energy 135 (2014) 182-191.

[4] D. Ciolkosz, R. Wallace, *A review of torrefaction for bioenergy feedstock production*, Biofuel Bioproducts and Biorefining 5 (2011) 317-329.

[5] M. Wilk, A. Magdziarz,*Hydrothermal carbonization, torrefaction and slow pyrolysis of Miscanthus giganteus*, Energy 140 (2017) 1292 -1304.

[6] M. Jakubiak, W. Kordylewski, *Toryfikacja biomasy*, Archiwum spalania 10 (2010) 1-2:11-24.

[7] M. Wilk, A. Magdziarz, I. Kalemba, *Characterisation of renewable fuels' torrefaction process different instrumental techniques*, Energy 87 (2015) 259-269.

[8] M. Wilk, A. Magdziarz, I. Kalemba, P. Gara, *Carbonisation of wood residue into charcoal during low temperature process*, Renewable Energy 85 (2016) 507-513.

[9] M. Śliz,*Procesy karbonizacji paliw odnawialnych*, BSc thesis, Wydział Energetyki i Paliw, Akademia Górniczo-Hutnicza w Krakowie (2017).

[10]European Standard EN 14774-2, *Solid biofuels – Determination of moisture content – Oven dry method – Part 2: Total moisture – Simplified method*, CEN 2009.

[11]European Standard EN 14775, *Solid biofuels – Determination of ash content*, CEN 2009.

[12]European Standard EN 15148, *Solid biofuels – Determination of the content of volatile matter*, CEN 2009.

[13]A. Friedl, E. Padouvas, H. Rotter, K. Varmuza, *Prediction of heating values of biomass fuel from elemental compositon*, Analytica Chimica Acta 544 (2005) 191-198.

[14]M. Wilk, A. Magdziarz, M. Gajek, M. Zajemska, K. Jayaraman, I. Gokalp, *Combustion and kinetic parameters estimation of torrefied pine, acacia and Miscanthus giganteus using experimental and modelling techniques*. Bioresource Technology 243(2017) 304–314.

Ultra-high temperature thermal energy Storage and other thermal energy storage systems: A review

Shemin Sagaria[1]

[1]faculty of Power and Environmental engineering, Silesian University of Technology,

e-mail:sheminsagaria@gmail.com

Abstract

With advancement in technologies, renewable energy have the potential of replacing fossil fuels for a better and greener future. But still fossil fuels are ruling the market and it is because of inconsistency of renewable energy production. By using the energy storage methods, we can facilitates effective utilization of intermittent renewable sources and can be combined into smart integrated energy system. In addition to this, energy storages helps to reduce need for increased peak generation capacity and enhances the grid reliability. In this paper, ultrahigh temperature thermal storage system is reviewed and is compared with other thermal storage system which is operational now in terms of overall round efficiency.

Keywords: Thermal energy,thermal energy storage,energy storage, High temperature thermal storage

1. Introduction

Renewable energy source is creating a new potential future in the energy sector, and energy storage make a vital contribution to energy security in the future. The aim is to supply energy that is free from carbon dioxide production while sustainable and not dependent on a finite energy supply.As now, the world is generating more renewable electricity as ever before. However, most of the renewable power are weather dependent and varies according to the availability of the resources. For example in case of solar energy, it depends upon the solar rays and time while in case of wind turbine, it depends on the availability of wind over the region, which both these scenarios are unpredictable.Unfortunately their full potential is reduced by their intermittency.

Currently we have large number of renewable energy sources whose power output cannot be controlled during their peak performance time having high renewable energy generation, surplus energy thus created get lost. On the other side, during low renewable energy generationthey won't be able to produce the demanded energy and this creates a gaps betweenconstant energy distributions. For the former problems and other developing renewable technologies, such as tidal current energy and wave energy, to make a real difference we need to find effective ways to store this energy.

In Fig. 1, load curve diagram shows the electricity demand for continuous 24/7 supply (base-load) in the polish power system [1]. We can observe that the energy required during each hour is varying simultaneously.During day time (peak hours: 0800-2200) the required amount of energy is much higher than that of night time (off peak hours: 2200-0800). While a day in summer and winterfollows the same trend, nevertheless, during winter more energy is required for district heating purpose.In order to make effective distribution of energy, it is wise to store energy during the off-peak hours and distribute in peak hours which allows a constant generation of energy from the fossil fuel source, else on peak hours more energy has to be produced. On comparing with Fig. 1, Fig.2 shows an example of using excess energy produced during off peak hours on peak hours. The same method can be followed in order to meet the requirements during different seasons. The excess energy produced during summers can be stored using different techniques and we can recover stored energy during summers or when high load is required in the grid [2][3].

Energy storage facilitates us to capture/store the excess energy produced during peak performance time and to distribute it during the weak performance time. The energy storage techniques balances between generation and

demand and improves the overall stability and reliability of power system and could defer the costs need to improve the transmission and distribution capacity to meet ever growing power demand.
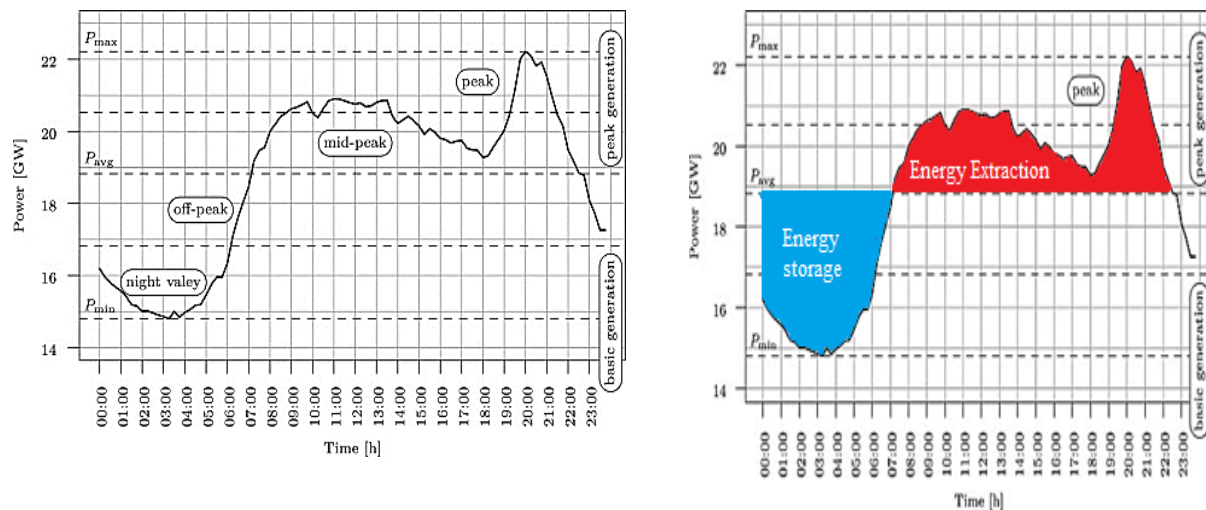
Fig. 1. Load curve of polish energy system on 01/03/2014   Fig. 2. Load curves with energy storage system [1]

There are many types of storage technologies available at present. Although examining all these technologies is necessary, this papers concentrate only on thermal storage technologies and gives an overview of

➢ Different types of thermal energy storage technologies available at present

➢ State some of the features of the thermal energy storage technologies

➢ Do a comparison study of various thermal energy storage technologies

2.   Thermal Energy Storage Systems

Thermal energy storage (TES) is mostly used to store the excess available energy as heat or cold to be used when required later under varying conditions such as temperature, place or power. Thermal energy storage system helps us to fill the gap between energy supply and energy production during peak hours [4] [5]. In TES system, energy storage take place in 3 sequential steps: charging, storage and discharge, giving a complete storage cycle (Fig.3)

The main necessities for designing a TES system are high energy density in the storage material (storage capacity), good heat transfer between the heat transfer fluid (HTF) and the storage material, mechanical and chemical stability of the storage material, compatibility between the storage material and the container material, complete reversibility of a number of cycles, low thermal losses during the storage period, and easy control. In addition to this, the most significant design principles are the operation strategy, the nominal temperature and enthalpy drop, and the integration into the whole application system. The advantages of implementing thermal energy storage to the grids are:

• better economics: reducing capital and operational costs

• better efficiency: achieving a more efficient use of energy

• less pollution of the environment and less CO_2 emissions

• better system performance and reliability.

Fig. 3. TES storage cycle

2.1.   Thermal energy storage principles

The basic thermodynamics of energy storage is done by following mainly three principles: sensible heat storage, latent heat storage, and thermochemical storage.

2.2.   Sensible heat storage

In sensible heat storage devices, the energy is stored as heat in the substance, by changing the temperature of substance to higher value or lower value. The commonly used storage material are water, air, oil, bedrock, brick, concrete, etc. even though each material has its own advantages and disadvantages, the material selection is done based on the heat capacity and the available space for storage [6]. The amount of energy stored is calculated following Eq. [1]:

$$Q = m * cp * \Delta T \qquad\qquad [1]$$

Where -Q is the amount of heat stored in the material (J),m is the mas of storage material (kg),

cp is the specific heat of the storage material (J/kg·K), andΔT is the temperature change (K).

The material used for sensible heat storage should have high thermal capacity and it has to be abundant and cheap. The basic properties that are evaluated while considering a material are density, specific heat, thermal conductivity and diffusivity, vapour pressure, compatibility with container materials, and chemical stability [8]. Sensible heat is usually stored in solid or liquid, but gas media can also be used, but they are much more bulky.

2.3.   Latent heat storage

In Latent heat storage, energy is stored in to a material by transition of the phase of the material. Usually solid–liquid phase change is used, by the process of solidification and melting of the material. When material is solidified, heat is released, energy extraction can take place and on melting, heat is taken into the material. Using this principle storing large amounts of heat at constant temperature is possible. Usually materials that are used to store energy as latent heat are called phase change materials (PCM). The amount of heat stored is calculated following Eq. [2]:

$$Q = m * \Delta h [2]$$

Where - Q is the amount of heat stored in the material (J), m is the mass of storage material (kg), and

Δh is the phase change enthalpy (J/kg).

The commonly known and used PCM is water, used as ice for cold storage since early times. Even though many materials have been studied to storage energy as latent heat, but only a few of them have been succeeded for the former [4][6][7], mainly due to problems such as phase separation, sub cooling, corrosion, long-term stability, and low heat conductivity, that have not yet been totally solved.

2.4.   Thermochemical energy storage

Thermochemical energy storage works with the assistance of a reversible reaction, when a chemical reaction with high energy elaborate in the process is used to store energy. The products from the reaction is stored separately and the heat is retrieved from the system when the reverse reaction takes place [6]. Therefore, only reversible reactions can be used for this storage process. The material used should have energy storage density and reversibility in order to store energy efficiently [9]. It is to be noted that chemical energy conversion has superior energy storage performance than that of other methods such as sensible and latent heat storage. But it is also difficult to find proper reversible chemical reaction for the energy storage.

Thermochemical reactions are used as thermos chemical materials (TCM) at high temperatures (more than 400°C) and the enthalpy of the reaction is located in a high range (80–180 kJ/mol). Moreover, thermochemical energy storage devices are considered as seasonal energy storage system as the products of the reaction are store separately [10].The most common and studied reversible reactions for energy storage are the carbonation reaction, ammonia decomposition, metal oxidation reactions and sulphur cycles [11] [12] [13].

In addition to this, sorption is used to store energy in thermochemical energy storage systems. In sorption, binding of a gas or liquid on to the inner surface of a porous material is carried out. While on removing the absorbent from the surface, heat is given in to the system, acts as charging cycle. Energy is extracted on the absorption process when binding is carried out, is the discharging process of the storage cycle.Adsorption on solid materials or absorption on liquids is used in sorption systems [12] [13].

3. Types of TES systems

3.1. Ultra high temperature energy storage systems (UHTS)

Until now thermal energy storage has been limited to a temperature of around 800 K [14], making it uncompetitive in terms of energy density and round-trip efficiency from heat to electricity. By storing energy as heat at ultra-high temperatures (> 1100 K), it is possible to raise energy density and round-trip efficiency to the point where grid-scale thermal storage becomes technically and economically feasible. But, the operating temperature of thermal storage has been limited by heat loss that rises exponentially with increasing temperature, by the radiative power losses [18].

Metals have been previously proposed as an energy storage media due to their high specific heat capacity and heat transfer properties [15]. There have also been proposals to use molten alkali metals for storage within the 800–1000 K temperature range in combination with concentrated solar power [16]. Metals would be advantageous as the primary storage materials for UHTS because they:

> Can be common and inexpensive.

> Have high specific heat capacities.

> Have superior thermal conduction properties to other feasible materials, which improve resistance to thermal shock and differential expansion during charging and cooling.

A major consideration for any thermal storage system is the rate at which energy is lost to the surrounding environment. Conductive loss for a planar surface is given by Eq. [3], Radiative losses for a sphere within a spherical volume are calculated with Eq. [4] [17]

$$P_c = \frac{kA\,(T_2 - T_1)}{d} \quad \text{------ [3]} \qquad\qquad P_r = \frac{\sigma A\,(T_1^4 - T_2^4)}{\frac{1}{\varepsilon_1} + \frac{1 - \varepsilon_2}{\varepsilon_2}\left(\frac{r_1}{r_2}\right)^2} \quad \text{-------- [4]}$$

Where k is the thermal conductivity, A is the surface area, d is the thickness, T1 is the lower temperature, and T2 is the higher temperature, ε the emissivity and σ isthe Stefan–Boltzmann constant, while r is the radius of the sphere. In Eq. (2) the subscript 1 denotes the inner sphere and 2 the outer sphere.

By using a medium strength vacuum around the storage vessel, thermal conduction can be reduced to the point where conduction losses become negligible compared to radiative losses. The footprint of the plant relative to the energy stored will also be less for a larger sphere. These results are a consequence of the fact that storage capacity is a function of volume and thermal losses are a function of area[18].

3.1.1.   Charging cycle of UHTS

For the charging cycle heat is given in to the system. The heat pump charge cycle begins with nitrogen at a pressure of 0.76 MPa and a temperature of 600 K. This gas is heated to 795 K through a series of heat exchangers connected to the collector stages and ending in the labyrinth heat exchanger built around the storage core. The nitrogen is then piped inside the storage core where it enters the multi-stage compressor with inter-stage heat exchangers. Again, compressing the nitrogen raises the temperature above that of the storage medium, allowing energy to be transferred to the storage core. At the end of this process the nitrogen exits the final heat transfer stage with a temperature of 810 K and a pressure of 3.19 MPa; the total compression ratio is 2.88 as before. As the storage core charges its temperature increases until it reaches the state shown in Fig. 4 (1800 K). If the collector stages are depleted during the charge or the COP is low, direct electric heating of the core will be used instead of the heat pump. The nitrogen exiting the final inter-stage heat exchanger expands through a turbine back to 0.76 MPa and 600 K. The nitrogen exiting the turbine is directed through insulated pipes back to the first storage stage heat exchanger to continue the closed cycle.

3.1.2.   Energy storage

A schematic of the UHTS system in the storage phase of operation, numbered at each stage of the thermodynamic process, is shown in Fig. 4 and inFig. 5. At the centre of this storage system is the storage medium, which is contained within a spherical platinum-coated alumina vessel; this will be referred to as the UHTS core. The storage core is surrounded by a labyrinth heat exchanger, which is part of the heat pump used to recover energy lost through radiation from the core. Outside of this heat exchanger is a sequence of insulated and isolated thermal masses that are used to capture energy lost from the labyrinth heat exchanger, known as the collector stages.
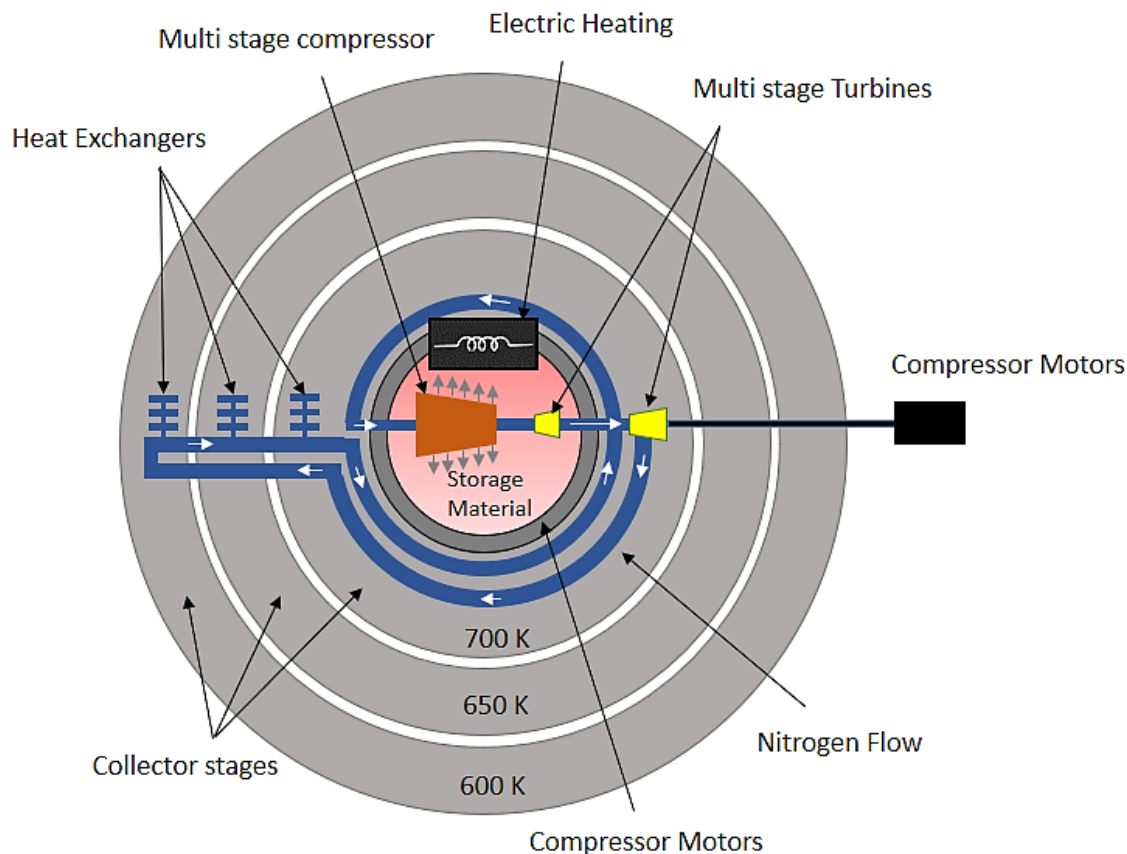
Fig. 4. UHTS system in storage mode
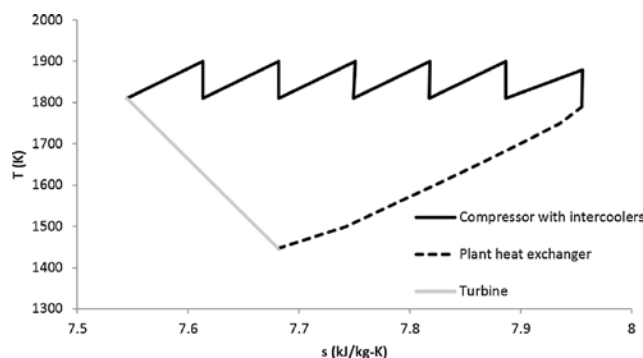
Fig. 5. T-s diagram of the heat pump during storage model. (Compression process are not isentropic)
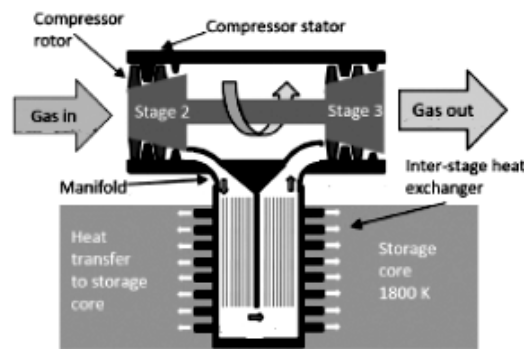
Fig. 6. configuration of compressor with inter stage heat exchanger

The UHTS cycle begins with nitrogen, at a pressure of 2.12 MPa and a temperature of 1446 K, entering a labyrinth heat exchanger built around the storage core to collect lost thermal radiation. Heat is transferred to the gas from the heat exchanger through convection and conduction. A representation of this heat exchanger is shown in Fig. 6, which has a final wall temperature of 1800 K. Upon leaving this heat exchanger the nitrogen has a temperature of 1790 K. Reaching 1800 K is not critical and would require a significantly larger and more expensive heat exchanger.

Following the labyrinth heat exchanger the nitrogen is then piped inside the storage core where it enters a multi-stage compressor with inter-stage heat exchangers connected to the storage core. Compressing the nitrogen raises the

temperature above that of the UHTS medium, allowing energy to be transferred to the storage core. At the end of this process the nitrogen exits the final heat transfer stage with a temperature of 1810 K and a pressure of 8.43 MPa. The total compression ratio is 2.88.During compression process energy will be losses by friction or turbulence, In the case of UHTS, this energy could be transferred back to the storage core, thereby increasing the effective efficiency of the compressor closer to 100%.After the final storage core heat exchanger the nitrogen is expanded through a turbine back to 2.12 MPa. This decompression also lowers the temperature of the nitrogen. The turbine is connected to the compressor and can be expected to recover a significant proportion of the energy used to compress the nitrogen in stage 2–3. The extra power required to run the compressor will be provided by a separate motor (Fig. 4) and will represent the main use of externally supplied power to the UHTS storage system whilst in storage mode.The nitrogen exiting the turbine is directed through insulated pipes into the labyrinth heat exchanger to continue the closed cycle.

3.1.3.   Energy Extraction

Energy recovery from UHTS uses identical configuration to existing Combined Cycle Thermal Power Plants (CCPP) and will be independent from the thermodynamic cycles used for storage and charging. Energy released from the storage core is used to heat the working fluid, which passes through a gas turbine operating on the Brayton cycle. The remaining heat from the exhaust of the gas turbine is used to generate steam, which is then utilised to drive a steam turbine operating on the Rankine cycle which to extract additional energy from the working fluid.
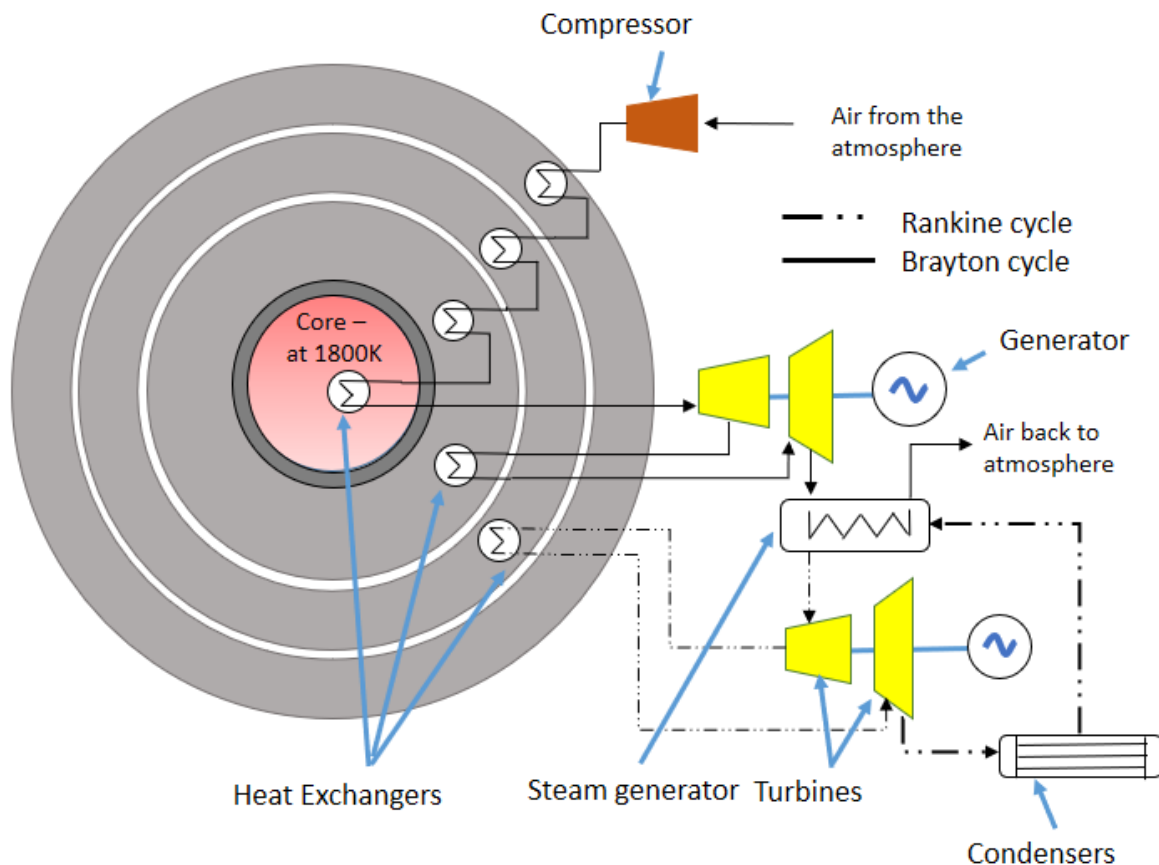

Fig. 7. UHTS in discharge mode

The turbines of both the topping Brayton cycle and the bottoming Rankine cycle are used to turn electric generators. The energy extraction from UHTS is shown in Fig.. The gas passessequentially through a series of heat exchangers connected to each of the collector stages, thereby absorbing energy and reduces heat loss.

The temperature of each of the collector stages will be dependent on the transient nature of the previous extraction, charging and storage cycles. Once the air is heated to the temperature of the storage core, it is transported through an insulated pipe outside the UHTS to feed a multi-stage turbine. The air enters the gas turbine at 1800 K and leaves at 900k air from the turbine is used to provide heat to the steam generator that drives the bottoming Rankine cycle. Once this steam exits the turbine it is cooled and condensed to supply a water pump, thus beginning the cycle again. The UHTS architecture may afford the use of many inter-stage reheats to increase efficiency. Heat exchangers can theoretically have an efficiency of 100% but are limited from achieving this by practical and economic considerations [20]. In real-world gas-to-gas heat exchanger efficiencies of 95% are reported in open-cycle gas turbine recuperates [21] and 93% in closed-cycle gas turbines [15]. The solid-to-gas heat exchanger used in UHTS should be significantly more efficient than gas-to-gas heat exchangers used in existing gas turbines.

3.2. Molten-salt technology

Molten salts are a special class of compounds that have immense potential as thermal energy storage and heat transfer media. Their use for solar energy applications is mainly due to the following properties:

- o   liquid state over a large range of temperatures and high thermal stability,

- o   Ability to dissolve a large amount of inorganic and organic compounds,

- o   High heat capacity per unit volume.

In addition, many salts have low production costs, compared with other liquid materials, which positively impacts the total cost of the storage system with a round trip efficiency of 70% [19], which can be used to store energy at 1100K. The types of molten salt storages are:

3.2.1.   Direct Heating with molten salt

When the heat transfer fluid (HTF) used in the solar field is also used as a storage material, the system is considered as a direct storage system, while in an indirect system, a different medium is used for storing the heat. Molten salt (solar salt, 60% $NaNO_3$, 40% KNO_3) is recognized as the most successful material for solar heat transport. This eutectic mixture melts at 220°C and remains a liquid at 290°C in an insulated storage tank, called a 'cold tank'. The operating principle is as follows (see Fig. 8): 'cold' molten salt (at a temperature of 292°C), entering the tower receiver, is heated by the concentrated sunlight reflected from the heliostats. Hot salt (at a temperature of 565°C) moves downward through the tower into a special storage tank. When energy is required, hot salt from the tank passes through the heat exchanger to generate superheated steam, which further turns the turbine and produces electricity. The advantage of this type of plant is that it can be used to achieve higher temperatures than solar power plants using organic storage media (565°C vs 400°C). Thus, due to the greater temperature difference between the cold and hot molten salts, a tower plant can store more energy in the same amount of salt as a trough plant. The disadvantage is a very high risk of solidification of storage medium, because molten solar salt has a relatively high freeze point.
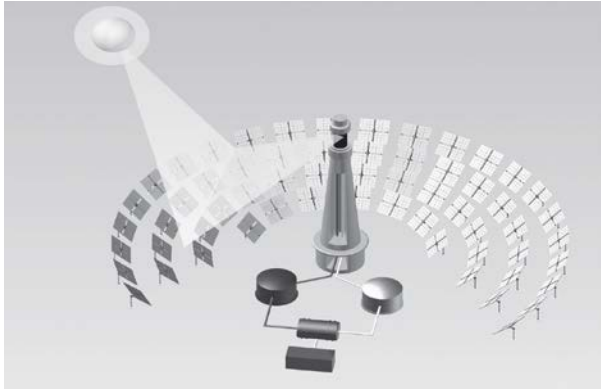
Fig. 8. Direct heating of molten salt
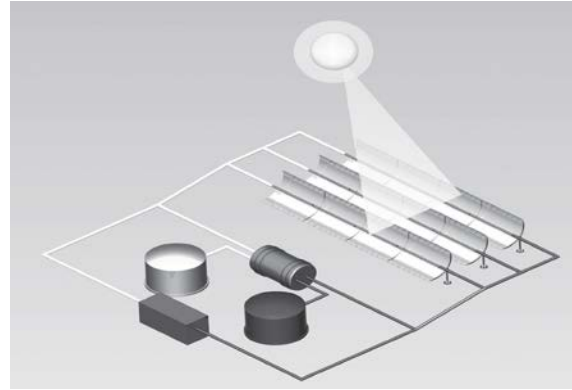
Fig. 9. Two tank indirect storage system

3.2.2. Two tank indirect storage system

Unlike direct two-tank storage, there is an extra heat exchanger (HX) between the oil and molten salt circulation loops (see Fig.9). The thermal oil circulates in the solar field (e.g., parabolic trough collector), is heated and passed through the oil–salt HX. At the same time, the thermal storage fluid from the cold tank flows through this HX and is heated by the high-temperature HTF. In this way, the high-temperature storage fluid flows back to the cold storage tank. The HTF output from the heat exchanger re-enters the solar collector field to raise the temperature. Using one-tank TES instead of two, the costs of construction, pipelines and related equipment can be reduced. Recently, a single-tank storage system for molten salt has been tested commercially through parabolic plant Valle 2 by SENER.

4. Ice/snow storage technology

Ice and snow have been used for cooling since ancient times. Plato mentions that ice was harvested in the mountains during the winter and stored in thermally insulated buildings for cooling in the summer. Sir John Chardin reports in his 'Travels in Persia 1673–1677' how ice is produced, stored, and sold for cooling of drinks in the summer[23].

Snow and ice have extraordinary properties for cooling applications. Its melting point at 0°C (normal ice at normal pressure) together with its very high latent heat of fusion makes it suitable in particular for space cooling and for cooling of foodstuffs. Water's latent heat of fusion (0.093 kWh/kg) means that 0.093 kWh of heat is required to melt 1 kg of 0°C ice into 0°C water. If the melt water can be used for cooling up to a temperature of 6°C, then 1000 kg of ice contains 100 kWh of cold [24].

4.1. Snow storage in thermally insulated buildings

Thermally insulated buildings have been used for seasonal snow storage since ancient times. Though the building is thermally insulated also the snow/ice is usually also insulated. The most commonly used natural material is sawdust, but other natural thermal insulation materials and also manufactured thermal insulation material are being used. Part of the storage building's volume (25–50%) is filled with snow during the winter. Snow blowers and/or tractors are used to fill the snow storage room. The main part of the building is used for storage of root vegetables, fruit, rice, etc., which means that the object to be cooled is placed in the same building. Such buildings could have a snow storage volume of 45,000 m3.
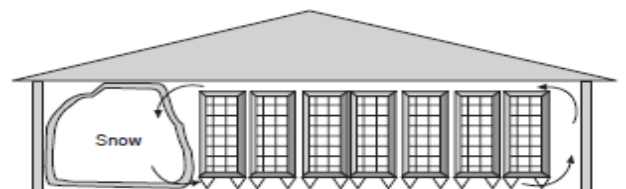
Fig. 10. Snow storage in thermal insulated building

4.2. Snow storage in thermally insulated pits

The principle of this system, which is usually located partly below the ground surface, is outlined in Fig. 12. Snow is stored during the winter in a shallow watertight pit. When the storage is filled up, it is covered by thermal insulation. Because of natural snowmelt caused by heat leakage from the surrounding snow, melt water is formed at the bottom of the storage. This water, which is close to 0°C, is used for cooling. It is pumped through a heat exchanger where it cools the cooling circuit, as it absorbs its heat. The warmed water is now pumped back to the snow storage.
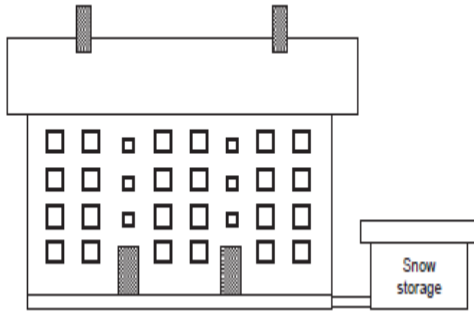
Fig. 11. Storage system integrated with structure   Fig. 12. Thermally insulated pit
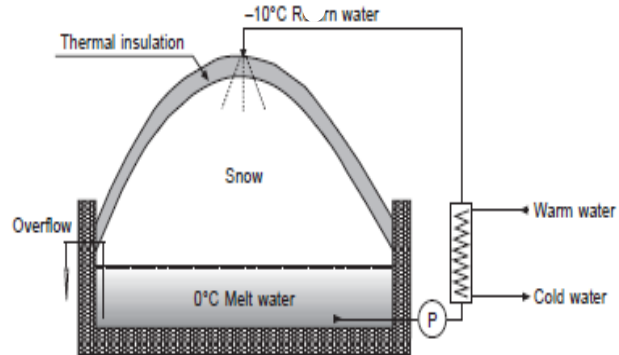
The is cooled after being spread onto the snow where it melts more snow and new 0°C melt water is formed. As the process continues, increasingly more melt water is formed at the bottom of the snow storage. The melt water, which is more or less polluted, is then let out of the snow storage through the overflow. Polluted melt water from snow dumps usually causes considerable environmental problems. About 90% of the pollutants in a snow dump will fall out as the snow melts and about 10% will be dissolved in the melt water.

5. Aquifer thermal energy storage system (ATES)

ATES systems are used to store cold from the winter for use to cool buildings in the warmer months of the year and to store heat from the summer to heat buildings in the colder months. ATES systems appear, at times, as open loop geothermal systems since they might incorporate heat pumps in the winter to supply heating demand and at the same time store cold thermal energy.

The principle of energy storage in aquifers is very simple, shown in Fig. 14. If there is natural cold in the winter, this can be stored in an aquifer. In summer the stored cold can be used for cooling purposes. It requires a minimum of two wells, a warm well and a cold well. In larger systems it requires several warm and cold wells. When cooling is demanded by the user, cold water is extracted from the cold well(s) and utilized to meet the cooling demand. The water is then returned to a warm well(s) at an elevated temperature. When there is a demand for heating, water is extracted from the warm well(s) to provide the heating load. The water is then injected into the cold well(s) at a low temperature (as in Fig. 14). In this manner thermal energy is stored seasonally.
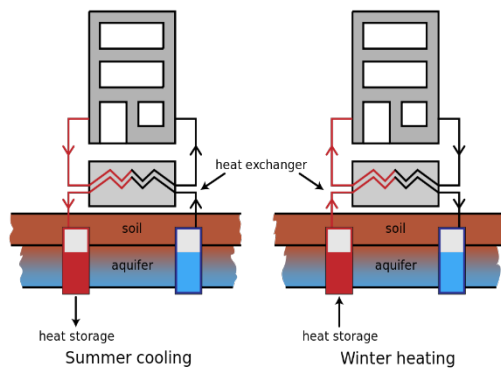
Fig. 13. Schematics of ATES
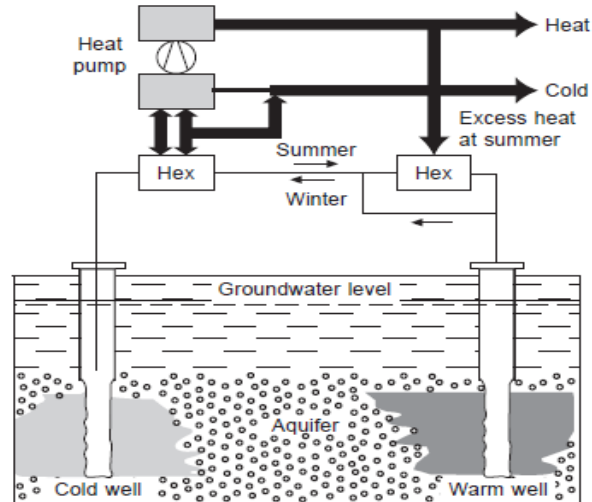
Fig. 14. Flow diagram of working principle of ATES [24]

6. Cryogenic energy storage

Cryogenic energy storage (CES) uses of low temperature (cryogenic) liquids such as liquid air or liquid nitrogen as energy storage.Process. When the energy availability is cheaper (usually at night), electricity is used to cool air from the atmosphere to -195 °C using the Claude Cycle to the point where it liquefies, as shown in Fig. 15. The liquid air, which takes up one-thousandth of the volume of the gas, can be kept for a long time in a large vacuum flask at atmospheric pressure. At times of high demand for electricity, the liquid air is pumped at high pressure into a heat exchanger, which acts as a boiler. Air from the atmosphere at ambient temperature, or hot water from an industrial heat source, is used to heat the liquid and turn it back into a gas. The massive increase in volume and pressure from this is used to drive a turbine to generate electricity [25].

In isolation the process is only 25% efficient, but this is greatly increased (to around 50%) when used with a low-grade cold store, such as a large gravel bed, to capture the cold generated by evaporating the cryogen. The cold is re-used during the next refrigeration cycle. Efficiency is further increased when used in conjunction with a power plant or other source of low-grade heat that would otherwise be lost to the atmosphere. *Highview* Power Storage claims an AC to AC round-trip efficiency of 70%, by using acold storage, thermos storages and otherwise heat source at 115 °C [26].
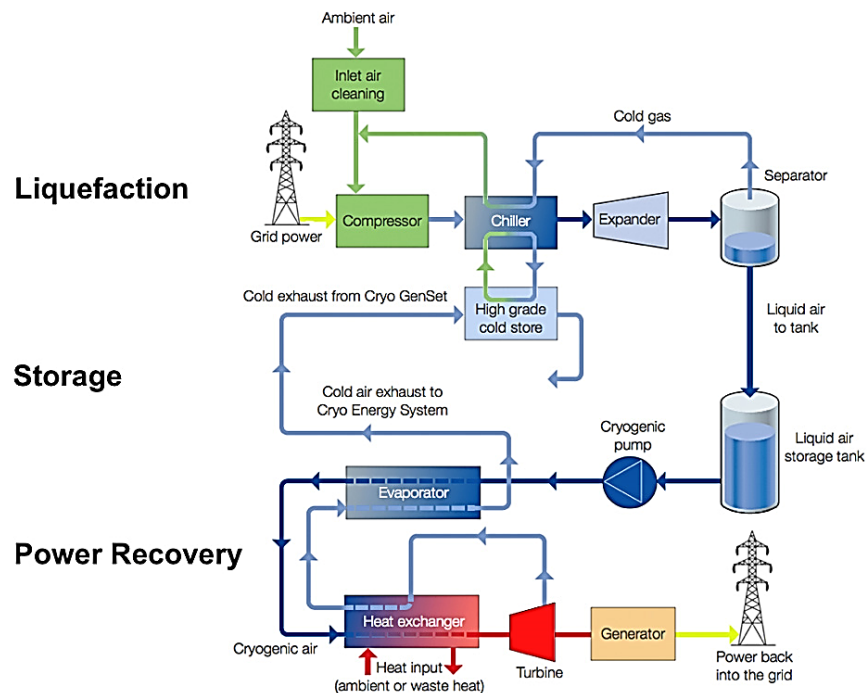
Fig.15. Cryogenic liquid air storage system

7. Using Phase changing materials (PCM)

A phase change material (PCM) is a material that changes phase at a certain temperature. During the phase change process, a PCM absorbs or releases a large amount of heat in order to carry out the transformation, as shown in Fig. 16. This action is known as the latent heat of fusion or vaporisation, and through this process energy is stored. The PCMs used can be organic and inorganic materials. Relative to sensible energy storage, the main advantages of such storage systems are the large storage capacity and the potential recovery of thermal energy at almost constant temperature,and is the ability to store large amounts of energy where the temperature difference between the heat source and sink is low. This property makes them useful for thermal comfort in buildings, solar heater systems, low energy cooling, concentrating solar power (CSP) plants and many other applications [24].
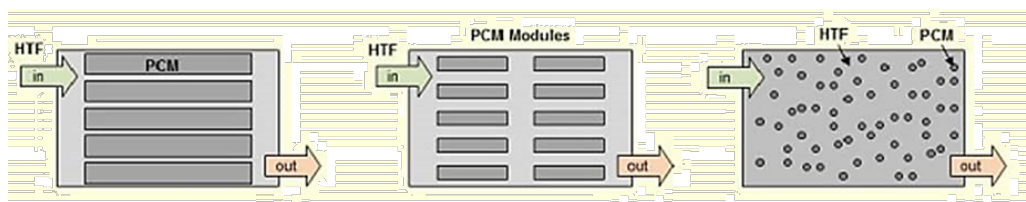
Fig. 16 : Phase changing of PCM material on storing energy

7.1. Moderate-Temperature PCMs

Many PCMs, including many salt hydrates, have their phase transitions in the moderate-temperature range, 40 °C to just over 100 °C. Salt hydrate materials consist of an inorganic or organic salt with one or more waters of hydration. Salt hydrates were the first materials to be investigated for use as PCMs [27].

Moderate temperature PCM's are used in solar thermal water heaters, to heat up the water for domestic applications.Heat transfer fluid, such as water or glycol, circulated through a flat plate or an evacuated tube solar collector, collects solar radiation as heat to be used to heat water for household use.

It is also used for seasonal heat storage. Long-term "seasonal" heat storage is characterized by multi-month to multiannual heat storage retention. Two principal mechanisms contribute to the ability of a PCM heat storage system to accomplish seasonal heat storage: insulated thermal mass and stable super cooling. The first mechanism is common to all heat storage media and not unique to PCMs, whereas stable super cooling is a unique property of PCM storage [28].

7.2.   High-Temperature PCMs

For high-temperature heat storage, in the range of several hundred to well over1000 °C, the PCMs used are metals and anhydrous salts. For the latter, variouscarbonates, chlorides, sulphates, nitrates, and nitrites are commonly used, as well as their eutectic mixtures [29].Molten salts are corrosive to many steels and their vapours are often reactive, and therefore expensive alloys and coatings are required to achieve an acceptable lifetime for the system. Salts also have low thermal conductivity, so metal or graphite rods or fins are required to transfer heat within the bulk of the PCM [30].

High temperature PCM's are used for concentrated solar stations, use large volumes of molten salt for thermal energy storage. The use of thermal storage in concentrated solar power (CSP) plants decouples power production from solar radiation availability [31]. In most thermal storage systems for solar thermal power plants, only the sensible heat of the molten salt is used. The Andasol Solar Power Station in Andalusia (Spain) is one such example. Andasol consists of three 50 MW projects, each producing about 165 GWh of energy annually. Andasol is a parabolic trough-type solar thermal station and operates just under 400 °C [31]. In this configuration, parabolic mirrors focus solar radiation onto a system of pipes containing biphenyl–diphenyl oxide eutectic as a heat transfer fluid, which carries heat to a steam generator and turbine, and to tanks of molten salt for storage.

Another application of high temperature PCM is Industrial Heat Scavenging. Excess process heat in continuous processes is routinely and economically captured in heat exchangers called economizers and using combined or cogeneration cycles. Sensible heat storage masses (e.g., bricks) are presently used to store excess heat from exhaust gases in large furnaces, then used to preheat inlet gases to active furnaces. Suitably encapsulated PCMs could be readily deployed to substitute bricks for thermal mass and improve the heat storage densities in these processes since operating temperatures are well defined and storage durations are short

8. Summary

A review on ultrahigh temperature energy storage is given and comparison study is done with other thermal energy storage devices is done. It can observe that when energy is stored at high temperature, the round efficiency has been increased comparatively with other thermal storage systems. By storing the excess energy on these storage devices definitely improves the energy loss inside the storage system and helps to improve the performance of the storage devices. In addition to this, facilitates effective utilization of intermittent renewable sources and can be combined into smart integrated energy system.

References

[1] Werminski Szymon, Jarnut Marcin, Benysek Grzegorz, Bojarski Jacek; Demand side management using DADR automation in the peak load reduction; journal: Renewable and Sustainable Energy Reviews, vol:67, pp-998-1007, 2017

[2] www.oxfordenergy.org/wpcms/wp-content/uploads/2018/04/Natural-gas-demand-in-Europe-in-2017-and-short-term-expectations-Insight-35.pdf

[3] Dostál, Zdeněk&Ladányi, Libor(2018) : Demands on energy storage for renewable power sources-pp. 250-255-Journal of Energy Storage-volume 18;

[4] Dincer, I. and Rosen, M.A. (2002) Thermal energy storage (TES) methods. In: Dincer, I. and Rosen, M.A. (eds) Thermal Energy Storage: Systems and Applications, pp. 93–212. New York: John Wiley & Sons.

[5] Cabeza, L.F. (2012) Thermal energy storage. In: Sayigh, A. (ed.) Comprehensive Renewable Energy, Vol. 3, pp. 211–253. Oxford: Elsevier

[6] Mehling, H. and Cabeza, L.F. (2008) Heat and Cold Storage with PCM: An Up to Date Introduction into Basics and Applications. Heidelberg, Berlin: Springer.

[7] Zalba, B., Marín, J.M., Cabeza, L.F. and Mehling H. (2003) 'Review on thermal energy storage with phase change: materials, heat transfer analysis and applications', Applied Thermal Engineering, 23, 251–283.

[8] Fernandez, A.I., Martinez, M., Segarra, M., Martorell, I. and Cabeza, L.F. (2010) 'Selection of materials with potential in sensible thermal energy storage', Solar Energy Materials and Solar Cells, 94, 1723–1729

[9] Kato, Y. (2007) Chemical energy conversion technologies for efficient energy use. In: Paksoy, H.O. (ed.) NATO Sciences Series, II. Mathematics, Physics and Chemistry, Vol. 234: Thermal Energy Storage for Sustainable Energy Consumption: Fundamentals, Case Studies and Design, pp. 377–391. Dordrecht: Springer.

[10] Michel, B., Mazet, N., Mauran, S., Stitou, D. and Xu, J. (2012) 'Thermochemical process for seasonal storage of solar energy: characterization and modeling of a high density reactive bed', Energy, 47, pp. 553–563.

[11] Tatsidjodoung, P., Le Pierrès, N. and Luo, L. (2013) 'A review of potential materials for thermal energy storage in building applications', Renewable and Sustainable Energy Reviews, 18, 327–349.

[12] N'Tsoukpoe, K.E., Liu, H., Le Pierrès, N. and Luo, L. (2009) 'A review on long-term sorption solar energy storage', Renewable and Sustainable Energy Reviews, 13, pp. 2385–2396.

[13] Hauer, A. (2007) Sorption theory for thermal energy storage. In: Paksoy. H.O. (ed.) NATO Sciences Series, II. Mathematics, Physics and Chemistry, Vol. 234: Thermal Energy Storage for Sustainable Energy Consumption: Fundamentals, Case Studies and Design, pp. 393–408. Dordrecht: Springer.

[14] Gil, et al., State of the art on high temperature thermal energy storage for power generation. Part 1—Concepts: materials and modellization, Renew. Sustain. Energy Rev. 14 (1) (2010) 31–55.

[15] S.M. Hasnain, Review on sustainable thermal energy storage technologies, Part I: heat storage materials and techniques, Energy Convers. Manage. 39 (11) (1998) 1127–1138.

[16] W. Hering, R. Stieglitz, T. Wetzel, Application of liquid metals for solar energy systems, EPJ Web of Conferences, EDP Sciences, 2012.

[17] Y. Cengel, Introduction to Thermodynamics and Heat Transfer+ EES Software, McGraw Hill Higher Education Press, New York, 2007.

[18] Robinson, Adam, Ultra-high temperature thermal energy storage. Part 1: concepts, Journal of Energy Storage, volume 18, pp. 333-339, 2018.

[19] https://www.technologyreview.com/s/525121/molten-salts-might-provide-half-price-grid-energy-storage/

[20] R. Shah, D. Sekulic, Heat exchangers, Handbook of Heat Transfer, (1998) , pp. 3.

[21] L.A. Catalano, et al., A high-efficiency heat exchanger for closed cycle and heat recovery gas turbines, ASME Turbo Expo 2010: Power for Land, Sea, and Air, American Society of Mechanical Engineers, 2010.

[22] H. Frutschi, Closed-Cycle Gas Turbines. Operating Experience and Future Potential, ASME Press, New York, 2005.

[23] Edward Morofsky, history of thermal energy storage, DOI: 10.1007/978-1-4020-5290-3_1, January 2007

[24] Luisa_F_Cabeza, Advances_in_thermal_energy_storag, 2015, ISBN: 978-1-78242-088-0

[25] https://en.wikipedia.org/wiki/Cryogenic_energy_storage

[26] https://www.engineering.com/ElectronicsDesign/ElectronicsDesignArticles/ArticleID/5780/Cryogenic-Energy-Storage.aspx

[27] Telkes M. Thermal energy storage in salt hydrates. Sol Energy Mat 1980;2:381–93.

[28] Pinel P, Cruickshank CA, Beausoleil-Morrison I, Wills A. A review of available methods for seasonal storage of solar thermal energy in residential applications. Renew Sust Energy Rev 2011;15:3341–59.

[29] Guillot S, Faik A, Rakhmatullin A, Lambert J, Veron E, et al. Corrosion effects between molten salts and thermal storage material for concentrated solar power plants. Appl Energy 2012;94:174–81.

[30] Liu M, Saman W, Bruno F. Review on storage materials and thermal performance enhancement techniques for high temperature phase change thermal storage systems. Renew Sust Energy Rev 2012;16:2118–32.

[31]   Dinter F, Gonzalez DM. Operability, reliability and economic benefits of CSP with thermal energy storage: first year of operation of ANDASOL 3. Energy Proc 2014;49:2472–81.

Study on Controllable Turbocharging System of Diesel Engine

Shanlin Chen[1]

[1]Faculty of Energy and Environmental Engineering, Silesian University of Technology,E-mail: chen.shanlin@hotmail.com

Abstract

Controllable Pulse Turbocharging System can optimize the whole performance of the diesel engine at a low-speed or a high-speed condition, through switching the turbocharging system with a controlled valve. In this paper, the research object is D6114 diesel engine, the model is simulated by GT-POWER and validated with the data from experiments. This research aims to obtain the changing traits of the pressure waves of different turbocharging system and different operating speeds, compare the two different turbocharging systems, evaluate the performance of the diesel engine with controllable pulse turbocharging system, and find the appropriatecondition to open the controlled valve to improve the performance and efficiency.

Keywords: Controllable Pulse Turbocharging, pressure waves, diesel engine.

1. Introduction

Turbocharging system can obviously improve the overall performance of diesel engine. At present, there are two different turbocharging system of diesel engine[1], the first one is constant pressure turbocharging system, which has a smaller pumping loss, high turbine efficiency, and can achieve a better performance at a high-speed condition; the second one is pulse turbocharging system, which has a high air intake pressure, can make full use of the energy of the exhausted gases and has a superior performance at a low-speed condition. However, a fixed turbocharging system can hardly take into account the performance of power, economy and emissions requirements of high and low speed conditions at same time, there are some limitations and deficiencies in practice.

As a new type of turbocharging system, controllable pulse turbocharging system can combine the advantages of both constant pressure turbocharging system and pulse turbocharging system by switching the turbocharging systems with a controlled valve or some other mechanical structures, so it can make the engine operate well at both high and low speed conditions, but it is different from MPC[2] and MIXPC[3], when the engine is at a low-speed or in a speed-up process, close the controlled valve to make the turbocharging system as pulse turbocharging, so it can make full use of the pulse energy of the exhaust gas and decrease the fuel consumption as well as emission levels; when the engine is at a high-speed condition, open the controlled valve to make the turbocharging system as semi-constant pressure turbocharging, so it can lower the exhaust back pressure, reduce the pumping lossand improve the efficiency and performance of the engine[4-7].

In this paper, the research object is D6114 diesel engine, the model is simulated by GT-POWER and validated with the data from experiments. This research aims to obtain the changing traits of the pressure waves of different turbocharging system and different operating speeds, compare the two different turbocharging systems, evaluate the performance of the diesel engine with controllable pulse turbocharging system, and find the appropriate condition to open the controlled valve to improve the performance and efficiency.

2. Construction and validation of simulation model

In practice, the six-cylinder diesel engine generally adopts a three-pulse turbocharging system, and it has a good performance when the speed is slow,however, in high-speed working conditions, the pumping loss is large and the performance is deteriorated. If the controllable pulse turbocharging system is adopted, the controllable valve willbe opened to connect the exhaust pipes, thereby reducing the exhaust back pressure, reducing the fuel consumption, and improving the engine's performance. This chapter is mainly about the research and analysis of the pressure wave characteristics of the exhaust gaswhen the engine is under a steady-state with controllable pulse turbocharging system.

2.1. Construction of simulation model

The main parameters of the engine used in the calculation are shown in Tab..2.1. In order to realize the controllable pulse turbocharging system, a controlled valve is installed in the middle of the two exhaust pipes. When the controlled valve is closed, the engine's turbocharging system is pulse turbocharging; when the controllable valve is open, the engine's turbocharging system is semi-constant turbocharging, while there are certain differences between the semi-constant pressure turbocharging and the constant pressure turbocharging system. The diesel engine was simulated by GT-POWER software. The simulation model is shown in Fig.2.1. The schematic diagram of the exhaust pipe system and the controlled valve is shown in Fig.2.2.

Tab. 2.1. Parameters of the engine

Type	6 cylinders, turbocharging, intercooling
Cylinder diameter $\times$ stroke	114mm $\times$ 135mm
Swept volume	8.26 L
Compression ratio	17.7:1
Rated power	184kW(2200 rpm/min)
Maximum torque speed	1400 rpm/min
Firing order	1-5-3-6-2-4
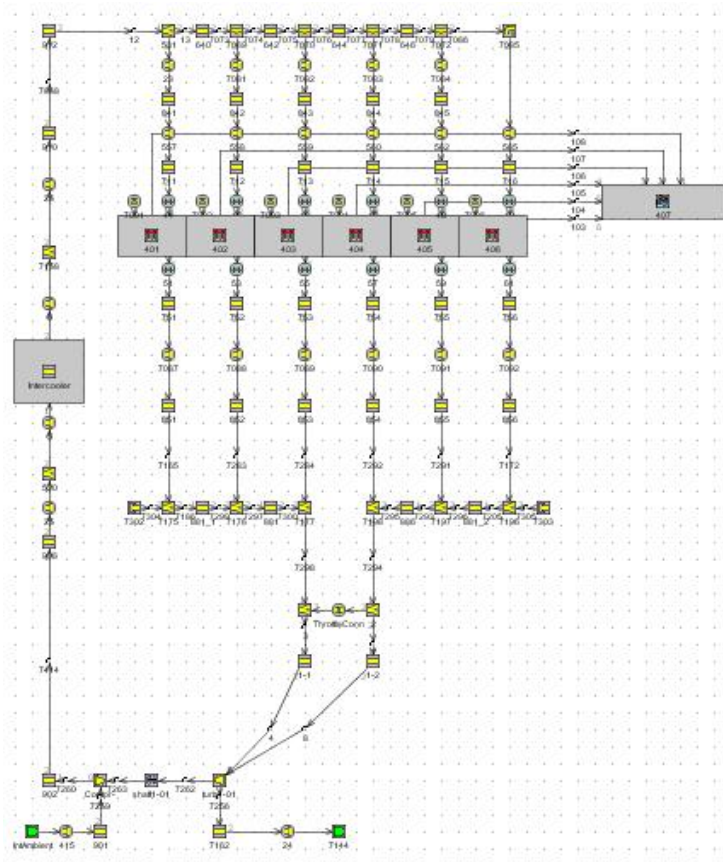
Fig. 2.1. Simulation model of controllable turbocharging system
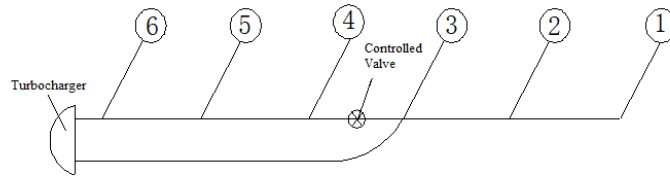
Fig.2.2. Schematic diagram of the exhaust pipe system and controlled valve

2.2. Validation of simulation model

The simulation model of diesel enginewasvalidated by the experiment data of the original turbocharging system, which is pulse turbocharging. The comparison results between the experiment and the simulation dataare shown in Fig.2.3 and Fig.2.4.
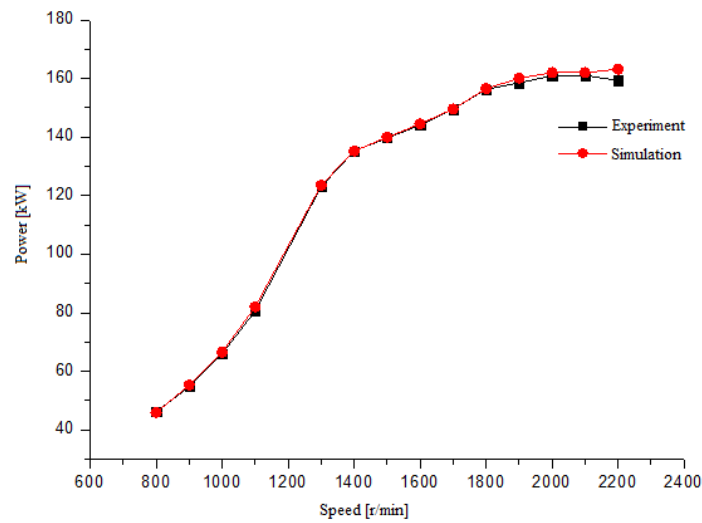
Fig.2.3. Comparison of power between experiment and simulation
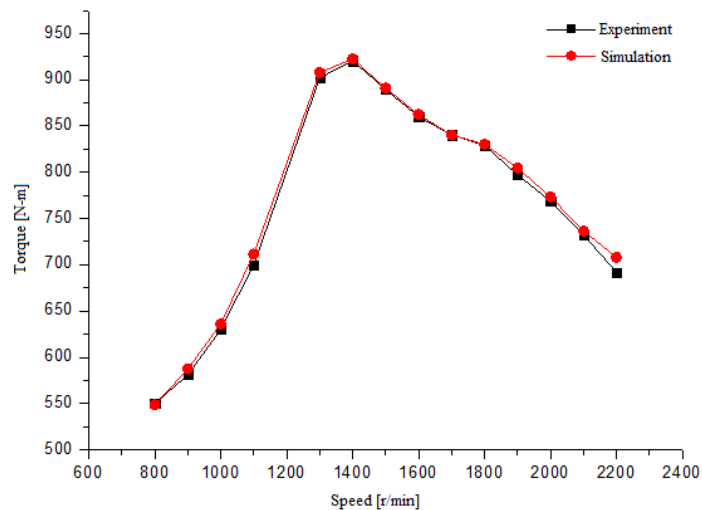
Fig.2.4. Comparison of torque between experiment and simulation

The comparison results demonstrate the experiment power values of the original engine and the power values fromsimulation modelagree well, and the maximum differenceis 2.35% when the speed is 2200 rpm. The experiment torque values of the original engine and the torque values calculated by the simulation model are

very close, and the maximum difference is 2.32%. Therefore, the errors of power and torque on the originalengine and the simulation model areless than 3%; although the effective fuel consumption rate is larger in low speed conditions, the error is below 5% in high speed conditions, so the established GT Power simulation model is in good agreement with the real diesel engine.

3.   Comparison and analysis ofpressure waves with two different turbocharging systems

3.1. Analysis of pulse turbocharging system

In the simulated calculation, low speed 800RPM, high speed 2200RPM and the maximum torque speed 1400RPM were selected as three main study conditions. The main studiedcharacteristicsof pressure waves are the pressure changes in exhaust gas pipe,before the turbine and after the compressor. Taking the first cylinder exhaust gas branch pipe as the research object, the exhaust pressure waves at different speeds is shown in Fig.3.1.
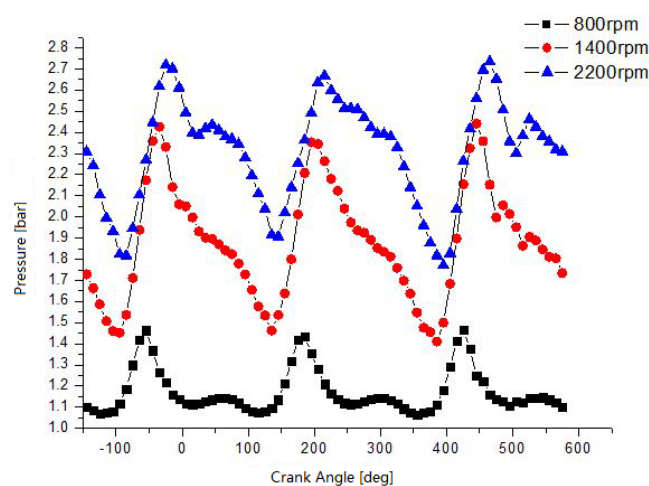
Fig.3.1.The exhaust pressure wave of pulse turbocharging system

By using pulse-turbocharged mode, the first, second and third cylinders share one exhaust branch pipe, since the exhaust interference between cylinders is relatively small with three-pulse turbocharged system, the exhaust process in cylinders will not proceed at the same time, thus, in one working cycle there are three peaks in one cylinder exhaust process, one of which is due to the cylinder's own the exhaust process, and the other two are formed by the pressure waves generated by the exhaust processes of the other two cylinders.

According to the Fig.3.1, the exhaust pressure will increase as the engine speed increases. This is because when the engine speed is rising, engine's power will also increase and gradually reach the rated power, and the engine needs to increase the output work of the cylinder, theamount of fuel injection and intake air will increase accordingly, resulting in an increase in engine exhaust pressure. In addition, as the engine speed increases, the exhaust pressure rises, the crank angle of the largest peak will be delayed accordingly, because the pressure wave in the exhaust pipe is transmitted at the speed of sound, and the length of the exhaust pipe is constant, and the pressure wave propagation time is constant, but the engine speed increases, and the crank angle calculated in the same time will correspondingly increase. When the maximum speed is reached, the cylinder discharge pressure will appear a second small amplitude fluctuation after a peak wave occurs, which is caused by forced exhaust, and this situation doesn't occur at low speed, with the speed raise, the influence of force exhaust on exhaust pressure waves are becoming more and more obvious. As the speed increases, the peak value of the pressure wave increases more than thetrough value in the cylinder, which means that the fluctuation intensity of the exhaust pressure wave is increasing.

The exhaust branch pipe is shared by the first, second and third cylinders,the pressure before the turbine will be slightly smaller than the pressure out of the cylinder due to the influence of the internal resistance of the exhaust pipe,and the heat transferbetween the atmosphere and the pipe wall. The characteristics of pressure wave before turbine are similar with the exhaust pressure wave. As the speed increases, the pressure before the turbine will also increase, the volatility of the pressure becomes stronger and the energy of the exhaust pulse is also increased,

so that the available energy of the exhaust gas also increases, as a result, the turbocharger can increase the intake air pressure, thereby increase the intake air amount, and ensurethe engine works effectively.
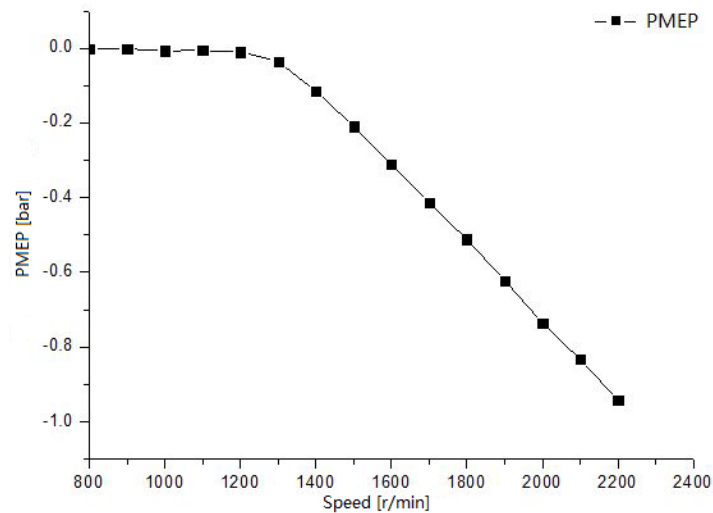
Fig.3.2.The PMEP curve with pulse turbocharging system

When the controlled valve is closed, thepumpingmean effective pressure (PMEP) corresponding to the external characteristic speed of the diesel engine is shown in Fig.3.2. The PMEP values actually reflect the pumping loss. The smaller the PMEP value is, the greater the pumping loss. It can be seen from the Fig. that the PMEP value is large when engine is at low-speed working condition with the pulse turbocharging system. As the diesel engine's speed increases, the PMEP value gradually decreases, and the pumping loss is also becoming more and more serious.

3.2. Analysis of semi-constant pressure turbocharging system

In the simulated calculation, the same conditions were selected aslow speed 800RPM, high speed 2200RPM and maximum torque speed 1400RPM. The main studied pressure wave characteristics are the exhaust pressure wave, the pressure wave before turbine and after compressor. Taking the first cylinder exhaust branch pipe as the research object, the exhaust pressure waves at different speeds with semi-constant turbocharging system are shown in Fig.3.3.

According to theFig., there are 6 peaks on the exhaust pressure curves with semi-constant turbocharging system, because the controlled valve is open. With two branch pipes are connected to each other, so that the exhaust pressure waves of the cylinders can be transmitted to each other in the exhaust branch pipe, one of the six peaks is generated by the cylinder's own exhaust process, and the other five are generated by the other cylinders exhaust pressure transmission. Compared with the general constant pressure turbochargingsystem, the exhaust pressure of semi-constant turbocharging system has a higher fluctuation range, but it is much lower than the pulse turbocharging system, which illustrated thatthe engine's turbocharging system can be switched by the controlled valve.

The exhaust pressure of the cylinder increases when the rotational speed goes up, and the fluctuation amplitude of the exhaust pressure wave also increases with speed, but the variation of the exhaust pressure is small, and the overall pressure tends to be sTab.. The peak value of the pressure wave caused by the forced exhaust of each cylinder of the semi-constant pressure turbocharging system is not much different from the peak value of the pressure wave caused by free exhaust, so the pulse energy of the exhaust is small.
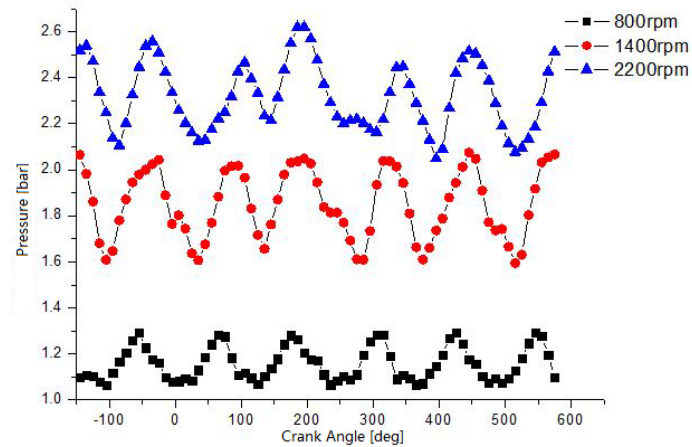
Fig.3.3.The pressure wave of semi-constant pressure turbocharging system

The pressure wavebefore the turbine pressure of the semi-constant pressure turbocharging system is basically the same as the pressure changesafter the cylinder, apart from some differences, because there are some heat loss and resistance in the exhaust branch pipe, so the pressure value before the turbine will decrease, and the fluctuation amplitude of the pressure wave and the available pulse energy will also decrease accordingly.
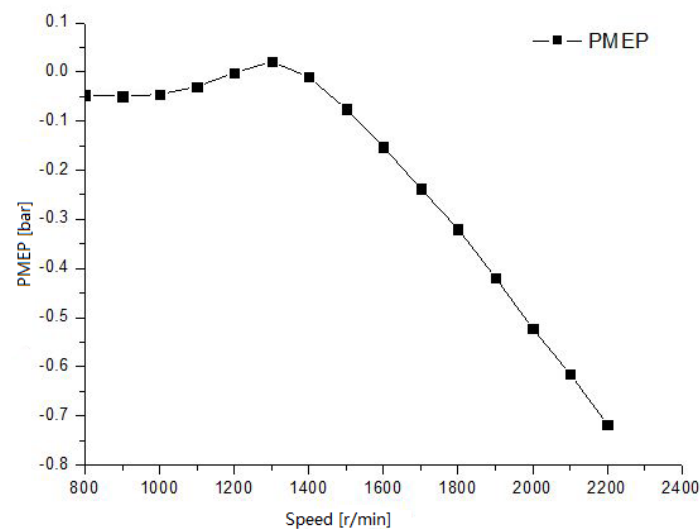
Fig.3.4.The PMEP curve with semi-constant pressure turbocharging system

Semi-constant pressure turbocharging system has a lot in common with constantpressure turbocharging system. Therefore, the turbocharging performance is poor at low speed condition, the utilization of exhaust energy is relatively low, and the low-speed torque characteristics and acceleration performance are not good. However, at high rotational speeds, the utilization of exhaust energy is high, and the intake air pressure is also relatively large. The PMEP curve of the semi-constant turbocharging system with speedis shown in Fig.3.4. As the speed increases, the PMEP value increases first and then decreases, indicating the pumping loss of semi-constant pressure turbochargingdecreases first and then increases. The maximum PMEP value appears at the speed of 1300 rpm, the pumping loss is the smallest. The pumping loss is smaller at low speed compared to high speed conditions, but the working speed of the engine is at medium and high speed, so it is necessary to make the pump loss at the working speed of the engine as small as possible, but this is not the only evaluation parameter. To optimize the overall performance of the diesel engine, the influence of other parameters should also be considered.

3.3. Comparison of pulse and semi-constant pressure turbocharging system

Pulse turbocharging and semi-constant pressure turbocharging systems have their own advantages. The semi-constant pressure turbocharging system is obtained after the controlled valve is opened on the basis of pulse turbocharging system. The connection of the branch pipes causes some changes in the performance of the engine. The changes in the intake and exhaust system are mainly reflected in the cylinder exhaust pressure, the pressure before turbine and the intake pressure after the compressor. Semi-constant pressure turbocharging and pulse turbocharging systemhave different performances at different speeds. In order to evaluate the advantages of pulse turbocharging and semi-constant pressure turbocharging under different operating conditions, comparing and analyzing the performance under the same working conditions with different turbocharging systems are required, the main contents of comparison and analysis are exhaust pressure, pressure before turbine and intake pressure. By analyzing the above parameters, the adaptability of semi-constant pressure turbocharging and pulse turbocharging system under different working conditions can be determined.

Fig.3.5.Comparison of exhaust pressure with different turbocharging system at speed of 800 rpm

Comparison of exhaust pressurewith pulse turbocharging and semi-constant pressure turbochargingsystem at 800 rpm, 1400 rpm and 2200 rpm are shown in Fig.3.5, Fig.3.6 and Fig3.7. The exhaust pressure increases with the increase of the rotational speed. Compared with the pulse turbocharging, the pressure of the semi-constant pressure turbocharging is smaller and more sTab.. When using pulse turbocharging, the peak values and the trough values of the exhaust pressure increase with the increase of the rotational speed, but the increased degree of the peak is much larger than the trough value. Therefore, as the rotational speed increases, the intensity of the pulsed exhaust pressure wave increases. Thepressure fluctuation intensity of semi-constant pressure turbocharging system is smaller than the pulse turbocharging system. Therefore, the exhaust pulse energy of the semi-constant pressure turbocharging system is smaller than the exhaust energy of the pulse turbocharging system.

The difference between pulse turbocharging and semi-constant pressure turbocharging is that the volume of the exhaust pipe and the pressure before turbine are different. The pressure at the turbine inlet does not change much due to the stabilizing effect of the exhaust pipe with semi-constant turbocharging system. As forpulse turbocharging, periodicpressure fluctuations arisebefore the turbine due to the periodic pulse in the exhaust pipe.
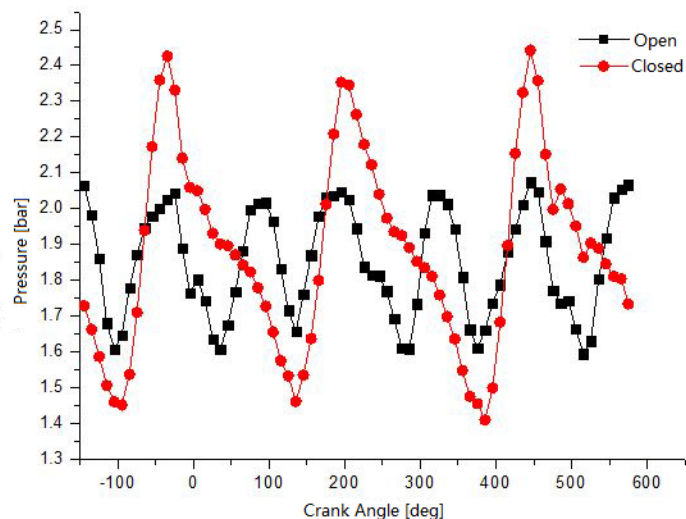
Fig.3.5.Comparison of exhaust pressure with different turbocharging system at speed of 1400 rpm
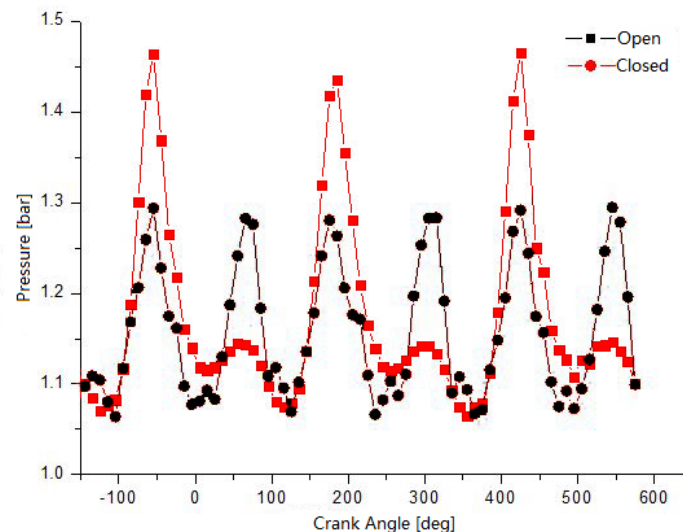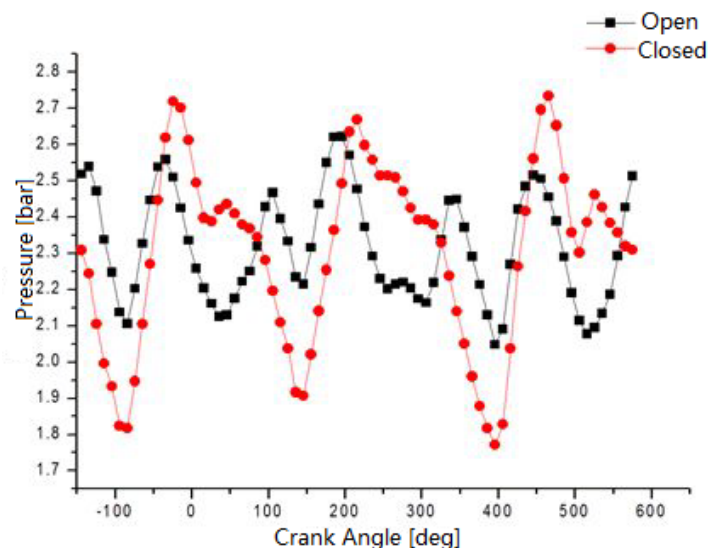

Fig.3.6.Comparison of exhaust pressure with different turbocharging system at speed of 1400 rpm
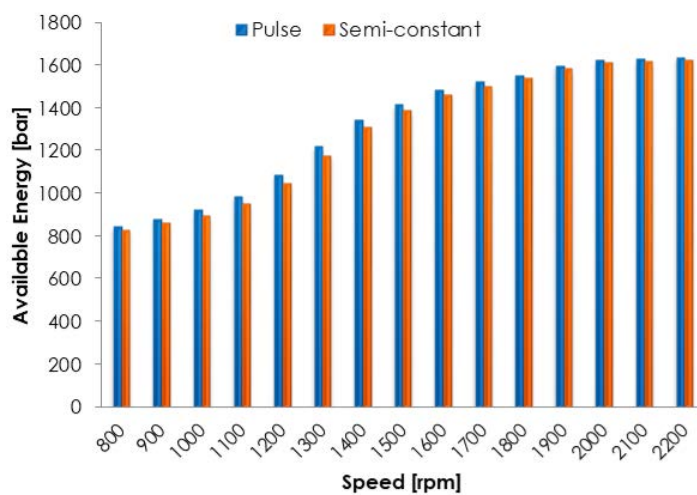
Fig.3.7.Available energy before turbine with different turbocharging system

As the engine speed increases, the pressure before turbine will gradually increase. Compared with pulse turbocharging, the pressure wave before turbine of the semi-constant pressure turbochargingsystem is more regular, and the variation is not high. It can be explained that pulse turbocharging can provide more pulse energy, and semi-constant pressure turbocharging can ensure stabilities. In order to analyze the pressure before turbine under the two turbocharging systems, it is necessary to calculate the available energy before the turbine under different working conditions, and results are shown in Fig.3.7.Although the pressure waves before turbine of pulse turbocharging and semi-constant pressure turbochargingsystems are very different, the available energybefore turbine is not much different.

4. Performance study of controllable pulse turbocharging system

During the actual operation of the engine, the controllable pulse turbocharging system can use the controlled valve to realize the conversion of the turbocharging mode, so that the engine can adopt the appropriate turbocharging system under different working conditions to optimize the performance. When the engine is in a low speed condition or an accelerated loading condition, the total volume of the exhaust pipe corresponding to a single cylinder is relatively small by closing the controlled valve, thereby the turbocharging mode is pulse turbocharging, so it can fully utilize the exhaust pulse energy; when the engine is in high-speed working condition, the total volume of the exhaust pipe is relatively enlarged by opening the controlled valve, so that the turbocharging mode is converted into semi-constant pressure turbocharging, it can reduce the exhaust back pressure andpumping loss,improve the turbine efficiency.

The three operating conditions of high speed, low speed and maximum torque speed are selected as the studied cases. When calculating and analyzing the controllable pulse turbocharging system, the fuel injection amount is the same before and after the opening the controlled valve in each case. The calculation results of each case are shown in Tab. 3-1. When the rotation speed is 2200 rpm, the fuel consumption becomes smaller after the valve is opened, and the power and torque values become larger. The fuel consumption is reduced because the PMEP is larger after the valve is opened, which means that the piston has to overcome a smaller work to push the exhaust gas out. After the valve is opened, the pumping loss is reduced, the pressure after the compressor becomes larger, and the engine's air intake amount is increased, so that the power and torque of the engine are correspondingly increased. The excess air ratios in the cylinder after the valve is closed and opened are 1.976 and 1.986, respectively, so the fuel mixture can be fully burned in the cylinder, so the indicate mean effective pressure(IMEP) values under these two turbocharging systems are similar. Therefore, in the high-speed working condition, the fuel consumption is small after the valve is opened, and the power and torque are higher.

Tab. 3.1. Calculation results of controllable pulse turbocharging system

	2200 rpm		1400 rpm		800 rpm	
	Closed	Open	Closed	Open	Closed	Open
Fuel consumption [g/kW-h]	240.748	235.819	209.395	208.434	243.589	246.558
Power [kW]	162.843	166.246	135.39	136.014	46.4061	45.8473
Torque [N-m]	706.833	721.605	923.486	927.743	553.932	547.262
IMEP [bar]	12.5441	12.7738	15.5455	15.6049	9.49556	9.38781
PMEP [bar]	-0.94218	-0.71695	-0.11525	-0.0106	-0.00117	-0.04685
Pressure after compressor [bar]	2.17515	2.19927	2.07869	2.06053	1.18953	1.16405
Air-fuel ratio	28.2581	28.4019	25.1662	24.7214	21.0848	20.5411
Excess air ratio	1.976	1.986	1.76	1.73	1.474	1.436

When the speed is 800 rpm, the controlled valve is closed, the fuel consumption is small, and the power and torque are larger. Although the PMEP value becomes larger after the valve is closed, the IMEP becomes larger, resulting in a reduction in fuel consumption. In low-speed conditions, the valve is closed and the turbocharging system is pulse turbocharging, which can make full use of the pulse energy, so that the engine intake pressure and intake air flow are both larger, and the power and torque values will be correspondingly larger. The excess air coefficients in the cylinder after the valve is closed and opened are 1.474 and 1.436, respectively. At this time, the larger the excess air coefficient in the cylinder, the more compete the combustion of the mixture is, and the larger the IMEP in the cylinder is. Therefore, the fuel consumption is smaller when the excess air ratio in the cylinder is larger.When the engine is working at low speed condition, closing the controlled valve will make the fuel consumption smaller, make power and torque greater.

When the speed is 1400 rpm, the performance indicators of the engine are not showing many differences no matter the controlled valve is open or closed; the values of power, torque and fuel consumption are very close. This means that when pulse turbocharging systemandsemi-constant turbocharging systemare used alone, there will be an intermediate speed which makes the performance of the engine similar no matter which turbocharging system is used, and the pulse turbocharging system is better when the rotational speed is lower than the intermediate rotational speed; meanwhile, when the rotational speed is greater than the intermediate rotational speed, semi-constant pressure turbocharging is superior. Therefore, in this study, 1400 rpm can be the speed for switching the turbocharging systems by opening or closing the controlled valve.

5.   Conclusions

For the D6114 diesel engine, a platformwith the controllable pulse turbocharging system was built, and the simulation model was established and verified by experiment data. Through simulation calculations and experimental studies, the following conclusions are obtained:

1) The exhaust pressures of the pulse turbocharging system and the semi-constant pressure turbocharging system increase with the increase of the rotational speed; the fluctuation of the exhaust pressure wave is enhanced with the increase of the rotational speed; the fluctuation intensity of the semi-constant pressureturbocharging system is less than the pulse turbocharging system's, the pulse turbocharging can provide more pulse energy, and the semi-constant pressure turbocharging can ensure the stability.

2) As the rotational speed increases, the exhaust pressures before the turbine of the pulse turbocharging system and the semi-constant pressure turbocharging system increase, and the available energy for the turbine increases. At low speeds, the pulse energy utilizationof the pulse turbocharging system is high; at high speeds, the semi-constant pressure system has higher turbine efficiency and higher overall energy utilization.

3) At high speeds, after the controlled valve is open, fuel consumption is reduced, power and torque are greatly increased; at low speeds, when the controlled valve is closed, fuel consumption is reduced, power and torque are increased; there is no big influence on the engine's performance when the controlled valve is openor closed at the speed of 1400 rpm. Therefore,it can be used as a control boundary for switching the turbocharging system.

Acknowledgment

References

[1] Heywood J B, Internal combustion engine fundamentals, New York, McGraw-Hill Science Engineering, 1988

[2] Yang SY, Deng KY, Cui Y, Simulation and experimental research on a mixed pulseconverter turbocharging system, Proceedings of the Institution of Mechanical Engineers,Part D: Journal of Automobile Engineering , 2007, 221, 215–223

[3] Yang SY, Wang LS, Gu HZ, MIXPC turbocharging system for diesel engines, SAE Paper , 2006-01-3390, 2006

[4] Vlaskos I, Codan E, Alexandrakis N, et al, Design and performance of a controllable turbocharging system on marine diesel engines. Proceedings of ICEF06, ASME Internal Combustion Engine Division 2006 Fall Technical Conference,5-8 November, 2006,California,USA.

[5] Papalambrou G, Alexandrakis N, Kyrtatos N, Smokeless transient loading of medium or highspeed engines using a controllable turbocharging system, Proc.CIMAC Cong., Vienna, Austria, May 2007, International Council on Combustion Engines, Paper 22

[6] Codan E,Vlaskos I,Kyrtatos N, Alexandra N, The charging of a medium/high speed 5-cylinderdiesel engine with controllable pulse turbocharging.10th Supercharging Conference,22-23 September 2005,Dresden,Germany

[7] Livanos G, Kanellopoulou E, Kyrtatos N, Marine Diesel engine rapid load acceptance without smoke emissions, 7th International Symposium on Marine Engineering (ISME Tokyo 2005), 24- 28 October 2005, Tokyo, Japan

Potential of Microbial Fuel Cell for Bioelectricity Production using Waste Water: A Review

Talal Ashraf[1], Shaheen Aziz[2]

[1]*AGH University of Science and Technology Krakow, e-mail:talal@student.agh.edu.pl*

[2]*Mehran University of Science and Technology Pakistan, e-mail:Shaheen.shaikh@faculty.muet.edu.pk*

Abstract

Microbial fuel cell is emerging and innovative technology for simultaneous energy production and wastewater treatment. This paper will give an overview about problems related to adopt this technology, comparison with other conventional wastewater treatment processes. Practical implementation and adoption of Microbial fuel cell is challenging for different processes. However, it is more efficient than energy negative aerobic treatment. Various key factors that has effect on process efficiencies are discusses in this review. Challenges facing by this technology are high cost of electrodes, high capital investment, low return rate and low power density. Meanwhile, its positive impacts are environmental friendly with no carbon footprint, no energy intensive and possibility to integrate with other treatment technologies.

Keywords: Wastewater, Microbial Fuel Cell, Bioelectricity, Energy Saving, Aerobic Treatment

1. Introduction

Conventional treatments for waste water such ach activated sludge isn't capable to recover full potential due to energy intensivist and residuals problems. Anaerobic digesters have significant capability but sometimes it doesn't meet the regulatory standards although it can be self-energy sustain process. Waste water treatment requires a self-efficient sustainable technology for both water and energy saving. In fact, water reuse is quite implemented in dry regions with waste water treatment but issues are concerned with water quality criteria for domestic usage. Wastewater is now recommended as a vital resource for water reuse. An emerging technology microbial fuel cell is under consideration due to its multifunctional ability of waste water treatment and clean energy production [1]. Problems caused by disposal of waste water directly from industrial, agricultural and domestic applications, imposes greater environmental problems like algal blooms and eutrophication of fresh water. Technologies currently adopted for waste water treatment requires high energy input and capital costs without revenue generations, Almost 0.5-2 KWh/m^3 energy is consumed for removing nitrogen and carbon from waste water. Which on other hand, emits a large fraction of greenhouse gases and volatile compounds in degrading ecosphere. Furthermore, carbon footprint for these conventional technologies are higher as each KWh of electricity releases 0.9kg of CO and 155 tons of greenhouse gases emitted with every 1000 tons of treating wastewater[11]. Addressing energy and environmental challenges in far remote areas, microbial fuel cell acts as promising technology for bio hydrogen production, direct electricity generation, bio remediation and waste water treatment. Special advantages for adopting microbial fuel cell technology are no energy input, independent of atmospheric constraints even works at low temperature, direct electricity production, less sludge with no gas treatment and can be applicable in remote locations without excessive electrical systems [2-5]. Microbial fuel cell can be extended into Bio electrochemical cells with a combination of biological catalytic redox activity and abiotic electrochemical reactions. As compared to other fuel cell (direct methanol fuel and proton exchange membrane fuel cell), microbial fuel cell can operate at relatively low temperature (14-45C) almost near to atmospheric conditions, appropriate pH conditions (neutral) [6-7]. Indeed, previous researches about microbial fuel cell shows great achievements using milliliters volume reactors. Problem lies within scaling of this technology on commercial level due to non-uniform properties of domestic waste water with low conductivity and biodegradability. Bioactivity could be reduced by low biodegradability and concentration as organic matter degraded and catalyzed by microorganisms at electrodes. This could affect greatly the output which causing hurdles to scale up this technology for municipal waste water treatment [8]. Sustainability of microbial fuel cells can been for waste water treatment through direct conversion to electricity, reduction of activated sludge as compared to conventional treatment technologies and insensitivity towards ambient conditions. Energy can be saved and storages a byproduct which makes this process more self-sustain. Challenge lies in the mechanism of

electron transfer and bio scale formation and production of bio anodes at macroscale. This innovative technology for simultaneous waste water treatment and electricity generation show great potential in terms of industrial context at lab scale. Moreover, the effectivity can be increased by merging this technology with other treatment processes creates more opportunities and effectiveness of systems [9]. Energy extracted from domestic and waste water can be classified into chemical and thermal energy. Almost 26% of chemical energy is bounded in the form of Carbon which can be determined by Chemical Oxygen Demand. Major portion lies with thermal energy with potential of 74%. Extraction of chemical energy is quite efficient method but extremely difficult for thermal energy. So, while reducing environmental impacts by extracting this chemical energy, waste water technology can be converted into energy yielding or self-sufficient processes [10].

2. Features and Performance of Microbial Fuel Cellfor Wastewater Treatment

Conventional aerobic treatment generates a lot of activated sludge by municipal and domestic waste water but also contains a large amount organics which can be utilized for electricity generation in microbial fuel cell. Meanwhile, operating cost sludge treatment can reach to more than 50% of waste management investments. As sludge is valuable and this decrement in treatment cost will impact great potential with emerging technologies. Animal Manure is suiTab. due to high organic content and strength and can be collected in large volume from crop faring and livestock. Treating agricultural waste water containing high nitrate and phosphate concentration through microbial fuel cell technology can avoid odor problems and met with environmental regulations. High carbohydrate, starch and protein component of food industry waste water act as a good substrate for microbial fuel cell. Brewery waste water with high COD content act as a suiTab. substrate for microbes which could result in high electricity production. Milk and dairy processing waste water contains a higher number of biodegradable organics which can be utilized as an efficient electrolyte for microbial fuel cell technology. Textile and dyes industrial waste water can also be treated for water discoloration, pollutants removal and electricity production as previous research has been carried out for activated carbon based microbial fuel cell which results in 70-77% of color elimination and 71-76% of COD removal with a power density of $1.7 W/m^2$ [12-15].

Tab. 1 Comparison of Conventional Anaerobic Digestion with Microbial Fuel Cell [16]

	Anaerobic Digester	Microbial Fuel Cell
Systematic configuration	Anaerobic Migration, Upflow sludge blanket reactor and internal circulator reactors	Single and dual Chamber, Cylinder, tube and stack reactors
Bio Catalyst	Food chain type	Axenic/mixed culture
Input	High/low concentration COD biomass	Low strength influents containing glucose etc
Output	1Kg of COD to 1 KWh	1 Kg of COD to 4 KWh
Power Density	400 W/m^3	250 W/m^3
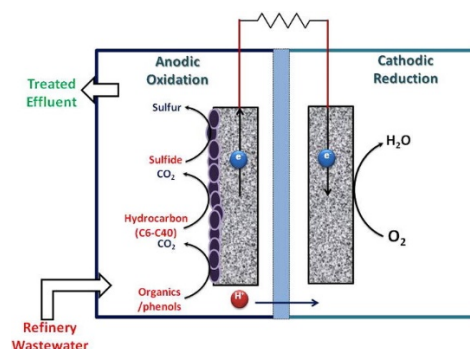
Fig. 1. Refinery Waste Water Treatment using Microbial Fuel Cell (adopted from [31])
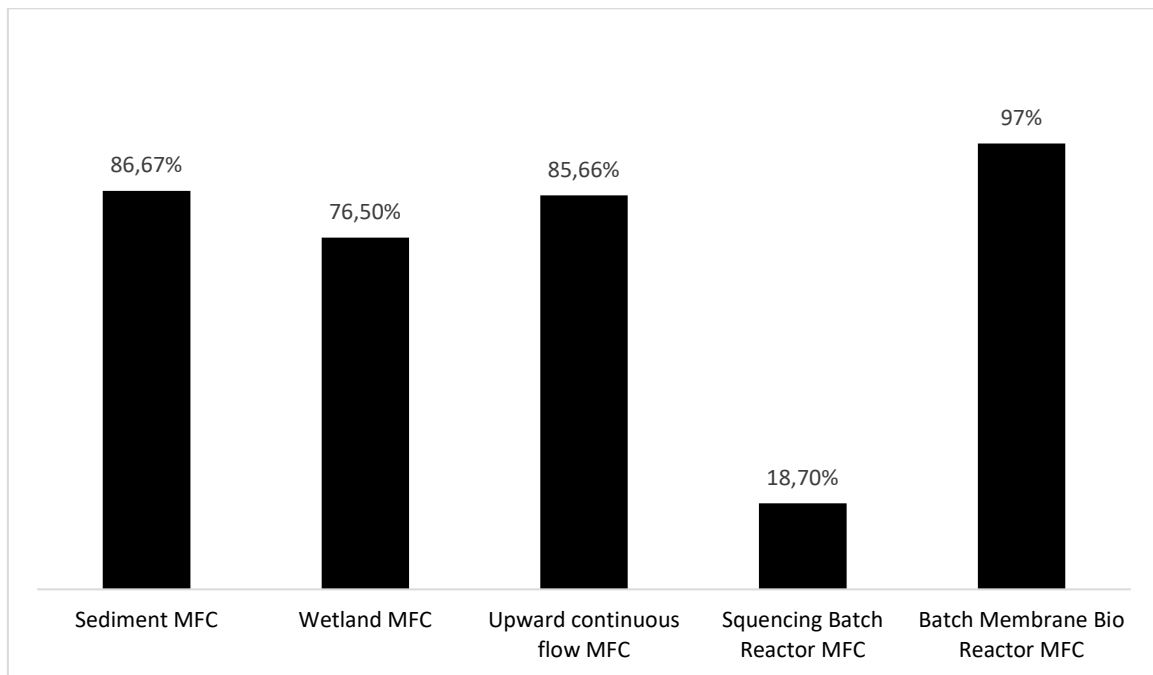
Fig. 2. Microbial Fuel Cells coupled with wastewater treatment [17-19]

3.   Framework for High Power Generation Using Wastewater

To oxidized organic compounds, bacterial colonies have ability to transfer electrons. However, it is more problematic to have mixed cultures that have more possibilities to cause disturbances because resistivity of mixed culture is comparatively higher for substrate consumptions. In some studies, it has been found that pure culture produce more consistency in power output. However, for some waste water treatment, it has been found that mixed culture is suiTab. for wide range of substrate. Almost, every bacterial colony doesn't have any effect because of temperature sustainability of cell. However, Klebsiella pneumonia special kind of bacteria is more suiTab. for electron transfer and hence more applicable for microbial fuel cell. Design of microbial fuel cell technology also impose a significant impact on performance and efficiency of fuel cell. The biological reactions in which redox mediator takes place are always supported by batch reactor. Problematic situation mostly happens in flow reaction due to large species/ colonies of bacteria tends to deposits on electrodes and hence forming biofilms. Affinity and colonial structure of bacteria is also affected by anolyte which has the direct impact on power generation density and coulombs efficiency. Durability and proper electronic transfer and bacterial deposition is effected by the proper use of electrodes. Electrodes should have high conductivity and large surface area and better structure. Other desired properties of electrodes are non-reactive (inert and non-toxic) to microorganisms, long lasting and economically feasible. Efficiency and performance of microbial fuel cell technology can be optimized by selecting different materials for electrodes. Usage of internal separator membrane to separate cathode and electrode have a significant impact on performance as the membrane has its own resistance which could drastically reduce the efficiency of system. To minimize concentration gradient across electrodes, low pH is utilized for proton movement towards cathode. However, methanogens can be suppressed by increasing pH which could significantly increase power generation [21-27].

4.   Expenditure Analysis for Microbial Fuel Cell

Numerous MFC waste water treatment system has shown a significant potential for producing 1000mW/m2. A case study has been done with population of 100,000 producing 16.4 billion liters of wastewater can produce 2.3MW of electricity based on avaergae BOD value (300mg/l). However, if we compare MFC with activated sludge and other treatment technologies, activated sludge doesn't have revenue generation system which anaerobic digestion has greater potential for generating net worth which s comparably very high as compared to other technologies. While MFC can overcome it's 50% of capital cost for its life time. Major cost distribution

for MFC is taken place by electrode material which could affect the economic impact of MFC. When it comes to economical effectiveness for energy positive/neutral system, MFC cannot stand against them at current stages. Using advanced schemes, MFC integration with other technology to produce bioethanol, bioelectricity can show a significant return on investment in 20 years[28-30].

5. Conclusion

Microbial fuel cell is one of the promising technology that generates no sludge, save and produce energy, innovative in wastewater treatment technologies. Some of its unique features have leading edge over other technologies. Problems lies with amount of power generation and , biofouling, high membrane cost and very less return of investment. TO overcome this problem, microbial fuel cell shows vital performance when merged with other technologies. Performance dependence on mixed organism culture results in better power density as compare to pure inoculation. Stability and capital investment impose a great challenge for scaling up of this technology. COD removal efficiency is significantly high that it can achieve 92 % removal. Further research has to be done to make this technology more cost effective by improving design and change of electrodes

Acknowledgment

References

[1] Venkata Mohan, S., Mohanakrishna, G., Chiranjeevi, P., 2011. Sustainable power generationfrom floating macrophytes based ecological microenvironment through embeddedfuel cells along with simultaneous wastewater treatment. Bioresour. Technol.102 (14), 7036–7042.

[2] Venkata Mohan S, Velvizhi G, Annie Modestra J, Srikanth S. Microbial fuel cell:critical factors regulating bio-catalyzed electrochemical process and recent advancements.Renew Sust Energ Rev 2014;40:779–97.

[3] ElMekawy A, Hegab HM, Vanbroekhoven K, Pant D. Techno-productive potentialof photosynthetic microbial fuel cells through different configurations. Renew SustEnerg Rev 2014;39:617–27.

[4] Kumar R, Singh L, Zularisam AW. Exoelectrogens: recent advances in moleculardrivers involved in extracellular electron transfer and strategies used to improve itfor microbial fuel cell applications. Renew Sust Energ Rev 2016;56:1322–36.

[5] Mercuri EGF, Kumata AYJ, Amaral EB, Vitule JRS. Energy by Microbial FuelCells: scientometric global synthesis and challenges. Renew Sust Energ Rev2016;65:832–40.

[6] D. Pant, G. Van Bogaert, L. Diels, K. Vanbroekhoven, Bioresour. Technol. 101(2010) 1533-1543.

[7] P. Pandey, V.N. Shinde, R.L. Deopurkar, S.P. Kale, S.A. Patil, D. Pant, Appl.Energy 168 (2016) 706e723.

[8] Logan, B.E., 2010. Scaling up microbial fuel cells and other bioelectrochemicalsystems. Appl. Microbiol. Biotechnol. 85 (6), 1665e1671.

[9] Kim, J.R., Jung, S.H., Regan, J.M., Logan, B.E., 2007. Electricity generation and microbialcommunity analysis of alcohol powered microbial fuel cells. Bioresour. Technol. 9 (13), 2568–2577.

[10] Gude, V.G., Kokabian, B., Gadhamshetty, V., 2013. Beneficial bioelectrochemicalsystems for energy, water, and biomass production. J. Microb. Biochem. Technol.6, 2.

[11] EIA, 2009. http://www.eia.gov/tools/faqs/faq.cfm?id¼474&t¼11 (accessed online on05.08.15.).

[12] Xiao B, Yang F, Liu J. Enhancing simultaneous electricity production andreduction of sewage sludge in two-chamber MFC by aerobic sludge digestion andsludge pretreatments. J Hazard Mater 2011;189:444–9.

[13] Maekawa T, Liao CM, Feng XD. Nitrogen and phosphorus removal for swinewastewater using intermittent aeration batch reactor followed by ammoniumcrystallization process. Water Res 1995;29:2643–50.

[14] Sharma S, Malaviya P. Bioremediation of tannery wastewater by chromiumresistant novel fungal consortium. Ecol Eng 2016;91:419–25.

[15] Kalathil S, Lee J, Cho MH. Granular activated carbon based microbial fuel cell forL. He et al. *Renewable and Sustainable Energy Reviews 71 (2017) 388–403*401simultaneous decolorization of real dye wastewater and electricity generation.New Biotechnol 2011;29:32–7.

[16] Pham, T.H., Rabaey, K., Aelterman, P., Clauwaert, P., De Schamphelaire, L., Boon, N.,Verstraete,W., 2006. Microbial fuel cells in relation to conventional anaerobic digestiontechnology. Eng. Life Sci. 6 (3), 285–292.

[17] Venkata Mohan, S., Mohanakrishna, G., Chiranjeevi, P., 2011. Sustainable power generationfrom floating macrophytes based ecological microenvironment through embeddedfuel cells along with simultaneous wastewater treatment. Bioresour. Technol.102 (14), 7036–7042.

[18] Zhao, Y., Collum, S., Phelan, M., Goodbody, T., Doherty, L., Hu, Y., 2013. Preliminary investigationof constructed wetland incorporating microbial fuel cell: batch and continuousflow trials. Chem. Eng. J. 229, 364–370.

[19] Fang, Z., Song, H.-l., Cang, N., Li, X.-N., 2015. Electricity production fromazo dye wastewaterusing a microbial fuel cell coupled constructed wetland operating under differentoperating conditions. Biosens. Bioelectron. 68, 135–141.

[20] Deng Q, Li X, Zuo J, Ling A, Logan BE. Power generation using an activatedcarbon fiber felt cathode in an upflow microbial fuel cell. J Power Sources2010;195:1130–5.

[21] P. Choudhury et al. *Renewable and Sustainable Energy Reviews 79 (2017) 372–389*

[22] Zhang F, Cheng S, Pant D, Van Bogaert G, Logan BE. Power generation using anactivated carbon and metal mesh cathode in a microbial fuel cell. ElectrochemCommun 2009;11:2177–9.

[23] Lu M, Li SFY. Cathode reactions and applications in microbial fuel cells: a review.Crit Rev Environ Sci Technol 2012;42:2504–25.

[24] Gil G-C, Chang I-S, Kim BH, Kim M, Jang J-K, Park HS, et al. Operationalparameters affecting the performance of a mediator-less microbial fuel cell.Biosens Bioelectron 2003;18:327–34.

[25] Rozendal RA, Hamelers HV, Buisman CJ. Effects of membrane cation transport onpH and microbial fuel cell performance. Environ Sci Technol 2006;40:5206–11.

[26] Zhang X, Cheng S, Huang X, Logan BE. The use of nylon and glass fiber filterseparators with different pore sizes in air-cathode single-chamber microbial fuelcells. Energy Environ Sci 2010;3:659–64.

[27] Min B, Román ÓB, Angelidaki I. Importance of temperature and anodic mediumcomposition on microbial fuel cell (MFC) performance. Biotechnol Lett2008;30:1213–8.

[28] Logan, B.E., 2005. Simultaneous wastewater treatment and biological electricitygeneration. Water Sci. Technol. 52 (1), 31-37.

[29] Rozendal, R.A., Hamelers, H.V., Rabaey, K., Keller, J., Buisman, C.J., 2008. Towardspractical implementation of bioelectrochemical wastewater treatment. TrendsBiotechnol. 26 (8), 450e459.

[30] Pham, T.H., Rabaey, K., Aelterman, P., Clauwaert, P., De Schamphelaire, L., Boon, N.,Verstraete, W., 2006. Microbial fuel cells in relation to conventional anaerobicdigestion technology. Eng. Life Sci. 6 (3), 285e292.

[31] SandipamSrikanthManojKumarDheerSinghM.P.SinghB.P.Das, Electro-biocatalytic treatment of petroleum refinery wastewater using microbial fuel cell (MFC) in continuous mode operation. https://doi.org/10.1016/j.biortech.2016.09.034

A numerical analysis of current–voltage characteristics of a Solid Oxide Fuel Cell

Piotr F. Raczkowski

Energy and Fuels, AGH University of Science and Technology, p.f.raczkowski94@gmail.com

Abstract

The article presents numerical analysis of current-voltage characteristics of a single Solid Oxide Fuel Cell depended on microstructure's features of electrodes. The issue of SOFC and the role of its microstructure wasintroduced.A description of mathematical model and its main assumption were included. Presented model was validated using an experimental data for ensuring its correct performance. Subsequently the results were presented and discussed. Taking into consideration that SOFC performance strongly depends on its microstructure, obtained results can be a precious information when considering an optimal SOFC working conditions.

Keywords: Solid Oxide Fuel Cell, Mathematical modeling, Microstructure

1. Introduction

Solid Oxide Fuel Cells are expected to play an important role in ongoing energy utilization, their work parameters enables to cooperate either with a renewables or conventional power stations supplied with carbon (IGFC). Although as each emerging technology requires to fulfil energy industry expectation. Therefore this paper covers the topic of enhancing SOFC performance by manipulation of its microstructure parameters. This research

is based on"Parametric study approach"- is a method used in mathematical modeling that helps us artificially examine the relationship between input and output data. More precisely, in the mathematical model of a given phenomenon, we check how the change of only one input parameter will affect the output results. Thanks to this method, we are able to identify in which direction and to what extent particular parameters affect our model, so we can more effectively determine which parameters have a significant impact on the given phenomenon to check it experimentally, rationalizing the costs of our project.One can hardly find suchstudies. Similar researches were presented in [1].

2. SOFC and its microstructure

High temperature solid oxide fuel cells are one of the most efficient devices directly converting chemical energy into electricity, they work in the high temperature ranges, around 600-1000 ℃. Due to the operating temperature, it is possible to use internal reforming and use of various fuels (hydrogen, carbon monoxide, methane and other hydrocarbons) to supply the cell. There is no need to use expensive catalysts, while maintaining sufficiently high rates of electrode reactions, what is a huge advantage. The idea of this type of links was proposed by Nerst at the end of the 19th century. [2]

2.1. The characteristics of SOFC electrodes microstructure

The main characteristic of SOFC is a solid electrolyte, composed ofY_2O_3 stabilized ZrO_2 called (YSZ), which at a temperature range of 600-1000 ℃ is an ion conductor (here: O^{2-}) and is impenetrable for electrons. The characteristics that this material should have in order to be a good electrolyte are: a high density for preventing the penetration of gases between the electrodes and high stability in oxidation and reduction environment. It is also important that the material has a strong chemical durability in the high oxygen partial pressure and good mechanical properties allowing it to work within the range of 600-1000 ℃. [3]

The anode material is responsible for fuel oxidation which reacts withoxygen ions flowing from the cathode through electrolyte. Features that this material should perform are; high conductivity for ions and ions, chemical stability in reducing atmosphere and catalytic activity for hydrogen oxidation reaction. A well-functioning anode provides a constant supply of reactants to catalytically active sites (TPB) while efficiently draining the products of this reaction (eg water vapor). The most popular anodic material used for SOFC is a nickel-zirconium cermet

(Ni + YSZ) with a porous structure allowing gas to flow. The role of the ion conductor is played by YSZ, and the electron conductor is nickel. [3]

In the Cathode material an electrochemical oxygen reduction is performed. Oxygen ions O^{2-} formed during the reduction are incorporated into the electrolyte via oxygen vacancies. The challenges the cathode fulfill are catalytic activity for oxygen reduction, high ionic and electronic conductivity, physical and chemical stability, and compatibility with other components. Materials that meets these criteria are generally complex oxides with a perovskite structure of the formula $LaMO_3$. Symbol "M" in this case is an atom or mixture of transition metal atoms such as Cu, Ni, Fe, Co, Mn. To increase the ionic and electron conductivity, these metals are partially replaced with lanthanum ions with acceptor additions such as Sr and Ca. One of the most commonly used cathode materials are LSM (Lanthanum strontium manganite): $La_{1-x}Sr_xMnO_{3-\delta}$ or LSCF (Lanthanum strontium cobalt ferrite): $La_{0.8}Sr_{0.2}Co_{0.8}Fe_{0.2}O_3$. [3]

All of these materials should be chemically and physically compatible with each other. Working at such a high temperature is associated with the occurrence of high mechanical stresses in the materials and their connections. It is important to adjust the coefficients of thermal expansion, due to the fact that a high tightness is required from the cell in order to prevent the penetration of gases between the materials. In addition, these materials cannot create intermediate phases that interfere the cell's operation.[3]

2.2. Solid Oxide Fuel Cell operation
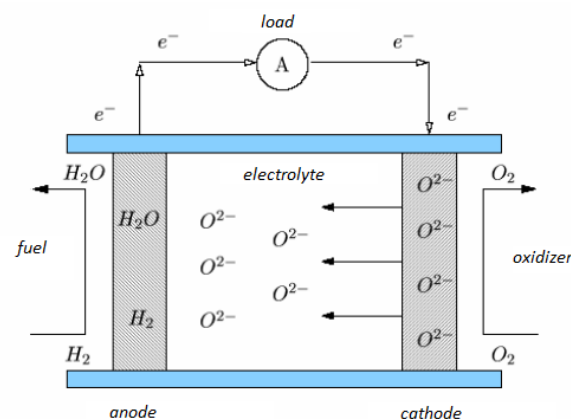
Fig. 2.1 The scheme of Solid Oxide Fuel Cell operation [4].

Fuel (here: hydrogen) is supplied to the anode where it is oxidized by oxygen ions that are able to penetrate the cathode electrolyte according to the following reaction:

$$H_{2(g)}+O^{2-}=H_2O_{(g)}+2e^-$$
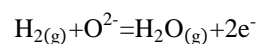
Cathode is supplied by air which contains oxygen. Free electrons flowing through the outer circuit from the anode reduce the molecular oxygen at the cathode to the oxygen ions according to the cathode reaction:

$$O_{2(g)}+2e^-=O^{2-}$$
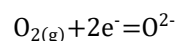
The reaction product (here: water vapor) is produced on the anode. Hydrogen oxidation and oxygen reduction reactions take place in a region called **TPB** (*Triple Phase Boundary*), this is the zone where the electrode, electrolyte and gas phase are in contact.

Total reaction:

$$H_2+\frac{1}{2}O_2=H_2O$$
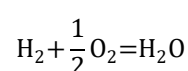
2.3. Triple Phase Boundary Region
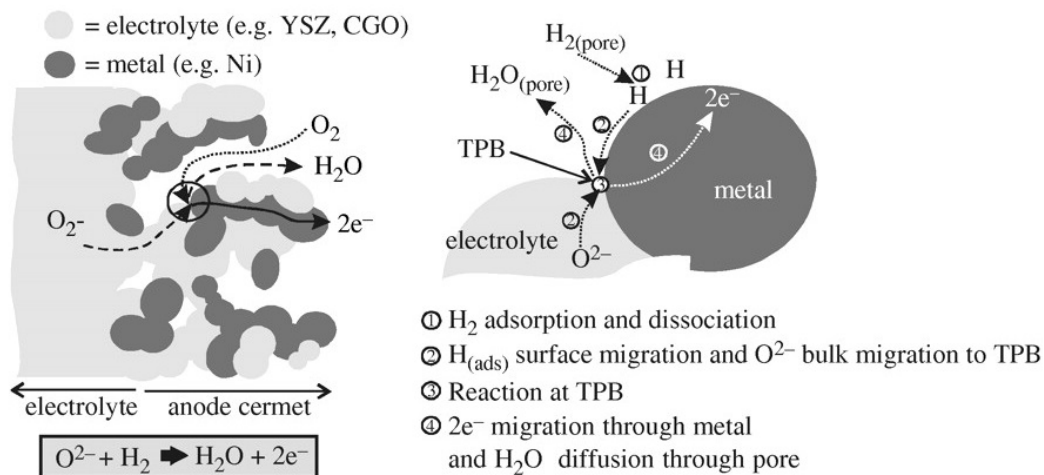
Fig. 2.2 Chemical and physical processes taking place on electrodes in *TPB* region.[5]

The *TPB* surface (Fig. 2.2) is the region occupying a small portion of the electrode, however, the reactions occurring in this area are much more complicated than those listed above. Generally, the mechanisms that influence transport in the gas phase within the cell are convection and gas diffusion in the channels of porous electrodes, molecular diffusion, adsorption and desorption of gaseous components, dissociation, surface and mass diffusion, surface reactions and charge transfer. [6]

Parameters of microstructures affecting the processes occurring in the TPB area are:

- length of the TPB area - the size describing the amount of the active surface of the electrode,
- tortuosity (τ) - it is a parameter describing the complexity of the structure in the electrodes,
- porosity (ε) - the share of free spaces in the volume of electrodes which are the flow channels for reagents,
- the contribution of individual materials forming the electrode in its total volume.

3. Mathematical model

In order to examine the influence of selected microstructure parameters on current-voltage characteristics of the cell, a one-dimensional version of the numerical model described in the article [7] was used. It is an isothermal model of a single SOFC, implemented in MATLAB. This code calculates the volumetric current density, ionic and electron potential of the conductive phase, all three parameters were measured along the cell. Model takes into account to the composition of substrates given to the electrodes, cell operating temperature, and the microstructure parametees of electrode materials and electrolyte. These are among others:

- volume fraction of individual substances in electrode materials (ε),
- length of TPB region inside the electrode (active surface on electrode),
- tortuosity (τ) the degree of microstructure complexity , defined as [8]:

$$\tau = \frac{L_{\text{eff}}}{L_0}$$

Where,

L_{eff} - mean length of the curve (m),
L_0-distance between the ends of the curve (m).

The code calculates current density according to given voltage difference. Thanks to this method, determining a few points between the set voltages, current-voltage characteristic of the entire cell are obtained.

a) Ions and electrons transports

The essence of fuel cells operation is the cooperation between two conductors, ionic and electric. Therefore, there must be an exchange current i_{tpb}, which is passed between the two conducting phases in the area Triple Phase Boundary for an anode or Double Phase Boundary that only consists of a porous LSCF. Transport equations look like this:

Ions transport, respectively for the anode, electrolyte and cathode:

$$\sigma_{ion}^{eff}\frac{\partial^2\phi_{ion}}{\partial x^2} = i_{ano}^{ct}$$

$$\sigma_{ion}^{eff}\frac{\partial^2\phi_{ion}}{\partial x^2} = 0$$

$$\sigma_{ion}^{eff}\frac{\partial^2\phi_{ion}}{\partial x^2} = -i_{ano}^{ct}$$

Electrons transport, respectively for the anode and cathode:

$$\sigma_{el}^{eff}\frac{\partial^2\phi_{el}}{\partial x^2} = -i_{ano}^{ct}$$

$$\sigma_{el}^{eff}\frac{\partial^2\phi_{el}}{\partial x^2} = i_{cat}^{ct}$$

Where,

ϕ_{ion} – ionic potential in ionic conductor (V),

ϕ_{el} - electric potential in electron conductor (V),

$i_{cat/ano}^{ct}$ – volumetric current density $(\frac{A}{m^3})$,

σ_{i-ion}^{eff} – effective ionic conductivity, i - component of electrode $(\frac{S}{m})$,

σ_{i-el}^{eff} - effective electric conductivity, i - component of electrode $(\frac{S}{m})$,

Effective ionic and electric conductivities for electrode materials (YSZ, LSCF, Ni) are calculated using the equations:

For anode it is:
$$\sigma_i^{eff} = \frac{V_i}{\tau_i}\sigma^{bulk}$$

$$\sigma_{Ni}^{eff} = \frac{V_{Ni}}{\tau_{Ni}}\sigma_{el}^{bulk}$$

$$\sigma_{YSZ}^{eff} = \frac{V_{YSZ}}{\tau_{YSZ}}\sigma_{el}^{bulk}$$

Where conductivity of a pure material is calculated from:

$$\sigma_{Ni}^{bulk} = 3.4\times10^4 - \exp\left(-\frac{10350}{T}\right)$$

$$\sigma_{YSZ}^{bulk} = 3.27\times10^6 - 1065.3T$$

For calculating the conductivity for LSCF the model proposed by Matsuzaki et al. were used [9].

b) Diffusion of gas species

Gas diffusion was modeled using Fick's equation:

For hydrogen:

$$\frac{D_{H_2}^{eff}}{RT}\frac{\partial^2 P_{H_2}}{\partial x^2} = -\frac{i_{ano}^{ct}}{2F}$$

For nitrogen,

$$\frac{D_{N_2}^{eff}}{RT}\frac{\partial^2 P_{N_2}}{\partial x^2} = 0$$

For water vapour,

$$\frac{D_{H_2O}^{eff}}{RT}\frac{\partial^2 P_{H_2O}}{\partial x^2} = \frac{i_{ano}^{ct}}{2F}$$

Assuming that cathode is supplied by air which is an oxidizer, there is a diffusion of oxygen and nitrogen. Diffusion on the cathode:

For oxygen:

$$\frac{D_{O_2}^{eff}}{RT}\frac{\partial^2 P_{O_2}}{\partial x^2} = \frac{i_{cat}^{ct}}{4F}$$

For nitrogen:

$$\frac{D_{N_2}^{eff}}{RT}\frac{\partial^2 P_{N_2}}{\partial x^2} = 0$$

Where,

F - Faraday's constant ($\frac{C}{mol}$),

R – gas constant ($\frac{J}{mol\,K}$),

T - temperature (K),

P_j – partial pressure of j-compound (Pa),

D_j^{eff} – effective diffusion coefficient off j −compound ($\frac{m^2}{s}$) depending on microstructure according to equation:

$$D_j^{eff} = \frac{V_{pore}}{\tau_{pore}}\,D_j^{bulk}$$

For the equation above, volumetric diffusion coefficient was calculated using Fuller's method [10].

c) Electrochemical reactions

Volumetric current density for the hydrogen oxidation is obtained from Bulter-Volmer equation, it is calculated in every grid point throughout the cell. Respectively for anode and cathode it is:

$$i_{ano}^{ct} = i_{0,ano}^{tpb}l_{ano}^{tpb}\left(\exp\left(\frac{2F}{RT}\eta_{ano}^{act}\right) - \exp\left(-\frac{F}{RT}\eta_{ano}^{act}\right)\right)$$

$$i_{cat}^{ct} = i_{0,cat}^{dpb}A_{cat}^{dpb}\left(\exp\left(\frac{1.2F}{RT}\eta_{ano}^{act}\right) - \exp\left(-\frac{F}{RT}\eta_{ano}^{act}\right)\right)$$

Where,

l_{ano}^{tpb} -długość obszaru $TriplePhaseBoundary$ w anodzie ($\frac{m}{m^3}$),

A_{cat}^{dpb} - powierzchnia obszaru $DoublePhaseBoundary$ w katodzie ($\frac{m^2}{m^3}$),

$i_{0,ano}^{tpb}$ exchange current density on the anode derived by de Boer'a ($\frac{A}{m}$),[11].

$$i_{0,ano}^{tpb} = 31.4 \cdot p_{H_2}^{-0.03} \cdot p_{H_2O}^{0.4} \cdot \exp\left(-\frac{18300}{T}\right)$$

$i_{0,\text{cat}}^{\text{dpb}}$ - exchange current density on the cathode derived by de Esquirol et al. $\left(\frac{A}{m^2}\right)$, [12].

$$i_{0,\text{cat}}^{\text{dpb}} = 1.47 \cdot 10^6 \cdot P_{O_2}^{0.2} \cdot \exp\left(-\frac{85859}{RT}\right)$$

$\eta_{\text{ano}}^{\text{act}}, \eta_{\text{cat}}^{\text{act}}$ – activation overpotentials for anode and cathode (V) defined as:

$$\eta_{\text{ano}}^{\text{act}} = \phi_{\text{el}} - \phi_{\text{ion}} - \eta_{\text{ano}}^{\text{conc}}$$

$$\eta_{\text{cat}}^{\text{act}} = \phi_{\text{ion}} - \phi_{\text{el}} - \eta_{\text{cat}}^{\text{conc}}$$

Concentration overpotential (η^{conc}) were calculated according to:

$$\eta_{\text{ano}}^{\text{conc}} = \frac{RT}{2F} \ln \frac{P_{H_2}^{\textbf{bulk}}}{P_{H_2}} \frac{P_{H_2O}}{P_{H_2O}^{\textbf{bulk}}}$$

$$\eta_{\text{cat}}^{\text{conc}} = \frac{RT}{4F} \ln \left(\frac{P_{O_2}^{\textbf{bulk}}}{P_{O_2}}\right)$$

Current density is obtained by integrating volumetric current density (i^{ct}) throughout the electrodes, according to:

$$i_{\text{cell}} = \frac{1}{L_{\text{cell}}} \int i^{\text{ct}} \, dx$$

The values of i_{cell} combined with respective voltage drops were used to build current-voltage characteristics of SOFC.

4. Numerical method

The discretization method used for that problem was Control Volume Method presented in [13]. The obtained system of algebraic equations were solved using Gauss-Seidel method.

5. Results

The model has been verified by experiment conducted in the fuel cell laboratory at the Department of Fundamental Research in Energy Engineering in AGH UST. The measurements were carried out for a temperature of 700 ºC and 750 ºC with fuel composed from 60 % of H2 and 40 % of N2, and an oxidant mixture composed of 21 % of O2 and 79 % of N2. Moreover we can clearly see a strong dependence between the SOFC performance and operating temperature. The higher temperature we have the more efficient our cell is.
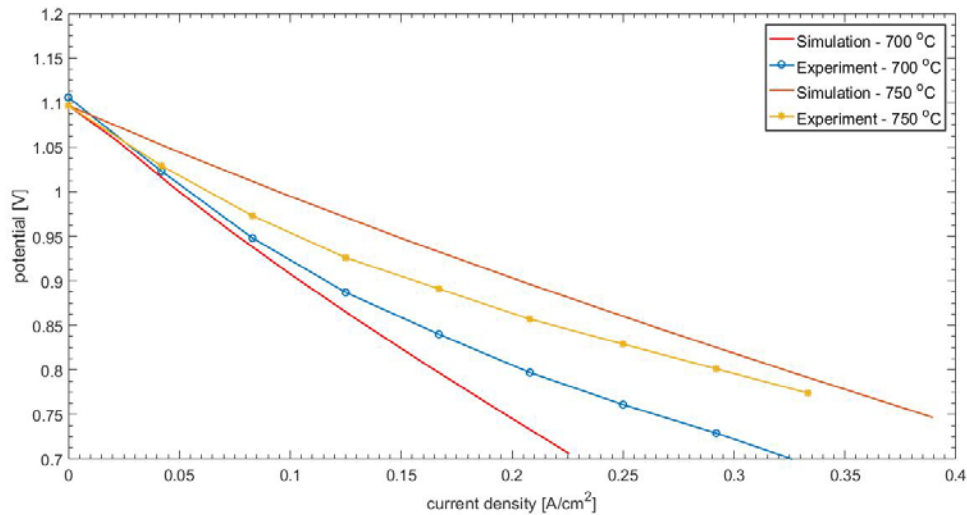
Fig. 5.1 Comparison of model output with experiment

5.1. Changes in anode microstructure parameters

Because of the TPB region where fuel oxidation takes place, the structure of the anode is essential for SOFC efficiency. This relation can be seen at the figure below. One can observe that with an increase of TPB length inside the anode current density rises significantly. The shape of the current-voltage characteristic for the highest density of TPB (black line) is also important, it is a straight line, which indicates a much smaller activation polarization.
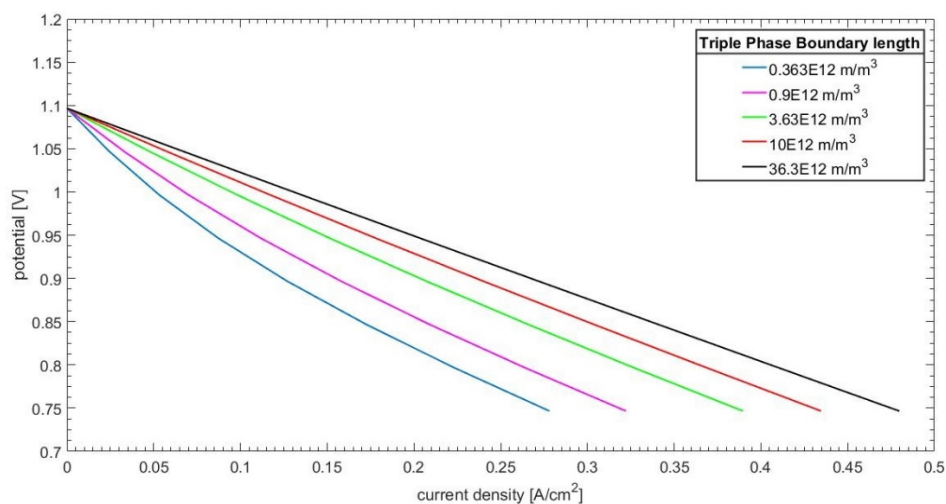
Fig.5.2 Current voltage characteristic depending on TPB length.

In subsequent investigated cases, the influence of the amount of YSZ in the anode material at nickel cost was calculated (Fig. 5.3) and at a porosity cost (Fig. 5.4) and the impact of YSZ tortuosity   (Fig. 5.5) and nickel (Fig. 5.6) for a cell performance. Presented plots indicate a strong tendency for the cell's efficiency to increase when the volume fraction of YSZ is increased which, being an ion conductor, has a significant impact on the cell's operation. Because of the fact that ionic conductance is the main factor for diminishing the SOFC performance. Analyzing the graph (Fig. 5.4), we can see that in the last case (for anode composition(8 % pores, 64 % YSZ, 28 % nickel), the increase in current density is small in comparison to the previous composition, this is due to decrease in the share of pores in the cell structure, making the flow of reagents difficult, what may rise the concentration polarization. In the reality the performance in that case could be even lower, because of the lack in pore phase continuity. Therefore, slightly better results are presented in the graph (Fig. 5.3) where the

share of YSZ is increased at the cost of nickel participation.The nickel content should be adjust to the lowest possible level in which the continuity of the phase will be preserved.
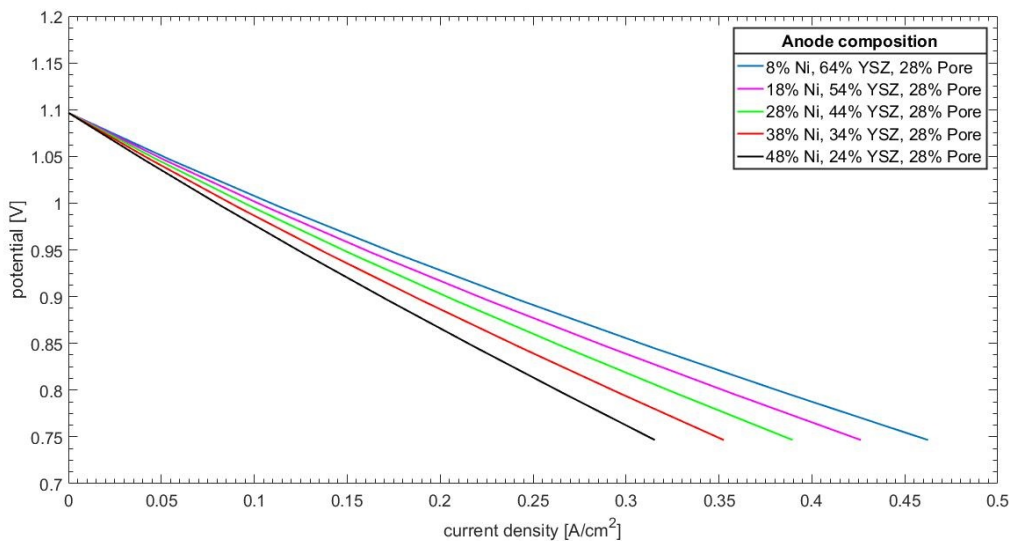
Fig. 5.3 Current voltage characteristic depending on anode composition I.
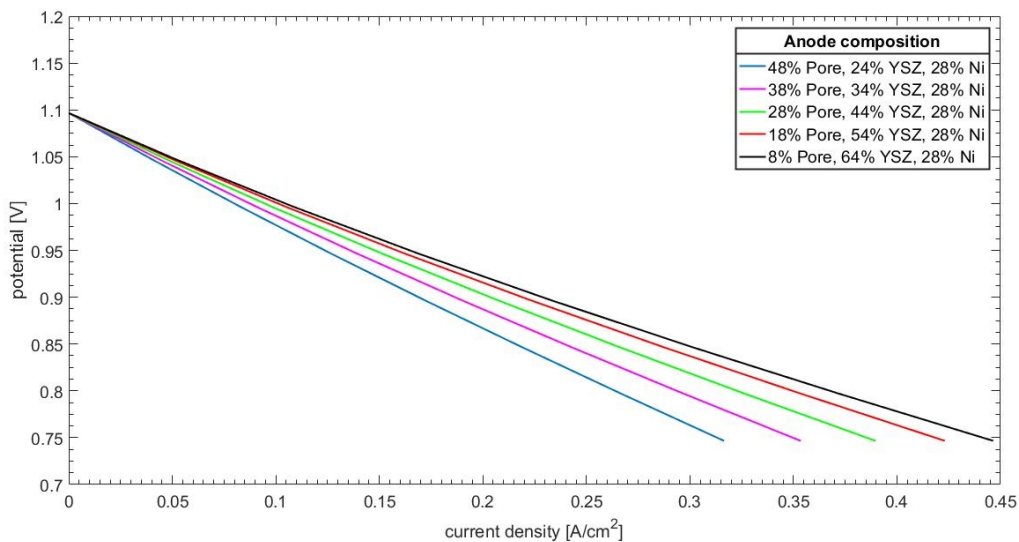
Fig. 5.4 Current voltage characteristic depending on anode composition II.

At the plots (Fig. 5.5) and (Fig. 5.6)   it is easy to notice that the nickel tortuosity in the microstructure does not affect the obtained current density, as opposed to the YSZ tortuosity which plays a very important role in cell performance. The smaller the YSZ volume fraction, the better the performance of the cell is. For the theoretical tortuosity, equal to 1, the link is more efficient about 40% than in the case of tortuosity factor equal to 2.28 assumed as reference. Although, as it was mentioned at the beginning of the chapter, low tortuosity factor is not possible in the real cell microstructure, because it limits the complexity of the cell, thereby TPB length which is undesirable.
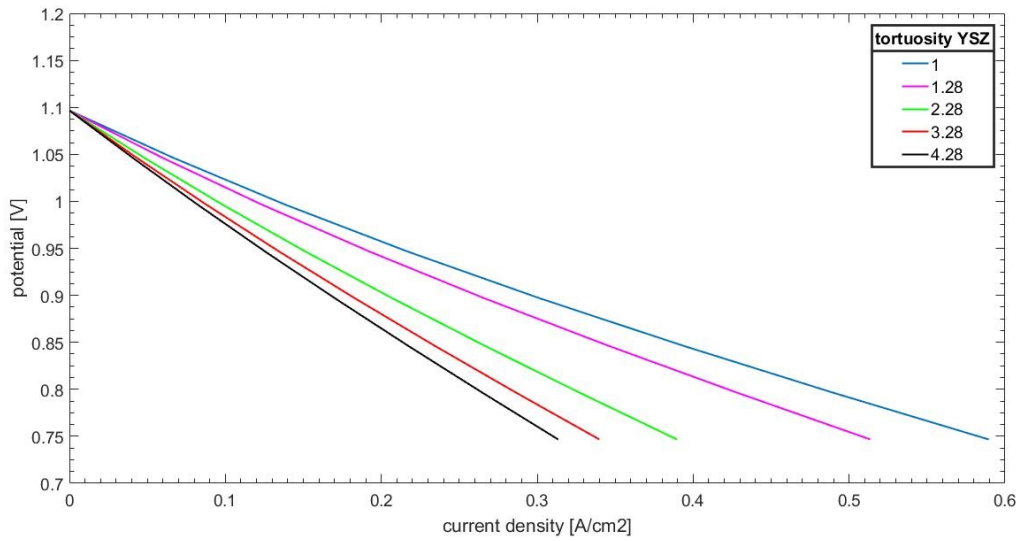
Fig. 5.5 Current voltage characteristic depending on YSZ tortuosity factor.
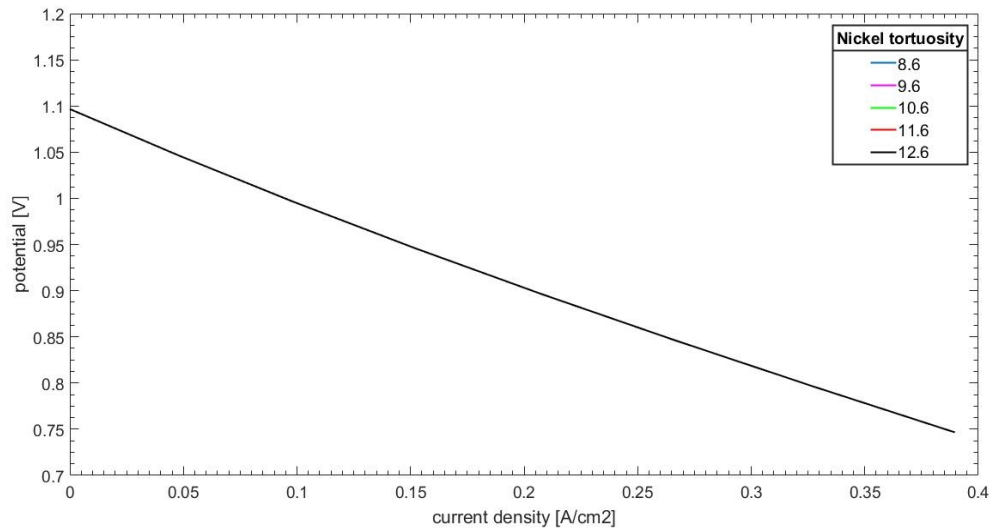
Fig. 5.6 Current voltage characteristic depending on Ni tortuosity factor.

5.2. Changes in cathode microstructure parameters

The microstructure of the cathode material has also a significant effect on the performance of the SOFC. In this model, for cathode material LSCF is used. This type of material belongs to group called *MIEC* (Mixed Ion and Electron Conductor). Thereby the most important region here, is called *Double Phase Boundary* in which the electrons transported by the outer circuit reduce oxygen, from where oxygen ions are directed towards the anode. As shown in (Fig. 5.7) the increase in the surface area of the DPB rise the density of the current produced by the cell, although not in such a significant way as the increase of TPB length.
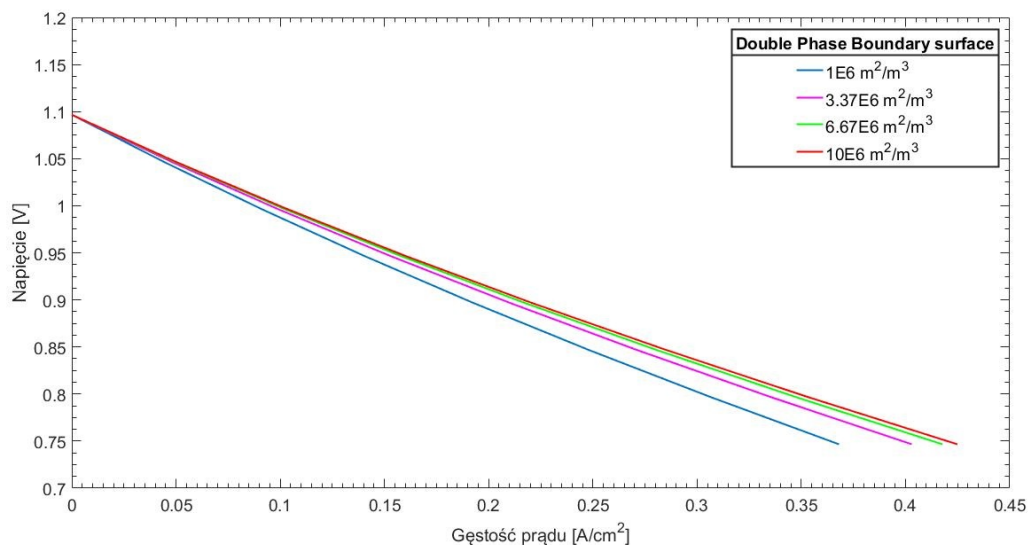
Fig. 5.7 Current voltage characteristic depending on DPB surface area.

The next examined parameters were the porosity of the cathode material and the tortuosity of the LSCF. As shown in Fig. 5.8for a higher volume of LSCF fraction, the cell achieves more effective operating performance. In Fig. 5.9it can be observed that the decrease in LSCF tortuosity increases the density of the current produced by the fuel cell, what, as in the case of YSZ tortuosity factor, is the resultof the relation for the effective diffusion coefficient in the material.
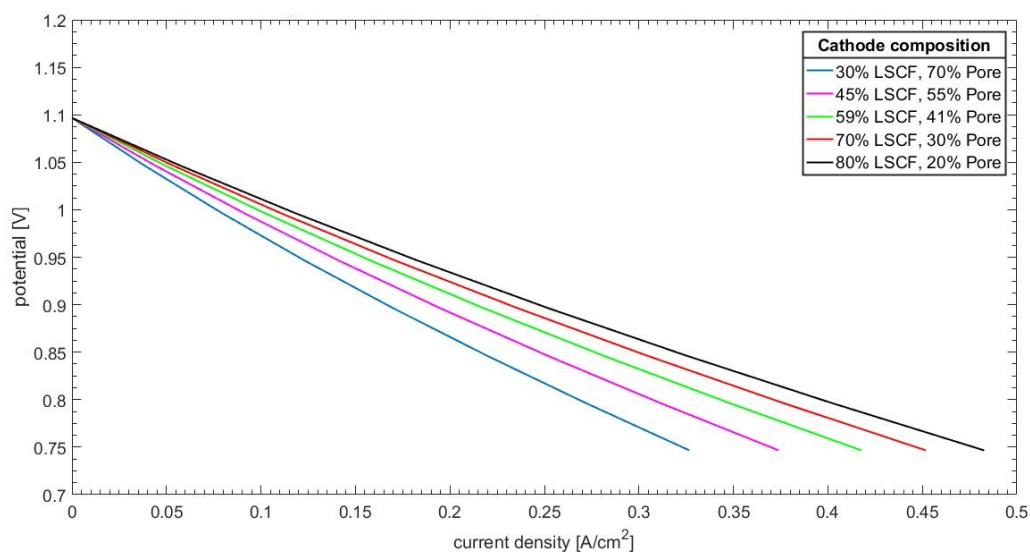
Fig. 5.8 Current voltage characteristic depending on LSCF volume fraction.
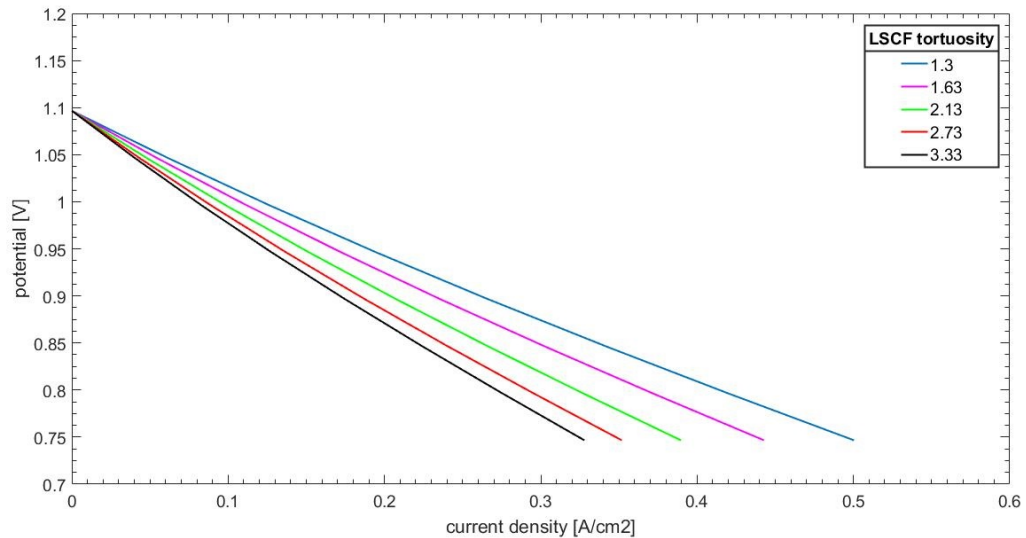
Fig. 5.9 Current voltage characteristic depending on LSCF tortuosity factor.

6. Conclusions

Analyzing the current-voltage characteristics of the SOFC cells presented in the previous chapter, made for 9 different microstructure parameters as well as operating temperature, itcan be seen a close interaction between some parameters and cell efficiency. The presented validation of the model shows that it can be a reliable source of information, because the current-voltage characteristics obtained from the simulation of the model and data from experiments carried out in a laboratory are very similar and show common features.

From the analysis made for different operating temperatures, we can see that this is the most-important parameter in the context of SOFC fuel cell performance. An increase in the working temperature of the cell by 100 ºC increases the current density by about two times. Unfortunately, this way of growing the SOFC efficiency is problematic due to the fact that high mechanical stresses occur inside the cell when operating at high temperatures. This fact results in the problem of adjusting the thermal expansion coefficients for the materials from which the cell is made and the interconnectors used in the fuel cells system.

Based on the results obtained by changing the parameters of the microstructure, we can notice some important regularities affecting the density of the energy produced by the cell. Both for the anode and the cathode, the increase in the density of the TPB regions(DPB in the case of the cathode).TPB length is the factor that the most effectively improves the cell's performance, which is simply caused by the upswing of reaction rate inside the electrodes. Other important parameters which have a positive effect on the density of produced current in the cell are the volumetric fractions of ionic conductors within the electrodes (YSZ for the anode and LSCF for the cathode, which is also an electron conductor), which can be explained by the fact that the process of ion transport inside the cell is the slowest process and the source of concentration losses. In addition, the decrease in the tortuosity of the YSZ and LSCF volume fractions also significantly improves the efficiency of the cell.Unfortunately this parameter should not be decreased because of the fact that, the lower tortuosity we have the less complex our microstructure is. Because of that we observe a significant drop in area of active surface (TPB and DPB) in electrodes. In the case of the anode for the volume fraction of nickel fraction and its tortuosity, no significant change in the appearance of the current-voltage characteristic was observed.

In conclusion, the results presented in the above study clearly show that the features and parameters of the SOFC fuel cell microstructure have a very significant impact on the efficiency achieved by this device and should serve as a guide in designing and manufacturing components for SOFC cells.

Acknowledgment

References

[1] Yosuke Sakamoto et al., Effects of electrodes microstructure on polarization characteristics of SOFC anode, Proceedings of FuelCell2008, Six international Fuel Cell Science, Engineering and Technology Conference, June 16-18,2008,Denver, Colorado, USA

[2] Mariusz Krauz, Opracowanie technologi wytwarzania stałotlenkowych ogniw paliwowych, PhD, AGH University of Science and Technology, 2008.

[3] Marian Soltanzadeh, Modelling Triple Phase Boundary (TPB) in Solid Oxide Fuel Cell (SOFC) Anode, Master thesis, University of Ottawa 2010.

[4] Michał Karcz, Problemy numrycznego modelowania przepływów z reakcjami elektrochemicznymi w ogniwie paliwowowym SOFC, V Warsztaty „Modelowanie przepływów wielofazowych w układach termochemicznych zaawansowane techniki pomiarowe”, Zakład Konwersji Energii, Instytut Maszyn Przepływowych PAN, Stawiska 2005.

[5] N.P Brandon , D.J Brett, Engineering porous materials for fuel cell applications, The Royal Society, 5.Fuel cells electrode,2006.

[6] R. Bove and S. Ubertini, Modeling Solid Oxide Fuel Cells, Methods, Procedures and Techniques, ©Springer Science+Business Media B.V., Cleveland, 2008.

[7] MarcinMozdzierz, Yosuke Komatsu, Motohiro Saito, Hideo Yoshida, Hiroshi Iwai, Janusz S. Szmyd, GrzegorzBrus, Combining structural, electrochemical, and numerical studies to investigate the relation between microstructure and the stack performance, Journal of Applied Electrochemistry(2017), 47,9.

[8] Wei Kong, Qiang Zhang, XiuwenXu, Daifen Chen, A Simple Expression for the Tortuosity of Gas Transport Paths in Solid Oxide Fuel Cells' Porous Electrodes, Energies, 2005.

[9] Matsuzaki K , Shikazono N , Kasagi N, Three-dimensional numerical analysis of mixed ionic and electronic conducting cathode reconstructed by focused ion beam scanning electron microscope. Power Sources (2011),196,6.

[10] Poling BE, Prausnitz JM, O'Connell JP, The properities of gases and liquids 5th edition, McGRAW-HILL, 2011.

[11] de Boer B., SOFC anode-hydrogen oxidation at porousnickel and nickel/yttria-stabilised zirconia cermet electrodes, University of Twente, 1998.

[12] Esquirol A, Brandon NP, Kilner JA, Mogensen M, Electrochemical characterization of La0. 6Sr0. 4Co0. 2Fe0. 8 O 3 cathodes for intermediate-temperature SOFCs, J ElectrochemSoc (2004), 151,11.

[13] Suhas V. Patankar, Numerical heat transfer and fluid flow, McGraw-Hill, ISBN 0-07-048740-5.

The future of energy storage. Insight into the advancement of batteries and analysis of charge transfer process at the electrolyte-cathode interface in all-solid-state lithium cells.

Bartłomiej Rak[1]

[1]*Faculty of Energy and Environmental Engineering, Silesian University of Technology, bartlomiejrak95@gmail.com*

Abstract

This article contains basic facts about lithium-ion all-solid-state batteries and presentation of the research results. The aim of this research was to prepare electrolyte-cathode interfaces by impregnation of asymmetrically porous electrolyte pellet with liquid cathode precursor, which was subsequently calcinated and construction of Li-ion cells with the use of fabricated junctions. Later, electrochemical performance of the cells was measured. Material used as electrolyte was perowskite $La_{2/3-x}Li_{3x}TiO_3$, cathode – spinel $LiNi_{0,45}Cu_{0,05}Mn_{1,5}O_4$ and anode – metallic lithium. Electrochemical impedance spectroscopy and cyclic woltammetry methods were used to measure cells performance. In order to compare the cells with each other, parameters of equivalent circuit were fitted to impedance spectra, which allowed to choose the best performing cell. This work also shows how purity of produced materials, particular construction steps and hermetic storage of electrochemical cells can affect their performance and utilization.

Keywords: energy storage, lithium-ion cells, all-solid-state batteries

1. Introduction

In the light of ever growing demand for energy, depletion of fossil fuel reservesand pressure on utilization of renewable energy sources, one of the main challenges scientists face today findingnew, reliable and efficient ways to store energy. Over the recent years there has been significant progress in development of electrochemical energy storage systems such as Li-ion batteries or supercapacitors which are widely used in porTab. electronic devices, electric vehicles, grid energy storage and many other. Requirements addressed to new technologies are safety of use, reliability of performance, low production cost and harmless influence on natural environment [1,2]. Today the state-of-the-art LIBs offer volumetric and gravimetric energy densities up to 770 Wh l^{-1} and 260 Wh kg^{-1}, respectively. For comparison, energy accumulated in water at 100 m dam height is equal to 0.278 Wh l^{-1} and 0.278 Wh kg^{-1}, in wood 5000 Wh kg^{-1} and in biodiesel 11 722.2 Wh l^{-1} and 9 166.7 Wh kg^{-1} [3]. Although conventional Li-Ion batteries (LIBs) have proven their performance, the technology is well known and production cost is reasonable it is predicted that there is little room for improvement since their energy density will soon reach its electrochemical limit. In addition, the vast majority of conventional LIBs use organic liquid electrolytes which cause a risk of self-ignition or explosion if used improperly. A good example that proves the safety concerns are real is the widely known issue with Samsung Galaxy Note 7 which batteries occasionally exploded even though smartphones were used properly. Many scientists believe that the answer to the above problems could be replacement of combustible liquid electrolyte with inflammable solid one. Application of such electrolyte would not only bring significant benefits in terms of safety but also would enable the use of lithium metal electrode increasing energy and power density of the battery and simultaneously decreasing its size. Another positive features of solid state electrolyte are improvement of electrochemical, mechanical and thermal stability, lack of dangerous leakage and increased lifespan [4]. Since the task of electrolyte in battery is to transport positive metal ions between electrodes with concurrent flow of electrons through external circuit, the sought electrolyte material must poses high ionic conductivity, infinitesimal electron conductivity and be chemically compatiblewith electrodes [5].

History of solid ion conductors begins in the fifties years of the XX century when Li$^+$ conduction was discovered in solid lithium nitride Li_3N. Over the next years other compounds of different structures and better conduction properties were unveiled. Few examples are perovskite oxides $Li_{1/2}La_{1/2}TiO_3$ (LLTO), NaSICON oxides $Li_{1+x}Al_xTi_{2-x}(PO_4)_3$ or garnet type $Li_7La_3Zr_3O_{12}$. In 2016 it was discovered that Li$^+$ conductivity of

$Li_{9.54}Si_{1.74}P_{1.44}S_{11.7}Cl_{0.3}$ can reach 25 mS cm^{-1} which confirmed the former assumptions that solid electrolytes will outbalance ionic conductivity of their liquid counterparts [6]. In recent years perovskite oxide LLTO has gained huge interest due to its ionic conductivity at the level of 1 mS cm^{-1} in room temperature. Because of that it is considered as one of key electrolyte materials for development of Li-ion all-solid-state batteries [7].

The aim of the research presentedin this article was the synthesis of electrolyte-cathode interfaces via impregnation of asymmetrically porous solid electrolyte with liquid cathode precursor, its calcination and construction of lithium ion cells based on the synthesised interface and lastly measurements of cells electrochemical performance. The subject of observation was how the method of the electrolyte-cathode interface synthesis influenced performance parameters of cells. The applied electrolyte was hybrid system: perovskite oxide $La_{2/3-x}Li_{3x}TiO_3$ (LLTO) for x = 0.11 from cathode side and liquid solution of $LiPF_6$ in organic aprotic solvent. Material used as cathode was lithium manganese spinel with an admixture of nickel and copper $LiNi_{0.45}Cu_{0.05}Mn_{1.5}O_4$, and lithium metal as anode material. The applied electrochemical measurements were open circuit voltage (OCV), electrochemical impedance spectroscopy (EIS) and cyclic voltammetry (CV).

2. Research methodology

The research covered the synthesis of electrolyte material $La_{2/3-x}Li_{3x}TiO_3$, formation of asymmetrically porous electrolyte sinter, synthesis of liquid cathode precursor $LiNi_{0.45}Cu_{0.05}Mn_{1.5}O_4$ via sol-gel process, formation of electrolyte-cathode interface and cell construction. At the final stage electrochemical measurements of cells were carried out to determine their performance. The measurement methods applied to the cells were electrochemical impedance spectroscopy (EIS) were cyclic voltammetry (CV). Open circuit voltage (OCV) measurement were done before each EIS. Upon synthesis of electrolyte and cathode material their samples were analyzed in terms of their phase composition to estimate the content of unwanted compounds using X-ray diffraction method. The applied test procedure of the electrochemical properties of cells is shown in the diagram below.

Fig. 2.1. Procedure of electrochemical properties of cells measurements.

All cells have undergone an identical measuring cycle with the same settings of the measuring devices. OCV and EIS measurements were made using the Solartron Analytical 1252A frequency response analyzer. The settings for OCV are: 2 minutes and frequency 2 points per second, while for EIS it is the frequency range of 0.3 MHz – 1mHz, with an amplitude of 0.1 V over the voltage obtained when measuring OCV. The next step was to perform two CV cycles for the voltage range 3.5 - 4.9 V with a scanning speed of 0.1 mV s^{-1} using the MULTI AUTOLAB M204 (MetrohmAutolab) device. Finally, the OCV and EIS tests were repeated for the same settings as before. The results of EIS measurements were developed using the ZView2 program issued by Scribner Associates Inc. This program is used to model equivalent circuits to describe the impedance of the materials tested. During the analysis of the obtained impedance spectra, anequivalent circuit was used, which was taken from the scientific work devoted to the analysis of impedance spectra of Li-ion cells with liquid electrolyte [8]. On the basis of the electrochemical nature of the individual processes taking place inside the cell during the charge transfer, in the literature it was found that using such a system of elements (Fig. 2.2.), a Li-ion cell can bereliably modeled.
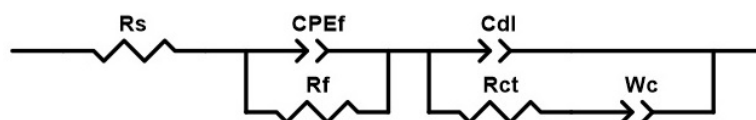
Fig. 2.2. The equivalentcircuit adopted to analyse results of EIS. Rs – internal cell resistance, Rf and CPEf – resistance and capacity of passivation layer (SEI), Rct – cathode charge transfer resistance, Cdl – capacity of double layer, Wc- Warburg element [8].

3. Materials synthesis and construction of all-solid-state cells

This chapter is devoted to a detailed description of the procedure for the production of electrolyte material - $La_{2/3-x}Li_{3x}TiO_3$ perovskite for x = 0.11 cathodic - lithium manganese spinel with an admixture of nickel and copper $LiNi_{0.45}Cu_{0.05}Mn_{1.5}O_4$ (LMNO) and their use in the construction of all-solid-state cells.

3.1. Synthesis of electrolyte material

The electrolyte material used in this work is a compound of the $La_{2/3-x}Li_{3x}TiO_3$ perovskite structure (LLTO) obtained as a result of high-temperature synthesis. The summary synthesis reaction is described by the following equation:

$$\frac{3x}{2}Li_2CO_3 + TiO_2 + \left(\frac{\frac{2}{3}-x}{2}\right)La_2O_3 \rightarrow La_{\frac{2}{3}-x}Li_{3x}TiO_3 + \frac{3x}{2}CO_2$$
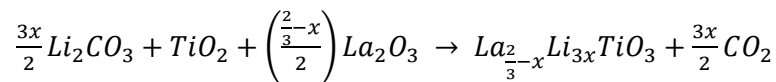
for x = 0.11.

For the synthesis of 20 g of the electrolyte material the following amounts of reagents were used: 1.40376 g Li_2CO_3 (99% POCH); 9.10364 g TiO_2 (99.6% Alfa Aesar);10.33588 g La_2O_3 (≥99.9% ALDRICH). Due to hygroscopicity of La_2O_3, it was preheated for 12 hours at 1000 °C in argon atmosphere, heating speed was 5 °C / min. Reactants with 20 ml propanol addition were being grounded in the SpexSamplePrep 8000M rotary-vibrating mill for 20 min. The product was then dried in a HERAEUS Vacuum Oven (Thermo Scientific) oven at 70 ° C, 30 mbar until complete propanol evaporation. The pellets were formed (20 mm diameter, pressure of 39,2 kN) using a Specac 15t single-axle hydraulic press. The material prepared in this way was calcined at 1000 °C. The pellets were placed in a ceramic boat and put into the oven. The heating took place in a synthetic air atmosphere ata rate of 5 °C / min for 3 hours 20 minutes to reach the temperature of 1000 °C, which maintained for another 12 hours, then the furnace was self-cooled. Then the pellets were broken into powder and re-homogenized in a mill with 20 ml of propanol addition for 20 minutes, dried and pressed. This time pellets of 13 mm diameter were formed with pressure of 19,6 kN. The proper synthesis of electrolyte material (perovskite LLTO) took place at 1150 °C in synthetic air. Heating rate was at a rate of 5.2 °C / min to 1150 °C (3h 40min),which was maintained for another 12 hours and then self-cooling. The tempered pellets were homogenized in a mill with 20 ml of propanol and dried in a vacuum oven. In order to check the purity of the obtained material, it was subjected to X-ray diffraction analysis using an Empyrean powder diffractometer from PANalytical. Phase composition analysis was performed using the HighScore Plus program by matching the entries in the ICDD database (International Center of Diffraction Data) to the received diffraction pattern.
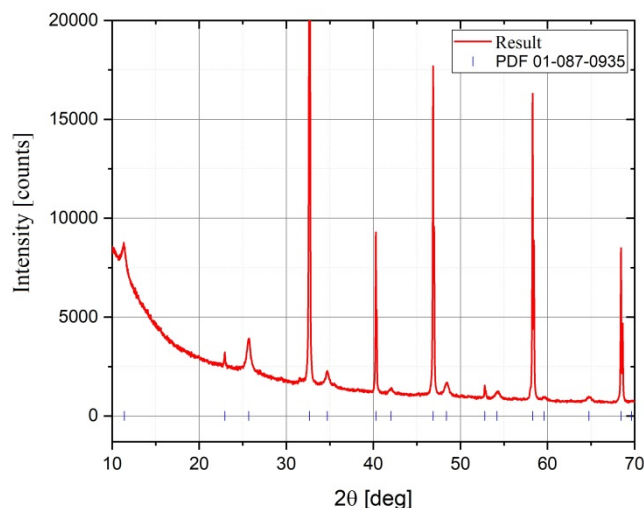
Fig. 3.1.1. X-ray diffractogram with phase analysis developed together with Aleksandra Bombała and Anna Lasak for $La_{2/3-0.11}Li_{0.33}TiO_3$ obtained in high-temperature synthesis.

Obtained peaks are compliant with the data contained in the PDF 01-087-0935, which characterizes the compound $La_{2/3-0.11}Li_{0.33}TiO_3$ with a perovskite structure (space group P4 / mmm).

3.2. Synthesis of cathodematerial

Cathode material$LiNi_{0.45}Cu_{0.05}Mn_{1.5}O_4$ (LMNO) was synthesised via low-temperature sol-gel method, reagents used for 10 g of final product were as follows: 0.16877 g $Cu(NO_3)_2$ (99.999% ALDRICH chemistry); 3.56649 g $Ni(NO_3)_2$ (99% ACROS ORGANICS); 3.36157 g $LiNO_3$ ($\geq$99,0% SIGMA); 10.29077 g $Mn(NO_3)_2$ (100% POCH). The process of synthesis was conducted in two ways: in synthetic air atmosphere and in argon atmosphere.

Method (1): Surplus weights were dissolved in a glass platter with a magnetic stir bar in 6 ml of distilled water. Then 4.5 ml of 25% ammonia solution (POCH) was added to reach pH = 9.The cathode precursor in form of slurry was dropped onto porous side of electrolyte pellets using Pasteur pipette. The synthesis was carried out in an oven in a synthetic air atmosphere according to the program: heating to 400 °C for 4h (drying out the LMNO precursor), heating from 400 °C to 800 °C for 1 h 20 min, maintaining temperature 800 °C for 8h (synthesis of cathode material), self-cooling.

Method (2): To prevent contact of nitrates with oxygen, a two-necked round-bottom flask was used to prepare the solution, through which argon was passed. Surplus weights were dissolved in the flaskwith a magnetic stir bar in 6 ml of distilled water. The water was previously degassed in a vacuum oven. Then 4.5 ml of 25% ammonia solution (POCH) was added to reach pH = 9. The cathode precursor in form of slurry was dropped onto porous side of electrolyte pellets using Pasteur pipette. The synthesis was carried out in an oven in argon atmosphere according to the program: heating to 400 °C for 4h (drying out the LMNO precursor), heating from 400 °C to 800 °C for 1 h 20 min, maintaining temperature 800 °C for 8h (synthesis of cathode material) self-cooling.

Cathode materials were subjected to X-ray diffraction measurements to estimate their purity. During the phase composition analysis, the HighScore Plus program identified three compounds consisting mainly of both diffractograms obtained: desired LMNO (01-080-2162) and two lithium nickel oxides with various stoichiometry $Li_{0.45}Ni_{1.05}O_2$(01-087-1548) and $Li_{0.4}Ni_{1.6}O_2$(01-081-0095). The estimation of their content was carried out using the semi-quantitative analysis method using the scale factors given by the program and the RIR (reference intensity ratio) found in the catalog's datasheets. The weight percentageis shown inTab. 3.2.1.

Tab. 3.2.1. Weight percentage of compounds in cathode material.

Synthesis Method	Weight percentage [%]		
	$LiNi_{0.5}Mn_{1.5}O_4$	$Li_{0.45}Ni_{1.05}O_2$	$Li_{0.4}Ni_{1.6}O_2$
Method (1) – synthesis in synthetic air	47	44	8
Method (2) – synthesis in argon	65	30	5

The analysis shows that the cathode compounds produced in both ways are contaminated. It is evident, however, that the limitation of oxygen access during the preparation process resulted in a higher proportion of the desired cathodic compound $LiNi_{0.5}Mn_{1.5}O_4$and a smaller proportion of impurities.

3.3. Construction of cells

Preparation of the electrolyte in the form of one-sided porous pellets

In order to improve the efficiency of the cells, the interface engineering method was used to create an artificial porosity in the outer layer of the electrolyte which was impregnated with the liquid cathode precursor. The first attempts to make one-sided porous pellets constituting the electrolyte layer began with the preparation of samples: 0.1 g of pure LLTO electrolyte phase and 0.3 g of a mixture of pure LLTO and starch in a volume ratio (LLTO): (starch) → 1: 1. The starch used in this step was the SIGMA-ALDRICH rice starch, the LLTO-starch mixture was prepared by weighing the reagents in the appropriate ratios and then homogenizing them in a mortar for about 15 minutes. The next step was to create pellets by properly compressing the prepared samples. For this purpose, 0.1 g of pure LLTO phase was placed on the basis of a punch of a hydraulic press with a diameter of 13 mm and spread evenly over its entire surface. Then this layer was pressed under pressure of 14.7 kN for 30

seconds and then a prepared mixture of 0.3 g LLTO-starch was added to the top of the pressed LLTO layer and the whole was pressed under a pressure of 19.6 kN for 30 seconds. The obtained pellets were placed in a ceramic boat with a layer of pure LLTO facing down and sintered at 1200 °C according to the program: heating the furnace to 1200 °C for 4 h - heating rate 5 °C / minute, maintaining 1200 °C for 12 h, and then automatic cooling. Heating and sintering took place in the atmosphere of argon, while during self-cooling the flowing gas was changed to synthetic air to burn out the starch and create the desired pores. Due to the cracking and deformation of the pure LLTO side of obtained pellets some of them were rejected and only three were taken to further work (cells were numbered 1; 2; 3).

Preparation of electrolyte-cathode interface

Asymmetrically porous electrolyte pellets were impregnated with cathode precursor by placing droplets on the porous side of the pellets using Pasteur pipette.Three droplets of cathode precursor obtained in method (1) were put on the cell no. 1 and only two droplets obtained in method (2) for cells no. 2 and 3. Then they were placed in a vacuum dryer to pre-remove the water. The process was as follows: a negative pressure was created at room temperature, sucking air from the dryer chamber, thereby drawing air from the pores of the pellets and allowing them to be filled with cathodic material, reaching a vacuum of 100 mbar the pump was turned off and the valve opened to refill the chamber with air, then negative pressure of 20 mbar was created and pellets were dried under such conditions for 1 minute. Subsequently pellets were put into the FRIOCELL FC 55 dryer of BMT Medical Technology and dried for 1 hour at 90 °C under atmospheric pressure. The next step was the synthesis of the cathode material in the furnace in a synthetic air atmosphere for cell no. 1 and in argon for cells no. 2 and 3 according to the program: heating to 400 °C for 4h (drying out the LMNO precursor), heating from 400 °C to 800 °C for 1 h 20 min, maintaining temperature 800 °C for 8h (synthesis of cathode material), automatic cooling.In order to enhance cathode-current collector contact in cells no. 2 and 3the cathode side was coated with 100 nm Au layer in a Quorum Q150R S atomizer.

Construction of complete cells

The construction of the cells consisted in the application of a metallic lithium anode on the dense LLTO side of the pellets and placing them in the Swagelok casing. In order to prevent perovskite reduction when in contact with metallic lithium, a separator was used - glass fiber impregnated with liquid LiPF6 dissolved in EC / DEC. The whole construction process took place in a sealed argon chamber.

4. Findings

The aim of this work is to analyze the efficiency of charge transfer in the produced electrolyte-cathode interface. The object of observation is the change of the resistance of the cells depending on the preparation of the cathode material and its method of impregnation on a porous electrolyte pellet. Based on the literature, a suiTab.equivalent circuit was selected and fitted to the obtained impedance spectra by determining the values of the characteristic parameters of its elements. This allowed for the projection and identification of resistances associated with individual processes taking place in different layers of the cell. Current responses of the cells to the applied voltage during the CV measurement were also observed.

4.1. Results of the electrochemical measurements of the cells

The adjustment of the equivalent circuitparameters to the measured impedance spectrum consisted in appropriate selection of the values of individual elements. The result of such a match was a graph which coincides with the measured spectrum as it can be seen in Fig. (4.1.1.). The obtained adjustment parameters are summarized in Tab. 4.1.1. and Tab. 4.1.2..

Tab. 4.1.1. Voltage of cells obtained during first OCV measurement.

	Measured voltage [V]
Cell no. 1	2.97
Cell no. 2	1.34
Cell no. 3	1.67

The literature states that the potential value between the LMNO cathode and the metallic lithium reaches up to 4.7 [V] for the open circuit [9-11]. The obtained values are therefore 2-3 times lower than expected. The probable cause of such a low voltage may be contamination of the cathode or anode material, or to a lesser extent, insufficient contact of the cathode and anode with current collectors. Cell no. 1 has a much higher voltage compared to the others.The result of the first EIS measurement are the impedance spectra listed in Fig. 4.1.2.
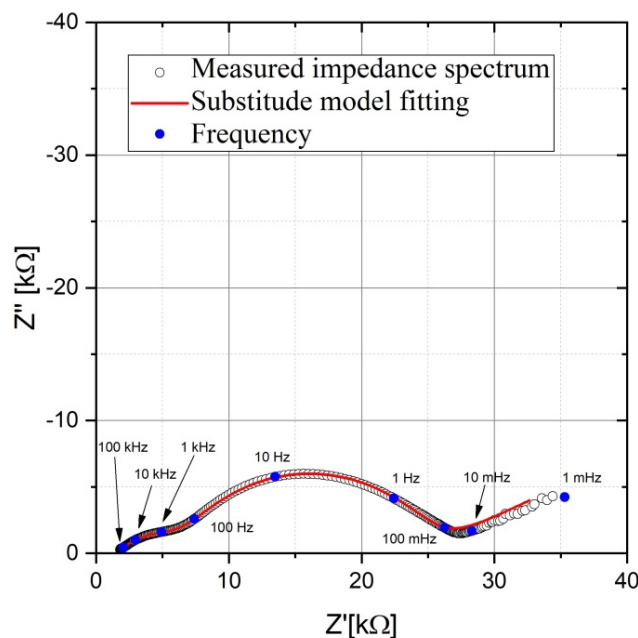
Fig. 4.1.1. An example of matching the equivalent circuit parameters to the measured impedance spectra of cell 1 at the second EIS measurement.

In the high frequency range - near the origin of the coordinate system in Fig. 4.1.2., the shapes of the impedance spectra of cells 1 and 3 are more similar to the spectra typical for lithium cells with liquid electrolyte. Semi-circle impedance responses are in the frequency range 50 kHz - 1 Hz. In particular, two characteristic overlapping half-circles can be seen in the spectrum of cell no. 3. The first one, occurring in the higher frequency range, reflects the resistance and capacity of the SEI (solid electrolyte interphase) layer, while the second one - the charge transfer and double layer capacity. Cell no. 2 has one very distinct semicircle corresponding to anode processes and virtually imperceptible semicircle associated with cathodic processes. Only in cell no. 1 it is possible to notice the "tail" deviated almost by 40 ° in relation to the X axis (theoretical value is 45°) resulting from mass transport in the cell, which describes the substitute element of Warburg. At lower frequencies, measurement errors starts to appear from approx. 10-2 Hz.
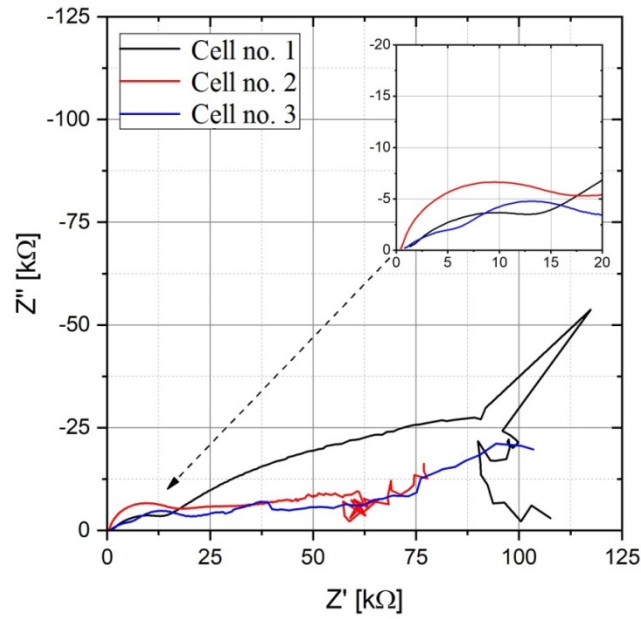
Fig. 4.1.2. Nyquist plot for first EIS measurement for cells no. 1;2;3.

Fig. 4.1.3. Impedance module as a function of frequency (upper graph) and theta angle as a function of frequency (lower graph) – Bode plots for first EIS measurement.

Tab. 4.1.2. Equivalent circuit parameters adjusted to the impedance spectra of cells. C1_1 means Cell no. 1, first measurement.

	Rs [Ω]	CPEf-T [Fcm^{-2}s^{P-1}]	CPEf-P	Rf [Ω]	Cdl-T [Fcm^{-2}s^{P-1}]	Cdl-P	Rct[Ω]	Wc-T [Fcm^{-2}s^{P-1}]	Wc-P
C1_1	1231	9,09·10^{-7}	0,5642	11363	2,47·10^{-5}	0,4455	1,32·10^5	5,02·10^{-4}	0,2932

Error [%]	0,64	2,19	0,45	0,95	0,37	0,64	1,31	-	-
C2_1	298,8	$4,01 \cdot 10^{-8}$	0,8646	15120	$1,30 \cdot 10^{-5}$	0,4419	44824	$5,49 \cdot 10^{-4}$	0,5
Error [%]	4,51	7,90	1,08	2,20	3,17	1,91	2,22	5,76	-
C3_1	760,9	$1,02 \cdot 10^{-5}$	0,6305	15588	$2,61 \cdot 10^{-6}$	0,5228	5407	$3,26 \cdot 10^{-4}$	0,5
Error [%]	3,24	2,73	2,28	3,20	10,44	2,26	5,99	4,46	-

On the basis of the above diagrams and parameters' values in Tab. 4.1.2., there are significant differences between the resistance of individual processes taking place in the cells. For the resistance Rs being the internal resistance of the cell, the determined value of 1231 Ω for O1_1 is four times greater than that for O2_1 (298.8 Ω). An even greater discrepancy can be observed for the resistance value Rct, which reflects the load transfer resistance. The smallest value (5407 Ω) was fitted for cell no. 3, which is 24 times smaller than the resistance value for cell no. 1 ($1.32 \cdot 105 \ \Omega$). However, the direct comparison of resistances is not reliable, since analyzing the course of the impedance module as a function of frequency (Fig.4.1.3.) the differences between the cells are 3 - 4 times the highest value in relation to the smallest. Such disparity may support the creation of a better quality electrolyte-cathode interface in cells no.2 and 3, as it is of key importance during the charge transfer process. The resistance of the passivation layer Rf is the smallest for cell no. 1 (11363 Ω) and it does not deviate too much from the value assigned to the other cells. The angular characteristics of the Bode plot (Fig. 4.1.3.) allow to note that for the frequency of $2 \cdot 10^5$ Hz in cell no. 1 and 3 there were some difficult to identify side processes, represented by small arcs. At a frequency close to 10^4 Hz, the spectrum characteristic for the resistance and capacity of the anodic passivation layer was formed in all the cells (most clearly visible for cell no. 2). For cell no. 3 another arc associated with the charge transfer resistance and double layer capacity is visible at 10 Hz, while for cell no. 1 at 1 Hz. At this stage, it is difficult to clearly indicate which of the tested cells is significantly better than the others.

In the next step, two cycles of cyclic voltammetry were performed, the results of which are presented in Fig. 4.1.4. All curves differ significantly from those typical for electrochemical cells. It can be assumed that the voltammetric curve of cell no. 1 tends to create a peak that would be at a higher potential. When the 4.9 V potential is reached, the current reaches its maximum and then starts to decrease with the voltage drop. A faster rate of current growth is visible than the rate of its subsequent decline. For cells no. 2 and 3 scan 1 starts with a higher current than the one obtained for the voltage of 4.9 V. Scans 2 of these cells show a very small increase in current from the voltage of 3.5 V to 4.9 V, and then its decrease (in the cell 3 the current change for this range of potential is virtually unnoticeable, the resistance is too high).
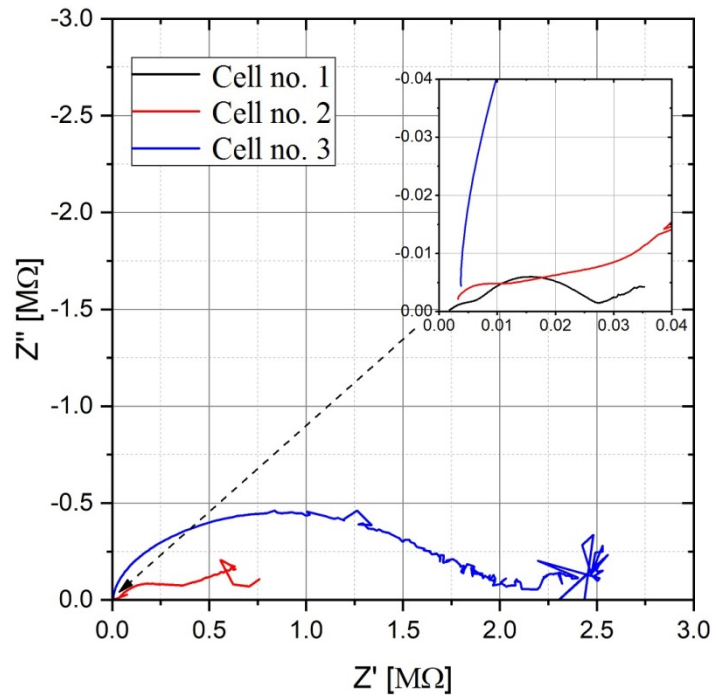
Fig. 4.1.4. Collation of voltamperograms from two cycles of measurements using the CV method.

It is assumed that in the first cycles of charging / discharging the transport of charge between the electrodes can cause morphological changes in the structure of materials and the formation of new passivation layers. The possible effects of these processes can be seen in Fig. 4.1.4.due to the discrepancy between the scans and the impedance diagrams for fresh cells. Perhaps the cell housings were unsealed, which could have caused changes in the materials from which the cells were made.
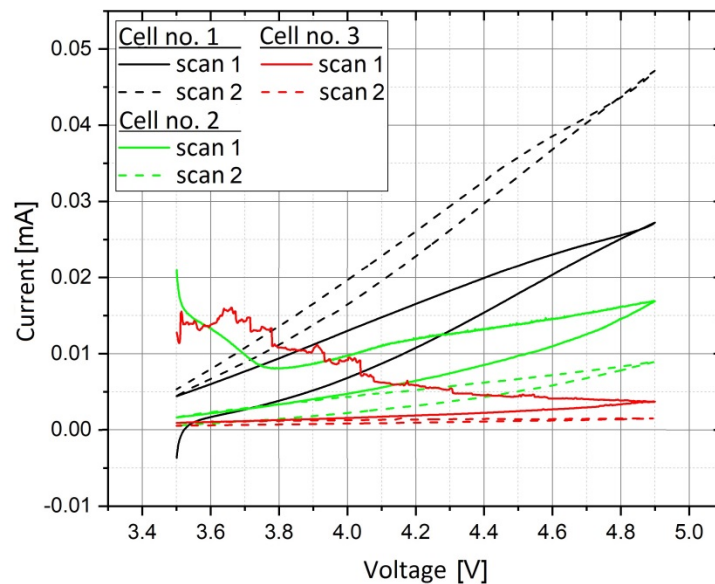
Fig. 4.1.5. Nyquist plot for second EIS measurement for cells no. 1;2;3.

In cell no. 1, the voltage increased slightly compared to the first OCV measurement, while for cells 2 and 3 it decreased to around 0 [V].

Tab. 4.1.3. Voltage of cells obtained during second OCV measurement.

	Measuredvoltage [V]
Cell no. 1	3.11

Cell no. 2	0
Cell no. 3	0
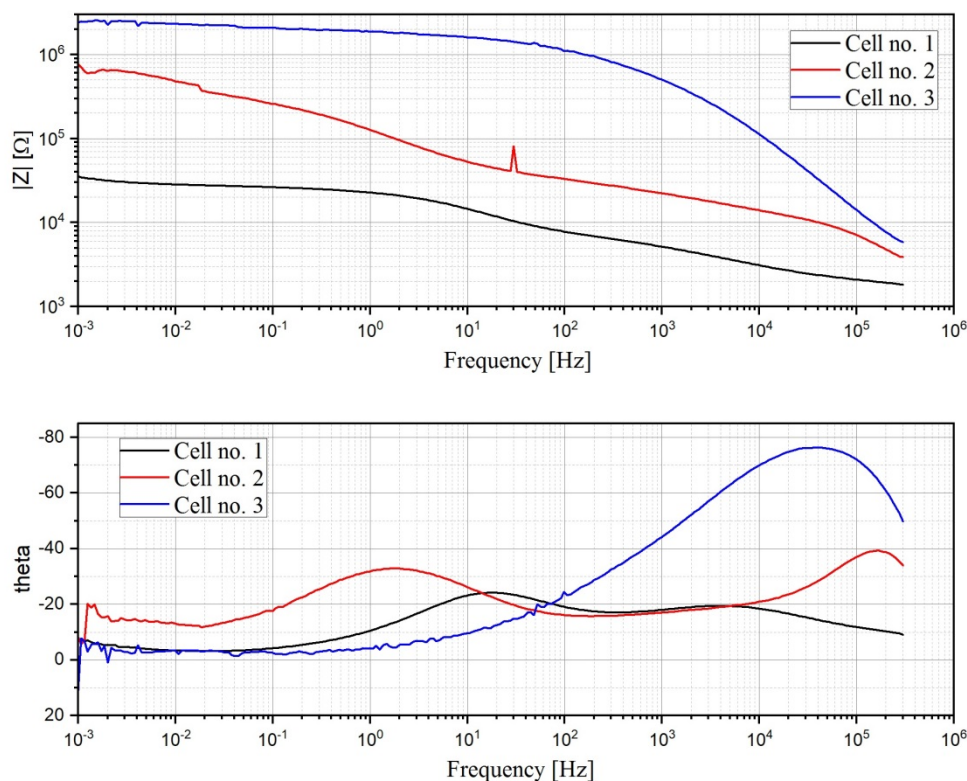
Fig. 4.1.6. Impedance module as a function of frequency (upper graph) and theta angle as a function of frequency (lower graph) – Bode plots for second EIS measurement.

The impedance spectra obtained during the second measurement of EIS are significantly different from those obtained for fresh cells. The graph from Fig. 4.1.6.shows a large increase in the impedance of the cell no. 3, which module reaches values of the order of MΩ at the frequency of 10^2 Hz (for the fresh cell it was 6 kΩ at 10^2 Hz). It is also difficult to identify individual processes in this cell because the spectrum consists of one large arc and significant measurement errors at the end. The spectra of cells no. 1 and 2 consist of overlapping semi-circles in the frequency range 10^5-1 Hz, and in cell no. 2 three processes can be distinguished represented by three half-circles occurring at frequencies $2 \cdot 10^5$, 2000 and 2 Hz visible in Fig. 4.1.6. Impedance spectrum of cell no. 1 definitely best suits the typical shape of the lithium cell spectrum. Its semi-circles symbolizing the resistances and capacities of individual processes are more distinct and occur in similar frequencies as in the first measurement. It is noticeable that the characteristic deviation of its curve in the low frequency range and the lack of measurement errors.
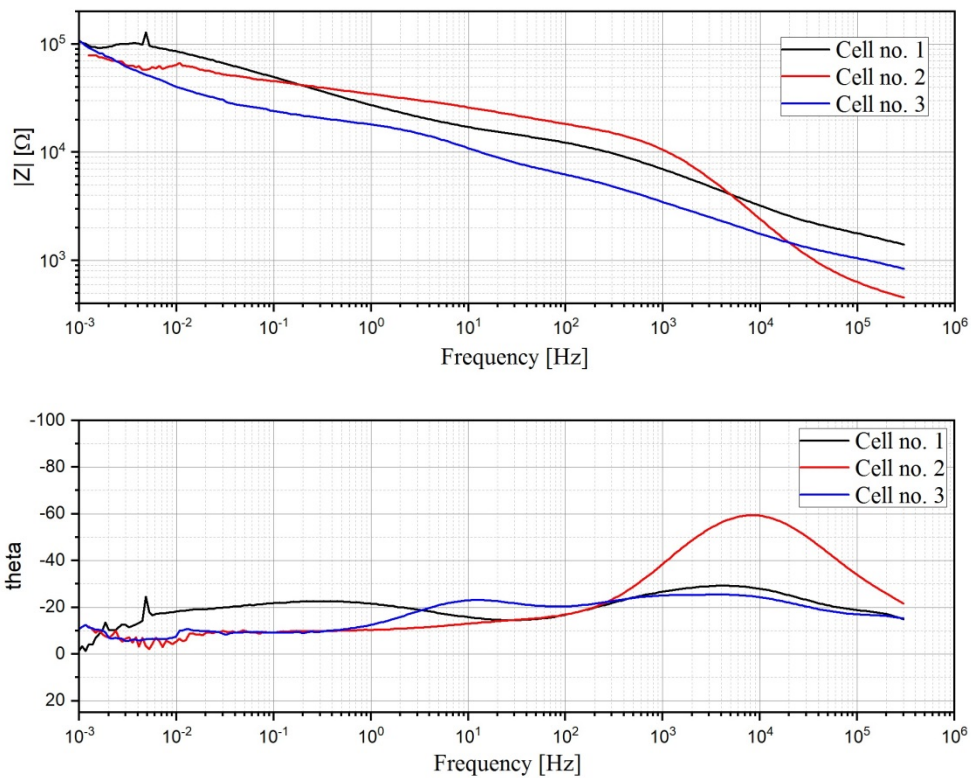
Tab. 4.1.4. Equivalent circuit parameters adjusted to the impedance spectra of cells for second EIS measurement.

	Rs [Ω]	CPEf-T [Fcm^{-2}s^{P-1}]	CPEf-P	Rf [Ω]	Cdl-T [Fcm^{-2}s^{P-1}]	Cdl-P	Rct[Ω]	Wc-T [Fcm^{-2}s^{P-1}]	Wc-P
C1_2	1682	1,25·10^{-6}	0,5448	5229	4,25·10^{-6}	0,7106	17873	5,02·10^{-4}	0,2932
Error [%]	1,26	6,87	1,36	2,17	1,73	0,79	1,36	6,47	3,42
C2_2	1822	4,14·10^{-10}	1	5331	2,75·10^{-6}	0,6138	3,48·10^5	1,38·10^{-4}	0,5

Error [%]	4,53	3,03	-	2,76	0,59	0,52	0,72	-	-
C3_2	1851	$4,72 \cdot 10^{-10}$	0,9203	567870	$1,13 \cdot 10^{-8}$	0,7365	$1,41 \cdot 10^{6}$	$1,63 \cdot 10^{-5}$	0,5
Error [%]	11,60	13,76	1,95	8,45	7,36	2,96	3,79	5,50	-

The internal resistance of cells represented by the Rs element in the equivalent circuit for all cells assumes a similar value, the maximum difference is about 160 Ω. However, they are larger than those measured at the first EIS measurement, the largest increase in resistance Rsis for cell no. 2 and equals 1523.2 Ω. The resistance of the passivation layer Rf for cells no. 1 and 2 is similar (approximately 5300 Ω) which corresponds to a 2-3 times decrease in relation to the first measurement. In cell no. 3, the Rf element reaches the value of 568 kΩ, which significantly differs from the others. The charge transfer resistance Rct for cell no. 1 is the smallest (17873 Ω) while for cells no. 2 and 3 it has increased tremendously to the value of $3.48 \cdot 10^{5}$ and $1.41 \cdot 10^{6} \Omega$ respectively.

For the purpose of projection the impedance spectrum of cell no. 2, it was necessary to modify the previously adopted equivalent circuit. Between resistance RC and RCf additional element of resistance RCct was added in series. It reflects an additional sequential occurrence at the frequency of 2000 Hz, which can be observed in the diagram of Bode from Fig. 4.1.6. as a small convexity between neighboring arches. The determined parameters of this resistance are: $R_{f2} = 24055 \Omega$, $CPE_{f2}\text{-}T = 3.93 \cdot 10^{-7}$ [$F \cdot cm^{-2} \cdot s^{P-1}$] and $CPE^{f2}\text{-}P = 0.5126$.

Both the Bode charts from Fig. 4.1.3. and 4.1.6. and the data in Tab.s 4.1.2. and 4.1.4. show that cell no. 1 exhibits the most favorable electrochemical parameters compared to the others. It is the only cell in which positive changes in electrochemical properties have been observed along with CV measurement. Its own resistance Rs slightly increased from 1231 Ω to 1682 Ω, while the resistance of the anodic passivation layer Rf decreased from 11363 Ω to 5229 Ω, and the resistance of the charge transfer Rct from $1.32 \cdot 105 \Omega$ to 17873 Ω. The value of its impedance module dropped three times in the low frequency range compared to that before CV measurement and is significantly lower in the entire frequency range compared to other cells (Fig. 4.1.6.) However, it is necessary to identify such huge changes in electrochemical properties of cells no. 2 and 3to be able to present reliable conclusions.

5.   Identification of reasons for discrepancies in results.

In order to visually check the condition of the cells, it was decided to disassemble the housings and remove the cells from them. This was done on the laboratory Tab. in the atmospheric air. In cell no. 1 and 2, a white powder deposited on the current collector was observed as a residue of the metallic lithium anode. No more detailed analysis of this substance is shown in Fig. 5.1. Compounds that can be formed from metallic lithium when in contact with atmospheric air are mainly LiO_2, $LiOH$ and $LiCO_3$. The presence of this powder indicates the contact of the lithium anode with oxygen contained in the air, thus leaks in the cell housings are probable. No special changes were observed on the cathode side of any of the cells. In cell no. 3, the metallic lithium anode looks as if it has been covered with a rust-colored substance and visible mechanical damage of the cell in the form of cracks in the layer of dense electrolyte substrate.

The leakage in cell housings is considered the most probable cause of oxidation of the metallic lithium being an anode in the cell. In the event that the metallic lithium is oxidized and forms a chemical compound, a further oxidation reaction, the product of which are Li^+ ions and electrons is impossible. This is equivalent to the inability to generate an ionic current in the cell in order to obtain electron current in the external circuit. In this situation, the cell loses its electrochemical energy storage properties and is useless.
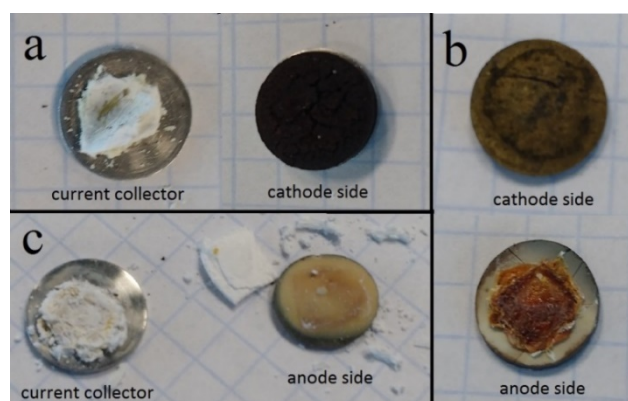
Fig. 5.1. Visual examination of the cells after removal from the casings in the air atmosphere a) cellno. 1: white powder (residue after lithium anode) collected from the current collector and cathode side, b) cellno. 3: cathode and anode side, c) cell no. 2: white powder (residue from lithium anode) collected from the current collector and the anode side.

6. Conclusions

In this work, an attempt was made to create a electrolyte-cathode interface in all-solid-state cells using one of the interface engineering methods and analysis of cells' electrochemical properties was done. There are several important stages of work that have had a decisive influence on the final result of the research. The first of these was the successful synthesis of the pure compound $La_{2/3-x}Li_{3x}TiO_3$, from which one-sided porous pellets constituting the electrolyte material of the cells were successfully produced. Next, the $LiNi_{0.45}Cu_{0.05}Mn_{1.5}O_4$ cathode precursor was synthesized by sol-gel method and attempts were made to impregnate it into porous electrolyte substrates, which were subsequently heated to produce the desired electrolyte-cathode interface. Cells were constructed by applying a separator and a metallic lithium anode to the dense side of the electrolyte pellet and they were locked in a special housing enabling electrochemical measurements. To the impedance spectra obtained, anequivalent circuit was selected, on the basis of which the obtained cells were compared and their electrochemical properties were analyzed: open-circuit voltage measurement (OCV), impedance spectroscopy (EIS) and cyclic voltammetry (CV). Cell no. 1 showed the most favorable parameters of work in relation to the others and the course of its impedance spectrum was closest to the typical spectrum of lithium cells. In addition, favorable changes in electrochemical properties were observed on the basis of impedance spectra obtained before and after the cyclic voltammetry test. For these reasons, it can be treated as a reference cell. Probably the unsealing of its housing was so small that during the research most of the anodic material was not destroyed yet, which affected the measurement results. This work illustrates how the purity of the materials being prepared and the individual construction stages can affect the final properties of the cells produced. It was shown that the lack of contact of the cathode precursor with oxygen during its synthesis caused a decrease in impurities in the final cathode material. From the point of view of mechanical strength, the pressing process is of great importance, as it was often found that the uneven distribution of material on the basis of the press die resulted in cracking and deformation of the pellets after baking in the oven. Maintaining the final cells in a sealed housing is crucial to ensure its long-term work and prevent degradation of materials.

Acknowledgment

References

[1] W. Liu, M.-S. Song, B. Kong, Y. Cui, Flexible and Stretchable Energy Storage: Recent Advances and Future Perspectives, Adv. Mater. 29 (2017) 1603436

[2] J. Janek, W.G. Zeier, A solid future for battery development, Nat. Energy. 1 (2016) 16141

[3] "Energy density", https://en.wikipedia.org/wiki/Energy_density, date of access (20/11/2018)

[4] Y. Wang, W.D. Richards, S.P. Ong, L.J. Miara, J.C. Kim, Y. Mo, G. Ceder, Design principles for solid-state lithium superionic conductors, Nat. Mater. 14 (2015) 1026–1031

[5] C. Sun, J. Liu, Y. Gong, D.P. Wilkinson, J. Zhang, Recent advances in all-solid-state rechargeable lithium batteries, Nano Energy. 33 (2017) 363–386

[6] B. Wu, S. Wang, W.J. Evans IV, D.Z. Deng, J. Yang, J. Xiao, Interfacial behaviours between lithium ion conductors and electrode materials in various battery systems, J. Mater. Chem. A. 4 (2016) 15266–15280

[7] K. Ohara, Y. Kawakita, L. Pusztai, L. Temleitner, S. Kohara, N. Inoue, S. Takeda, Structural disorder in lithium lanthanum titanate: the basis of superionic conduction., J. Phys. Condens. Matter. 22 (2010) 404203

[8] S.R. Narayanan, D.H. Shen, S. Surampudi, a. I. Attia, G. Halpert, Electrochemical impedance spectroscopy of lithium-titanium disulfide rechargeable cells, J. Electrochem. Soc. 140 (1993) 1854–1861

[9] J. Ma, P. Hu, G. Cui, L. Chen, Surface and Interface Issues in Spinel $LiNi_{0.5}Mn_{1.5}O_4$: Insights into a Potential Cathode Material for High Energy Density Lithium Ion Batteries, Chem. Mater. 28 (2016) 3578–3606

[10] M. Kunduraci, G.G. Amatucci, The effect of particle size and morphology on the rate capability of 4.7 V $LiMn_{1.5+\delta}Ni_{0.5-\delta}O_4$ spinel lithium-ion battery cathodes, Electrochim. Acta. 53 (2008) 4193–4199

[11] G. Gabrielli, M. Marinaro, M. Mancini, P. Axmann, M. Wohlfahrt-Mehrens, A new approach for compensating the irreversible capacity loss of high-energy $Si/C|LiNi_{0.5}Mn_{1.5}O_4$ lithium-ion batteries, J. Power Sources. 351 (2017) 35–44

Advantages and development tendencies of HVDC lines

Marcin Dolata

Faculty of Energy and Environmental Protection, Silesian University of Technology,dol.marcin@gmail.com

Abstract

In this paper the author describes the most important advantages of HVDC (High Voltage Direct Current) lines determining their usefulness and tries to assume development tendencies thereof.Growing electric power demand results in the need of modernizations in energy industry. Among others, transmission sector requires new investments.In terms of bulk power transmission over long distances or submarine connections the HVDC technology is usually a reasonable and profiTab. choice. First, advantages of HVDC lines over traditional HVAC(High Voltage Alternating Current) lines were described,which among others include asynchronous AC networks integration capacity, power flow control, transmission energy losses and right-of-way width. Furthermore, development tendencies of HVDC lines were assumed. First one is a Light technology developed by ABB company which uses VSC converters and cables with insulation extruded from modified cross-linked polyethyleneXLPE-DC. The second is an idea of extensive, meshed HVDC grid which can enhance renewable energy sources utilization and international power trade.

Keywords:energy transmission; high voltage; HVDC.

1. Introduction

The increasing consumption of electricity is a serious challenge for contemporary energy industry. The future of the electricity productionrelies onimprovement of renewable energy sources utilization and the gradual decommissioning of generation units using fossil fuels combustion technologies. Theelectric power transmission sector must also undergo expansion and modernization in the coming years. HVDC lines with their excellent performance are more and more often an optimal choice for large scale investments.

HVDC transmission systems have unique features, thanks to which their construction is often from the technical point of view the best, and in some cases even the only possible solution. Examples of such situations are, among others, systems which enable exchange of power between asynchronous networks or sea connections over distances of hundreds of kilometers. However there are also some drawbacks of HVDC systems, for example big costs of converter stations or generation of harmonics which require expensive filtering devices. Moreover, voltage transformation is impossible for direct current and HVDC circuit breakers technology still needs improvements.

Despite this HVDC power lines have numerous advantages that encourage investors to build them. The choice of HVDC technology in most cases is motivated by economic profitability or technological reasons. The advantages of HVDC over traditional HVAC transmission lines in certain cases are described in following chapter.

2. Advantages of HVDC lines

2.1. Asynchronous networks integration capability

The nominal frequencies of neighboring networks can have different values i.e. 50 Hz or 60 Hz. Moreover, in some countries, such as Japan, both frequencies are used. The technology of high voltage DC lines solves the problem of transferring electricity between asynchronous systems, i.e. systems with different nominal frequencies, and also operating independently with the same frequency. At both ends of the HVDC line there are converter stations. The converters installed in them are made of semiconductor devices capable of withstanding high voltage, such as transistors or thyristors switched by a gate pulse [1]. At the beginning, alternating voltage is changed to DC voltage. Then the energy is transmitted through the direct current line (so-called point-to-point connection) to the second station, where the voltage is changed back to sinusoidal. In some cases the voltage is rectified and alternated to the desired frequency in the same station. This type of solution (so-called back-to-back

connection) is usually an optimal one for integrating neighboring asynchronous networks or covering the needs of customers located near a converter station. The station converting DC to AC thanks to PWM (Pulse Width Modulation) with a sufficiently high transistor switching frequency is able to provide the output alternating voltage with the appropriate quality parameters.

2.2. Simple active and reactive power flow control
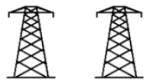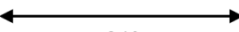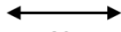
The advantage of VSC (Voltage Source Converter) converters is the ability to quick and easy active and reactive power flows control. High IGBT (Insulated Gate Bipolar Transistor) switching frequency and the use of the PWM modulation method allows almost arbitrarily shape the course of the AC output voltage (with some limitation of the maximum amplitude). As a result, it is possible to control the phase angle and the amplitude of the voltage which determine respectively active and reactive power flowing through the transmission line. Both powers can be controlled independently. HVDC stations made in VSC technology can therefore act as reactive power compensating devices at the ends of the line. In addition, the high switching frequency of IGBT transistors up to 2 kHz reduces the generation of higher harmonics. As a result, VSC terminals require much less space for filtering devices in relation to traditional LCC (Line Commutated Converter) terminals.

Active power control in DC lines contributes to the stability of the system. The ability to immediately adjust the frequency and voltage level allows you to maintain synchronism during transient states. When combining small systems with larger ones, the high-capacity HVDC line balances the active power and provides support for maintaining the desired voltage and frequency levels.

2.3. Narrow ROW (right-of-way) – smaller visual impact on the environment

High-voltage DC power lines require a narrower ROW (right-of-way) technology belt, compared to an AC line capable of transmitting comparable power. This is an advantage of both overhead lines and DC cables, while for overhead lines this fact plays a much more important role. A narrower stripe of land required by DC lines enables supplying energy where area for transmission towers or cable path is limited, for example by high buildings density [2]. In Tab. 2.1 a comparison of the ROW width for different transmission lines is presented.

Tab. 2.1. Comparison of ROW width for DC and AC overhead lines capable to transmit 6000 MW [2]

Voltage	765 kV AC	500 kV DC	800 kV DC
Number of transmission paths			
Width of ROW	~ 240 m	~ 110 m	~ 90 m

In the case of overhead lines, the narrower right-of-way is associated with smaller dimensions of high-voltage lines and limitation of the visual impact on the environment as well as lower investment costs described in subsequent point.

2.4. Smaller transmission losses – lower exploitation costs

Both overhead and cable high voltage DC lines are characterized by lower power losses compared to AC lines. For both types of lines, the losses are proportional to their length. Total power losses consist of losses in the lines and losses in the converter stations which does not depend on the transmission distance. In HVDC technology, losses in converter stations are bigger than losses in AC transformer stations. It means that only for the relatively long lines the total losses in the HVDC transmission system will be lower than losses in the AC system with the same transmission capacity. Fig. 2.1. presents a comparison of total losses in AC and HVDC transmission systems capable of transmitting comparable capacities.
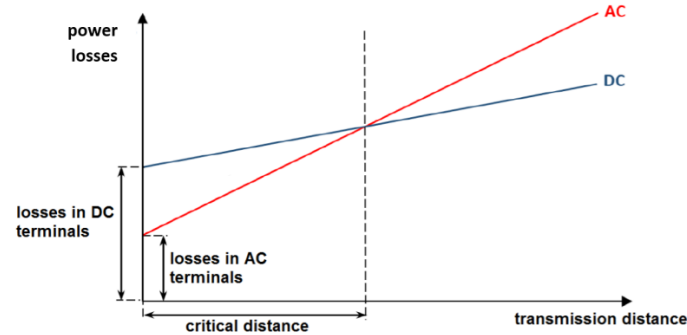
Fig. 2.1. Total power losses for AC and DC technology as a function of transmission distance [4]

In Fig.2.1 the transmission distance above which the total losses in the DC transmission system are smaller than in the AC transmission system is called the critical distance. Value of this distance depends strongly on various factors characteristic for particular case.

2.5. Smaller demand for materials – lower unit costs of overhead line construction

The choice of AC or DC technology is made primarily on the basis of economic analysis. The cost of converter stations which are the key element of HVCD transmission systems may be several times higher than the cost of standard AC transformer stations. The situation is different in the case of unit costs of overhead lines construction. DC high voltage lines require fewer wires. The most common are bundledconductors. Depending on the type of transmission system, one or two wire bundles are required. For comparison, one line of a three-phase AC transmission path always consists of three phase lines.

There is no skin effect at direct current, which means that the conductors have a lower resistance. This results in increased load capacity or reduced cross-section compared to the AC line. A smaller number (and weight) of wires also requires the use of fewer insulators. As a result, the loads that have to withstand the supporting structures, most often steel lattice towers, are reduced [3]. Thanks to this, they can be lighter and their construction requires fewer building materials. HVDC overhead line construction costs are lower than the construction costs of the same HVAC line length with comparable transmission capacity, as shown in Fig. 2.2.
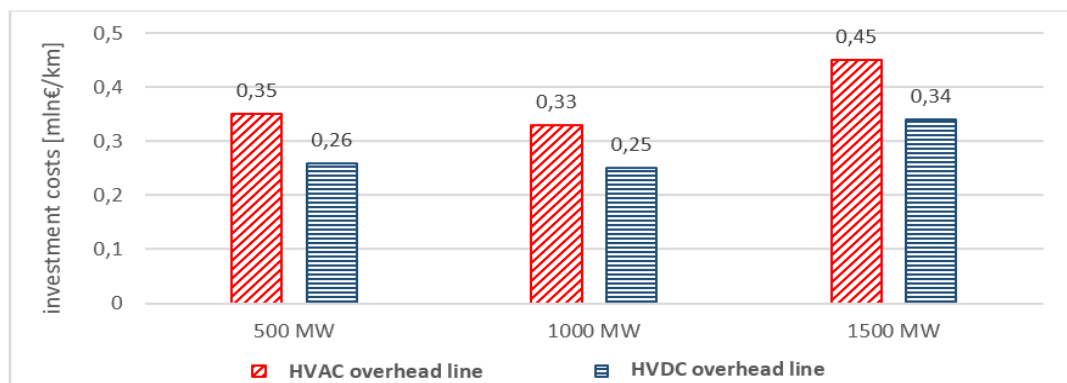
Fig. 2.2. Comparison of investment costs per kilometer for AC and DC technology [5]

The construction costs of DC terminals are much higher than those of AC terminals. However, similarly to power losses, above the certain line length, the total cost of building the HVDC transmission system is lower. It is estimated that for overhead lines this distance is 550÷800 km [1]. It means that this technology is economically viable when it is necessary to transmit energy over long distances.

2.6. Renewable energy sources integration

The energy policy of the European Union puts a strong emphasis on improving energy efficiency and reducing greenhouse gas emissions to the atmosphere. It is assumed, among others to reduce primary energy consumption by 20% by 2020 [6]. Investments in renewable sources are a solution to cover the growing demand for electricity while limiting the use of fossil fuels.

In European countries wind turbines are the most popular among renewable energy sources due to geographical and weather conditions. However, the possibilities of using the potential of kinetic energy of wind on the land may be limited, for example by the terrain shape, the presence of areas covered by the Natura 2000 environmental protection program or strong urbanization. In addition, local communities living in rural areas often protest against the construction of new wind farms near their properties, because of possible noise or negative impact on the landscape.

A good solution to the problems described above is the construction of offshore wind farms. In some countries, such as the Netherlands, it is forbidden to build such installations at a distance of less than 12 nautical miles (approximately 22 km) from the shore in order to eliminate their negative visual impact on coastal territories. In addition, the potential of wind energy at sea is much higher than on land. Excellent conditions in the North Sea and Baltic Sea such as high average wind speed at the height of the wind turbine nacelle and a large number of hours during the year in which the turbine can work with rated power make those areas very useful for obtaining clean wind energy [7].

An another important issue is transmission of energy generated in offshore wind farms to shore and its delivery to the local power system of alternating current. HVDC submarine power cable lines are the perfect solution here. Wind turbines generate alternating voltage with frequency changing over time, which is a result of variable wind speed moving the rotor blade. In order to deliver the generated energy to the AC network, it must be provided with the correct frequency. It is necessary to rectify the generated voltage, and then to use inverter to producesine wave with the synchronous frequency. The converter stations installed on both sides of the DC power line solve this problem.

An example of using the HVDC line to connect large clusters of renewable energy sources with the power grid is the DolWin1 connection. It makes it possible to supply 800 MW of power from the wind farms located in the North Sea to the German transmission network. This system, with a DC voltage of ± 320 kV, is composed of two parallel cables with a length of 165 km (2x75 km of DC submarinecable, 2x90 km of land overhead line). DC cables using Light technology with extruded insulation made of modified cross-linked polyethylene were produced by ABB [8].

2.7. Offshore oil platforms power supply

Supplying power to offshore constructions (so-called power from shore) brings many benefits. The elimination of gas turbines as an electricity generators on the oil platform can reduce noise and vibrations as well as exhaust fumesemissions. Additionally, it reduces the risk of explosion or fire. Electrical installations have fewer moving parts. This is associated with a lower need for maintenance and repair, as well as a smaller number of expeditions for service teams [9]. All this allows to reduce negative environmental impacts, significantly reduce operating costs and increase employees safety.

The HVDC transmission system was firstlyapplied to delivery electricity for object locatedfar away from shore in 2005, when the construction of a two paths cable line in the Light system supplying power the Troll Aoil platformwas completed. This construction was built on the coast of Norway. Four cables with a length of 70 km and a nominal voltage of ±60 kV DC were laid. In 2015, two more lines were commissioned to increase total transmission capacity up to 188 MW [10, 11].

3. Examples of HVDC transmission system applications

3.1. Overhead line –Rio Madeira, Brazil

A good example of investment in which long distance was the main reason for choosing HVDC technology is the record-breaking Rio Madeira connection in Brazil put into use in 2013. The total distance on which electricity is transmitted is almost 2,400 km. This connection makes it possible to meet large power demand of area with huge population using very remote hydropower potential. A 600 kV direct current DC line is capable of transmitting 6,300 MW from hydropower plants located in the north-west of Brazil to the São Paulo city area at the coast of the Atlantic Ocean (Fig.3.1.).

Fig. 3.1. Rio Madeira HVDC overhead line, Brazil [12]

Two back-to-back connections on voltages of 230 kV and 500 kV, with a total capacity of 800 MW, were also implemented close to the power source in order to increase the stability of the local AC network [13, 14, 15]. The advantage of HVDC technology over HVAC for such a long connection consists in reduction of investment costs, transmission losses and the right-of-wayarea, as well as increasing the stability of the system.

3.2. Submarine cable line – NorNed, Norway-Netherlands

The NorNed line connecting the Norwegian network with the Dutch network (Fig. 3.2) is currently the longest cable line in the world, with a length of 2x580 km. Converter stations are located in Eemshaven (Netherlands) and the Feda (Norway).

Fig. 3.2. NorNed HVDC submarine cable line [16]

The connection consists of marine cables with impregnated paper insulation, placed on the bottom of the North Sea. The line is built of two types of cable, depending on the depth − the shallow part was supplied by ABB, while the part laid deeper by Nexans Norway AS. The bipolar system operates with a nominal voltage of ±450 kV DC, and its maximum transmission capacity is 700 MW. The NorNed connection purpose is to connect asynchronous AC transmission networks of both countries in order to enable energy trade, increase the flexibility and reliability of power supply, as well as better use of renewable energy sources, which will reduce carbon dioxide emissions [17].

4.   Expected development tendencies of HVDC lines

4.1. HVDC Light technology

The construction of the high voltage cable and its insulation type depend mostly on the line capacity as well as the environment the cable is laid in. The construction of the submarine cables includes additional layers responsible for protection against moisture and increase mechanical strength. However, DC cables consist of the same components as standard AC cables. It means that considering only the structure of the cable it is difficult to assess to what type of current it is intended for.

A key element in the design of HVDC cables is the insulation system. The basic types of insulation systems are made of paper, paper and polypropylene or are extruded from special type of polyethylene. The insulation thickness is influenced by such factors as the rated voltage level, the estimated values of overvoltages and the ability to change the polarity of the cable line [1].

Extruded insulation used in HVDC cables is made of modified cross-linked XLPE-DC polyethylene. In order to obtain it, the cross-linked polyethylene, used in AC power cables, is modified by adding inorganic fillers. As a result, it is possible to achieve the desired, very good electrical, thermal and mechanical properties, and above all, the tendency to create a space charge in this insulation decreases. Extruded insulation is characterized by more beneficial properties than oil impregnated paper insulation. At the same time, it eliminates the risk of environmental contamination associated with oil leakage, which can occur as a result of mechanical damage to the cable line. This is the reason why cables with extruded insulation are more and more willingly used in submarine cable lines exposed to breaking off by ship anchors.

An important advantage of cables with XLPE-DC insulation is their relatively low weight. This is why the technology of DC transmission systems using cables with extruded insulation made of modified cross-linked polyethylene, developed and patented by ABB, has been called light technology (HVDC Light). Light systems use converter stations made in VSC technology and bipolar system, built of two parallel cable lines with opposite voltage polarity (positive and negative). The bend radius of cable in Light systems is smaller compared to the bend radius of cables using other insulation types. The combination of relatively small mass, high flexibility and high durability considerably extends the possibilities of using DC transmission systems. Transport and laying of a cable line in a light system are less problematic, which results in a reduction of the costs of mentioned operations. The limited mass and bendradius, by reducing the required tensile force, facilitate the installation of both land and sea cables for which smaller vessels can be used. In addition, the lack of oil in the insulation system eliminates the risk of environmental contamination in the event of line damage. All these features make HVDC Light technology more and more used for sea connections, which include connections between countries, island power lines or oil platforms, as well as systems delivering energy from offshore wind farms to power systems. The relatively narrow technological land strip needed and small dimensions of converter stations in Light systems enable their use to power heavily built-up areas, at the same time limiting noise, the presence of electric and magnetic fields and a visual impact on the landscape [1].

4.2. HVDC grids

The hypothetical high-voltage DC network (HVDC grid) consists of a large number of converter stations connected by multiple HVDC lines. The effects of DC network operation (Fig. 4.1. a)) and the solution in which many HVDC point-to-point connections were installed in the AC network (Fig.4.1. b)) would be very similar in practice.
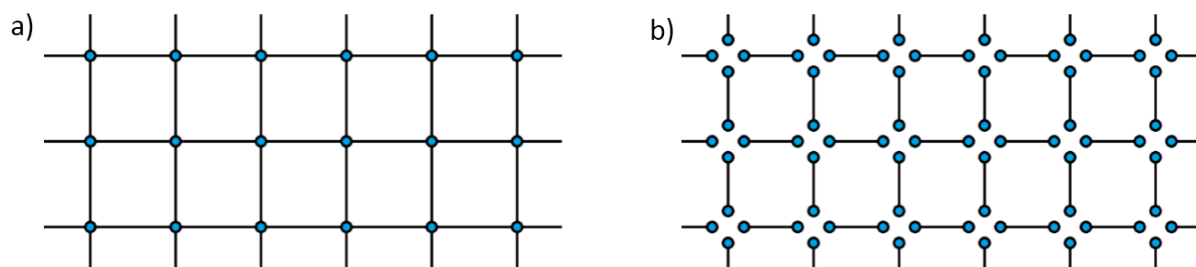
Fig. 4.1. a) HVDC grid; b) numerous point-to-point connections; blue points represent converter stations [18]

In the case of the solution from Fig. 4.1. b), all power flowing through the given line must be converted at the beginning and at the end of this line. Connecting more DC lines to a single node, shown in Fig. 4.1a), allows to transfer some of the power (transmitted with DC voltage) through the node without converting it. In this situation, the transmission capacity of the line is not limited by the rated power of the converter located in the node to which the line is connected, but only by the permissible load of lines and switches. This results in a reduction of losses accompanying the conversion process. The losses can also be reduced by the possibility of offloading the overloaded fragments of the overlapping DC and AC networks. At the same time, it involves

reducing the need to oversize installed devices, as well as increasing the reliability of power supply –to a certain extent AC and DC networks are insuring each other [18].

Among the power lines built over the last fifty years, connections using DC technology accounted are only around 2% of all investments. However, HVDC systems are often implemented in developing countries, where the demand for electricity is growing at a rapid pace. It is often necessary to send large powers over very long distances. In highly developed countries connections allowing better use of renewable energy, increase energy security and facilitate cross-border trade in electricity need to be provided [18]. The proposal of the HVDC network enabling the effective use of the potential of renewable energy sources in Europe, North Africa and the Arabian Peninsula is shown in Fig. 4.2.

Fig. 4.2. Idea of extensive HVDC grid integrating remote renewable energy sources [19]

An alternative to HVDC systems is the construction of a larger number of parallel AC overhead lines, which is unprofiTab., and often unfeasible due to the surface that would be occupied by such corridors. Problems related to the construction of new AC lines can be eliminated by modernizing existing lines by changing the type of voltage from alternating to direct. It is connected with the necessity to build converter stations and therefore high investment costs, but it allows to increase transmission capacity without the need to build new lines. Another solution is the construction of underground cable lines. In this casewhile, considering long distances,HVDC cable technology is the only possible solution. The need to build numerous new transmission "corridors" and obstacles in the construction of an alternating current lines such as long transmission distances, difficulties in obtaining permits for the construction of overhead lines and problems with the use of AC lines for sea connections encourage to consider the construction of DC transmission network as a solution corresponding to the existing and future needs of electricity consumers [18].

Before implementing a HVDC network, a full analysis of its feasibility and profitability must be carried out. Choosing the right configuration and obtaining the necessary arrangements and standardization will certainly be a very long-lasting process, requiring international cooperation at the technical and political level. The creation of a fully functional, complete (according to the initial assumptions) DC network can take several decades. The topic of constructiona DC network has been discussed for years at scientific conferences, considering available technologies in terms of usefulness in the context of the DC network and pointing out issues that must be subjected to further research and analysis.

5.   Conclusions

The growing demand for electricity creates a need for new energy corridors capable of satisfying the requirements of customers. In addition, modern regulations put a strong emphasis on protecting the natural environment and landscape, as well as reducing the emission of harmful exhaust components, better use of renewable energy sources and increasing energy efficiency - both in the manufacturing and transmission sectors.

HVDC transmission systems, thanks to their numerous advantages, are a solution that meets the requirements set for new and modernized power grids.

Several decades of HVDC lines tradition performed very positive operating experience. Thanks to the benefits of using them, they are gaining increasing popularity around the world. Therefore, the need to develop technologies used in high-voltage DC power lines becomes a natural issue.

One of the biggest breakthroughs in the history of DC transmission systems was the development by the ABB company of HVDC Light technology, using VSC transistor converter stations and DC cables with insulation extruded from modified XLPE-DC cross-linked polyethylene. Further development of this technology is expected, aimed at achieving higher transmission capacities (raising the voltage level), increasing the stability of the power system, reducing energy losses and negative conversion effects (such as generation of higher harmonics) on the AC transmission and distribution network.

Improving HVDC technologies, an increasing number of point-to-point connections as well as the requirements set for contemporary and future networks may in consequence lead to a situation when the construction of a large meshedHVDC gridwill be a suiTab. and cost-effective solution. Furthermore, in-depth study of this issue is expected due to the huge amount of work related to the preparation of appropriate regulations and the development of devices used in HVDC systems.

References

[1] Rakowska A., Linie kablowe prądu stałego. Zagadnienia wybrane, Wydawnictwo Politechniki Poznańskiej, Poznań, 2011.

[2] Heyman O., Weimers L., Bohl M.L., HVDC – A key solution in future transmission systems, in: World Energy Congress, Montreal, Canada, September 2010, p. 1-16.

[3] Kamrat W., Szczepański T., Wybrane zagadnienia budowy i eksploatacji sieci przesyłowych najwyższych napięć, Energetyka, 2009, nr 10.

[4] http://new.abb.com/systems/hvdc/why-hvdc/economic-and-environmental-advantages (03.12.2018).

[5] Voltage Source Converter (VSC) HVDC for Power Transmission – Economic Aspects and Comparison with other AC and DC Technologies, CIGRE WG-B4.46, Technical Brochure 492, April 2012.

[6] https://www.ure.gov.pl/pl/urzad/wspolpraca-miedzynarod/inne-akty-prawne-ue/4940,Dyrektywa-w-sprawie-efektywnosci-energetycznej.html (03.12.2018).

[7] Europe's onshore and offshore wind energy potential, EEA Technical report, No 6/2009, s. 32-34.

[8] ABB hands over Germany's DolWin1 offshore wind energy link, ABB press release, 28 July 2015.

[9] More sustainable power solutions for oil and gas, ABB press release, 15 March 2015.

[10] Troll A. Power from shore, broszura ABB, 2015

[11] Callavik E.M., Lundberg P., Bahrman M.P., Rosenqvist R.P., HVDC technologies for the future onshore and offshore grid, CIGRE Symposium Grid of the future, USA, 2012

[12] http://new.abb.com/systems/hvdc/references/rio-madeira (03.12.2018).

[13] ABB commissions world's longest power transmission link in Brazil, ABB press release, 27 August 2015.

[14] The world's longest HVDC link – bringing power to millions, ABB press release, 3 November 2014.

[15] Guarini A.P., Quintão P.E.M., Tenório A.R.M., Operational Experience of Madeira River Project in the Brazilian Interconnected Power System under Initial Configuration, in CIGRE Session, Paris, 2014, paper B4-104.

[16] http://new.abb.com/systems/hvdc/references/norned (03.12.2018).

[17] Skog J.E, Koreman K., Pääjärvi B., Worzyk T., Andersrød T., The NorNed HVDC cable link a power transmission highway between Norway and the Netherlands, http://search-

ext.abb.com/library/Download.aspx?DocumentID=9AKK101130D3006&LanguageCode=en&DocumentPartId=&Action=Launch (03.12.2018).

[18]   HVDC grid feasibility study, CIGRE WG-B4.52, Technical Brochure 533, April 2013.

[19]   https://www.siemens.com/press/pool/de/pressebilder/2009/power_transmission/300dpi/soept20091201-04_300dpi.jpg (03.12.2018).

Review of Sustainable Water Desalination Integrated with Renewable Energies

Talal Ashraf[1],Shaheen Aziz[2]

[1]*AGH University of Science and Technology Krakow, e-mail:talal@student.agh.edu.pl*

[2]*Mehran University of Science and Technology Pakistan, e-mail:Shaheen.shaikh@faculty.muet.edu.pk*

Abstract

Water and Energy Scarcity acting a barrier in development, living standards and flourishing life. With abundance of water in nature, desalination is one of the promising technologies for providing poTab. and palaTab. water, But the problem lies in energy intensive nature of process. Primary objective of this review is to determine a clear understanding of cost effective comparison and implementation water desalination technologies with and without coupling to renewable energy sources.Due to environmental constraints and growing demand of renewable, desalination coupled with renewable system can contribute to provide basic necessity of life: water with reduction in carbon footprint and hence reduction in greenhouse gases emission. However different desalination technologies have some limits and dependency on weather and location which makes them more applicable in remote areas. This review suggests that despite of barriers, renewables integrated with desalination have strong potential on a feasible, economic and environmental tolerant aspect

Keywords: Desalination, RenewableEnergy, PoTab. Water, Carbon footprint, Greenhouse gases

1. Introduction

Industrialization and population growth causing an impact on water shortage problems. Almost one third of residents in world are facing water scarcity problems. This can occurs when water supply drops below $1000m^3$ per person per year. In many promising solution, water desalination has a very good impact as 71% of earth's surface is covered with water and only 2.5% of water is fresh/drinkable water. Although desalination is energy demanding process and consumes 10000 tons of fossil fuels to produce 3600000 m^3 of water per year. To decrease greenhouse emissions and carbon footprints, it is vital to implement and integrate sustainable renewable energy sources [1-5]. Huge investment are required for installing a desalination plant which is way more challenging for developing countries. Almost 70% of desalination in world are located in Middle East as they have plenty of conventional fossil fuels and governmental policies which encourage investors for desalination technology implementation. Due to energy intensive process, desalination plant consumes 3-10 KWh of energy which is comparatively high for conventional water plants which consumes 1 KWh for $1m^3$ of water [6]. Globally, Saudi Arabia is utilization desalination technology on very large scale basis through multistage desalination which is quite energy intensive and consumes 10-16KWh/m^3 of water [7-8]. Australia, Europe and USA are utilizing reverse osmosis which consumes 3-4 KWh/m^3 as compared to conventional method which consumes <$0.5m^3$. Estimate, 3.8 kg of CO_2 emitted per desalination of $1m^3$ water. As an example, sea water desalination facility in Sydney utilizing reverse osmosis emitting 954 tons of CO2/day to desalination 250,000 m3/day water. Some desalination technologies are limited to serve centralized systems like reverse osmosis that makes it more economical. Sydney sea water reverse osmosis plant is taking power from national grid which is compensated by producing 132 MW from windfarms in outside location [9-12]. SWRO can be powered by solar energy by photovoltaics. In a joint venture of IBM and King Abdulaziz city of science and technology, a national solar desalination center has been built for desalinating water 30,000 m^3/day by 10 MW of energy consumption through photovoltaic cells [13-14]. Renewable energy market is limited to a large number of constraints related to financial, technical, regulation and lack of experience issues. This makes an implication for adaptability of renewable energy systems at cheap cost. Sometimes due to abundancy of produced energy, it can be either consumed or lost, but with water production through desalination, it will be consumed due to availability of sea water in abundance [15]. Combination of desalination with renewable systems offers a promising and technical feasible system than others. Some combinations are more suited for large scale like reverse osmosis while some are better for small scale units like electrodialysis. Appropriate selection of technology depends on variety of factors which include water quality parameters, availability of energy, plant. Desalination technology is adopted

by several countries, almost 80% of countries are facing water scarcity issues. Thermally driven technologies contributes to 27% of desalination plants exists. Multi stage flash desalination is suited for solar and thermal energy [19]. Development and governing the chain to civilization, water and energy combining plays an utmost role. Shortage of water can significantly impacts the energy availability and vice versa. in these conditions, governmental policy makers trying to focus on ground water recharge and waste water utilization. the main obstacle of desalination is the salinity, the more saline water is, the more energy intensive process utilized which drastically increase cost and water supple resilience of energy. Since, it is found that desalination technology future is chained to environmental impacts and availability of conventional energy sources and cheaper development of renewable energy sources [20-23]

2. Global Desalination Aspects

There are 18,500 desalination plant located in 150 different countries with maximum capacity of desalinating water 99.8 million m³/day. Algeria, UAE, KSA and Spain are dominant in desalination adopting countries. Although, this process is extremely energy intensive but widely applicable for remote areas when there is not any other alternative and for oil abundant countries which have cheap fuels but high poTab. and palaTab. water cost. Recent studies showed that 53% of desalination plant located in Middle East followed by North America, Asia, Europe, Africa as shown in Fig. 1.
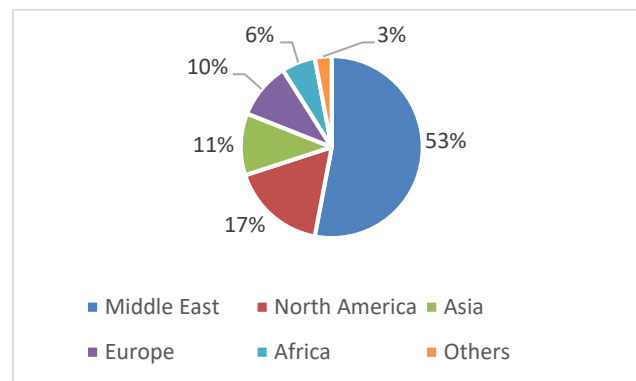
Fig. 1 Desalinationplants worldwide distribution adapted from [48]
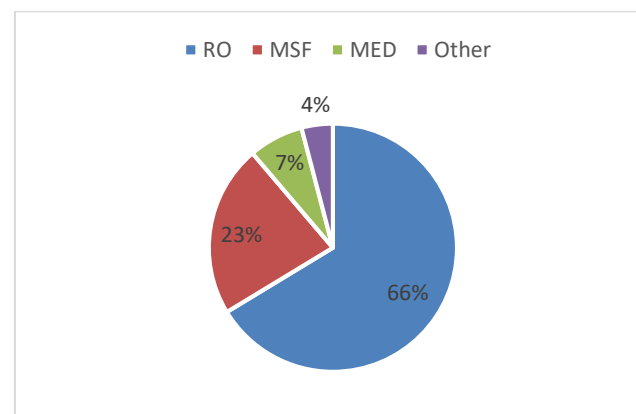
Fig. 2. Desalination systems installed in 2014

According to desalinationtechnology in 2012, RO took an edge for 55% followed by MSF and MED. In 2014, it has been drastically increased to 65% of desalination capacity as shown in Fig. 2. Use of reverse osmosis is rapidly growing because of versatility for both brackish and sea water desalination. In some cases, merging a thermal technology with RO impose a significant increment in efficiency of system. First RO plant was commissioned in Jeddah 1980 for sea water desalination and first hybrid RO and MSF plant was commissioned in Ra AlKhair with capacity if 728 million l/day desalinated water [49-52].Desalination without carbon footprint coupled with renewable sources is an emergingtechnology for poTab. water production. In 2014, desalination systems with renewable energy categorized as shown in Fig. 5. There are several small scale systems are

installed due to minimal maintenance cost, although output is quite negligible as compared to global capacities [53-56]. Solar PV is dominating its share coupling with 43% of total desalination followed by solar thermal and wind as shown in Fig. 3.
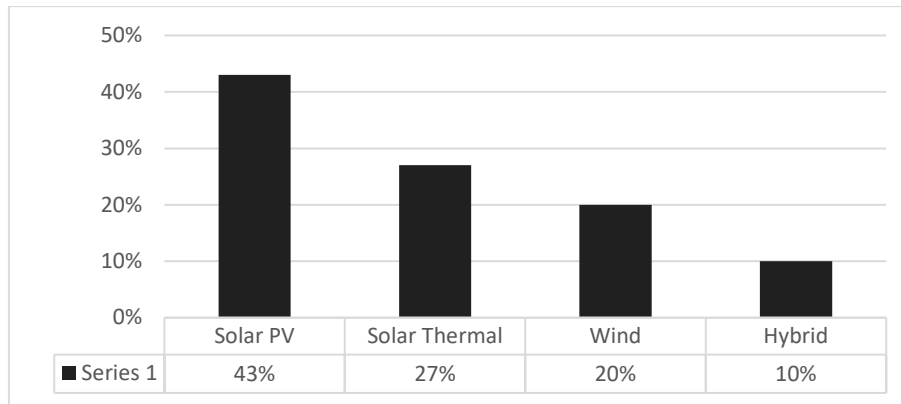
Fig. 5. Global Renewable Energy Desalination 2014

3.   Energy Utilization for Desalination Systems

To remove the dissolved salts from brackish water requires a lot of energy. It can be easily observed by estimating the amounts of conventional fossils fuels burned for producing palaTab. water and also it and poTab.'s contribution towards global warming. Thermodynamically, desalination requires more minimum energy as compared to the theoretical value but system configuration plays a vital role with technology for desalination. Mostly, the treatment units consumes 5 to 26 times more energy in order to desalinate water of 34,5000 ppm salinity with minimum theoretical energy of 0.85 KWh[26-27]. In estimation, 5 ton of crude oil is consumed to desalinate 1000 m3 of saline/brackish water which is able to generate 5000 m3 of greenhouse gases or about 10 tons of CO_2 [24-25].

Tab. 1. Energy consumption in desalination process [57-60]

	Multistage Flash Distillation	Multi Effect Distillation	Thermal Vapor Compression	Mechanical Vapor Compression	Reverse osmosis	Electrodialysis
Typical unit size (m³/d)	50,000-70,000	10,000-35,000	5,000-15,000	100-2500	24,000	145,000
Electrical Energy Consumption (KWH/m³)	4-6	1.5-2.5	1.5-2.5	7-12	3-7	2.6-5.5
Thermal Energy consumption (kJ/kg)	190-390	145-390	230-390	None	None	None
Electrical equivalent for thermal Energy (KWH/m³)	9.5-19.5	11-28	6.5-11	7-12	3-7	2.6-5.5
Total Equivalent Energy Consumption(KWH/m³)	13.5-25.5	11-28	6.5-11	7-12	3-7	2.6-5.5
Water Quality (ppm)	10	10	10	10	200-500	150-500

4.   Desalination Systems Coupled with Renewable Energy

Since last few years, more than 130 renewable energy desalination systems have been adopted and implemented worldwide, which shows a greater trend in RED systems. Various energy systems can be coupled with desalination (solar, tidal, wind and geothermal), but biomass energy system and hydropower are not easy to adopt in water scarce countries. In all renewable solar desalination systems operated in the world, 70% of the plant run by solar energy. Solar harvesting, photovoltaic are most promising technologies in this field. Wind energy is more compatible for coastal areas but it is more attachable to reverse osmosis and electrodialysis because these systems require electricity rather than heat. There are two considerable systems for merging renewable systems to desalination plants, it can be generating and adding electricity to the grid or by direct applications. Thermal desalination using distillation can be done by using geothermal and solar energy. But these proceses are very energy extensive which is reqired for phase phase along with the auxilary electricity for utilities. Solar themral systems are directly corelated to intensity of solar radiations and atmospheric conditions. Thses systems are applicable when low enthalpy energy is available. Instead of limitance of geothermal site, it is most feasible for thermal distillation systems. Solar Systems can be hybridized to reverse osmosis process via Photovolatics. The energy utilization is dependent of the no of solar cell, numbers of ro units and pressure driving pump. Wind energy system can be combined with electrical and mechanical primary energy systems such as RO and MVC [28-36].This technology has more implementation in far island and places with higher altitude, dependent upon weather conditions but stillsuiTab. to combine with desalination systems. Capital cost is dramatically increased, if batteries are utilized. In greek Island 2007, Ro technology is combined with wind turbine with a capacity if 3360m^3/day and providing water to municipality at the rate of $2.02/m^3. Desalination technology coupled with renewable systems impose great impact on future energy and water projects [37-40].Solar Energy is widely applicable for desalination systems both for large and small scale, it can be used as a source for thermal energy or mechanical or electrical energy. It can be implemented via direct methods or indirect methods (TVC, MD, MSF etc). It can also be used as a source of electrical energy by photovoltaics to run reverse osmosis, electrodialysis systems [41-42]. In remote areas where water scarcity is a major issue and unavailability of grid systems, RO coupled with PV is a promising integration. With PV-RO desalination systems of 120m^3/day capacity, the average cost is estimated as $7.98-29/m^3. PV coupled with electrodialysis is a promising technology as it requires DC to power the electrode for initiation of desalination and issuiTab. for various environmental conditions. The applicability of electrodialysis is appropriate of brackish water (1500-3500ppm). Energy requirement via desalination for electrodialysis ranges $16-5.80/m^3. However, if coupled with solar system, it could be reduced to $10.40-11.70/m^3. Due to high brackish water recovery, expensive membrane, excessive energy consumption and huge capital cost, this technology is suffering from economic constraints [43-44]. Another well-known technology Solar thermal multi stage flash desalination can be integrated with thermal and mechanical energy. It utilizes solar collectors (plate, tube, parabolic, dish) to absorb solar radiation and converting it into heat. A new technology of coupling RO with tidal energy resulted in saving 31-47% water cost as comparison to RO systems as feed pressure of tidal RO system is higher than conventional RO systems which would increase life time of plant. But tidal system is mainly depended on periodic motion and phases of moon and sun which effect the rotational force of earth [45].It is the most sTab. and consistent supply of geothermal heat by means of high temperature geothermal fluids. Due to stability of geothermal systems, the water desalinated by this system have high quality. For good operational life tie, geothermal coupled with RO is a cost effective solution for GCC countries[46]. Estimation of $0.73-1.46/m3 rate, a plant in Queensland showed excellent performance with a capacity of 100-100,000 m3/day. Geothermal can also be coupled with MED, a pilot has been working in Greece with a capacity of 80m3/h at the rate of $1.69/m3. Indeed, the applicability of geothermal is valid in particular locations, however, transportation of geothermal fluids or desalinations increases capital costs in those far remote areas[47].

Tab. 2. Energy Requirements in Renewable enrgy Desalination System

	Typical Capacity (m^3/day)	Energy Demand (KWHe/m^3)	Water Production cost (US $/m^3)
Solar Still	<100	Solar Passive	1.3-6.5
Solar MEH	1-100	Thermal 29.6, Electrical 1.5	2.6-6.5
Solar MD	0.15-10	45-59	10.5-19.5

Solar Pond/MED	20,000-200,000	Thermal 12.4 -24.1 Electrical 2-3	0.71-0.89
Solar Pond/RO	20,000-200,000	Sea Water 4-6 Brackish Water 1.5-4	0.66-0.77
Solar CSP/MED	>5,000	Thermal 12.4-24.1, Electrical 2-3	2.4-2.8
Solar PV/RO	<100	Sea Water 4-6 Brackish Water 1.5-4	11.7-15.6 6.5-9.1
Solar PV/EDR	<100	1.5-4	10.4-11.7
Wind/RO	50-2,000	Sea Water 4-6 Brackish Water 1.5-4	6.6-9.0 small capacity 1.95-5.2 for 1000 m^3/day
Wind/MVC	<100	7-12	5.2-7.8
Geothermal/MED	80	Thermal 12.4–24.1Electrical 2-3	2- 2.8

5. Conclusions

Depletion of water and conventional fuel resources causing an alarming situation with greenhouse emissions. Renewable energy mixes with water desalination technologies to enhance the concept of water production using clean energies. This paper addressed some of the significant technologies integrated with water desalination. These innovation coupling are energy efficient and producing no carbon footprint that causes environmental degradation. Significant criteria for such alternatives are experience and maturity of technology at commercial level with availability of sources and local support. PV-RO desalination system is most promising especially in remote areas with no grid connections and it's efficiency can be increased by specialized solar array and angle adjustment. Although, it is light dependent process but it can be continuous operating by attaining solar thermal storage. Despite of geographical restriction of geothermal, it shows great efficiency when combining with desalination technologies to produce high quality fresh water and excess heat. Similar situation with wind energy as it is more suiTab. near to shore side but it could be coupled with other renewable technologies to attain limiting factor of wind energy. To minimize the cost reduction, more work on pilot scale has to been done for hybrid renewables integrated with desalination systems.

Nomenclature

MFD Multistage flash distillation

MEF Membrane effect distillation

RED Renewable energy desalination

References

[1] Wong KV, Pecora C. Recommendations for Energy–Water–Food Nexus Problems. Journal of Energy Resources Technology. 2015; 137(3):32002-7.

[2] Jimenez-Cisneros B. Responding to the challenges of water security: the Eighth Phase of the International Hydrological Programme, 2014- 2021. Proceedings of the International Association of Hydrological Sciences. 2015; 366:10-19.

[3] Rijsberman FR. Water scarcity: Fact or fiction?. Agricultural Water Management. 2006; 80(1-3):5-22.

[4]   Micale G, Cipollina A, Rizzuti L. Seawater Desalination for Freshwater Production. Seawater Desalination: Conventional and Renewable Energy Processes. 2009; 1:1-15.

[5]   Rao SM, Mamatha P. Water quality in sustainable water management. Current science. 2004; 87(7):942-7.

[6]   Al Hashemi R, Zarreen S, Al Raisi A, Al Marzooqi F, Hasan S. A review of desalination trends in the Gulf cooperation Council countries. IntInterdiscip J Sci Res 2014;1:72–96.

[7]   Ghaffour N, Missimer TM, Amy GL. Technical review and evaluation of the economics of water desalination: current and future challenges for better water supply sustainability. Desalination 2013;309:197–207.

[8]   Maurel A. Seawater/brackish water desalination and other non-conventional processes for water supply. 2nd ed. Lavoisier; 2006.

[9]   Lattemann S. Development of an environ impact assessment and decision support system for seawater desal plants (PhD thesis). CRC Press/Balkema; 2010.

[10] Ghaffour N, Reddy KV, Abu-Arabi M. Technology development and application of solar energy in desalination: MEDRC contribution. Renew Sustain Energy Rev 2011;15:4410–5.

[11] Mahmoudi H, Saphis N, Goosen M, Sablani S, Ghaffour N, Drouiche N. Assessment of wind energy to power solar brackish water greenhouse desalination units – a case study. Renew Sustain Energy Rev 2009;13:2149–55.

[12] Ayoub GM, Malaeb L. Developments in solar still desalination systems: a critical review. Crit Rev Environ SciTechnol 2012;42:2078–112.

[13] Al-Harbi O, Lehnert K. Al-Khafji solar water desalination. In: The Saudi international water technology conference 2011, and KACST website

[14] GWI. Solar solutions point Saudis towards RO, www.globalwaterintel.com, Middle East, December 2012. p. 8.

[15] Desalination guide using renewable energy sources. JOULETHERMIE;1998.

[16] E. Tzen and R. Morris, Renewable energy sources for desalination, Solar Energy, 75 (2003) 375–379.

[17] J. Rheinländer, E. Perz and O. Goebel, Performance simulation of integrated water and power systems—software tools IPSEpro and RESYSpro for technical, economic and ecological analysis, Desalination, 157 (2003) 57–64.

[18] E. Mathioulakis, V. Belessiotis and E. Delyannis, Desalination by using alternative energy: Review and state-of-the-art, Desalination, 203 (2007) 346–365.

[19] Dagdas, Performance analysis and optimization of double-flash geothermal power plants, Journal of Energy Resources Technology 129 (2007) 125–133.

[20] KaragiannisIC,SoldatosPG.Water desalination cost literature :review and assessment.   Desalination 2008;223(1–3):448–56.

[21] Blanco J,MalatoS,Fernández-IbañezP,AlarcónD,GernjakW,Maldonado MI. Review of feasible solar energy applications to water processes. Renew Sustain EnergyRev2009;13(6–7):1437–45.

[22] GrubertE,StillwellA,WebberM.Where does solar-aided sea water desalination make sense? A method for identifying sustainable sites Desalination 2014;339:10–7. [23] Garcia rodriguez L. Sea water desalination driven by renewable energies :a review.Desalination2002;143:103–13.

[23] SourceOECD (Online service). World energy outlook. OECD/IEA; 2006.

[24] Gude VG, Nirmalakhandan N, Deng S. Renewable and sustainable approaches for desalination. Renewable and Sustainable Energy Reviews. 2010; 14(9):2641-54.

[25] Energy Requirements of Desalination Processes. ⟨http://www.desware.net/ Energy-Requirements-Desalination-Processes.aspx⟩; n.d. [accessed 16.09.15].

[26] Al-karaghouli A, Kazmerski LL. Comparisons of technical and economic performance of the main desalination processes With and Without renewable energy coupling. Proc Am Sol Energy Soc World Renew Energy Forum 2012:1–8.

[27] Hasan E. Desalination Integration with Renewable Energy for Climate Change Abatement in the MENA Region. Recent Progress in Desalination, Environmental and Marine Outfall Systems. 2015; 1:159-173.

[28] Xevgenos D, Moustakas K, Malamis D, Loizidou M. An overview on desalination & sustainability: renewable energy-driven desalination and brine management. Desalination and Water Treatment. 2016; 57(5):2304-14.

[29] Moser M, Trieb F, Fichter T. Potential of concentrating solar power plants for the combined production of water and electricity in MENA countries. Journal of Sustainable Development of Energy, Water and Environment Systems. 2013; 1(2):122-40.

[30] Shatat M, Worall M, Riffat S. Opportunities for solar water desalination worldwide: Review. Sustainable Cities and Society. 2013; (9):67-80.

[31] MA Q, LU H. Wind energy technologies integrated with desalination systems: Review and state-of-the-art. Desalination. 2011; 277(1-3):274-80.

[32] Dorn JG. World Geothermal Power Generation Nearing Eruption. World; 2008.

[33] Council CE. Clean energy Australia report 2014. Economic Analysis and Policy; 2015.

[34] Eltawil MA, Zhengming Z, Yuan L. A review of renewable energy technologies integrated with desalination systems. Renewable andSustainable Energy Reviews. 2009; 13:2245-62.

[35] Huttner KR. Overview of existing water and energy policies in the MENA region and potential policy approaches to overcome the existingbarriers to desalination using renewable energies. Desalination and Water Treatment. 2013; 51(1-3):87-94.

[36] Dehmas DA, Kherba N, Hacene FB, Merzouk NK, Merzouk M, Mahmoudi H, et al. On the use of wind energy to power reverse osmosis desalination plant: a case study from Téns (Algeria). Renew Sustain Energy Rev 2011;15:956–63.

[37] Ma Q, Lu H. Wind energy technologies integrated with desalination systems: review and state-of-the-art. Desalination 2011;277:274–80.

[38] Kondili E, Kaldellis JK Wind energy based desalination processes and plants. In:Proceedings of the Xth world renewable energy congress; n.d. p. 1–7.

[39] Fernández-López C, Viedma A, Herrero R, Kaiser AS. Seawater integrated desalination plant without brine discharge and powered by renewable energysystems. Desalination 2009;235

[40] M. Darwish, H. Abdulrahim, A. Hassan, A. Mabrouk, PV and CSP solar technologies & desalination: economic analysis, Desalin. Water Treat. 57 (36) (2016), 16679–16702.

[41] M.T. Ali, H.E. Fath, P.R. Armstrong, A comprehensive techno-economical review of indirect solar desalination, Renew. Sust. Energ. Rev. 15 (8) (2011) 4187–4199,

[42] Al-Karaghouli A, Renne D, Kazmerski LL. Technical and economic assessment ofPhotovoltaic -driven desalination systems. Renew Energy 2010;35:323–8

[43] Sharon H, Reddy KS. A review of solar energy driven desalination technologies. Renew Sustain Energy Rev 2015;41:1080–118.

[44] C. Ling, Y. Wang, C. Min, Y. Zhang, Economic evaluation of reverse osmosis desalination system coupled with tidal energy, Front. Energy Power Eng. Chin

[45] Loutatidou S, Arafat HA. Techno-economic analysis of MED and RO desalination powered by low-enthalpy geothermal energy. Desalination 2015;365:277–92.

[46] Kalogirou SA. Seawater desalination using renewable energy sources. Prog Energy Combust Sci 2005;31:242–81.

[47] Zotalis K, Dialynas EG, Mamassis N, Angelakis AN. Desalination technologies: hellenic experience. Water (Switz) 2014;6:1134–50..

[48] Renewable energy desalination an emerging solution to close the water gap in the Middle East and North Africa. World Bank. 2012. pp. 1–236.

[49] Greenlee LF, Lawler DF, Freeman BD, Marrot B, Moulin P. Reverse osmosis desalination: water sources, technology, and today's challenges. Water Res2009;43:2317–48

[50] Gude VG, Nirmalakhandan N, Deng S. Renewable and sustainable approaches for desalination. Renew Sustain Energy Rev 2010;14:2641–54

[51] Osman AH. Overview of hybrid desalination systems — current status and future prospects. Desalination 2005;186:207–14.

[52] Ras Al Khair Desalination Plant - Water Technology n.d. ⟨http://www.watertechnology. net/projects/-ras-al-khair-desalination-plant/⟩ [Accessed 14 October2017].

[53] Kalogirou SA. Seawater desalination using renewable energy sources. Prog Energy Combust Sci 2005;31:242–81.

[54] Chaibi MT. An overview of solar desalination for domestic and agriculture water needs in remote arid areas. Desalination 2000;127:119–33.

[55] Goosen MFA, Mahmoudi H, Ghaffour N. Today's and future challenges in applications of renewable energy technologies for desalination. Crit Rev Environ SciTechnol 2014;44:929–99.

[56] Energy Requirements of Desalination Processes. ⟨http://www.desware.net/ Energy-Requirements-Desalination-Processes.aspx⟩; n.d. [accessed 16.09.15].

[57] CLLEEN Water and Power™ Stationary and Mobile Water Treatment Solutions. ⟨http://waterdesalinationplants.com/wp-content/uploads/2012/02/CLLEENdesalination- doc.pdf⟩; n.d.:29 [accessed 16.09.15].

[58] Al-karaghouli AAM. Renewable energy applications in water desalination. In: Proceedings of the 56th annual NM water conference, new water new energy a conference linking desalination and renewable energy; 2011. p. 79–87.

[59] Al-karaghouli A, Kazmerski LL. Comparisons of technical and economic performance of the main desalination processes With and Without renewable energy coupling. Proc Am Sol Energy Soc World Renew Energy Forum 2012:1–8.

Possibilities for biodiesel production using heterogeneous catalysts derived from wastes – A short literature review

Joao Victor de Oliveira Pontes[1], Teresa Grzybek[2]

[1]Affiliation: Student, EIT KIC InnoEnergy Clean Fossil and Alternative Fuels Energy (CFAFE) Master's Program, Akademia Górniczo-Hutnicza im. Stanisława Staszica w Krakowie (AGH)/ AGH University of Science and Technology (AGH UST), e-mail: joaovictorpontes_br@hotmail.com

[2]Affiliation:WydziałEnergetyki i Paliw (WEiP)/ Faculty of Energy and Fuels,Akademia Górniczo-Hutnicza im. Stanisława Staszica w Krakowie (AGH)/ AGH University of Science and Technology (AGH UST), e-mail: grzybek@agh.edu.pl

Abstract

Biofuels can be obtainedvia a chemical reaction, usually, esterification or transesterification, from a broad type of waste materials, such as vegeTab. oils, animal fats or waste frying oils. Its availability is dependent, besides other factors, on national and regional characteristics of agricultural and industrial activities. There are many factors influencing the quality ofproduced biodiesel and still some challenges which have to be met to make it an even more sustainable source of energy. For instance, improvements in purification process that usually apply water, better management of wastes (mainly wastewater and glycerol) and lower costs of reagents are first-hour challenges, still needing innovative ideas and proposals. The application of heterogeneous catalysts instead of homogeneous ones is suggested in order to diminish some of the above mentioned problems, mainly those connected with the purification stage and water consumption. Hence this brief review presents selected results reported in literature regarding the possibilities of the development of heterogeneous catalysts for biodiesel production starting from wastes from different industries, such as energy and power, and iron and steel sectors. This type of wasteis produced in high amounts, and considered a problem that needs to be taken care of.

1. Introduction

The renewable energy industry is growing, reaching more relevant role in local economies and impacting the common citizen day-by-day life. Among the renewable energies available for economically viable use there are wind, solar, hydroelectric, biomass and biofuels (mostly, biodiesel and ethanol).The latter is utilized in connection withgreenhouse emissions problem, as an answer to the arising demands for greener practices and true dedication to environmental protection.

Biodiesel canbe produced from a multitude of oleaginous plants,such soybean, corn, cotton, sunflower, castor bean and palm, but also from wastes, such as beef and swine tallows, fish viscera and waste frying oil (WFO). It should be taken into account, however, that the current methods of biodiesel production using homogenous catalysts lead to high amounts of waste, thus making it necessary to switch to heterogenous catalytic processes. This short literature review deals with new ideas of catalysts for biodiesel production based on waste materials from other types of industry – power and steel.

2. Biodiesel Production

To produce biodiesel, there are two main methods, transesterification and esterification. A typical reaction is illustrated, respectively, by (I) and (II) in Fig. 2.1.The esterification reaction occurs between molecules of fatty acids (FA) and an alcohol, most commonly, ethanol or methanol, producing a Fatty Acid Ethyl (FAEE) or Methyl Ester (FAME) and water, besides some impurities. In the transesterification reaction, triglyceride (TG)and alcohol molecules are substrates, FAEE or FAME are products, and glycerol is a by-product.The first reaction is more suited for very acidic raw materials, which are naturally rich in free fatty acids (FFA), a common characteristic oftallows and WFO, and also very oxidized (degraded) vegeTab. oils.
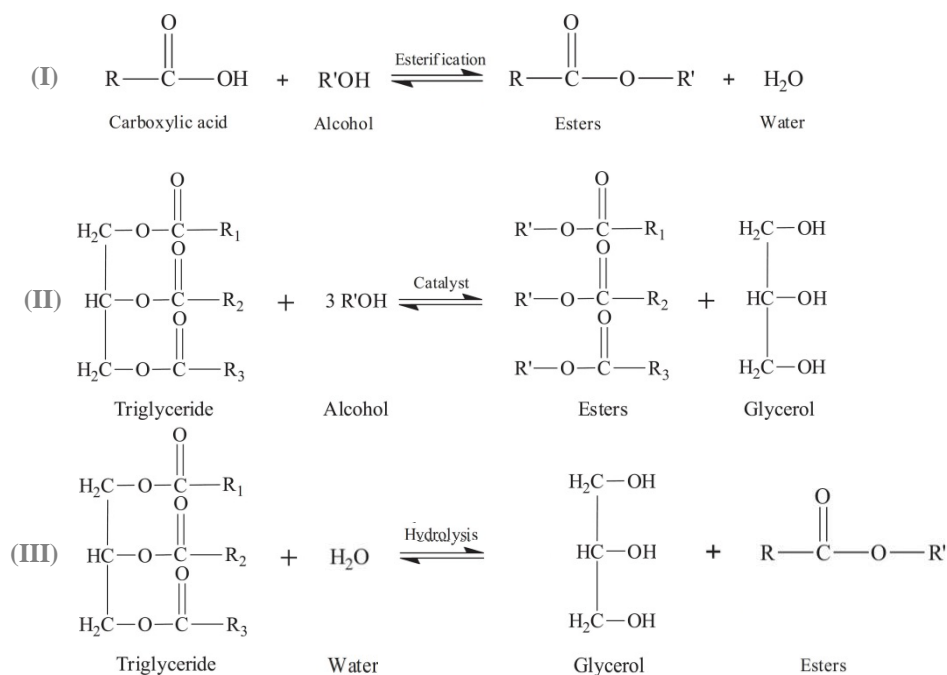
Fig. 2.1. Main reactions in biodiesel production. (I) esterification, (II) transesterification and (III) hydrolysis. Source: PEREIRA *et al.* (2014).

3. Homogeneous versus heterogeneous catalysts – advantages and disadvantages

In biodiesel production bothabove reactions can be carried out with homogenous and heterogenous catalystsaccording to MA and HANNA (1999) andHELWANI *et al.* (2009). The process is described schematically in Fig. 3.1.The homogenous catalysts may be ofacidic, basic or enzymatic type (used in solution) while the heterogenous catalystsare solids with different structures, characteristics and compositions with acidic or basic proprieties[ROBLES-MEDINA *et al.* (2009)]. BERRIOS and SKELTON (2008)also included types such asion-exchange resins and supercritical fluids. Generally, the biodiesel production reactions can be influenced by many factors such as, temperature, time of reaction, amount of catalysts and oil: alcohol ratio, purity of reagents, vegeTab. oil acidity index, mixing and also type of catalysts applied.

According to WRIGHT *et al.* (1944) there are constraints for transesterification reactionsin order to reach high yields using homogeneous alkali sodium hydroxide catalystsregarding the acidity and water contents .The water content needs to be as low as possible (which means high purity of alcohol reagent) and acidity index (related to the amount of FFA) needs to be below 1 mgKOH/ g, as suggested by DEMIRBAS (2002).

Some other authorsclaim thatthe content of FFA should be even more restricted, around 0.5 mgKOH/ g, in order to reach biodiesel conversions near 100 % using different types of alkali metal catalysts, including sodium hydroxide [HARTMAN (1956) as cited in FREEDMAN, PRYDE and MOUNTS (1984)]. On the other hand, ATADASHI *et al.* (2012) and LEUNG, WU and LEUNG (2010) reportedthat the content of FFA could be up to2.5 % in weight of oil.
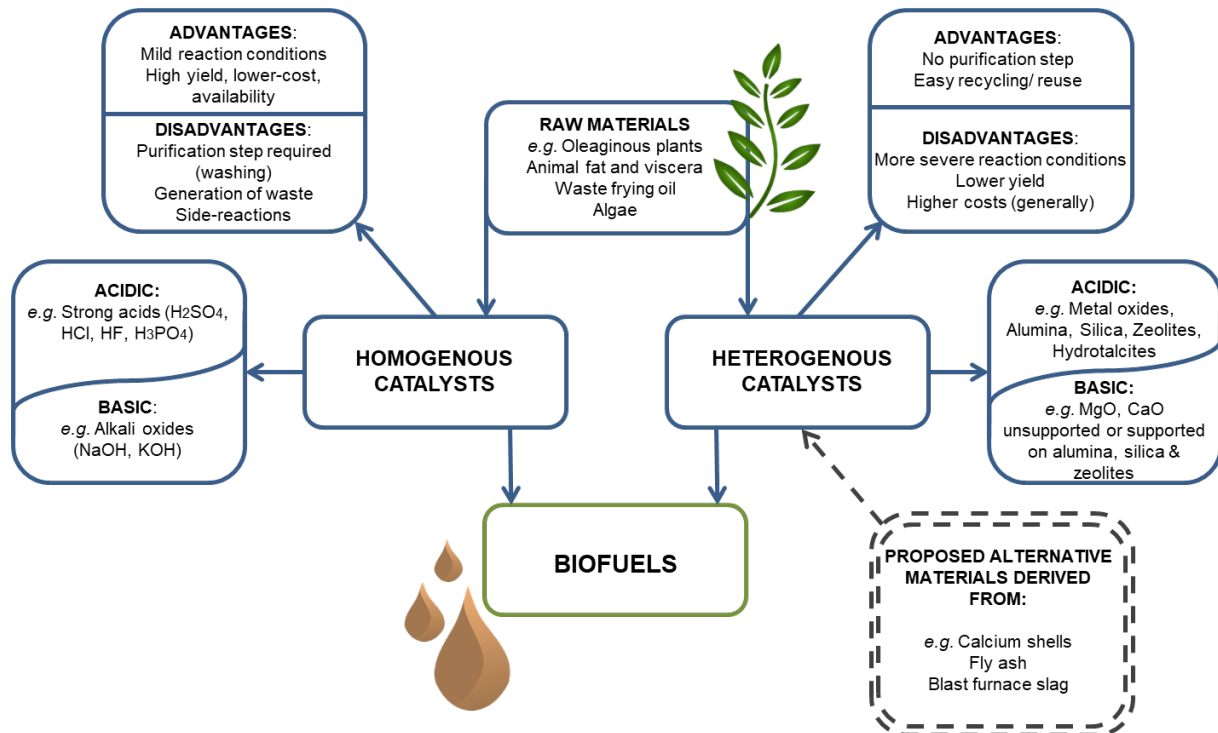
Fig. 3.1. Biodiesel production catalysts – advantages, disadvantages and alternatives. Source: Authors.

Theabove mentioned factors decrease conversion and increase the possibility of occurrence of side reactions, such as production of emulsions and/ or saponification.The most commonly used catalysts for biodiesel production are homogenousalkali catalysts, containing potassium and sodium hydroxides.Theirhigh efficiency in yielding esters under very mild conditions and also its relatively cheap price are advantages, as supported by MA and HANNA (1999), BERRIOS and SKELTON (2008), ATADASHI *et al*. (2011, 2012), and ISSARIYAKUL and DALAI (2014). After the reaction, there is a need, however, to remove substances, such as glycerol, unreacted alcohol, as well as catalysts and sometimes water, which are realized via washing steps using high quality water with low content of salts. This generates considerable amount of waste.

Transesterification can also be catalyzed by acid homogenous catalysts, such as strong acids – sulphuric (H_2SO_4), sulfonic (R-SO_3H), hydrochloric (HCl), fluoric (HF), phosphoric (H_3PO_4), as well as boron trifluoride (BF_3). However, these reactions are slower when compared to those catalyzed by alkali catalysts[SCHWAB, BAGBY and FREEDMAN (1987),MA and HANNA (1999), LEUNG, WU and LEUNG (2010) and ISSARIYAKUL and DALAI (2014)]. Moreover, much more severe operational conditions are required, higher temperatures and longer times.Alsothe cost of catalysts is higher and a demand for a neutralization step exists, which requires huge quantities of water, generating waste and equipment corrosion issues.

After homogenous-catalyzed reactions, a purification step is required in order to separate the ester phase. In transesterification, glycerol, unreacted alcohols and catalysts, sometimes water and impurities, must be removedvia washing step using water to remove all the polar residues. The esterification reaction needs similar purification step in order to remove the unreacted acids and to neutralize the ester phase. So both homogenous-catalyzed reactions produce a huge amount of waste, especially waste water that needs to be properly treated. This is, definitely, one of the biggest disadvantages of the biodiesel industry. To overcome this problem, heterogeneous catalysts have been proposed.

Heterogenous catalysts need to fulfill requirements such as selectivity, high yield of biodiesel, stability, physical characteristics, such asappropriate specific surface area and porosity, as well as economic feasibility. Theadvantages of such catalysts in comparison to the homogenous onesare no emulsions formed, no necessity for a purification step using huge amounts of water, the possibility of recycling (reuse) afterregeneration and aneasy recovery of glycerol. However, the rate of reaction is lower than when using the homogeneous catalysts [LEUNG, WU and LEUNG (2010) and ATADASHI (2012)]. There is also a tendency for leaching, mainly for acid catalysts, and basic catalysts were found to be less suiTab. to oils with high levels of FFA [ISSARIYAKUL

and DALAI (2014) and MANSIR *et al.* (2018)]. Similarly as in homogenous processes, both alkaline and acidic catalysts can be applied in a biodiesel production.

According to SHARMA, SINGH and KORSTAD (2011),acid catalysts are more demanded due to the fact that they are less susceptible to free fatty acids, an argument also supported by ISSARIYAKUL and DALAI (2014), but counterbalanced by the fact that these catalysts have lower activity than the basic ones, thus needing higher temperatures and longer time of reaction. Besides that, acid catalysts produce leachate to the biodiesel, which requires purification procedures and results in waste formation.

Among those found appropriate were metal oxides, of calcium, magnesium, zinc and tin, doped or unpromoted, different sulphated oxides, hydrotalcites(layered-double hydroxides, LDHs), alumina and silica, pure or used as supportsfor different compounds, such as carbonates, oxides and phosphates, or zeolites[MADSEN and FEHRMANN (2011), SOARES DIAS *et al.* (2013), ISSARIYAKUL and DALAI (2014) and MANSIR *et al.* (2018)].CaO based catalysts were found to be especially interesting as they can be obtained eitherat a reduced or even zero cost starting from wastes, e.g. calcium carbonate ($CaCO_3$),from different sources –egg, crab, oyster and mussel shells [MANSIR *et al.* (2018)].

PUNA *et al.* (2010) investigated some solid basic catalysts for biodiesel, such as alumina supported with potassium and calcium, magnesium and aluminum oxides pure and with strontium (Sr). All of them were under some specific pre-treatment (calcination) and results were high conversion (around and above 80 %) for all samples except magnesium oxide with Sr and commercial alumina. When submitted to a regeneration and reuse, pure calcium oxide and CaO doped with lithium showed conversions above 92 %.Other examples are zeolites, and some layered-double hydroxides (LDH) which contain Al and Mg, or hydrocalumites (HC), composed mostlyof Al and Ca.

GOMES *et al.* (2011), DI SERIO *et al.* (2012) and SOARES DIAS *et al.* (2012) investigated the capacity of hydrotalcites (HT) as catalysts for biodiesel production. The first two evaluated pure samples in a batch and a continuous packed-bed reactor and the latter reported results forHT promoted with cerium. The results were promising – 97 % efficiency was obtained in the batch reactor and ca. 80 % in a fixed bed flow reactor and above 90 % for doped HT. On the other hand, ALBUQUERQUE *et al.* (2008) investigated three types of zeolites as supports for calcium oxide for biodiesel production and yields of 65.7 % (castor bean oil) and 95 % (sunflower oil) were reached for the 14 % calcium supported on SBA-15.

4.   Fly ash a starting material for biodiesel catalysts

Some of the heterogenous catalysts mentioned in the previous Chapter may be obtained from waste materials, as discussed above for CaO-based materials. Somecan be also produced from flyash (FA),a waste from combustion processes, among them arezeolites and hydrotalcites.Hence, this waste is being evaluated, according to POLLARD et al. (1992), IYER and SCOTT (2001) and AHMARUZZAMAN (2010)as a raw material suited for many different applications, such asremoval of heavy metals, pesticides, dyes and toxic ions in general, and as an adsorbent for industrial wastewaters, flue gas purification, mine backfill, light weight aggregate and cement construction industries.

Fly ash from coal fired power plants and other industries forms a serious problem where waste is concerned due, primarily, to its extremely high amounts produced all over the world and, specifically, in countries with an energy generation basedon coal.According to IYER and SCOTT (2001), the total amount of coal ash generated around the globe in 1997 was around 600 million tons with 75 – 80 % being fly ash.The use of FA was around 3 – 57 % depending on the country, with an average of only 16 %. Fly ash is classified in two main classes, C and F, according to the type of coal they are derived from and the presence of certain components. Class C (cementitious) are produced by low-ranking coals (usually sub-bituminous) and have high content of silica, alumina and lime (CaO), while class F (pozzolanic) are produced by high-ranking coals (usually bituminous and anthracite) and have high content of silica and alumina, and a very low quantity of lime. The difference in lime content among the two classes is a very relevant point for differentiation and classification.

Fly ashis composed mostly of silica (60 – 65 %), alumina (25 – 30 %) and magnetite,Fe_2O_3 (6 – 15 %), but, depending on the type and amount of feedstock used in the combustion unit, the composition of fly ash can differ [AHMARUZZAMAN (2010)].This is the case of fly ash from biomass combustion and co-combustion of coal

and biomass.   According to MICHALIK and WILCZYNSKA-MICHALIK (2012), the content of silicainstrawand beech ashes is high (> 66 %wt. and ca. 56 %wt.) while it is low for sunflower husk and corn barn ashes (2.4 %wt. and 8.3 %wt.).

The important feature is also the presence of alkalis, such as e.g. K_2O,which is around 27.6 – 31.4 % wt. and 24 – 26.7 % wt.for sunflower and corn barn, respectively. Also calcium oxide content 15.4 – 17.7 %wt. for beech barn ash and above 10 %wt. for straw and corn barn. The content of alkalis, especially of CaO, makes such materials interesting where the preparation of basic heterogenous catalysts for biodiesel production is concerned. On the other hand, high contents of silica and alumina allow preparing zeolites, another type of heterogenous catalysts of interest for biodiesel industry.

This brief literature review aims at discussing reports on catalysts obtained from fly ash from different industries, such as iron and steel, agriculture and energy and power, and studied as catalysts for biodiesel production. Special attention was paid to hydrotalcites and hydrocalumites.Tab. 2.1 summarizes selected preparation details for waste-derived catalysts studied for biodiesel production. The reaction data and the best results from selected reports describing the application of fly ash-derived layered double hydroxides (hydrotalcites) in the production of biodiesel are listed in Tab. 2.2.

KUWAHARA *et al*. (2010) proposed a method based on Blast Furnace Slag (BFS) to produce hydrotalcites, while MURIITHI *et al*. (2017), adapted a similar method to preparehydrotalcites from fly ash. VOLLI and PURKAIT (2015) prepared hydrotalcite-like materials containing magnesium and aluminiumfrom FA and investigatedtheirpotential as basic heterogeneous catalyst for biodiesel production via transesterification reaction.

The latter research was based on the methodology proposed by KONDAMUDI *et al*. (2011). Commercial Mg-Al hydrotalcite (C-HT), fly ash-based hydrotalcite (F-HT) and fly ash-based zeolite hydrotalcite (FZ-HT) were compared as catalysts. The efficiency of converting TG into FAME for all developed catalysts was good. The highest conversion of 93.4 % was obtained for FZ-HT, followed by 90.5 %for commercial (C-HT) and 71.2 % for hydrotalcite prepared from fly ash (F-HT).

It should be mentioned here, that the performance of hydrotalcite-based catalysts can be enhanced by promotion with other compounds, as proven for traditionally obtained materials of this type e.g. bySOARES DIAS *et al*. (2012) whotested the production of soybean-derived biodiesel using a cerium doped Mg-Al hydrotalcite catalyst. Transesterification reaction tests indicated that the doping with cerium increased soybean oil conversion to biodiesel, reaching the levels similar to those obtained with homogeneous catalysts

KUWAHARA *et al*. (2012) proposed a method to produce hydrocalumite catalyst starting from blast furnace slag. The catalyst was tested in soybean conversion. The efficiency of the catalysts depended on the appropriate choice of calcination temperature. Conversion was 0.8, 65.8 or 97.0 % for the sample calcined at 400, 600 or 800 °C, respectively. The sample calcined at 800 °C could be re-used, though with yields decreasing from 95 % for the first trial to 85.7 % and 68.6 % for the second and third trials, respectively

Tab.. 2.1. Selected materials derived from waste, studied as catalysts for biodiesel production. Source: Authors.

Catalyst Nomenclature	Final Catalysts	Origin of Raw Material	Preparation Procedure	Reference
Fly ash-derived hydrotalcite (HT$_{FA}$) Regular hydrotalcite (HT$_{CONTROL}$)	Calcite Hydrotalcite	Class F fly ash (coal-fired power plant)	Acid leaching precipitation	[36]
Mg-Al hydrotalcite (C-HT) Fly ash-based hydrotalcite (F-HT) Fly ash-based zeolite	Amorphous alumina MgO (periclase)	Class F fly ash (Saraca Laboratories Limited)	Co-precipitation	[50]

hydrotalcite (FZ-HT)				
BFS-based LDH (slagHC), Ca–Al–Cl hydrocalumite	CaO Mayenite MgO	Blast Furnace Slag (unclassified)	Acid dissolution Coprecipitation	[26]
CaO-supported fly ash	Dicalcium silicate Mullite Hematite α-quartz	Class F fly ash (coal-fired power plant)	Impregnation	[8]
Sodalite (zeolite)	Mullite Quartz Sodalite	Class F fly ash (coal-fired power plant)	Hydrothermal	[32]

Focusing on other types of residues, CHAKRABORTY, BEPARI and BANERJEE (2010) proposed the production of a low-cost catalyst based onfly ash used as a support for CaO obtained from waste eggshells for transesterification of soybean oil to biodiesel production. The registered conversion was 96.97 %, and the catalyst could be reused in 16 runs. MANIQUE *et al.* (2017) prepared a fly ash-based zeolite (sodalite) heterogenous catalyst for biodiesel production using a hydrothermal method, similarly as proposed by PETKOWICZ *et al.* (2008).

Tab.. 2.2. The performance in biodiesel production of selected waste-derived heterogenous catalysts – feedstock.
Source: Authors.

Catalysts	Feedstock	Qty. of Oil (g)	MeOH/ Oil Ratio	Cat. (%wt.)	Time (h)	Temp. (°C)	Conversion	Ref.
Mg-Al hydrotalcite (C-HT) Fly ash-based hydrotalcite (F-HT) Fly ash-based zeolite hydrotalcite (FZ-HT)	Mustard (refined)	20	12:1	7	6	65	93.4 % (FZ-HT) 90.5 % (C-HT) 71.2 % (F-HT)	[50]
BFS-based LDH (slagHC), Ca–Al–Cl hydrocalumite	Soybean	7	12:1	1	Variable	60	0.8 % (400 °C) 65.8 % (600 °C) 97.0 % (800 °C)	[26]
CaO-supported fly ash	Soybean	89.8	6.96	1	5	70	96.97 %	[8]
Sodalite (zeolite)	Soybean	–	12	4	2	65	95.5 %	[32]

Besides provingthe method's viability and efficiency to produce zeolitic catalysts from FA, the authors studied their behavior intransesterification reaction of soybean oil. Generally, the data collected showed that

catalystswere efficient in the reaction, giving relatively high conversions (above 60 %) for all samplesunder the reactional conditions applied (6, 9 and 12:1 methanol/ oil ratio and 1, 2, 3 and 4 % wt. of catalyst), and a higher conversion of 95.5 %under optimized conditions. However, the used sodalite catalyst was characterized by a very quick deactivation, from 95.5 % to 60.9 % after the first run.

5. Conclusions

Biodiesel can be produced from different waste feedstock. The development and optimization of heterogeneous catalysts can result in decreasing the amount of waste arising from traditional industrial processes carried out with the application of homogenous catalysts. This short review gives examples from literature, indicating that such heterogenous catalysts can be prepared from certain sorts of waste e.g. from power or steel industries. Especially, it was shown that double layered hydroxides (called also hydrotalcites) and zeolites derived from slag from steel industry or fly ash from power plants can be the starting material for preparation of efficient heterogenous catalysts for biodiesel production. Taking into account huge amount of the latter waste, a new direction of its useful application is thus indicated.

References

[1] Ahmaruzzaman, M., A review on the utilization of fly ash, Progress in Energy and Combustion Science, v. 36, p. 327-363, 2010.

[2] Albuquerque, M. C. G., Jiménez-Urbistondo, I., Santamaría-González, J., Mérida-Robles, J. M., Moreno-Tost, R., Rodríguez-Castellón, E., Jiménez-López, A., Azevedo, D. C. S., Cavalcante Jr., C. L. and Maireles-Torres, P., CaO supported on mesoporous silicas as basic catalysts for transesterification reactions, Applied Catalysis A: General, v. 334, p. 35-43, 2008.

[3] Atadashi, I. M., Aroua, M. K., Abdul Aziz, A. R. and Sulaiman, N. M. N., The effects of water on biodiesel production and refining technologies: A review, Renewable and Sustainable Energy Reviews, v. 16, p. 3456-3470, 2012.

[4] Atadashi, I. M., Aroua, M. K., Abdul Aziz, A. R. and Sulaiman, N. M. N., Refining Technologies for the purification of crude biodiesel, Applied Energy, v. 88, p. 4239-4251, 2011.

[5] Berrios, M. and Skelton, R. L., Comparison of purification methods for biodiesel, Chemical Engineering Journal, V. 144, p. 459-465, 2008.

[6] Canakci, M. and Van Gerpen, J., Biodiesel production via acid catalysts, Transactions of the American Society of Agricultural Engineers (ASAE), v.42, p. 1203-1210, 1999.

[7] Canakci, M., Senel, F. and Van Gerpen, J., Biodiesel pilot plant & glycerin production and purification,Final Freedman, B., Pryde, E. H. and Mounts, T. L., Variables affecting the yields of fatty esters from transesterifiedvegeTab. oils, Journal of the American Oil Chemists Society (JAOCS), v. 61, Issue 10, p. 1638-1643, 1984.

[8] Gomes, J. F. P., Puna, J. F. B., Gonçalves, L. M. and Bordado, J. C. M., Study on the use of MgAlhydrotalcites as solid heterogeneous catalysts for biodiesel production, Energy, v. 36, Issue 12, p. 6770-6778, 2011.

[9] Hartman, L., Methanolysis of triglycerides, Journal of the American Oil Chemists Society (JAOCS), v. 33, Issue 3, p. 129-129, 1956.

[10] Helwani, Z., Othman, M. R., Aziz, N., Kim, J. And Fernando, W. J. N., Solid heterogeneous catalysts for transesterification of glycerides with methanol: A review, Applied Catalysis A: General, v. 363, p. 1-10, 2009.

[11] Issariyakul, T. and Delai, A. K., Biodiesel from vegeTab. oils, Renewable and Sustainable Energy Reviews, v. 31, p. 446-471, 2014.

[12] Iyer, R. S. and Scott, J. A., Power station fly ash – a review of value-added utilization outside of the construction industry, Resources, Conservation and Recycling, v. 31, p. 217-228, 2001.

[13] Kondamudi, N., Mohapatra, S. K. and Misra, M., Quintinite as a bifunctional heterogeneous catalyst for biodiesel synthesis, Applied Catalysis A: General, v. 393, p. 36-43, 2011.

[14] Kuwahara, Y., Tsuji, K., Ohmichi, T., Kamegawa, T., Mori, K. and Yamashita, H., Transesterifications using a hydrocalumite synthesized from waste slag: an economical and ecological route for biofuel production, Catalysis, Science & Technology, v. 2, p. 1842-1851, 2012.

[15] Kuwahara, Y., Tsuji, K., Ohmichi, T., Kamegawa, T., Mori, K. and Yamashita, H., A novel conversion process for waste slag: synthesis of a hydrotalcite-like compound and zeolite form blast furnace slag and evaluation of adsorption capacities, Journal of Materials Chemistry, v. 20, p. 5052-5062, 2010.

[16] Leung, D. Y. C., Wu, X. and Leung, M. K. H., A review on biodiesel production using catalyzed transesterification, Applied Energy, v. 87, p. 1083-1095, 2010.

[17] Ma, F., Hanna, M. A., Biodiesel production: a review, Bioresource Technology, v. 70, p. 1-15, 1999.

[18] Madsen, A. T. and Fehrmann, R., Catalytic production of biodiesel, PhD Thesis, Technical University of Denmark (DTU), KongensLyngby, Denmark, 2011.

[19] Manique, M. C., Lacerda, L. V., Alves, A. K. and Bergmann, C. P., Biodiesel production using coal fly ash-derived sodalite as a heterogeneous catalyst, Fuel, v. 190, p. 268-273, 2017.

[20] Mansir, N., Teo, S. H., Umer, R., Mohd, I. S., Tan, Y. P., Alsultan, G. A. and Taufiq-Yap, Y. H., Modified waste egg shell derived bifunctional catalyst for biodiesel production from high FFA waste cooking oil. A review, Renewable and Sustainable Energy Reviews, v. 82, p. 3645-3655, 2018.

[21] Michalik, M. and Wilczynska-Michalik, W., Mineral and chemical composition of biomass ash, European Mineralogical Conference, v. 1, p. 423-423, 2012.

[22] Muriithi, G. N., Petrik, L. F., Gitari, W. M. and Doucet, F. J., Synthesis and characterization of hydrotalcite from South African coal fly ash, Power Technology, v. 312, p. 299-309, 2017.

[23] Pereira, C. O., Portilho, M. F., Henriques, C. A. and Zotin, F. M. Z., SnSO$_4$ as catalyst for simultaneous transesterification and esterification of acid soybean oil, Journal of the Brazilian Chemical Society, v. 25, No. 12, 2014.

[24] Petkowicz, D. I., Rigo, R. T., Radtke, C., Pergher, S. B. and dos Santos, J. H. Z., Zeolite NaA from Brazilian chrysotile and rice husk, Microporous and Mesoporous Materials, v. 116, p. 548-554, 2008.

[25] Pollard, S. J. T., Fowler, G. D., Sollars, C. J. and Perry, R., The Science of the Total Environment, v. 116, p. 31-52, 1992.

[26] Puna, J. F., Gomes, J. F., Correia, M. J. N., Soares Dias, A. P. and Bordado, J. C., Advances on the development of novel heterogeneous catalysts for transesterification of triglycerides in biodiesel, Fuel, v. 89, p. 3602-3606, 2010.

[27] Robles-Medina, A., González-Moreno, P. A., Esteban-Cerdán, L. and Molina-Grima, E., Biocatalysis: towards ever greener biodiesel production, Biotechnology Advances, v. 27, p. 398-408, 2009.

[28] Schwab, A. W., Bagby, M. O. and Freedman, B., Preparation and properties of diesel fuels from vegeTab. oils, Fuel, v. 66, p. 1372-1378, 1987.

[29] Sharma, Y. C., Singh, B. and Korstad, J., Advancements in solid acid catalysts for ecofriendly and economically viable synthesis of biodiesel, Biofuels, Bioproducts & Biorefining, v. 5, p. 69-92, 2011.

[30] Soares Dias, A. P., Bernardo, J., Felizardo, P. and Correia, M. J. N., Biodiesel production over termal activated cerium modified Mg-Al hydrotalcites, Energy, v. 41, p. 344-353, 2012.

[31] Soares Dias, A. P., Puna, J., Correia, M. J. N., Nogueira, I., Gomes, J. and Bordado, J., Effect of the oil acidity on the methanolysis performances of lime catalyst biodiesel from waste frying oils (WFO), Fuel Processing Technology, v. 116, p. 94-100, 2013.

[32] Volli, V. and Purkait, M. K., Preparation and characterization of hydrotalcite-like materials from flyash for transesterification, Clean Technologies and Environmental Policy, v. 18, p. 529-540, 2015.

[33] Wright, H. J., Segur, J. B., Clark, H. V., Coburn, S. K., Langdon, E. E. and DuPois, R. N., A report on ester interchange, Glycerine Producers' Association Research Laboratories, Oil & Soap, v. 21, p. 145-146, 1944.

[34] Report Grant No. 98-06, Department of Mechanical Engineering – Iowa State University, 2000.

[35] Chakraborty, R., Bepari, S. and Banerjee, A., Transesterification of soybean oil catalyzed by fly ash and egg shell derived solid catalysts, Chemical Engineering Journal, v. 165, p. 798-805, 2010.

[36] Demirbas, A., Biodiesel fuels from vegeTab. oils via catalytic and non-catalytic supercritical alcohol transesterifications and other methods: a survey, Energy Conversion and Management, v. 44, p. 2093-2109, 2003.

[37] Di Serio, M., Mallardo, S., Carotenuto, G., Tesser, R. And Santacesaria, E., Mg/Al hydrotalcite catalyst for biodiesel production in continuous packed bed reactors, Catalysis Today, v. 195, Issue 1, p. 54-58, 2012.

Modeling phytoremediation – main opportunities and limitations

Marta Jaskulak[1], Aneta Kowalska[1], Anna Grobelak[1];

[1]Politechnika Częstochowska, Wydział Infrastruktury i Środowiska, Instytut Inżynierii Środowiska, adres; ul. Brzeźnicka 60A, tel. 728547285, e-mail: martajaskulak@gmail.com

Abstract

Contamination of soils with heavy metals (HMs) is a growing concern since HMs are not biodegradable and can accumulate in living organisms causing a hazard to plants, animals, and humans. Phytoremediation is a cost-efficient technology that uses plants to remove, transform or detoxify contaminants from water, sediments, soils, and atmosphere. During the last years, phytoremediation entered the stage of modeling such process on a large scale by using mathematical models. Such models can be useful tools to further understand processes that influence the efficiency of phytoremediation and to precisely plan such actions on a large scale. When dealing with extremely complicated and challenging processes like the interactions between the climate, soil, and plants, modeling phytoremediation before starting an operation can significantly reduce the time and cost of such process by granting us the accurate prediction of possible outcomes. The primary objective for modeling phytoremediation is to check the time necessary for remediation of specific contaminated sites and assess the extent of contaminant removal under given circumstances.

Keywords: phytoremediation, soil pollution, modeling, DSS, heavy metals, soil remediation

1. Introduction

The rapid increase in soil contamination in recent years causes a major problems to the environment and also human health.Exposure to heavy metals (HMs) in different forms can inflict a vast variety of threats to humans including damage to the nervous system which is irreversible [1]. The removal of HMs from soils requires effective technological approaches and cost-efficient solutions, especially since HMs are considered a unique group of pollutants since they cannot be broken down into safe, non-toxic forms [1,2]. The areas with soil contamination by HMs has dramatically risen in past years mostly as a result of industrialization and discharge of waste and wastewater [2,3]. Among HMs, cadmium, lead, nickel, and mercury were shown to appear more frequently in soil samples through the world [2]. Due to the growing health concerns associated with heavy metals and its broad distribution in soils and water, more attention has been directed to identify the sources of such pollution and remediate contaminated sites [3]. The use of physical and/or chemical methods to deal with heavy metal contaminated soils includes the use of ion exchange, reverse osmosis, chemical reduction, precipitation, and evaporation. All of them can be successfully applied for remediation by they require a lot of external resources and in most cases are too expensive for a large scale use [1,4]. Due to those reasons, in recent decades, more and more attention is given to phytoremediation processes in which plants absorb and transform HMs in order to detoxify the site and clean up polluted environments [4]. It is worth mentioning that such a method can also be applied to other contaminants like pesticides, explosives, and oil. Overall, phytoremediation can take advantage of natural processes, and it requires less equipment and labor than other technologies [5].

Phytoremediation can also be divided into a couple of main groups: phytoextraction, phytodegradation, phytovolatilization, phytotransformation, phytostabilization, and rhizofiltration [6]. In the process of phytoextraction (which is also sometimes called phytoaccumulation), plants uptake, translocate from roots to shoots and accumulate heavy metals. Phytodegradation involves breaking down the contaminants mostly as a direct consequence of catalytic enzymes produced by the roots. In phytovolatilization after the uptake of a contaminant, it is released through the transpiration process to the atmosphere. Phytostabilization mostly refers to immobilization of pollutant in a root-zone while rhizofiltiation uses the processes of adsorption and/or absorption of contaminants in plants roots [6,7].

All phytoremediation technics has been tested to clean up heavy metals, but overall, their efficiency varies significantly between species [8]. To increase such efficiency plants can also be genetically modified in order to accumulate higher concentrations of metals or to obtain higher tolerance to their toxic effects [8,9]. Overall the implementation of such modifications has been shown to still be much less expensive in comparison to physical

and/or chemical methods for cleaning up contaminated soil. On the other hand, since a wide variety of contaminants and soils properties that can affect the process, phytoremediation is often viewed as a site-specific technology [9].

Phytoremediation, despite being still a young technology has already entered the stage of modeling of biological and chemical processes for this purpose. Currently, there are several models available and more in current development that can be applied for this purpose [10]. Overall, a vast variety of such models is mostly caused by different outcomes that can be modeled, for example, we can model the phytoremediation by heavy metal accumulation in the selected part of the plant or by its overall distribution among all plant compartments [11].

2.   Modeling phytoremediation

Modeling the process of phytoremediation is a specific process mostly due to some unavoidable assumptions as well as some limitations and the complicated nature of interactions. Therefore, most models differ in their level of complication and extent of possible applicability [12].

The selection of a model for phytoremediation planning depends mostly on the objectives of the operator but also on the main advantages and drawbacks of such models and overall the comprehension level of given results [13]. Different models can also be chosen by different operators, for example, an environmental researcher can choose a different model than the environmental officer or the owner of the contaminated site, depending on their experience and primary objectives. As an example, the researcher can be focused on the concentration of a selected chemical in plant tissues and use a model that involves mechanisms of the uptake, translocation and final accumulation of such substance. A model operator from food industry would be mostly focused on models that give a detailed forecast of contaminant concentration in plants parts used as a food source which can predict the risk of selected contaminant to enter the food chain. An environmental protection officer would look for models that could assess the ecological risks posed by contaminated site whereas the owner of such sites would like to use models that can predict the time of decontamination and its cost [13,14].

Overall all phytoremediation models can be divided into two main groups [15]:

- the steady-state models;

- dynamic models;

The first group provides a forecast for an infinite time while the second group is more useful in assuming the time period needed before the modeled variables will reach the target values [15]. Depending on the main objectives, the operator has to choose a model with an appropriate level of details suitable for planning such a process. It is worth mentioning that the major disadvantage of complex models is that the input data is often incomplete and the final data can be a rough estimation. Therefore, simpler models have the advantage of a smaller need for preliminary data input but it that case, proper modeling requires more theoretical basis including a detailed understanding of processes occurring in the selected site [16]. Such models are therefore better suitable for site-specific, regional application whereas more complex models can be used the asses the process in an arbitrary location but with less precision [15, 16].

In order to evaluate the phytoremediation process of a specific regional site, the best way is to use a relatively simple model with a basic description of processes occurring on such site. It needs to be remembered that there are always consequences of selected simplifications such as not taking into consideration specific processes (for example the pH change, changes in humidity, content or lack thereof some specific, etc.) [17]. Therefore, to avoid such consequences and gain more insight into our model choice, it is often recommended to perform modeling with a couple of different models using various parameters and compare the given results. By doing this, we can also gain valuable insights into the differences in the sensitivity of selected parameters and the overall relevance of different processes in the systems [17,18].

3.   Basic element uptake modeling – the main opportunities and limitations

Models described in this chapters present different modeling approaches for a selected element uptake by plants.

3.1. Models focused on plants

3.1.1.   Decision Support System model - DSS

One example of a model designed for the assessment of plants uptake (for example heavy metals uptake) is a Decision Support System – DSS [19]. In its original form, it was strictly intended for evaluation of phytoextraction including the overall absorption and distribution of selected metals in plants tissues [20]. The use of this model can also provide insights into the economic feasibility of phytoextraction process and compare it to other land reclamation methods [19].

The Phyto-DSS was created in 2000 at the Instituto de RecursosNaturales y Agrobiología de Sevilla, Spain. Subsequently, the Phyto-DSS was developed at HortResearch, Palmerston North, New Zealand (2001 - 2004), and the Swiss Federal Institute of Technology, Zurich, Switzerland (2005 – 2007) [21].

In summary, the DSS model is based on the processes involved in the transfer of metals through transpiration flow and as a consequence water transfer through plant tissues [21]. It is mostly focused on metal concentration in soil and the change of it after the use of plants, and with taking into the consideration the soil density, plants roots distribution and root-absorption factor [22]. Since soil solution is up taken via roots and transported into different plants tissues, any component taken up by the roots will accumulate in plants tissues [20]. It is also possible for such component to migrate to other tissues and get accumulated in different places [19]. The DSS model also depends on the fact that the metal translocation from roots to the shoots of plants is driven by plant water uptake. The DSS overall can predict the amount of component (M) that will be removed by plants taking into the account its transpiration rate (T) over a selected period of time (t) (equation 1) [22]. Also, the amount of component is a function the component concentration in soil solution (C) due to the fact that total amount of metal that accumulates in the plant is proportional to the metal concentration in soil solution and not to the metal concentration in bulk soil by itself. (equation 2) [22,23].

$$M \propto \int_0^t T \, dt \qquad (1)$$

$$M \propto [C] \qquad (2)$$

Where:

M –the overall amount of selected component (mg/kg)

t – selected period of time

C – component concentration in soil solution (mg/kg)

3.1.1.1. Root absorption factor

It is well established that the total concentration of metal that accumulates in the plant tissues does not easily equal the concentration in soil solution times volume of transpired water since metals have to be translocated to the shots via apoplastic or symplastic pathways where it can be percolated and or filtrated. Due to this reason, the DSS defines the root absorption factor (f) which represents the metal concentration divided through the root xylem/soil solution system (equation 3) and other different factors that can influence the metal uptake in the roots [24].

$$f = \frac{[Cr]}{[C]} \qquad (3)$$

Where:

f – root absorption factor

Cr – soluble concentration of contaminant in roots (mg/L)

C – soluble concentration of contaminant in soil (mg/L)

The processes like temperature, moisture, pH, microbial activity and concentration of competing ions can affect the value of f. This issue is even more complicated due to the fact that root absorption factor can also change depending on the metal concentration in the soil solution [23,24].

3.1.1.2. Plants stress and root absorption factor

In DSS model plant species has been divided into three main groups depending on their capability to store metals in shoots in relation to metal concentration in soil [22]. For toxic and non-essential elements including lead, cadmium, and nickel, plants that have low values of f are consider being 'excluders'. Most plants species belong to that first group. The second group consists of plant species that have a close to constant f values for a wide range of metal concentrations. They are considered 'indicators' due to the almost linear relationship to metal concentration in soil. In the third group, there are plants which are able to tolerate high concentrations of metals in their shoots and/or possess active uptake mechanisms for such metals. Plants in this group are known as 'hyperaccumulators' [23,24].

For hyperaccumulators and excluders, the f value is constant only for just a narrow concentration rate [23]. After a certain threshold, the protective mechanisms will break down, and metal will flood into the plant causing high toxicity symptoms, reduced biomass, and even plants death [21]. Overall, the plant species-specific f can be assessed using the plants' water use, dry biomass of shoots and the metal concentration in the soil solution. (equation 5). Which is why the DSS model ads constant 'decay constant K' (equation 4) [24,25].

$$f(C) = \frac{f_1 C_1}{C_1 + K(C - C_1)} \quad (4)$$

Where:

f(C) – root absorption factor at specific concentration of component in soil (mg/L)

f_1 – measured root absorption factor at component concentration C_1 (mg/L)

K – decay constant (0 < K < 1)

$$f \cong \frac{MB}{TC} \quad (5)$$

Where:

f - root absorption factor for the component

M - component concentration in the above-ground dry plant biomass (mg/kg)

B - whole above-ground dry biomass (kg)

T - the total water use (L)

C - concentration of component in soil solution (mg/L)

3.1.1.3. Contaminant distribution

The distribution of contaminants in soils is never uniform through the depths of it, and highest concentrations are typically found close to the surface layer of soil [8]. The DSS model considers soil to be divided into three zones [22]:

- contaminated zone – usually the surface layer - maximum concentration of contaminant;
- intermediate zone – in which mixingcontaminated and uncontaminated soils occurs;
- uncontaminated soil – mostly deeper layers that are unaffected by the contamination on given time;

The uptake of contaminant by plants causes changes in soil concentration of such contaminant (mg/kg) at specific depth d. This change is calculated by the following formula [23]:

$$\Delta[M]_z = \frac{1}{\rho_z} \int_0^t R_z TCf \ \ dt \quad (6)$$

Where:

$\Delta[M]_z$ – change in component concentration at certain depth (mg/kg)

ρ_z– soil bulk density at depth z (g cm^{-2})

t – time (usually in days)

R_z – root density (root mass at depth z) / (total mass of roots)

T – total water use (L/day)

C – concentration of selected component in soil solution (mg/L)

f – calculated root absorption factor

Alternatively, the f values and overall phytoextraction process can be enhanced by selective breeding, gene manipulation or by increasing the concentration of available contaminants for example by the use of chelates [20].

3.1.1.4. Limitations of DSS model

The DSS model is relatively simple but provides general information about the whole process of contaminant uptake by plants [21]. The main drawback of using this kind of models is that environmental conditions such as drought, winter weather, rapid changes in temperature are not taken into consideration. Moreover, the f factor for a pollutant uptake can be different for plants grown on different soil types mostly due to the presence of various ions and pH [22].

After entering the root, DSS model assumes that the contaminant will be translocated and stored in plants shoots, but many researchers demonstrated that metals stored in shoots could be relocated back to the roots which in that case will result in an overestimation of the component that is up taken [24,25].

Another drawback to this model is the fact that is considers same moisture distribution in soil with ich almost never the case in the natural environment and will influence the uptake of metals by roots [25]. Given these limitations, the DSS model can actually indicate a shorter time of remediation then will occur on a natural site. Therefore, it is advised to apply caution and not mislead potential clients. Overall, inusing the DSS model, the precise input data is required to predict future biomass and metal accumulation. The environmental conditions must be considered very precisely because DSS model is susceptible to changes in water content [24,25].

3.1.1.5. Calculating the economic viability of phytoextraction by the DSS model

In the DSS model, the economic viability of phytoextraction is compared to the best alternative technology and the cost of complete inaction. The model determines the probable costs by the formula (equation 7) [25]:

$$V = A * \left(\int_0^t (C1 + C2 - P1 \ x \ V1) \ dt + \sum_{x=1,2,3\ldots t} \int_0^x (C1 + C2 - P1 \ x \ V1) \ dt \ x \frac{I}{100} \right) \quad (7)$$

Where:

A – contaminated area (ha)

C1 – cost of planning ($ ha^{-1})

C2 – cost of production ($/ha)

P1 – biomass that can be sold (t/ha)

V1 – value of biomass ($/t)

I – interest rate (%)

After that the costs are compared to an alternative technology by the following formula (equation 8) [25]:

$$V_a = A * \left(C \left(1 + \frac{I}{100} \right)^{t1} - L \left(1 + \frac{I}{100} \right)^{(t2-t1)} \right) \quad (8)$$

Where:

A – contaminated area (ha)

t1 – time necessary for different technology to remediate site (years)

t2 – time for phytoremediation of site (years)

C – cost of different technology ($ ha^{-1})

I – interest rate (%)

L – profit from the land ($)

The final step included the comparison of selected technology to the cost of doing nothing. Such price is determined mostly by specific legislation but also as a loss of income from land [24].

3.1.2. Other plant-oriented models

Another model that can be used in phytoremediation planning is the PLANTX model which considers the dynamic transfer of compounds from soil to plants and air and also the metabolism of contaminants including their final accumulation in stems, leaves or fruits. It is mostly useful for organic contaminants [26].

The other model that can predict the uptake of contaminants from soil was described by Hung and Muckay [27]. It can evaluate the whole circle of contamination transfer including the translocation from soil to roots than through stem to leaves, from leaves to air, air to leaves, leaves to stem and finally from stem to roots [28]. The uptake of the selected contaminant is based on balancing chosen factors which can describe the distribution of pollutants and the rate of plants metabolism. Moreover, the time of plants growth is also evaluated [27,28].

In this model the parameters taken into the consideration are as follows [28]:

- Leaves surface area;

- Growth and metabolisms – duration of exposure to contaminants, the growth rate of all organs;

- Metal characteristics – concentration of pollutants, its molecular mass;

- Physio-chemical analysis of plants – the density of leaves and roots, transpiration rate;

3.2. Models focused on soil

BALANS model was developed in Tomsk State University (Russia) to simulate the processes involved in the self-purification of soils from metals [29]. These processes include mostly metal uptake and its removal by harvesting of plants and the removal of metals as a consequence of its natural migration in the soil. The total amount of metals bioaccumulated in crops is estimated in this model as biomass removed and metal concentration in the biomass [30]. The natural removal of metals from contaminated soils is calculated using annual migration rates after taking into the consideration climatic zone and the type of soil. The program uses annual metal leaching rates for lead, chromium, copper, zinc, and nickel chosen from a vast range of literature which can divide soils into selected typed including *Podzols* and *Albeluvisols* [29,30].

The main advantages of the BALANS model:

- A clear difference between the removed metals by phytoremediation and by the natural migration of metals by leaching;

- Determination of the balance of metals in the soil-plant system for short and long-term with is essential for sustainable development;

4. Conclusions

The use of mathematical models in environmental studies can improve the evaluation of different outcomes in order to make an objective decision about the most suitable process for the selected contaminated site. In the last three decades, several mathematical approaches have been used to better understand the interaction between soil and plants which then can be applied for modeling the process of phytoremediation [31,32]. Contaminant absorption and accumulation models can play a main role in understanding processes occurring in soils and plant which can allow as to manage contaminated sites [33].

Acknowledgements

References

[1] Arthur EL, Rice PJ, Rice PJ, Anderson TA, Baladi SM, Henderson KLD, Coats JR. *Phytoremediation—An overview.*Crit Rev Plant Sci 24:109–122, 2005;

[2] Doty SL, *Enhancing phytoremediation through the use of transgenics and endophytes.* New Phytol 179:318–333, 2008;

[3] Lebeau T, Braud A, Je´ze´quel K. *Performance of bioaugmentation assisted phytoextraction applied to metal contaminated soils. Environ Pollut* 153:497–522, 2008;

[4] Van Nevel L, Mertens J, Oorts K, Verheyen K. *Phytoextraction of metals from soils: How far from practice?* Environ Pollut 150:34– 40, 2007;

[5] Schro¨der P, Scheer CE, Diekmann F, Stampfl A. *How plants cope with foreign compounds: Translocation of xenobiotic glutathione conjugates in roots of barley (Hordeumvulgare).* Environ SciPollut Res 14:114–122, 2007;

[6] Khaitan S, Kalainesan S, Erickson LE, Kulakow P, Martin S, Karthikeyan R, Hutchinson SLL, Davis LC, Illangasekare TH, Ng'oma C. *Remediation of sites contaminated by oil refinery operations.* Environ Prog 25:20–31, 2006;

[7] Boominathan R, Doran PM. *Cadmium tolerance and antioxidative defenses in hairy roots of the cadmium hyperaccumulator, Thlaspicaerulescens.*BiotechnolBioeng 83:158–167, 2003;

[8] Anning, A.K., Akoto, R., 2018. Assisted phytoremediation of heavy metal contaminated soil from a mined site with Typhalatifolia and Chrysopogonzizanioides. Ecotoxicol. Environ. Saf. 148, 97–104.

[9] Grobelak, A., Placek, A., Grosser, A., Singh, B., Almås, Å., Napora, A., Kacprzak, M., 2017. Effects of single sewage sludge application on soil phytoremediation. Journal of Cleaner Production. 155. 189-197.

[10] Davari, M., Homaee, M., 2015. An analytical deterministic model for simultaneous phytoremediation of Ni and Cd from contaminated soils. Environ. Sci. Pollut. Res. 22 (6), 4609–4620.

[11] Lindstrom, F.T., Boersma, L., McFarlane, C., 1991. Mathematical model of plant uptake and translocation of organic chemicals: development of the model. Journal of Environmental Quality 20, 129–136

[12] Boersma, L., McFarlane, C., McCoy, E.L., 1988a. Uptake of organic chemicals by plants: a theoretical model. Soil Science 146, 403–417.

[13] Yetilmezsoy, K., Demirel, S., Vanderbei, R.-J., 2009. Response surface modeling of Pb(II) removal from aqueous solution by Pistaciavera L.: Box–Behnken experimental design. J. Hazard. Mater. 171, 551–562.

[14] Oporto, C., Arce, O., Van den Broeck, E., Van der Bruggen, B., Vandecasteele, C., 2006. Experimental study and modelling of Cr (VI) removal from wastewater using Lemna minor. Water Res. 40 (7), 1458–1464.

[15] Khan FI, Husain T (2003) Evaluation of a petroleum hydrocarbon contaminated site for natural attenuation using 'RBMNA' methodology. Environmental Modeling and Software 18: 179-194.

[16] RAAG (2000) Evaluation of risk based corrective action model remediation alternative assessment group, Memorial University of newfoundland St. John's NF, Canada.

[17] Yeh, G.-T., Burgos, W.D., Zachara, J.M., 2001. Modeling and measuring biogeochemical reactions: system consistency, data needs, and rate formulations. Adv. Environ. Res. 5, 219–237.

[18] Whiting, S.N., Broadley, M.R., White, P.J., 2003. Applying a solute transfer model to phytoextraction: zinc acquisition by Thlaspicaerulescens. Plant Soil 249, 45–56.

[19] Liang, H.M., Lin, T.H., Chiou, J.M., Yeh, K.C., 2009. Model evaluation of the phytoextraction potential of heavy metal hyperaccumulators and nonhyperaccumulators. Environ. Pollut. 157, 1945–1952

[20] Ouyang Y (2002) Phytoremediation: modeling plant uptake and contaminant transport in the soil-plant-atmoshere continuum. J Hyrol 266:66-82

[21] Verma, P., George, K.V., Singh, H.V., Singh, S.K., Juwarkar, A., Singh, R.N., 2006. Modeling rhizofiltration: heavymetal uptake by plant roots. Environ. Model. Assess. 11, 387–394.

[22] Thoma, G.J., Lam, T.B., Wolf, D.C., 2003. A mathematical model of phytoremediation for petroleum-contaminated soil: model development. Int. J. Phytoremediation 5, 41–55

[23] Burken, J.G., Schnoor, J.L., 1996. Phytoremediation: plant uptake of atrazine and role of root exudates. Journal of Environmental Engineering 122, 958–963.

[24] Spiteri, C., Slomp, C.P., Regnier, P., Meile, C., Van Cappellen, P., 2007. Modelling the geochemical fate and transport of wastewater-derived phosphorus in contrasting groundwater systems. J. Contam. Hydrol. 92, 87–108

[25] Dietz A. C., Schnoor J. L. 2001 Advances in phytoremediation Environ. Health Perspect. 109. 163-168.

[26] Koopmans G. F., Romkens P., Song J., Temminghoff E. J. M., Japenga J. 2007 Predicting the phytoextraction duration to remediate heavy metal contaminated soils Water Air Soil Pollut. 181. 355-371.

[27] Mathur S. 2004 Modeling phytoremediation of soils Pract. Periodical Hazard. Tox. Radioact. Waste Manag. 8. 286-297.

[28] Ouyang Y. 2002 Phytoremediation: modeling plant uptake and contaminant transport in the soil–plant–atmosphere continuum J. Hydrol. 266. 66-82.

[29] Brennan M. A., Shelley M. L. 1999 A model of the uptake, translocation, and accumulation of lead (Pb) by maize for the purpose of phytoextraction Ecol. Eng. 12. 271-297 .

[30] Briggs G. G., Bromilow R. H., Evans A. A. 1982 Relationships between lipophilicity and root uptake and translocation of non-ionized chemicals by barley Pesticide Sci. 13. 495-504.

[31] Seuntjens, P., Nowack, B., Schulin, R., 2004. Root-zone modeling of heavy metal uptake and leaching in the presence of organic ligands. Plant Soil 265, 61–73

[32] Rainbow, P.S., 2007. Trace metal bioaccumulation: models, metabolic availability and toxicity. Environ. Int. 33, 576–582.

[33] Park, S.S., Jaffe, P.R., 1996. Development of a sediment redox potential model for the assessment of postdepositional metal mobility. Ecol. Model. 91, 169–181.

Experimental and Mathematical Investigation of Water Desalination by Capacitive Deionization and Electrodialysis with Heterogeneous Membranes

Talal Ashraf[1], Shaheen Aziz[2]

[1]*AGH University of Science and Technology Krakow, e-mail:talal@student.agh.edu.pl*

[2]*Mehran University of Science and Technology Pakistan, e-mail:Shaheen.shaikh@faculty.muet.edu.pk*

Abstract

Water scarcity is globally a challenege and problematic. Several researches are carried out to overcome this issue by introducing cost effective and efficient technologies. In this research work, the experimental and mathematical studies were carried out to observe the phenomena of water desalination.Technology adopted for desaltion is coupling of two concepts fo water desalination with electrodialysis. Heterogeneous membranes were prepared from glass fiber polymer with coating of sulfonic and ammonium acid group resin. The capacitive electrodes were prepared from activated carbon coated over a copper wire to adsorb ones from concentrate section. As the voltage increased, the desalination and deionization also increases. 96.4% of TDS reduction and 95.92% of conductivity reduction was observed. Scaling up of this technology will be effectively feasible on small scale/domestic purposes.

Keywords: Desalination; Electrodialysis; Capacitive electrode; deionization; Conductivity; Activated Carbon.

1. Introduction

Electrodialysis technology can be used for water production [1]. The main possible benefit for Electrodialysis is that it can be utilize as off grid desalinated water provider as it can be merged with the renewable energy sources like wind and solar. For the wind energy, the desalination rate is directly dependent on the wind turbine speed [2]. Electrodialysis module work cheaply if the system is hybridized with photovoltaics. The sustainability of this hybridization with photovoltaics eliminates the environmental hazard for disposal of batteries [3]. Membrane methods for water desalination emerges as a solution for water scarcity across the world. Integration of electrodialysis with other technologies can increase its sea water desalination from 94.8 to 99.4 for half of it optimum time [4]. Shock electrodialysis utilizes the shock waves for disinfection of water. 99% of Escherichia coli bacteria can be removed and killed causes the water disinfection by electrodialysis [5]. In Electrodialysis, the passage of sodium and hydrogen ion across cationic exchange membrane and chlorine with hydroxide ion across anion exchange membrane using a module of three partitions [6]. The electrodialysis can also be used for ionic and non-ionic separation of material. The membranes in the electrodialysis system are of two classification that is homogeneous and heterogeneous membranes. This classification is purely done on the basis of membrane structure and heterogeneous degree of membranes that are polymeric inter and block along with snake in cage structures. Preparation of homogeneous membrane was done by the crosslinking of formaldehyde using the condense monomers, showed low mechanical stability and excellent electrochemical behaviour [7]. The electrical resistivity of sea water and currently density determination by ohms law, the transportation of ions becomes efficient throughout membrane when the current efficiency reaches to 48 and this will leads to efficient use of electrodialysis for sea water desalination. At higher flow rates, the current efficiency remain elevated [8]. Mathematical modelling approach by using the nonlinear programming can be used estimating membrane characteristics, desalination efficiency and energy requirements to estimate the operation cost and investment [9]. Mathematical modelling can be used for the predictive development of electrodialysis system. This can be done on the consideration that system is on steady state and negligible resistance by ionic membranes. Differential Equations can be used for mass balance of the system [10]. To simulate the electrodialysis module, a two dimension structure can be used. The concentration polarization and its effects on the ionic transport can be studied using Nernst Plant, Continuity and Navier Stokes models in steady state approaches. The solution of this two dimensional model has to be computed by the usage of computational fluid dynamics for prediction of ionic transport per unit area with concentration potential in the cell [11]. The activated carbon can be as a capacitive

electrode to adsorb the ions from concentrate section. Their durability can be done by assessment of environmental cycle and life cycle of capacitive material [12]. Capacitive deionization have strong capabilities for desalination of ground water. The cloth electrode coated with the activated carbon have a great impact on the usage of capacitive deionization technology to control the water contaminants that are organic in nature and microbes because capacitive electrode have a wide surface area with the chemical inertness [13]. Membrane based separation is one of the state of the art technology that the membranes made from polyvinyl ideneflouride and polymers of ethylene and propylene, polytetrafluoroethylene, polysulfone, polyether sulfone, polyacrylonitrile, polyamide, polyester and cellulose acetate. These materials are non-charged and chemically inert. To make them capable for ion exchange, resins are coated on them to make them heterogeneous membranes [14]. The preparation of ion exchange membrane having heterogeneous nature involves the steps like mould and compressing of polymeric nature powder then fusing with hot roll along with the blending of solvents on the material for ion exchange of polymeric matrix. The heterogeneous membrane found out to be mechanically highly sTab. as compared to the homogeneous membrane because of cross linked structure but they gets rapidly exhausted [15].

2. Materials and methods

2.1. Preparation of Heterogeneous Membranes

Two glass fibre membranes were purchased. Pore size of membranes are 1.6 µm. The area of single membrane is 0.00025 m2 as shown in Fig. 2 . The initial weight of each membrane is 5 g. These membranes are coated with the 12 g of cationic resin and 12g of anionic resin with 6 g of conductive epoxy resin binder. The cationic resins are sulfonic group resin and anionic resins are ammonium group resin. These resin have the range to transfer ions at entire pH range. The membranes are dried in an electric oven at 80ºC for 15 minutes and air cooled for 1 hour at room temperature 31ºC. Due to heat, the cross linked structure of resins melted and the two joined sheets are bounded. Cationic exchange membrane named as CEX while anionic exchange membrane named as AEX.
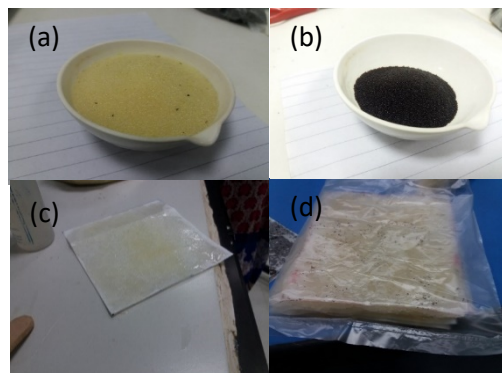
Fig.1 (a) Sulfonic group Cationic resin (b) Ammonium group anionic resin (b) resin coating on membrane (d) set of prepared dried membran es

Fig.2: Glass Fiber Membrane

2.2. Preparation of Capacitive Electrodes

Two Copper wires were bought from the market. The weight of copper wire is 3.175 g and the length of copper wires are 6.5 µm inch each. Activated carbon was pulverized in the ball mill with the particle size of 10 µm. The 8 grams activated carbon is mixed with the 2 grams of conductive epoxy resin binder and coated over the copper wires. The capacitive electrodes were dried in an electric oven at 80⁰C for 30 minutes. The electrodes are then cooled for 5 hours at room temperature.
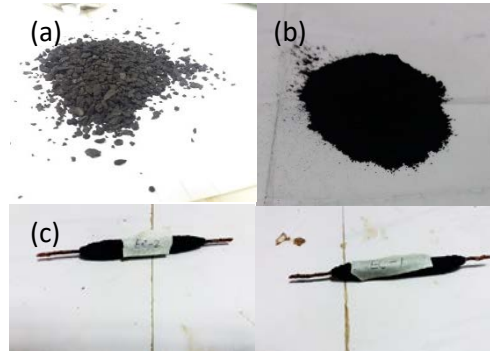
Fig.3(a) raw activated carbon (b) pulverized activated carbon (c) prepared capacitive electrode

2.3 Preparation of Module

The electrodialysis module is made from the white plane glass. The dimensions of this module are 0.12945 m length, 0.13208 m width and 0.14224m height. The holdup volume of module is calculated as 2.433 L. The volumetric weight that this module can withhold is 0.4056kg. The thickness of glass 5.08 mm.

2.4 Water Sample Collection

The water samples were collected from Aquafina Mineral water plant Karachi using online sampling method. The qualitative characteristics of water sample is shown in

Tab. 1. Sample water qualitativ parameters

TDS (mg/L)	Conductivity (mS/cm)	Temperature(⁰C)	pH
4540	9.07	31	7.37

2.5 Experimentation Procedure

CEX and AEX were placed in the module. The module is filled with 1liter of water sample. The Electrodes were placed besides the membrane. The electrodialysis module consists of three compartments. One is dilute that is middle one, while the other two are concentrate compartment. The CEX was placed after Cathode while AEX was placed after Anode. The electrodes are connected with DC power supply. The voltages are set to 8, 10, 12, 14 V respectively. The variation of voltages were done after 15 minutes each. Before each variation of voltage, online sampling of water is done to determine the TDS, Conductivity, Temperature and pH at their respective Voltages. The angle of capacitive electrode is such that only 25% of electrode is dipped in water.

Tab.1. StandardizedSaltsconcentration in watersample

Compound	Meq/l
Sodium	197.39
Potassium	116.41
Chloride	127.89

Bicarbonate	74.43
Calcium	227
Phosphorus	292.9
Iron	162.14
Magnesium	378.33
Sodium Chloride	77.61
Sodium Bicarbonate	54.05
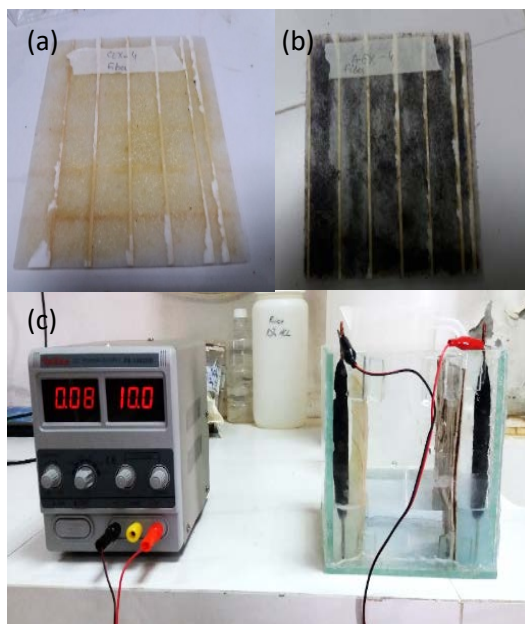
Fig.4 (a) Prepared double layered cationic and anionic membrane (b) Open batch electrodialysis with capacitive deionization system

2.6 Mathematical Modelling Using Interpolation Technique

When the values at four different voltages are found, then there needs to be development of model on the experimental basis to determine at each instant how much changes takes place. The boundaries values are set to be minimum at 8 volts while maximum at 14 volts using the algorithm Lagrange interpolation technique is for unequal spaced data points. Value at desired point is calculated with the help of Lagrange coefficients. By using Lagrange coefficients formula will be:

$$F(x) = L_0 f(a_0) + L_1 f(a_1) + L_2 f(a_2) +........... L_n f(a_n) \qquad \textit{Equation 1}$$

3. Results and Discussions

The current variation using the sample 2 of water with cationic and anionic exchanges membrane CEX and AEX using a DC-supply were to be found as:

Tab.2 Voltage, ampere and resistance of CDED of SAP with CEX and AEX

Voltage (V)	8	10	12	14
Current (amp)	0.06	0.08	0.10	0.12
Resistance (Ω)	133.33	125	120	116.66

By considering the above data, it is estimated that the during first 15 minutes, the resistivity of module (Water sample + electrodes + cationic and anionic membranes) is very high, but after 30 minutes the water resistivity tends to be lower. This is because of ionic transport. At first instant, the module resistivity is high because the most energy utilizes in the activation energy for ionic transport. As the ionic transport starts, the resistivity of module gets low after 45 minutes, using a high intense 14 V, the ionic transport gets at its peak and the resistivity gets minimum. From the observation, we analysed that there is maximum ionic transport at highest voltages because at high voltage, the ions are able to move faster towards their respective electrodes

3.1 TDS reduction using CDED with CEX and AEX of SAP

The initial TDS of water sample 2 was found from HACH Company TDS meter is 4540 mg/l. During the desalination of SAP-2, the TDS is checked after each 15 minutes at the voltage regulation of 8, 10, 12 and 14 V. The TDS of the dilute compartment seems to be decreased as the voltage increases along with time as shown in Fig. 5. The TDS of dilute becomes lower at the 14 volts after 1 hour. This is because of the ionic transport from the dilute section to the concentrate section. The TDS of the concentrate increases as the increase in concentration of ions in the concentrate section. There is the gradual increment in the TDS, this is because of the capacitive electrodes, as they adsorbs some ions but after 45 minutes, they are about to exhausted and that's why the TDS of concentrate section increases. This is the sign for the need of polarity reversal (capacitive electrode regeneration) of electrodes

3.2 Conductivity reduction using CDED with CEX and AEX of SAP

The initial conductivity of water sample 2 was found from HACH Company EC meter is 9.07 mS/cm. During the deionization of SAP-2, the conductivity is checked after each 15 minutes at the voltage regulation of 8, 10, 12 and 14 V. During the second sample analysis, the conductivity of dilute water decreases as we increase the voltages. The conductivity of concentrate water increases by increasing the voltages as shown in Fig.6. This increment in the concentrate section and decrement in the dilute section is because of the ionic transport from dilute to concentrate one. Reduction of conductivity in the dilute section is also referred as deionization.
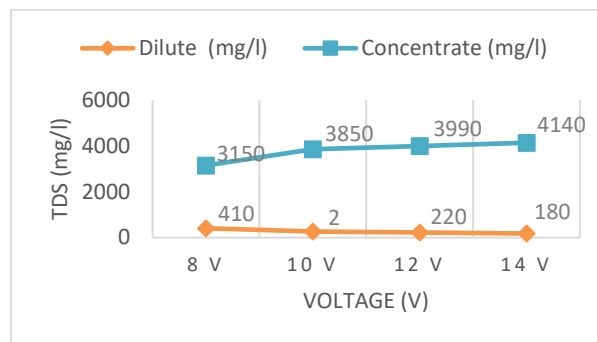
Fig.5 Comparative TDS analysisof SAP 1
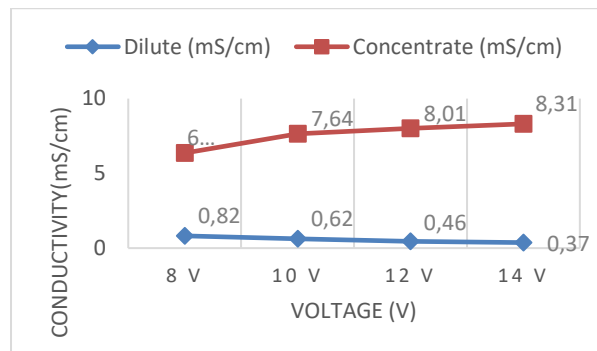
Fig.6 Comparative Conductivity analysis of SAP-2
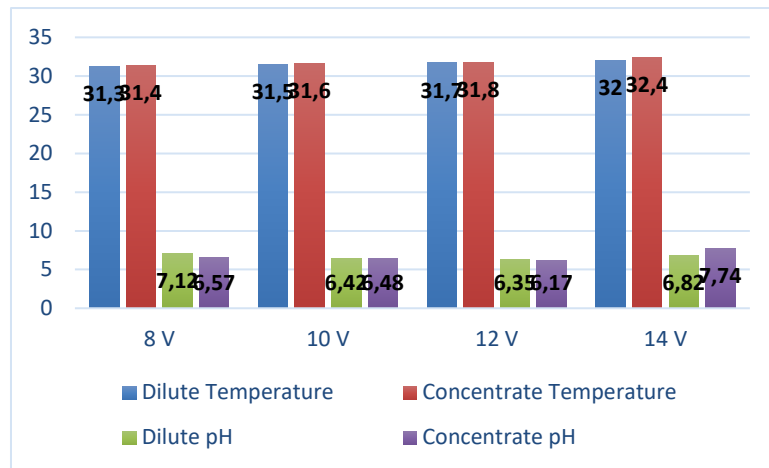
Fig.7 Temperature and pH variation at different voltages

Fig.8 Desalination efficiency
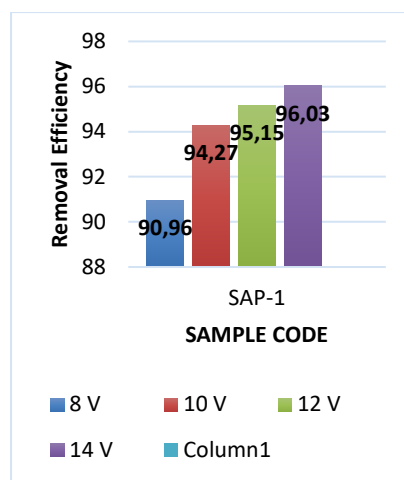
	SAP-2
8 V	90,959
10 V	93,164
12 V	95,038
14 V	95,9206
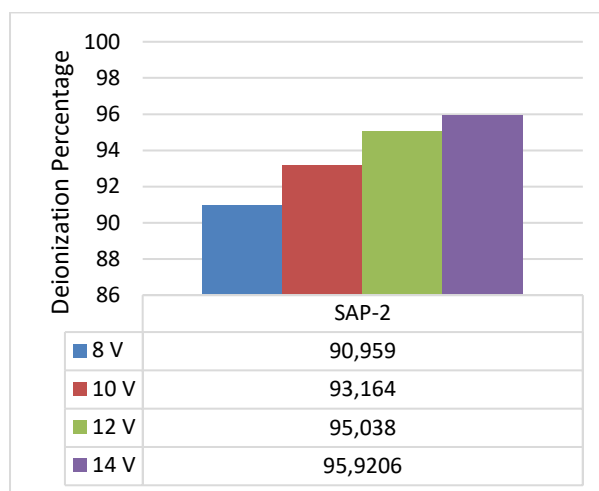
Fig.9 Deionization efficiency at different voltages
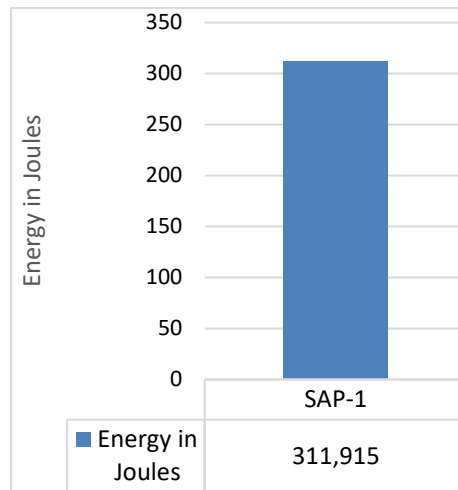
Fig.10 Minimum Energy required to start desalination
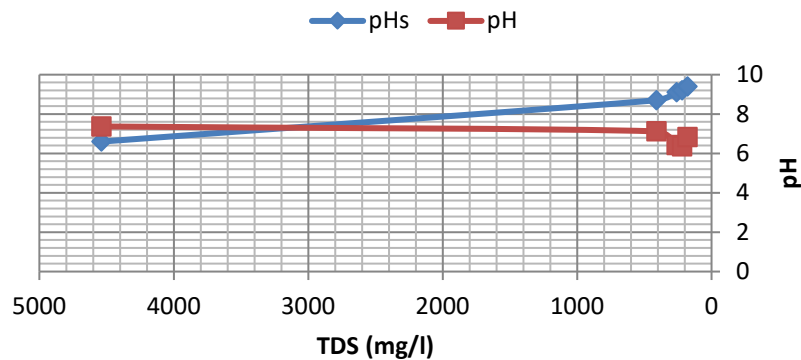
Fig.11Comparison of predicted and experimental pH values of SAP-2

By plotting the values of TDS and pH of product water of sample 2, at initial point and after saturation, the graph indicates a little bit increment in pH and then a point comes where it become linear and finally decreases pH_s of water decreases continuously as Fig. 11. From the graph it has been concluded that the there is a minute change in both values. To initialize the desalination and deionization process, the minimum amount of energy required that is known as Gibbs free energy is calculated using equation. The minimum energy required to desalinate the SAP-2 is 311.915 joules or 0.086643 watts as shown in Fig. 9 and Fig. 10 The temperature variation and pH of Concentrate and dilute sections were not changing so much. The temperature of concentrate seems a very bit higher than dilute because of the ionic transport movement. The movement of ions causes a bit increase in temperature because of their kinetic energy is responsible for this increment. The pH variation of dilute and concentrate is very much smaller. This pH increment is due to a very much splitting of water that causes the increment in the hydrogen ions concentration as shown in Fig. 7. CEX and AEX of SAP-2 was very high form 8V and a gradual increasing till 14 V as shown in Fig. 7. At the lowest voltage of our system that is 8 volts, SAP-2 has got the maximum deionization that is 90.959%. As we increasing the voltage, the deionization efficiency also increases that shows that the free ions removal in the dilute section is directly dependent on the voltage applied ash shown in Fig. 9.

4. Conclusion

Merging of capacitive deionization with the electrodialysis helps to improve the overall cost effects and low saline by-product for desalination. Because of use of activated carbon as a capacitive electrode that also works as an adsorbent, the concentrated water salinity becomes decreased. The resistivity of the CDED system varies with the change it voltages. As the desalination and deionization takes place, their rate is directly proportional to the resistivity of the whole module (dilute, membranes, and concentrate. The TDS of the dilute water decreased as

the voltage increased and the TDS of concentrate water increased as the voltage increases. The amount of desalination is directly dependent to current applied in a certain time. As the time increases the desalination rate reduces due to the maximum ionic transport so that there is no charge left to carry out the current. The deionization rate also directly depend on the amount of current supplied but as the time passes, the deionization rate reduced due to the low concentration of free ions to move the electrons. There is a slightly up and down in the pH due to the increasing of hydrogen ion concentration in concentrate section while the reduction of hydrogen ion in concentrate section. There is slightly up and down in the temperature due to flow of electrons that causes the increment in the kinetic energy. Salt removal efficiency are low at low voltages while at high voltage that is 14 V, the salt removal efficiency reaches up to 96.4%. Despite of high electric resistance of the membranes, the system performed more than 92% for high voltages. By the development of mathematical model as an equational system of the linear third degree polynomial by using Lagrange's Interpolation Technique, we can determine the value of TDS and Conductivity at any voltages between our boundary values. Maximum 4.194 watts of power consumed to desalinate a litre of water, the final TDS is 300 mg/l. The total amount of maximum 2.335 PKR/liter were consumed to desalinate and deionized the water up to 96%. It has been found that the more capacitive activated carbon electrode dipped in the water, the less will be TDS and Conductivity of concentrate. The concentrated water has other non-environmentally aspects, so the use of capacitive also helped to reduce this waste water salts. The free ions moves rapidly towards concentrate section as the voltage increases, that causes the reduction of ions in the dilute section and hence the deionization of dilute takes place. It has been found that at 14 volts there is up to 97% deionization takes place. The Gibbs free energy equation can be used for the estimation of theoretical minimum energy required to start the process of desalination and deionization. The hybridization of capacitive deionization and electrodialysis emerges as a cheap low voltage system that has potential to solve the water scarcity problems.

Nomenclature

SAP: Sample

AEX: Anion Exchange Membrane

CEX: Cation Exchange Membrane

CDED: Capacitive Deionization Electrodialysis

TDS: Total Dissolve Solids

Acknowledgment

References

[1]   T. Sirivedhin, J. McCue, L. Dallbauman, " Reclaiming produced water for beneficial use, salt removal by electrodialysis", Journal of Membrane Science, Volume 243, Issues 1–2, 1 November 2004, Pages 335–343

[2]   P. Malek, J.M. Ortiz, H.M.A. Schulte-Herbrüggen, "Decentralizeddesalination of brackishwaterusinganelectrodialysis system directlypowered by wind energy", Desalination, Volume 377, 1 January 2016, Pages 54–64

[3]   Juan Manuel Ortiz, Eduardo Expósito, Francisco Gallud, VicenteGarcía-García, VicenteMontiel, Antonio Aldaz, "Electrodialysis of brackishwaterpowered by photovoltaicenergywithoutbatteries, directconnectionbehavior", Desalination, Volume 208, Issues 1–3, 5 April 2007, Pages 89-100

[4]   E.A. Abdel-Aal , M.E. Farid, Fatma S.M. Hassan , Adila E. Mohamed, "Desalination of Red Sea water using both electrodialysis and reverse osmosis as complementary methods", Egyptian Journal of Petroleum, Volume 24, Issue 1, March 2015, Pages 71–75

[5]   DaoshengDeng,WassimAouad, William A. Braff, Sven Schlumpberger, Matthew E. Suss, Martin Z. Bazant, "Waterpurification by shockelectrodialysis, Deionization, filtration, separation, and disinfection",Desalination , Volume 357, 2 February 2015, Pages 77–83

[6] M. Chérif , I. Mkacher , L. Dammak , A. Ben Salah , K. Walha , D. Grande , V. Nikonenko, "Waterdesalination by neutralizationdialysis with ion-exchange membranes, Flowrate and acid/alkaliconcentrationeffects", Desalination, Volume 361, 1 April 2015, Pages 13–24

[7] M.Y. Kariduraganavar*, R.K. Nagarale, A.A. Kittur, S.S. Kulkarni, "Ion-exchange membranes" preparative methods for electrodialysis and fuel cell applications",Desalination, Volume 197, 2006 Page 225-246

[8] MohtadaSadrzadeh, TorajMohammadi, "Treatment of seawaterusingelectrodialysis, Currentefficiencyevaluation", Desalination, Volume 249, Issue 1, 30 November 2009, Pages 279–285

[9] PanagiotisTsiakis, Lazaros G. Papageorgiou, "Optimal design of an electrodialysis brackish water desalination plant", Desalination, Volume 173, Issue 2, 10 March 2005, Pages 173-186

[10] MohtadaSadrzadeh, TorajMohammadi, "Sea water desalination using electrodialysis ", Desalination ,Volume 221, Issues 1–3, 1 March 2008, Pages 440-447

[11] ZahraZourmand, FarzanehFaridirad, NorollahKasiri , TorajMohammadi, "Mass transfer modeling of desalinationthroughanelectrodialysiscell", Desalination, Volume 359, 2 March 2015, Pages 41–51

[12] Faisal A. Al Marzooqi , Amal A. Al Ghaferi , Irfan Saadat , Nidal Hila, "Application of CapacitiveDeionisation in waterdesalination, A review ",Desalination, Volume 342, 2 June 2014, Pages 3–15

[13] KarthikLaxman , MyoTayZarMyint , Mohammed Al Abri , PriyankaSathe , SergeyDobretsov , JoydeepDutt, "Desalination and disinfection of inlandbrackishgroundwater in a capacitivedeionizationcellusingnanoporousactivatedcarbonclothelectrodes", Desalination, Volume 362, 15 April 2015, Pages 126–132

[14] Claus Vogel, JochenMeier-Haack, "Preparation of ion-exchange materials and membranes", Desalination, Volume 342, 2 June 2014, Pages 156–174

[15] Gunther E. Molau, "Heterogeneous ion-exchange membranes", Journal of Membrane Science, Volume 8, Issue 3, 1981, Pages 309-330

[16] Benefield, L., Judkins, J. & Weand, B. 1982. Process Chemistry for Water and Wastewater Treatment. Prentice-Hall, Inc. Englewood Cliffs, New Jersey.

[17] Metcalf & Eddy, Inc. Wastewater Engineering Treatment and Reuse, Fourth Edition

[18] Kevin Raffert. July 1999, Scaling in geothermal heat pump systems, U.S. Department of Energy

Low-Temperature Effect on Water-Oil Systems Using The "Cold" Rod Method

Temiloluwa Ademuwagun[1], Anton Aleksandrovich Elpidinskiy[2]

[1]*Student: Department of Energy and Power, AGH University of Science and Technology, temiloluwa26@gmail.com:*

[2]*Associate Professor: Department Chemical Technology of Oil and Gas Refining, Kazan National Research Technological University, sinant@yandex.ru:*

Abstract

This article considered the impact of physical effects in this case the "Cold rod" (CR) method on oil and water-oil systems in the processes of dehydration and desalting of oil and its physicochemical characteristics. It is shown that with the help of cold, heavy and highly viscous components are removed from oils, which led to a decrease in pour point, viscosity and water content of the processed medium.

Keywords: viscosity, resins, asphaltenes, paraffins, water-oil system

1. Introduction

Oil field equipment that is used to transport oil systems at the stage fluid formation from the well to the oil processing unit (OPU) is under high stress. It is at this stage that highly watered oil-water emulsion with high viscosity is being pumped over. In addition, the viscosity increases not only from the formation of an emulsion system, but also due to the high content of structural-forming components (asphaltenes, resins and paraffins). In the cold season, the problem of pumping is aggravated: leading to energy costs increase.

Currently, there is a wide range of methods for solving the problems described above. The classic method - the chemical method – involves the use of reagents for various functional purposes at almost every stage of pumping and oil processing, especially during dehydration. These reagents are effective, but are quite expensive and require both constant delivery to the facilities of the oil industry, as well as a special block installation for dosing into the stream. Alternative methods are physical methods, which consist of the introduction of a wide range of wave and other effects into field processes – from production to preparation.

In this article, the effect of low-temperature treatment by the "cold rod" method on the exploitational properties of oils and its emulsions is evaluated. This method consists in placing metal rods cooled to negative temperatures into oil, on which structural-forming components, resins, asphaltenes and paraffins crystallize out of the oil medium. It is assumed that this treatment will affect the various physical and chemical properties of oil and emulsion.

2. Experiment

We used oils under the label A, B, C. Their physicochemical characteristics of which are given in Tab. 2.1.

Tab. 2.1. Physicochemical characteristics of the studied oils

Oil	Density ρ_{20}, kg/m³	Kinetic viscosity v_7, cCt	Components composition, %		
			Paraffins	Asphaltenes	Resins
Oil A	889	349,3	1,13	0,8	12,1
Oil B	903	367,1	0,72	1,1	14
OIl C	846	86,9	9,6	1,8	7,5

The apparatus that implements this method consists of two block installations (Fig. 2.1):

- block "cold" rod with a water bath (1);

- cryostat unit (2), which ensures the creation of a temperature in the rods ranging from -30 to + 60ºC.

The "cold-rod" block includes 4 metal cups in which the tested substances are placed, and covers in which "cold rods" are mounted - U-shaped hollow stainless-steel tubes. The tubes are connected to the refrigerant supply and return system (Fig. 2.2).
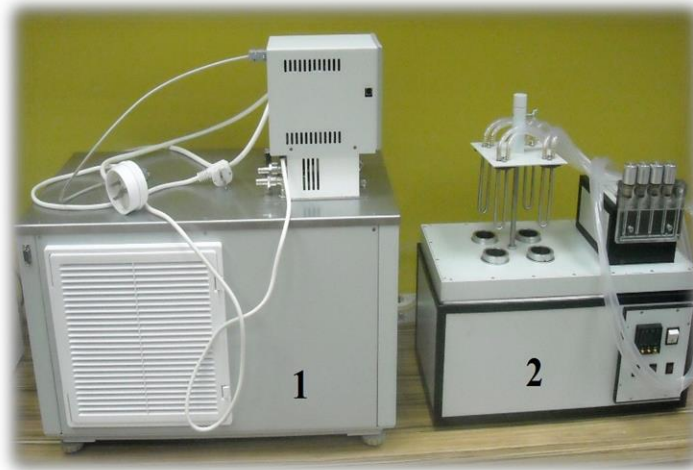
Fig. 2.1. Cold-rod treatment apparatus
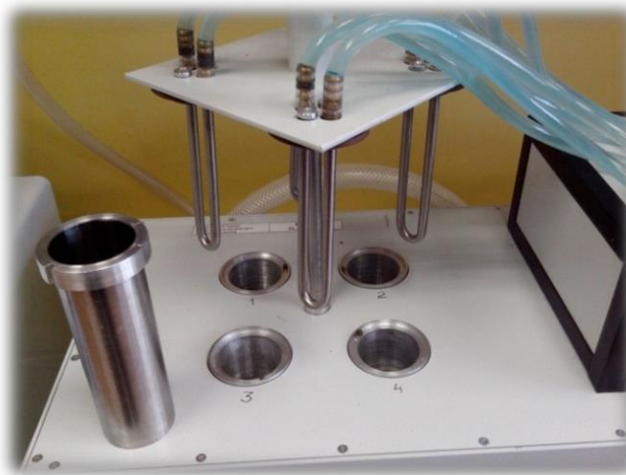
Fig. 2.2. Metallic glass and parallel U-shaped rods

During the experiment, the metallic glasses filled with oil rotate around the rods. After the immersion of the rods into the oil, they are removed from the metal cups and allowed to drain residual oil for 10-20 minutes. Then the temperature of the "cold rod" is set at + 50ºC and the melting deposits are collected in previously weighed collecting jar and weighed.

3. Discussion and Results

According to the results of the experiments to the following conclusions were deduced:

1) *The effect of temperature treatment on the deposit yield from oil.* The research was conducted at three temperatures: -10 °C, -20 °C and -30 °C. The lowest (less rigid) temperature was selected for -10 ° C, since with a further increase in temperature, the yield of structural components is insignificant. Also, the temperature was not lowered below -30 ° C for reasons of compliance with the energy efficiency of the technology.

Tab. 3.1 and Fig. s 3.1 show the results of deposit from the treatment temperature. The method of removal of asphaltenes is based on the sedimentation of asphaltene particles by washing the deposits with n-hexane in ratio of solvent:deposit = 40: 1 and further filtering and drying the separated deposit.

Tab. 3.1. Dependence of deposit yield from oil A, B and C on treatment temperature

Temperature, °C	Heavy oil deposit output, %			Asphaltene output, %					
				Dependence on initial composition of asphaltene			Dependence on oil		
	Oil A	Oil B	Oil C	Oil A	Oil B	Oil C	Oil A	Oil B	Oil C
-10	4,72	5,05	7,73	9,4	17,3	10,3	0,08	0,19	0,19
-20	5,87	14,17	23,83	11,5	25,6	40,00	0,09	0,28	0,72
-30	8,50	23,26	39,08	16,8	36,8	74,3	0,13	0,40	1,34
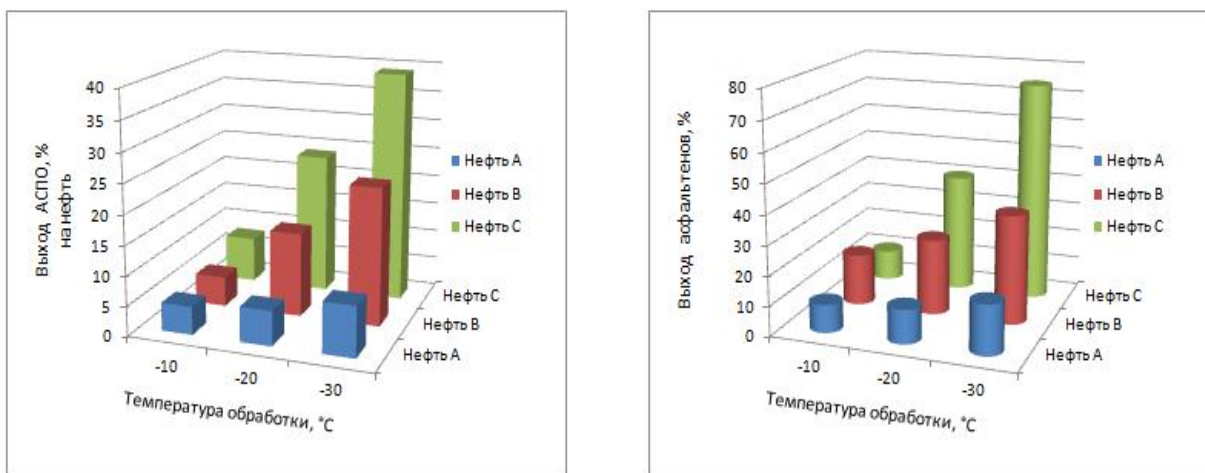
Fig. 3.1 – The dependence of the deposit outputs from oil A, B and C on the treatment temperature

The graphs revealed a general pattern: as the temperature decreases, the yield of both asphalt-resin-paraffin deposits and asphaltenes increases. The temperature at -30 ° C intensifies a greater release of structural components.

It can be noted that from oil A to oil C, with the same temperature parameter, an increase in deposit yield is observed. Apparently, this is due to the different content of paraffins in the oil, which are the centre of crystallization, initiating the formation of deposits. The highest content of paraffins is noted in oil C, which is correlated with the maximum deposition of this oil. Directly from oil A to oil C and from oil B to oil C, this increase is correlated with an increase in paraffin and asphaltene components in the original media. However, from oil A to oil B, the increase in deposits is due to the fact that at negative temperatures paraffins are capable of forming large crystals not only between their molecules, but also co-crystallize with precipitated associates of asphaltene components. Asphaltenes are probably an additional centre of crystallization, which favours the coprecipitation of solid paraffins.

2) The effect of watering on the yield of deposits in oil at a constant temperature. Oil emulsions was subjected to low-temperature treatment with different content of the aqueous phase. The results of the output of heavy oil deposits and asphaltenes in emulsions (based on oil C) of different watering after the "cold" rod are presented in Fig. 3.2. Fig. 3.2 shows the dependencies of heavy oil deposit output on emulsions at various process temperatures.
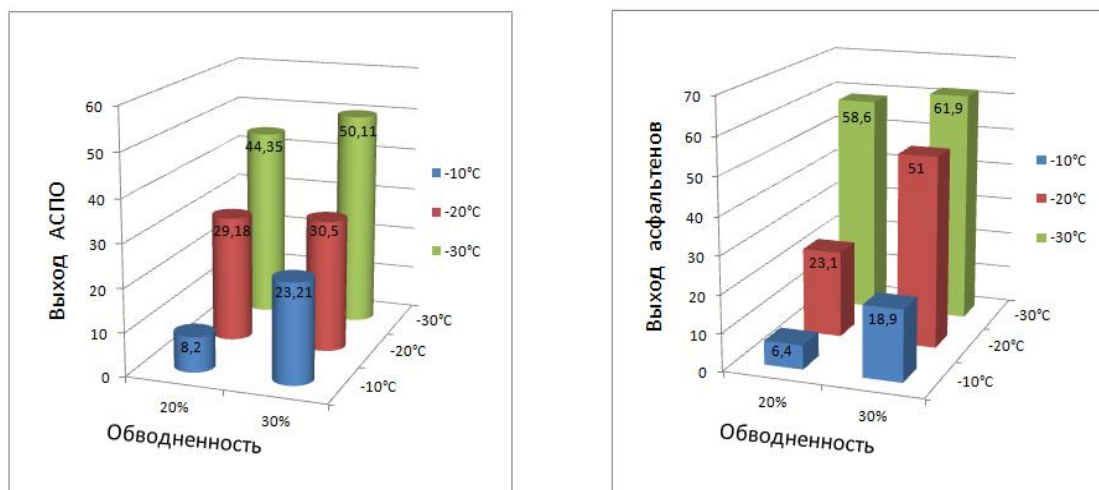
Fig. 3.2 - The dependence of the output of heavy oil deposit output and asphaltenes on the treatment temperature of the emulsions

At all temperatures, there is an increase in deposit yield as the water content of the emulsion increases. Perhaps, with a decrease in temperature and with an increase in watering, there is an intensive deposition of asphalt-resin-paraffins due to the concomitant active immobilization of the emulsified liquid phase (water) on the surface of rods.

Also, a greater decrease in the treatment temperature tends to have a higher concentration of asphaltenes in the deposits.

3) Evaluation of changes in the properties of oil after treatment of CR. The effect of different treatment temperatures on the change in viscosity of oils was reviewed and analyzed. Tab. 3.3 presents the obtained data on the viscosity of the raw and processed oil A.

Tab. 3.3. Change in viscosity of untreated and treated oil A

Speed rate (viscosimeter), rpm	Oil A	Treated oil, -10°C	Treated oil, -20°C	Treated oil, -30°C
	Dynamic Viscosity, cP:	Dynamic Viscosity, cP:	Dynamic Viscosity, cP:	Dynamic Viscosity, cP:
5	603	627	487	494
10	449	449	339	322
15	405	393	236	261
20	377	359	228	216
25	351	332	220	202
30	338	314	213	193
35	326	302	206	185
40	315	291	199	176

The rheogram (Fig. 3.3) graphically displays the change in viscosity for untreated and treated oil A from shear stress.

An improvement in viscosity properties is observed with a decrease in temperature. The lower the core temperature, the better the oil pumpability. From the point of view of the choice of treatment temperature, it can be seen that lowering the temperature below -20 ° C does not significantly change the rheological properties of the oil.
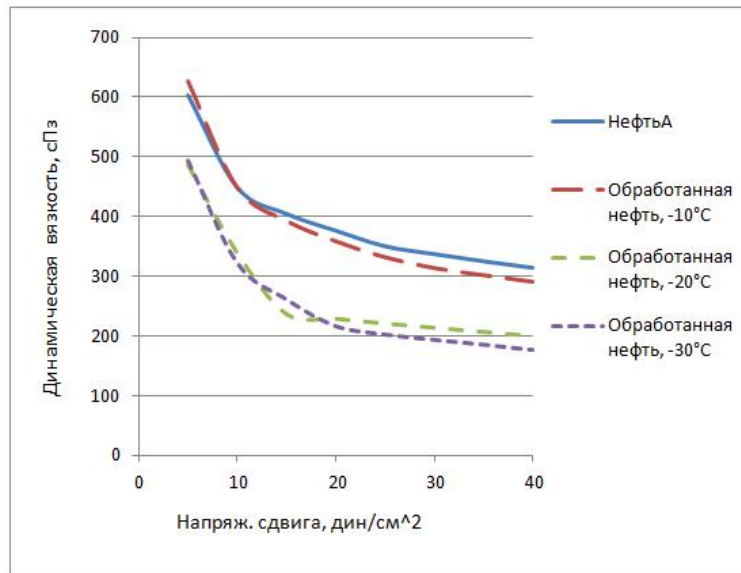
Fig. 3.3. Rheogram of crude and treated oil A

Tab. 3.4 and Fig. 3.4 present data on the change in the viscosity of the untreated and treated oils B.

Tab. 3.4. Change in viscosity of untreated and treated oil B.

Speed rate (viscosimeter), rpm	Oil B	Treated oil, -10°C	Treated oil, -20°C	Treated oil, -30°C
	Dynamic Viscosity, cP:	Dynamic Viscosity, cP:	Dynamic Viscosity, cP:	Dynamic Viscosity, cP:
5	355	235	158	530
10	354	237	160	472
15	351	237	159	465
20	347	237	159	450
25	344	237	159	446
30	340	237	159	442
35	335	237	159	434
40	333	237	159	428
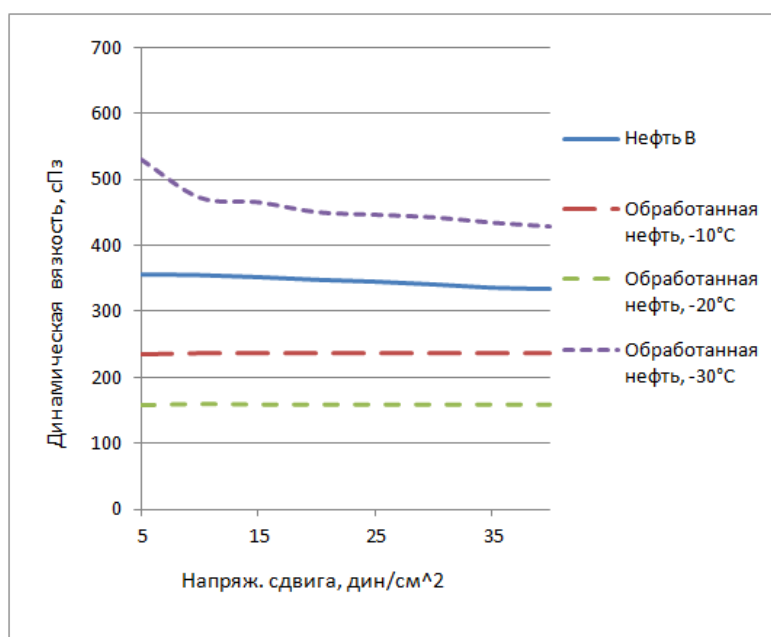
Fig. 3.4. Rheogram of crude and treated oil B

As in the case of oil A, treatment is preferable at –20 ° C. In this case, the viscosity of the oil also decreases by an order of magnitude with decreasing temperature. However, at a temperature of -30 ° C, the viscosity of the treated oil relative to the initial oil increases 1.5 times. This is probably due to the redistribution of supramolecular structures of the CAB, in particular asphaltenes. Tab. 3.5 presents data on the viscosity of the untreated and treated oil C. Fig. 3.5. shows the rheogram of the raw and processed oil C.

Tab. 5. Change in the viscosity of the untreated and treated oil C

Speed rate (viscosimeter), rpm	Oil C	Treated oil, -10°C	Treated oil, -20°C	Treated oil, -30°C
	Dynamic Viscosity, cP:	Dynamic Viscosity, cP:	Dynamic Viscosity, cP:	Dynamic Viscosity, cP:
5	116,6	116	121	642
10	82	70	84	185
15	53	38	64	131
20	24,6	3	44	91
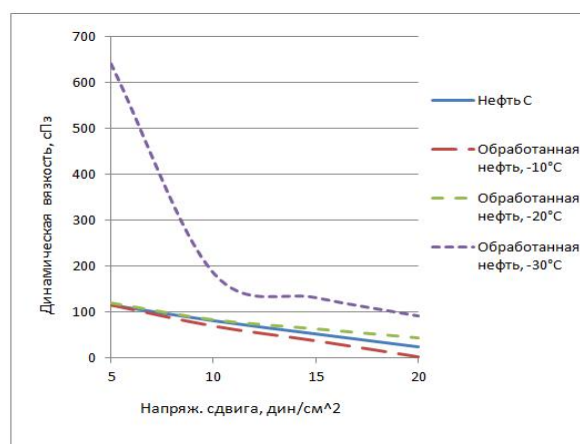
Fig. 3.5. Rheogram of untreated and treated oil C

Regarding this graph, it can be said that treatment at -10 ° C and -20 ° C does not affect the viscosity. As the temperature becomes more rigid (-30 ° C), viscosity increase is clearly noticeable, the nature of the curves also does not have flatness. These dependences are explained from the same positions that were described in the case of oil B.

4. Conclusions

During the course of this work, the influence of physical methods on oil and water-oil systems was studied. It is shown that the "cold" rod method: contributes to increase in the yield of the CAB with decrease in the treatment temperature and an increase in the water content; some decrease in viscosity at certain temperature of processing and at certain class of oil; using secondary treatment for removed sediments at -20 ° C, it allows extraction of entrained light oil components and returning them to the main stream.

References

[1] Электронный ресурс – Режим доступна: https://studfiles.net/preview/2181853/

[2] АСПО [Электронный ресурс]. – Режим доступа: http://mpk-vnp.com/neft/obrazovanie-aspo-i-parafinov

[3] Р.З. Сафиева. Химия нефти и газа. Нефтяные дисперсные системы: состав и свойства (часть 1). Учебное пособие. М.: РГУ нефти и газа им. И.М.Губкина. 2004.

[4] Дияров И.Н. Химия нефти. Руководство к лабораторным занятиям: учеб. пособие для вузов/ И.Н. Дияров, И.Ю. Батуева, А.Н. Садыков, и др. – Л.: Химия, 1990. -240с.

Catalytic applications of nickel coatings modify with palladium ions obtained by electroless metallization of 3D prints

Katarzyna Skibińska[1], Karolina Kołczyk-Siedlecka[1], Dawid Kutyła[1], Piotr Żabiński[1]

[1]Faculty of Non-Ferrous Metals, AGH University of Science and Technology, e-mail: kskib@agh.edu.pl

Abstract:

3D printing is a technology allows to produce elements of any geometry and made of plastic. According to application, the prints can be metalized to give them new properties such as conductivity, corrosion resistance or catalytic properties. This work shows the studies on the cementation process and thin palladium layers formation onto nickel coatings, which had been electroless deposited on 3D prints. Nickel coatings were catalytically deposited on elements printed from hard-lightened resin. Then they were modifyby the galvanic displacement method in $PdCl_2$ solution to obtain Ni/Pd layers. The morphology of surface was observed by scanning electron microscopy (SEM) and samples were analyzed by XRD method. The electrocatalytic properties of Ni and Ni/Pd coatings were analyzed and compared.

Keywords: electroless deposition, nickel, palladium, 3D prints, metallization

1. Introduction

Hydrogen evolution reaction at the cathode is one of the most frequent reactions in electrochemical industrial installations[1]. One of the newest uses of this reaction is "solar fuel"[2]. The integrated device would use sunlight absorbed by semiconductors connected to electrocatalysts to break down water. It would enable obtaining fuels using sunlight. All catalysts are deposited on various substrates, while their chemical activity is measured in electrolytes with different compositions, pH or temperature. This makes it difficult to assess the properties of these materials, but gives many possibilities for their use.

Nickel and its alloys is usually used as a catalysts for hydrogen evolution reaction[3]–[5]. In theliterature are many works dealing with electrodeposition these materials, for example: Ni-Cu [3], Ni-Co [6], Ni-W [7], Ni-S-Fe [8] and Ni-Co-W [9]. These coatings are characterized by better catalytic properties than pure nickel and in most cases they even could replace expensive noble metals.

3D printing is a technology in which materials are overlapped layer by layer. In this fast method samples could be obtained in any geometry directly from digital project. This technology is used in many industry sectors, for examples: the food [10], medical [11]–[13]and energy sectors [14]. Technology of metallization 3D prints is multi-stage process. K. Kołczyk-Siedlecka and co-workers [15] had electroless deposited copper and nickel on plastic samples. They investigated the influence of magnetic field on these coatings.

The coatings obtained in electroless deposition are different than the ones obtained by electrodeposition. They are characterized by good corrosion resistance and good solderability. In this way, for example, gold[16], silver[17], cobalt[18], palladium[19] as well as aluminum[20] can be deposited. The condition for the occurrence of electroless deposition of metals is the less noble nature of the oxidation potential of the reducing agent in comparison with the metal deposition potential.

For cementation method, the precursor is usually a less noble metal M according to the galvanic series with a standard electrochemical potential lower than the potential of Pd [21]. The cementation process is carried out by placing a metal M into a solution containing palladium ions. The metal M is oxidized by palladium ion, which are reduced and deposited atthe surface. The substitution of metal M by this palladiumions is irreversible. The driving force of this process is the positive value of the difference between the metal equilibrium potential on the surface and the potential of palladium balance in the presence of its complexes. The stoichiometry of the redox reaction thus allows determination of the amount of palladium deposited. K. Skibińska and co-workers [22] electroless deposited Pd on Co samples. Presence of palladium decreased the overpotential of hydrogen

evolution reaction. This method ofmodification of cobalt coatings is low cost and easy method to improve their catalytic activity for water splitting reaction.

The aim of this work is modification and measurement of the catalytic properties of Ni coatings deposited on plastic 3D printsmodified by Pd. The analyzed coatings may find a potential application in industrial catalytic processes, due to lightness and much lower price in compare to pure noble metals.

2.   Experimental section

In experimental work the substrate were 3D prints prepared by SLA technology on Formlabs Form 2 printer from light-hardened resin (Clear – GPCL02) characterized by chemical resistance. To remove the liquid resin from the surface the printed elements were cleaned in isopropyl alcohol, washed in deionized water and dried.

Preparation of the samples for the metallization is a multi-stage process. The compositions of individual electrolytes could be found in the Tab. 2.1. All reagents were characterized by analytical purity.

The first step was degreasing for 10 minutes at 70 $^{\circ}$C. After every step the samples were washed in deionized waterand dried. Then the samples were etched for t = 1min at 70 $^{\circ}$Cusingeatching solution (see Tab. 2.1). The next step was neutralizating. The samples were immersed into solution (Tab. 2.1) for 2 minutes at 23°C to remove chromium ions from the surface of the plastic. Adsorption of tin ions was carried out for 2 minutes. The next step was activating for 2 minutes in activating solution (Tab. 2.1). After that the samples were placed in a metallizing bath (Tab. 2.1)for 5 to 60 minutes at 65 °C. The pH of the solution was 9.

Tab. 2.1 The compositions of used electrolytes.

Stage of the process	Composition of electrolyte
Degreasing	5% wt. NaOH
Etching	95% H_2SO_4 (250 ml), Cr_2O_3 (50 g) and H_2O (150 ml)
Neutralizing	5% wt. HCl solution with an addition of 5% wt. $K_2S_2O_5$
Adsorption	50 cm^3/dm^3 HCl with 10 g/dm^3 $SnCl_2$
Activating	0.2 g/dm^3 $PdCl_2$ and 10 cm^3/dm^3 HCl
Metallization	30 g/dm^3 $NiCl_2 \cdot 6H_2O$, 20 g/dm^3 $NaH_2PO_2 \cdot H_2O$, 50 g/dm^3 $Na_3C_6H_5O_7$, 15 g/dm^3 NH_4Cl.

The electroless Pd deposition solution was prepared by weighing on the analytical balance and reconstituting a sufficient amount of hydrated palladium chloride in concentrated hydrochloric acid. The pH of the solutions was 1.3. The process time was 300, 600, 900, 1800and 3600 s.The catalytic efficiencyon obtained coatings was estimated from linear scan voltammetry. The determination of open circuit potential (OCP) was determined using the Bio-Logic SP-300 potentiostat. This value determines the anti-corrosive properties of coatings. Each of samples were placed into 1 M NaOH solution for 5 minutes to obtain a starting point for linear scan voltammetry (LSV) measurements. The LV curves weremeasured in a range from Open Circuit value to -2V vs saturated calomel electrode (SCE). Linear scans have been performed with a low scan speed (5mV/s) with non-stirred electrolyte. Hydrogen emitted on the surface of the coating oxidizes the deposited oxides and hydroxides to the metal form, it also allows to determine the overpotential of hydrogen evolution. The process of hydrogen evolution was carried out in a three-electrode cell containing a 1M NaOH solution. The electrolyte was deoxygenated by argon. The working electrode was metalized 3D print, the anode was a platinum plate. A saturated calomel electrode was used as a reference. In these measurements, the slope of polarization and onset potential for hydrogen evolution reaction curve are read.

Phase analysis of coatings was performed using the XRD method (Rigaku MiniFlex II). Microstructure and the compositions were observed using the SEM technique (JCM-6000 Plus Versatile Benchtop SEM).

3. Results and discussion

The electrocatalytic properties of nickel coatings obtained were determined by releasing hydrogen evolutionreaction on their surface. The coatings were deposited from the solution in different times.
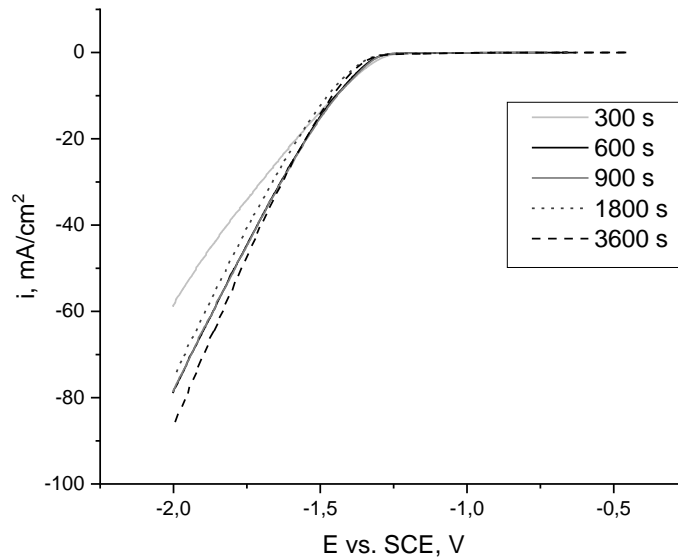
Fig. 3.1LSV curves of nickel coatings electroless deposited for times 300, 600, 900, 1800 and 3600 s, respectively.

Fig. 3.1 shows that based on LSV curves obtained for individual electroless deposited nickel coatings. Depending on the metallization time, there were obtained coatings with different catalytic properties. Nickel coating deposited in 300 s is characterized by worse catalytic properties than coating obtained in longer time, especially in 3600 s. It is a result of the content of phosphorus in coatings depending on the time of metallization. Nickel coatings, in the initial stage of the process, are characterized by higher concentration of phosphorous (7,5% mass.). The amount of phosphorus is decreasing to the value of approximately 3% mass. with the increasing time. Due to these facts, coatings obtained in t = 3600 s were chosen for modification by palladium ions.
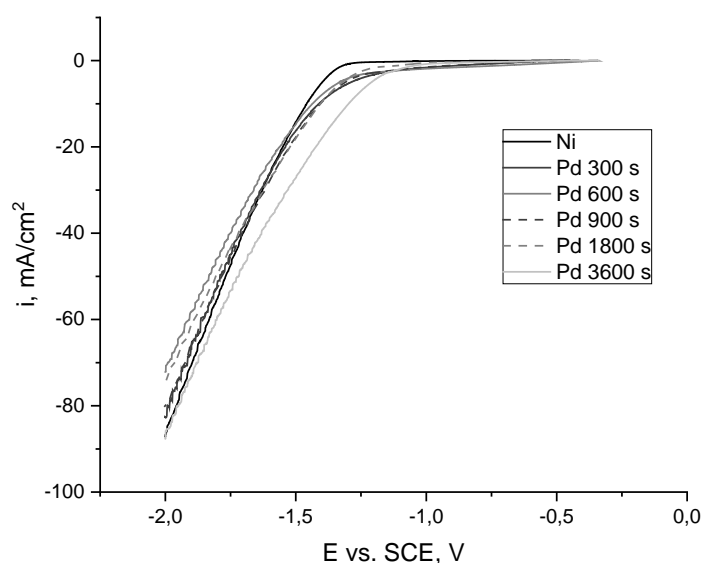
Fig. 3.2 LSV curves of nickel coatings modificated with palladium ions for times 300, 600, 900, 1800 and 3600 s, respectively.

Fig. 3.2 shows LSV curves for samples after modification by palladium ions the hydrogen evolution reaction started in higher potential than for nickel coatings.The process of modification allowed to increase catalytic activity of samples. It can be connected with increase of the surface area of sample and number of active sites, where overpotential for this reaction is lower.
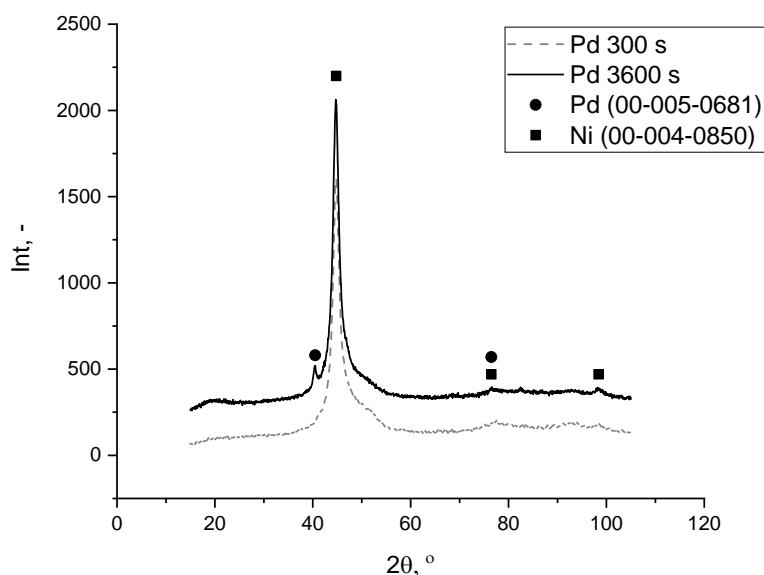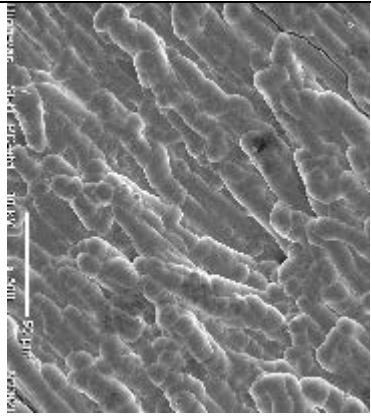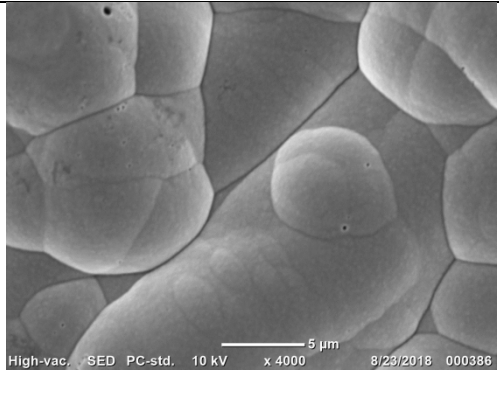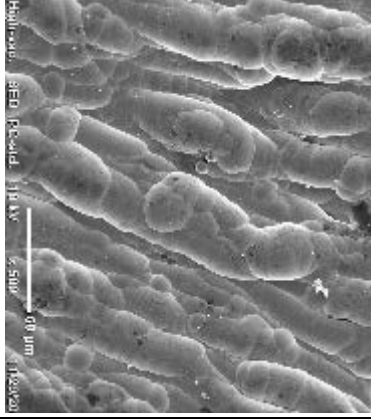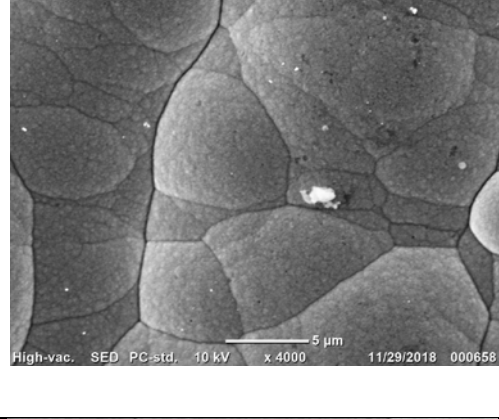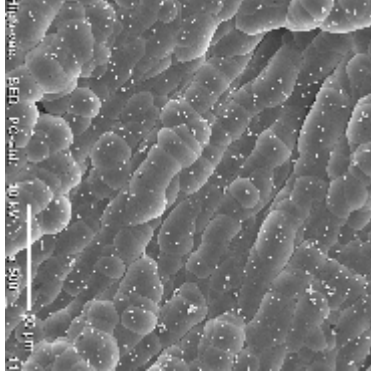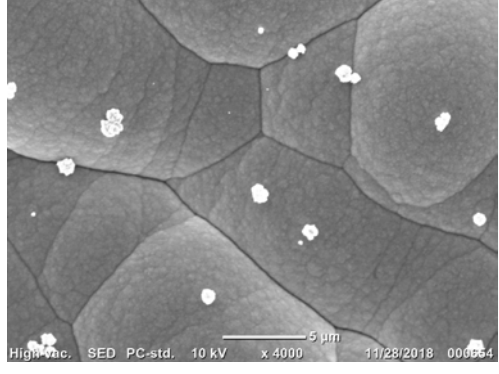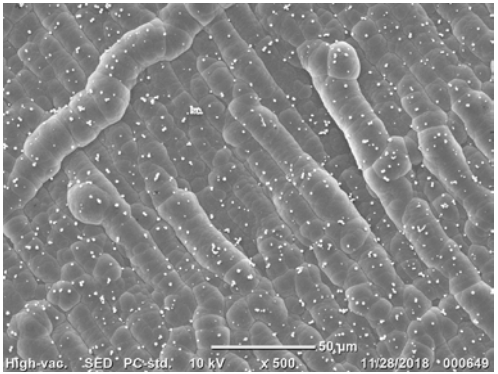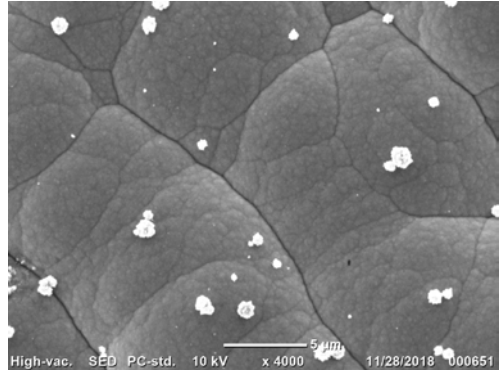
Fig. 3.3 X-ray diffraction patterns of Ni coatings after galvanic displacement by palladium ions for 300 and 3600 s.

Fig. 3.3 presents the phase composition of nickel coating after modification. For sample after longer time of cementation process, the new palladium peak is observed and the other two are higher in compare to coating obtained in 300 s. This is connected with ion exchange on the sample surface and increasing of palladium composition in Ni/Pd coatings.

	500x	4000x
Ni		
Pd 300 s		
Pd 600 s		
Pd 900 s		
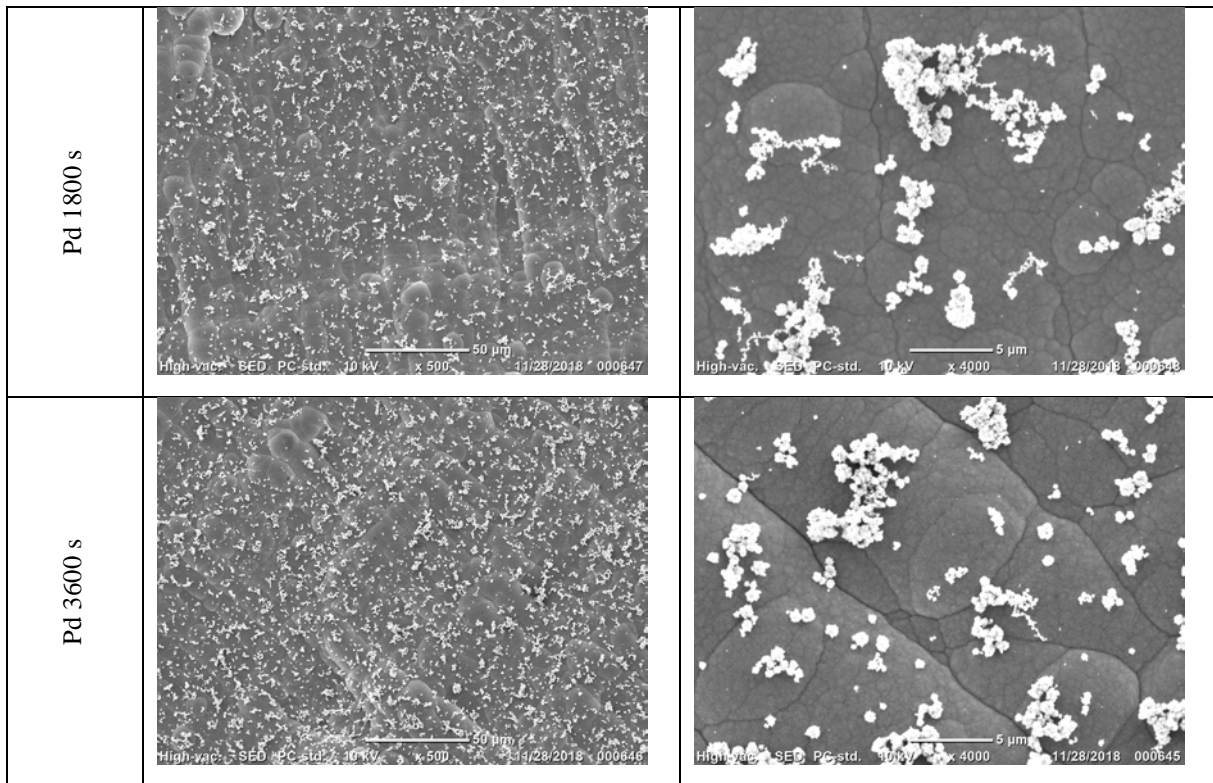
Fig. 3.4 Compared the SEM pictures of nickel with coatings modify for times 300, 600, 900, 1800 and 3600 s.

The SEM pictures showed on Fig. 3.4 present that number of nucleation sites of crystallization increased with increase of time of modification with palladium ions. In most cases they occurred on the border of grains. Deposited nickel coatings noticeable in the background is characterized by linearity which is connected with restoration of the substrate shape, coming from the resin layers obtained during the printing of the elements.
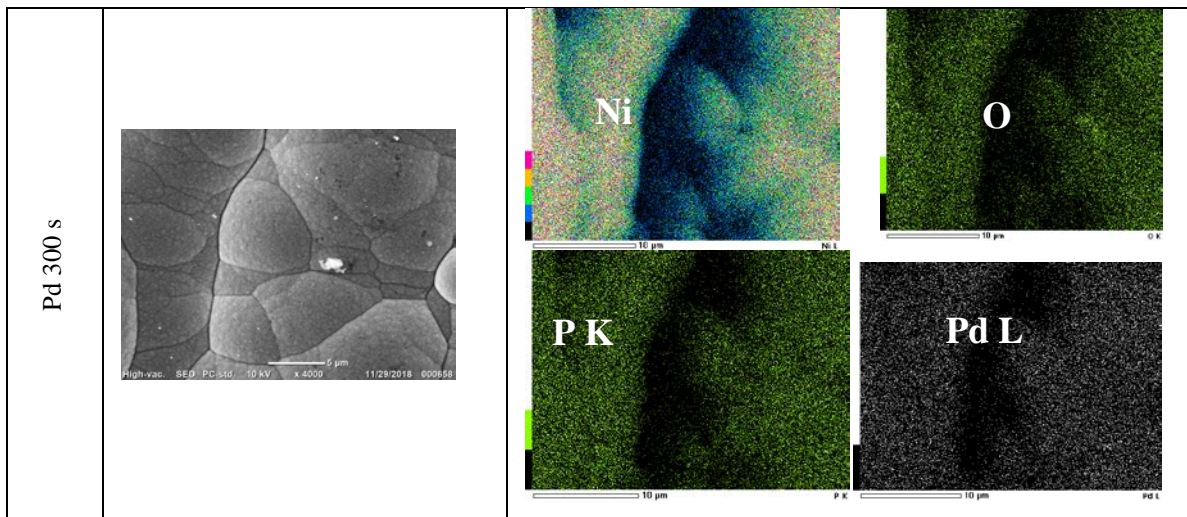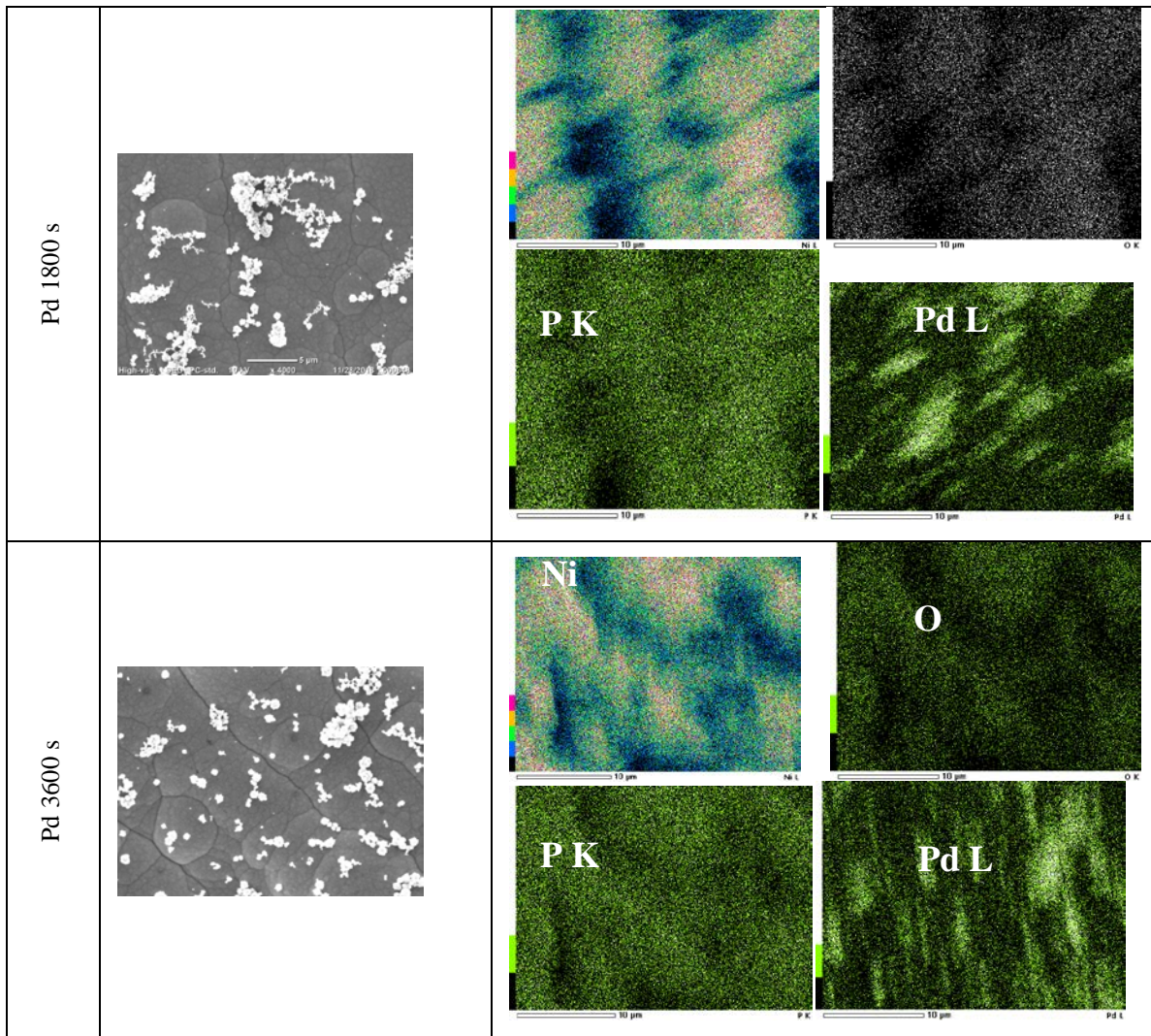
Fig. 3.5 SEM pictures and mapping of Ni samples obtained by cementation process for different times 300, 1800 and 3600 s.

Fig. 3.5 shows mapping of selected samples at a magnification of 4000x. It can be notice that palladium occurred only in selected places forming linear grains. The present phosphorus came from reductant.

4. Conclusions

The aim of this work was amodification of metallization nickel coatings to obtain better catalytic properties. Parameters of metallization for modification was choose based on the catalytic tests of nickel coatings. The cementation process improved these properties especially for the sample after modification time t = 3600 s for which the hydrogen evolution reaction was started at the highest potential value.

Phase analysis proved that with increase time of galvanic displacement more palladium occurred on the surface and the Pd peak was higher. SEM pictures and mapping show characteristic places – grain's bonders where palladium nucleation occur and increase. In every case nickel surfaces have characteristic linear structures.

Acknowledgment

References

[1] A. Kadier, Y. Simayi, M. S. Kalil, P. Abdeshahian, and A. A. Hamid, "A review of the substrates used in microbial electrolysis cells (MECs) for producing sustainable and clean hydrogen gas," Renew. Energy, vol. 71, pp. 466–472, 2014.

[2] Michael R. Nellist, Forrest A. L. Laskowski, Fuding Lin, Thomas J. Mills, Shannon W. Boettcher, "Semiconductor–Electrocatalyst Interfaces: Theory, Experiment, and Applications in Photoelectrochemical Water Splitting," Acc. Chem. Res., vol. 49, no. 4, pp. 733–740, 2016.

[3] K. Ngamlerdpokin and N. Tantavichet, "Electrodeposition of nickel-copper alloys to use as a cathode for hydrogen evolution in an alkaline media," Int. J. Hydrogen Energy, vol. 39, no. 6, pp. 2505–2515, 2014.

[4] K. S. Bhat and H. S. Nagaraja, "Nickel selenide nanostructures as an electrocatalyst for hydrogen evolution reaction," Int. J. Hydrogen Energy, vol. 43, no. 43, pp. 19851–19863, 2018.

[5] G. Barati Darband, M. Aliofkhazraei, and A. Sabour Rouhaghdam, "Nickel nanocones as efficient and sTab. catalyst for electrochemical hydrogen evolution reaction," Int. J. Hydrogen Energy, vol. 42, no. 21, pp. 14560–14565, 2017.

[6] Y. Li, X. Zhang, A. Hu, and M. Li, "Morphological variation of electrodeposited nanostructured Ni-Co alloy electrodes and their property for hydrogen evolution reaction," Int. J. Hydrogen Energy, vol. 3, 2018.

[7] S. H. Hong et al., "High-activity electrodeposited NiW catalysts for hydrogen evolution in alkaline water electrolysis," Appl. Surf. Sci., vol. 349, pp. 629–635, 2015.

[8] Y. Wu and H. He, "Direct-current electrodeposition of Ni-S-Fe alloy for hydrogen evolution reaction in alkaline solution," Int. J. Hydrogen Energy, vol. 43, no. 4, pp. 1989–1997, 2018.

[9] C. Lupi, A. Dell'Era, and M. Pasquali, "Effectiveness of sodium citrate on electrodeposition process of Ni[sbnd]Co[sbnd]W alloys for hydrogen evolution reaction," Int. J. Hydrogen Energy, vol. 42, no. 48, pp. 28766–28776, 2017.

[10] Z. Liu, M. Zhang, B. Bhandari, and Y. Wang, "3D printing: Printing precision and application in food sector," Trends Food Sci. Technol., vol. 69, pp. 83–94, 2017.

[11] A. Marro, T. Bandukwala, and W. Mak, "Three-Dimensional Printing and Medical Imaging: A Review of the Methods and Applications," Curr. Probl. Diagn. Radiol., vol. 45, no. 1, pp. 2–9, 2016.

[12] Q. Yan et al., "A Review of 3D Printing Technology for Medical Applications," Engineering, vol. 4, no. 5, pp. 729–742, 2018.

[13] D. H. Ballard et al., "Clinical Applications of 3D Printing: Primer for Radiologists," Acad. Radiol., vol. 25, no. 1, pp. 52–65, 2018.

[14] F. Zhang et al., "3D printing technologies for electrochemical energy storage," Nano Energy, vol. 40, no. May, pp. 418–431, 2017.

[15] Karolina Kołczyk-Siedlecka, Wojciech Zborowski, Dawid Kutyła, Anna Kwiecińska, Remigiusz Kowalik, Piotr Żabiński, "Investigation of two-step metallization process of plastic 3D prints fabricated," Arch. Metall. Mater., vol. 63, no. 2, pp. 1031–1036, 2018.

[16] S. J. Bell et al., "Comparison of the surfaces and interfaces formed for sputter and electroless deposited gold contacts on CdZnTe," Appl. Surf. Sci., vol. 427, pp. 1257–1270, 2018.

[17] C. N. Grabill, D. Freppon, M. Hettinger, and S. M. Kuebler, "Nanoscale morphology of electrolessly deposited silver metal," Appl. Surf. Sci., vol. 466, no. June 2018, pp. 230–243, 2019.

[18] M. G. Ortiz, E. B. Castro, and S. G. Real, "Effect of cobalt electroless deposition on nickel hydroxide electrodes," Int. J. Hydrogen Energy, vol. 39, no. 11, pp. 6006–6012, 2014.

[19] N. Nobari, M. Behboudnia, and R. Maleki, "Palladium-free electroless deposition of pure copper film on glass substrate using hydrazine as reducing agent," Appl. Surf. Sci., vol. 385, pp. 9–17, 2016.

[20] S. Poges, J. Jin, C. Guild, W. N. Li, M. Birnkrant, and S. L. Suib, "Preparation and characterization of aluminum coatings via electroless plating onto nickel nanowires using ionic liquid plating solution," Mater. Chem. Phys., vol. 207, pp. 303–308, 2018.

[21] O. Ghodbane, L. Roué, and D. Bélanger, "Study of the electroless deposition of Pd on Cu-modified graphite electrodes by metal exchange reaction," Chem. Mater., vol. 20, no. 10, pp. 3495–3504, 2008.

[22] Katarzyna Skibińska, Dawid Kutyla, Karolina Kołczyk-Siedlecka, Anna Kwiecińska, Remigiusz Kowalik, Piotr Żabiński "Electrocatalytical properties of palladium-decorated cobalt coatings obtained by electrodeposition and galvanic displacment," Arch. Metall. Mater., vol. 63, no. 3, pp. 1517–1521, 2018.

Lactic acid - preparation by fermentation with the participation of *Lactobacillus*

Edyta Strzelec[1], Grzegorz Jodłowski[2]

[1]*AGH University of Science and Technology /Faculty of Energy and Fuels /Department of Fuel Technology, al. Mickiewicza 30 30-059 Cracow, strzelec@agh.edu.pl,*

[2]*AGH University of Science and Technology /Faculty of Energy and Fuels /Department of Fuel Technology, al. Mickiewicza 30 30-059 Cracow, jodlowsk@agh.edu.pl,*

Abstract

One of the ways of using a waste glycerol fraction is its conversion to lactic acid. Lactic fermentation, or the proper process responsible for this pathway of glycerol transformation, is a biochemical process that uses enzymes in its essence - proper biocatalysts. Thanks to their undemanding working conditions, they are able to cooperate in obtaining compounds that are attractive from the point of view of the chemical industry. Such a process can be safely connected to the part of biodiesel technology, as one of the elements of the closed circuit of the existing technology.

Key words: biotechnology, lactic acid bacteria, glycerol, lactic acid

1. Introduction

At the turn of a dozen or so years, you can see developing trends that reduce the impact of technologies and waste generated from production.

White biotechnology is developing delightfully quickly. Everything happens for purely economic and ecological reasons. For example, it is primarily waste management or planning experiments that will be related to the use of microorganisms or will allow for implementations related to changes in refinery processes in "biorefinery", and thus will change the face of already existing refineries in a more friendly environment and man. White biotechnology is often called industrial, and this is because it was created for this purpose to introduce changes leading to lowering the negative effects of heavy technologies serving the industry.

In the production of biofuels, especially alcohol esters of fatty acids (obtained in the transesterification reaction with methanol with the participation of a catalyst) waste is also produced in addition to the main product. This is a problem for many industrial companies that are doing everything to prevent or reduce the production of unwanted waste that entails the costliness of processes. Glycerin waste in the production of biodiesel is cumbersome, even after purification for later development. The cosmetics industry, which is overloaded with this product, does not meet the maximum use of available glycerine in order to make up for these overproduction.

The search for new management solutions for this waste starts with the less attractive chemical methods for modern biotechnology methods. One of these last methods is fermentation. It is a reaction in which the product can be many compounds chemically needed. It depends on the biocatalysts that will be used. This task is met by microorganisms, especially bacteria (fungi can also be used). The desired raw material obtained from fermentation using lactic acid bacteria is lactic acid. Microorganisms willing to cooperate metabolize raw materials selected in their metabolic pathways to waste, useful from our point of view (such as lactic acid).

2. Lactic acid

Lactic acid is one of the simplest organic acids containing hydroxyl and carboxylic groups in its structure. The orientation of the hydroxyl group allows for two optical isomers (L and D lactic acid). Chemical routes usually produce racemic lactic acid, while biological pathways usually approach enantiomeric purity (L variant is more common). Bifunctionality enables inter-esterification of lactic acid molecules to form dimers, trimers and longer oligomers of this acid. Lactide, as one specific dimer, arises when two molecules of lactic acid undergo inter-esterification at the substituent positions (-OH and -COOH). The result is a heterocyclic ring and this is called

ring opening polymerization of the lactide. This leads to the formation of polymers of lactic acid (*ineng. PLA, polylactic acid*) [1].
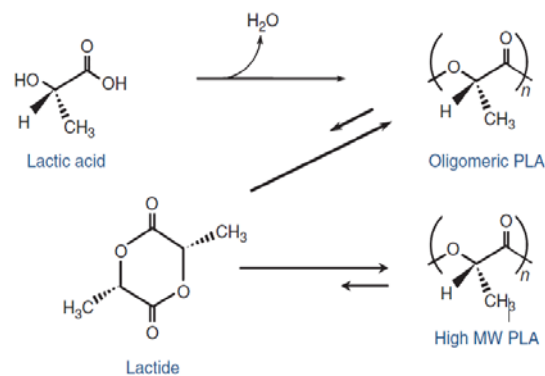
Fig. 2.1. PLA production from lactic acid(*'High MW PLA' - high molecular weight of polylactic acid*) [1].

2.1.   Chemical method for obtaining lactic acid

The commercial chemical synthesis process is based on lactonitrile. Hydrogen cyanide is added to the acetaldehyde in the presence of a base to give the lactonitrile. This reaction occurs in the liquid phase at high pressures. The crude lactonitrile is recovered and purified by distillation. It is then hydrolysed to lactic acid with concentrated hydrochloric acid or sulfuric acid (VI) to produce the corresponding ammonium and lactic acid. The esterification of lactic acid with methanol then gives ethyl lactate, which is removed and purified by distillation and hydrolyzed with water in an acidic catalyst to form lactic acid. Methanol is recycled back. The following picture 2.2. presents a short scheme for the production of lactic acid chemically [2].
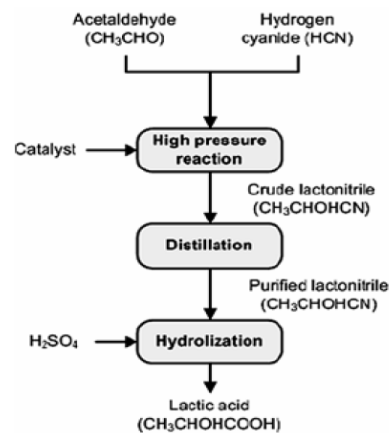
Fig. 2.2. Chemical synthesis of lactic acid production [2].

2.2.   Biotechnological method of obtaining lactic acid

The chemical synthesis method produces a racemic mixture of lactic acid. Two Musashino companies (Japan) and Sterling Chemicals Inc. (USA) are using this technology. Another way to obtain lactic acid is the method of lactic fermentation [3].

This chapter focuses on the microbiological fermentation of lactic acid. The first commercial factory was founded by Avery in the USA in 1881. Currently, raw materials for the production of lactic acid are renewable resources and waste, which is very desirable and beneficial for industry [3].

The enzymes are the most important in fermentation. They are contained in microorganisms, which are needed for further life are raw materials such as molasses, whey, glycerine and others. Microorganisms containing enzymes capable of producing interesting lactic acid called lactic acid bacteria (LAB). In order for them to be used in the process, they need to be expanded and prepared beforehand. For this purpose, a production medium

containing a source of nitrogen and vitamins is prepared. Optimal production conditions vary depending on the production strain, but generally the pH is maintained at 5-7, well above the pKa of lactic acid, which is 3.86. The temperature of bacterial lactic acid fermentation varies between 37-45 ° C [1].

However, certain limitations are known in bacterial processes. The use of rich substrates for the cultivation of microorganisms carries high costs both related to the nutrient solution and post-fermentation purification. This is because it connects to unused nutrient components in the process. It is complicated and raises the price of the process considerably. Another limitation of the process is its sterility. Bacteria surround us. It is therefore difficult to maintain a sterile environment so that the system does not infect. Techniques for maintaining sterility of systems are difficult to control especially in the case of larger lactic acid fermentations on an industrial scale, in which chiral purity, by-products and nutrient requirements have to be well defined. There are different methods to correct these difficulties. These include, among others: improvement of bacterial strains in genetic modification, development of media with additions of chemical compounds to improve breeding or development of a method for obtaining one, pure lactic acid variety. For example, having a Lactobacillus strain, its genome was improved so that the production of lactic acid in its share tripled [1] [4] [7].

Due to the fact that pKa of lactic acid is 3.86, more than 95% of lactic acid produced in a traditional microbiological process must be neutralized in order to maintain the pH in terms of bacterial viability. On an industrial scale, this is usually done with calcium hydroxide or calcium carbonate, added to the fermentation broth. Subsequently, the recovery of lactic acid from the salt formed with calcium (calcium lactate) consists in its reaction with sulfuric acid (VI). In this reaction, in addition to lactic acid, calcium sulfate (or gypsum), useful in the construction industry, is also formed. Purification, during which the recovery of lactic acid by means of physical and chemical processes is the most expensive stage in obtaining lactic acid. The ideal solution would be to eliminate the calcium lactate production stage, and instead lactic acid would be obtained directly from the fermentation. This would eliminate costs and unit operations, as a result, shortening the duration of the process. Unfortunately, it is impossible to introduce such an action. Lactic fermentation cannot work efficiently at pH values less than five because of the inhibitory effect of bacterial metabolism, and more specifically the activity of enzymes contained in them [1] [8].

2.3.   Biocatalysts of lactic fermentation

Bacteria and fungi (including yeast) are responsible for the catalysts of the lactic fermentation process. This article, however, focuses on lactic acid bacteria. They belong to the most researched microorganisms, among which there are those with the most desirable industrial characteristics. These features include the ability to quickly and completely ferment the available (and therefore cheap) raw material, minimum nitrogen demand, ensuring high yields of the preferred stereospecific lactic acid at low and high pH conditions (ie resistance to reaction changes). The choice of a microorganism depends primarily on the carbohydrate or compound that is to be fermented, i.e. on the fermentation. For example, the product may contain sucrose, lactose or glucose. Due to the metabolic pathways and lactic acid bacteria metabolism products obtained, they can be divided into three groups:

I.   homofermentative (the product is only lactic acid)

II.   optionally heterofermentative (the product is lactic acid or / and acetic acid, carbon dioxide)

III.   heterofermentative (products are lactic acid, acetic acid and carbon dioxide)

These groups show what possible routes of fermentation are available and possible to use and explain the mechanism of formation of metabolites, and thus products after the process [2] [4].

3. Laboratory research

As mentioned before, microorganisms dedicated to this process are needed for the production of lactic acid. They can be obtained from ready-made commercial farms or to reduce the total costs, a microbiological culture can be set up.

On the basis of fermented milk, more than four hundred types of dairy products are obtained, of which the leading ones are: kefir, buttermilk, yogurt and sour milk. Dairy produced by lactic fermentation has in its

composition some cultures of lactic acid bacteria that ensure proper functioning of the digestive system in humans.

3.1.   Initial screening of microorganisms

To detect and isolate microorganisms contained in the selected dairy, the necessary dairy products were purchased and samples were prepared in flasks with skimmed milk. After an incubation test lasting three days, organoleptic determination was determined in which the sample was clot. This indicated the microbiological activity of lactic acid-producing organisms derived from fermentation, i.e. from the breakdown of lactose from milk to lactic acid.

Below picture 3.1. shows the appearance of the clot (sample on the left) and no clot, i.e. bacteria inactive in the sample (sample on the right).

Pic .3.1. Clots in flasks after three days of incubation.

To confirm the presence of bacteria in the samples, microscopic preparations were prepared for further testing. A light microscope with a bright field of view is used to observe the bacteria. Cells stained with special reagents are identified in the field of view of the microscope. That's why different dyeing methods are used. One of these methods is the use of a Loeffler reagent, i.e. methylene blue, whose functional group reacts with the chemical compounds contained in the bacterial envelope. This results in a color and allows the confirmation of the existence of microorganisms.

Microscopic preparations in the experiment were created by applying bacterial cells in an antiseptic environment. Preparations prepared in this way were fixed and examined using an armed eye (Pic 3.2).

The staining of the preparations favored the observation of the size, shape and structure of the bacteria. Bacteria took forms of kernels and sticks. They testified, along with the dairy products indicated by the producers, with the presence of *Lactobacillus* bacteria (the most numerous group in the samples, apart from the less interesting *Streptococcus* bacteria detected).

sample 1   sample 3   sample 6

sample 4   sample 8
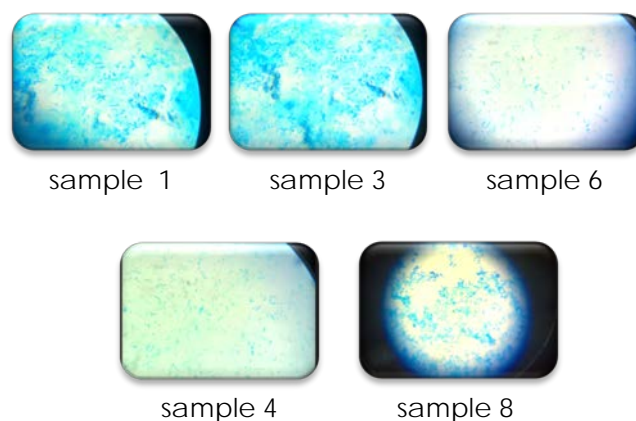
Fig. 3.2. Selected microscopic preparations.

3.2.   Preparation of nutrients

One of the simpler nutrients is food agar. It is a multi-sugar obtained from sea algae and exactly from algae. Together with additives providing nutrients, it is prepared in the form of agar plates or slants. The second medium was Demeter's medium. It also consists of agar, but the additional ingredient is a coloring compound. Both media were prepared according to the recipe found in the book "Handbook of Microbiological Media" 2nd edition, by R.M. Atlas, CRC - Press, 1996 (pp. 56-57 and 930). Subsequently, microbiological media were sterilized in Koch and autoclaves.

3.3.   Culture of material on culture media

The prepared media were poured into Petri dishes, in a sterile condition they solidified, and then the bacterial material was applied three times to each of the plates. There were three sources of bacteria:

a.   From dairy products (Pic 3.3)

b.   From glycerine (bank of the Department of Microbiology, University of Agriculture)

c.   Refreshed strains of lactic bacteria from the collection of the Department of Microbiology at the University of Agriculture
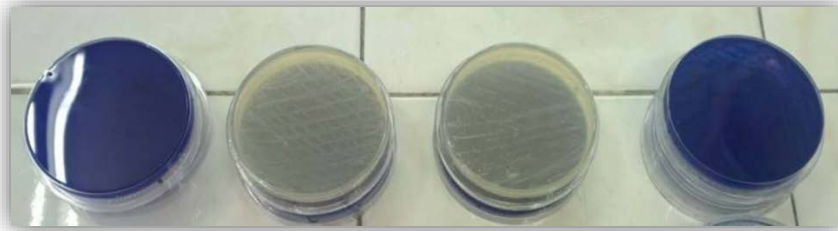
Fig. 3.3. Plates of sown bacteria isolated from commercial products.

3.4.   Isolation of pure strains and multiplication

After the subsequent incubation period of the growing bacterial cultures, each pan contained strains of various microorganisms. To isolate those that are needed for fermentation, the method of reduction cultures was used. This method allows to determine the morphology of the colonies and also allows the maximum probability of obtaining pure cultures. According to picture 3.4. the method of polygonal passage has been clearly presented.
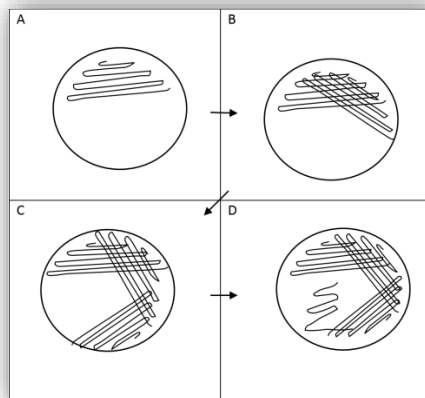
Fig. 3.4. Method of surface reduction cultures.

After the next incubation period, those that gave the best result of isolated strains were selected. Subsequently, these samples were multiplied, duplicating them several times. The cultures so prepared were ready for use in the right biotechnological process.

3.5.   Fermentation

A kit containing a water bath with six fermenters was assembled to carry out the fermentation process. A substrate for reactors (molasses, glycerin) - previously prepared, which was subsequently inoculated with appropriate bacteria [5] [6]. The tubes leaving the fermenters were used to collect any biogas that could be formed (picture 3.5).

Fig. 3.5. Research stand for fermentation.

The pH and process temperature were optimized, and samples were taken during and after the process for further analysis. The process was monitored all the time. After a certain time, the conducted fermentations were completed and the results obtained from the analyzes were summarized. Among the methods of purification and analysis of lactic acid in samples taken, the most available ones were selected.

They have led to further studies, during which the criterion and principles of analyzing and determining lactic acid are established. On the basis of the spectrophotometric method, after the initial analysis, it is possible to determine the presence of the desired product. This initiates the process of successive repetitions of the above-described tests and validation of the method for qualitative and quantitative determination of lactic acid.

4. Summary

The fermentation process as a way to obtain precious lactic acid seems to be the right way to process industrial and food waste. This widens the horizons associated with waste management, and thus reduces the cost of their disposal, but also somehow allows for the optimization of the circulation of matter in nature, which is currently considered the basis of the circular economy.

The laboratory scale of the research (which is translated on a technical scale, but under different conditions and with the use of other biocatalysts) presented the fairness of managing available waste materials. The results of the research may indicate a rational approach to the problem. It starts a cause and effect sequence, which entails further development of previously unknown areas of the described topics.

Acknowledgements

Bibliography

[1] Miller C. et al, *Industrial Production of Lactic Acid;* Cargill Incorporated, Biotechnology Development Center, Elsevier B.V.;179-188; Minneapolis, MN, USA, 2011

[2] Lii Y., Cui F., *Microbial Lactic Acid Production from Renewable Resources;* Sustainable Biotechnology, Springer; 211-228; Ohio, USA, 2010

[3] Jim Jem K et al, *Microbial Lactic Acid, Its Polymer Poly(lactic acid), and Their Industrial Applications;* Plastics from Bacteria; Natural Functions and Applications, Springer; 323-346; Berlin, 2010

[4] Narayanan N. et al, *L (+) lactic acid fermentation and its product polymerization;* Electronic Journal of Biotechnology; 7(2), 2004

[5] Kośmider A., Czaczyk K., *Perspektywywywykorzystaniaglicerolu w procesachbiotechnologicznych;* Post. Mikrobiol.; 48, 4, 277-287, 2009

[6] Ciriminna R. et al, *Understanding the glycerol market;* Eur. J. Lipid Sci. Technol.; 116, 1432-1439, 2014

[7] Wee Y.J. et al, *Pilot – Scale Lactic Acid Production via Batch Culturing of Lactobacillus sp. RKY2 Using Corn Step Liquor As a Nitrogen Source;* Food Technol. Biotechnol.; 44, 2, 293-298, 2006

[8] Hong A. et al., *Strain isolation and optimization od proces parameters for bioconversion of glycerol to lactic acid;* J. Chem. Technol. Biotechnol.; 84, 1576-1581, 2009

Modified zeolites as alternative catalysts for syngas production

Marta Kamienowska[1], Natalia Czuma[1], Bogdan Samojeden[1], Paweł Baran[1], Monika Motak[1], Katarzyna Zarębska[1]

[1]*AGH University of Science and Technology in Cracow, Faculty of Energy and Fuels, kamienowskamarta@gmail.com*

Abstract

Carbon dioxide is the best-known greenhouse gas, which may be considered as the main cause of global warming. Nowadays, numerous activities are undertaken to reduce CO_2 emissions into the atmosphere. One of the best ways to reduce CO_2 emission is to use it for a syngas production. It is a gas mixture of carbon monoxide (II) (CO) and hydrogen (H_2) and is used as a raw material for production e.g. methanol, ethanol or in the Fischer-Tropsch synthesis. Syngas can be produced in the steam and dry reforming of methane. Due to the problem of deactivation of catalysts, e.g. sintering or the formation of carbon deposits, new materials have to be examined in order to become active and sTab. catalysts, which could be used in the above-mentioned processes. The aim of this paper is to present a literature review about catalysts for steam methane reforming and dry methane reforming.

Keywords: dry reforming of methane, steam reforming of methane, catalysis

1. Introduction

In order to reduce the emission of CH_4 and CO_2 in the atmosphere, many processes have been tested. One of the most popular industrial processes of syngas production is reforming. There are three types of reforming: steam reforming of methane (SRM), dry reforming of methane (DRM) and partial oxidation of methane (POM). The differences between the above techniques are the energy and kinetics of the reaction, oxidant used and the H_2/CO ratio of the syngas[1].

One of the most dangerous materials generated by coal-fired power plants is fly ash[2]. The amount of solid waste residue produced by the large-scale industrial processes has been increasing every year and nowadays the total annual production of coal fly ash is around 500 million tones worldwide[3]. Small particles of fly ash are regarded as truly hazardous pollutants, especially those with size below 10 μm as well as 2.5 μm, which are extremally dangerous for the respiratory system of the human body. This is why many detailed studies have been conducted on the alternative application of the fly ash in order to decrease the environmental impact of solid wastes originating from power plants [2]–[4]. Zeolites, which may be obtained from the fly ash, could become an effective catalyst for certain chemical prosses e.g. dry and steam reforming of methane [5].

2. Production of syngas

2.1. Dry reforming of methane

DRM is a process which has been of interest for scientists for a long time. DRM has been also considered as a promising alternative to steam reforming of methane (SRM) and partial oxidation of methane (POM) [1]. In DRM reaction the ratio of obtained H_2 and CO is close to 1, therefore it could be industrially advantageous for example for Fischer-Tropsch synthesis, which is used for liquid hydrocarbons production. DRM is also less expensive than the other methods of reforming and can be developed to utilize biogas as feedstock to produce eco-friendly fuels [6]. Nevertheless, the main reaction of DRM is highly endothermic as shown below:

$$CH_4 + CO_2 = 2CO + 2H_2 (\Delta H_{298K} = +247 \text{ kJ/mol})$$

Thus, the catalysts which can work at high temperatures are required. Higher temperatures may render that process uneconomical for an industrial use and cause the risk of unwanted side reactions, such as coke formation, which is the main reason for catalysts deactivation[7]. DRM is accompanied by side reactions which appear depending on the temperature of the process.

Over the past decade, a great number of studies have been published concerning the catalysts for the DRM. The most popular catalysts for the DRM are supported noble metals such as Rh, Ru and Pt, as well as supported transition metals, for example, Ni and Co[8]. Additionally, hydrotalcites-derived materials havebeen recently investigated as promising catalysts for DRM [9]–[11]. Noble catalysts have high activity and resistance to coking, but they are expensive and not widely available. These are the reasons why Ni-based catalysts are the most promising ones, which can be used at industrial scales installations for DRM as well as SRM[12].

The role of active component

In general, transition metals of 8, 9 and 10 groups of the periodic Tab. are usually chosen for active materials in DRM[13].Many researchers have investigated the influence of the active component on the activity and stability of catalysts in DRM [14]–[16]. It can be noticed that the noble metal-based catalysts are active and selective during DRM. Moreover, Rh- and Ru-based catalysts perform with higher activity than the others. Because however, rhodium is more expensive than ruthenium, Ru is more likely to become an industrial catalyst. Among non-noble metals, comparable activity and selectivity have been shown only for nickel-based catalysts. What is more, according to [14], [17], the activity of the nickel-based catalyst can be boosted by the introduction of higher loadings of active phase in comparison to noble metals [13]. However, non-noble metals demonstrate the tendency to enhance carbon-forming reactions during the process. Thus the catalyst may be deactivated and the reactor may be plugged. It must be mentioned that Ni dissolves carbon to a higher extent than noble metals and it is the reason of low resistance of nickel-based catalysts to coke formation in comparison to noble metal ones. Nevertheless, nickel-based catalysts have received a great deal of attention because of their low price and good accessibility [13], [18]–[21]. Nickel is considered the most appropriate non-noble catalyst for DRM [8]. Nowadays, the main effort is to increase the stability of Ni-based catalysts, i.e. to avoid sintering of nickel particles (caused the high temperature of the process) and carbon deposition (resulting from carbon-forming reactions which proceed more easily on large nickel crystallites)[8], [13].

The role of support

A support is a very important component of the catalyst. It may be inert or participate in the reaction. The support regulates the dispersion of active material, enhances resistance to sintering, and usually provides a large surface area [13], [22]. The supports most commonly tested for DRM are single oxides e.g. Al_2O_3 and MgO, mixedoxidessuch as $MgO-Al_2O_3$ and $CeO2-ZrO_2$, hydrotalcitesbased materials, ordered mesoporous silica – SBA-15, zeolites, clays and carbon-based materials [8], [9], [13].

Magnesia – MgO

Magnesia is one of the most popular supports for dry reforming of methane in case of Ni-based catalysts[8], [10], [17], [23], [24], because of its strong Lewis basic sites, which enhance CO_2 adsorption. Moreover, due to the possibleformation of NiO-MgO solid phase, the catalysts are likely to be prevented from deactivation via sintering [13].

Alumina – Al_2O_3

Alumina was also a commonly studied as the support for nickel-based catalysts [20], [25], [26]It is due to its cheap price, high specific surface area, high thermal stability in case of α-Al_2O_3 phase and acidic-basic character. On the other hand, the resistance of Ni/Al_2O_3 to carbon formation depends on many factors e.g. calcination conditions and composition [13], [25].

Hydrotalcite-based materials

One of the promising materials examined in DRM ishydrotalcites. They are considered as good catalysts for the DRM because of their basic properties [9]. Moreover, it is possible to improve hydrotalcites by different modifications, among others, such as introducing new active sites. In addition, they have a fairly high specific surface area of ca. 100-300 m^2/g, show the high dispersion of metal species and exhibit good anti-sintering properties. What is even more, their synthesis is simple and can be easily controlled to create the desired catalyst [9], [13].

The role of promoters

In general, promoters are added to catalysts because they may improve their selectivity, stability and activity by modification of catalyst structure [8]. The promoters in DRM are divided into three groups [13]:

- Alkali and alkalinemetals – Li, K, Mg, Ba, Ca – added because of their basic properties, ability to oxidize carbon deposits and suppress coking,

- Raremetals – Zr, Ce, La – added to improve redox properties, ability to oxidize carbon deposits

- Othersmetals – Sn, Au, Ag, As – used to create new active sites or modify existing ones.

Alkali metals are used because of their high basicity, which improves activity in DRM. Moreover, they may form a solid solution with NiO, which enhances the interaction between the active phase and support (smaller nickel crystallites) [13].

Summary of catalysts applied in DRM studies

Tab. 1 presents the effect of combining different active metals and supports for DRM. For industrial application of a catalyst in DRM, a lot of factors must be met. It should be noted, that experiments (cp. Tab. 1) were carried out under completely different conditions and therefore a direct comparison is not possible. On the whole, during the process, the catalyst has to perform with reasonable activity and stability, as well as possess appropriate resistance to sintering and low carbon formation[8].

Tab. 1. Comparison of selected catalyst for dry reforming of methane

Active material	Supporter or carrier	Reaction conditions	Methane conversion [%]	References
1 wt.% Pd, Rh, Ir, Ru	Al_2O_3	Temp. 500˚C $CH_4/CO_2=1/1$	>66	[27]
2 wt.% Pt	Al_2O_3	Temp. 500 ˚C $CH_4/CO_2=1/1$	63	
2 wt.% Ru, Rh, Ir	Hydrotalcite-derivered Mg(Al)O	Temp. 800 ˚C $CH_4/CO_2/N_2=23/23/35$	95	[16]
2 wt.% Pt	Hydrotalcite-derivered Mg(Al)O	Temp. 800 ˚C $CH_4/CO_2/N_2=23/23/35$	76	
5 wt. % Ni	$MgO – Al_2O_3$	Temp. 700 ˚C $CH_4/CO_2=1/1$	77	[25]
10 wt. % Ni	$MgO – Al_2O_3$	Temp. 700 ˚C $CH_4/CO_2=1/1$	74	[28]
2 wt. % Ni	ZrO_2	Temp. 650 ˚C $CH_4/CO_2=1/1$	22	[29]
13 wt. % Ni	$\gamma\ Al_2O_3$	Temp. 750 ˚C $CH_4/CO_2=1/2$	94	[30]
10 wt. % Ni	MgO	Temp. 650 ˚C $CH_4/CO_2=1/1$	63	[31]

2.2. Steam reforming of methane

Steam reforming of methane is a typical technology for production of hydrogen, approximately ¾ of H_2 is derived from this process. SRM needs high energy input because of the endothermic nature of the reaction presented below[32]:

$$CH_4 + H_2O = CO + 3H_2 (\Delta H_{298K} = +228 \text{ kJ/mol})$$
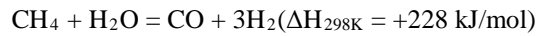
Moreover, a higher H_2O/CH_4 ratio is required to obtain a higher H_2 yield, which causes the process energy inefficient and speeds up the catalyst deactivation [33]. In addition, SRM installation needs additionally a desulphurization unit because of corrosion issues [21].

In case of steam reforming of methane similar catalysts as for the dry reforming of methane have been tested - due to really comparable required reaction conditions. Nickel-based catalysts require usually higher active material loading in comparison to noble metals[34]. Ru-based catalysts had high activity and selectivity [35]. Moreover, they were resistant to coking and sintering even at high temperatures (800°C). Ru-based catalysts were also studied on different supports e.g. MgO. It was proven that catalysts supported on MgO had high CH_4 conversion[36]. Mixed oxides of cerium and titanium were also tested in the SRM process and performed quite good activity[37]. In Tab. 2 some selected catalysts for SRM are presented.

Tab. 2. Comparison of selected catalyst for steam reforming of methane

Active material	Supporter or carrier	Reaction conditions	Methane conversion [%]	References
9.8 wt. % Ni	Al_2O_3	Temp. 700 °C $H_2O:CH_4:air=2.5:1:3.5$	99	[38]
10 wt. %Ni	SiO_2	Temp. 700 °C $H_2O:CH_4=2:1$	35	[39]
7 wt.% Ni	Al_2O_3	Temp. 600°C, $H_2O:CH_4=2:1$	80	[32]
1.5 wt. % Ru	Al_2O_3	Temp. 699 °C $H_2O:CH_4=3.5:1$	99	[35]
1.1 wt.% Pt	CeO_2	Temp. 800 °C $H_2O:CH_4=3.5:1$	80	[35]
Ru	MgO	Temp. 750 °C $H_2O:CH_4=2.8:3$	98	[36]
Ni	50%Ce 50%Ti	Temp. 500°C $H_2O:CH_4:N_2=1:1$	60	[37]
NCZO	La	Temp. 900°C $H_2O:CH_4:N_2=1:1:3$	95	[40]

2.3. Zeolites

Zeolites may be considered as quite cheap and sTab. materials, which are used in many branches of industry [41], [42]. Due to their properties such as relatively high thermal stability and acid-basic properties, they were also studied as the catalysts either in dry or steam reforming of methane [43]–[47]. Zeolites synthesized from fly ash may be a promising substitute of the tested materials [48]. Modification of zeolites may increase their thermal stability as well as activity, therefore they may be studied in both processes.

3. Conclusions

Research on sTab., active and selective catalysts for both steam and dry reforming of methane is focused on the nickel-based catalysts, which are supported on modified basic oxides. A lot of well-performed catalysts were investigated, nevertheless, most of them are expensive, difficult to obtain as well as to implement to industrial scale. One of the possible materials, which may be tested as the catalysts could be modified zeolites obtained from the fly ash. They might be an interesting and cheap alternative to the others tested catalysts.

Acknowledgement

References

[1] B. Abdullah, N. A. AbdGhani, and D.-V. N. Vo, 'Recent advances in dry reforming of methane over Ni-based catalysts', J. Clean. Prod., vol. 162, pp. 170–185, Sep. 2017.

[2] R. M. Cuéllar-Franca and A. Azapagic, 'Carbon capture, storage and utilisation technologies: A critical analysis and comparison of their life cycle environmental impacts', J. CO2 Util., vol. 9, pp. 82–102, Mar. 2015.

[3] Z. T. Yao et al., 'A comprehensive review on the applications of coal fly ash', Earth-Sci. Rev., vol. 141, pp. 105–121, Feb. 2015.

[4] J.-H. Wee, 'A review on carbon dioxide capture and storage technology using coal fly ash', Appl. Energy, vol. 106, pp. 143–151, Jun. 2013.

[5] 'Shape-Selective Catalysis: Zeolites', in Industrial Catalysis, Wiley-Blackwell, 2015, pp. 239–260.

[6] M. Mohamedali, A. Henni, and H. Ibrahim, 'Recent Advances in Supported Metal Catalysts for Syngas Production from Methane', ChemEngineering, vol. 2, no. 1, p. 9, Mar. 2018.

[7] L. Yao, Y. Wang, M. E. Galvez, C. Hu, and P. Da Costa, 'Ni–Mo2C supported on alumina as a substitute for Ni–Mo reduced catalysts supported on alumina material for dry reforming of methane', ComptesRendusChim., vol. 21, no. 3, pp. 247–252, Mar. 2018.

[8] N. A. K. Aramouni, J. G. Touma, B. A. Tarboush, J. Zeaiter, and M. N. Ahmad, 'Catalyst design for dry reforming of methane: Analysis review', Renew. Sustain. Energy Rev., vol. 82, pp. 2570–2585, Feb. 2018.

[9] R. Dębek, M. Motak, M. E. Galvez, P. D. Costa, and T. Grzybek, 'Catalytic activity of hydrotalcite-derived catalysts in the dry reforming of methane: on the effect of Ce promotion and feed gas composition', React. Kinet. Mech. Catal., vol. 121, no. 1, pp. 185–208, Jun. 2017.

[10] A. R. González, Y. J. O. Asencios, E. M. Assaf, and J. M. Assaf, 'Dry reforming of methane on Ni–Mg–Al nano-spheroid oxide catalysts prepared by the sol–gel method from hydrotalcite-like precursors', Appl. Surf. Sci., vol. 280, pp. 876–887, Sep. 2013.

[11] D. Y. Kalai, K. Stangeland, H. Li, and Z. Yu, 'The effect of La on the hydrotalcite derived Ni catalysts for dry reforming of methane', Energy Procedia, vol. 142, pp. 3721–3726, Dec. 2017.

[12] M. M. Nair and S. Kaliaguine, 'Structured catalysts for dry reforming of methane', New J. Chem., vol. 40, no. 5, pp. 4049–4060, May 2016.

[13] R. Dębek, 'Novel catalysts for chemical CO2 utilization Nowekatalizatory do chemicznejutylizacji CO2 Design de nouveaux catalyseurs pour la valorisationchimique de CO2', p. 273.

[14] S. Barama, C. Dupeyrat-Batiot, M. Capron, E. Bordes-Richard, and O. Bakhti-Mohammedi, 'Catalytic properties of Rh, Ni, Pd and Ce supported on Al-pillared montmorillonites in dry reforming of methane', Catal. Today, vol. 141, no. 3, pp. 385–392, Mar. 2009.

[15] K. Asami et al., 'CO2 reforming of CH4 over ceria-supported metal catalysts', Catal. Today, vol. 84, no. 1, pp. 27–31, Aug. 2003.

[16] A. Tsyganok, M. Inaba, T. Tsunoda, S. Hamakawa, K. Suzuki, and T. Hayakawa, 'Dry reforming of methane over supported noble metals: A novel approach to preparing catalysts', Catal. Commun., vol. 4, pp. 493–498, Sep. 2003.

[17] H. Ay and D. Üner, 'Dry reforming of methane over CeO2 supported Ni, Co and Ni–Co catalysts', Appl. Catal. B Environ., vol. 179, pp. 128–138, 2015.

[18] A. Albarazi, P. Beaunier, and P. Da Costa, 'Hydrogen and syngas production by methane dry reforming on SBA-15 supported nickel catalysts: On the effect of promotion by Ce0.75Zr0.25O2 mixed oxide', Int. J. Hydrog. Energy, vol. 38, no. 1, pp. 127–139, Jan. 2013.

[19] Y. Duan, R. Shang, X. Zhong, W. Xie, X. Wang, and L. Huang, 'In-situ synthesis of NiMo2C/Al2O3 catalysts for dry reforming of methane', Int. J. Hydrog. Energy, vol. 41, no. 47, pp. 21955–21964, Dec. 2016.

[20] Y. L, G. Me, H. Cw, and D. C. P, 'Mo-promoted Ni/Al2O3 catalyst for dry reforming of methane', Int. J. Hydrog. Energy, vol. 42, no. 37, pp. 23500–23507, 2017.

[21] P. Djinović, I. G. OsojnikČrnivec, B. Erjavec, and A. Pintar, 'Influence of active metal loading and oxygen mobility on coke-free dry reforming of Ni–Co bimetallic catalysts', Appl. Catal. B Environ., vol. 125, pp. 259–270, Aug. 2012.

[22] A. Neiva and A. Gama, 'A study on the characteristics of the reforming of methane: A review', Braz J Pet Gas, vol. 4, Sep. 2010.

[23] M. M. Barroso-Quiroga and A. E. Castro-Luna, 'Catalytic activity and effect of modifiers on Ni-based catalysts for the dry reforming of methane', Int. J. Hydrog. Energy, vol. 35, no. 11, pp. 6052–6056, Jun. 2010.

[24] M. C. J. Bradford and M. A. Vannice, 'Catalytic reforming of methane with carbon dioxide over nickel catalysts I. Catalyst characterization and activity', Appl. Catal. Gen., vol. 142, no. 1, pp. 73–96, Aug. 1996.

[25] L. Xu, H. Song, and L. . Chou, 'Ordered mesoporousMgO–Al2O3 composite oxides supported Ni based catalysts for CO2 reforming of CH4: Effects of basic modifier and mesopore structure', Int. J. Hydrog. Energy, vol. 38, pp. 7307–7325, Jun. 2013.

[26] 'Natural clay-based Ni-catalysts for dry reforming of methane at moderate temperatures', Catal. Today, vol. 306, pp. 51–57, May 2018.

[27] F. Solymosi, G. Kutsán, and A. Erdöhelyi, 'Catalytic reaction of CH4 with CO2 over alumina-supported Pt metals', Catal. Lett., vol. 11, no. 2, pp. 149–156, Mar. 1991.

[28] Z. Alipour, M. Rezaei, and F. Meshkani, 'Effect of Ni loadings on the activity and coke formation of MgO-modified Ni/Al2O3 nanocatalyst in dry reforming of methane', J. Energy Chem., vol. 23, no. 5, pp. 633–638, Sep. 2014.

[29] F. Pompeo, N. N. Nichio, O. A. Ferretti, and D. Resasco, 'Study of Ni catalysts on different supports to obtain synthesis gas', Int. J. Hydrog. Energy, vol. 30, no. 13, pp. 1399–1405, Oct. 2005.

[30] Y. Chen and J. Ren, 'Conversion of methane and carbon dioxide into synthesis gas over alumina-supported nickel catalysts. Effect of Ni-Al2O3 interactions', Catal. Lett., vol. 29, no. 1, pp. 39–48, Mar. 1994.

[31] L. Li, L. Zhang, Y. Zhang, and J. Li, 'Effect of Ni loadings on the catalytic properties of Ni/MgO(111) catalyst for the reforming of methane with carbon dioxide', J. Fuel Chem. Technol., vol. 43, no. 3, pp. 315–322, Mar. 2015.

[32] M. A. Nieva, M. M. Villaverde, A. Monzón, T. F. Garetto, and A. J. Marchi, 'Steam-methane reforming at low temperature on nickel-based catalysts', Chem. Eng. J., vol. 235, pp. 158–166, Jan. 2014.

[33] A. Iulianelli, S. Liguori, J. Wilcox, and A. Basile, 'Advances on methane steam reforming to produce hydrogen through membrane reactors technology: A review', Catal. Rev., vol. 58, no. 1, pp. 1–35, Jan. 2016.

[34] E. le Saché, L. Pastor-Pérez, D. Watson, A. Sepúlveda-Escribano, and T. R. Reina, 'Ni stabilised on inorganic complex structures: superior catalysts for chemical CO2 recycling via dry reforming of methane', Appl. Catal. B Environ., vol. 236, pp. 458–465, Nov. 2018.

[35] U.-E.-S. Amjad, A. Vita, C. Galletti, L. Pino, and S. Specchia, 'Comparative Study on Steam and Oxidative Steam Reforming of Methane with Noble Metal Catalysts', Ind. Eng. Chem. Res., vol. 52, no. 44, pp. 15428–15436, Nov. 2013.

[36] U. Amjad, G. GonçalvesLenzi, N. R. Camargo Fernandes-Machado, and S. Specchia, 'MgO and Nb2O5 oxides used as supports for Ru-based catalysts for the methane steam reforming reaction', Catal. Today, vol. 257, pp. 122–130, Nov. 2015.

[37] E. T. Kho, E. Lovell, R. J. Wong, J. Scott, and R. Amal, 'Manipulating ceria-titania binary oxide features and their impact as nickel catalyst supports for low temperature steam reforming of methane', Appl. Catal. Gen., vol. 530, pp. 111–124, Jan. 2017.

[38] I. Bobrova, N. Bobrov, and A. Davydov, 'Catalytic methane steam reforming: novel results', Catal. Today, vol. 24, pp. 257–258, 1995.

[39] Y. Zhang, W. Wang, Z. Wang, X. Zhou, Z. Wang, and C.-J. Liu, 'Steam reforming of methane over Ni/SiO2 catalyst with enhanced coke resistance at low steam to methane ratio', Catal. Today, vol. 256, pp. 130–136, Nov. 2015.

[40] H.-M. Kim et al., 'Low temperature steam reforming of methane using metal oxide promoted Ni-Ce0.8Zr0.2O2 catalysts in a compact reformer', Int. J. Hydrog. Energy, vol. 43, no. 1, pp. 262–270, Jan. 2018.

[41] N. Koshy and D. N. Singh, 'Fly ash zeolites for water treatment applications', J. Environ. Chem. Eng., vol. 4, no. 2, pp. 1460–1472, Jun. 2016.

[42] C. Colella, 'Recent advances in natural zeolite applications based on external surface interaction with cations and molecules', in Studies in Surface Science and Catalysis, vol. 170, R. Xu, Z. Gao, J. Chen, and W. Yan, Eds. Elsevier, 2007, pp. 2063–2073.

[43] A. Luengnaruemitchai and A. Kaengsilalai, 'Activity of different zeolite-supported Ni catalysts for methane reforming with carbon dioxide', Chem. Eng. J., vol. 144, no. 1, pp. 96–102, Oct. 2008.

[44] A. Al-Ubaid and E. E. Wolf, 'Activity, FTIR studies and catalyst characterization during methane steam reforming on Ni/Y-zeolite catalysts', Appl. Catal., vol. 34, pp. 119–134, Jan. 1987.

[45] A. N. Pinheiro, A. Valentini, J. M. Sasaki, and A. C. Oliveira, 'Highly sTab. dealuminated zeolite support for the production of hydrogen by dry reforming of methane', Appl. Catal. Gen., vol. 355, no. 1, pp. 156–168, Feb. 2009.

[46] D. Yao, H. Yang, H. Chen, and P. T. Williams, 'Investigation of nickel-impregnated zeolite catalysts for hydrogen/syngas production from the catalytic reforming of waste polyethylene', Appl. Catal. B Environ., vol. 227, pp. 477–487, Jul. 2018.

[47] R. Alotaibi, F. Alenazey, F. Alotaibi, N. Wei, A. Al-Fatesh, and A. Fakeeha, 'Ni catalysts with different promoters supported on zeolite for dry reforming of methane', Appl. Petrochem. Res., vol. 5, no. 4, pp. 329–337, Dec. 2015.

[48] X. Querol et al., 'Synthesis of zeolites from coal fly ash: an overview', Int. J. Coal Geol., vol. 50, no. 1, pp. 413–423, May 2002.

Is it possible to fulfill electric energy needs by a PV on-grid system?

Andrzej Boduch

Affiliation: Faculty of Energy and Fuels, USTAGH, andboduch@gmail.com

Abstract

The article presents the analysis of the possibility to fulfilenergy needs of the five-storey office building in Gliwice throughout the existing 40 kWp PV system and whether the investment was economically viable. The analysis was based on the energy audit, the configuration of annual renewable energy production and its self-consumption by the building, details of subsidy obtained from the VFEP&WM, the structure of investment financingand payback calculations. To make the results credible, due to the high impact of weather conditions and seasons on the system, the research covered a period of 12 months.The tool used in the economic analysis is a method for assessing the economic effectiveness of the investment projects: the payback period of capital expenditures.

The On-grid PV system**is not able** to fully meet the energy needs of the building. The analysed system may improve the investor's financial results, however, it will not eliminate the costs related to the purchase of energy from the grid. The results showed that the capital expenditure will pay off in 7.5 years of exploitation, compared to 25 years estimated lifetime can be considered as economically viable.

Keywords: renewables, photovoltaics, On-gridPV system

1. Introduction

Analysingseveral forecasts modelled by global energy organizations and concerns, including The US governmental body - Energy Information Agency (EIA) [5] or petrochemical BP [3], it is easy to see that the demand for energy, including electricity, will continue to grow. The reason for such assumptions is the increase of population and growing access to energy bydeveloping countries. According to analysts' researches, the share of individual sources in the production of electricity willalso not remain unchanged [6]. Emissions of undesirable chemical compounds to the atmosphere and depletion of fossil fuel resources result in a drop in the presence of conventional thermal power plants in the structure of electricity production in the world. This trend can be closely related to environmental regulations and the rapid development of renewable energy, which share in the same forecasts clearly increases [7].

In contrast to fossil fuels, which reproduction lasts millions of years, renewable energy sources are not exposed to total depletion. The high degree of dependence on atmospheric conditions, which prevents the standalone operation of such technologies, is the biggest barrier to the total resignation from conventional fuels. The solution may appear in the near future with a development of smart grids and a dropin prices of highly efficient energy storage systems. Currently, the irregular work of electricity-generating devices negatively affects the operation of electrical grids.

One of the basic energy sources, which is classified as Renewable Energy Sources (RES), is the Sun. The energy potential of photons, which reaches the Earth, exceeds 10,000 times the current energy demand[4]. Using photovoltaic cells, you can directly convert solar into electricity without emitting harmful compounds and noise.Individual countries or unions conducting environmental policy accelerate the development of technology through co-financing and promotion programs, thus globally installed capacity from smaller systems and larger solar power plants is growing. Based on annual reports prepared by the International Energy Agency (IEA), it can be concluded that production capacity based on solar cells increases exponentially. In 2015, approximately 50 GW of installed power in photovoltaic power plants was globally built, while in 2016 it was as much as 75 GW, and the total amount was at a level slightly above 300 GW of power [7]. For comparison - such installed power would be able to satisfy Poland's needs more than seven times [12].

Poland is committed to the European Union that by 2020 the use of energy from renewable sources in final gross energy consumption would be 15% [14]. In the case of non-compliance, Poland will be obligated to reach the

expected share of RES by importing clean energy from the neighbouring countries. According to statistical data from the Central Statistical Office, the share of energy from renewable sources is fluctuating. In 2012, it accounted for 11.7%, to reach 13.1% in 2015. Unfortunately, with the law entry into force regulating the distance of wind farms from residential buildings and forests,there has been a huge step back in the share of RES to 11.3%, which results in hindering the achievement of the 15% target [11].

2. Theoretical background – On-grid system

2.1. On-grid system

Systems integrated with the power grid are the most commonly used. They are used in urban and suburban zones, as well as in industrial areas. They consist of photovoltaic modules, an inverter, a supporting construction, fuses, a bi-directional meter and connection to the grid (*Fig. 2.1.*). The on-grid system allows for the current use of the generated power for own needs. The unused energy is not accumulated, thus immediately sold to the power grid, while in the event of adverse weather conditions, during the night or insufficient installed power of PV system, it is also possible to flow the current in the opposite direction. If too much of self-generated energy is being transferred to the grid, the payback period of the investment is significantly longer, because currently in Poland the value of 1 kWh of electricity delivered to the grid is lower than the same amount of energy collected from the distributor. The main disadvantage of such a system is dependence on a failureof the external power system. If there is no voltage in it, the inverter with anti-islanding protection causes the modules to be disconnected for security purposes. An important element necessary for proper operation of the system is also the required high-qualityelectrical grid that is able to balance the surplus of energy entering the system.
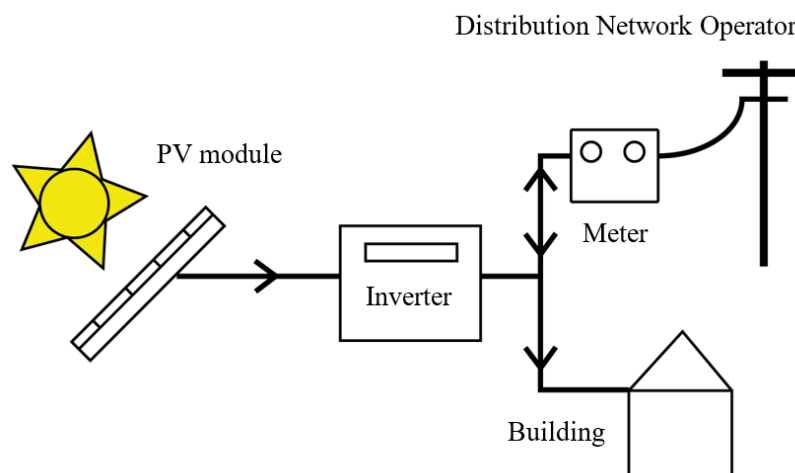
Fig. 2.1. PV on-grid system components

2.2. Connecting modules and cells into circuits

In order to ensure adequate output power and parameters of the photovoltaic power plant, the modules can be wired into series, parallel or a combination of the two.

Integration of modules in a series array (*Fig. 2.2.*) is performed to obtain higher voltages. The resultant voltage of a system is the sum of voltages of individual cells. The main disadvantage of this connection is the dependence on the flowing current from the weakest working module, which, for example, has been subject to shadowing. [13]

A parallel circuit (*Fig. 2.3.*) is used in case of the need to increase the current because the resultant current is the sum of generated currents in all connected modules. The voltage is constant and the shading does not exert significant influence on a system's operation. [13]

In the series-parallelcircuit, current-voltage characteristic curves depend on the configuration and number of modules connected with each other. In the figure below (*Fig. 2.4.*) there is a parallel connection of three chains,

which consist of three modules connected in series. Thanks to the characteristics, it is easy to trace what effect individual connections have on the voltage and current values. [13]
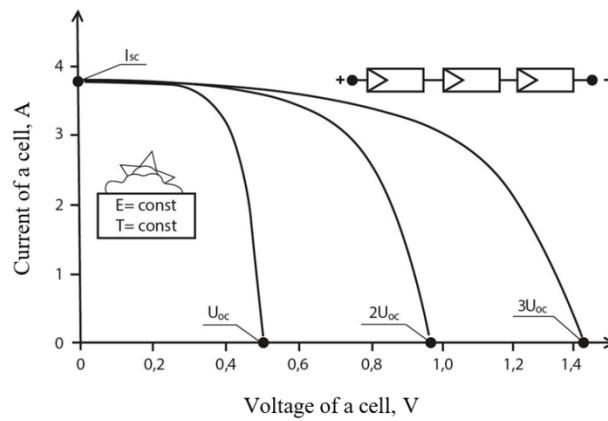
Fig. 2.2. The impact of the series combination of three PV cells on the resultant current-voltage characteristics (own elaboration based on [13])
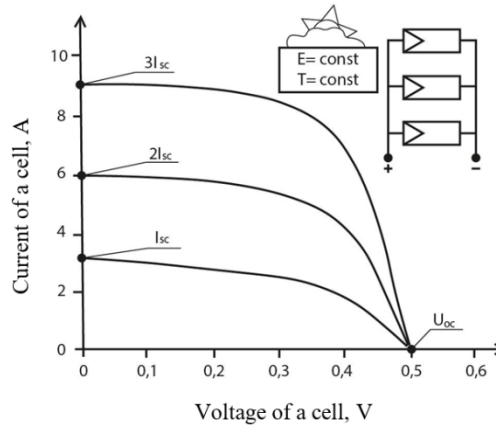
Fig. 2.3. The impact of the parallel combination of three PV cells on the resultant current-voltage characteristics (own elaboration based on [13])
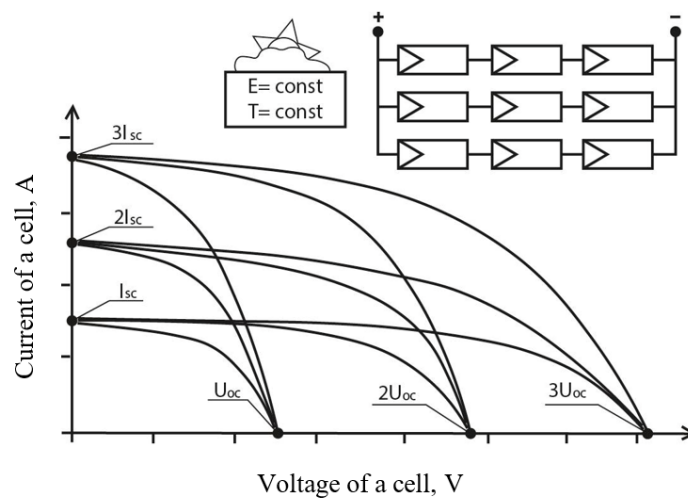
Fig. 2.4. The current-voltage characteristics of PV cells wired in a series-parallel combination (own elaboration based on [13])

3. Investment support systems summary

The increase in interest in the photovoltaic industry in Poland resulted from instruments supporting the development of new technologies. Subsidies granted by the National Fund for Environmental Protection and Water Management, the Voivodship Fund for Environmental Protection and Water Management or the European Union programmes include:

- grants,

- loans on preferential terms,

- credits on preferential terms,

- R&D (Research & Development),

- tax breaks.

Due to large budgets, the NFEP&WM programmes are very popular, e.g.,*Prosument* [9] (budget: PLN 800 million; projects: inter alia photovoltaic systems with installed power up to 40 kWp) or*Bocian*[8] (budget: PLN 420 million; projects: Distributed Energy Resources).

From October 1, 2015, the Tradable Green Certificates System operates in Poland, which is a mechanism for supporting the production of electricity from renewable sources. Green certificates are property rights issued by the President of the Energy Regulatory Office in exchange for proving in the registration system certificates that energy was generated from clean sources, i.e., wind, sun, geothermal, water and biomass. They are being traded on the Polish Power Exchange, which results from the obligation imposed by the Energy Law on the Transmission and Distribution System Operators to purchase energy from RES. In addition, energy companies that produce and sell electricity are required to demonstrate a certain number of green certificates or to pay a replacement fee, as far as EU requirements concerning emissions are not fulfilled. [10]

4. Investment decision and characteristics of thePV system

Due to the height of electricity bills, the investor decided to build a PV installation on the five-storey office building to lower its operational costs. The most important incentive to make the decision was acceptance of participation in the Renewable Energy Sources support programme financed from the budget of the Voivodeship Fund for Environmental Protection and Water Management in Katowice, which offers grants to investors and loans on preferential terms.

The installation consists of 152 silicon polycrystalline modules with STC (Standard Test Conditions) power - 260 W, which translates into a total value of less than 40 kW. The two installed three-phase inverters from KACO with two separate MPPT maximum power tracking points are connected to four chains of interconnected modules in series and parallel wiring systems.

A unidirectional meter, overvoltage,andovercurrentprotection are located in the main PV switchboard. In the distribution board of the building, electricity from photovoltaic generators is prioritized to facilitate the building, however excess of electrical energy is measured by a bi-directional meter and sold to the Distribution Systems Operator (in this case TauronDystrybucja S.A.).

C21 tariff, which is valid in the building, is characterized by a constant price of electricity per day (which means the number 1), and its connection power exceeds the value of 40 kW (which means the number 2). The tariff is targeted at medium-sized enterprises whose electricity consumption often coincides with the peak times of energy demand in Poland.

5. Analysis of the annual work of the PV installation

PV systems depend to a large extent on atmospheric conditions and a season of a year. It effects with fluctuating electrical energy production, thus to make calculations more credible, the research covered the period of 1 year - from 1 December 2016 to 30 November 2017. Based on the below graph (*Fig. 5.1.*), it can be stated that the most favourable period for electricity generation is from May to August when the sun towers above the northern hemisphere.
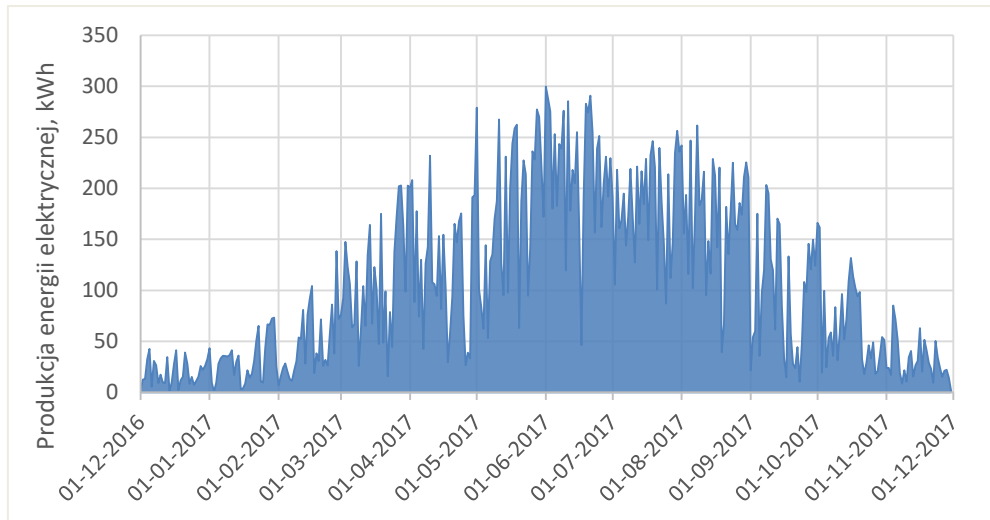
Fig. 5.1. Daily production of electricity from the PV system (own elaboration)

Tab. 5.1.List of production, consumption,and sales of electricity generated from the 40 kWp PV installation and a purchase of energy from a distributor (own elaboration)

	El. energy production (**PV**), kWh	El. energy consumption (**PV**), kWh	El. energy sale (**PV**), kWh	El. energy purchase, kWh
Dec 2016	555	541	14	10,927
Jan 2017	940	864	76	11,667
Feb 2017	1,248	1,213	35	11,547
Mar 2017	3,249	2,946	303	11,613
Apr 2017	3,516	2,725	791	9,905
May 2017	5,311	4,575	736	8,519
June 2017	6,482	5,661	821	7,961
Jul 2017	5,539	4,498	1,041	8,262
Aug 2017	5,250	4,767	483	9,772
Sep 2017	2,748	2,519	229	10,498
Oct 2017	1,985	1,807	178	10,848
Nov 2017	864	787	77	11,734
Σ	37,687	32,903	4,784	123,253

The limited roof area,insufficient financial capabilities of the investor and the characteristics of the On-grid PV system **do not allow to meet the energy needs of the facility in 100% renewable energy**. It is required to buy electricity from external sources, and even periodicallyto sell it due to the current lack of electricity needs.

As a result of the high demand for electricity during the day, there is no surplus of energy production from the photovoltaic installation. The column *El. energy sale, kWh* appearing in the table (*Fig. 5.2.*) shows the excessive energy resulting from the functioning of the installation on public holidays or during weekends. For the period considered, the ratio of energy produced to sold reaches the value of 8, which means that the building consumes

energy to its own needs to a high degree. This ratio has a significant impact on the return period of the investment, as currently, the sale of energy from RES takes place at unfavourable conditions for the investor.

6.   Economic analysis of the investment

6.1. Calculation assumptions

Since the investor deducts VAT, all prices quoted in the paper are net prices (they do not include VAT). In addition, the amount of electricity consumed by the PV system in standby mode was not taken into account, due to the almost insignificant impact on the analysis result.

Pursuant to Art. 4j of the Energy Law Act, the recipient has the right to conclude two separate agreements: a sales contract and a contract for the provision of distribution services [2]. The investor resigned from the comprehensive agreement for two separate ones. Such a procedure generates savings that shorten the payback period.

TheRenewable Energy Act of Poland and its amendment of 1.06.2016 does not allow entrepreneurs to award the title of a *Prosumer*, i.e. "final consumer purchasing electricity on the basis of a comprehensive contract, producing electricity only from renewable energy sources in micro-installation for its own consumption, not related to the business (...) "[1]. An owner of a micro-installation (*prosumer*)from 10 to 40 kWp settles the energy introduced into the grid in a quantity ratio of 1 to 0.7. This means that by introducing 100 kWh of surplus electricity to the grid, the prosumer is authorized to take 70 kWh of energy from the producer within a year. For micro-installations of not more than 10 kWp, this ratio is 1 to 0.8.

In the case of an office building in Gliwice, which is not a subject to the *Prosumer*law, the surplus of energy entered into the grid is being sold at a price equal to 100% of the average electricity sales price on the competitive market in the previous quarter announced by the President of ERO. The arithmetic mean of prices from 2017 was used for the calculation. There is an advantage addressed to entrepreneurs, which cannot be used by an individual, is the support system in the form of green certificates. Unfortunately for the investor, the market for green certificates in 2016 experienced an oversupply phenomenon, which resulted in a decrease in the price of the certificate from almost PLN 300/MWh of produced clean energy to about PLN 30/MWh. In further calculations, the price of the certificate (property rights PMOZE_A) from December 28, 2017, on the website of the Polish Power Exchange (TGE) was taken into account - PLN 45.29.

The calculations consider each income source, however, the main factors resulting in investment payback period are the savings due to the reduction of electricity consumption from the distributor, which corresponds to the value of energy consumption from PV. Only variable fees were considered: purchase of energy, variable component of network rate, quality rate, renewable energy (purchase –PLN 0.357/kWh, distribution –PLN 0.14595/kWh). Permanent fees are inevitable for On-grid installations and related to the grid connection capacity (in the case of the office building: 50 kW).

It was assumed that the generated amount of electricity for the subsequent years of the installation operation will remain at the same level, reduced only by the maximum efficiency drop expected by the producer, i.e. after 10 years - a drop to 90% efficiency, after 25 years - a drop to 80% efficiency. It was also assumed that the structure of energy consumption and its size, as well as the ratio of energy taken from the PV installation to the one received from the distributor, will not change. Assumptions are subject to a small error limit, because the investor does not plan to change the installed capacity, and the risk of system failure is low. In the event of an unexpected problem, the system's live performance monitoring allows for rapid intervention. All office premises available in the building are rented under long-term rental contracts, therefore it is expected that its electricity consumption will not change dramatically.

The period taken for the analysis results from the typical 25-year warranty for solar modules [15]. Inverters are statistically worn after 15 years of operation, thus their replacement is included in operating costs. The other costs related to the functioning of the installation consist of the cost of periodic quality inspections, cleaning,and possible service.

The structure of costs related to the financing of a 39.52 kWp photovoltaic system consists of:

- secured own funds: PLN 65,189;

- the loan granted by VFEP&WM in Katowice: PLN 11,533;

- the subsidy granted by VFEP&WM in Katowice: PLN 59,240.

The total investment cost was **PLN 236,962**

6.2. Payback period method

Tab. 6.1. Loan (3% - interest)

Years	Loan instalment, PLN	Interest, PLN
1	-	-
2	22,506.60	3,375.99
3	22,506.60	2,700.79
4	22,506.60	2,025.59
5	22,506.60	1,350.40
6	22,506.60	675.20
Σ	112,533.00	10,127.97

Tab. 6.2. Amortization (7% - amortization rate)

Years	Annual amortization instalment, PLN	Total amortization amount, PLN	Value of the fixed asset, PLN
1	0	0	177,721.92
2	12,440.53	12,440.53	165,281.39
3	12,440.53	24,881.07	152,840.85
4	12,440.53	37,321.60	140,400.32
5	12,440.53	49,762.14	127,959.78
6	12,440.53	62,202.67	115,519.25
7	12,440.53	74,643.21	103,078.71
8	12,440.53	87,083.74	90,638.18
9	12,440.53	99,524.28	78,197.64
10	12,440.53	111,964.81	65,757.11
11	12,440.53	124,405.34	53,316.58
12	12,440.53	136,845.88	40,876.04
13	12,440.53	149,286.41	28,435.51
14	12,440.53	161,726.95	15,994.97
15	12,440.53	174,167.48	3,554.44
16	3,554.44	177,721.92	0

Pursuant to the PIT Act, the obligation to pay income tax will not occur in a situation in which the generated electricity will be used for own needs, but income derived from the sale of surplus electricity not used for the own needs of the taxpayer is subject to the income tax. For this reason, the sum of the net profit from investments exceeds over one and a half times the sum of gross profit. The sale of certificates of origin of electricity from renewable sources is also subject to the obligation to pay income tax. The income tax rate applicable to the investor is 19%.

Tab. 6.3. Gross and Net Incomes (own elaboration)

Years	Gross Income, PLN	Net Income, PLN	$ZN_i + A_i + O_i$, PLN
1	-	-	-
2	- 19,464.13	-12,599.52	3,217.00
3	- 18,980.52	-12,239.46	2,901.86
4	- 18,496.91	-11,879.40	2,586.72
5	- 18,013.31	-11,519.35	2,271.57
6	- 17,529.70	-11,159.29	1,956.44
7	5,460.51	7,431,11	19,871.64
8	5,268.92	7,244.26	19,684.79
9	5,077.33	7,057.41	19,497,94
10	4,885.74	6,870.56	19,311.09
11	4,694.15	6,683.70	19,124.23
12	4,502.56	6,496.85	18,937.38
13	4,365.57	6,363.25	18,803.78
14	4,228.59	6,229.65	18,670.18
15	4,091.60	6,096.06	18,536.59
16	- 6,859.30	-2,796,81	757.63
17	16,258.16	15,905.69	15,905.69
18	16,121.17	15,772.09	15,772.09
19	15,984.18	15,638.49	15,638.49
20	15,847.20	15,504.89	15,504.89
21	15,710.21	15,371.29	15,371.29
22	15,573.22	15,237.69	15,237.69
23	15,436.24	15,104.09	15,104.09
24	15,299.25	14,970.49	14,970.49
25	15,162.26	14,836.89	14,836.89
26	15,025.28	14,703.29	14,703.29
Σ	99,648.29	151,323.91	339,173.74

$$ZB_i = P_i \cdot C_i - (K_i + A_i + O_i)$$

$$J = \sum_{i=1}^{Tz} (ZN_i + A_i + O_i)$$

P_i – Electricity consumed (from the PV system)

C_i – Electricity distribution and sell rate

ZB_i – Gross income

ZN_i– Net income

A_i – Amortization

O_i – Loan interest

$$T_z \leq 25 \; years \; (estimated \; system \; lifetime)$$

$$7.5 \; years \; \leq 25 \; years$$

Criterium is met

Capital expenditures reach PLN 65,188.92, while the net profit after 25 years of operation is PLN 208,339.07. According to calculations, the investment will be returned after 7.5 years of operation.

7. Conclusions

The increase in global demand and the decline in prices of solar systems proves that investment profitability is constantly growing. The economic analysis of the installation on the office building with the method of the payback period proved that the return on investment will take place after a short time in comparison to the entire period of operation assumed for 25 years. The relatively young technology of obtaining energy from RES improves increasingly its results in terms of lifetime and efficiency of individual components, which leads to the conclusion that the period of exploitation can be significantly extended, generating further profits for the investor.

The short payback period can be attributed to thesubsidy equals 25% of the total investment cost and the loan, the interest of which is significantly lower than proposed by banks. However, the main advantage of the investment is the structure of the energy demand of the building itself. Numerous devices, lighting system, pumps, ventilationand air conditioning installationsallow for the consumption of almost whole energy generated from PV, which, as proved in the previous sections, brings the largest profits. Oversizing of the installation or poor selection of technology to the electricity demand could lead to an extension of the investment return period or even to determine aninvestment as unprofitable.

It should also be noticed, that the calculated profits may change positively as a result of a forecasted rapid increase in unit energy prices.However, adverse weather conditions, a failure of the system or a change in legal regulations regarding the connection of distributed installations to the grid may affect system performance negatively.

The On-grid PV system**is not able** to fully meet the energy needs of the building. The analysed system may improve the investor's financial results, however, it will not eliminate the costs related to the purchase of energy from the grid, especially in the case when the investor is not subject to prosumer law.

References

[1] Art. 2 ustawy z dnia 20 lutego 2015 r. o odnawialnych źródłach energii (Dz.U. 2015 poz. 478).

[2] Art. 4j ustawy z dnia 10 kwietnia 1997 r. – Prawo Energetyczne Dz.U. 1997 nr 54 poz. 348)

[3] BP, *Energy Outlook 2017,* access: 21.11.2017 r.,https://www.bp.com/content/dam/bp/pdf/energy-economics/energy-outlook-2017/bp-energy-outlook-2017.pdf

[4] Ciok Z., *Ochrona środowiska w elektroenergetyce*, Podstawowe Problemy Współczesnej Techniki, PWN, Warszawa 2001

[5]   EIA, *International Energy Outlook 2017,* access: 21.11.2017 r.,https://www.eia.gov/outlooks/ieo/pdf/0484(2017).pdf

[6]   IEA, *PVPS Annual Report 2016,* data dostępu:21.11.2017 r., www.iea-pvps.org/index.php?id=9&eID=dam_frontend_push&docID=3951

[7]   IEA, *Renewables 2017,* data dostępu: 8.01.2018 r., https://www.iea.org/publications/renewables2017/

[8]   Information regarding Bocian programme, NFEP&WM, access: 11.12.2017 r., http://www.nfosigw.gov.pl/oferta-finansowania/srodki-krajowe/programy-priorytetowe/bocian-rozproszone-odnawialne-zrodla-energii/

[9]   Information regarding Prosument programme, NFEP&WM, access: 11.12.2017 r., https://nfosigw.gov.pl/oferta-finansowania/srodki-krajowe/programy-priorytetowe/prosument-dofinansowanie-mikroinstalacji-oze/informacje-o-programie/

[10] Kowara M., Lasocki K., Trepka M., *Analiza polskiego systemu wsparcia produkcji energii elektrycznej z odnawialnych źródeł energii w postaci Zielonych Certyfikatów na podstawie pomocy publicznej,*K&L Gates, 2014

[11] CSO Report, *Energia ze źródeł odnawialnych w 2016 roku,* access: 25.11.2017 r., http://stat.gov.pl/obszary-tematyczne/srodowisko-energia/energia/energia-ze-zrodel-odnawialnych-w-2016-roku,3,11.html

[12] Report PAIiIZ S.A., *Sektor energetyczny w Polsce,*access: 25.11.2017 r., www.paih.gov.pl/files/?id_plik=19609

[13] Sarniak M. T., *Podstawy fotowoltaiki,* Oficyna Wydawnicza Politechniki Warszawskiej, Warszawa 2008

[14] Schnell Christian, *Wykonanie celu OZE 2020. Analiza stanu obecnego i prognoza,* SOLIVAN, Warszawa 2016

[15] Heckert Solar NeMo 60P 260 Wp module specifications, access: 8.12.2017 http://www.heckertsolar.com/en/products/solar-modules/solar-module-nemor-60-p.html

Modeling the Seismic Reservoir Response to CO2 Injection at the Ketzin CO2 Storage Site, Germany.

Mayra Alvarez

[1]*Faculty of Energy and Environmental Engineering, Silesian University of Technology, e-mail: mayra.alvarez.rivero@gmail.com*

Abstract

Carbon Capture and Storage (CCS) is an immediate option to reduce the amount of anthropogenic CO2 emission in the atmosphere. To guarantee the effectiveness of CO2 injection and storing is crucial to monitor the evolution of the CO2 plume. One technique is to use 3D time-lapse seismic technology. The success of the seismic monitoring is determined by the magnitude of the change of the elastic properties of the reservoir; therefore, the change of the reflection coefficient at its top. For this purpose, fluid replacement modeling is performed at the injection well at the Ketzin pilot site for CO2 storage to quantify and predict the changes in the elastic properties of the reservoir for different CO2 concentrations in the pore space. Additionally, it was estimated the extension of the CO2 plume and its maximum saturation using the CMG reservoir simulation software. The results of this research indicate that monitoring the CO2 plume with seismic methods is feasible even after injecting small amounts of CO2.

Keywords: Fluid substitution, carbon capture and storage, CO2 sequestration, time-lapse, numerical simulation, Ketzin pilot site.

1. Introduction

Nowadays, the world depends strongly on energy, electricity in particular. Most of this energy is provided through fossil fuels combustion (gas, coal and oil) which is the largest source of emissions of carbon dioxide, that contributes to radiative forcing and global warming. The challenge today is that we are almost entirely dependent on fossil fuels and even considering the best scenario it will take decades to move fully to alternatives.

In this sense, scientists have tried to understand for decades how can we continue to meet our energy needs while preventing further damage to the climate. According to the International Energy Agency (IEA), Carbon Capture and Storage (CCS) will be an essential technology to apply in order to achieve this ambition. CCS can contribute to 13 % of the cumulative emission reduction or one-sixth of total CO2 reduction by 2050 (I. E. Agency, 2015). It is the only solution for deep emissions reductions from industrial processes and from fossil fuel use in the power sector.

To guarantee the effectiveness of CO2 injection and storing, some characteristics must be met. The reservoir should be a porous permeable sedimentary layer located at a depth of more than 800 meters (the supercritical state of CO2 is preferred) below a cap rock or impermeable formation in order to be effectively stored for thousands of years. Furthermore, it is crucial to monitor the evolution of the CO2 plume and detect any leakage after injection into the upper geological formations to ensure that the CO2 injected will be stored permanently in the reservoir (Yordkayhun et. al., 2009; Götz et. al., 2014).

One of the methods used for monitoring the sequestered CO2 is 3D time-lapse monitoring using seismic surface methods. The propagation of the seismic waves through the subsurface depends on several factors that are affected when CO2 is injected in the porous media: the density, bulk modulus, and seismic velocities are reduced. For this reason, is possible to use seismic methods to analyze the evolution of CO2 during and after the injection phase given that the change of these properties can be detected in the seismic data, specifically the change of the reflection coefficient and time shift (Morado and Lawton, 2012).

The goal of this research is to model the effect of injected CO2 on the seismic response using the well data from the Ketzin site for CO2 storage in order to investigate the theoretical detectability of CO2. For this purpose, Fluid Replacement Modeling (FRM) module of Hampson-Russell software is used to estimate the change in seismic velocities and density at different CO2 saturations in order to evaluate how the seismic response (the

acoustic impedance and reflection coefficient) varies in the vicinity of the well with the injection of CO2. Additionally, the numerical simulation of the reservoir is performed using CMG Software to evaluate how would it be the evolution of the CO2 plume over time.

2. Background

2.1. Carbon Capture and Storage (CCS)

Carbon Capture and Storage (CCS) is a technology that can capture CO2 emissions that result from the use of fossil fuel at industrial scale preventing the carbon dioxide to get to the atmosphere; therefore, reduces the emissions of greenhouse gasses due to human activities. This solution consists of three parts: capturing, transporting, and injecting CO2 into deep rock formations (e.g. depleted oil and gas fields and deep saline aquifers formations) (Yang, 2012).

This technique is relatively a new concept but for several decades CO2 has been injected into geological formations for the purpose of enhanced oil recovery, which is a technique used to increase the amount of crude oil that can be extracted from an oil field. The information and experience gained from projects where fluids have been injected on a massive scale underground indicate that it is feasible to store CO2 in geological formations (IPCC, 2005).

2.2. Seismic methods

Seismic acquisition involves an energy source such as a vibrator unit, dynamite or air gun, and a receiver such as a geophone or a hydrophone. The energy coming from the source is used to obtain information about the subsurface. As a result, the energy is transmitted into the ground as an elastic wave which propagates by the movement of rock particles; when a ray encounters an interface, some energy is reflected back and is recorded as seismic data, the other part of the energy is refracted or transmitted to the next layer.

The product of the density and the wave velocity in a medium it is called acoustic impedance (Z), and the difference of acoustic impedances between consecutive rock layers affects the reflection coefficient, which for normal incidence case is given by

$$RC = \frac{Z_2 - Z_1}{Z_2 + Z_1} = \frac{\rho_2 v_2 - \rho_1 v_1}{\rho_2 v_2 + \rho_1 v_1}$$

where RC is called reflection coefficient, v_1 and v_2 are the seismic velocities of the wave in each medium and ρ_1 and ρ_2 are the densities of each medium. From the previous equation one can notice the larger the impedance contrast between two layers, the higher the amplitude of the reflected wave will be.

3. Geologic setting

3.1 Area of study

The research site is located near Ketzin, a town situated about 25 kilometers west of Berlin on the southern Northeast German Basin, which is part of the Central European Basin System. During the CO2SINK, the borehole Ktzi 201 served as the injection well and three observation wells, Ktzi 200, Ktzi 202 and Ktzi 203 (figure 1), where drilled down to a depth of 800 m.

Fig. 1. Geographic location and aerial view of Ketzin site and its facilities.

3.2. Geological background

The CO2 storage reservoir is situated on the southern flank of the Ketzin anticline with a dip angle of around 15 degrees (Huang et. al., 2016). The Upper Triassic Stuttgart Formation is the target for CO2 injection, which thickness is about 75 to 80 meters at a depth of 500 to 700 meters and consists of flood plain siltstones and mudstones with embedded channel sandstones. At the formation depth, the measured pressure is between 6.21 and 6.47 MPa and the temperature varies from 34˚C to 37˚C (Kazemeini, 2009). According to the well-log analyses within the Stuttgart Formation, permeability is in the range of 0.02 to 5000 mD and porosity in the range of 5 to 35% (Huang et. al., 2016).

The Weser and Arnstadt formations are the cap rocks that complete the appropriate trapping system to accommodate and store the carbon dioxide. The immediate caprock, consisting of Weser formation overlaid by the Arnstadt Formation, is 210 m thick (Ouellet et. al., 2011). A 10 to 20 meters thick layer of anhydrite is present at approximately 80 m above the Stuttgart Formation (K2 reflector) and acts as a strong marker in the seismic sections that can be easily seen in the sonic logs (Yang, 2012).

4.   Data description

In this work the data set from the injection well Ktzi 201, specifically the sonic and density logs, was used to build the Fluid Replacing Model at the depth of the Stuttgart Formation. In addition, a 3D baseline seismic survey with 12 km^2 extension and nominal fold of 25 was used to generate a geological model needed for the numerical simulation of the reservoir.

The 3D seismic *ak_base_orig.sgy* is constituted by 216 inlines and 206 crosslines, starting from inline 1069 to 1284 and from crossline 1020 to 1225, both with an increment of 1. The spacing between inlines is 132.8 m and between crosslines is 103 m. The recording time is up to 1.2 seconds.

In order to bound the data sets previously described the seismic-well correlation was performed. This resulted in a depth-time relationship that is of great importance taking into account that one of the objectives of this research is the creation of synthetics seismograms to study the change of the amplitude at the top of the reservoir for different CO2 saturations. For this purpose, first calibration was done with the statistical wavelet and then it was improved using the extracted wavelet at the well vicinity. The final calibration showed a correlation coefficient of 0.8753 that suggests that the correlation between events of the synthetic data of zero offset (blue trace in figure 2) and the seismic data (red traces in figure 2) was close in depth.
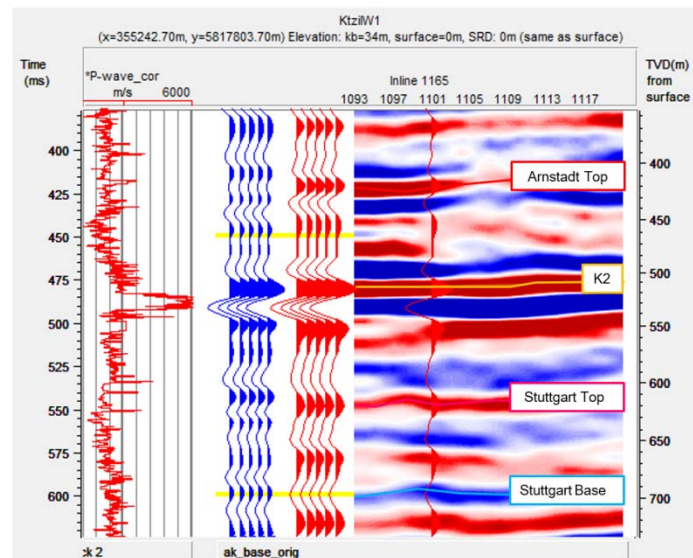
Fig. 2 Correlation between the zero offset synthetic trace (blue) and the pilot trace extracted from the seismic (red). On the right the real seismic is displayed with the pilot trace (red) imposed over the position of the injection well.

5. Fluid Replacement Model (FRM)

A three-layer model was created by averaging P-wave velocity and density logs of Ktzi 201 at the depth of interest. In figure 3 the layer in yellow corresponds to the cap rock (Weser Formation), the layer in blue corresponds to the reservoir (upper part of the Stuttgart Formation) and the layer in green includes the rest of the Stuttgart Formation and part of the Grabfeld Formation.
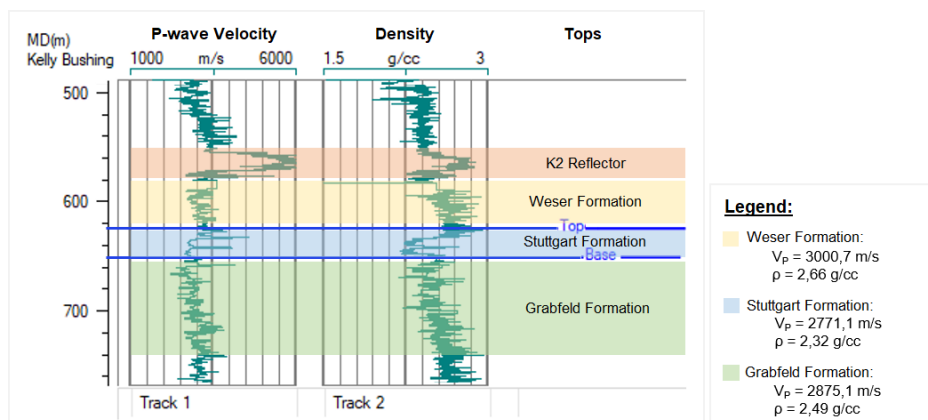
Fig. 3. 1D model with the average P-wave velocity and density obtained from the P-wave velocity log and density log of the injection well Ktzi 201. The reservoir interval is marked with a blue rectangle.

To develop a fluid substitution model it was necessary to first create a base scenario in order to evaluate if the parameters used for the generation of the synthetic seismogram gave a similar response when compared with the real data. The input parameters that were used to generate this scenario corresponds to the ones presented in figure 3. The synthetic seismogram generated (figure 4) was created assuming an initial water saturation of 100 % in the porous space of the reservoir.

The maximum depth difference between the top and the base horizon in the original and synthetic seismic is 6 m and 4 m respectively. The small difference between the arrivals of the synthetic and the real seismic indicates a good fit.
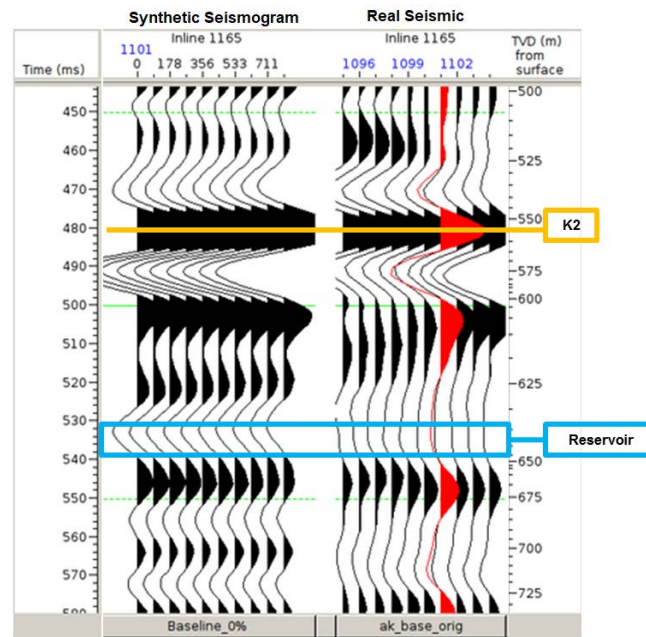
Fig. 4. Synthetic and seismic data for the baseline case. The reservoir interval is marked with a blue rectangle. The baseline seismic trace located in the vicinity of the injection well where inline 1165 intersects crossline 1101 is marked red. The K2 reflector is highlighted in orange.

After verifying that the properties used to generate the synthetic seismic for 100 % water saturation produced similar results when compared to the real seismic, fluid substitution was applied over 637-651 m depth in the injection well by replacing brine with CO2. The variation of the elastic parameters in the reservoir was computed in this interval because the properties of the formations that overlay and underlie the reservoir are not affected during the CO2 injection; consequently, their properties and seismic response remain constant during the simulation.

The P-T condition was fixed at 6.2 MPa and 34 ºC that corresponds to the condition measured before the injection of CO2 (Ivanova et. al., 2013). Furthermore, two saturation patterns are considered: homogeneous and patchy. Eleven scenarios from 0 % to 100 % CO2 saturations was created with an increment of 20% to evaluate the change of the elastic properties of the medium. Figure 5 shows the P-wave velocity, S-wave velocity and density logs for 0, 20, 40, 60, 80 and 100 percentages to illustrate these changes.

The values obtained for the computed logs in figure 5 are presented graphically in the following sections in order to evaluate the effects of fluid replacement on each variable under study.

6.   Effect of fluid substitution on P-wave velocity

The P-wave velocity (Vp) in the reservoir decreases when CO2 is injected for both homogeneous and patchy cases (figure 6.a). The displacement of brine by CO2 causes a drop in Vp because CO2 is more compressible than brine. For the homogeneous saturation pattern case, the injection of just a few percents of CO2 (10 % of CO2 saturation) causes a drop in P-wave velocity of 1855 m/s, corresponding to 33 % of the P-wave velocity of the baseline case. This is a result of the fast filling of the pores at the beginning of injection for the homogeneous scenario. At 50 % of CO2 saturation the P-wave velocity value starts to increase. These observations agree with the results of Vera and Lawton (2010), where Vp drops abruptly by 20 % and the behavior of Vp values is similar to the one displayed in figure 6.a for the homogeneous saturation pattern.

The variation of P-wave velocity depends on the change of the rock bulk modulus (K_{sat}) and bulk density values. The rock bulk modulus and the fluid density decreases with the increase of CO2 saturation. In this case, from 0 % to 50 % of CO2 saturation (low to intermediate saturation), the decrease of K_{sat} is larger than fluid density decrease resulting in Vp decrease. However, from 50 % CO2 saturation (intermediate to high saturation) the lower density values cause a subtle increment in the Vp.

The situation is completely different when saturation is patchy (green points in figure 6.a); in this case, P-wave velocity steadily decreases with increasing CO2 saturation. The gradual decrease of Vp for patchy saturation is a result of no pressure communication between different fluid patches.
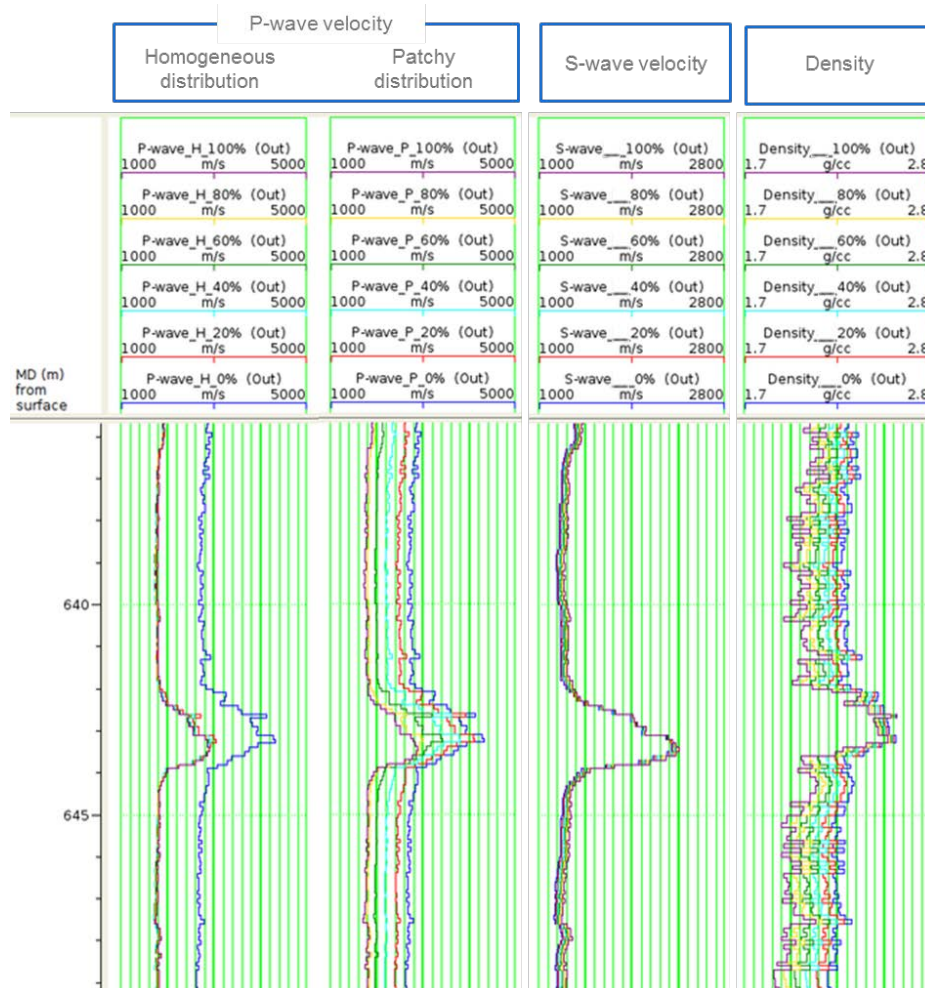
Fig. 5. From left to right, the simulation of P-wave velocity log, S-wave velocity log and density log within the reservoir calculated using Gassmann fluid substitution at different CO2 saturations considering homogeneous and patchy pattern saturation.
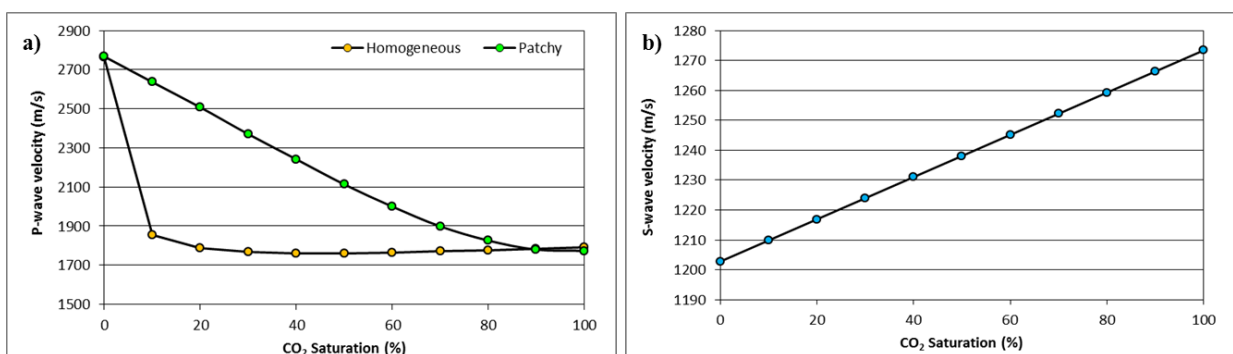
Fig. 6. a) P-wave velocity and b) S-wave velocity values as a function of the CO2 saturation.

7.   Effects of the fluid substitution on the S-wave velocity

Gassmann theory predicts a constant shear modulus after fluid substitution. In the Ketzin case, the modeling predicts a density drop by 10.8 % at 100 % CO2 saturation in comparison to the pure brine scenario. In other words, the change of S-wave velocity is only a result of the change in the density of the reservoir and its values increase directly proportional to CO2 saturation.

However, the increase of the S-wave velocity is not as significant as the P-wave velocity change (figure 6.b), because shear modulus is sensitive to the lithology and pore space but not to the fluid type present in the pores. The maximum change of Vs is 4.8 % when compared with the baseline scenario.

8. Effects of the fluid substitution on the Reflection Coefficient

The injection of CO_2 has a significant effect on the seismic impedances; therefore, on the reflection coefficient. For the homogeneous saturation pattern, the CO_2 saturation of 10 % causes a reflection coefficient change of 170 %. At 100 % of CO_2 saturation the reflection coefficient changes for 224 % when compared with the baseline scenario. Furthermore, the modeling shows that when a certain amount of CO_2 is injected into the reservoir, the change of the reflection coefficient is highly notable, but at higher saturation levels the change is only subtle (yellow points in figure 7). This is a result of the fast filling of the pores that are all connected in the homogeneous scenario. For patchy saturation pattern, the reflection coefficient gradually decreases until it reaches the value for the homogeneous case at 100 % (green points in figure 7). Such a gradual change of RC thus allows identifying saturation levels within the reservoir more easily than in the case of the homogeneous saturation.
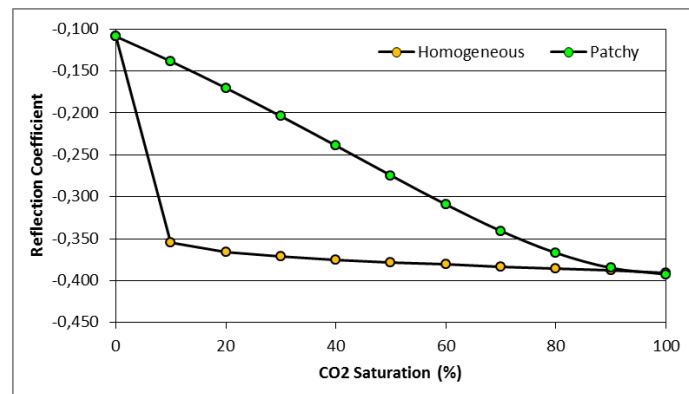
Fig. 7. Zero offset reflection coefficient versus CO_2 saturation for homogeneous and patchy saturation pattern.

In summary, the change in the reflection coefficient is totally dominated by the behavior of the P-wave velocity. Furthermore, the same value for CR at 100 % CO_2 saturation is obtained for both saturation patterns. It is important to highlight that in this study both saturation patterns are evaluated in order to understand their behavior and differences. However, Ivanova et al. (2013) expose on their investigation that in the case of Ketzin site, there is a linear dependence of the P-wave velocity with the saturation of the fluid according to laboratory measurements made in cores. Hence, irregular saturation is the distribution pattern that best models the response at the Ketzin site, and therefore will be the saturation pattern that will be considered from now on.

9. Synthetic traces generation

In order to model the changes in the amplitudes associated with the top of the reservoir after injecting different concentration of CO_2, the logs presented in figure 5 are used as input data to generate the synthetic seismic trace at the position of the injection well.

Figure 8 presents the baseline seismic trace located at the injection well, near the intersection of inline 1165 and crossline 1101 of the 3D seismic survey with the modeled synthetics for 20, 50 80 and 100% CO_2 saturation scenarios considering a patchy saturation pattern.
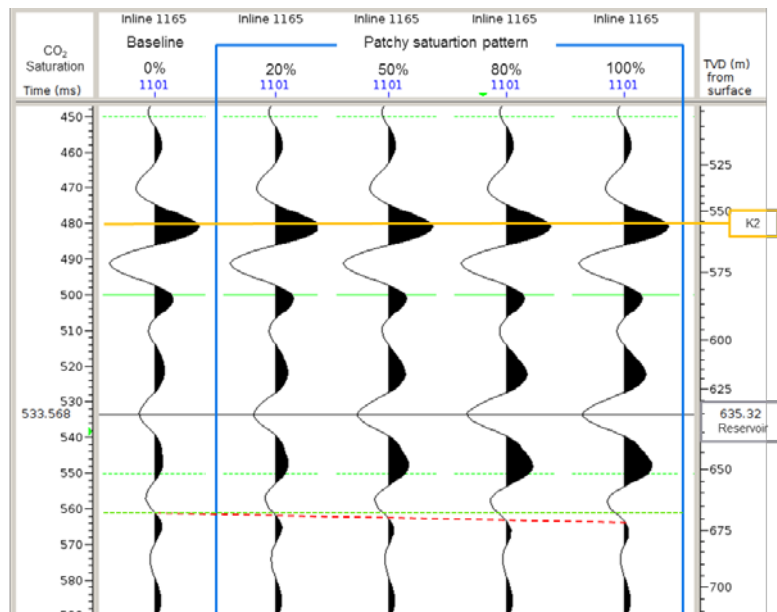
Fig. 8. The response of the seismic modeling for different CO2 concentrations for patchy saturation pattern at the injection well. The K2 reflector is highlighted in yellow and the top of the reservoir is marked with a gray line. Time delay effect is indicated by a red dashed line.

In the patchy saturation case, the absolute amplitude at the top of the reservoir (gray line in figure 8) increases almost linearly. The amplitudes at the top of the reservoir are -0,114 (baseline), -0,173 (20%), -0,269 (50%), -0,352 (80%) and -0,375 (100%). Below the reservoir the change of the amplitudes is negligible, but there is a time delay effect due to the velocity decrease within the reservoir (red dashed line in figure 8). A zoom of a zone below of the reservoir is shown in figure 9. The time delay is nearly linear with the increase of CO2 saturation and at the maximum CO2 concentration the push down effect is 2,5 ms.
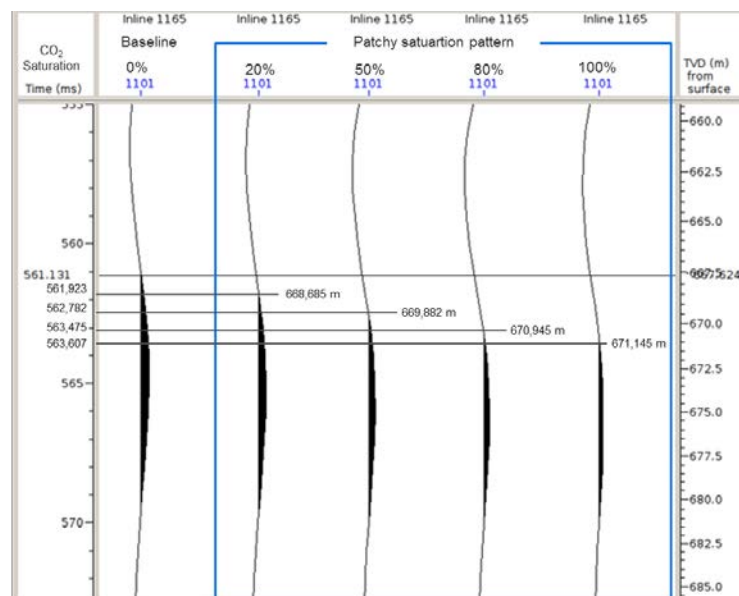
Fig. 9. Zone below the reservoir that illustrates the push-down velocity time delay for different CO2 saturations considering patchy saturation pattern.

10. Seismic interpretation

In this section the seismic interpretation is shown over the entire seismic cube in figure 10. Due to the continuity of the horizons and the simplicity of the seismic, it is easy to see that there are no significant faults within the

extension of the seismic cube that could leak the injected CO2 to overlying layers. This agrees with what exposed by Juhlin et. al. (2007).
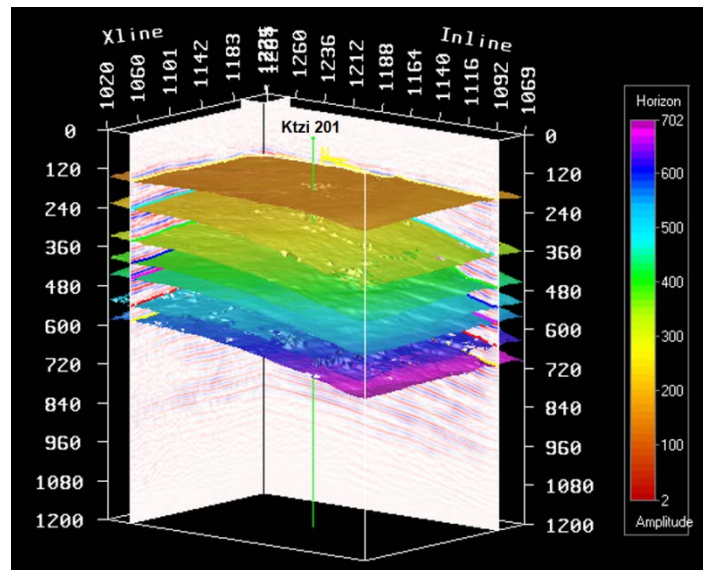
Fig. 10. Three-dimensional view of the extent of the horizons interpreted on the seismic cube. From top to bottom are shown: the base of the Tertiary, top of the Sinemuriense, top of the Triassic, top of the Arnstadt Formation, top of the Stuttgart Formation and its base.

11. Numerical simulation of the reservoir

The geological model of the Ketzin field created in CMG-Builder was developed using the interpreted horizons to build the geometry of the model. Additionally, Figure 11 summarizes the values of porosity and permeability introduced that were taken from Schmidt (2010).
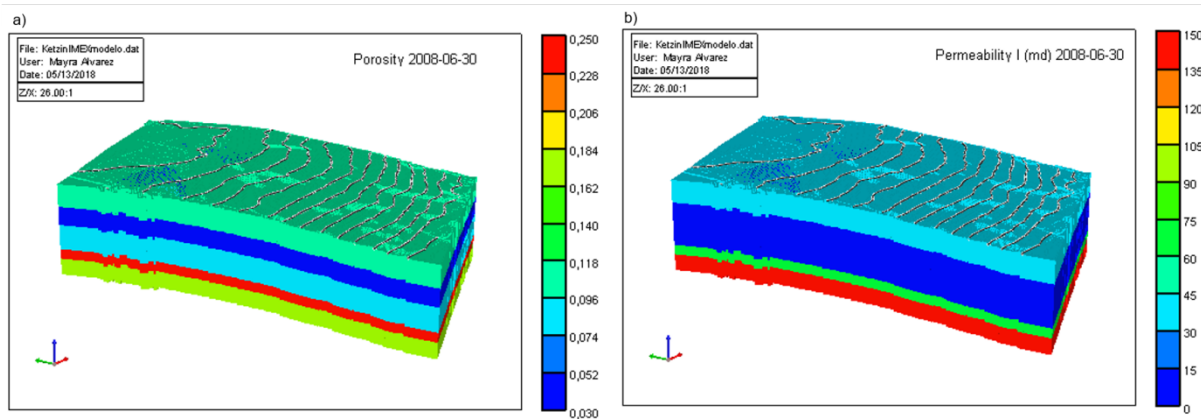
Fig. 11. 3D view of the model created CMG-Builder highlighting (a) the porosity and (b) permeability of the layers.

In order to optimize the time required to successfully finish the simulation it was necessary to decrease the surface size of the model and reduce the depth interval to the one covered by the Stuttgart Formation (figure 12). An additional reason for this decision is that the relative permeability curves available corresponded only to this Formation. Furthermore, the continuity of the seal and its low permeability (Schmidt et al., 2010) are enough to limit the simulation to the reservoir rock and decrease the computation time.
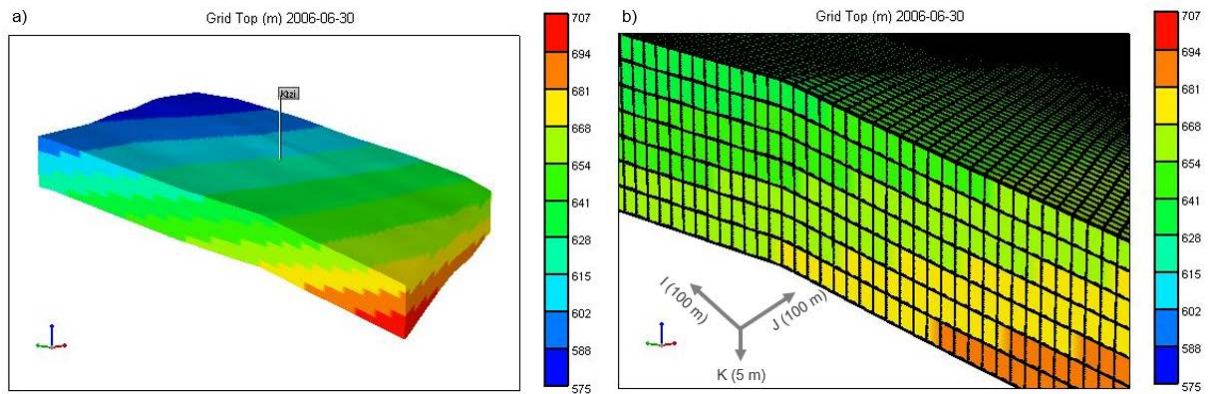
Fig. 12. a) New model of the reservoir created to reduce computation time. The injection well Ktzi 201 is shown in gray. b) Geometry of the mesh whose blocks are of dimension 100mx100mx5m (scale 1:38).

The numerical simulation in this study is used to fulfill the objectives of estimating the evolution and extension of the CO_2 plume and the change of saturation in the rock. The criteria used to establish the variables that control the injection well were fixed to obtain a pressure close to 7 MPa at the end of 2009 because this was the only pressure value accessible from Ivanova et al., 2013. After making several runs changing the controlling variables of the well, the desired pressures were obtained by establishing a limit rate of injection of 100,000 m3/day, a pressure limit of 10,000 kPa and an injection period of 5 years and one month (project execution period). In this sense, the evolution of the CO_2 plume during the CO_2 injection and after the injection until year 2025 is presented in the figures 13 and 14.
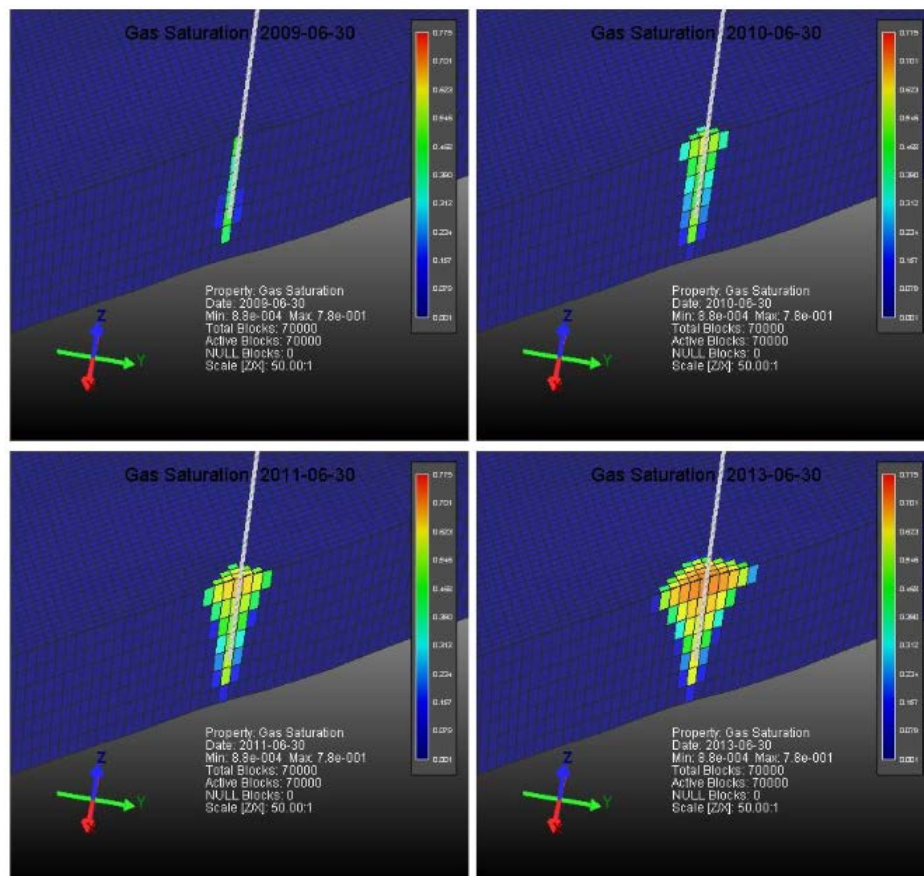
Fig. 13. Evolution of CO_2 saturation after the CO_2 injection for the years 2009, 2010, 2011 and 2013.
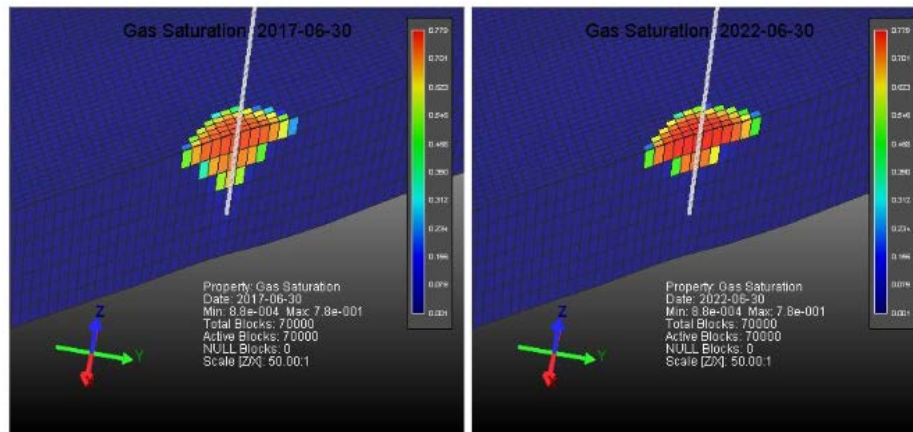
Fig. 14. Evolution of CO2 saturation after the CO2 injection for the years 2017 and 2022.

From Figures 13 and 14 it can be seen that the flow trend is radial around the bottom of the well with a vertical flow that expands laterally when approaching the overlying cap rock. The maximum radius reached for the CO2 at the bottom of the well and below the seal rock is approximately 100 meters in June 2013 and 600 meters by January 2025 respectively. From the simulation result, it is observed that the maximum saturation of CO2 is 71% in the year 2025. Additionally, the average saturation of CO2 of at the top of the reservoir was of 50 % at the end of 2009, which coincides with the results presented by Ivanova et. al. (2013).

It should be noted that the limit values of the injection rate and bottom pressure are assumed and do not save a relation with real production. However, for the purposes of this investigation is sufficient to estimate that the possible extension of the CO2 plume can reach 1.1 km^2 at the top of the reservoir. This extension is sufficient to be detected in seismic acquisitions using the same geometry as in the baseline acquisition due to the proven impedance change presented in this investigation.

12. Conclusions

The purpose of the current study was to estimate the change of the elastic properties of the reservoir after the injection of different concentrations of CO2 considering two different fluid saturation patterns. For this purpose, fluid substitution was applied to replace the wet zone of the reservoir with different CO2 saturation scenarios that allowed to estimate new well logs for each CO2 concentration. The generated well logs were used to create synthetic seismograms for the evaluation of the change of the seismic response at the top of the reservoir.

The results of this study suggest that the saturation pattern of the rock used in the fluid substitution model plays an important role in the estimation of the elastic properties of the reservoir. Depending on the saturation pattern under consideration the value of the P-wave velocity will be different, resulting in large differences when comparing the results for different saturation patterns. Hence, the change of the CR could be gradual (patchy saturation) or abrupt (homogeneous saturation) as the CO2 is injected into the reservoir. The same idea describes the effect of the velocity push down, consequently the variation of the delay time below the reservoir. Both results highlight the importance of identifying the saturation pattern that is closest to reality in order to correctly calculate the bulk modulus of the rock to predict seismic velocities more accurately.

The results showed that the extension and change of CO2 saturation of the reservoir are sufficient to generate a change in its seismic response. This implies that it is possible to monitor the evolution of the CO2 plume using 3D time-lapse seismic technique.

In further studies, it is recommended to use a petrophysical model as input data in the numerical simulation of the reservoir that indicates the variation of porosity and permeability over the entire volume. Additionally, it is suggested to include in the simulation the variables associated with trapping mechanisms since it will vary the porous space of the reservoir and the mineral content of the rock over the time.

Acknowledgment

References

[1] Huang, F., Bergmann, P., Juhlin, C., Ivandic, M., Lüth, S., Ivanova, A., Kempka, T., Henninges, J., Sopher, D., Zhang, F., 2016. The First Post-injection Seismic Monitor Survey at the Ketzin Pilot CO2 Storage Site: Results from Time-lapse. Analysis. Geophysical Prospecting. Retrieved from: http://urn.kb.se/resolve?urn=urn:nbn:se:uu:diva-301005

[2] IPCC, 2005. IPCC Special Report on Carbon Dioxide Capture and Storage. Prepared by Working Group III of the Intergovernmental Panel on Climate Change [Metz, B., O. Davidson, H. C. de Coninck, M. Loos, and L. A. Meyer (eds.)]. Cambridge University Press, Cambridge, United Kingdom and New York.

[3] Ivanova, A., Juhlin, C., Lengler, U., Bergmann, P., Lüth, S., Kempka, T., 2013. Impact of temperature on CO2 storage at the Ketzin site based on fluid flow simulations and seismic data. International Journal of Greenhouse Gas Control, 19, 775–784. Retrieved from https://doi.org/10.1016/j.ijggc.2013.05.001 Johnson, K., 2009. "Climate Debate: IPCC Head Pachauri Joins the 350 Club". The Wall Street Journal. Disponible en https://blogs.wsj.com/environmentalcapital/2009/08/25/climatedebate-pcc-head-pachauri-joins-the-350-club/.

[4] Juhlin, C., Giese, R., Zinck-Jørgensen, K., Cosma, C., Kazemeini, H., Juhojuntti, N., Lüth, S., Norden, B., Förster, A., 2007. 3D baseline seismics at Ketzin, Germany: the CO2SINK project. Geophysics 72, B121–B132.

[5] Kazemeini, S. H., 2009. Seismic Investigations at the Ketzin CO2 Injection Site, Germany: Application to Subsurface Feature Mapping and CO2 Seismic Response Modeling. PhD dissertation, Uppsala University. Retrieved from http://urn.kb.se/resolve?urn=urn:nbn:se:uu:diva-105032

[6] Morad, S., and Lawton, D., 2012. Time-lapse seismic modeling of CO2 sequestration at Quest CCS project. CREWES Research Report, Volume 24. Retrieved from: https://www.crewes.org/ForOurSponsors/ResearchReports/2012/CRR201272.pdf

[7] Ouellet, A., Bérard, T., Desroches, J., Frykman, P., Welsh, P., Minton, J., Pamukcu, Y., Hurter, S., Schmidt-Hattenberger, C., 2011.Reservoir geomechanics for assessing containment in CO2 storage: A case study at Ketzin, Germany", Energy Procedia, Volume 4, 2011, Pages 3298-3305, ISSN 1876-6102. Retrieved from http://dx.doi.org/10.1016/j.egypro.2011.02.250.

[8] Vera, V. and Lawton, D., 2010. Fluid substitution and seismic modelling in a sandstone aquifer. CREWES Research Report, Volume 22.

[9] Yang, C., 2012. Time-Lapse Analysis of Borehole and surface Seismic Data, and Reservoir Characterization of the Ketzin CO2 Storage Site, Germany. Digital Comprehensive Summaries of Uppsala Dissertations from the Faculty of Sciences and Technology 887.

Technical and economical assessment of small-scale renewable hydrogen production within Europe

David Allen Johnson[1], MaciejSobczyk[2]

[1]*AGH University of Science and Technology, e-mail: davidallenjohnson08@gmail.com*

[2]*AGH University of Science and Technology, e-mail: msobczyk@student.agh.edu.pl*

Abstract

The aim of this research is to perform a technical and economical analysis in order to determine the most cost competitive methods of producing hydrogen available on the market. Gaseous hydrogen will be than used in Fuel Cell Vehicles (FCV's) or co-generation of heat and power applications within a specifically chosen location in Europe. Hence small-scale unit, already available for the market, of both WE and SMR will be compared under operational conditions and costs. Pre-evaluation of the most convenient country for the facility implementation was performed based on statistical data provided by "Eurostat" regarding total share of Renewable Energy Sources (RES) in gross final energy consumption among EU-28 countries and price levels of both electricity and natural gas respectively. According to currently observed forecasts and governmental incentives aiming development of hydrogen refueling stations (HRS's), hydrogen production might, to greater extent, play a pivotal role as of the fuel for FCV's and as an energy carrier.

Keywords: hydrogen production, water electrolysis (WE), steam methane reforming (SMR), renewable energy sources (RES), SimSci PRO/II

1. Introduction

Renewable energy sources (RES) are going to play a pivotal role in electricity power generation mix within EU countries, challenging targets to decrease GHG's emission established by European Commission. Forecasts claim, that levels of the GHG's are about to be reduced 30% until 2020 and 50% until 2050, according to IPCC 2018 report.

Therefore, gaseous hydrogen (H2), as an energy carrier, poses marvelous properties such as high mass energy content, high combustion energy content, elemental abundance and long-term storability. In addition, in air combustion no greenhouse gases, such as CO2 or N2O are formed. Nevertheless, low volumetric energy content seems to be its weakest point. Furthermore, due to lack of infrastructure to store and deliver gaseous hydrogen, as it is not apparently easy process, further development of hydrogen production affordability still requires significant economic breakthroughs.

As a consequence of previously mentioned aspects, being at the edge of transition from fossil fuels towards zero-emission alternatives, technologies evaluated in this work aim to tackle a promising, affordable way to produce pure hydrogen at competitive prices. Hydrogen production via water electrolysis (WE) and steam methane reforming (SMR) was performed based on simulations conducted by scientific software - SimSci PRO II and statistical data provided by European Statistical Office (Eurostat). Final comparison of obtained results regarding final costs of hydrogen production (€/kgH2) based on efficiency of evaluated installations, widely used in industry nowadays.

NOMENCLATURE:

WE - Water Electrolysis

SMR - Steam Methane Reforming

PEM - Proton Exchange Membrane

FCV - Fuel Cell Vehicle

RES - Renewable Energy Sources

HRS -Hydrogen Refueling Station

WGS -Water-Gas-Shift

2. Metodologycal Framework

The framework proposes selecting a specific EU country with the most overall favorable conditions for renewable hydrogen production. After country selection, the minimum cost of production of hydrogen that covers the cost of raw materials is determine under optimal conditions for each technology. Hence the proposed framework can be summarized in three main points as follows:

- Country Selection Methodology

- Selected approach for Water Electrolysis analysis

- Selected approach for Steam Methane Reforming analysis

However, it is important to note that methodology only compares the cost of production of hydrogen based on the raw feed and resources used under operational condition. However, the analysis does not include compressions cost or capital expenditures costs. Hence, the methodology only works for determining the minimum price of hydrogen to cover raw materials and resources for each case study.

2.1. Country Selection Methodology

Additionally, the categories were chosen to represent as whole the cost of raw materials and resources, the likelihood of production via a renewable source and the hydrogen market growth within a specific the country. The six categories selected and their respective scores are presented as follows:

1) **Natural Gas Price:** This parameter represents the cost of raw materials for the SMR process. The prices of natural gas in €/kWh where obtained for each EU country based on statistical information provided by Eurostat [1]. The data set obtained was divided in 4 quartiles, where the first quartile (Q1) represents the countries with lowest price while the fourth quartile (Q4) represents the countries with the highest prices. Hence, for this category scores from 1 to 4 were chosen in a manner that countries with highest prices located in the set Q4 receive a score of 1, while countries with lowest prices located in Q1 receive a score of 4.

2) **Electricity Price:** This parameter represents the cost of resources for both the Electrolysis process and the SMR process. Analogues to the previous category, the prices for each country are also obtained by Eurostat in €/kWh [2]. Furthermore, the scoring system is also developed in the same fashion as the aforementioned category.

3) **Water Price:** This parameter represents the cost of raw materials for both the Electrolysis process and the SMR process. The data for the prices presented in €/m3 for this category are obtained from reports of the "Governance of water services in Europe" [3]. Furthermore, the scoring system is also developed in the same fashion as the aforementioned categories.

4) **Renewable Share:** This parameter represents the likelihood of producing renewable hydrogen using electricity derived form a renewable source. The category takes into account the share of energy production from renewables in a specific country, since the more renewable share within a country the more likely the electricity use for the process will come from a renewable source. The renewable share data is obtained from Eurostat [4]. Similar to previous categories the data was divided in 4 quartiles, where the first quartile (Q1) represents the countries with lowest share while the fourth quartile (Q4) represents the countries with the highest shares. Hence, for this category scores from 1 to 4 were chosen in a manner that countries with highest shares located in the set Q4 receive a score of 4, while countries with lowest shares located in Q1 receive a score of 1.

5) **Number of Bio-gas plants:** This parameter represents the likelihood of producing renewable hydrogen from SMR by using Bio-gas instead of natural gas. The category takes into account the number of Bio-Gas plants within a country that are connected to the gas grid in order to ensure that hydrogen produced from SMR comes from a renewable source. Additionally, the category assumes that bio-gas prices are or will be competitive and interchangeable with natural gas prices for each country in the near future.

The number of Bio-Gas plants in each country connected to the gas grid are obtained from GIE/EBA European Bio-Methane map of 2018 [5]. However, since most countries don't have bio-gas plants connected to the grid the scoring meninism was adjusted. This adjustment was made so that countries without plants received a score of 0. Furthermore, from the remaining countries the data was divided in 4 quartiles, where the first quartile (Q1) represents the countries with the lowest number of plants while the fourth quartile (Q4) represents the countries with the highest number of plants. Hence, for this category scores from 1 to 4 were chosen in a manner that countries with highest number of plants located in the set Q4 receive a score of 4, while countries with lowest numbers of plants located in Q1 receive a score of 1.

6) **H2 mobility score:** This parameter represents the market growth of hydrogen based on Fuel Cell Vehicles and other hydrogen installation infrastructure forecast increases. Hence, it is one of the most valuable parameters since it assures a market for the product. However, only a small minority of EU countries are considered major hydrogen players within the framework of H2-mobity [6]. In this sense, countries that have a hydrogen market are of special interest and receive an additional score of 4.

2.2. Selected approach for Water Electrolysis analysis

Gaseous hydrogen production via water electrolysis (WE) is a commercially available process to obtain desired product with satisfactory purity and with low by-products emission. A phenomenon of electrolysis process lays in a formation of both gaseous hydrogen (H2) and oxygen (O2) molecules via splitting water molecule (H2O) by passing electricity as DC (Direct Current). Oxygen is produced at the anode (+) and comparatively hydrogen at the cathode (-). The voltage of direct current provided by the electrode need to be greater than Gibbs free energy of formation of water (equal to -237,14 kJ/mole H2O) at standard ambient temperature and pressure conditions – SATP (T = 293.15K, p = 1013,25 hPa), relative activation process and ohmic losses before water molecule decomposition. Nowadays there are three mainly used technologies of electrolytic hydrogen production available on the market.

In this study both PEM (Protone Exchange Membrane) and alkaline electrolyzers were taken into consideration, as the most convenient to operate and less demanding according to water purity and chamber separators. Based on the data provided by National Renewable Energy Laboratory (NREL) in United States of America, four facilities aimed to produce four different volumes of hydrogen were assessed. These technologies are provided to the market by following companies: Stuart IMET®, EC Proton Hogen®, AvalenceHydrofiller® and Teledyne MC®. Each of them produces hydrogen at small or large scale, depending on hourly volumetric H2 formation, forecasted capacity of vehicles to serve and unit size range.

Water feed to the electrolysis unit ought to fulfil specific requirements regarding purity, therefore small water treatment before electrolyser should be implemented. After purification process, injection of potassium hydroxide solution (KOH) with concentration equal to 25% (v/v) is necessary to provide conductive agent. If needed, sodium chloride (NaCl) or sodium hydroxide (NaOH), may be used as an electrolyte instead of KOH solution. The aim of this process is to provide highly soluble chemical agent in order to achieve fair conductivity of the solution. After electrolyser injection, electrolysis process take place, and then two gaseous agents – H2 and O2 will appear in biphasic state (gaseous-liquid). Hence, the undesired oxygen is discharged to the atmosphere, when hydrogen flows further to two alumina dryers when final purity of gas is achieved, up to 99,99%. No compression of gaseous hydrogen and its storage were evaluated.
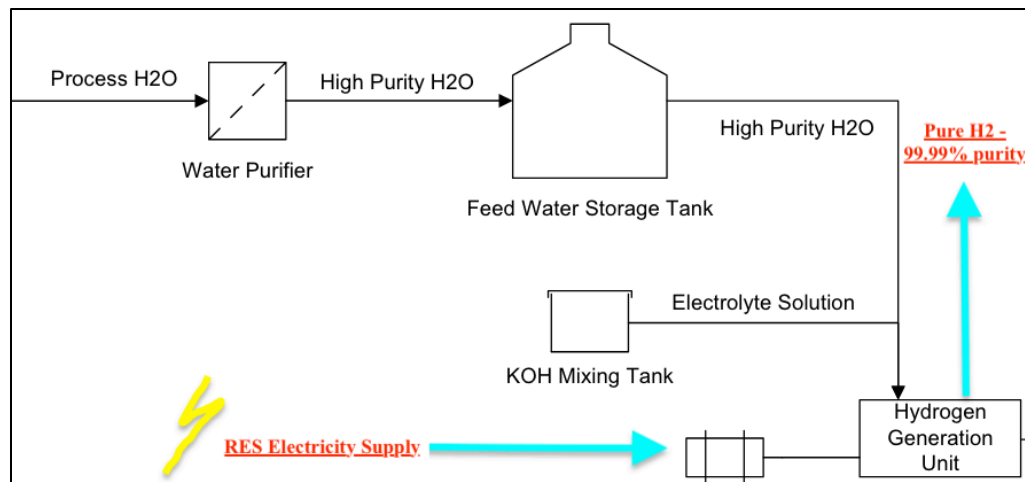
Fig. 1. Conceptual sketch of the electrolysis system[7] (date of access to the online source: 18/11/18)

Generally, overall electrolysis process can be described by following chemical equation:

$$H_2O + e- \rightleftharpoons H_2 + \frac{1}{2}O_2$$
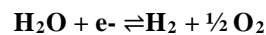
In alkaline system where, to greater extent, potassium hydroxide (KOH) solution is used as an electrolyte, chemical reactions at each electrode are:

Cathode (-) $2H2O + 2e^- \rightleftharpoons H2 + 2OH^-$ (Water reduction process)

Anode (+) $2OH^- \rightleftharpoons \frac{1}{2}O2 + 2H_2O + 2e^-$ (Oxidation process)
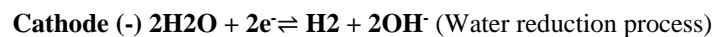
In PEM electrolysers water electrolysis is slightly different, due to lack of electrolytic base solution. Chemical formula presented below describes electrolysis in PEM systems:

Cathode (-) $2H^+ + 2e- \rightleftharpoons H2$ (reduction process)

Anode (+) $H_2O \rightleftharpoons \frac{1}{2}O_2 + 2H+ + 2e^-$ (oxidation proces)
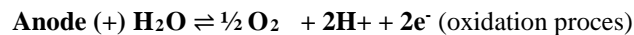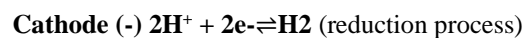
Fig. 2 shows water electrolyser with unipolar bath system.
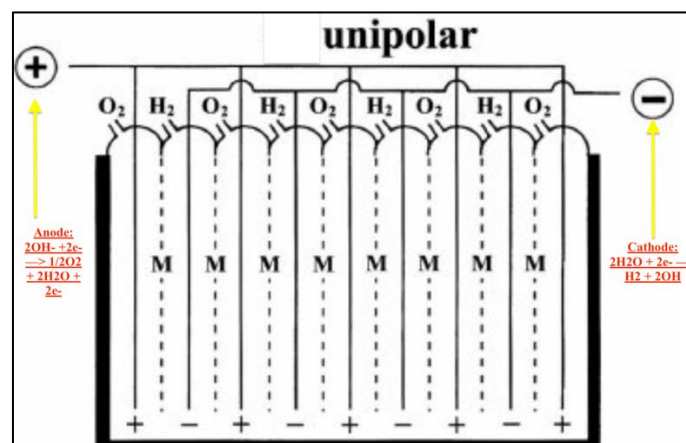
Fig. 2. Unipolar alkaline electrolyser bath system [8]

2.2.1.   Description of units for the Water Electrolysis process

In connection with the data provided by NREL four electrolysers were chosen in order to cover as wide range of hydrogen production as available on the market. Two of them are PEM technology, and two of them are unipolar, alkaline respectively. Station sizes will cover the requirements for hydrogen production for variety of areas including small neighborhood, neighborhood and small forecourt. It is worth to emphasize that we want to provide affordable hydrogen to smaller area during the first step of facility implementation and incrementally

expand to become more competitive on a larger scale market. Small forecourt installation will cover the demand for hydrogen at the level up to 91 kg per day. Tab. 1 shows the a summary list of commercially available units

Commerciallyavailableelectrolyzers	kgH$_2$/day	kg H$_2$/hr	kgH$_2$/annum	Number of carsserved	Station Size
Proton Hogen 380®	28	1,17	7875	39	Small Neighbourhood
Teledyne EC-750®	91	3,79	33000	165	Small Forecourt
AvalancheHydrofiller 175®	10	0,42	3000	18	Small Neighbourhood
Stuart: IMET 1000®	65	2,71	23000	118	Heighbourhood

In order to calculate the final cost of hydrogen production via water electrolysis one of the crucial parameter of the whole operation is an efficiency of the unit. All units presented in this frame exhibit efficiency within the range of 80% to 95%. The energy efficiency of the unit was determined by dividing higher heating value (HHV) of the hydrogen, equal to 39,5 kWh/kgH2 by the electrolysis system energy demand per one kilogram of hydrogen derived. No compression energy requirement was included in calculations. Apparently the efficiency would decrease significantly if we compress the hydrogen to desired storage value, equal to 410 bar (6000psi) [7].

2.3. Selected approach for Steam Methane Reforming analysis

The technical and economical assessment of hydrogen production using SMR was done by minimizing the cost of production based on the cost of raw materials and resources under optimal operation conditions. The simulation was carried out using SimSci Pro/II. The thermodynamic model chosen was Soave-Redlich-Kwong (SRK) for all components except pure liquid water for which Tab. properties where chosen. Additionally, in order to ensure comparable results to the WE process, the same four aforementioned case studies for hydrogen production rate where selected and optimized. Furthermore, the main scheme for small scale hydrogen production using SMR was based on commercial technologies presented by the National Renewable Energy Laboratory (NREL) in the US [9]. Such a scheme is presented in the PRO/II simulation flow diagram shown in Fig. 3.
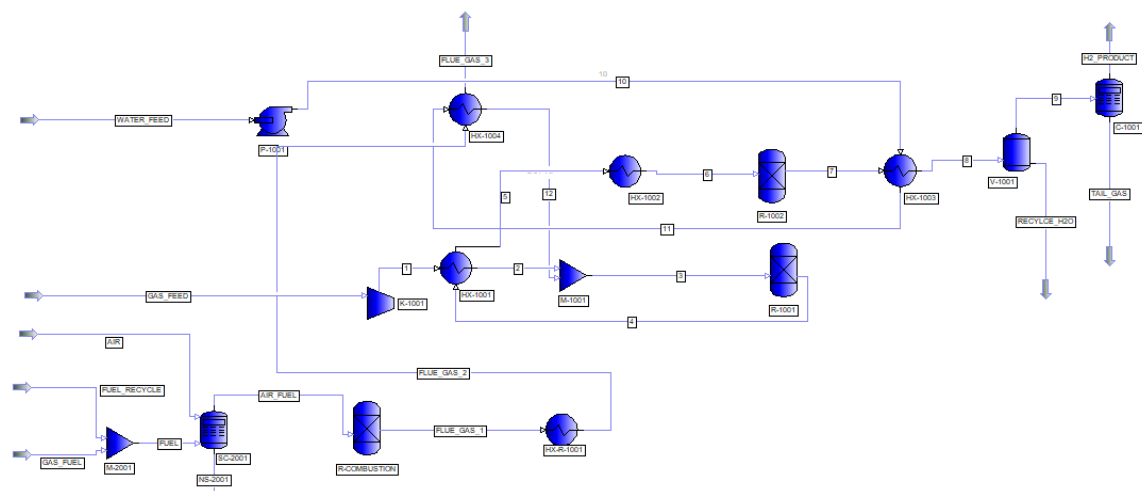
Fig. 3. Simulation Scheme for Small Scale SMR using SimSci PRO/II

The optimization consists of minimizing a cost function which is dependent of the sum of raw materials such as water and natural gas, as well as the electricity consumed by the process. Furthermore, the optimization is accomplished by varying operational conditions such as the amount of feed and the temperature of the reformer. In this sense, the optimization function algorithm can be written as:

Step 1 Minimize

$$F_{cost} = \frac{(C_1 * HHV * (\dot{M}_{NG} + \dot{M}_{Fuel}) + C_2(W_{pump} + W_{comp}) + C_3 * \dot{V}_{H_2O})}{\dot{M}_{H_2}}$$

Where,

C1   Cost of Natural gas (kWh)

C2   Cost of Energy (kWh)

C3   Cost of Water (m3)

HHV   High heating value of natural gas (kWh/kg)

$\dot{M}_{H_2}$ Mass flow of hydrogen (kg/day)

$\dot{M}_{Fuel}$ Mass flow of natural gas used as fuel (kg/day)

$\dot{M}_{NG}$ Mass flow of natural gas used as chemical feed (kg/day)

$\dot{V}_{H_2O}$ Volume flow of water (m3/day)

W comp   Work of the compressor (kWh/day)

W pump   Work of the pump (kWh/day)

Step 2 Vary

The following flowsheet parameters are varied to reach the minimum value of the cost function, while at the same time ensuring the specific production rate of hydrogen:

A)   **Feed of natural gas**: Control the price by regulating the amount of natural gas use as reactive.

B)   **Feed of water**: Controls the price by regulating the amount of natural gas.

C)   **Temperature of the reformer reactor**: Controls the price by regulating the amount of gas used as fuel.

On the other hand, all other operational conditions for the remaining equipment of the process fixed based on commercially available experience. However, pressure drop of the equipment's is not considered under the study. Additionally, since the operation considered is small scale reforming with PSA, only one small scale shift reactor is used for the process [10]. Additionally, since PRO/II cannot simulate adsorption processes an equipment that separates the desired products is used as the PSA and the feed in considered Sulphur free. A summary of this operational parameters is presented in Tab. 2.

Tab.2. Summary of operational conditions for the main equipment's of the SMR process [10].

Equipment	Simulation Considerations	Fixed values
Reformer (R-1001)	- Gibbs reactor - Isothermal - Inlet Temperature	- Inlet Temperature :450 °C - Fixed Temperature: 700-900 °C
Shift Reactor (R-1002)	- Gibbs reactor - Adiabatic - Temperature range	- Outlet CO concentration: 0,5 %vol - Temperature range: 210-330 °C

PSA Column (C-1001)	• Component splitter • Inlet Temperature • Pressure outlets	• Purity of hydrogen on the top: 99.99% • Hydrogen Recovery on the top: 90% • Inlet Temperature: 40°C

3. Results

3.1. Matrix of localizationresutls

From the relevant data reviewed a localization matrix for country selection was made. The EU countries for which data was available are shown in Tab. X listed in order from most favorable to least favorable in terms of conditions for implementing hydrogen production within the country.

Tab. 3. Localization Matrix for country selection

EU Country	Electricity Price	GasPrice	Water Price	Renewable Share	# of BiogasPlants	H2 Mobility	Total Score
Finland	4	1	1	4	2	4	16
Sweden	4	1	1	4	2	4	16
United Kingdom	1	4	2	1	4	4	16
Denmark	2	1	1	4	3	4	15
Hungary	4	4	3	2	1	0	14
Germany	1	2	1	2	4	4	14
France	3	1	1	2	3	4	14
Bulgaria	4	4	2	3	0	0	13
Spain	2	3	4	3	1	0	13
Croatia	3	4	3	3	0	0	13
Netherlands	4	3	2	1	3	0	13
Portugal	2	3	4	4	0	0	13
Romania	3	3	4	3	0	0	13
Czech Republic	4	4	2	2	0	0	12
Estonia	3	3	2	4	0	0	12
Slovenia	4	2	3	3	0	0	12
Italy	1	3	4	3	0	0	11
Latvia	2	2	3	4	0	0	11

Lithuania	3	1	4	3	0	0	11
Austria	2	1	2	4	2	0	11
Poland	3	3	3	2	0	0	11
Greece	1	2	4	2	0	0	9
Slovakia	2	2	3	2	0	0	9
Belgium	2	4	1	1	0	0	8
Ireland	1	2	4	1	0	0	8
Luxembourg	3	2	1	1	1	0	8

From the previous Tab. we can notice that the preliminary screening shows that the EU countries with most favorable conditions for hydrogen production are Finland, Sweden and the United Kingdom with a total score of favorability of 16. However, taking into consideration a more subjective analysis of these three countries it was decide that political aspects that Finland was the most suiTab. for implementing this technology since the UK will no longer from part of the EU, and Sweden presents higher market barriers than Finland.

3.2. Results of the technical andeconomical analysis for the Water Electrolysis process

Based on the localization matrix results, the Finnish water and electricity cost for each case study were used. Furthermore, Tab. 4 shows the results of the production of hydrogen for each commercially available technology chosen.

Tab. 4. Cost of hydrogen production via Water Electrolysis

Commerciallyavailableelectrolysers	Production rate of H2 [H2/day]	Price of energy [€/kgH2]	Price of water [€/kgH2O]	Cost of hydrogen production (€/kgH2]
Proton Hogen 380®	28	4,74	0,0558	4,80
Teledyne EC-750®	91	4,21	0,0663	4,28
AvalancheHydrofiller 175®	10	4,09	0,0596	4,15
Stuart: IMET 1000®	65	3,61	0,0663	3,68

3.3. Results of the technical andeconomical analysis for the SMR process

Based on the localization matrix results, the composition feed used for the SMR simulation was that of the pipeline specification provided by the Finnish Gas Association as shown in Tab. 5[11]. Additionally, feed temperatures and pressure used in the simulation were also chosen based on the data provided by the Finnish Gas Association.

Tab. 5. Composition of the natural gas in Finland [11]

Component	Composition (%mol)
Methane (CH_4)	98,00
Ethane (C_2H_6)	0,8
Propane (C_3H_8)	0,2
Butane (C_4H_{10})	0,02

Nitrogen (N_2)	0,9
Carbon Dioxide (CO_2)	0,1

Furthermore, based on the composition of the Finnish natural gas the reactions within the reformer and the shift reactors are considered as shown in Tab. 6.

Tab. 6. Main chemical reactions of the SMR process Reactions.

Reactions	Chemical formula of the reaction
Methane reforming	$CH_4+H_2O \rightleftharpoons 3H_2 +CO$
Ethane reforming	$C_2H_6+2H_2O \rightleftharpoons 5H_2 +2CO$
Propane reforming	$C_3H_8+3H_2O \rightleftharpoons 7H_2 +3CO$
Butane reforming	$C_4H_{10}+4H_2O \rightleftharpoons 9H_2 +4CO$
Water gas shift reaction	$CO+H_2O \rightleftharpoons H_2 +CO_2$

Using the Finnish gas composition, the optimization process with SimSci PRO/II where done. The optimization results are shown in Tab. 7.

Tab. 7. Results of the SMR technical and economicalanalysis for optimal conditions

Production rate of H2 (kg/day)	Feed of Gas (kg/day)	Feed of Water (kg/day)	Steam to Gas ratio (kg_{vapor}/kg_{gas})	Temperature of Reformer (°C)	Price of H_2(€/kgH$_2$)	Efficiency[A] (%)
10,00	29,27	119,91	4,10	793,43	3,05	75,66
28,00	79,99	294,50	3,68	814,83	3,04	75,74
65,00	195,3	705,26	3,61	800,13	3,03	75,84
91,00	261,84	1186,36	4,53	786,90	3,06	75,51

[A]   Efficiency refers to the fuel efficiency, hence it is the heating value of the product in respect to the heating value of the feed.

From the previous Tab. we can calculate that the average value for production hydrogen is 3,05 €/kgH2.

4. Analysis of results

4.1. Analysis of hydrogen production prices in Finland via WE

Analyzing Tab. 4 from Section 3.2 we can notice that the price of hydrogen produced via commercial electrolysis varies from 3,68€/kgH$_2$ to 4,80 €/kgH$_2$. In particular, it can be noted Alkaline electrolysers units are costlier in terms of production cost than PEM electrolysers. This can be attributed to the lower efficiency of the PEM electrolysers. Furthermore, from Tab. 4 we can notice that water cost is almost negligible in comparison to the electricity prices for all electrolysers.

4.2. Analysis of hydrogen production prices in Finland via SMR

Analyzing Tab. 7 from Section 3.3 we can notice that in particular for all case studies the average price of hydrogen is around 3,05 €/kgH2. Additionally, we can notice that for all case studies the average fuel efficiency of the process is around 75%, the steam to gas ratio is in the range of 3,6 to 4,5, and the optimal temperature of the reformer is around 800 °C. The similarities within the results are as expected since most of the equipment's used to optimize the cost function in the simulation are based solely on thermodynamic models. Hence the results from section 3 corroborate that under optimal operational conditions in terms of cost effectiveness the process is thermodynamically feasible.

On the other hand, compering the results in Tab. X of the optimal operation conditions of the small-scale reforming process with typical commercial operation conditions we can notice three important factors:

1) The optimal operational temperature of the reformer corresponds to typical temperature operation of commercial reforms (700°C to 900 °C) [10]

2) The steam to natural gas ratio is relatively high in respect to the typical commercial operations of 3.2 to 3.5 [12]. This is due to the fact that gas prices in Finland are considerably higher than water hence, adding more vapor improves conversion and reduces the amount of natural gas needed, and therefore the overall cost of the process.

3) The fuel efficiency of the process is considerably low in comparison to commercial efficiencies (>95%). This is due to the fact that commercial efficiencies reported usually include the heat recovery and integration systems to create steam. This integration improves the overall efficiency of the process however was not included within this study.

4.3. Comparison of hydrogen production prices in Finland via WE and SMR

The main results regarding the hydrogen production price in Finland for each production process are summarized in Tab. 8 for comparison.

Tab. 8. Comparison of cost of hydrogen production via WE and SMR within Finland.

Production rate of H2 (kg/day)	Production cost via WE (€/kgH$_2$)	Production cost via SMR (€/kgH$_2$)
10,00	4,15	3,05
28,00	4,80	3,04
65,00	3,68	3,03
91,00	4,28	3,06

Analyzing the results in Tab. 8 we can notice that in general the process producing hydrogen within Finland is considerable cheaper for the Steam Methane Reforming process in comparison with the Water Electrolysis process. This is mostly due to the fact that the amount of electricity needed by WE process is considerably high, making the net cost of electricity used in WE exceed the net cost of natural gas used for SMR.

On the other hand, it is important to notice that the result in Tab. 8 only imply that in terms of costs of raw material and resources, the production of hydrogen in Finland is cheaper using SMR technology. Hence, further research that takes into account capital expenditure, as well as operational and maintenance cost, must be considered in order to definitely determine which process is more economically favored within Finland for a specified demand of hydrogen production. Additionally, tracing the renewability of WE process is considerably easier than for SMR process connected to the gas grid. Hence, further research should also consider the feasibility of the study in a specific location in Finland where renewability of both the electricity and natural gas source can be confirmed.

5.   Conclusions

From the technological and economical analysis for renewable hydrogen production via Steam Methane Reforming and Water electrolysis within the European Union it can be concluded that:

- The most favorable countries for hydrogen production are Finland, Sweden, and the UK with a specific emphasis in Finland.

- Using Water Electrolysis for Hydrogen production within in Finland it was determine that the lowest production price to cover costs of raw material and resources is of 3,68€kgH$_2$for a production rate of 65 kg/d using the commercially available Stuart: IMET 1000®electrolyser

- The average price of hydrogen production to cover the costs of raw material and resources via SMR in Finland is 3,05 €kgH$_2$

- The lowest production price to cover raw materials in Finland using SMR is 3,03€kgH$_2$ for a production rate of 65 kg/d

- In general, for all case studies it can be concluded that the price of hydrogen to cover the costs of raw material and resources is lower for the process of SMR in comparison to WE in Finland.

References

[1] Eurostat Statistics Explained, https://ec.europa.eu/eurostat/statistics-explained/index.php/Natural_gas_price_statistics, date of access (28/10/2018).

[2] Eurostat Statistics Explained, https://ec.europa.eu/eurostat/statistics-explained/index.php/Electricity_price_statistics , date of access (28/10/2018).

[3] EurEau, https://www.asoaeas.com/sites/default/files/Documentos/2018-04-10%20-%20Report-on-the-governance-of-water-services-in-Europe.pdf , date of access (28/10/2018).

[4] Eurostat Statistics Explained, https://ec.europa.eu/eurostat/tgm/Tab..do?tab=Tab.&init=1&language=en&pcode=t2020_31&plugin=1 , date of access (28/10/2018).

[5] Gas Infrastructure Europehttps://www.gie.eu/index.php/gie-publications/maps-data/gse-storage-map, date of access (28/10/2018).

[6] CertifHy, http://www.certifhy.eu/images/3__Certifhy_Market_outlook_presentation-Daniel_Fraile_Final.compressed.pdf, date of access (30/10/2018).

[7] National Renewable Energy Laboratory (NREL), https://www.nrel.gov/docs/fy04osti/36734.pdf , date of access (30/10/2018)

[8] Research Gate, https://www.researchgate.net/Fig./Electrolyzer-modules-with-a-unipolar-and-b-bipolar-cell-configurations_fig8_262617097 , date of access (30/10/2018)

[9] National Renewable Energy Laboratory (NRE) https://www.nrel.gov/docs/fy06osti/39943.pdf , date of access (30/10/2018)

[10] Rase, H.F. "Handbook for commercial catalyst: heterogeneous catalysts". CRC Pres Boca Raton, FL 2000

[11] Maakaasukäsikirjhttp://www.kaasuyhdistys.fi/sites/default/files/pdf/kasikirja/kasikirja_20110307.pdf, date of access (4/11/2018)

[12] Kent, J.A. "Riegel's Handbook of Industrial Chemistry", New York, NY, Litton Educational Publishing,1974. Print

Cost-effectiveness of thermomodernization of existing residential buildings in order to meet EU regulations for 2017 and 2021 by the example of single-detached dwelling located in Poland

Kacper Kozioł[1], Jakub Starczewski[2]

[1]Department of Energy and Fuels, AGH University of Science and Technology

[2]Department of Energy and Fuels, AGH University of Science and Technology

Abstract

Nowadays, a great attention is paid to solving environmental problems, for example by aiming for the lowest possible emissions of harmful compounds into the atmosphere resulting from the combustion of conventional energy sources such as coal. For this reason, the European Union has introduced strict legal regulations aimed at gradual implementation of the idea of low-energy constructions. The article presents the cost-effectiveness of thermomodernization in the economic, energy and ecological context.

Keywords: thermomodernization, thermo-efficiency, EU Legislation

1. Introduction

Nowadays, there is an increasing concern for the environment. One of the main problems is the emission reduction of pollutants and greenhouse gases released into the environment through the combustion of energy carriers. The goal of minimizing the emission of harmful compounds can be achieved by reducing energy consumption. The fundamental plan of the European Union is the commitment of Member States to implement a strategy of gradual energy consumption, so that by 2021 all newly constructed buildings are energy-efficient or zero-energy. In order to implement EU directives, the relevant state authorities create laws and regulations that regulates the parameters of modernized and newly constructed buildings. In case of Poland, laws and regulations are in place defining the technical conditions that buildings should meet. Since 2014, particular attention has been paid to the EP coefficient $[kWh/m^2y]$, which determines the demand for non-renewable primary energy for heating, ventilation and hot water preparation in the facility, and thermal insulation of building partitions determined by the heat transfer coefficient U $[W/m^2K]$.

The introduction of ever more stringent legal provisions makes the population aware of the problem related to the need to use highly effective and alternative energy systems in buildings and popularizes the idea of reducing energy usage. Rising energy prices and the operation of residential buildings significantly affect the interest in solutions which reduce the energy expenditure of buildings. The article presents the ideas and problems posed by energy-saving construction and the use of high-efficiency heat sources to reduce energy consumption.

2. Energy-efficient construction

Energy-efficient construction, as the name suggests, is characterized by low energy consumption, but there are a number of requirements to meet. Such facilities are operated with less energy consumption than traditional construction facilities, through the use of design and technical solutions to increase the energy efficiency of the house and reduce the financial outlays associated with its heating. The possibilities are created by the development of technology, manifested by the implementation of new structural solutions, as well as those related to heating, preparation of hot tap water, ventilation and the use of Renewable Energy Sources. Such construction ensures high comfort of use and energy efficiency. We consider a building energy-efficient, when it meets the insulation requirements of building partitions, i.e. external and internal walls, doors, windows, floors, roofs and ceilings in accordance with current standards and regulations regarding the technical conditions of buildings and their location [1]. The requirements include the heat transfer coefficient U $[W/m^2K]$ and the EP index $[kWh/m^2y]$, which determines the building's demand for primary energy for heating, domestic hot water preparation and ventilation. These coefficients should not exceed the limit values shown in Tab.1 and Tab.2. In Polish conditions, an energy-efficient house is a building whose seasonal energy needs for heating and ventilation are lower than $40kWh/m^2$ for energy-efficient buildings and $15kWh/m^2$ for passive buildings [3].

Tab.1 Maximum value of the EP indicator for heating, ventilation and domestic hot water preparation [1]

Type of building		Partial maximum value of the EPH+W indicator for heating, ventilation and hot water preparation [kWh/(m^2 · year)]		
		od 01.01.2014 r.	od 01.01.2017	od 01.01.2021
	Residential building			
1	a) single-family	120	95	70
	b) multi-family	105	85	65
2	Collective residential building	95	85	75
	Public building			
3	a) healthcare	390	290	190
	b) other	65	60	45
4	Manufacturing, storage and farm buildings	110	90	70

3. Thermomodernization methods

By applying a number of possibilities related to energy saving, we can significantly reduce the energy demand of the building even at the design stage, or by carrying out thermo-modernization of an existing building. Continuous energy price increases cause the need for construction solutions, central heating installations and hot water preparation, ventilation as well as the use of Renewable Energy Sources in order to minimize the costs necessary for the household use and the user's comfort. The structure of energy consumption in 2015 [5] (Fig.1) presented below shows that over 80% of energy is used for space and water heating. Households in Poland had up to 20% share in the national energy consumption, which is unfavourable among EU Member States, where the average is 16%. [5]
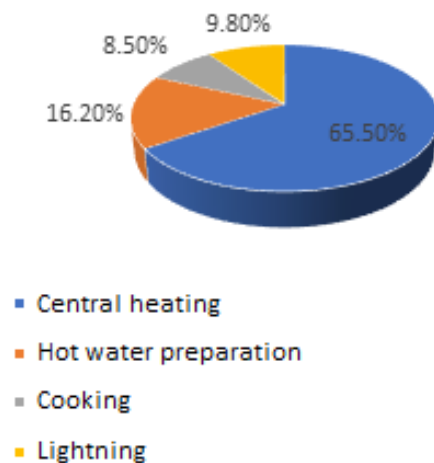
Fig. 1 The structure of energy consumption in Polish households in 2015 [5]

3.1. Construction solutions

A compact structure is a typical feature of an energy-efficient building. It is shown by low A/V shape factor, which is a ratio of the surface area of the snal partitions to the volume of the heated building. A cube-like structure reduces the building surface needed to be insulated. Selection of appropriate and even thermal insulation of external walls, roof and floor on the ground helps to eliminate heat losses by penetration through

external partitions. When building a facility, it is also important to choose proper materials. Materials like cellular concrete or silicate brick in combination with a frame structure are becoming more and more common, because of excellent heat transfer coefficients and an affordable price. Heat losses due to improperly built partitions cause waste of energy intended for heating at the level of up to 70%. [2] Estimated construction of an energy-efficient house is 5-15% more expensive (15-25% for passive house) than a house based on traditional technologies [2]. However, despite the higher cost incurred in the early phase of construction, it still makes the investment viable due to the much lower financial outlay for later use. In order to use solar radiation, objects should be located on sunny slopes towards the south, and glazing should be oriented from south-east to south-west.

3.2. Solutions for central heating

The 2010/30/EU Directive of the European Parliament and Council [4] imposes requirements on the minimum efficiency, permissible level of pollutant emissions and the level of noise emitted for commercially placed energy production equipment. It is called Ecodesign or Ecoproject. Heat sources with high efficiency supported or based on Renewable Energy Sources and heat pumps characterized by minimal energy consumption and zero emission of oxides and dusts are increasingly used. Appliance selection is of key importance for the cost of building use due to the fact that heating has about 65% share in the energy consumed during home use [5]. The installation is supported by automatic regulation devices, which generates lower costs of system use. The control system measures the given parameters and accordingly optimizes the work of the source to the needs of user at a given moment. It includes controllers that manage pump operation, weather automation, thermostatic radiator valves or pressure regulators. It is also important to select the proper insulation of the central heating system pipes and their quality, which allows you to reduce losses to the environment through the transport of heat. The length of pipes should be as short as possible, limiting losses of heat energy and pressure. The use of valves with thermostatic heads individually adjusts the flow rate of the heating medium, thereby adjusting the heat consumption. The latest thermostats available on the market allow you to set the temperature in a given room with an accuracy of 0.5°C, and adjust the parameters to the current needs of user during the day and week. Savings related to the use of thermostatic valves reach 25% of total heat consumption [6].

3.3. Solutions for ventilation

Widespread gravitational ventilation in Poland is not energy efficient, and losses associated with its use account to 50% of all losses in an insulated house [2]. The most sensible solution is the mechanical supply and exhaust ventilation with a recuperator, i.e. a device that heats the inflowing air with the recovered heat from the used air. This installation ensures air exchange in the building regularly every 2-3 hours and minimal energy losses. Thanks to the reduction of heating costs, the investment returns within a few years. However, the introduction of this type of ventilation in an existing building is associated with its reconstruction and large financial outlays related to it. It is recommended to introduce this type of solution already at the design phase.

3.4. Application of RES

Looking through the prism of recent years, the use of renewable energy is becoming more and more affordable, numerous funding allows individual users to support central heating installations or domestic hot water preparation with ecological devices, if they find their economic justification. The installation of a pellet boiler is an affordable option. Modern devices operate without maintenance for several days, and during combustion, a minimum amount of pollutants and ash (which can be used as a fertilizer) is generated. Thanks to solar collectors, by converting solar energy into heat, we offload the main source of heat by collecting hot utility water in a storage tank or by supporting central heating. However, in Polish weather conditions, high efficiency is ensured between April and September. The heat pump extracting heat from the ground or air is a good alternative to a condensing gas boiler in the absence of a gas connection to the building. It is estimated that a heat pump powered by 1 kWh of electricity gives 3 kWh of heat energy. Unfortunately, we encounter some obstacles related to the need of cooperating with low-temperature underfloor heating and relatively high initial investment costs.

4. Thermomodernization

4.1. Existing condition

To carry out the thermomodernization included in the subject of the work, an existing single-family building was used, located in Kraków, Lesser Poland voivodship with an area of 113.9 m^2 (usable area - 103.16 m^2). The building is a detached, 2 storey and it does not include basement. The attic is unheated. The building has 3 rooms, a kitchen, a bathroom, a pantry, a corridor and a boiler room. All rooms outside the pantry are heated. The usable height of residential premises is 2.6 m. The windows are characterized by a low (0.9) heat transfer coefficient U [W/m^{2}K]. They are made of plastic, have double glazing and high-quality joinery. Similarly, external doors made of wood were chosen, where the U [W/m^{2}K] coefficient equals 1.3. In the modernized building, a 4th class 18kW boiler with a PEREKO feeder is installed. It is a universal boiler that allows you to burn solid fuels like coal, eco-pea coal, wood, pellets, fine coal or brown coal. We use steel radiators type VK-UN-33 from BRUGMAN and a bathroom heater type GKR from BRUGMAN with integrated thermostatic valves with pre-setting - RA-U type from Danfoss with an electronic head. All pipes of the central heating system and hot water preparation have been insulated with PE 1 polyurethane lagging, and the Grundfos ALPHA2 electronic circulation pump is installed - energy class A.
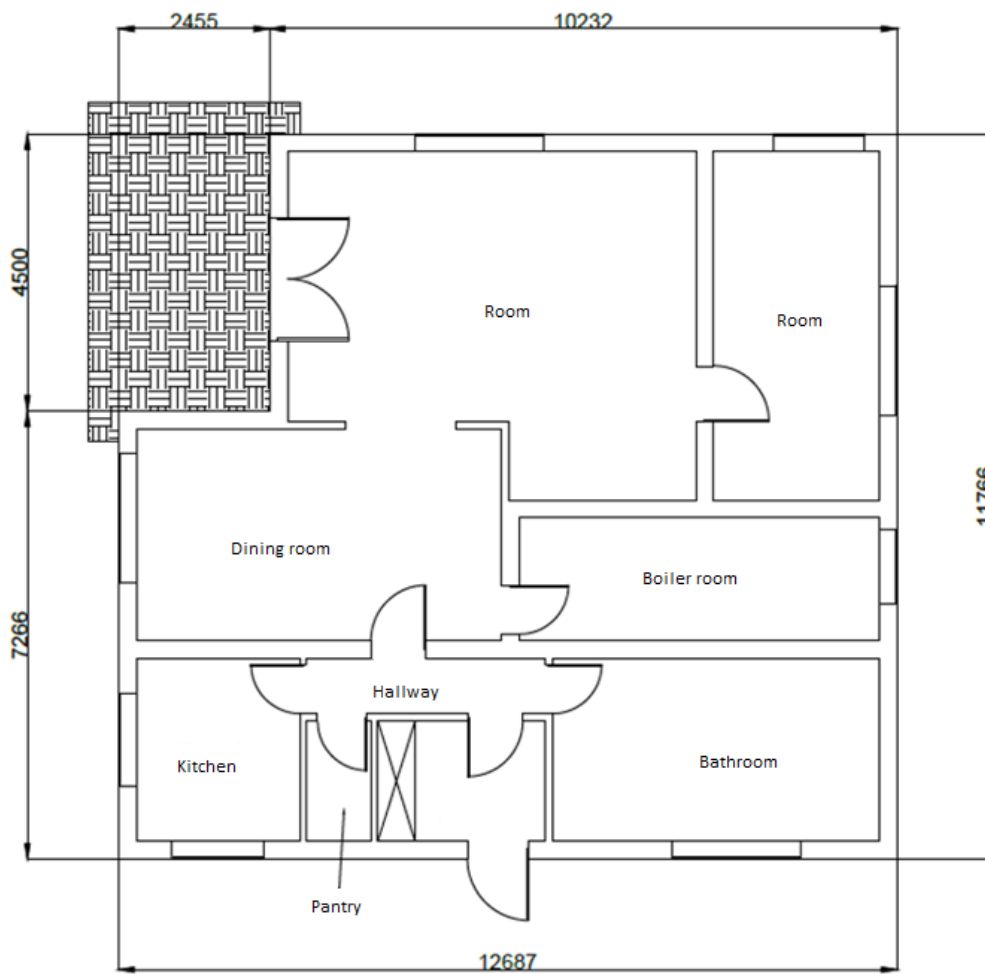
Fig.2 Simplified project of modernized building

4.2. Characteristics after thermomodernization

In order to meet the requirements of WT2021 [1], an appropriate selection of materials with a low heat transfer coefficient λ [W/mK] was needed to reduce the heat demand for heating. External walls and ceiling under the unheated attic have been modernized. To this end, the materials presented in the table below (Table 7) were selected:

Tab.2 Material used for thermomodernization of external walls and ceiling under the unheated attic

Layer	Thickness [m]	λ [W/mK]
External wall		
Kooltherm K5, wall isolation	0,20	0,021
Limestone plaster	0,01	0,7
Ceiling under the unheated attic		
S-VENT boards + mineral wool	0,12	0,031
S-VENT boards + mineral wool	0,18	0,031

4.3. Investment cost estimate

The materials used are high quality and their prices reflect this fact. Accepting the price of Kooltherm about €112/m^2 and the surface of the walls thermomodernization of external walls costs around 16 450 € The prices of mineral wool boards from the official manufacturer website (ISOVER) for the thickness of 12 mm and 18 mm, are ca. €17/m^2 and €24/m^2 respectively, which in total translates into nearly 4 000 € The overall investment is predicted to be 24 500 € assuming an extra 20% for the needs of additional materials such as adhesives, grids and the order for thermomodernization itself.

4.4. Design thermal load and design calculation temperatures

The modernized building is located in Kraków, according to the guidelines set out in the standard [8], climatic data corresponding to the third zone were adopted, i.e. outdoor air temperature equal to -20°C and average annual outdoor temperature of 7.6°C. For the aforementioned building, calculations of the design heat load were made using the Auditor Edu OZC 6.8 Pro program in accordance with the standards [7] and [8], taking the following internal temperatures: 20°C for the room, bedroom, dining room, kitchen, hallway, boiler room, 14°C for pantry and 24°C for bathroom. As a result, we obtained project thermal loads prior to (9056 [W]) and after thermomodernization (4692 [W]). The changes made have reduced primary energy consumption by almost half.

4.5. Hot tap water

In both cases, the seasonal primary energy demand for the preparation of hot tap water is identical. It has been calculated on the basis of PN-EN 15316-3-1: 2007 [9] and is equal to $Q_{cwu} = 44,79$ [kWh/(ym^2)].

5. Economic and ecological analysis

With the help of the Edu EKO 1.0 Auditor software, an economic and ecological analysis has been carried out for the purpose of choosing the appropriate source of heat. We analysed the change of the source of heat fired with the fourth-class coal to a condensing gas boiler or connecting the building to the Municipal Thermal Energy Enterprise in Krakow (MPEC). The research includes investor's costs for the purposes of implementing the solutions, estimated operating costs and emissions of carbon, sulfur and nitrogen oxides, soot, dusts and aromatic hydrocarbons. The analysis was based on data generated from the AudytorEdu OZC 6.8 Pro software.

PALIWO		WARIANT OBLICZEŃ	ZUŻYCIE
ENERGIA ELEKTRYCZNA			
	Kocioł węglowy		324,32 zł/rok
	MPEC Kraków		324,32 zł/rok
	Piec gazowy		324,32 zł/rok
PALIWO		WARIANT OBLICZEŃ	ZUŻYCIE
GAZ MIEJSKI			
	MPEC Kraków		4 103,25 zł/rok
PALIWO		WARIANT OBLICZEŃ	ZUŻYCIE
GAZ ZIEMNY MŚ			
	Piec gazowy		2 028,31 zł/rok
PALIWO		WARIANT OBLICZEŃ	ZUŻYCIE
WĘGIEL KAMIENNY 0,7/13			
	Kocioł węglowy		2 994,61 zł/rok
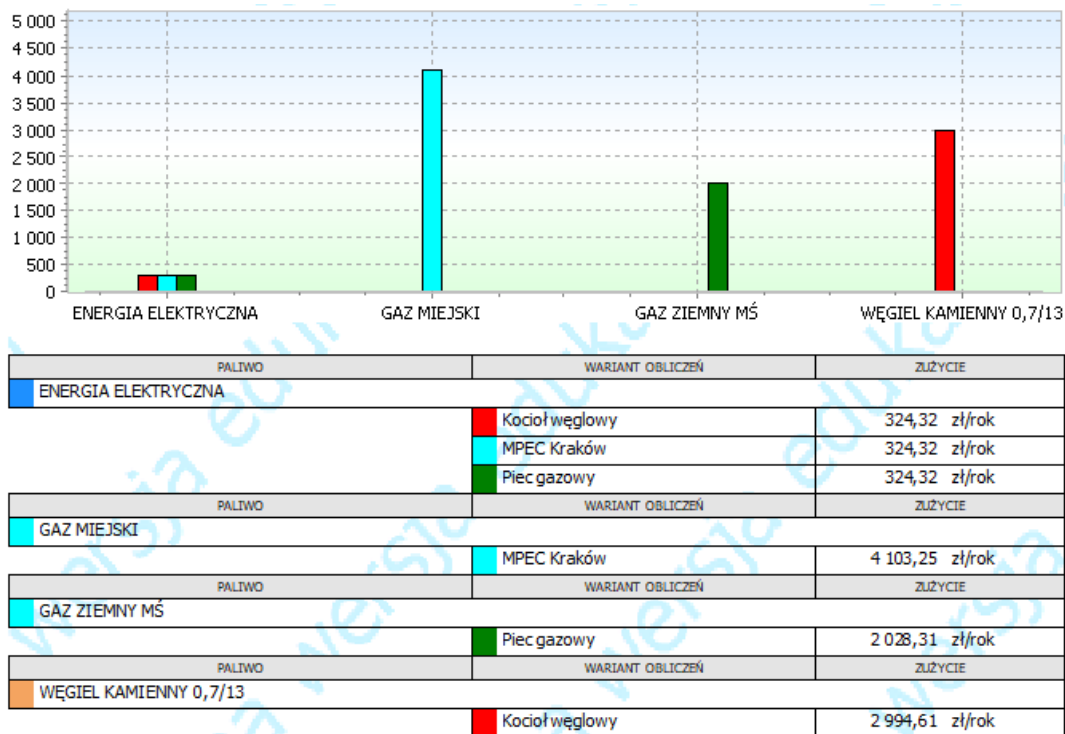
Fig. 3 - The results of cost analysis – Audytor EKO 1.0

The investment costs of connection to MPEC are almost zero in our case due to already existing central heating installation in place and the preparation of hot utility water meeting the requirements set by MPEC. On the other hand, the investment costs related to the replacement of a heat source with a condensing gas boiler are about 1000 €- in this case, the Valliant dual-mode gas condensing boiler with the appropriate power has been selected. The consumption and costs of electricity used to support central heating and hot water installations in all options are identical, because they were not modernized. Comparing the annual costs for the fuel purchase, a dual-purpose, condensing gas boiler was chosen as the best solution. The high annual fees for connection to MPEC Kraków are almost twice as high due to the use of natural gas with a lower calorific value than the one purchased directly from PGNiG for supplying the gas boiler. The best option is to install a gas heat source due to annual savings compared to the base variant, which will pay back after 4-5 years(exchange of heating source).

OPIS	SO₂ kg/rok	NO₂ kg/rok	CO kg/rok	CO₂ kg/rok	PYŁY kg/rok	SADZA kg/rok	BAP kg/rok
Kocioł węglowy	33,848	2,635	91,320	9 261,86	32,8947		0,0003
MPEC Kraków	1,785	3,618	0,575	4 339,85	0,0279		
Piec gazowy	1,750	2,277	0,309	2 574,96	0,0275		
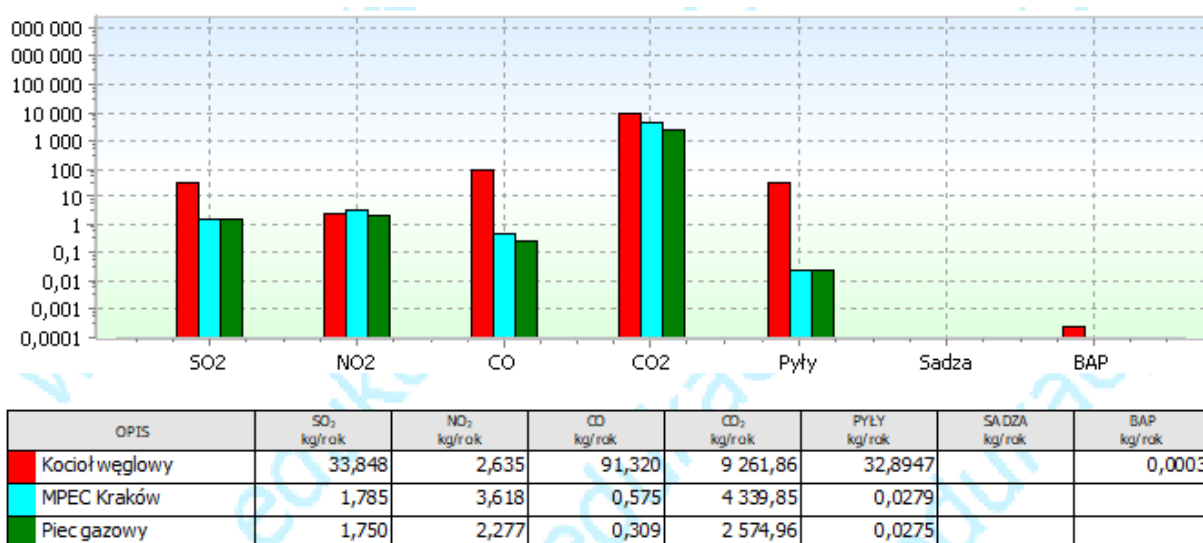
Fig. 4The results of pollutants emission analysis – Audytor EKO 1.0

Based on the above results, it was found that the change of the heat source from the coal boiler diametrically reduces the emission of pollutants into the environment. The biggest change can be seen in the emission of CO

and dust, which are practically not produced in both solutions. Comparing variants after thermo-modernization of the building, their results are similar in favour of a gas boiler.

6. Conclusions

Requirements contained in the regulation of the Minister of Transport, Construction and Maritime Economy on technical conditions which should be met by the buildings and their location [1] are extremely strict and practically impossible to meet in Polish conditions. To meet the appropriate standard of an energy-efficient building, the investor is forced to incur large financial outlays, which are not profitable when looking at the investment return time, significantly exceeding the life-cycle of a given solution. Thermomodernization presented in the article is one of the examples. Despite using 20 cm high quality insulation of external walls and 30 cm insulation with mineral wool ceiling under unheated attic with low thermal conductivity λ [W/mK], the building still does not meet the legal requirements for energy efficiency of buildings 2021. Exchanging the heat source is associated with high investment costs, but also a significant saving on a yearly basis. It is also often necessary to modernise the heating installation in order to introduce new heat source, which results in additional financial outlays. An undeniable advantage is the Significantly lower emission of pollutants into the environment is an undeniable advantage of moving to a gas heat source, which is presented in the paper. In the case of solutions such as a heat pump, biomass boiler or photovoltaic panels, the emission of pollutants is virtually zero.To sum up, it seems that with modernization of the building external partitions and the exchange of a heat source it is still impossible to obtain the coefficient EP = 70 $[\frac{kWh}{m^2*year}]$, despite many possibilities of obtaining subsidies from the State.

References

[1] Rozporządzenie Ministra Transportu, Budownictwa i Gospodarki Morskiej z dnia 5 lipca 2013 r. w sprawie warunków technicznych, jakim powinny odpowiadać budynki i ich usytuowanie.

[2] Krajowa Agencja Poszanowania Energii S. A.: Wytyczne do weryfikacji projektów budynków mieszkalnych, zgodnych ze standardem NFOŚiGW, Warszawa 23 sierpnia 2012 r

[3] Dyrektywa Parlamentu Europejskiego i Rady 2012/27/EU z dn. 25.10.2012 r. w sprawie efektywności energetycznej.

[4] Dyrektywa Parlamentu Europejskiego i Rady 2010/30/UE z dnia 19 maja 2010 r. w sprawie wskazania poprzez etykietowanie oraz standardowe informacje o produkcie, zużycia energii oraz innych zasobów przez produkty związane z energią

[5] Zużycie energii w gospodarstwach domowych w 2015 r., Informacje i opracowania statystyczne. GUS, Warszawa 2017.

[6] Koczyk H., Ogrzewnictwo praktyczne, SYSTHERM SERWIS, Poznań 2009 r.

[7] PN-EN ISO 6946:2008 „Komponenty budowlane i elementy budynku. Opór cieplny i współczynnik przenikania ciepła. Metoda obliczania."

[8] PN-EN 12831:2006. „Instalacje ogrzewcze w budynkach. Metoda obliczania projektowego obciążenia cieplnego."

[9] PN-EN 15316-3-1:2007 „Instalacje ogrzewcze w budynkach. Metoda obliczania zapotrzebowania na energię instalacji i sprawność instalacji. Część 3-1: Instalacje centralnej ciepłej wody, charakterystyka zapotrzebowania (wymagania dotyczące rozbioru wody)."

Agricultural biogas as a sustainable alternative for current energy need

Paulina Harazin[1], Mateusz Proniewicz[2]

[1]Silesian University of Technology, Faculty of Energy and Environmental Engineering ,Clean Fossil and Alternative Fuels Energy, KIC, Master's Degree, paulina.harazin@onet.eu

[2]Silesian University of Technology, Faculty of Energy and Environmental Engineering,Clean Fossil and Alternative Fuels Energy, Master's Degree, matproniewicz@gmail.com

Abstract

At present, the depletion of fossil fuels and the environmental compliance concerning the reduction of the greenhouse gases have attracted the interest in non-conventional fuel from bio-resources and waste. Production of biogas from anaerobic digestion has the potential to be part of the transition to a renewable based energy system and plays a vital role in rural development. This work presents basic problems connected with effective use of the energy potential of biogas from the agricultural waste in the aspect of biogas production efficiency in methane fermentation in Poland. Private investment is a critical factor for the polish biogas sector to fulfill its expected role. Under this circumstance, the major part of this article focuses on the existing agricultural micro biogas installation in Studzionka, biogas production capacity, followed by thermal and electric electricity production in a co-generator and its impact on the environment and society.

Keywords: biogas, biogas plant, methane fermentation, anaerobic digestion, renewable energy

1.   Introduction

Nowadays most of the energy is provided by fossil fuels amongst which oil has the biggest share in energy provision [4]. However due to problems connected with global climate changes and prices fluctuations which are the result of finite quantity of fossil fuels it is crucial to search for independent sources of energy, in particular nuclear and renewable. These facts have been behind the tendency known as active climate policy. According to European Commission, by the 2030 at least 27% of energy production should be delivered from carriers known as "green sources". One of the most approachable technologies to meet this demand, amongst others, is biogas delivered from agricultural biogas plants. Such plants are thought to be sTab. as they are capable of delivering electric power to the grid for more than 8,300 hours per year and e.g. wind stations deliver electricity for 2,700 hours. This clearly proves this technology to be worth considering.

2.   Biogas

Biogas is a natural, colorless and odorless gas released during the anaerobic digestion. The composition of biogas varies with type of feedstock and operating condition of the digester. In general, biogas consists of 50–75% CH_4 and 25–50% CO_2 along with other trace components like water vapor (H_2O), hydrogen sulfide (H_2S), and ammonia(NH_3). Typical compositions of raw biogas and the properties of the components are summarized in the Tab. 1.Methane is the only component that contributes to the heating value. Biogas is formed as a result of methane fermentation which is the decomposition of organic substances under anaerobic conditions, with the appropriate nutrient content and at temperature, conducted by fermentation bacteria. As a result of the decomposition of organic substances, biogas and digestate is produced, which may be a good fertilizer. It ia a complex biochemical process, which consists of four basic phases: hydrolysis, acidophilic phase, acetate phase and methanogenic phase. Each is carried out by specific types of bacteria under appropriate conditions. Each subsequent phase consists in the decomposition of compounds from which the substrates are made, to an increasingly simpler form, and in the final stage to methane, carbon dioxide and other compounds,i.e. biogas [1].

Tab. 1. Chemical composition of biogas and properties of components [1].

Components	Concentration	Properties

CH$_4$	50-75%	Energy carrier
CO$_2$	25-50%	Decreases heating value, corrosive especially in presence of moisture
H$_2$S	0-5000 ppm	Corrosive, Sulfur dioxide emission during combustion
NH$_3$	0-500 ppm	Nox emissions during combustion
N$_2$	0-5%	Decreases heating value
Water vapour	1-5%	Facilitate corrosion in presence of CO$_2$ and SO$_2$

The calorific value of a such biogas reaches between 19-26 MJ/m^3. Biogas with a high methane content can be used for energy purposes or other technological processes such as [9]:

- productionofelectricityinspark-ignitionenginesorturbines,
- thermalenergyproductionin adapter gasboilers,
- productionofelectricityandheatinassociatedunits,
- introductionafterappropriatecleaningtothenaturalgasnetwork,
- useasfuelfortractionmotorsorvehicle,
- useintechnologicalprocesses,e.g. fortheproductionofmethanol.

3. Substrates for biogas production

The methane fermentation process has been known for a long time and used by humans in processes of varying degrees of advancement. The biogas plant uses biomass, or renewable raw material, that is why the obtained biogas is treated as a renewable ecological source of energy. Basic sources for biogas production are [9]:

- fermentation of the activated sludge in the fermentation chambers of the sewage treatment plant,
- fermentation of organic municipal and industrial waste,
- fermentation of slurry and manure from farms,
- fermentation of plant biomass,
- fermentation of the abovementioned substrates in various proportions.

The raw material for methane fermentation in a biogas plant can be almost all easily biodegradable organic substances. However, the individual materials differ significantly in terms of their decomposition rate and methane production efficiency. The substrate used in a biogas plant should be obtained mainly locally. Therefore, local availability of raw materials is a key aspect in the design of a biogas installation, and the substrates used in a biogas plant are most often classified on the basis of origin. What is more, detailed analysis of the substrate feed is necessary to determine the parameters of individual elements of the biogas plant technological line.

4. The advantages of biogas technologies

Biogas is a renewable, as well as clean source of energy. Gas generated through biodigestion is non-polluting, because no combustion takes place in the process, meaning there is zero emission of greenhouse gasses to the atmosphere. Therefore, using gas from waste as a form of energy is actually a great way to combat global warming. Moreover, Biogas production is associated with another positive environmental effect. It ia an effective way to dispose the waste, because an input material are the products from various industries and agriculture activities, which are usually cumbersome to the environment. What is more, as a result of the biogas plant operation, a digestate is obtained which is a good fertilizer, richin easily digestible biogenic components that does not cause soil acidification, as in the case of raw slurry. It reduces the emission of nitrogen to the

atmosphere, in the form of ammonia, and inactivates the weed germination and also removes odor-causingcompounds. Another advantage of biogas energy is its various conversion possibilities.Chemical energy contained in biogas can be transformed into thermal energy, electricity and chemical energy of other compounds. Thanks to this, there are also numerous possibilities of using energy generated from biogas. One of them are stationary applications, i.e. any non-moving installations using properly transformed biogas. Another application is the possibility of powering car engine engines with biomethane obtained from the processes of proper biogas purification. In addition, compared to other renewable energy sources, biogas production takes place continuously, regardless of the weather, asopposed to variability in wind or solar energy. Therefore, the potential of biogas is huge,but it is not yet fully used [10].

5. Renewable sources of energy for Poland

The goal which is set to Poland is to increase the share of renewable sources in energy production up to 15% by 2020r. Current state in Poland is presented in the Tab. 2 (state for 30.06.2018) [5].

Tab. 2. Power from renewable sources of energy in Poland.

Renewable source	Installed power [MW]			
	2005	**2010**	**2015**	**2018**
Biogas	31.97	82.88	212.50	240.97
Biomass	189.79	356.19	1,122.67	1,363.67
Solar	-	0.03	71.03	126.00
Wind	83.28	1180.27	4,582.04	5,874.78
Hydro	825.50	937.04	981.80	979.14
Total	1,157.54	2,556.42	6,970.03	8,584.52

Since 2005 significant changes have appeared. All of the technologies have been developed and as a result over these 13 years the total amount of power produced from renewable sources has risen by 741,6%. Level of implementing between particular technologies differ due to geographical, climate and economic conditions in Poland yet all of them have been installed delivering energy to some extent. The highest share belongs to wind power, as for 2018 around 70% of power generated from renewable source is energy from wind.

Special attention should be focused on energy delivered from biogas stations. Such stations, unlike other technologies using renewable sources, do not depend on weather or geographical conditions but only on the supply of substrates which in terms of agricultural stations is considered rather constant. Polish farms and agricultural industry produce sufficient amount of organic waste so that it is beneficial to transform them into biogas which then can be used to generate electricity or heat. It is additional advantage that such stations can be easily used for cogeneration purposes.

6. Market situation for agricultural biogas plants

Considering the market of biogas stations in Poland and distinguishing the capacity of such stations we can recognize agricultural biogas stations and agricultural microbiogas plants. Microbiogas units are adjusted to the size of particular agricultural plants and their waste production. Power these units deliver is usually up to 50 or even 150 kW according to definition [6] and the typical substrates are: slurry and maize silage. Bigger biogas stations are located close to large-area farms and they are adjusted to use different substrates which increases the level complexity of technology there. They are capable of producing power from around 1MW up to over a dozen of MWs.

Special attention should be given to microbiogas stations as they are cheaper than typical biogas stations. According to [6] installation with power capacity about 5kW costs around 150 thousands of euro and units with power about 40kW is evaluated to cost around 300 thousands of euro. There is also a special system of support

for such installations: energy produced in installation of power up to 40 kW can be used for own purposes without the need of registering as a producing power company if these units belong to ARR (AgencjaRynkuRolnego). Excess of power can be sold to network at price equal to 80% of the energy price from previous year. In case of installation that produces biogas for electricity and heat purposes implementing a gas network for local consumers do not cause any trouble, moreover generated heat power is usually higher than electric one. Many examples of such installations can be found for example in Asia where, due to beneficial conditions, simple aboveground tanks for waste utilization are often combined with microbiogas stations. In case of Poland and middle Europe due to existing conditions such tanks should be insulated and then such units are most profiTab..

Larger plants of biogas installations are also being developed in Poland. They are located close to large agricultural farms and are adjusted to delivering bigger amount of power, typically from few hundred of kW up to few hundred of MW. Therefore, technology chain might be more complicated comparing to simple microbiogas stations, however way of working is the same (fermentation chambers). In order to increase the benefit from these plants, they are connected to each other in a separate electric network creating energetic knots. Sources of energy are located close to consumers so it lowers losses and help to optimize energy distribution. Linking of these installations delivers complement of power for all plants that are included in such knot and only one unit is connected to global distribution network. Consumers are linked to both global network and local biogas supplied knots and they have "double supply" contracts. Excess of power within such knot is sold to a global network.

The issue that still causes difficulties for these technologies to grow on larger scale is the investment analysis. Even though there is a system of support for renewable sources of energy known as colored certificates which main idea is that producers of energy from renewable sources can obtain a certificate that can be later sold in stock exchange. This mechanism supports investors and increases the profitability of such investments but in case of agricultural biogas the reference price for MWh produced from this gas is still lower than the cost of production [7]. The situation on the market however changes and for companies that require a lot of energy for their own needs, such installations may prove to be beneficial.

7. Review of biogas technologies in Poland

According to the data from URE (UrządRegulacjiEnergetyki) in 2016 there were 303 biogas plants in Poland (state for 30.09.2016) [7]. Tab. 3 provides division of these plants by feedstock used to produce biogas.

Tab. 3. Division of biogas plants by feedstock.

Type of biogas plant	No. of installations	Share %
Wastewater treatment	106	35
Agricultural	93	31
Landfill	100	33
Mixed origin	4	1

Comparing this data with 2015 the biggest rise took place for agricultural biogas plants, as 36 new units appeared, however due to changes in law and definitions (microinstallations appeared) in 2018 there are 86 producers of agricultural biogas (state for 30.06.2018) [8], despite the fact that the general tendency for such technologies is to increase.

Considering the arrangement of the biogas processing units, more of the installations is located in industrial and generally developed areas. Specific data are provided in theTab. 4 [7].

Tab. 4. Areas with highest concentration of biogas plants.

Voivodeship	Type of biogas plant	Total

	Wastewater treatment	Agricultural	Landfill	Mixed	number
mazowieckie	13	5	20	0	38
śląskie	17	2	15	1	35
wielkopolskie	7	8	10	0	25
dolnośląskie	10	9	9	1	29
zachodniopomorskie	4	13	8	1	26

Other voivodeships than shown in Tab. 3 contain less than 20 units of biogas plants, however there are no provinces with 0 biogas plants. This is due to the fact that according to document "PolitykaenergetycznaPolski do 2030 roku" each community should have at least 1 of such installation by the 2020. This is a very demanding goal to achieve due to uncertain profitability for such technologies.

8.   Analysis of biogas plant in Studzionka

Biogas plants can become an opportunity for the development of agricultural holdings by increasing and diversifying sources of income, becoming independent from electricity suppliers and managing agricultural by-products in accordance with environmental protection regulations. Moreover, it is a good way of efficient and effective management of leftovers from agricultural production while protecting the environment also in smaller farms. A pioneering installation of this scale is a biogas plant in the Bibianna and GrzegorzPojda's farm in Studzionka village (near Pszczyna, Silesia Voivodship), which will be analysed in this paper. Presented biogas plant should be considered as a prototype for sucha n invetstement in Poland. Due to the pilot nature, lack of all necessary technological solutions and regulations on the domestic market and deficiencies in the micro-source promotion system in the period when it was created, should not be considered as a model for further micro-biogas plants. Nevertheless, experiences gained during its construction and operation are extremely valuable.

It was the first agricultural biogas plant in Poland of such a small scale. It was launched in November 2009. The installation is adapted to the scale and needs of the farm in which it is located. The installation uses waste from a 40-hectare farm in which the laying hens and pigs are farmed. The installation uses annually approx. 560 tons of chicken manure and 335 t of pig slurry, plus additionally, silage maize, grass and organic waste from the farm. The idea for the construction of micro-biogas plant was born in 2006. That would be the time when EU requirements imposed on farmers the construction of reinforced concrete slabs for collecting manure and tanks for animal excrements. The owners saw the drawbacks of such a solution and began to look for an alternative that would at the same time meet the requirements of the European Union, as well as effectively use the resulting waste in agricultural production. Encouraged by German biogasifiers, they decided to build a similar installation in their farm. Thus, in October 2007 construction of a biogas plant began and lasted two years. It was carried out mainly by farmers themselves in cooperation with Wolf System. Biogas production leads to energy production. The installation uses a converted diesel engine as a cogeneration unitand in that way produces about $30kW_{el}$ and approximately $40\ kW_{th}$ [2].

Electric energy is used for the needs of biogas plant and within the farm. The heat heats up residential and livestock buildings. The by-product of biogas production is used as a natural fertilizer for feeding the crops, what we can observe at the Fig.1.
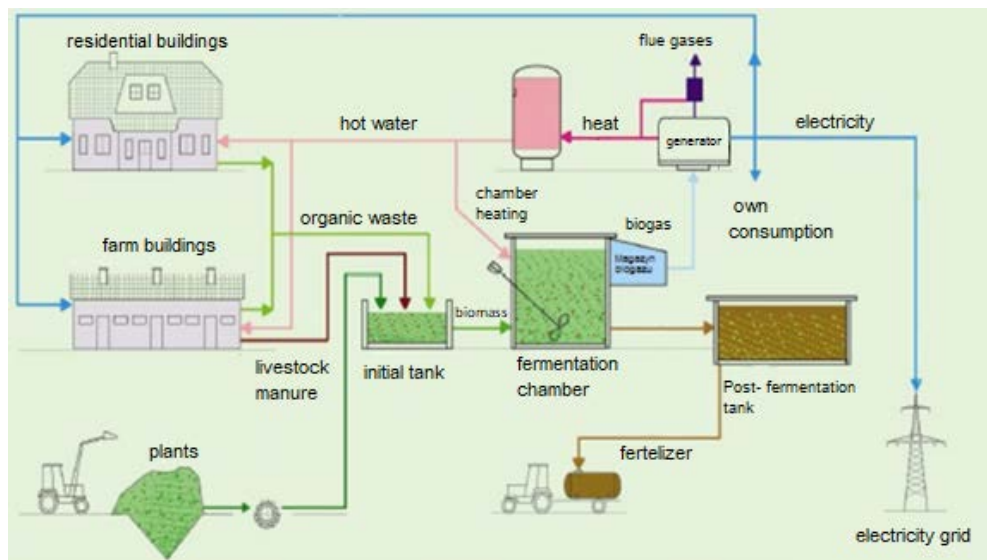
Fig. 1. Schematic diagram of biogas plant in Studzionka

9. The biogas production and substrates supply

The size of the farm is an average of 14,000 laying hens, 12 sows and 250 pigs. Every year, analysed biogas plant consumes the following amounts of raw materials:

- chicken droppings - 560 tons,

- pig slurry - 335 tons,

- pig manure - 36 tons,

- cuttings - casual,

- waste – casual,

- root crop waste - periodically.

The general principle underlying the economics is the use of waste from animal husbandry in the first place, and still as an additive, energy crops and agricultural waste. Supplementing animal faeces with other substrates increases the efficiency of the fermentation process, thus increasing the production of biogas.

The Tab. illustrates data on dry matter content and dry organic matter from individual animal faeces as well as on the characteristic potential of biogas production. On the basis of the data contained in the Tab. 5, the annual yield of biogas from the vital substrates subjected to fermentation was calculated [3].

Tab. 5. Characteristics of selected substrates with biogas production potential[11]

Basis	Dry-matter content, %	Organic matter content, % d.m.c	Biogas yield, m^3/t o.m.c.	$[CH_4]$,%
Pig slurry	6,6	76,1	301	60
Pig manure	25	8	350	55
Chicken manure	32	75,6	320	60
Maize silage	32	95	600	52

- Biogas production, B_p

$$B_p = M_s \cdot C_d \cdot C_o \cdot Y_b$$

Where,

B_p Biogas production, m3

M_s Mass of substrates, t

C_d Dry-matter content, %,

C_o Organic matter content, % d.m.c,

Y_b Biogas yield, m³/t o.m.c.

- Biogas production, M_p

$$M_p = B_p \cdot [CH_4]$$

Where,

M_p Methane production, m³

$[CH_4]$ Methane content.

As a result of the calculations made, results were obtained, which are presented in the Tab. 6.

Tab. 6. Biogas and methane production in Studzionka biogas plant

Basis	Biogas production, m³	Methane production, m³
Pig slurry	43 352,06	26 011,24
Pig manure	2 520,00	1 386,00
Chicken manure	5 064,54	3 038,72
TOGETHER	50 936,60	30 435,96

By adding plant substrates to the fermentation chamber, especially those with high energy potential, e.g. fodder and sugar beets, maize and grass silages, biogas production increases two or even three times a year.

10. Electricity and heat production

The biogas production leads to the calculation of the possible electricity and heat generation. In connection with the promotion of "green energy", the most popular method of biogas management and used in the discussed agricultural farm is the use of a co-generator, that is electricity and heat generating unit.

For the analysys of the annualy energy production in a co-generator, the following parameters were taken into account: aggregate efficiency: thermal- 45%, electric- 34%, aggregate operation time- 12 h/day, which gives 4380 h / year. The following formulas were used to carry out the calculations[3].

a) for the heat production

- Theoretical thermal power, P_{th}

$$P_{th} = V_{CH4} \cdot \eta_{th} \cdot W_{op}$$

Where,

P_{th} theoretical thermal power, kW

V_{CH4} methane production per hour, 3,47 m³/h

η_{th} thermal efficiency in cogeneration, 45%

W_{op} calorific value of methane, 9,17 kWh/m³

- Gross heat production, Q_{gross}

$$Q_{gross} = P_{th} \cdot t_p \cdot 3,6$$

Where,

Q_{gross} gross heat production, GJ/year

t_p operational time, 2920 h/year

- Heat consumption for process purposes, $Q_{process}$

$$Q_{process} = Q_{gross} \cdot 30\%$$

Where,

$Q_{process}$ heat consumption for process purposes, GJ/year

- Net heat production, Q_{net}

$$Q_{net} = Q_{gross} - Q_{process}$$

Where,

Q_{net} net heat production, GJ/year

b)   for theelectricity production

- Theoretical electric power,P_{el}

$$P_{el} = V_{CH4} \cdot \eta_{el} \cdot W_{op}$$

Where,

P_{el} theoretical electric power, kW

V_{CH4} methane production per hour, 3,47 m³/h

η_{el} electrical efficiency in cogeneration, 34%

W_{op} calorific value of methane, 9,17 kWh/m³

- Gross electricity production, Eel_{gross}

$$Eel_{gross} = P_{el} \cdot t_p$$

Where,

Eel_{brutto} theoretical electrical power, MWh/year

t_p operational time 2920 h/year

- Electricity consumption for process purposes,$Eel_{process}$

$$Eel_{process} = 9\% \cdot Eel_{brutto}$$

Where,

$Eel_{process}$ electricity consumption for process purposes, MWh/year

- Net electricity production, Eel_{net}

$$Eel_{net} = Eel_{gross} - Eel_{process}$$

Where,

Eel_{net} net electricity production, MWh/year

The results of the computations related to the electricity and heat production are presented in the Tab. 7.

Tab. 7. Heat and electricity production in Studzionka

Paremeter	Heat	Electricity
Theoretical power	14,34 kW	10,83 kW
Gross production	226,07 GJ/year	47,45 MWh/year
Consumption for process purposes	67,82 GJ/year	4,27 MWh/year
Net production	158,25 GJ/year	43,18 MWh/year

11. Conclusions

Bioenergy production, as part of a bio-based economy, has the potential to contribute significantly to the development of a green, low carbon economy. Moreover, itfavors the development of rural areas and encourage creating new supply chains for biomass feedstock, especially based on the use of waste and residues from agriculture. The potential of biogas contribution to renewable energy generation with various waste and residues is significant, both in terms of energy supply and in terms of the greenhouse gases emission reduction.

An example of a micro biogas plant in Studzionka proves that a biogas plant is not only a solution for large enterprises, but also for small farms. An appropriately designed installation can significantly contribute to reducing the problem of greenhouse gases and odor emissions from the farm, enabling utilization of waste and producing a high quality natural fertilizer. In addition, the farm receive electricity and heat, which can be properly managed as needed. The analyzed installation currently does not resell electricity. All produced energy is consumed for the needs of biogas plant and the needs of the farm. For process purposes, the biogas plant consumes approx. 9% of the electricity produced, which is mainly related to the operation of the stirrers. Annually it is around 4.27 MWh. The rest of the energy in an average amount of 43.18 MWh/year is allocated to meet the needs of the farm. This energy contributes to reducing energy consumption and related expenses. When it comes to heat, all of it, in the amount of about 266.07 GJ/year is used for the purposes of own biogas plant and heating of livestock, farm and residential buildings, as well as for domestic hot water. Therefore, the hosts reduced the amount of coal, that was used before for the heating purposes and also gave up the gas furnace, that heated up domestic water. This shows that the biogas plant can become an additional source of income or generate savings. The farmers from Studzionka are precursors when it comes to small biogas plants. Due to the investment talent of the owners in the use of non-dedicated devices, the biogas plant in Studzionka is not an idea for replication, because its components may prove difficult or impossible to apply in other conditions. Nevertheless, their example may encourage farmers from all over Poland to take actions aimed at both protecting the natural environment and increasing the profitability of agricultural farm production. It is worth noting that it was created at the time when energy from renewable energy sources was not very popular in our country, and biogas technology was even unknown. There was also lack of financial and legal support in this area. However, now the situation has changed. There are favorable conditions in Poland to invest the capital in a biogas installation, which could bring a lot of benefits.

References

[1] Węglarzy Karol, PodkówkaWitold (red.), Agrobiogazownia: opracowaniezbiorowe, InstytutZootechniki - PaństwowyInstytutBadawczy, GrodziecŚląski 2010.

[2] Latocha Ludwik,*Materiały własne biogazowni, dokumentacja techniczno-opisowa*, 2007,2014

[3] Curkowski Andrzej, *Przewodnik dla inwestorów zainteresowanych budową biogazowni rolniczych*, Instytut Energetyki Odnawialnej 2011

[4] Deublein D., Steinhauser A., *Biogas from Waste and Renewable Resources*, 2nd Ed., WILEY-VCH Verlag GmbH & Co.KGaA, p. 5, 2011

[5] www.ure.gov.pl,

https://www.ure.gov.pl/pl/rynki-energii/energia-elektryczna/odnawialne-zrodla-ener/potencjal-krajowy-oze/5753,Moc-zainstalowana-MW.html, 01.12.2018

[6] Tucki K., Piątkowski P., Wójcik G., *Wybrane aspekty z zakresu analizy sektora biogazowni rolniczych w Polsce*, „Rynek Energii", 02.2016

[7] www.cire.pl,

https://www.cire.pl/item,141910,2,0,0,0,0,0,stan-biogazowni-w-polsce.html?fbclid=IwAR3jLtLYVYQzgCWC6knhTq1RXPhUdaXIVc5WDdt6m6A6xndG-QJXH73tNnw, 01.12.2018

[8] www.kovr.gov.pl, http://www.kowr.gov.pl/uploads/pliki/oze/biogaz/7.%20Rejestr%20wytw%C3%B3rc%C3%B3w%20biogazu%20rolniczego%20z%20dnia%2005.01.2018%20r..pdf, 01.12.2018

[9] Grzybek Anna (red.), Biogazownieszansądlarolnictwa i środowiska, FundacjanaRzeczRozwojuPolskiegoRolnictwa, Warszawa 2013.

[10] Grzesik Katarzyna, *Wykorzystanie biogazu jako źródła energii*, Zakład Kształtowania i Ochrony Środowiska, Wydział Geodezji Górniczej i Inżynierii Środowiska AGH w Krakowie, Kraków 2005.

[11] Czasopismo Techniczne, Wydawnictwo Politechniki Krakowskiej, 2-Ch/2012, Zeszyt 17, Rok 109, Przegląd technologii produkcji biogazu różnego pochodzenia, Justyna Kwaśny, Marcin Banach, Zygmunt Kowalski]

Cooperation of renewable energy sources with a heat pump on the example of single-family house

Paulina Wienchol[1]

[1]*Silesian University of Technology/Faculty of Energy and Environmental Engineering, e-mail:paulinawienchol@onet.pl*

Abstract

The EU Policy until 2030 is mainly aimed to reducing greenhouse gas emissions, increasing the share of renewable energy sources and increasing energy efficiency. The implementation of the plan requires making the necessary investments in the communal-living sector. This is due to the significant amount of pollutant emissions that come from local boilers. The purpose of this work is energy analysis of the cooperation of renewable energy sources with a heat pump on the example of a selected single-family home, located in the province of Upper Silesia. During the analysis, two cases were examined. In the first, building is heated only with a ground heat pump and in the second with the air heat pump. Then the operation of both pumps was compared in terms of energy efficiency. In the ecological analysis, the impact on the natural environment of using alternative energy sources to power the heat pump was checked. The analyzed sources of renewable energy are solar and wind energy. Based on their basic characteristics and real environmental data on solar radiation, wind speed and ambient temperature, the amount of energy produced in selected installations was calculated. The obtained results will allow to determine which heating device works more efficiently and ecological.

Keywords: heat pump, renewable energy sources, carbon dioxide

1. Introduction

Nowadays, the sector of key role in terms of air pollution is the communal-living sector. It is caused by heat consumption in households which accounts 37% of total heat consumption [1] and due to the fact that in households the most frequently used heating devices are outdated furnaces and low efficient boilers. Moreover, low-quality fuels are burnt, as well as various types of municipal waste, especially plastics. This makes the household sector one of the largest sources of air pollution in Poland.

According to the European Union's Climate and Energy Policy until 2030, the main objectives include: a reduction of at least 40% of greenhouse gas emissions (compared to 1990), ensuring at least a 27% share of energy from renewable sources in total energy consumption and an increase of at least 27% energy efficiency [2]. Achieving these regulations requires end users to use sustainable heating systems, i.e. those whose use does not adversely affect the natural environment. In this work, the heat demand of a typical single-family home was examined. It was assumed that the heat for the central heating and domestic water system is covered in the first case by an air heat pump, and in the second - a ground heat pump. The electricity which is supply to the heating system and all other electrical equipment in the household is taken from the grid and supplemented by a household wind turbine, photovoltaic panel installation or both.

2. Analyzed building

The main purpose of the design study of heat demand is to select the power of heating devices. In addition, energy analysis will help to locate weak points of the structure that bring the biggest heat losses to the environment. The analyzed building is a traditional house which is inhabited by a family of three. The house is without basement. The area of the building is 207 m^2. The analyzed object is shown in Figure 2.1.
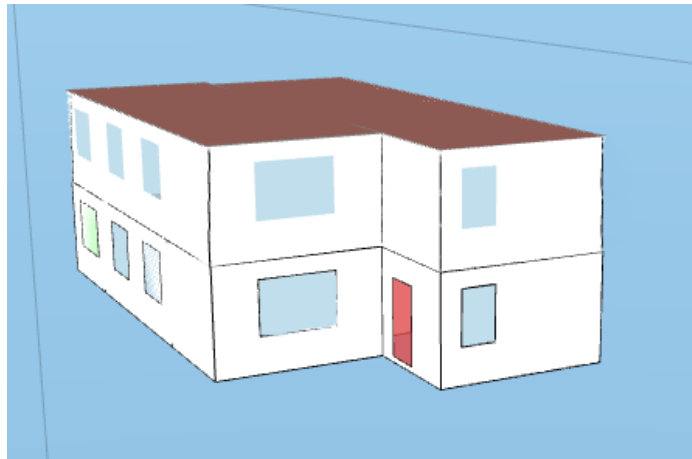
Fig. 2.1. Analyzed building

In order to determine the heat demand of the building, thePurmo OZC 6.7 Basic program was used. The program is based on applicable standards and regulations. The first stage of determining the heat demand is to introduce basic data about the building to the program.

Tab.. 2.1. Data

Parameter	
Location	Upper Silesia
Climatzone	III
Design outsidetemperature	-20°C
Averageannualoutdoortemperature	7.6°C

In the next step, the heat transfer coefficients$U$ were determined forall building partitions. It isa coefficient that determines the heat transfer through the walls. The lower is the heat transfer coefficient of wall, the better are its thermal properties.They are calculated in the OZC Purmo program based on the PN-EN ISO 6946. The results are presented in the Tab.2.2.

Tab.. 2.2. Heat transfer coefficient for all building partitions

Type of wall	Heat transfer coefficient U, W/m^2K
Outer Wall	0.121
Inner Wall	0.940
Groundfloor	0.217
Ceilling	0.751
Roof	0.137
Externaldoor	1.500
Interior door	1.500
Windows	1.500

Analyzing the results of calculations, it can be concluded that walls which are in direct contact with the environment have lower values of the heat transfer coefficient. It is beneficial in the terms of energy efficiency, because there are smaller heat losses to the environment.

Then, existing thermal bridges from the catalog available in the program were selected. Thermal bridge is a phenomenon involving the local increase of heat transfer through the building wall. It is related to the heterogeneity of the structure. In the analyzed building the most typical natural ventilation is used, which is called gravitational ventilation. The drive for natural ventilation is the difference in the density of cold air that comes from outside to the rooms and the warm air which is inside. For natural ventilation to work properly, a sufficient amount of fresh air must be supplied to the room.

The total heat demand wascalculated by equation (1). It is the sum of heat losses through all heated spaces excluding the heat exchanged inside the building, ventilation heat loss of all heated spaces excluding heat exchanged inside the building and excess heat output of all heated spaces required to compensate for the effects of heating weakness.

$$\phi_{HL} = \sum \phi_{T,i} + \sum \phi_{V,i} + \sum \phi_{RH,i} \tag{1}$$

where: $\phi_{T,i}$design heat loss of the heated space (i) by diffusion, W; $\phi_{V,i}$ - design ventilation heat loss of heating space (i), W; $\phi_{RH,i}$ - excess heat output to compensate for the effects of weakening heating of the heated zone (i), W

The design heat load of a building is the basic tool for selecting heating devices and for preparing domestic water. The results of the energy analysis, which are the basis for further considerations, are presented in Tab. 2.3.The calculated value of the heat output of a building means the maximum heat needed to the house heating, with a minimum outside temperature of -20°C.

Tab.. 2.3. Heat output for Analysed building

Parameter	Heat output, W
Design heat loss by diffusion	6894
Design ventilation loss of heat	3548
Excessheatoutput	2276
Design thermal load of the building	12718
Heat output to domestic water	2613

2.1. Heat demand in the year

The thermal load of the building varies within a year, because it is related to the outdoor air temperature. The lower is the outdoor temperature, the higher is the energy needs of the house. This is due to the necessity to maintain the thermal comfort of residents staying indoors. Thermal power variability was calculated based on real environmental data for Katowice from 2016 [3] and using the following formula (2).

$$\dot{Q}_g = \dot{Q}_{gmax} \cdot \frac{t_{in} - t_{out}}{t_{in} - t_{outmin}} \tag{2}$$

$\dot{Q}_{gmax}$ - maximum heat output, kW, t_{in}–internal temperature (20°C), t_{out} - outdoor temperature, °C, t_{outmin} - minimum outdoor temperature (-20°C).

Equation (2) is correct if the outside temperature is below 14 ºC, otherwise $\dot{Q}_g$ = 0. Figure 5 presents an ordered chart of the demand for thermal power, based on the results of calculations.
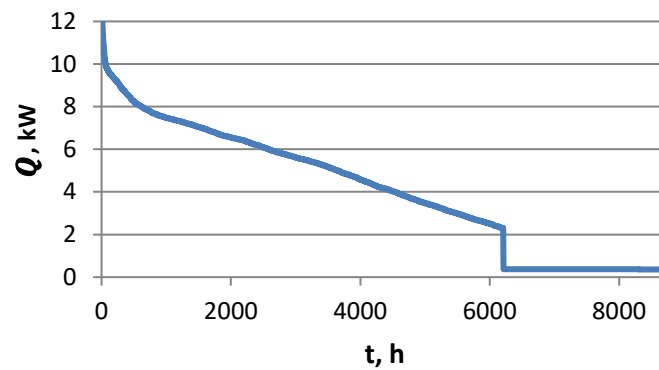
Fig. 2.3. Orderly graph of the heat demand for the building

In the Fig. 2.3.is clearly seenthe end of heating season, i.e. the period when the outside temperature is lower than 14ºC. It can also be seen that the maximum thermal load of a building occurs only a few days in a year. During the summer, the heat demand is associated only with the preparation of domestic water.

3. Selected heating systems

As a source of heatfor the analyzed single-family house an air-heat pump and a ground heat pump was used. The heat pumps were selected to cover all heat demand. The aim of this part of the analysis is to compare two heat pumps in terms of energy efficiency.

The main task of the heat pumps is to transfer heat from the lower heat source to the upper source. As it is known that such process cannot proceed spontaneously. Therefore it is implemented in a forced thermodynamic cycle, in which the work is provided to drive a compressor [4]. A characteristic quantity describing the energy efficiency of a heat pump is COP (Coefficient Of Performance). It is the ratio of useful heat to the energy needed to power the heat pump, as shown in the formula (3).

$$COP = \frac{Q_h}{E_{el}}$$

(3)

Q_h - useful heat, J, E_{el} – electricity consumption, J.

3.1. Air heat pump

In the first variant of the analysis, the Vitocal 200-S heat pump from Viessmann company was selected [5]. It is an air-to-water heat pump (power is 10.60 kW). Figure 3.1 presents values of the energy efficiency coefficient as a function of the temperature of the lower source, which in this case is outdoor temperature.

Figure 3.2shows that the efficiency coefficient changes linearly depending on the outside temperature, i.e. the lower heat source. If the temperature of the lower heat source increases, the COP increases. The value of the energy efficiency coefficient is also dependent on the temperature of the upper source. The lower the domestic water temperature, the higher the COP coefficient.
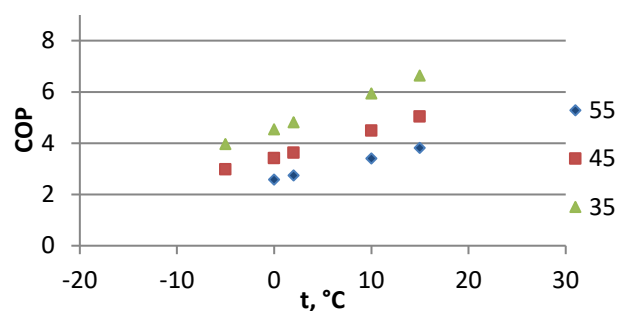
Fig. 3.1. COP values for the air pump depending on the outside temperature

3.2. Ground heat pump

In the next variant of the analysis, the energy efficiency of the Viessmann Vitocal 300-G ground heat pump was examined [6]. It is a brine-to-water heat pump with a thermal rated power of 12.95 kW. Figure 3.2. presents the values of the energy efficiency coefficient as a function of the temperature of the lower source, which is the ground.
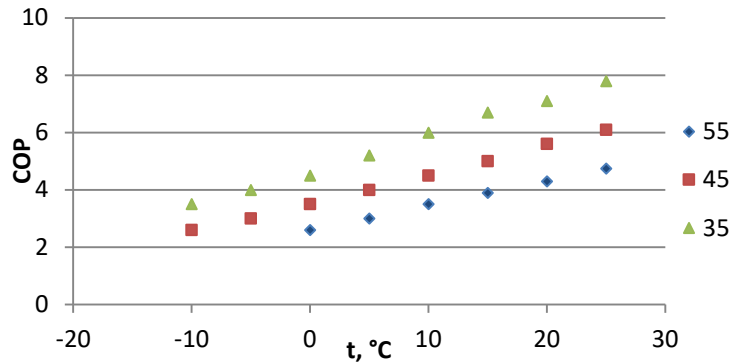
Fig. 3.2. COP values for the ground pump depending on the brine temperature

Similarly to the air heat pump, in figure 3.1 it can be noticed that the smaller the difference between the temperature of the lower and upper heat sources, the higher the value is the energy efficiency coefficient. In the energy efficiency study of a ground source heat pump, it was assumed that the brine temperature is constant during the year and is 10°C.

3.3. Comparison of selected heat pumps

Figure 3.3. shows a graph of the annual electricity consumption by heat pumps. It can be clearly seen that a ground heat pump consumes less electricity than air heat pump. The only exception is the summertime, when the air temperature is higher than the ground temperature. Then, the air heat pump consumes less electricity. After energy analysis of heat pumps, it can be concluded that a more efficient heating device is a ground pump, especially in winter.
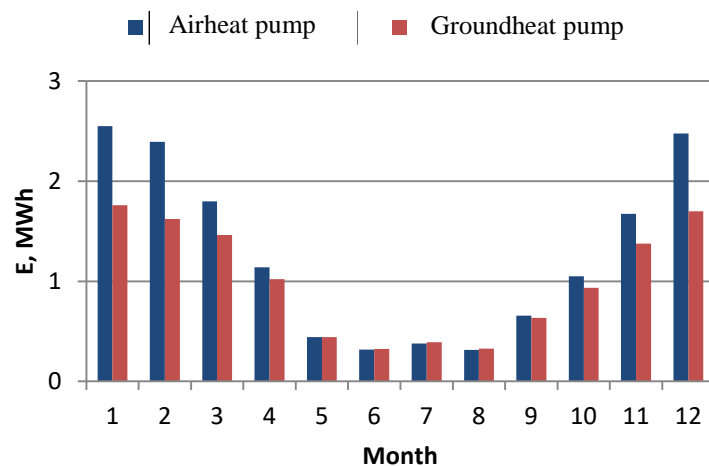
Fig. 3.3. Electricity consumption from the grid by heat pumps: air and ground

4.   Renewable energy sources

The basic types of renewable energy include solar, wind, water, geothermal, nuclear and biomass energy. In Poland, according to [7], the total share of renewable energy sources in final gross energy consumption in 2015 was at the level of 12.70%.

In this part of the analysis, two sources of renewable energy were examined. It was calculated how many electricity each plant is able to produce in a year in Silesia [3].

4.1. Photovoltaics

Analyzed photovoltaic installation consisting of 12 panels produced by SELFA GE S.A.company. The total power of installation is 3.3 kW. Figure 4.1. shows a graph showing the annual production of electricity in the photovoltaic system.
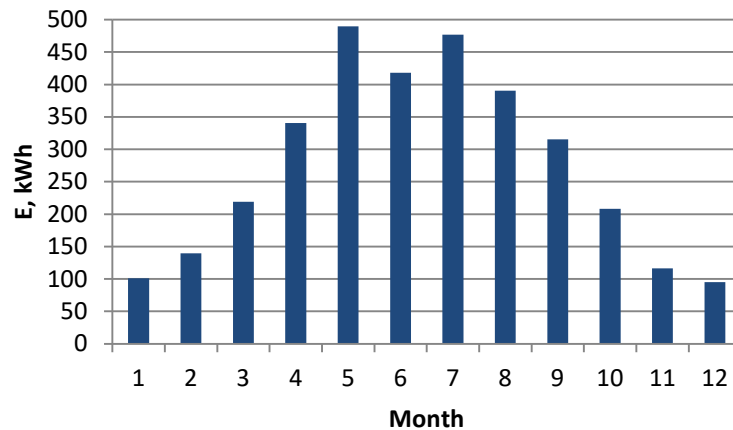
Fig. 4.1. Electricity production in photovoltaic panels during the year

In Fig.4.1. it can be easily seen that the photovoltaic plant is able to generate electricity throughout the year, however, the largest energy production is in the summer months. It is related to the value of the intensity of solar radiation reaching the surface of the Earth, which is the highest in these months.

4.2. Wind turbine

The analysis assumes that electricity production takes place in a 3 kW wind turbine [15]. It is a 2-rotor turbine with a vertical axis, its height is 3.5 m and the weight is 415 kg. Figure 4.2. shows the calculated production of electricity in the discussed wind turbine in the following months of the year.
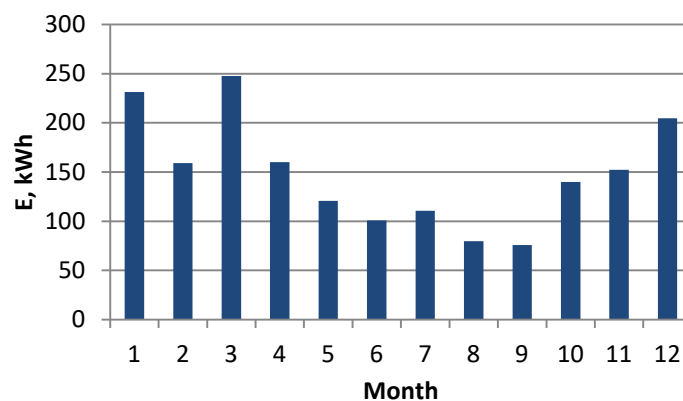
Fig. 4.2. Electricity production in a 3kW wind turbine during the year

Figure 4.2. shows that the production of energy in a wind turbine during the year is variable and it cannot be predicted. In some winter-spring months, electricity production is higher, but it is not a permanent dependence.

5. Cooperation renewable energy sources with heat pumps

In order to calculate the primary energy savings and to study the carbon dioxide emissions, depending on the heat pump used and the electricity source, the energy balance was used. The energy balance results from the first law of thermodynamics, which states that in the steady state the energy supplied to the system is equal to the

energy derived [8]. The walls of the analyzed building form the control cover of the system, the energy supplied to the system is electric energy (from the grid, photovoltaic system or wind turbine), while the energy derived from the system is energy used for heating purposes and preparation of domestic water.

During the analysis, the followingvariants were examined:

- Variant "0" - electricity to supply all electrical equipment comes only from the grid,

- Variant "1" - electricity comes from photovoltaic installations and grid,

- Variant "2" - electricity comes from a wind turbine and grid,

- Variant "3" - electricity comes from both renewable energy sources and the grid.

Each variant was tested for an air and ground heat pump. In Figures 3.3., 5.1-3. the results of energy balances for all possible variants are presented. On the left side there is a balance of energy for the photovoltaic installation and on the right there is a balance of energy for the wind turbine.

In Figures 5.1-3. it can be easily seen that in each of the variants, the production of electricity in micro-installations is not able to fully cover the demand for electricity throughout the year. The exception is the installation of photovoltaic panels. During the summer period PV produces electricity in an amount greater than the energy demand of the building, which presents red bars, which are below zero. This means that the electricity produced could be returned to the grid. Similarly, when both photovoltaic installation and wind turbine work. This is due to the fact that the heat demand is small in the summer and the photovoltaic installation produces the most electricity in this period. Although a wind turbine cannot provide the entire energy independence of a house, in the winter-spring period it is able to produce slightly more electricity than photovoltaic panels.
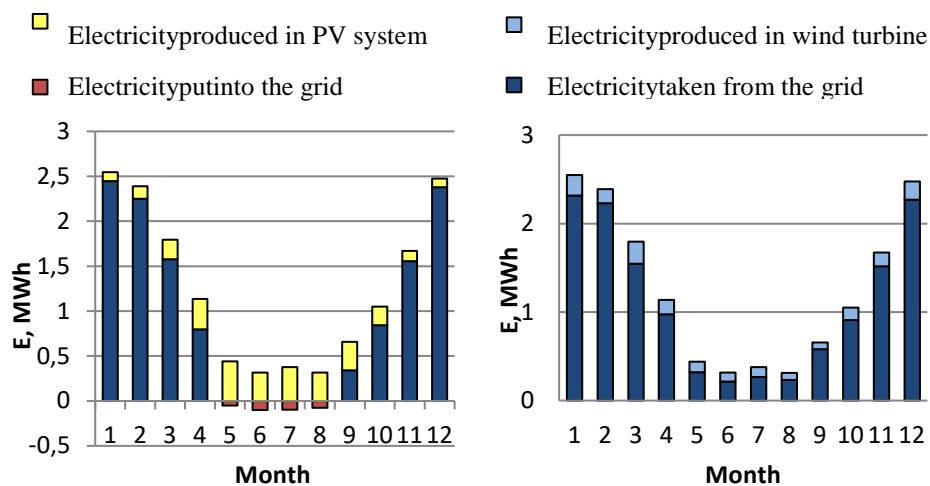
Fig. 5.1. Energy balance for an air heat pump and renewable energy sources
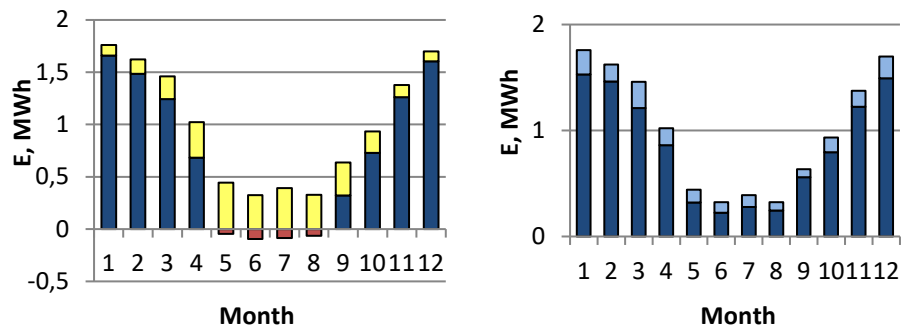
Fig. 5.2. Energy balance for a ground heat pump and renewable energy sources
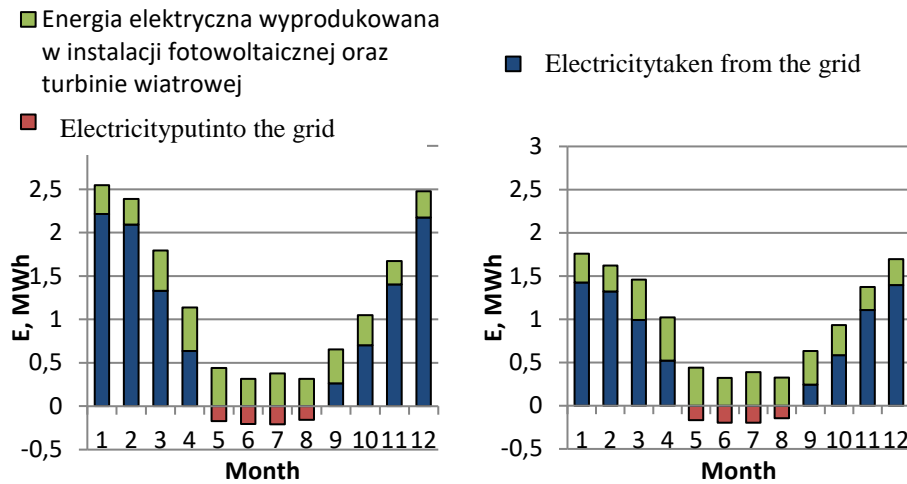
Fig. 5.3. Energy balance for an air and ground heat pump and the sum of electricity produced in the analyzed installations

6. Ecological analysis

6.1. Primary energy consumption

Primary energy is energy derived from nature in a renewable or non-renewable form. In energy performance certificates, it is defined as the amount of energy extracted at the source and needed to cover the heat demand of the house (heating, preparation of domestic water). In order to calculate the primary energy consumption for the tested variants, formulas (4) and (5) were used:

$$E_{chem,pal} = \frac{E_{el}}{\bar{\eta}_{Eel}} \cdot 100\% \tag{4}$$

where: $\bar{\eta}_{Eel}$ - average net transformation efficiency,%; E_{el} - electricity consumption to supply electrical equipment in the home, J.

The annual value of electricity consumption E_{el} is electricity used to the heat generation in heat pumps. This analysis uses the average net efficiency $\bar{\eta}_{Eel}$ of energy conversion in thermal power stations, which according to [9] is 37.5%.

$$E_P = E_{chem,pal} \cdot w_i \tag{5}$$

where: w_i - coefficient of nonrenewable primary energy input on generation and delivery of energy (or energy) carrier to the building, -.

The coefficient of non-renewable primary energy input for generation and delivery of the energy carrier to the building should be made available by the supplier of this energy carrier, otherwise it can be read from the Tab. [10]. For the electrical grid, the coefficient w_i is 3.0.

e_{EP} is the ratio of the amount of primary energy needed for heat production in the variants studied to the annual heat consumption in the building, as shown in the formula (6). Tab. 6.1. presents the results of calculations of primary energy consumption and the index of unitary primary energy consumption for heat production for the analyzed variants.

$$e_{EP} = \frac{E_p}{Q_a} \tag{6}$$

where: Q_a - annual heat consumption, GJ

Tab.. 6.1. Results of ecologicalanalysis

Variant	Primary energy consumption, GJ		Indicator of unitary primary energy consumption, GJ/GJ	
	Air heat pump	Ground heat pump	Air heat pump	Ground heat pump
0	447,59	355,80	3,53	2,80
1	352,24	260,45	2,78	2,05
2	395,55	303,76	3,12	2,39
3	300,20	208,42	2,37	1,64

Considering the results of primary energy consumption, it can be concluded that renewable energy sources allow saving the primary energy. Because the indicator of unitary primary energy consumption, in the cases 1-3 is lower than the variant 0. Solar energy in comparison with a wind energy is better in analyzed area. The variant 3 is the best solution from the ecological point of viewand the idea of sustainable development.However, an economic analysis should be made before making the investment decision.

6.2. Carbon dioxide emission

The by-products of combustion of natural fuels are flue gas, ash and slag.In solid fuels combustion, the main component is carbon dioxide. The impact of CO_2 on the environment is complex, because it is an essential gas in the process of photosynthesis and on the other hand is one of the factors that contribute to thegreenhouse effect. In order to calculate the emission of carbon dioxide to the environment (7), the value of electricity used to supply electric devices and the carbon dioxide emission factor, which according to [11] is 810 kg/MWh, are taken into account.

$$E_{CO_2} = E_{el} \cdot W_e \tag{7}$$

where: W_e - CO2 emission factor for electricity, kg / MWh.

Figure 6.1. presents carbon dioxide emission values for the analyzed variants. It can be seen that in the reference system, in which electricity comes only from the electric network, carbon dioxide emissions are the highest, especially for air heat pumps. Comparing solar and wind energy, it can be stated that using the photovoltaic plant, the carbon dioxide emission is lower. This means that solar energy in the studied area brings greater environmental benefits. The use of both sources of renewable energy brings the best ecological effects.
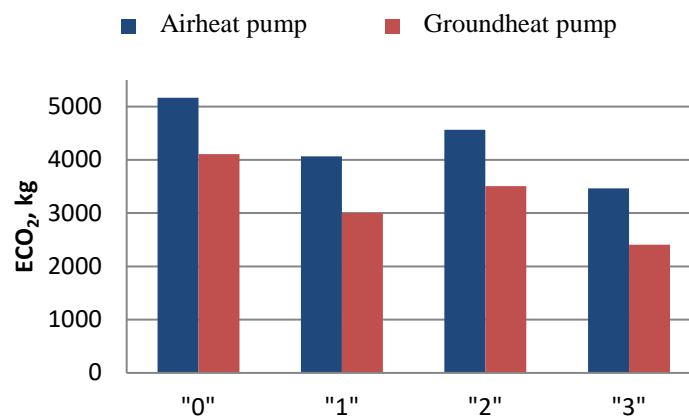
Fig. 6.1. CO_2 emissions during the year for the variants tested

7. Conclusions

The subject of this analysis was a single-family house with a usable area of 207 m², inhabited by a family of three and located in the province of Silesia. Two heat pumps were analyzed in the analysis: brine-to-waterand air/water. The aim of the work was to examine the efficiency of both pumps and compare them.

The ground heat pump is better in terms of energy efficiency. This is due to the sTab. temperature of the ground during the year, which along with the depth, is getting higher. The results of the ecological analysis show that the use of renewable energy sources clearly reduces the emission of carbon dioxide to the environment and allows a significant saving of primary energy.

After the analysis, it can be also concluded that renewable energy sources are consistent with the assumptions of sustainable development, because they contribute to the reduction of greenhouse gas emissions and the use of alternative energy sources does not significantly reduce reserves of non-renewable energy sources. This is especially importantdue to the compliance with the provisions of the EU Policy until 2030.

The presented analysis has shown that new and sustainable methods of heating buildings should be sought. This is important not only because of the goals of EU Policy until 2030, but also of global importance. We should rationally manage natural resources so that future generations can continue to use their wealth.

References

[1] Central Statistical Office, Consumption of fuels and energy carriers in 2015, Warsaw, 2016.

[2] Communication from the Commission to the European Parliament and the Council, Energy efficiency and its contribution to energy security and the political framework for climate and energy by 2030, Brussels, 2014.

[3] http://mib.gov.pl/2-Wskazniki_emisji_wartosci_opalowe_paliwa.htm

[4] W. L. Lewandowski, Proecological renewable energy sources, Scientific and Technical Publishers, Warsaw, 2001, pp. 285-303.

[5] https://www.viessmann.pl/pl/budynki-mieszkalne/pompy-ciepla/pompy-ciepla-powietrzewoda-w-wersji-split/vitocal-200-s.html, data dostępu: 2.10.2017 r.

[6] https://www.viessmann.pl/pl/budynki-mieszkalne/pompy-ciepla/pompy-ciepla-solankawoda/vitocal-300-g.html, data dostępu: 2.10.2017 r.

[7] Energy from renewable sources in 2015 Central Statistical Office, Warsaw, 2016.

[8] J. Szargut, Technical Thermodynamics, Wydawnictwo Politechniki Śląskiej, Gliwice, 2011, pp. 44-70.

[9] GUS, Fuel and Energy Economy in 2015 and 2016, Warsaw, 2017.

[10] Regulation of the Minister of Infrastructure and Development of June 3, 2014 on the methodology for calculating the energy performance of a building and a dwelling or a part of a building constituting an independent technical and utilitarian whole and the method of drawing up and models of energy performance certificates, Dz. U. of July 2, 2014.

[11] Emission factors CO2, SO2, NOX, CO and TPS for electricity on the basis of information contained in the National Database on greenhouse gas emissions and other substances for 2015, KOBiZE, February, 2017.

Economic and ecological analysis of the use of photovoltaic panels for the electricity production in a low-energy building

PrzemysławDygas

Faculty of Energy and Environmental Engineering, Silesian University of Technology, przemek.dygas@gmail.com

Abstract

The purpose of the work was to make economic and ecological analysis of the use of photovoltaic panels for the electricity production in a low-energy building that meets the requirements that will apply from 01.01.2021. on the basis of the Regulation of the Minister of Transport, Construction and Maritime Economy regarding technical conditions which should be met by buildings and their location. All of the electricity produced by PV system was intended to meet the needs of the building.In the theoretical part, low-energy building has been described, standards and requirements set for construction are presented, as well as solutions that allow to reduce energy consumption for buildings are mentioned.In the practical part of the article there is a characteristic of analyzed building with its project, construction of partitions and ventilation system. Further, there are calculations and their results for design thermal load of the building, central heating installation and electricity production. The final part is analysis of two different options in economic and ecological aspects and their comparison.

Keywords: low-energy buildings, photovoltaic, renewable energy sources

1. Introduction

Nowadays, due to the great concern for the natural environment, we strive to reduce emissions of pollutants and greenhouse gases. The idea of sustainable development causes that more and more attention is paid to the rational use of energy and respect for energy resources. We can do this by reducing energy consumption in the construction sector. It is a very energy-intensive sector of the economy. There are a number of legal acts issued by Parliament or the European Council, which set requirements and objectives for improving the energy efficiency of buildings. The Member States of the European Union, until 2021, must meet the requirements of TC 2021**.** This means that by that time, all newly constructed buildings must be low, possibly zero-energy. Starting from 2014 and TC 2014 requirements, the most attention should be paid to two coefficients. The first of these is $PE\frac{kWh}{m^2*year}$, the coefficient of demand for non-renewable primary energy for heating, ventilation and domestic hot water preparation. The second one is the heat transfer coefficient through building partitions $U\frac{W}{m^2*K}$.

Introducing more and more new and stricter requirements, forces investors to establish energy-saving power systems and use materials that have higher resistance to heat transfer. An additional incentive is the increasing prices of conventional fuels. Opting out of them and investing in, for example, renewable energy sources allows significantly reduce the cost of building exploitation. What's more, in many cases, you can receive funding for them, which allows you to reduce investment costs.

2. Low-energybuildings

Low-energy construction is a construction characterized by a much lower energy demand (intended for heating, cooling, hot water preparation and ventilation) than traditional construction. This is thanks to modern designs and technical solutions. With slightly higher investment costs, which are caused in most cases by a more expensive source of heat and better thermal insulation, it provides greater thermal comfort and generates much lower operating costs.

2.1. Standards and regulations

According to the regulation of the Minister of Infrastructure on technical conditions which should be met by buildings and their location [2], a low energy building is an object that meets the given requirements:

1. The values of heat transfer coefficients U [$\frac{W}{m^2*K}$] for partitions: outer walls, inner walls, floors, roofs, ceilings and flat roofs are calculated according to Polish Standards for calculating thermal resistance and heat transfer coefficient and ground heat transfer and do not exceed maximum U (max) in the Tab. below:

Tab.. 1.The value of heat transfer coefficients U for outer walls, inner walls, floors, roofs, ceilings and flat roofs [2].

Lp.	Type of partition and temperature in the room	Heat transfer coefficient U(max) [W/m2*K]		
		01/2014	01/2017	01/2021
1	2	3		
1	Outer walls			
	t >=16°C	0,25	0,23	0,2
2	Inner walls			
	Δt<8°C	no requirements		
3	Roofs, flat roofs and celings under an unheated attic			
	t>=16°C	0,2	0,18	0,15
4	Groundfloor			
	t>=16°C	0,3	0,3	0,3
Heated room - a room in which, due to the heating system operation or as a result of the balance of heat losses and profits, the temperature is maintained. t- temperature of heated room				

*values in above Tab. are only those which are used in following calculations, completed Tab. can be fond in the reference 2.

2. The PE [$\frac{kWh}{m^2*year}$] value determining the seasonal energy demand coefficient for heating, ventilation and domestic hot water preparation, calculated according to the methodology for calculating the energy performance of buildings, does not exceed the partial maximum values of the PE index heating, ventilation and hot water preparation, which for analyzed building, in 2021 will be equal 70 [$\frac{kWh}{m^2*year}$] according to [2].

3. Another value which needs to meet requirements is heat transfer coefficients U [$\frac{W}{m^2*K}$] for such partitions as: windows, balcony doors, exterior doors. In analyzed building there are only two of mentioned partition: exterior door with U(max)= 1.3 [$\frac{W}{m^2*K}$] and windows with U(max)= 0.9 [$\frac{W}{m^2*K}$] according to [2].

2.2. Solutions for low energy buildings

Low-energy constructions are becoming more and more popular. Environmental protection and increasing prices of conventional fuels encourage to be energy-saving. As the reports of the Central Statistical Office in 2015 show [3], we use the most energy for heating rooms and preparing hot domestic water. Thanks to investment during the design phase in low-energy solutions, we can significantly reduce the thermal demand of the building.
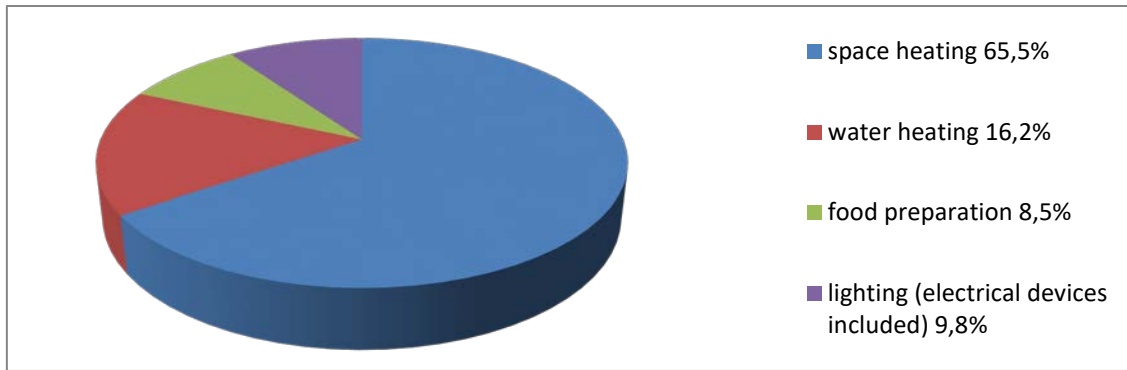
Fig. 1. Structure of energy consumption in households by the direction of use. Prepared on the basis of a report by the Central Statistical Office on energy consumption in households in 2015 [3].

Construction solutions:

1   Low ratio of the surface area to its cubic capacity,

2   Selection of materials with a correspondingly low thermal conductivity coefficient λ (investing 1% more in materials with better coefficients can save up to 30% on heating in subsequent years so it is a contribution that returns after 2-3 years and then generates profits for the investor [4],

3   Location of the building on the plot (maximum use of solar energy).

3. Energy characteristic of the building

To make the analysis, a single-family house building project with an area of $132.92\ m^2$ located in Cracow, Malopolska was used. It is a detached, one-storey building, without a basement, designed for a family of four.

The entrance to the building is located on the north side, and is separated from the living part by a hall. All rooms inside are heated. In order to minimize thermal bridges, in the northern part of the building there are rooms that do not require a lot of light, such as a dressing room and a boiler room. These are also the only rooms where radiators were installed. In the rest of the rooms there is underfloor heating. On the north wall there are only two small windows that provide light to the corridor. In order to make better use of solar energy in the southern and eastern part of the building, there are rooms for day use, including a living room and bedrooms, which have a larger number of glass surfaces than the rooms in the northern part. The usable height inside the building is 2.6 m.
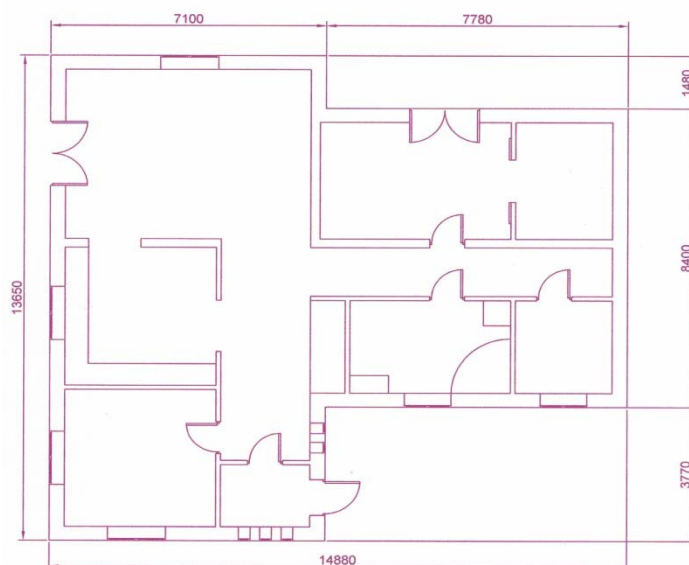
Fig. 2. Plan of the building

3.1. Construction of building partitions

All walls of the analyzed building were built with cellular concrete blocks. For the thermal insulation of outer walls, a material with a very low thermal conductivity coefficient Kooltherm k5-180 was used. The ground floor has the same construction everywhere. The only difference is the exterior layer. In one case, they are ceramic tiles, in the second case ash panels. The floor were laid on medium sand, and tightly stacked polystyrene was used for insulation. Insulation of foundations against water and moisture is ensured by the position of two layers of polyethylene foil. The ceiling under the unheated attic was made of reinforced concrete, insulated with polyurethane foam and mineral wool. In this case, polyethylene foil was also used to provide vapor barrier.

For all partitions, based on the standard [1], in accordance with formulas (3.1-3.3), the value of the coefficient U $[\frac{W}{m^2 * K}]$ was calculated, and the values of resistance to heat transfer were adopted in accordance with the standards.

$$R = \frac{d}{\lambda} (3.1)$$

$$R_T = R_{si} + \sum R + R_{se} (3.2)$$

$$U = \frac{1}{R_T} (3.3)$$

d- meterial thickness [m]

λ- design heat transfer coefficient $\frac{W}{mK}$

R_{si}- resistance to heat transfer on the internal surface $\frac{m^2 K}{W}$

R_{se}- resistance to heat transfer on the external surface $\frac{m^2 K}{W}$

R_T- total thermal resistance $\frac{m^2 K}{W}$

U- heat transfer coefficient $\frac{W}{m^2 K}$

In the calculations, the Auditor OZC 6.8Pro Edu program was used, and the results obtained from it, compared with the limit values for them, are presented in the Tab.s below.

Tab. 2. List of multilayer partitions for the analyzed building

Layer	Thickness [m]	λ [W/(m·K)]	TC 2021
Multilayerpartitions			
Exteriorwall 39cm			
Cement-lime plaster	0,01	0,82	
Blocks of cellularconcrete	0,20	0,25	
Kooltherm k5-180	0,18	0,021	
Total thickness	0,39m		
Heat transfer coefficient U [W/m2·K]	0,105		0,2
Inner wall 24cm			
Cement-lime plaster	0,01	0,82	

Blocks of cellularconcrete	0,22	0,25	
Cement-lime plaster	0,01	0,82	
Total thickness	0,24m		
Heat transfer coefficient		0,859	-
Inner wall 12cm			
Cement-lime plaster	0,01	0,82	
Blocks of cellularconcrete	0,1	0,25	
Cement-lime plaster	0,01	0,82	
Total thickness	0,12m		
Heat transfer coefficient U [W/m2·K]		1,461	-
Groundfloor 1			
Ash panels	0,01	0,174	
Lean concrete	0,07	1,05	
Polyethylenefoil	0,0005	0,2	
Styrofoam	0,08	0,04	
Polyethylenefoil	0,0005	0,2	
Lean concrete	0,1	1,05	
Medium sand	0,15	0,4	
Total thickness	0,411		
Heat transfer coefficient U [W/m2·K]		0,204	0,3
Groundfloor 2			
Ceramictitles	0,02	1,05	
Lean concrete	0,07	1,05	
Polyethylenefoil	0,0005	0,2	
Styrofoam	0,08	0,04	
Polyethylenefoil	0,0005	0,2	
Lean concrete	0,1	1,05	
Medium sand	0,15	0,4	
Total thickness	0,411		
Heat transfer coefficient U [W/m2·K]		0,206	0,3
Ceiling under unheated attic			
Reinforcedconcrete	0,2	1,7	

Polyethylenefoil	0,0005	0,2	
Polyurethanefoam	0,08	0,025	
Polyethylenefoil	0,0005	0,2	
Reinforcedconcrete	0,05	1,7	
Mineralwool	0,12	0,035	
Polyethylenefoil	0,0005	0,2	
Total thickness	0,452m		
Heat transfer coefficient U [W/m2·K]	0,143	0,15	

Tab. 3. Typical partitions for the analyzed building

Tipicalpartitions		
Partition	U [W/m2·K]	TC 2021
Exteriordoor	1,3	1,3
Inner door 90x200	4	-
Window 120x90	0,9	0,9
Window 30x180	0,9	0,9
Window 150x150	0,9	0,9
Window 180x235	0,9	0,9

The data presented in the Tab.s show that the values of heat transfer coefficients obtained from the calculations for particular partitions will meet the ones coming into force on 01/01/2012 TC 2021 requirements [2] regarding thermal insulation of buildings.

3.2. Ventilation system

In the analyzed building, a supply-exhaust ventilation system with a recuperator was selected. For a house with an area of 150-200 m2, the cost of such installation is about PLN 10,000 - 15,000 more expensive than the exhaust ventilation system, but thanks to the use of heat recovery in the discharged air, you can save about 1,000-1500 PLN per year on heating costs [5]. This ventilation works on the basis of the work of fans that force the air flow in the room. Its variant with heat recovery is the best solution for energy-saving construction, because it is a compromise between an energy-efficient installation and one that ventilates the building in a proper way. In addition, the recuperator recovers heat from the removed air and transfers it to the fresh air. This process of energy transfer allows you to recover from 50 to 80% of heat removed from the building. The problem occurs when the outdoor temperature is below -10 ° C. Then direct blowing of the air is uncomforTab. and the interior of the building is too cool. In order to heat it, electric heaters are installed in recuperators. They also have a thawing system when the water condensing in the exchanger freezes. The whole device can be operated manually or automatically. Attached to various sensors that check the air condition at home, they can automatically regulate the efficiency, adapting it to the prevailing conditions so as to maintain comfort and adequate ventilation. In summer, when the outside temperature of the building is higher than the inside, the recuperator cools the air blown inward [5].

Using the Auditor OZC 6.8Pro Edu program, results regarding ventilation were obtained for the design heat load and those which are needed for further calculations are presented in paragraph 4.3.

4. Design thermal load of the building

The design heat load of a building is the thermal power of the building is needed to maintain the thermal comfort inside the building. The calculation methodology is defined in the PN-EN 12831: 2006 standard [6]. The following calculations were made to determine the amount of energy compensating for losses caused by energy diffusion through the heated space and ventilation losses, and then on this basis, a central heating installation was designed and an appropriate heat source with the required power was selected.

$$\Phi_{HL,i} = \Phi_{T,i} + \Phi_{V,i} + \Phi_{RH,i} \quad (4.1)$$

$\Phi_{HL,i}$- design heat load [W],

$\Phi_{T,i}$- heat loss by diffusion of the heated surface (i) [W],

$\Phi_{V,i}$- ventilation heat loss of heated space (i) [W],

$\Phi_{RH,i}$- surplus thermal power required to compensate for the effects of weakening heating of the heated zone[W].

4.1. Seasonal energy demand for heating

The seasonal energy demand for heating determines the amount of energy needed to be delivered per m^2 in a year to ensure thermal comfort in the building. It has been calculated based on the monthly method, using the PN-EN ISO 13790 standard [7] based on formulas (4.2-4.3). Tab. 5 presents the results of calculations obtained with the Auditor OZC 6.8Pro Edu program. They allowed designing a central heating installation and selection of an appropriate source of heat.

$$Q_{H,nd} = \sum_n Q_{H,nd,n} \quad (4.2)$$

$$Q_{H,nd,n} = Q_{H,ht} - \eta_{H,gn} * Q_{H,gn} \quad (4.3)$$

$Q_{H,nd}$- seasonal energy demand $[\frac{kWh}{year}]$

$Q_{H,nd,n}$- energy demand in particular months $[\frac{kWh}{month}]$

$Q_{H,nt}$- monthly heat loss through penetration and ventilation $[\frac{kWh}{month}]$

$Q_{H,gn}$- monthly internal solar heat gains $[\frac{kWh}{month}]$

$\eta_{H,gn}$- coefficient of profit utilization in heating mode

4.2. Calculation of energy demand for domestic hot water preparation

The amount of energy used to preparation of domestic hot water was calculated on the basis of EN 15316: 2007 [8], according to the formula:

$$Q_{hdw} = (c * n * d * \rho * V * \frac{t_h - t_c}{10^6 * P * \eta}) / 0,0036 \, \text{GJ} \quad (4.3)$$

Q_{hdw}- seasonal energy demand for the preparation of domestic hot water $[\frac{kWh}{year*m^2}]$,

c- specific heat of water $[\frac{kJ}{kg*K}]$,

ρ- density of water $[\frac{kg}{m^3}]$,

V- water volume per person [m³],

t_h- hot water temperature [°C],

t_c- cold water temperature [°C],

d- number of days in a year,

P- surface area of the building [m²],

n- the number of inhabitants,

η- system efficiency.

Tab. 4. Assumptions for calculations for hot utility water

Parameter:	c	ρ	V	th	tc	d	P	n	η

Value:	4,19	1000	0,04	55	10	365	132,92	4	0,52

The result was obtained: $44,25 \frac{kWh}{year*m^2}$

On the basis of the same standard, the formula (4.4) calculates the power demand for preparing domestic hot water.

$$\Phi_{cw} = \frac{V_{h\acute{s}r}*Q_{cw}*N_h*277,7}{\eta} \quad (4.4)$$

Φ_{hw}- power needed to prepare hot domestic water [kW],

Va- volume of hot domestic water in disposable time [$\frac{m^3}{h}$],

Q_{hw}- heat for heating 1m³of water [$\frac{GJ}{m^3}$],

N_h- coefficient of unevenness of hot water partition ($9,32*n^{-0,244}$)
Average daily use time of domestic hot water- 18h

The calculated power needed to prepare hot domestic water is 5,8 kW.

4.3. Results

Tab. 5. Results of calculations of seasonal thermal load and seasonal demand for thermal energy of the building generated by the Audytor OZC 6.8Pro Edu program.

Basic calculationresults	
Heated area of the building	132,9 m2
Heated volume of the building	345,6 m3
Design heat loss by diffusion	2532 W
Design ventilation loss of heat	1314 W
Total heatloss	3846 W
Designheatload	3846 W
Seasonal energy demand for heating	
Ventilation air flow for heating	224,5 m3/h
Energydemand for heating	$6224 \frac{kWh}{year}$
Seasonalheatdemand	$46,8 \frac{kWh}{m^2*year}$

The results placed in the Tab. above show the value of the coefficient of seasonal heat demand for energy for heating and ventilation $PE_{H+V} = 46,8 \frac{kWh}{m^2*year}$. Summing this value up with seasonal energy demand for preparation of domestic hot water total seasonal heat demand is $91,05\frac{kWh}{m^2*year}$.

5.   Central heating installation

The building uses a water, two-pipe system with a pump module with the following parameters: 55 ° C / 45 ° C. Two rooms in the whole building are heated radiators. The rest of the house has underfloor heating installed. In the bathroom there is also a bathroom radiator, which provides 35% of the required heat. Appropriate thermal powers were also selected, taking into account heat gains and appropriate cable diameters for all radiators.

5.1. Heat source

The central heating system is very important considering the energy efficiency. It absorbs about 70% of the energy consumed during the operation of the building. What's more, to meet the requirements of modern construction, the heat source should be ecological. For low-energy buildings, heat sources that do not require a large investment, such as electric heating, are a good choice. Taking into account Polish conditions and investment and operating costs, a gas boiler is a good solution in our country. [1]

As a source of heat for the analyzed building, a Junkers Cerapur Midi condensing, dual-function gas boiler with a capacity of 7.3-26.6 kW for central heating and 24 kW for the preparation of hot domestic water were selected. It has a high efficiency of 103%. [9]

5.2. Results

Thermal power of central heating installation needed for further analysis was calculated and generated using the HERZ C.O 4.0Basic program. Its value is equal 4211 W.

6. Electricity production for heating, ventilation and hot water preparation

A photovoltaic installation was selected for the analyzed building, which task is to provide electricity for the central heating, ventilation and hot water preparation system. Due to the power of the panel, its energy efficiency, which is higher than conventional panels and modern technology, the BenQSunForte PM096B00 model with a rated power of 330Wp, module efficiency of 20.3% and dimensions of 1559x1046x46 mm was chosen. [10]

The power of the photovoltaic installation was calculated on the basis of the method presented in the article [11].

$$P_{pv} = \frac{\eta * E_{el}}{E_{pv}} \ (6.1)$$

P_{pv}- required photovoltaic power [kWp],

η- correction coefficient of the optimal power range [from 0,9 to 1,2],

E_{el}- power consumption for central heating, ventilation and hot water installations [kWh],

E_{pv}- electricity production by PV installation $980[\frac{kWh}{kWp}]$

For the extreme values of the correction coefficient, the optimal power range was used to calculate the power of the photovoltaic installation. It should be in the range from 1.43 kWp to 1.92 kWp. Based on these results, an average value of 1.65 kWp was selected. For 330Wp photovoltaic panels, this gives the number of 5 panels.

$$A_{pv} = n * A_p \ (6.2)$$

A_{pv}- surface area of PV installation [m²],

n- number of PV panels,

A_p- surface area of PV panel[m²].

The calculated area of a photovoltaic installation is 8.20 m². It meets the same requirements as for the available space, because the building has a roof area of 48.5 m², which is directed towards the south. The entire photovoltaic installation has been designed for a roof with a 45 ° angle of inclination.

A simplified method from the article [11] was adopted to calculate the costs of a photovoltaic installation. It assumes the installation cost from 6000 to 8000 $[\frac{PLN}{kWp}]$ if the PV installation's power varies between 1 and 3 kWp and the price ranges from 5000-6000 $[\frac{PLN}{kWp}]$for 3-10 kWp. For the selected installation power of 1.65 kWp, the cost of 8000 $[\frac{PLN}{kWp}]$was assumed.

$$K_c = P_{pv} * K_j \ (6.3)$$

K_c- total installation cost [PLN],

P_{pv}- power of photovoltaic installation [kWp],

K_j- cost of 1kWp of photovoltaic plant power [$\frac{PLN}{kWp}$]

Based on above assumptions ondformula (6.3), the approximate, total cost of the PV installation was calculated to be approximately PLN 13200.

7. Economic and ecological analysis

Using EKO 1.0 EduAudytor program, an economic and ecological analysis of the applied solutions was carried out. The system with condensing, dual-function gas boiler powered with electricity from network and an installation with the same heat source, but with electricity produced by a solar installation built on the roof of the building, were compared. The consideration includes approximate investment costs that must be beared by the investor, estimated operating costs related to the prices of energy carriers and environmental impact understood as the emission of SO2, NOx, dusts, soot, carbon oxides and BaP or aromatic hydrocarbons.

Tab. 6. Basic data used for economic and ecological analysis obtained from above calculations

Information about the building for base variant	
Power demand for heating and ventilation	4211 W
Usable energy demand for heating and ventilation	7895 [$\frac{kWh}{year}$]
Final energy demand for auxiliary equipment for the ventilation and air conditioning system	866 [$\frac{kWh}{year}$]
Power demand for the system for preparing domestic hot water	5798 [W]
Usable energy demand for preparing domestic hot water	5356 [$\frac{kWh}{year}$]
Final energy demand for auxiliary equipment for preparing domestic hot water	352 [$\frac{kWh}{year}$]

What is more, the price of fuel, which was natural gas, was assumed as $2,1\frac{PLN}{m^3}$ and its lower heating value was equal $48\frac{MJ}{kg}$. For the case with gas boiler powered with electricity from the grid the additional assumption that the price of 1kWh was 0,54 PLN, was made. Additionally, cost of PV system taken into account in this analysis was higher than cost of just PV panels due to assumed, additional cost of installation.

7.1. Evaluation of ecological analysis

In the economic analysis, SO2, NOx, dust, soot, carbon oxides and BaP emissions, using condensing, dual-functional gas boiler powered with energy from network and the same energy source powered by electricity from photovoltaic panels were compared. Below is a comparison of two variants generated in the form of charts in the Auditor EKO 1.0 Edu program.
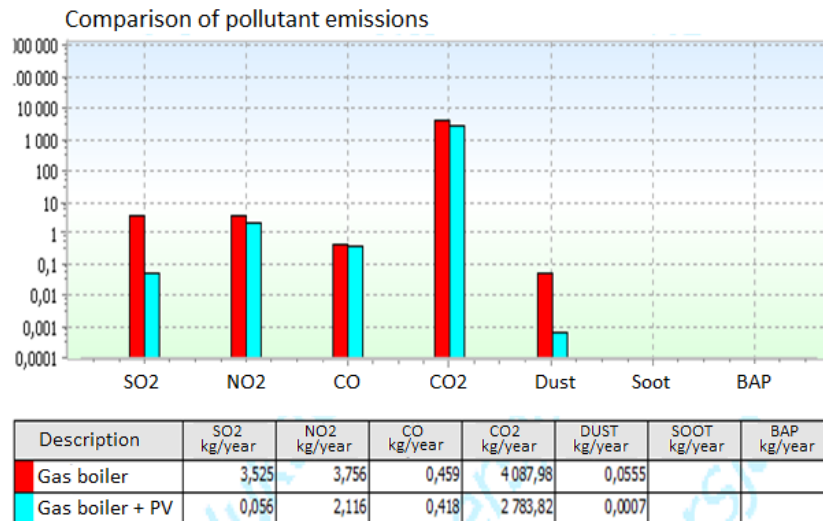
Fig. 3. Comparison of pollutant emissions for the analyzed variants

On the basis of the obtained results, it was found that the installation with the installed solar system is much more ecological. Emissions of all pollutants in this variant are lower than in the case of a boiler powered by electricity from the network. While in the case of NO2, CO and CO2 these differences are small, in the case of sulfur dioxide and dust, emissions are reduced almost 100 times.

7.2. Evaluation of economic analysis

As part of the economic analysis, investment costs and annual operating costs related to fuel and electricity costs were compared. The results in the form of charts in the Audytor EKO 1.0 Edu program are presented below.
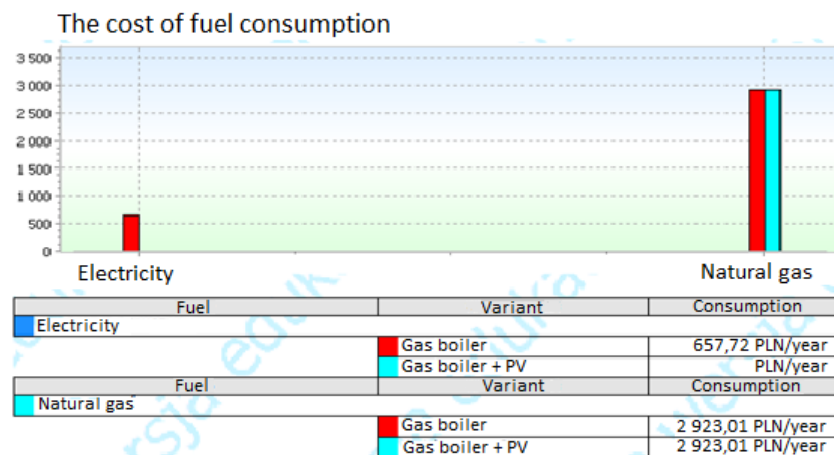
Fig. 4. Comparison of fuel consumption costs

The cost of natural gas will be the same in both cases, however, the electricity cost in the case of a solar installation will be equal to $0 \frac{PLN}{year}$ while the cost of electricity from the network will be $657.72 \frac{PLN}{year}$.

Assumptions

Calculation period	[years]	30
Discount rate	[%]	4

Total cost

Variant		Gas boiler	Gas boiler + PV
Total cost	[PLN]	87734	99145
Payback period	[years]	-	72,3
Increase of investment cost	[PLN]		15000
Annual savings	[PLN]		208

Fig. 5. Summary of economic analysis results

In the above economic set-up, installation with solar panels is definitely more beneficial in terms of operation. It will generate profits in the amount of 208 $[\frac{PLN}{year}]$. Unfortunately, the cost of installing a solar system is so high that, adding up all expenses, the installation would return after 72.3 years.\

8.   Conclusions

The requirements set by the ordinance of the Minister of Transport, Construction and Water Management are rigorous and difficult to achieve in Polish conditions. The more so that the systems required to meet these requirements are very costly, and by comparing the payback period of the investment and life cycle of the solution, it is easy to conclude that they are unprofiTab., as in the case of photovoltaic panels for the analyzed building.

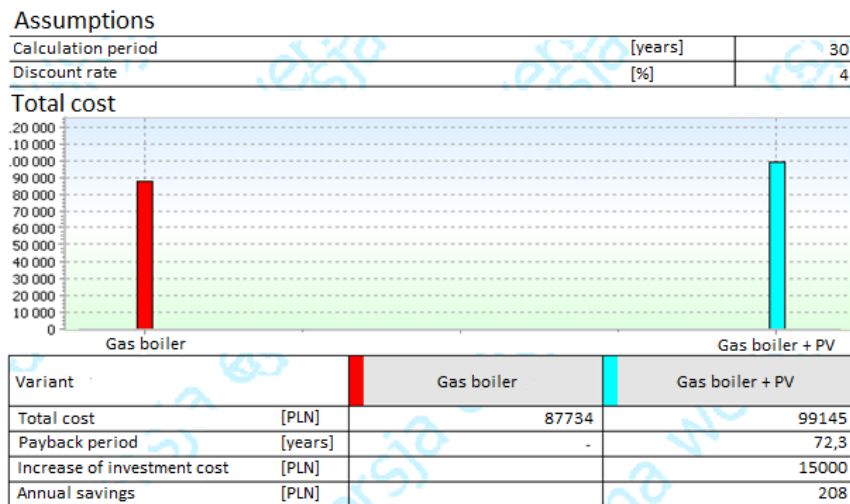It seems that when the requirements of TC2021 come into force, the only possibility to obtain the coefficient PE = 70 $\frac{kWh}{m^2*year}$ or less will be the use of solar system and solar collectors to reduce the consumption of conventional energy for the production of electricity and hot water and the use of heat pump systems co-operating with the above-mentioned systems for heating purposes. Another possibility that seems promising in this respect are biomass boilers, which also use renewable energy sources. It will be necessary to install ventilation systems with a recuperator with high efficiency of heat recovery.

It is all connected with high costs and despite the fact that it is possible to receive a number of subsidies due to environmental protection, designers face a difficult task of reconciling the most effective solutions with low prices that would be tempting for potential customers and encourage them to invest in these systems.

Acknowledgment

References

[1] "Energooszczędnydom i mieszkanie" ("Energy-saving house and flat") Brochure published as part of the project „Z energetykąprzyjaznąśrodowiskuza pan brat" ("To be friendly with environment friendly energy") with the financial support of the National Fund for Environmental Protection and Water Management, Warsaw 2011

[2] "ObwieszczenieMinistraInfrastruktury   i   Rozwoju   z   dnia   17   lipca   2015   r.   w sprawieogłoszeniajednolitegoteksturozporządzeniaMinistraInfrastruktury w sprawiewarunkówtechnicznych,

jakimpowinnyodpowiadaćbudynki i ichusytuowanie" ("Decree of the Minister of Infrastructure and Development of 17 July 2015 about publication of a uniform text of the Regulation of the Minister of Infrastructure on the technical conditions to be met by buildings and their location"), Warsaw 2015r.

[3] "Zużycieenergii w gospodarstwachdomowych w 2015r."("Energy consumption in households in 2015")Statistical information. Central Statistical Office, Warsaw 2017r.

[4] prof. Jerzy A. Pogorzelski, Department of Thermal Physics ITB, Brochure "Dom energooszczędny" ("Energy-saving house"), 2002r.

[5] www.wentylacja.org.pl, http://wentylacja.org.pl/pages-41.html, Date of use: 03.11.2017r.

[6] M. Strzeszewski, P. Wereszczyński, "Norma PN-EN 12831:2006. Nowa metoda obliczania projektowego obciążenia cieplnego- poradnik "("Norm PN-EN 12831:2006. New method of calculating the design heat load- gudie"), Warsaw 2009

[7] PN-EN-13790 "Metodykaobliczeńsezonowegozapotrzebowaniaciepła" ("Methodology for calculating seasonal heat demand")

[8] EN 15316: 2007 "Systemygrzewcze w budynkach - metodaobliczaniazapotrzebowanianaenergięinstalacji i sprawnośćinstalacji" ("Heating systems in buildings - the method of calculating the energy demand of the installation and the efficiency of the installation ")

[9] www.tanie-ogrzewanie.pl,   https://www.tanie-ogrzewanie.pl/piece-gazowe-junkers/piec-gazowy-dwufunkcyjny-junkers-cerapur-midi-7-24kw-kondensacyjny,,rid,13064.html Date of use: 05.12.2017

[10] www.sunsol.pl, http://sunsol.pl/produkty/panele-fotowoltaiczne/benq-solar/benq-sunforte-330w, Date of use:05.12.2017r.

[11] www.ladnydom.pl, http://ladnydom.pl/budowa/56,106580,19985382,panele-fotowoltaiczne-i-pompa-ciepla-dobrana-kompania.html, Date of use: 05.12.2017r.

Modeling biomass pyrolysis

Zuzanna Kaczor [1], Zbigniew Buliński[2*], Sebastian Werle [3*]*

*Institute of Thermal Technology, Silesian University of Technology, Gliwice, Poland

[1] *e-mail: zuzanna.kaczor@polsl.pl*

[2] *e-mail: zbigniew.bulinski@polsl.pl*

[3] *e-mail: sebastian.werle@polsl.pl*

Abstract

The paper presents a summary of numerical research on various phenomena occurring in the solar biomass pyrolysis process. The analyses are intended to verify the initial assumptions regarding the construction and work parameters of the laboratory rig, on which the pyrolysis will be experimentally investigated. The first model focuses on the phenomenon of concentrating solar radiation with mirrors of different curvatures. The next models are built to reflect the processes occurring in the pyrolytic reactor. The analyses concern the process of reactor heating, with and without taking into account the occurrence of chemical reactions in the biomass deposit. The results indicate significant differences between both models. This indicates an essential need of further developing the model with important phenomena taking place in the reactor. The next stages of the model's development are an update to the final concepts regarding the reactor construction, provision of suitable kinetic parameters and fortifying the model with other important phenomena, like mass loss and changes in the feedstock condition.

Keywords: biomass, pyrolysis, model, CFD, radiation, chemical reactions

1. Introduction

Facing stricter legal regulations in relation to the CO_2 emission levels from the heat and electricity production process and aiming to more and more wide use of renewable energy sources the possibility of using biomass is currently being studied all over the world. Biomass is classified as renewable energy sources, in addition, it is considered to have a zero CO_2 balance as a fuel.

Of the many known renewable energy sources, most occur in strictly defined places, as being connected with a geographical location, lay of the land, proximity of seas and oceans, occurrence of rivers, mountainousness of the terrain. This group includes geothermal energy, wave and tidal energy, hydropower. Biomass is also not widely available in large quantities, but occurs in places of intensive plant production (agricultural and wood) or near municipal waste treatment plants or sewage treatment plants (industrial waste, sewage sludge). In addition, the biomass in its raw form has a very low energy content due to high humidity and low density, therefore, its transport over long distances is energetically unjustified. However, the disadvantages of biomass as transportable fuel can be reduced in several ways, i.e. by drying, pelletization and thermal methods such as torrefaction, gasification, pyrolysis or liquefaction.

Pelletization requires the heat to drying or water to moisturization the raw material (in the case of excessively dry materials) and mechanical energy for crumbling and pressing into compact portions, pellets. Although drying or pelletization improve the issue of humidity, low density or milling properties, however, the fuel composition remains unchanged [1]. Only thermal methods allow the transformation of chemical content by decomposition into solid, liquid and gaseous fractions and further combustion of such processed biomass in gas or coal installations. All these methods require thermal energy and most often electrical energy for the automation and mechanization of the process. Therefore, the idea of biomass thermal processing is commonly combined with a use of concentrated solar radiation as a heat source. In very windy places, solar radiation can be replaced by electrical heating supplied by wind turbine generators

This work is a summary of the numerical tests carried out so far as part of experimental and numerical works on the solar pyrolysis of waste biomass process. Models and analyses concerning the component phenomena of the

pyrolysis process are presented here briefly. The work has been summarized in the context of the final goal which is the overall simulation of biomass pyrolysis.

2. Pyrolysis of biomass

Torrefaction, gasification and pyrolysis are, as mentioned earlier, methods of thermal biomass processing. The torrefaction is a roasting of biomass in temperature range 200-300 ° C in an inert atmosphere. As a result a partial thermal decomposition occurs and the torificatt is obtained - so-called biocarbon, characterized by reduced humidity, raised brittleness, a slight loss of volatile parts and thus, a small loss of chemical energy in relation to the raw material [1,2].

Pyrolysis is also a roasting without an oxygen access, but the range of temperatures used is higher, 400-1000 °C so that the material is completely decomposed into a solid, liquid and gaseous fraction. Depending on many factors, among others, process temperature, heating rate, material residence time in the reactor, the proportions and composition of pyrolysis products are different [3].

Gasification is carried out in the temperature range 800-1300°C by use of a hot medium, air and/or water vapor, so with an oxygen access. In this way, some of the combustible substances undergo oxidation, but in return, most of the input material is transformed into a gas form and a significant part of the toxic substances is neutralized [4–6].

Liquefaction occurs due to hydrogen reduction, as a result of which a liquid product is obtained - combustible oils - containing mainly hydrocarbons [3].

The subject of this work is the pyrolysis process. An overview of the literature performed in paper [7] allows to state that the most often studied type of biomass pyrolysis is a pyrolysis in a bed of particles, (catalytic) fast pyrolysis in fluidal reactor and solar pyrolysis.

2.1. Substances in biomass pyrolysis

As a result of biomass pyrolysis, three factions are obtained, so-called char, tar and gas. The char consists mainly of carbon and minerals (ash); tar is a mixture of water, hydrocarbons, acids and alcohols; while the gas includes carbon monoxide and dioxide, hydrogen, methane and other hydrocarbons [3,6].

Composition of raw biomass strongly depends on its origin, because among plant (straw, tree chips, husk stones, etc.) biomass can also come from sewage sludge, industrial, urban and municipal waste. Biomass of plant origin consists essentially of three main ingredients: cellulose, hemicellulose and lignin. Cellulose has a fibrous structure and is a building component. Hemicellulose is a building and stock material. Lignin couples fibers of cellulose and provides hardness and strength to the plant structure. The other biomass components of biomass are generally moisture and mineral substance [8–10].

2.2. Idea of biomass pyrolysis

Thermal processing of biomass in the process of e.g. pyrolysis powered by solar energy is an idea that combines three important issues: use of renewable energy, energy storage and distributed energy production. In addition, among a wide range of renewable energy sources only wind and solar energy occurs in most places on Earth, and in most of human settlements there is also the biomass. Biomass is a waste product in practically every farm, so in objects 1) located in open spaces, conducive strong winds and high insolation 2) usually with a large area, on which it is possible to install wind turbine systems, solar concentrators or photovoltaic cells. Therefore, in rural farms would be possible systematic conversion of different types of biomass into fuel and supplying this process with fully renewable energy.

In addition, the pyrolysis process powered by renewable energy as biofuel production it's a way of adjusting to annual, seasonal, daily or even instantaneous changes in the intensity of solar radiation, using its potential and storing it in the form of fuels, ready to use anywhere, anytime.

2.3. Use of solar energy

Solar powered pyrolysis concept requires the use of a solar concentrator, the most commonly applied are solutions available on the market. Fernandez-Garcia et al. [11] proposed the division of concentrators into two

main groups: systems that focus the Sun's rays on a single line or point. Usually for systems with a pyrolytic reactor linear concentrators are used, because they allow continuous, flow processing of larger portions of biomass. Linear concentrators are divided into flat mirror systems and so-called parabolic troughs. Parabolic curvature is the most common curvature of concentrating mirrors. That is because the parabola is a mathematical

curve that ensures focusing of rays incident parallel to the symmetry axis of the mirror, at one determined point. Due to the large distance Earth end Sun, it can be assumed that after orienting the mirror towards the Sun, the rays fall parallel to its axis.

The phenomenon of focus is governed by optics law: the angle of incidence is equal to the angle of reflection. Parabola is not the only mathematical curve with the ability to concentrate rays. Generally, different second order curves have such properties. For example, the spherical mirror focuses the rays falling parallel to its axis of symmetry on this axis; the ellipse concentrates rays emitted in one of its focal points, always in the second. However, for solar radiation concentrating applications, a parabola is the most often chosen curvature.

2.4. Laboratory rig conception

Also in the literature there are descriptions of research on solar pyrolysis of biomass carried out with an assumption of use of parabolic concentrators [10,11]. Hereby presented numerical works relate

to experimental tests at a laboratory rig, in which a heat flux is supplied to the pyrolysis reactor within previously focused light beam. In the presented research, the rig concept assumes that the pyrolysis reactor will be a copper pipe, which outer surface is insulated, except for the place to which the focused light beam of the xenon lamp is directed. The pellet being the biomass deposit is flowed by a stream of nitrogen to provide an inert atmosphere for the process and receive gaseous pyrolysis products. Over time, a copper gauze was added to the reactor concept, to keep the biomass feedstock is its original position during the process. The feedstock has been also enlarged, to not only a single pellet, but a set of pellets. The reactor's diagram is shown in Fig. 2.1.
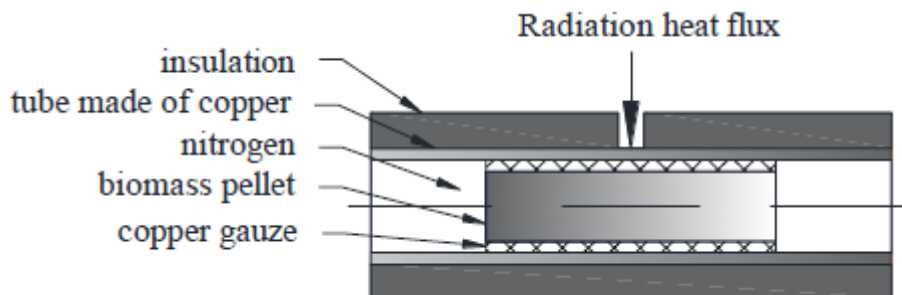
Fig. 2.1. Idea of pyrolytic reactor

The diagram shows an axisymmetric cross-section of the reactor. In the drawing, and later in the numerical model, it was assumed that the heat flux is supplied to the reactor through the surface around the circumference of the copper pipe. In a real experimental rig, it would not be a ring-shaped surface, but one selected place. The assumption of the axial symmetry greatly simplifies the reactor modeling.

3. Modeling phenomena of solar pyrolysis

In the process of solar pyrolysis of biomass there are many very complex phenomena: radiation from the source to the pyrolysis reactor, thermal decomposition of the bed in the reactor, gas flow inside the reactor (nitrogen, gas products), drying and heating of biomass, shrinkage of the deposit, changes of physical properties of all elements due to changes in temperature, structure and chemical composition. It is practically impossible to include all these phenomena in one model.

3.1. Focusing radiation

One of the first analyses carried out concerned the phenomenon of concentrating solar rays on the external surface of a pyrolysis reactor. Although laboratory tests do not include any focusing system (already focused artificial light is assumed to be used), however, an analysis of the mirror's ability for concentrating sunrays was performed.

The motivation for such studies was as follows: the basis of the parabola's ability to focus sunrays is the condition that these rays must fall parallel to the symmetry axis of the mirror. But in fact the rays of the Sun while passing through the atmosphere undergo partial scattering. Cloud cover, dustiness, humidity cause that in Poland the dispersed part if radiation states averagely in the year 48% [12].

Scattering is an absorption of a portion of energy by a molecule and its immediate emission in random direction. This means that the surface of the parabolic concentrator (even assuming its exact orientation towards the Sun) fall also rays from different, random direction and only part of the radiation falls parallel to the mirror axis of symmetry. So the question was posed: is a parabola the best solution for concentrating solar rays in conditions, when part of the radiation is dispersed? For this purpose, a parametric analysis was carried out, in which mirrors with different curves were examined.

3.2. Modeling of radiation focusing

The basic assumption adopted in the model of the solar concentrator mirrors was setting the mirror perfectly towards the Sun. It was also assumed that the essence of the research will be the curvature itself, thus the model was made as flat, two-dimensional. The influence of radiation properties of all elements of the system was also neglected, so it was assumed that the examined mirror is characterized by a reflexivity equal to 1 and that air is completely transparent to radiation. In addition, in order to simplify the evaluation of the calculations accuracy it was defined that the only source of radiation in the model is the Sun, therefore the temperature of all elements in the computational domain and beyond it is equal to 0 K. The analysis was carried out for two cases: 1) assuming that the Sun's rays fall completely directly, thus adopting the value of radiation intensity 1000 W/m^2 and 2) that a half of the radiation is scattered, thus defining the values of irradiation: direct 500 W/m^2 and diffuse 500 W/m^2. The geometry of the model is presented in Figure 3.1. The most important element is the **mirror**. Other surfaces represent openings in the domain (**pressure outlet**) or form a surface serving for definition of solar radiation intensity (**radiation window**).
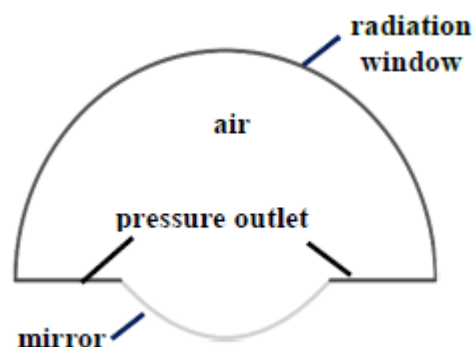
Fig. 3.1. Geometry of concentrating mirror model

Parametric analysis assumed the study on many different mirror curvatures under the same conditions. A parabola of the equation $y = 0.5x^2$ was chosen as basic curvature. The mirror width is limited by location of the focus of this parabola, so that the geometrical dimensions of the model were defined in accordance with Fig. 3.2. Parabola was described by 9 points, from which the top and ends were fixed and the remaining 6 were 3 pairs of symmetrical points. Then, in order to obtain different curves, the position of 3 pairs of points was modified by adding or subtracting the assumed value (1 cm) to their vertical position, keeping the horizontal position unchanged. Thus 3 possibilities of positioning 3 pairs of points were obtained which gave $3^3 = 27$ different curvatures of mirrors, including primary parabola.
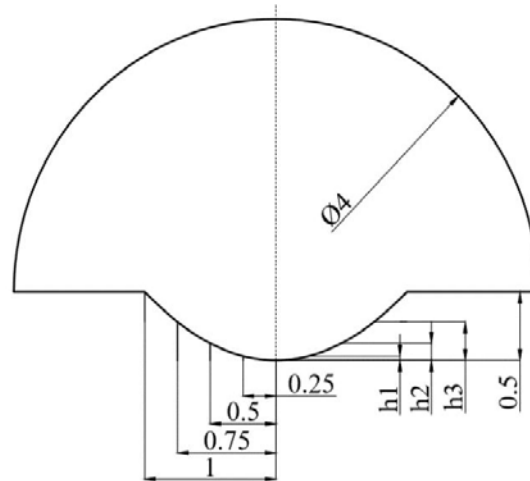
Fig. 3.2. Geometrical dimension of computational domain (given in meters)

As a result of calculations characterizing the mirror ability to concentrate solar radiation the maximum value of radiation intensity in the domain was chosen. The results are shown in the graph in Fig. 3.3. The shape of the obtained radiation intensity distributions was also evaluated. As the intensities observed in the distributions took values from a very wide range, distributions were studied assuming different color scales, for two reasons: firstly, by adopting one color scale, in some cases, the distributions would be almost uniform, without clear fields with increased radiation intensity; and secondly, the essence of the studying the distributions is the analysis of the shape and position of fields with maximum values, while, numerical data on maximum values are presented in the graph (Fig.3.3). The minimum value in the distributions results from the assumed intensity of solar radiation (1000 W/m^2). Examples of distributions for selected cases are shown in Fig. 3.4.
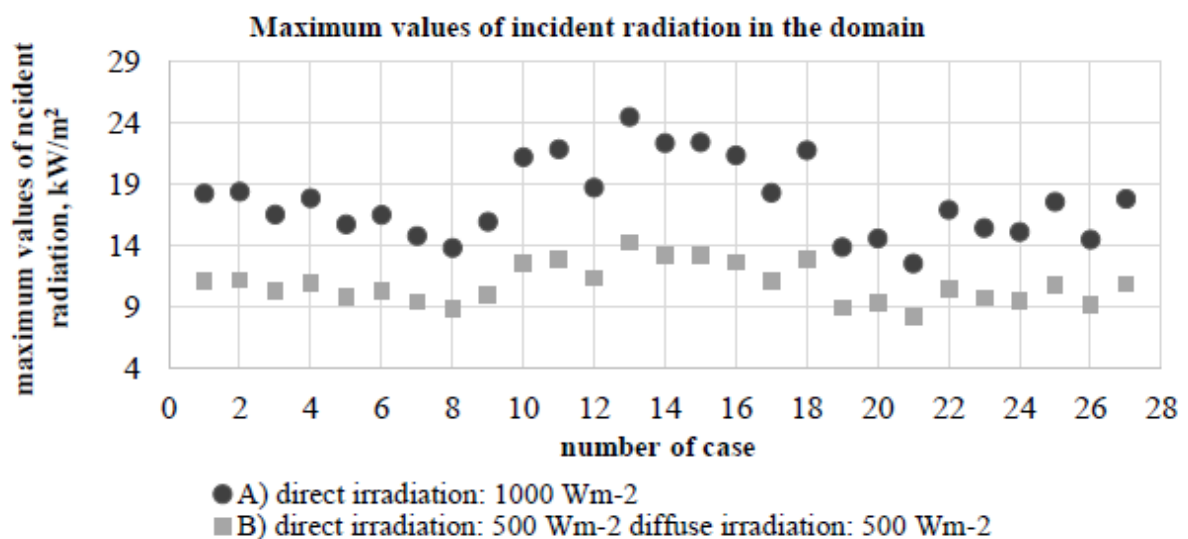
Fig. 3.3. Maximum values of incident radiation
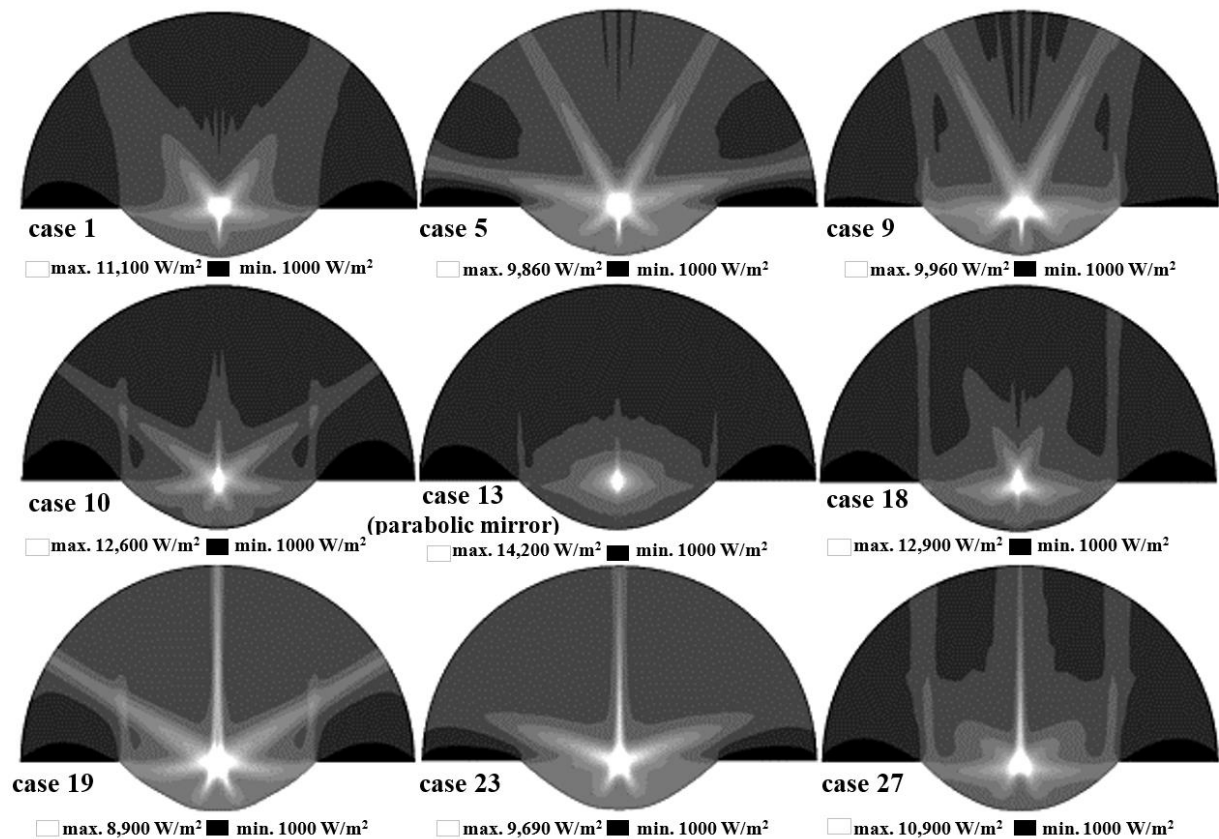
Fig. 3.4. Distribution of incident radiation for selected cases for irradiation direct: 500 W/m^2, diffuse: 500 W/m^2

The analysis revealed some interesting facts. Changes in the position of specific points in the mirror curvature caused similar changes in the distribution of radiation intensity. Of the 27 cases analyzed each subsequent 9 was a group with a similar distribution of radiation intensity and in every 9, every subsequent 3 showed even greater similarity. In addition, some curves ensured the occurrence of up to two areas with the highest intensity of radiation, which can be seen for example in Fig.3.4. case 19, 23, 27.

3.3. Thermal decomposition of biomass feedstock

Modeling of solar concentration provides very interesting results, however, the essence of the biomass pyrolysis process is a thermal decomposition of the feedstock in the reactor. So that the process could occur it is necessary to heat up the biomass to a certain temperature. It was assumed that these experiments will be conducted at temperatures above 400 °C. The most important parameters that affect the reactor heating, among occurring of endothermic reactions in a decomposing bed, is thermal power supplied to the reactor and the nitrogen flow rate, which provides an inert atmosphere, but also cools down the feedstock. The selection of appropriate thermal power and nitrogen flow rate is very important from the point of view of designing the laboratory rig.

In turn, the biomass distribution inside the reactor is a phenomenon so complex, that it is impossible to reflect it strictly in the numerical model. Therefore, a series of simplifications is commonly used, of which the most important consider chemical reactions.

Most often a complicated sequence of chemical reactions: endothermic decomposition reactions, reaction between products and exothermic reactions of tar cracking into the gas, are simplified by an equation, assuming that during the pyrolysis process occurs only one reaction (one or several). It is assumed that a substance called "biomass" transforms into substances named "tar", "gas" and "char". Sometimes biomass is divided into lignin, cellulose and hemicelluloses and for each of them the equation is written separately. The key to properly model pyrolysis is to introduce appropriate kinetic parameters and stoichiometric coefficients

into the reaction equation. Only taking into account chemical reactions, it is possible to simulate the actual reactor heating process and hence, take appropriate design assumptions for the laboratory rig.

3.4. Modelling reactor heating

First, the process of heating the pyrolysis reactor was analyzed. The most important model assumptions concerned the properties of the reactor and the biomass deposit. It was assumed that the reactor will be a copper pipe with a diameter of 10 mm, a wall thickness of 1 mm and a length of 45 mm. With the exception for the surface through which a heat flux enters the reactor, the external surface of the reactor is insulated with commercially available material. The biomass deposit is a single pellet, defined in the model as a porous medium composed of wood and nitrogen. Detailed assumptions of the analysis can be found in the paper [7].

The analysis checked how the reactor heating process was influenced by assumed values of the heat flux supplied to the reactor wall and values of the nitrogen flow rate. Analyzed values of nitrogen flow rate were $N_{min}=0.05l/min$ and $N_{max}=1l/min$, and adopted values of heat flux were $P_{min}=10W$ and $P_{max}=16.7W$. The results of calculations of the biomass feedstock average temperature over time are shown in Fig. 3.5.
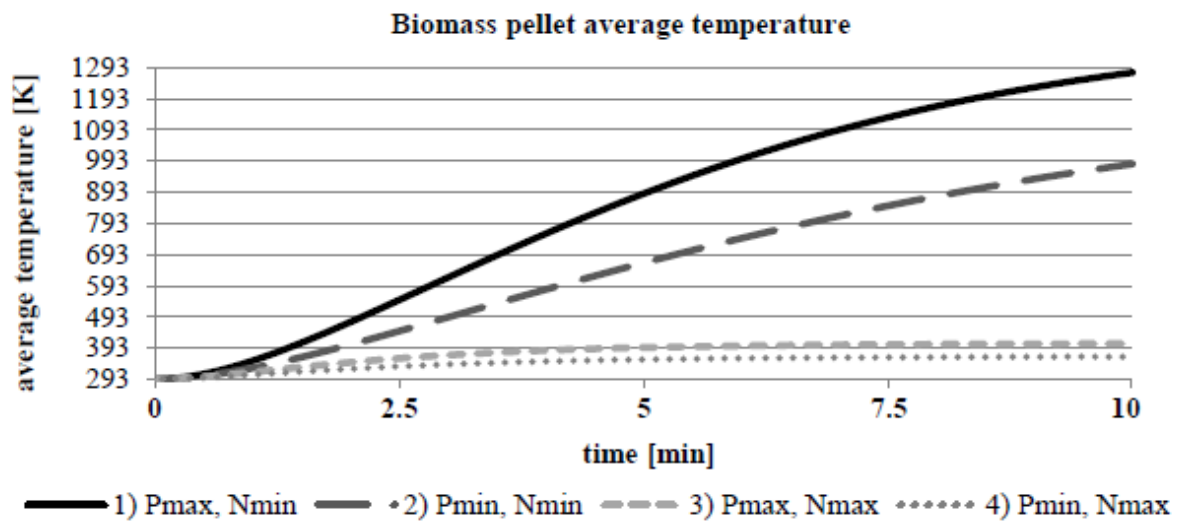
Fig. 3.5. Average pellet temperature for different values of provided heat flux and nitrogen flow rate

The analysis showed that for a larger value of the nitrogen flow rate the biomass deposit reaches an average temperature not higher than 120 ° C. This excludes the pyrolysis process.

3.5. Modelling thermal decomposition of biomass

In the next stage of research, the model was supplemented with new assumptions regarding the pyrolysis reactor construction and an initial chemical reaction model has been introduced. The most important change in the assumptions of the model is the significant enlargement of the biomass deposit to several pellets, so that the total length of the bed was 20 cm. Value of nitrogen flow rate has been kept equal to 0.15 l/min. In addition, the pellets were placed in a copper gauze, defined as a porous medium consisting of copper (70%) and nitrogen (30%).

The applied reaction model is a global kinetic model that captures biomass distribution according to the scheme [13]:
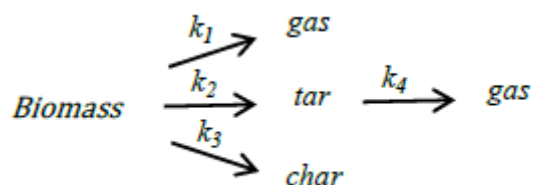
Where,

k_{1-4} rate coefficients, 1/s

Based on experimentally obtained data: frequency factors, activation energies and reaction heats, the rate coefficients can be calculated according to Arrhenius scheme:

$$k_i = A_i e^{Ei/RT}$$

Where,

A_i frequency factor (pre-exponential factor) characteristic for given reaction, 1/s

E_i activation energy, J/mol

R universal gas constant, R=8.3144 J/(mol·K)

T temperature, K

Followingly a specific heat flow rate of the reaction, J/(kg·s), can be calculated with the formula:

$$\dot{q} = \Delta h_i A_i e^{-Ei/RT}$$

Where,

Δh_i reaction heat, J/kg

As at this stage of the work, the TGA analysis of considered types of biomass are not available, the literature data were adopted for an initial simulation. This analysis uses kinetic parameters from the work of Gronil et al. [13]. The reaction model was introduced to the reactor model using the user-defined function UDF. In this way, based on the above calculations it is possible to obtain the amount of heat absorbed by the bed in the endothermic decomposition, taking into account the part of the heat produced in the reaction of tar cracking.

Such supplementation of simulations finally allows determining final temperature of the deposit. Fig. 3.6 presents the results of calculations of the average deposit temperature for selected values of the heat flux supplied to the reactor.
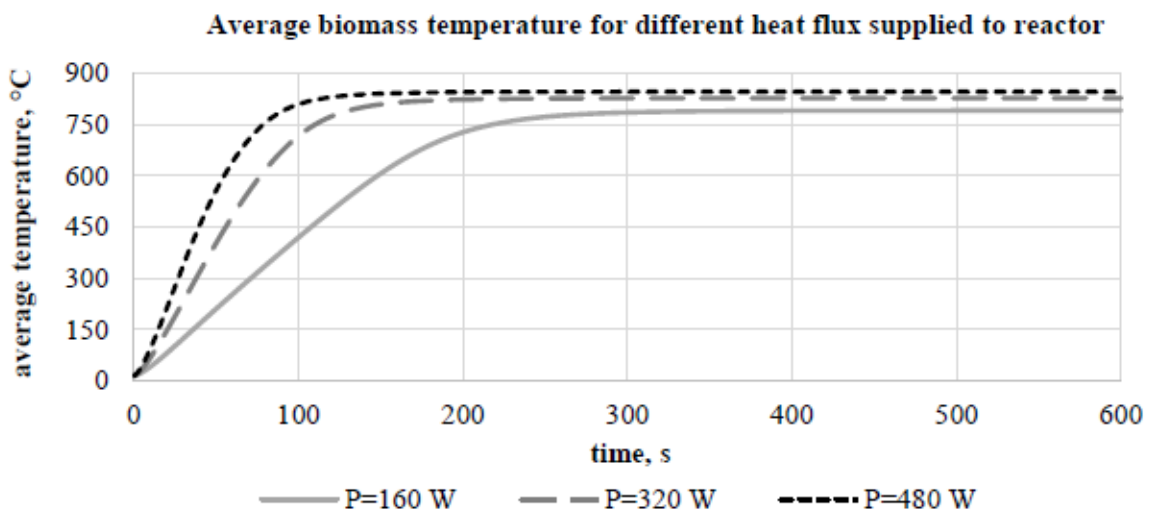
Fig. 3.6. Average biomass feedstock temperature for different values of provided heat flux

The analysis showed that providing a greater heat flux the temperature of the bed doesn't reach higher levels than for smaller heat fluxes. This is caused by the decomposition reactions, which take place more intensively under a larger heat flux, so they absorb more heat, which balances the increased heat flux supplied to the reactor.

4. Conclusions

The paper presents numerical studies of various aspects of the solar biomass pyrolysis process. The analyses are the components of the final model captivating phenomena occurring inside the pyrolysis reactor (reactor heating, thermal decomposition) or they can state a basis for future incorporating the radiation phenomenon from the light source to the reactor (radiation focusing).

Analyses show clear differences in simulation results with and without taking into account chemical reactions occurring during pyrolysis. This indicates an urgent need for the development of the model with further phenomena taking place in the reactor.

Numerical analyses have enabled the selection of appropriate ranges of values of the most important reactor operation parameters, necessary to design the final form of the laboratory rig.

The next step in numerical research is 1) updating the model with final assumptions regarding the construction of the reactor 2) implementing kinetic data related precisely to selected types of biomass 3) taking into account the changes in the state of the deposit during the process (loss of mass, change in porosity).

Acknowledgment

References

[1] M. Jakubiak, W. Kordylewski, Toryfikacja biomasy (ang. Biomass torrefaction), Arch. Spalania. 10 (2010) 11–25.

[2] J. Zuwała, M. Kopczyński, J. Robak, Ocena efektywnoœci techniczno-ekonomicznej sprężonego układu toryfikacja – peletyzacja – współspalanie biomasy, ENERGY POLICY J. 17 (2014) 147–158.

[3] D. Kardaś, J. Kluska, M. Klein, P. Kazimierski, Ł. Heda, Modelowe kompleksy agroenergetyczne: Teoretyczne i eksperymentalne aspekty pirolizy drewna i odpadów, Wydawnictwo UWM, Olsztyn, 2014.

[4] S. Stelmach, R. Wasielewski, J. Figa, Zgazowanie biomasy – przykłady nowych technologii, Arch. Waste Manag. Environ. Prot. 7 (2008) 9–20.

[5] P. McKendry, Energy production from biomass (part 2): conversion technologies, Bioresour. Technol. 83 (2002) 47–54.

[6] N.L. Panwar, R. Kothari, V. V. Tyagi, Thermo-chemical conversion of biomass - Eco friendly energy routes, Renew. Sustain. Energy Rev. 16 (2012) 1801–1816. doi:10.1016/j.rser.2012.01.024.

[7] Z. Kaczor, Z. Buliński, S. Werle, Preliminary study on computational modelling of slow solar pyrolysis of biomass, EPAE 2017 Conf. Mater. (2018) 161–171. doi:ISBN 978-83-950087-1-9.

[8] A. Anca-Couce, Reaction mechanisms and multi-scale modelling of lignocellulosic biomass pyrolysis, Prog. Energy Combust. Sci. 53 (2016) 41–79. doi:10.1016/j.pecs.2015.10.002.

[9] Ł. Szymański, B. Grabowska, K. Kaczmarska, Ż. Kurleto, Celuloza i jej pochodne – zastosowanie w przemyśle, Archvies Foundry Eng. 15 (2015) 129–132. http://www.afe.polsl.pl/index.php/pl/4323/celuloza-i-jej-pochodne-zastosowanie-w-przemysle.pdf.

[10] J. Soria, K. Zeng, D. Asensio, D. Gauthier, G. Flamant, G. Mazza, Comprehensive CFD modelling of solar fast pyrolysis of beech wood pellets, Fuel Process. Technol. 158 (2017) 226–237. doi:10.1016/j.fuproc.2017.01.006.

[11] M. Bashir, X. Yu, M. Hassan, Y. Makkawi, Modeling and Performance Analysis of Biomass Fast Pyrolysis In a Solar-Thermal Reactor, ACS Sustain. Chem. Eng. 5 (2017) 3795–3807.doi:10.1021/acssuschemeng.6b02806.

[12] W. Gogół, Konwersja termiczna energii promieniowania słonecznego w warunkach krajowych, Oficyna Wydawnicza Politechniki Warszawskiej, Warsaw, Poland, 1993.

[13] M.G. Grønli, M.C. Melaaen, Mathematical model for wood pyrolysis - Comparison of experimental measurements with model predictions, Energy & Fuels. 14 (2000) 791–800. doi:10.1021/ef990176q.

A Review of Waste to Energy Technologies

Shahmir Ali Nosherwani[1], Saifullah Nausherwani[2]

[1]*Faculty of Energy and Environmental Engineering, Silesian University of Technology,*

E-mail:shahmir.nosherwani@gmail.com

[2]*National University of Science and Technology, Karachi, Pakistan,*

Email: saifullah_23@hotmail.com

Abstract

Globalization is a key driver for rapid technological development and the already growing world population has resulted in an unprecedented increase in the amounts of Waste. Apart from that, it has increased energy demand which has further lead to environmental pollution or power outages. Clean Energy and Environment play a key role for the development of any nation. Hence, Waste-to-Energy (WtE) is seen as a viable option to fill the ever increasing energy gap with sustainable and clean energy. The current WTE options and how to get a benefit towards a more environmentally sustainable technology are discussed in this review along with their pros and cons.

Keywords: Waste to energy technologies, incineration, pyrolysis, plasma technology, anaerobic digestion, biogas, landfill technique

1. Introduction

The increase in population over the years have increased the amount of waste generated and made it an important issue for the urban world, especially in developing countries, where economic development and expansion have significantly increased the generation of waste. In recent years, proper waste management and generation of electricity from waste is gaining attention around the world.

Waste management refers to collection, transport, disposal and monitoring of waste materials. The harmless disposal of waste is important to reduce the burden on fossil fuels and to develop environment-friendly society, reduce pollution, improve the living environment and level of ecological civilization, and achieve scientific urban development. One safe way of disposing waste is through generation of electricity and moreover, the plants not only reduce the amount of waste sent to landfills, but also simultaneously producing useful energy (heat and/or power). [2,3,5]

2. Methods for waste to energy conversion

The WtE technologies aims at safe disposal of waste along with extraction of energy, however it has economic and environmental constraints. Therefore, it is necessary to select the best technology available. Since Waste varies along with climate and culture, the energy can be recovered to produce heat or electricity through two widely used pathways depending on the waste composition and moisture content. Fig. 1 depicts the two MSW conversion pathways to energy and the processes involved, and Tab. 1 shows the calorific value of MSW waste in different countries that can be extracted for useful purposes.[1]
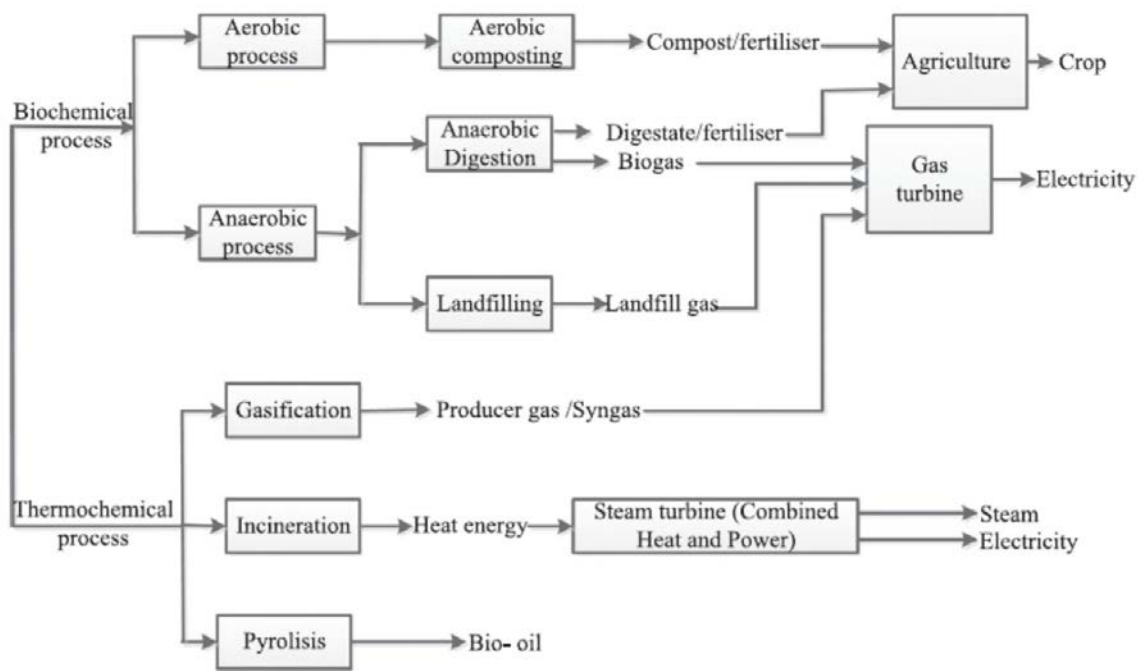
Fig. 1: Waste to Energy Technologies [6]

Tab. 1 :Calorificvalue of MSW in different countries [1]

Type of Countries	Countries	Calorific Value (kcal/kg)
Developing	Bangladesh	717
	China	1200-1600
	India	800-1100
	Malaysia	1500-2600
	Srilanka	950-1250
	Thailand	500-1500
Developed	Japan	2000-2200
	S. Korea	2600-3000
	UK	2200-3000

2.1. Incineration

The objective of incineration at the beginning was volume reduction and protecting the environment and ecosystem from the hazardous wastes, but with advances in the technology and right control measures for pollution, this process can also provide a means to extract the energy. Currently, it is an attractive waste treatment option due to both economical, legislature and environmental factors, especially in the developed countries (EU, US and Japan) and has resulted in reduction of waste disposal using landfilling.

Normally, Incineration is used for a variety of waste but usually it is utilized for less dense wastes with high percentage of organic non-biodegradable matter and low moisture content that subsequently reduces mass and volume can be reduced by 70% and 90% respectively. The waste, received is a mixture consisting of organic

substances, minerals, metals and moisture, which is combusted in an excess supply of air (1.2 to 2.5) leading to the production of hot flue gas having a temperature range of 800 -1000 °C. The hot flue gases are used in a high pressure feed-water boiler to produce steam that can be used to produce electricity from a steam turbine or for heating purposes (district heating) both heat and power (CHP). The process flow for incineration plant is shown in Fig. 2.Incineration technology have a net electrical efficiency of around 23–40%. [1, 6, 7]

Although incineration is considered successful in both developed and developing countries, the oxidizing process in incinerators are not always perfect and results in emissions which have serious impacts on environmental. The major components of flue gas from an incinerator are water vapour, nitrogen,carbon dioxide and oxygen and depending on the type of the waste combusted and operating conditions of the incinerator, small amounts of carbon monoxide, halogenated gases, oxides of nitrogen, oxides of sulphur, volatile organic compounds, furans, dioxins and heavy metal compounds are found in the flue gas too. [6, 7]
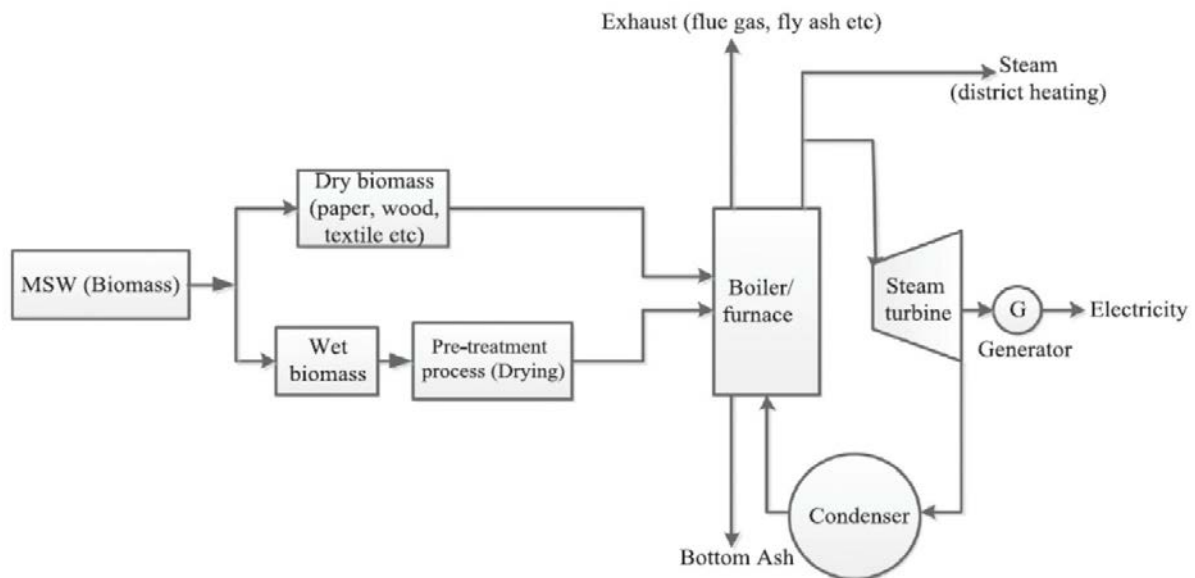
Fig. 2: Incineration of Waste [6]

2.2. Gasification

Gasification is a thermal conversion method to produce syngas. Waste is reacted with gasifying agent (air, oxygen or oxygen and steam) at 500-1800 °C or higher (endothermic process) in a controlled environment to produce combustible gases. The syngas can be used to produce heat or power or both heat and power. Furthermore, it can also be used for chemical processing. Process of gasification in generation electricity and heat from waste in shown in Fig.3.

The syngas produced is made up of flammable gases (CO, H2, CH4, small amounts of higher hydrocarbons), CO2, moisture, N2 if air is used, various contaminants such assmall carbon particles, ash and tars. However, the syngas composition and calorific value is depended on the conditions, type of waste and type of gasifying agent. Tab. 2 shows the effect of gasifting agent on syngas. Gasification with Air produces low heating value gas while with oxygen, it produces medium heating value gas.The gasification process always leads to decrement of energy - calorific value of gas received is lower than the calorific value of the fuel (waste). However if the next process after gasification is combustion of product gas this is much easier to carry out with higher energy efficiency and emission of pollutions is lower than from combustion of waste.

The emission and pollutants from Gasifier have both solid, liquid and water waste. This includes Ash,char, particulate matter, tars, nitrogen and Sulphur oxides, HCl, dioxins and furans, hydrocarbons, and carbon monoxide. Different methods can be applied to control the pollutants. Furthermore, the low level of oxygen in gasifier inhibits the production of dioxins and furans.
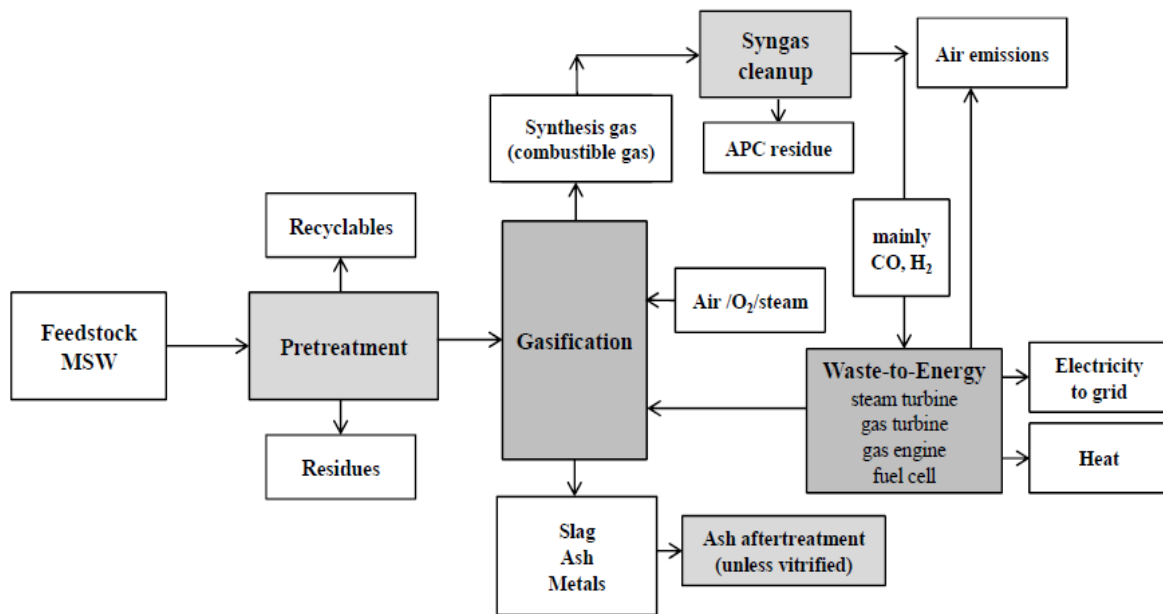
Fig. 3: Gasification of Waste [11]

Tab. 2:Gasificationprocess using different gasifying agents [9]

Process	Gasification agent	Producer gas heating value (MJ/Nm^3)
Direct Gasification	Air	4-7
Pure Oxygen Gasification	Oxygen	10-12
Indirect Gasification	Steam	15-20

2.3. Pyrolysis

Pyrolysis is a thermal conversion process of degradation of chemical particles under the influence of a sufficiently high temperature in anaerobic environment (or trace amounts of oxygen). Pyrolysis is the thermal conversion of fuel in a closed system, so there are no external supply of additional substrates (especially oxygen). It is also referred as thermal distillation and thermal de-polymerization. The main advantage of pyrolysis is that It can convert waste that are of no value or difficult to recycle into fuels, or other valuable products that can be further processed.

The products of waste pyrolysis include pyrolysis gas, oil and char including methane, hydrogen, carbon monoxide, and carbon dioxide. The conversion of waste to electricity and heat using pyrolysis is shown in Fig. 4. Depending on the thermal environment, residence time, temperature, type and size of waste, and reactor, composition of pyrolysis varies. However, pyrolysis yields mainly oil, wax andchar at low temperatures, less than 500 -550 ℃, when the heating rate is quite slow, and mainly gases at high temperatures, greater than 700 ℃, with rapid heating rates. Moreover, for good quality products, specific type of waste should be used.

The target contaminant groups for pyrolysis include volatile organic compounds (VOCs), including HCl, SOx, NOx, furans, dioxins, and PAHs. Although, it is expected to reduce emissions by retaining metals, Sulphur and chlorine within the process solid and liquid residues, prevent formation of dioxins, furans and NOx due to low temperatures and less availability of oxygenHCl and SOx may be found in gas yield. [11,17]
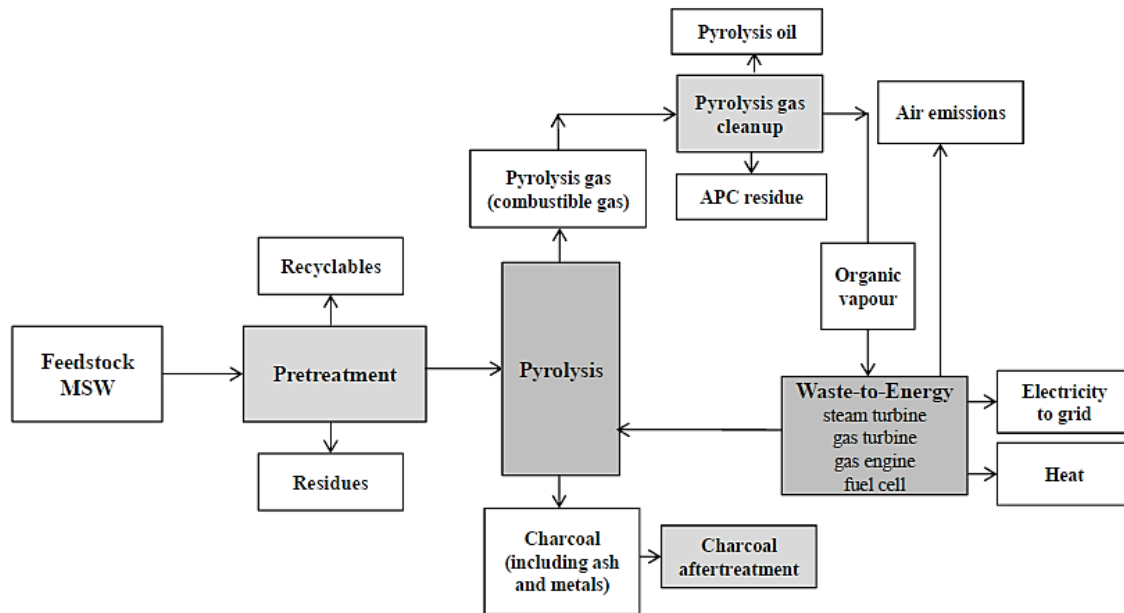
Fig. 4: Pyrolysis of Waste [7]

2.4. Plasma Technology

Plasma, also known as the fourth state of matter, uses high energy collision gaseous species with electrons results in its generation which behave significantly from other states of matter. Thermal energy, electric current or electromagnetic radiations can be used to create plasma. Depending upon the type of energy source and conditions, high temperature (fusion) plasma and low temperature (gas discharge) plasma is generated. The low temperature can be further divided into cold plasma and thermal plasma. The application of plasma technology in WtE systems is a relatively new, but it generates valuable products like syngas, hydrogen and electricity.

Plasma pyrolysis, plasma gasification, plasma compaction and vitrification of solidwastes, and combinations of the three already mentioned, are the technologies available for waste to energy conversion, but selection of plasma technology is highly depended on the type of waste.It can convert highly organic waste with high calorific value to syngas, highly halogenated waste streams to less toxic ones and inorganic solid material into non-leaching slag through melting.[7, 8, 11, 16]

2.5. Anaerobicdigestion

Anaerobic digestion is a bio-chemical process in which series of biological processes containing bacteria decompose the organic part of the waste in the absence of oxygen. This process leads to production of biogas composing of 50– 75% CH_4, 25–50% CO_2 and 1–15% of other gases (such as water vapor, NH_3, H_2S, etc.) and remaining solid-liquid residue that can be used as a fertilizer or converted into other products. The composition of biogas as shown in Tab. 3 and the content of digestate depends on the type of the waste. Biogas produced can be combusted to generate electricity and heat, or can be processed into biofuel. However, due to presence of undesirable components in the digestate, its use as a fertilizer has been prohibited by European Legislation.

In anaerobic conversion, the digestion of organic material into methane takes places in stages as shown in Fig.5. It begins with hydrolysis of complex waste compounds into simple and soluble compounds like sugar. This is followed by fermentation under anaerobic conditions leading to formation of simple organic acids, carbon dioxide and hydrogen. Finally the methanogenesis takes place in which methane is produced by reaction of carbon dioxide with hydrogen. Anaerobic process has net positive impact on environment by being a closed process in which means the gases are trapped and hence greenhouse emissions are controlled, and compact design which requires less land and can be done on small scale. [1,6]

Tab. 3 : Composition of Biogas [6]

Constituent	Composition (%)
Methane	55-75
Carbon Dioxide	30-45
Hydrogen Sulphide	1-2
Nitrogen	0-1
Hydrogen	0-1
Carbon Monoxide	Traces
Oxygen	Traces
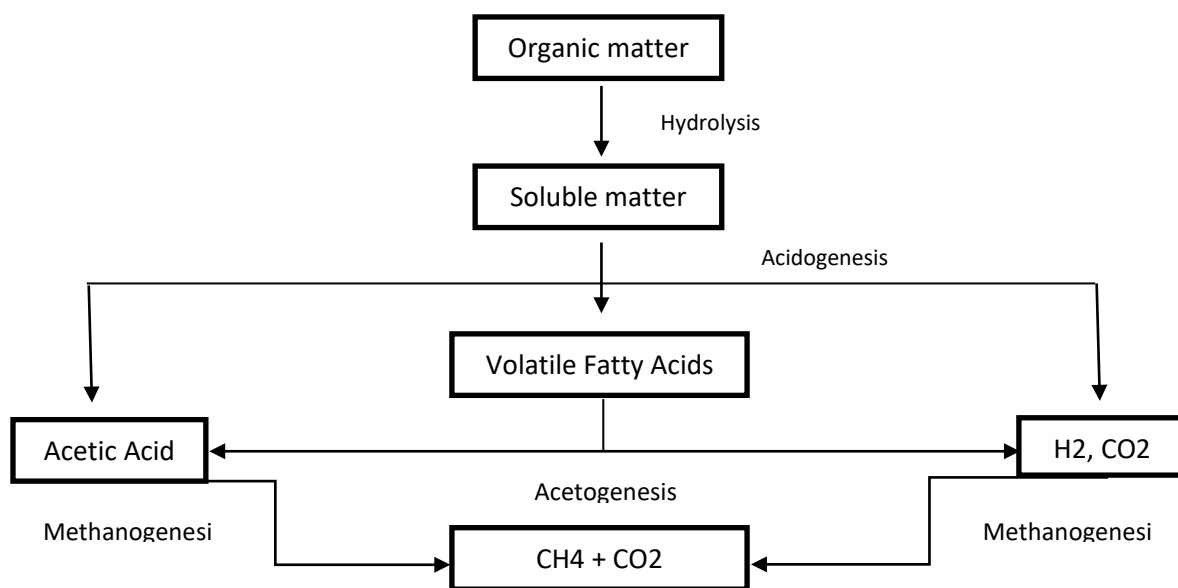
Fig. 5: Conversion of waste to biogas [1]

2.6. Landfill Gas

Waste disposal in unsanitary landfills have an adverse and everlasting effect on environment. Some problems such as water pollution through leachate, uncontrolled combustion and greenhouse gas emissions due to production of methane, unpleasant odor and causing asphyxiation. Although it is a simple and affordable method for waste disposal in developing countries, it is the worst option and poses a threat to environment. If this process is controlled under sanitary conditions, this can reduce the impact on environment by trapping the biogas and leachate management. LFG generated is extracted from the landfill and can either be flared or can be utilized in generating power in gas turbine, biofuel for vehicle or for further chemical processing.

Tab. 4 : Composition of Landfill Gas [6]

Constituent	Average Composition (%)
Methane	50
Carbon Dioxide	45
Hydrogen Sulphide	5
Nitrogen	<1

Non-methane organic compounds	2700 ppmv

Waste disposed in landfills is decomposed by undergoing bio-chemical reactions. The decomposition of organic part of waste generates Landfill gas (LFG). The conversion of waste takes place aerobically producing carbon dioxide till oxygen is consumed from the system. Then reactions proceed anaerobically resulting in generation of methane (around 55%) and carbon dioxide (around 45%) with trace amounts of volatile organic compounds, ammonia and hydrogen sulphide. The chemical composition of typical landfill gas is shown in Tab. 4 .Landfill gas is produced both under both aerobic and anaerobic conditions. Aerobic conditions are short-lived during the initial stage of waste conversion as a result of entrapped atmospheric air. The initial aerobic phase is short-lived and produces a gas mostly composed of carbon dioxide. Since oxygen is rapidly depleted, a long-term degradation continues under anaerobic conditions, thus producing a gas with a significant energy value that is typically 55% methane and 45% carbon dioxide with traces of a number of volatile organic compounds. Since it is naturally occurring phenomena, most of the methane is generated within 20 years while emissions from waste continues for 50 years or more. A typical landfill site with methane recovery is shown in Fig.6.[1, 6, 13]
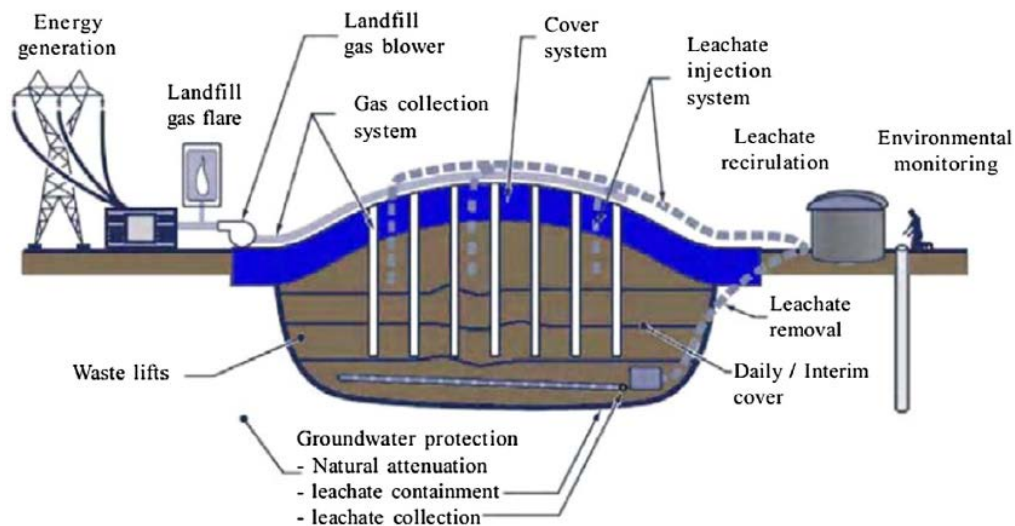
Fig. 6: Landfillsite with methane recovery [1]

3. Discussions

A major challenge and success of WtE technology depends on the efficiency, technical, environmental and economic feasibility. The analysis of different WtE technologies as shown in Tab. 5 taken from previously published articles. The capital costs is the investment in building up a project which includes purchasing/renting of land and equipment and supply of raw material, while operating costs includes maintenance and labor costs. There is range of costs which is highly depend upon the location of country, government policies and availability of raw material and labor. However, the lower value represents a developing country while higher value represents a developed country. In the following, a comparison is made between different WtE technologies but a real comparison requires in detailed life cycle assessment of each technology.

The incineration technology is most widely re-known and used commercially to combust for energy production in the form of heat, electricity or both. This is due to lower annual capital and operational costs as depicted in Tab. 5, less complex technology making it easier to operate, high efficiency, quick process, dealing with different types of waste and reducing volume by approximately 80 % and mass by approximately 70% of waste. However, it produces pollutants in both solid (highly leachable fly ash and bottom ash) and gaseous (NOx, SOx and formation of halogenated hydrocarbons). Hence requiring air pollution control devices (fabric filters, desulfurization, NOx abatement, activated carbon injection, etc.) and immobilization of solid waste to make it environmentally safe for landfill disposal.

Gasification technology is widely used in Japan, where 85 plants were operating till 2007 and around 100 plants globally, which is relatively a low number of plants worldwide that are operating commercially. Similarly, a number of *pyrolysis* projects exist in Europe and Japan. Gasification/pyrolysis has certain advantages over incineration due to less greenhouse emissions(meeting existing emissions limits) , reducing waste volumes by 95%, less energy required in flue gas cleaning and modern gasification units come with enclosures, which effectively reduce the chance of water and soil contamination. However, technical and economic issues, mainlyrelated to the heterogeneity of wastes (suiTab. for homogeneous wastes like used tyres, paper, electrical waste),power efficiency of plants and syngas cleaning systems, high operating and capital costs compared to incinerationplants as a result of ash melting in gasifiers or treatment of water waste or solid waste in pyrolysis or complexity of the plant as depicted in Tab. 5, are a hurdle for gasification/pyrolysis technologies to be established commercially worldwide.

Tab. 5: Economical and environmental factor comparison of WtE technologies [1,14]

Type of Technology	Type of waste	Capital cost (US$/tonne of Waste/Year)	Operational cost (US$/tonne of Waste/Year)	Global Warming potential (kg CO2 equivalent per unit MWh electricity generation)	Complexity of technology	Labor skill level
Incineration	General	400-700	40-70	424	Low	Low
Pyrolysis	Homogenous	400-700	50-80	412	High	Intermediate
Gasification	Homogenous	250-850	45-85	412	High	Intermediate
Anaerobic digestion	Organic	50-350	5-35	222	Low	Low
Landfilling with gas recovery	Inert	10-30	1-3	746 (if gases are not recovered)	Low	Low

Plasma technologies are relatively new compared to existing WtE technologies. Plasma processes uses electricity as a source of primary energy than thermal energy which makes the waste conversion process faster and providing system flexibility. It is gaining acceptance due to its positive impact on environment by avoiding landfill and lower emissions compared to conventional combustion technology. The solid residues, inorganic compounds and fly ash can be captured and vitrified to form non leaching slag (volume typically more than 5:1 for ash and more than 50:1 for solid waste) that can be used for making tiles or bricks. Moreover, the gases produced can be used to generate electricity and/or heat or for other chemical processes. Plasma technologies offer a sustainable way to treat waste and continued advances are being made as a viable alternative to conventional combustion. However, they use electricity as a source of energy which makes them expensive and pose an economic issue. Furthermore, there are a limited amount of data or literature which makes it difficult to compare plasma technologies with conventional waste to energy technologies.

Comparing to incineration and other thermal conversion technologies, anaerobic digestion process has the lowest capital and operating costs as shown in Tab. . The closed system makes it compact and promotes the use of this technology at small scale in rural areas. . Anaerobic digestion offers a lot of advantages as it is renewable source of energy producing small amount of solid (which can be used as a fertilizer), reduction of odors and production of important fuel known as biogas. Production of biogas from anaerobic digestion is faster as it is reported that it can produce 2-4 times more in 3 weeks than of landfill gas technique in 6-7 years. However, It has certain

disadvantages; It is suiTab. for organic waste only hence requiring waste segregation, Waste treatment is slower compared to thermal conversion (typically 20-40 of bacterial reactions), The plant has higher space requirements and finally, It is sensitive to process parameters like increase in ammonia and salt concentrations can stop the methanogensis process due to presence of nitrogen rich compounds and cations (such as sodium, potassium and calcium).

Landfill is mostly favorable in some developing countries because it is the least expensive process as shown in Tab. 5. Biogas produced can have variety of applications, skilled labor is not required, returning of natural resources to soil and conversion of marshy lands into useful areas. However, It has a lot of disadvantages apart from being a very slow process, requiring high costs for transporting waste and using a large land area, it adversely impacts environment as it risk the contamination of ground water or water streams nearby by leachate, highest greenhouse emissions (as methane has 21 times more global warming potential than CO2) and possible fires/explosion due to production of methane (if not trapped and used/flared). However, Landfill can be made environmentally friendly by using inert waste and using the biogas produced can used for different purposes.

Biogas produced can be stored and used for electricity and/or heat or biofuels in transport or transported using the already present nature gas infrastructure. Since it is a renewable source of energy, it can reduce the load on fossil fuels. For more commercial use, the quality of biogas can improved by removing carbon dioxide and other trace gases. Earlier, the process of anaerobic digestion was used for the treatment of different types of organic waste only, but it provides biogas which is economically and environmentally feasible making it a viable option for energy

4. Conclusion

This paper presents a review of different technologies that can be utilized to convert waste into useful energy. The ever increasing waste poses an environmental which can be solved using an economical, efficient and environmental favorable technology WtE technology is considered a renewable source of energy which not only decrease the dependence on fossil fuels and reduce greenhouse emissions but it also reduces the problems associated with uncontrolled landfill technique.

 An attempt is made to compare the current WtE technologies and after reviewing them the technologies can be used effectively depending upon the waste stream. For high organic waste (like food waste, animal manure) anaerobic is a suiTab. solutions, incineration for mixed waste, gasification and pyrolysis for homogenous waste (like tyres, wood or biomass waste) and landfilling for inert wastes. Lastly, Government policies and regulations, financial support and R&D programs across the globe can lead to develop and improve technologies like pyrolysis, gasification or plasma process in the future and pose a strong competitor to conventional incineration and landfillingtechniques.

References

[1] Atul Kumar, S.R. Samadder. A review on technological options of waste to energy for effective management of municipal solid waste,Waste Management 69 (2017) 407–422.

[2] Jun Dong , Yuanjun Tang , AngeNzihou, Yong Chi, ElsaWeiss-Hortala, MingjiangNi,Life cycle assessment of pyrolysis, gasification and incineration waste-to-energy technologies: Theoretical analysis and case study of commercial plants , Science of the Total Environment 626 (2018) 744–753.

[3] T.R. Ayodele, A.S.O. Ogunjuyigbe, M.A. Alao, Life cycle assessment of waste-to-energy (WtE) technologies for electricity generation using municipal solid waste in Nigeria, Applied Energy 201 (2017) 200–218

[4] JouniHavukainen , Mingxiu Zhan , Jun Dong , MiiaLiikanen , Ivan Deviatkin ,Xiaodong Li , Mika Horttanainen, Environmental impact assessment of municipal solid waste management incorporating mechanical treatment of waste and incineration in Hangzhou, China. Journal of Cleaner Production 141 (2017) 453-461.

[5] Zhao Xin-gang, JiangGui-wu,LiAng,LiYun, Technology,cost,and performanceofwaste-to-energy incineration industry in China, Renewableand Sustainable Energy Reviews 55(2016)115–130.

[6] A.S.O. Ogunjuyigbe, T.R. Ayodele, M.A. Alao, Electricity generation from municipal solid waste in some selected cities of Nigeria: An assessment of feasibility, potential and technologies.Renewable and Sustainable Energy Reviews 80 (2017) 149–162.

[7] A. Bosmans AND L. Helsen, ENERGY FROM WASTE: REVIEW OF THERMOCHEMICAL TECHNOLOGIES FOR REFUSE DERIVED FUEL (RDF) TREATMENT,Third International Symposium on Energy from Biomass and Waste, Venice 2010

[8] Umberto Arena, Process and technological aspects of municipal solid waste gasification. A review, Waste Management 32 (2012) 625–639.

[9] V. Belgiorno, G. De Feo, C. Della Rocca, R.M.A. Napoli, Energy from gasification of solid wastes, Waste Management 23 (2003) 1–15.

[10] Juan Daniel Martı´nez, NeusPuy, Ramo´n Murillo, Toma´ s Garcı´a, Marı´a Victoria Navarro , Ana Maria Mastral, Waste tyre pyrolysis–A review, Renewable and Sustainable Energy Reviews 23 (2013) 179–213.

[11] A. Bosmans, I. Vanderreydt, D. Geysen, L. Helsen, The crucial role of Waste-to-Energy technologies in enhanced landfill mining: a technology review, Journal of Cleaner Production 55 (2013) 10-23.

[12] Liqing Yang, Haojing Wang, Hongfei Wang, Dapeng Wang, Yue Wang, Solid waste plasma disposal plant, Journal of Electrostatics 69 (2011) 411-413.

[13] Montserrat Zamorano, Jorge Ignacio Pe´rez, Ignacio Aguilar Paves, Angel Ramos Ridao, Study of the energy potential of the biogas produced by an urban waste landfill in Southern Spain, Renewable and Sustainable Energy Reviews 11 (2007) 909–922

[14] Anwar Johari, Saeed Isa Ahmed, HaslendaHashim, Habib Alkali, Mat Ramli, Economic and environmental benefits of landfill gas from municipal solid waste in Malaysia, Renewable and Sustainable Energy Reviews 16 (2012) 2907– 2912.

[15] O.K.M. Ouda, S.A.Raza, A.S.Nizami, M.Rehan, R.Al-Waked, N.E.Korres, Waste to energy potential: A case study of Saudi Arabia, Renewable and Sustainable Energy Reviews 61 (2016) 328–340.

Utilization of Basic Acoustics in Measurements in Power and Heat Systems

Krzysztof Grzywnowicz[1]

[1]*M. Sc.: Institute of Power Engineering and Turbomachinery, Silesian University of Technology,e-mail:krzysztof.grzywnowicz@polsl.pl*

Abstract

In numerous processes, taking place in power and heat systems, quick and precise measurements of vital operational parameters state crucial issue, determining for instance staff safety. The measurements have to be often performed in tough environment of high humidity, extreme dust content of risk of explosion. Utilization of acoustic phenomena might introduce solution to this challenge. In the paper, a brief review of common acoustic phenomena, used in professional measuring equipment, is introduced. Short description of selected instruments exploiting discussed acoustic phenomena is provided.

Keywords: acoustics, acoustic phenomena, metrology, power and heat systems, power and heat plants

1. Introduction

Due to rapid development of information technologies, leading to vital soar in accuracy of measuring instruments, their digitalization and possibility of cooperation with fully automated control equipment, at the end of 20th century number of advanced measuring techniques, characterized by high sensitivity and low measurement uncertainty, were presented. Among those techniques, the gas chromatography, laser and semiconductor detection might be listed [1]. Quick introduction of mentioned technologies to the market took place mainly due to development of material sciences, enabling application of advanced materials (multi-layer ceramic-metallic oxides, for instance) in sensors of complete devices. Nevertheless, despite an essential advantage of minimized measuring uncertainty, stating main feature of the techniques being discussed, their application is often time-consuming. Furthermore, the instruments, utilizing mentioned methodology, are in general extremely sensitive to change in environmental parameters, and thus cannot be widely applied in heavy industrial conditions [1], introducing vital challenge for other measurement systems as well [2]. That fact states the reason for present focus on development of methods and instruments enabling quick and precise measurements of fundamental physical quantities, as temperature and composition, which could be simultaneously applied in dangerous conditions [3], as high-dust content, explosive or high-humidity zones, for instance [3]. One among the branches, which potentially might introduce solutions to discussed challenges and remains to be extensively investigated, is acoustics.

Utilization of acoustic waves might bring valuable techniques for different metrological issues. For instance, in the case of composition analysis of the gaseous mixture, which contains only two components (or when two components are dominant, comparing to other), shares of subsequent compounds might be identified on the basis of principal dependence of speed of sound propagation in the mixture on shares of its components [3]. Examples of that dependence, presenting speed of sound in binary methane-ethane and CO_2-propane mixtures as function of molar content of one of mixture components (methane and carbon dioxide, respectively) are presented on Fig.1 and Fig. 2. Use of those dependencies is especially efficient in the case of binary mixtures, containing components characterized by large difference in molar mass. In general, large increase in difference of molar masses of compounds, forming the mixture, results in soar in difference of nominal speed of sound in each of those compounds. This leads finally to higher accuracy of the method and simplification of instruments [4]. Nevertheless, in order to avoid complications connected with accurate determination of the sound speed, especially in the environment of high dust content (which is typical for industrial applications of discussed technique) in investigated mixture, that quantity might be estimated on the basis of measurement of the resonance frequency of the canal, filled with the mixture being analyzed [4].
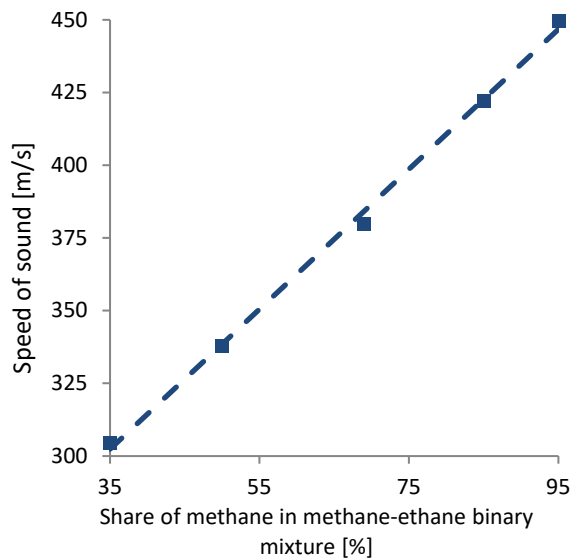
Fig. 1 Dependence of speed of sound in CH_4-C_2H_6 binary mixture on methane content [4].

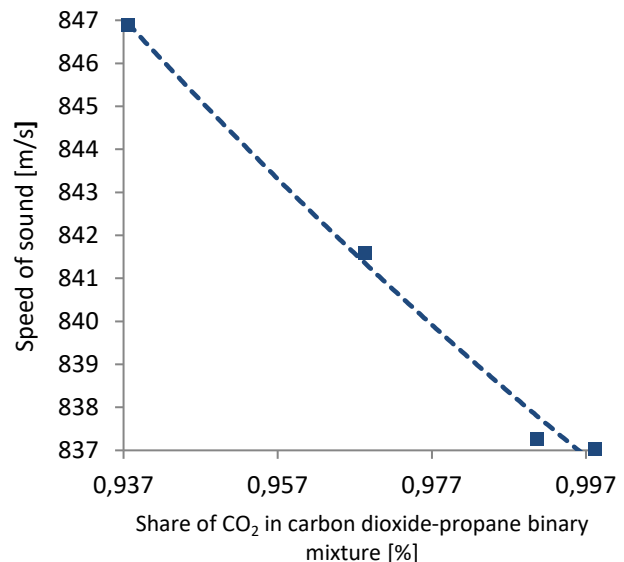Fig. 2 Dependence of speed of sound in CO_2-C_3H_8 binary mixture on carbon dioxidecontent [5].

In the case, where composition of the mixture is known (basing on the results from other equipment,as certified gas analyzer, for instance), the same dependence might be utilized to estimate its temperature. This concept states the basis of several techniques of contactless temperature measurement, used in industry [6,7]. Among those techniques, the acoustic pyrometry, stating the base for the computed tomography (CT) of a temperature field and an acoustic temperature gas measurement (AGAM) system, should be mentioned as the first one [6].

2. Phenomena and Their Principles

Let consider an empty canal, filled with gaseous mixture of investigated composition, called a resonator. If the resonator is covered with any source of the planar acoustic wave at its at least one side [3], the frequency of the emitted wave, forming the standing wave inside the canal, states function of the local sound speed in the mixture, described with equation (2.1):

$$f = \frac{c}{nL} \tag{2.1}$$

where: f – frequency of the acoustic wave, c – speed of sound, L – length of the resonator, n – integer describing of the order of harmonics.

Depending on the value of difference in sound speed between subsequent components of the investigated mixture, fluctuation of the resonant frequency with change in shares of those components might equal both few Hertz and one fifth of the initial frequency [4]. This fact is crucial to properly consider field of utilization of the discussed method: due to high inaccuracy, it cannot be used to determine humidity of inert light mixtures (humid air, for instance). On the other hand, in the case of mixtures of components characterized by large molecules, as hydrocarbons, change in speed of acoustic wave propagation leads to crucial change in resonant frequency. Thus, in the case of mixtures, which the mean sound of speed depends strongly on one of the components, there is possibility to construct simple device, executing quick and precise measurement of share of given component (as its concentration, partial pressure or other, proper for given application) using estimation of temporary resonant frequency of the resonator [3,7].

According to the basic idea, the postponed method utilizesindirect determination of the resonant frequency in open or closed acoustic resonator, filled with investigated mixture. The resonant frequency might be estimated both by iterative selection of parameters of the acoustic wave, emitted by the source (a membrane loudspeaker, for example), enabling occurrence of nodes and antinodes of acoustic pressure in predicted points along the resonator. Location of those covers locations of respective points, present in the case of an acoustic resonance appearance. Another possibility to estimate value of the resonant frequency includes determination of plane of

pressure nodes and anti-nodes by application of movable measuring instruments and the automatic regulation system, controlling their temporary location to the physical location of acoustic pressure nodes [1,4].

Nevertheless, speed of sound in given mixture depends not only on its composition. Basically, the speed of sound propagation in any gaseous compound or their mixture is related to temperature as well. General form of this relation is represented by Eq. (2.2) [6]:

$$c = \frac{\gamma \cdot R}{M} \cdot T \qquad (2.2)$$

where: c - speed of sound in a mixture in m/s, R - universal gas constant in J/(mol·K), γ - adiabatic index, T - temperature in K.

Thus, as long as shares of subsequent ingredients of the mixture might be accurately identified with other methods, and thus mean thermophysical properties of the mixture, the principle discussed may be involved in temperature measurements. Method presented is the acoustic pyrometry [6,7].The system for acoustic temperature measurement, used for in-furnace temperature identification, called AGAM, has been already introduced to the power generation units [6]. The system is dedicated to measure temperature distribution of combustion exhaust gases on horizontal cross-sectional planeinside the combustion chamber [6]. The complete system includes set of acoustic wave transmitters, performing the role of receiver as well, interconnected with computational unit to perform required control. The AGAM systemconsists of 8 single transmitters/receivers, creating 2 measuring paths across the horizontal plane of the furnace cross-section, forming together a complete measuring mesh. The system measurestemperature of the combustion gasesacross each path basing on time of the propagation of induced soundimpulse. While single transmitter generates specific acoustic impulse, other receivers stand by and wait for the incoming wave. After receiving the impulse, the computational unit, included in the system, calculates time of sound wave propagation [6]. The temperature distribution across the measuring mesh is calculatedbasing on the equation (2.3) [6]:

$$T = \frac{l^2}{\gamma \cdot R_M \cdot \tau^2} \qquad (2.3)$$

where: T - temperature in K, l - length of the measuring path in m, γ - adiabatic index, R_M - specific gas constant in J/(kg·K), τ - time of acoustic impulse propagation in s.

Accuracy of temperature measurement using the discussed method exceeds 98% [6,8]. Crucial part of error of the AGAM system is connected with changes in in-furnace exhaust gases composition (approximately 1.4%).Additional advantage of the system is insensitivity to instruments' influence on local heat transfer -due to the fact that AGAM technology utilizes contactless temperaturemeasurement, heat transfer between the transmitter/receiver and the exhaust gases does not vitally affect final measurementresults [6].

The acoustic pyrometry states the basis for advanced techniques of estimation of the temperature distribution as well. One of such techniques is the acoustic computed tomography (ACT).

Computed tomography (CT)is an efficient imaging method, including both industrial and medical CT. Basic tomography technique, based on performance of sequential X-ray scans, can be expanded to many other fields [7]. Nevertheless, measurement of sectional temperature distribution in large-scale furnaces or boilers using classical CT approach, with minute spatial resolution, is extremely challenging [7]. Thus, use of acoustic pyrometry to provide basis for further computation is of great significance. Basing on acoustic scans, the general methodology of computed tomography might be introduced to provide full image reconstruction [7]. If online monitoring of a two-dimensional temperature distribution is achieved, online diagnostics of the combustion state and optimization of the process might be performed [7]. Again, acoustic measurement methods, used to determine basic dataset for computational analysis, include the velocity method and frequency method [7]. Commonly, the method of infraredtemperature surveying is applied to industrial systems, due to its many advantages. If the dataset is gained from more instruments outputs, large number of average temperatures at numerous acoustic paths will be acquired [7]. Then, after collection of the required data, temperature distribution might be reconstructed by two-dimensional computed tomography (CT). Nevertheless, the reconstructed cross-sectional planar temperature distribution is discrete and further divided into mesh of non-overlapping regions of

pixels. Assuming, that exhaust gases in combustion chamber are the ideal gases, final temperature function is defined in the form of (2.4) [7]:

$$f(x,y) = \frac{1}{\sqrt{\frac{\gamma \cdot R}{M} \cdot T}} \tag{2.4}$$

where: $f(x,y)$ - function of the temperature distribution across the planar cross-section in x-y coordinates,γ - adiabatic index, R - universal gas constant in J/(mol·K), M - molar mass (kg/mol), T - temperature in K.

To represent the temperature distribution along prepared mesh, linear operator ofR_i is proposedand used in further computations, as shown in the equation (2.5):

$$\tau_i = R_i \cdot f(x,y) = \sum_{j=1}^{N} f_i \cdot w_{ij} \tag{2.5}$$

where: N is total number of measuring path installed,τ_i is the time of propagation of acoustic wave across the measuring path,w_{ij} is the weighted factor equal to the length of path$i$ that goes through cell$j$of final measuring mesh [7].

3. Instrumentation and Equipment

The complete measuring system, utilized to derive dataset required to perform acoustic computed tomography, includes set of ultrasonic transducers (microphones) linked with ultrasonic velocity measurement instrument (SBZ-A) and additional thermoelements for precise identification of temperature at the furnace walls. Ten thermocouples, used for wall-boundary temperature estimation,arwarranged in a straight line and bonded to the measured furnace wall to obtain the true temperature of the gas at the systems' boundary [7].The distance between the two test points in the same wall depends on local average speed of sound in the exhaust gases; in the case its value equalsapproximately 342 m/s, distance is set to the value of 3.764 m [7].The acoustic measurement is performed in two-channel mode [7] in order to obtain high quality of the output signal. Acoustic input, stating basis of the measurement, in general is assumed as sweeping signal in wide range of frequencies.

In the case of experimental measurement described in literature [7], the linear sweeping frequency signal of frequency changing from 500 Hz to 8kHz and sweepingcycle of 0.1 second period was used [7].The equipment, included in the complete measuring system, stated an industry control microcomputer (IPC610L) the external frequency generator card (PCI6722) anddata acquisition card (PCI4472).Instrumentation for performance of the acoustic measurement, forming the main measurement set, consisted from microphones (MPA201) able toresist environmentwith high-temperature and significant levels of dust, a power amplifier (MTC-300), loudspeaker (TORM-7300) and acoustic waveguides designed exclusively to perform the measurement. The system was controlled by common and full software system, implemented with NI LabVIEW™software and Microsoft™ Visual C++ environment [7].

In the case of previously mentioned AGAM measurement system, instrumentation required for its construction differs from the ACT equipment. As it was already stated, the AGAM system consists of 8 transmitters/receivers, creating 21 measuring paths across the furnace cross-sectional plane altogether. Depending on constructional features of specific combustion chamber, where the system is to be installed, the plane of measurement might to be assumed at different levels.In the case of experimental investigation, discussed in details in [6], the system was installed at the furnace exit, at 30.2 m level. Fluctuations of the combustion exhaust gases of the fire-ball shape might be calculated on a basis of twelve temperatures measurement [6]. Furthermore, the locations of the fluctuations might be estimated as well, since the temperatures hot spot indicates, whether the fire-ball is shifted to the left or right side of the furnace [6]. Intensity of those vertices might be estimated as the mean temperature for given temperature profile, whereas thedispersion is computed as standard deviation of identified AGAM temperatures. Since the fire-ball shaped fluctuations represent most efficient combustion [6], identification of their shape might be used to optimize the process. After defining shape categories, historical values of calculated temperatures, together with process parameters can be analyzed to find best values of the reference shapes of the mentioned fluctuations [6].

Similar system concept might be utilized to determine the composition of the gaseous mixture (combustion exhaust gases, for instance), as far as the temperature might be estimated with other means. In the case of usage

of iterative determination of resonant frequency of the resonator, filled with investigated mixture, implementation of the method in real instrument requires application of automatic computation-regulation unit. The main function of such unit is verification of either appearance or absence of the acoustic resonance in the duct, as well as regulation of the parameters of emitted acoustic wave to enforce the standing wave inside. Technical execution of such system might involve utilization of the feedback, which states one of the basis of the equipment including the photoacoustic generator of waves [3]. Simple scheme of this instrument is presented in Fig. 3.
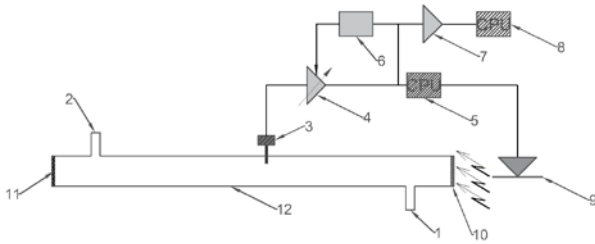
Fig. 3 Scheme of the instrument for determination of gaseous mixtures composition with photoacoustic generator (basing on [3]): 1,2 - mixture inlet/outlet, 3 - acoustic sensor (microphone), 4 - signal amplifier, 5 - photoacoustic unit controller, 6 - amplitude detector, 7 - integrator, 8 - microcontroller, 9 - LED diode, 10 - absorber, 11 - window, 12 - acoustic resonator.
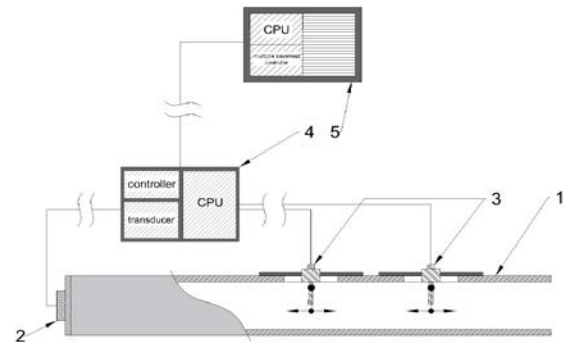
Fig. 4 Scheme of the mixture composition measurement system (basing on [4]): 1 - acoustic resnator, 2 - membrane acoustic emitter, 3 - movable sensors (microphones / piezoelectric transducers), 4 - control and data acquisition unit (transducer, microprocessor, controller), 5 - external data storage and analysis unit.

The second of the configurations of the instrument, utilizing the acoustic resonance for the determination of gaseous mixture's composition, involves application of numerous pressure transducers (microphones or piezoeletric transmitters, for example) to identify accurate location of nodes and/or anti-nodes of acoustic pressure inside the resonator [4]. In such configuration of the instrument, utilization of series (at least two) measuring points is beneficial, since it enables identification of the frequency of the wave basing on simultaneous determination of position of both node and anti-node. This leads to higher accuracy of the estimation performed, and thus lower uncertainty of final results [4]. Furthermore, due to movable location of microphones and mechanical/electromechanical regulation of their placement in void volume of the resonator, application of the feedback system is unnecessary. Lack of the feedback loop reduces number of elements creating the complete measurement system, comparing to the previously discussed one. Nevertheless, major disadvantage of that system might state inability of proper identification of the resonant frequency of the system in the case of sudden change in velocity of acoustic propagation in the investigated mixture. Such crucial change may occur in the case of rapid, impulse-type change in concentration of one of the investigated mixture's components [4].

4. Summary

Although the concept of utilization of acoustics in professional metrology might seem relatively old, its wide application has started recently, during first years of 21st century. Despite requirements for further investigation and optimization of postponed techniques, measuring systems based on the speed-f-sound measurement seem to be interesting alternative to conventional equipment, especially in tough conditions.

Main advantages of state-of-the-art systems, which have been already introduced to the experimental procedure at industrial installations, are insensitivity to radiative heat transfer (which is essential advantage for temperature measurement in furnaces and boilers) and enable estimation of planar distribution of temperature across given

plane, what might state vital help for process optimization. Nevertheless, currently developed systems require either quasi-static operational conditions, in the case of mixture composition-measurement instrumentation,or utilization of ultrasonic emitters/receivers, in the case of temperature determination equipment, which are comparatively more expensive than traditional wide-range loudspeakers. Independently on stated disadvantages, acoustic measurement methods are deemed to be continuously developed, and all of mentioned challenges might be solved in the nearest future.

References

[1] Crownhurst D., Manchester S.J.: *The measurement of methane and other gases from the ground*, CIRIA Report 131, Bulding Research Establishment/Construction Industry Research and Information Association, Watford, 1993

[2] Ostrowski P., Remiorz L.: *Measurement of gas flow in short ducts, also rectangular*, Flow Measurement and Instrumentation 30(2013), pp. 1-9

[3] Suchenek M., Borowski T.: *Measuring Sound Speed in Gas Mixtures Using a Photoacoustic Generator*, International Journal of Thermophysics 39(11)/2018 .

[4] Grzywnowicz K., Wiciak G.: *Wykorzystanie zjawisk akustycznych w pomiarze składu mieszanin gazu*, Napędy i Sterowanie 234(2018), pp. 90-94

[5] Lin C.-W., Trusler J.P.M.: *The speed of sound in (carbon dioxide + propane) and derived sound speed of pure carbon dioxide at temperatures between (248 and 373) K and at pressures up to 200 MPa*, Journal of Chemical Engineering Data 59 (2014), pp. 4099-4109

[6] Śladewski Ł., Wojdan K., Świrski K., Janda Tomasz, Nabagło D., Chachuła J.: *Optimization of combustion process in coal-fired power plant with utilization of acoustic system for in-furnace temperature measurement,* Applied Thermal Engineering 123(2017), pp. 711-720

[7] Zhang S., Shen G., An L., Niu Y.: *Online monitoring of the two-dimensional temperature field in a boiler furnace based on acoustic computed tomography*, Applied Thermal Engineering 75(2015), pp. 958-966

[8] M. Deuster:*Acoustic gas temperature measurement*, [in:] Proceedings of Wissenforum: temperature measurement technique Conference,Aldenhoven, 2009.

Biomass Gasification Techniques – A review

Shanlin Chen[1], Shemin Sagaria[1], Shahmir Ali Nosherwani

[1]Depatment of energy and environmental engineering,

e-mail:chen.shanlin@hotmail.com,sheminsagaria@gmail.com, Shahmir.nosherwani@gmail.com

Abstract

Biomass is known as a carbon-neutral and sustainable energy source. Biomass gasification is a mature technology pathway that uses a controlled process involving heat, steam, and oxygen to convert biomass to hydrogen and other products, without combustion. This papers reviews the various gasification processes for the biomass along with the advantages of these technologies, pretreatment, operation conditions and syngas cleaning processes.

Keywords: Biomass, Gasification, Gasifiers, Gasification technologies, Syngas cleaning

1. Introduction

Biomass gasification is a thermochemical transformation of solid biomass into syngas, which may contain H2, CO, CH4 and some other gases depending on the feedstock and gasifying agent. The gasification of biomass is a process for producing a combustible synthesis gas from solid biomass, this gas can then be used in a gas burner or a combustion engine.

Biomass is known as a carbon-neutral and sustainable energy source unlike coal. Because biomass is more reactive and has higher volatiles content than coal, biomass gasification occurs at a lower temperature. Lower temperature reduces the extent of heat loss, emissions and material problems associated with high temperatures.

Biomass gasification is considered to increase the use of biomass for energy production allowing widespread biomass utilization. The development of biomass gasification processes is pushed up by the growing awareness of the possible effects of fossil fuels on the climate and by the continuous increase in oil prices.

1.1. Advantages of biomass gasification technologies

- Mature technology: Biomass gasifier technology is a mature technology and gasifiers are available in several designs and capacities to suit different requirements.

- Small and modular: The technology is suiTab. and economical for small, decentralized applications, typically with capacities smaller than a megawatt.

- Flexible operation: A gasifier-based power system, unlike those based on other renewable sources such as the sun and wind, can generate electricity when required and wherever required. Biomass gasifier-based systems can be set up at almost any place where biomass feedstock is available.

- Economically viable: For small-scale systems, the cost of power generation by biomass gasification technology is far more reasonable than that of conventional diesel-based power generation.

- Socio-economically beneficial: Biomass gasifier-based systems generate employment for local people.

- Mitigate climate change: Biomass is a CO2 neutral fuel and, therefore, unlike fossil fuels such as diesel does not contribute to net CO2 emissions, which makes biomass-based power generation systems an attractive option in mitigating the adverse effects of climate change.

2. Type of biomass

The 2009/28/EC European Directive defines biomass as "the biodegradable fraction of products, waste and residues of biological origin from agriculture (including vegetal and animal substances), forestry and other related industries, including fisheries and the aquaculture, as well as the biodegradable fraction of industrial and municipal wastes". Tab. 1[1][9] shows the types of biomass and their properties.

Tab. 1. Types of biomass and their properties.

Biomass type	Cellulose	Hemi-cellulose	Lignin
Hardwood	42–48	27–38	16–25
Softwood	40–45	24–29	26–33
Straws	36–40	21–45	15–20

3.   Main process of biomass gasification

Biomass gasification involves the decomposition of a solid fuel, for example wood, by a reactive gas, air, to obtain a gaseous fuel. During this process, biomass is subjected to four successive thermochemical phenomena: drying, pyrolysis, oxidation and reduction. Fig. 1[1] shows the thermochemical phenomena, their products and byproducts.
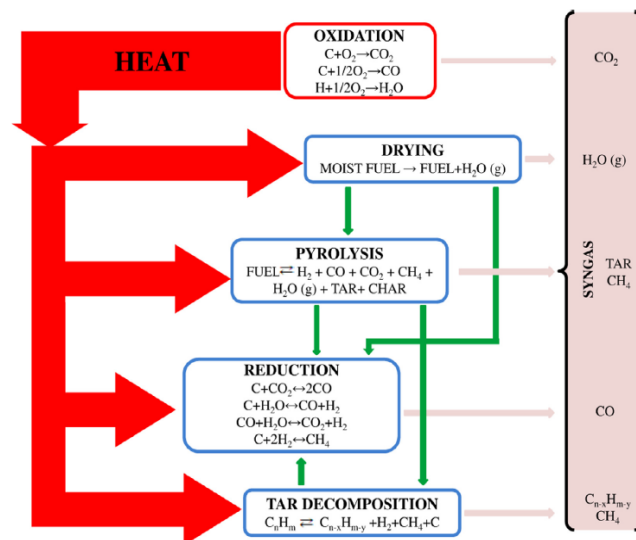
Fig. 1. thermochemical phenomena during gasification process.

Drying: The fuel moisture is removed by evaporation. This is an endothermic process, it occurs at a temperature between 100 °C and 160 °C.

Pyrolysis: As the temperature of the solid increases, gases are generated by dry biomass from 250 °C. These gases are constituted of non-condensable species (methane, hydrogen, carbon monoxide, carbon dioxide, etc.) and condensable vapors (tar). The solid residue from this operation is called coke and contains carbon and mineral materials.

Oxidation: Oxidation occurs in the presence of a reactive gas (air, steam, pure oxygen, hydrogen), which determines the calorific value of the gas leaving the gasifier. The use of air as reactive gas is more common. Oxidation is the phase that provides heat for the three phases of the gasification process.

Reduction: The coke reacts with water vapor and carbon dioxide, thereby forming hydrogen and carbon monoxide, principal constituents of the combustible gas produced.

The principal reactions of the gasification are endothermic and the necessary energy for their occurrence is, generally, granted by the oxidation of part of the biomass, through an allo-thermal or an auto-thermal phase. Thelowestheatingvalue(LHV)ofthesyngasrangesfrom4to13MJ/Nm3,   dependingon thefeedstock,thegasificationtechnologyandtheoperational conditions [6-8]

4.   Biomass gasification technologies

Different technological solutions can be implemented to obtain different plant configurations; in particular, the mode of contact of the biomass with the gasification agent canbe in counter-current, or co-current, or cross flow,

and the heat can be transferred from the outside or directly in the reactor using a combustion agent; the residence time can be hours (static gasifiers, rotary kiln) or minutes (fluidized bed gasifiers).

4.1. Fixed bed gasification technologies

Two types of fixed bed gasification technologies exist: updraft and downdraft.

4.1.1 Updraft gasifier

In an updraft gasifier, the biomass is supplied through the top of the reactor and the oxidizing agent is injected through the bottom of the unit through a gate, shown in Fig. 2a. Biomass undergoes partial oxidation that provides thermal energy needed for the various process steps. The gas passes through the areas of reduction and pyrolysis and is cooled down drying the biomass. This type of reactor does not allow for tar cracking, thus the syngas produced may contain a high concentration of tar.

4.1.2 Downdraft gasifier

The downdraft (also known as co-current) gasifier is the most common type of gasifier.In a downdraft gasifier, biomass and oxidizing agent flow in the same direction, as shown in Fig. 2b. The product gas passes through the hot zone which can crack tars formed during the reaction of pyrolysis. The product gas thus leaves the reactor at a high temperature, around 700 °C, with a minimum content of tar.
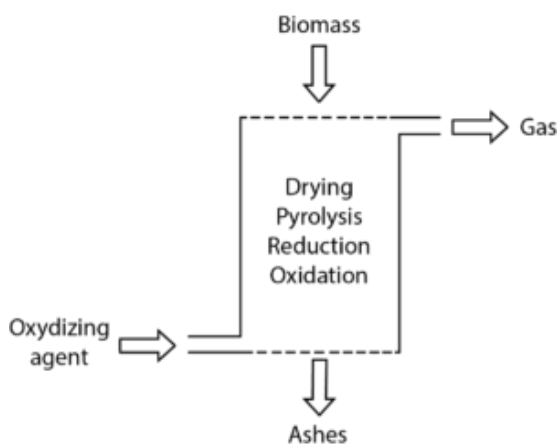
Fig. 2a. Updraft Gasifiers   Fig. 2b. downdraft gasifiers
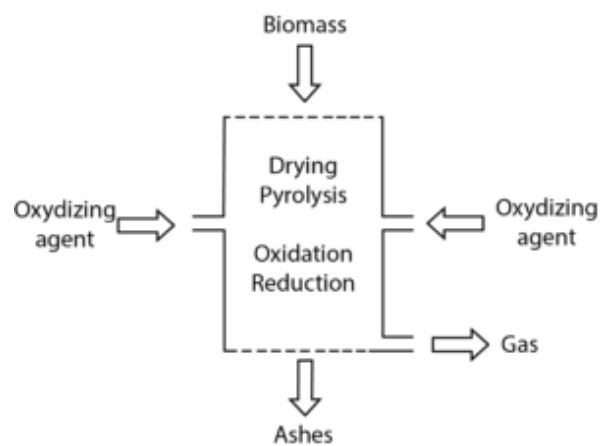
4.2. Fluid bed gasification technologies

These types of gasifiers are usually used for large power production.

4.2.1 Fluidized bed gasifier

The solid fuel is fluidized by the addition of air at high velocity into the bed which is made of small diameter particles such as sand or alumina to improve the fluidization. The solid thus behaves as a fluid for a good homogenization of temperature and reactants.Bubbling fluid bed (BFB-Fig. 3a) and circulating fluid bed (CFB – Fig. 3b) gasifiers are both capable of gasifying a wide range of biomass materials.
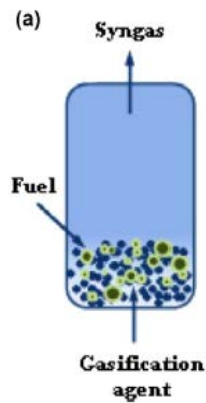
Fig. 3a. Bubbling fluidized bed   Fig. 3b. Circulating fluidized bed
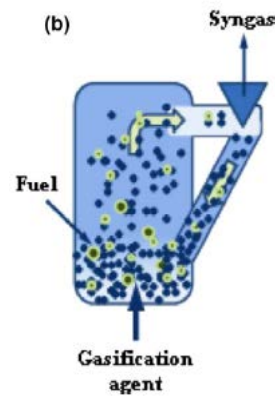
Fluidized bed gasifiers are better than dense phase reactors in that they produce more heat in short time due to the abrasion phenomenon between inert bed material and biomass, giving a uniformly high (800–1000 °C) bed temperature. A fluidized bed gasifier works as a hot bed of sand particles agitated constantly by gasifying agent. Gasifying agent is distributed through nozzles located at the bottom of the bed.

4.2.2 Entrained flow gasifier

In entrained-flow gasifiers, fuel and air areintroduced from the top of the reactor, and fuelis carried by the air in the reactor as shown in Fig. 4. The operatingtemperatures are 1200–1600 °C and the pressureis 20–80 bar. Entrained-flow gasifiers can beused for any type of fuel so long as it is dry (lowmoisture) and has low ash content. Due to theshort residence time (0.5–4.0 seconds), hightemperatures are required for such gasifiers.The advantage of entrained-flow gasifiers is thatthe gas contains very little tar.
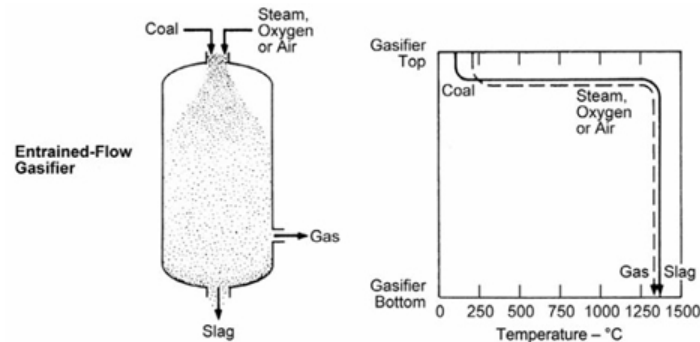
Fig. 4. Entrained flow gasifiers

The fuel is finely pulverized in the jet of gasifying agent (air, pure oxygen or air / water vapor) and the reaction proceeds at high temperature and high pressure, thereby preventing the formation of tar and methane.

Tab. 2 shows the advantages and dis advantages of different types of biomass gasifiers which is discussed above.

Tab. 2. Advantages and disadvantages of gasification technologies [5]

Type	Advantage	Disadvantage
Updraft	-High thermal efficiency -Different sizes feedstock -Higher humidity	-High tar content in syngas -Extensive gas cleaning is required
Downdraft	-Low tar production -High carbon conversion -Reliable	-Strict feedstock requirements -High ash and dust amount

Fluidized bed	-Uniform temperature profile -High conversions -Accepts fuel size variation -Low tar production	-Loss of carbon -Complex system and high cost -Gas stream contains dust particles
Entrained flow	-Applicable to large systems - Short biomass residence time	-High investment cost - Strict feedstock requirements

5. Pretreatment of biomass

The pre-treatment of biomass has the primary objective to ensure that the gasification process is conducted using a feedstock material that is homogeneous by size and composition. Other pre-treatments aim at reducing the initial moisture content that, in general, must not exceed 25–30 wt%; among these the main pre-treatments, besides drying, are torrefaction and hydro thermal upgrading (HTU).

5.1. Torre faction

Torre faction is a thermochemical process which is carried out at a temperature between 200 and 300 °C in the absence of oxygen. At these temperatures some chemical reactions take place; the biomass loses both the rigid fibrous structure and the moisture content, with a consequent increase in the energy content. In many cases the torrefaction process is performed with a system of palletization to increase the bulk density of the material.

5.2. Hydro thermal upgrading(HTU)

The HTU consists in the production of an oil, like crude oil, named "bio-crude" oil, by the decomposition of biomass in water. The pre-treatment is conducted, essentially, in two stages. The first one consists in treating the biomass with water at temperatures of 200–250 °C and a pressure of about 30bars. The second one is an increase both in temperature and pressure in a period of time variable from 5 to 10 min, in which the conversion of the biomass takes place by bringing the water at pressures of 120–180 bar and temperatures of 300–350 °C.

6. Effects of gasification operating conditions

There are many kinds of factors that can affect the biomass gasification process, such as temperature, pressure, gasifying agent and so on. To obtain the desired product gas composition, the least amount of impurities, and to increase the net energy conversion efficiency, the gasification operating conditions need to be optimized. The following section describes the effects of the main operating conditions on the quantity and composition of the product gas and its impurities.

6.1. Biomass type (composition, density, size)

The main constituents of lignocellulose biomass are cellulose, hemicellulose and lignin. The composition of these polymers in the biomass affects the product composition. Hanaoka observed that at 900 °C, carbon conversion efficiencies of cellulose, xylem and lignin were 97.9%, 92.2% and 52.8% [3], respectively. The product compositions from gasification of xylem and lignin were similar. Cellulose resulted in higher CO and CH4 but lower CO2 and H2 yields than those of xylem and lignin. Barreto observed that composting of biomass increased the lignin content in the compost, which resulted in up to 20% increased H2 production at a slow heating rate as compared to the original biomass at a fast heating rate.

A higher density of feedstock can also help with the biomass gasification process. For example, gasifying a high bulk density biomass pellet at 10% [3] moisture content can improve a gasifier production rate, efficiency, reliability, syngas quality compared with a lower density biomass. Feedstock density considerations are similar for both BFB and CFB gasifiers. Dense feedstock benefits both technologies in similar ways.

The size of biomass particles greatly affects the rate of gasification and the ability of the biomass to migrate to the center of the bed in a BFB design. The target feedstock size for both a BFB and CFB gasifier is approximately 2.0-2.5" with a thickness of ¼" to ½". Larger sizes are accepTab. if the thickness remains near ¼" to ½".

With small particles, the gasification is very quick, and unburned material might not make it to the center of the bed, resulting in oxygen slip and a void center in the BFB reactor. Smaller particles have larger surface areas per unit mass and larger pore sizes which facilitate faster rates of heat transfer and gasification.Smaller particles resulted in more CH4, CO, C2H4 and less CO2 [3] which led to higher gas yields, gas energy content (LHV) and carbon conversion efficiency.

6.2. Moisture content

The knowledge of biomass physical-chemical properties is fundamental for its use as sustainable resource for energy production. The moisture content is one of the most important parameters and critically affects the energy balance of the biomass gasification process. Fig. 5[1] shows the relation between moisture content and LHV .
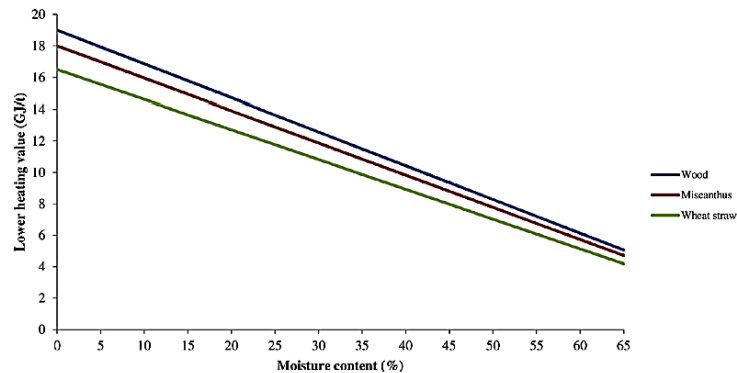
Fig. 5. Lower heating value vs Moisture content

Drying is needed to obtain a desired range of water content for the gasification processes. Drying is an energy intensive process which may decrease the overall energy efficiency of the process. However, in case of gasification, waste heat can be utilized to decrease the moisture content of the biomass which will increase the overall efficiency of the process.

The moisture content of bio-fuels is important for syngas quality. High moisture content reduces the thermal efficiency;therefore, heat is used to drive off the water from biofuels, and consequently this energy is not available for the reduction reactions and for converting the thermal energy into chemical bond energy in the syngas. Thus, high moisture content bio-fuels result in low heating values in syngas. In downdraft gasifiers, high moisture content gives rise to lower temperatures in the reactor, which leads to insufficient tar conversion, and thus further affects syngas quality. Operational problems in gasifiers occur if the fuel moisture content is too low or too high.

The biomass conversion efficiency and production rate typically decrease with increasing moisture content, because the process consumes more carbon (directly heated gasifier) or uses more of the available heat (indirectly heated gasifier) to heat and vaporize the water to the syngas temperature. Indirect gasification systems experience a drop-in temperature due to the consumption of additional heat, producing more char and subsequently increasing the amount of char combustion gases, which would ultimately increase the hot gas flow to the gasifier in a self-correcting type of action.Most gasifier technology providers require feedstock with a target range moisture content of 10-20%.

6.3. Biomass flow rate

Overfeeding of biomass can lead to plugging and reduced conversion efficiencies whereas starve-feeding results in less gas yield. Hence, an optimum biomass flow rate is desired for the gasification system to maximize energy efficiency. Optimum biomass flow rate is dependent primarily on the design of the gasifier and the properties of the biomass.

6.4. Air flow rate (equivalence ratio, ER or superficial velocity, SV)

Equivalence ratio (ER) and superficial velocity (SV) are measures of the air (or oxygen) flow rate. ER is the ratio of air flow to the airflow required for stoichiometric combustion of the biomass, which indicates extent of

partial combustion. The SV is the ratio of air flow to the cross-sectional area of the gasifier which removes the influence of gasifier dimension by normalization [11]. Hence, both ER and SV are directly proportional to the airflow. Air flow influences the gasification products in different ways. Air supplies the O2 for combustion (and fluidization in the case 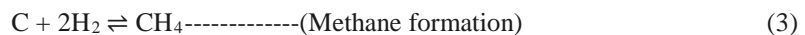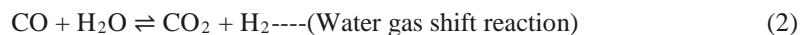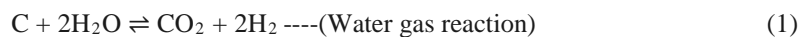of fluidized bed) and affects the residence time. By varying amount of the O2 supply, air flow rate controls the degree of combustion which in turn, affects the gasification temperature. Higher airflow rate results in higher temperature which leads to higher biomass conversion and a higher quality of fuel. But, an excess degree of combustion, on the other hand, results in decreased energy content of the gas produced because a part of biomass energy is spent during combustion. Higher airflow also shortens the residence time which may decrease the extent of biomass conversion.

All authors reported increases in gas yields with increases in ER (from 0.0 to 0.45). However, contradictory results of decreases in H2 and CO yields with increases in ER also have been reported [5]. The increase in gas yield with increase in ER implies that an increased airflow increases conversion rate. Some of the contradictory results on the effects of ER on the contents of H2, CO and CH4 (%) are logical because the percentage compositions of individual gases depend on both the yield of individual gases and the overall gas yield.

6.5. Steam flow rate (steam to biomass ratio, S/B)

Supplying steam as a gasifying agent increases the partial pressure of H_2O inside the gasification chamber which favors the water gas reaction (1), water gas shift reaction (2) and methane reforming reactions (3), leading to increased H_2 production.

$$C + 2H_2O \rightleftharpoons CO_2 + 2H_2 \text{ ----(Water gas reaction)} \tag{1}$$

$$CO + H_2O \rightleftharpoons CO_2 + H_2\text{----(Water gas shift reaction)} \tag{2}$$

$$C + 2H_2 \rightleftharpoons CH_4\text{-------------(Methane formation)} \tag{3}$$

However, the gasification temperature needs to be high enough (above 750–800 °C) for the steam reforming and water gas reactions to be favorable. Catalysts can lower the operating temperature needed for the above reactions to occur. Higher S/B also leads to higher biomass conversion efficiency.

Reduction in tar also is observed at higher steam to biomass ratios, which is attributed to steam reforming of the tar with an increased partial pressure of steam. Since the temperature of the steam supplied to the gasifier is lower than the gasification temperature, a significant amount of heat is needed to raise the steam temperature which, in turn, may lower the temperature of the gasifier bed. Hence an S/B ratio above a threshold, steam had negative effects on the product. Increasing the temperature of the gasifying agents leads to an increase in the heating value of the fuel gas, and reduces the tars, soot and char residues. A preheater is recommended before the introduction of gasifying agents (steam and air) to the gasifier to facilitate higher gasification bed temperature.

6.6. Temperature

Gasification temperature is one of the most influential factors affecting the product gas composition and properties. Higher temperature results in increased gas yield because of higher conversion efficiency, the contents and ratios of H2, CO, CO2 and CH4 in the product gas are affected by temperature and partial pressures of reactants.

At temperatures above 750–800 °C, the endothermic nature of the H2 production reactions (steam reforming and water-gas reactions) results in an increase in H2 content and a decrease in CH4 content with an increase in temperature. At temperatures above 850–900 °C, both steam reforming and the Boudouard reactions dominate (4), resulting in increases in CO content. High temperature also favors destruction and reforming of tar leading to a decrease in tar content and an increase in gas yield.

$$C+CO_2 \rightleftharpoons CO \text{ -------- (Boudouard reaction)} \tag{4}$$

The biomass gasification end products may be distinct in a solid phase and a gas/vapor phase. The gas phase usually is called syngas, which consists of CO, CO2, H2, CH4, and many other gases depending on the gasifying

agent. The solid phase usually is called tar, which contains several organic compounds, as shown in Fig. 6. In a gasification process, tars are formed in a series of complex reactions, which are highly dependent on the reaction conditions [10].
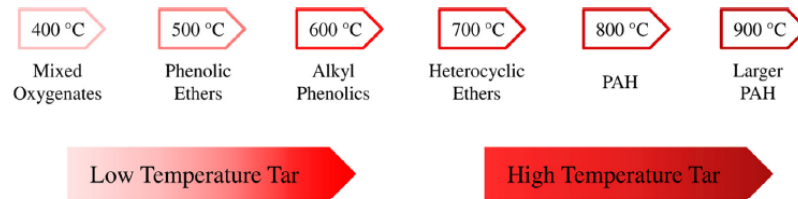
Fig. 6: Organic compounds in tar during different operating temperature.

Higher gasification and tar reforming temperatures would result in the following:

•Increase in carbon conversion

•Reduction in tar content

•Reduction in methane and higher hydrocarbons content

•Maximized H2 and CO production

•Increased slagging and agglomeration potential

6.7. Pressure

Pressure has a positive influence on the gasification process as the pressure goes higher, it improves the calorific value of the biomass. The increase in calorific value with increase in reactor pressure may be due to increase in temperature in the combustion and reduction zone which results in better reaction. But it reduces the residence time of gas, even reduces the conversion efficiency with increase in pressure

High pressure gasification favors hot, pressurized cleanup of the syngas and operation of downstream equipment at high temperature and sufficiently high pressure to accommodate flow control and equipment pressure drops. Tab. 3[2] the gas composition when gasification process is carried out at different pressures (bar).

Tab.3. An example, biomass gasification uses air as gasifying agent under different pressure.

Pressure (bar)	Gas composition (%)					
	H_2	N_2	O_2	CH_4	CO	CO_2
ATM	18.95	49.043	1.101	1.449	10.304	18.812
0.5	22.725	52.41	1.145	0.925	10.465	12.087
1	23.572	52.02	1.003	1.035	10.147	12.20
2	23.74	51.352	1.056	1.140	10.787	12.063
2.5	23.82	50.56	1.015	1.165	10.99	12.325

It was observed that the percentage of the combustible contents namely CO, CH4, H2 improved during the operation at 0.5, 1, 2 and 2.5 bar respectively as compared to atmospheric pressure. Also the calorific value of the producer gas improved with the increasing pressure. The gas production rate is increased at pressurized conditions as well. The conversion efficiency is decreased at a higher pressure, with the maximum at atmospheric condition. Tab. 4 shows the advantages and disadvantages of pressurizedgasification processes.

Tab. 4. Advantages and disadvantages of pressurized gasification

Advantages	Disadvantages
- Lower level of internal power consumption	- More complicated feed system
- Increases the syngas production rate	- Higher methane content in the syngas
- Decreased sintering of the ash	- Needs densified fuel

- Reduced reactor volume	- Higher investment

6.8. An example - Pressurized gasification of woody biomass

In this experiment, the parameters varied were temperature (720–900 °C), pressure (1–5 bar), air ratio (0.2–0.4), gasification agent (air, steam, oxygen), and the fluidization conditions of the reactor fluidized bed [4]. Tab. 5 and Tab. 6 shows the operating conditions and gas composition of wood biomass.

Tab. 5. Standard operating conditions

Gasification agent	Air
Gasification temperature	825 °C
Fuel	Wood pellets
Operating pressure	3 bar
Air ratio	0.3 (autothermal)
Bed material	Olivine
Fuel input	6 kg/h (30 kW)
Fluidization number	4–6

Tab. 6. standard producer gas composition

Component	Value	Unit
CO_2	14–17	[vol.% PG_{dry}]
CO	13–15	[vol.% PG_{dry}]
H_2	12–14	[vol.% PG_{dry}]
CH_4	4–5	[vol.% PG_{dry}]
N_2	50–60	[vol.% PG_{dry}]
O_2	0	[vol.% PG_{dry}]
Tars (GC-MS)	1–3	[g/Nm^3 PG_{dry}]
NH_3	500–1000	[ppm]
LHV	4–6	[MJ/Nm^3 PG_{dry}]

6.8.1 Pressure and temperature

The concentration of hydrogen is higher if the gasification temperature is over 820 °C and the pressure level is under 4 bars. Many articles also indicated that higher temperatures cause higher hydrogen content in the producer gas. The fact that the hydrogen production prefers low gasification pressure can be explained by the gasification reactions. At high pressure the chemical equilibrium of the hydrogen production reactions (heterogeneous water gas reaction, steam reforming reaction and methane reaction) are shifted to the duct side. For the enrichment of carbon monoxide in the producer gas, high temperatures and low pressures are required. To enrich the producer gas with methane moderate temperatures and high gasification pressures are required

6.8.2 Air ratio

The air ratio was varied between 0.2 and 0.4 at a constant pressure level of 3, 5 bar and a gasification temperature of 825 °C. The CO2 content increases, whereas the CO, H2, and CH4 content of the producer gas decrease with rising air ratio. A higher air ratio corresponds to a higher amount of O2, and therefore the exothermal combustion reactions are favored. The higher oxygen content implies that more CO2 and H2O are generated. In regard to the tar content means the higher amount of O2, that more hydrocarbon chains and aromatics can be oxidized and cracked. The tar content decreases as the air ratio increase. An increasing air ratio also causes a decreasing NH3 content.

6.8.3 Gasification agent

The biomass feed was held constant at a level of 4.5 kg/h as well as the gasification pressure at 3 bar. The addition of steam to the gasification agent led to an increasing hydrogen concentration whereas the carbon monoxide and the carbon dioxide concentrations are slightly decreasing. The producer gas composition

corresponds to the result shows the dependence of tar and ammonia on the steam to biomass ratio (SBR). The tar content increases whereas the ammonia content decreases with rising SBR. Regarding the operating conditions, the addition of steam to the gasification agent shows a better operating performance of the PRU compared to pure air gasification. Generally, the addition of oxygen to the gasification agent tends to result in lower tar and ammonia contents.

6.8.4 Conclusions

Many utilization routes for biomass gasification such as methanol and Fischer–Tropsch fuel synthesis need a pressurized syngas as raw material. Therefore, the pressure and temperature dependency of producer gas composition was investigated. Within some test series the best performance and operating points for biomass gasification in the investigated area were found. For power production high temperature (850 °C) is preferred and the pressure level should be an optimum for the gas engine entrance. To produce syngas for chemical synthesis the H2 to CO ratio should be about 2. Production of such a syngas requires a high gasification temperature and high steam to carbon ratio (0.7) [4]. The gasification pressure should be chosen to be moderate because of high investment and operating costs.

7. Syngas cleaning

The product gas from biomass gasification needs to be processed further for effective utilization. One of the most important processes is syngas cleaning [5].

7.1. Particulate removal

Cyclone separators are widely and routinely used to separate the larger particulates (above 5 μm in diameter) at the initial cleaning stage with little pressure drop.

Wet scrubbers remove particulates using liquid sprays (usually water) on the gas stream. These can remove 95–99% of over 1 μm particle size and 99% of over 2 μm with pressure across the venturi of 2.5 to 25 kPa. However, wet scrubbers are used at less than 100 °C which results in loss of sensible heat [5].

Electrostatic precipitators (ESP) apply electrical voltage to charge and then separate particulates. The separation efficiency depends on particulate resistivity, and sulfur and alkali contents. Because of its large size and high capital cost, it is suited for large-scale operations.

Barrier filters allow the gas to pass through various porous media collecting the particulates of 0.5 to 100 μm. However, because of the smaller pore size, it increases the pressure differential across the filter.

7.2. Alkali removal

Removal of alkali can be performed by cooling the gas and then passing it through barrier filters. Hot gas removal of alkali compounds holds promise, particularly for high temperature applications. However, research on hot gas alkali removal is still in the experimental stage.

7.3. Nitrogen compounds

When gasified, the nitrogen content of the biomass (0.5–3%) results primarily in ammonia (60–65%) and molecular nitrogen. If cold product gas is desired, ammonia can be removed by wet scrubbing. Hot gas cleaning for ammonia can be performed by destructing ammonia at higher temperature using dolomites, nickel-based catalysts and iron-based catalysts.

7.4. Sulfur compounds

Most biomass contains very little sulfur (<0.5%), which, during gasification, is converted to H2S and SO2. SO2 in syngas can be removed by wet scrubbing. Limestone, dolomite or CaO are used for SO2 and H2S removal because of their low cost and wide availability. Calcination processes are advantageous for SO2 removal whereas cleaning at 600–900 °C and regeneration of sorbents is the best scrubbing process for H2S removal from hot gas

7.5. Tar removal

Removal of tar is one of the biggest technical challenges facing the commercialization of gasification technology. Tar removal techniques are categorized as primary removal techniques and secondary removal techniques. Primary removal techniques refer to techniques that reduce the tar content in the syngas and are employed inside the gasifier without the need of a secondary reactor. Primary removal methods include design and optimization of the gasification operating conditions, and addition of catalysts in the gasifier bed (called in-bed catalysts). Secondary tar removal techniques use a separate reactor to destruct and reform the tar content below accepTab. level in the product gas. Secondary tar cleaning techniques are divided further into wet and hot gas cleaning.

8. Summary

Biomass combines solar energy and carbon dioxide into chemical energy in the form of carbohydrates via photosynthesis. The use of biomass as a fuel is a carbon neutral process since the carbon dioxide captured during photosynthesis is released during its combustion. Biomass includes agricultural and forestry residues, wood, byproducts from processing of biological materials, and organic parts of municipal and sludge wastes.

Biomass gasification is a promising technology to displace use of fossil fuels and to reduce CO_2 emission. Among other alternative energy conversion pathways, it has great potential because of its flexibility to use a wide range of feedstock, and to produce energy and a wide range of fuels and chemicals. Recently, the focus of its application has changed from production of combined heat and power to production of liquid transportation fuel. The technical challenges in commercialization of fuels and chemicals production from biomass gasification include increasing the energy efficiency of the system and developing robust and efficient technologies for cleaning the product gas and its conversion to valuable fuels and chemicals.

However, harvesting, collecting and storage of biomass adds another dimension of technical challenges to the use of biomass for production of fuels, chemicals and bio power. The main "bottlenecks" of the biomass gasification technology can be summarized in: feed material, syngas quality and development status. An entrained flow reactor requires specific features of the feed fuel, in terms of particle size (0.1–1mm), moisture content (<15wt %) and a constant composition, while biomass feed stock with light or without pre-treatment can be supplied to a plasma gasifier and a rotary kiln reactor. Fluidized and fixed bed reactors are more flexible than an entrained flow reactor operating with larger particle sizes(20–100mm) and a wider range of moisture contents (5%–55%), however a feed stock with low ash melting temperatures should be used. In terms of syngas quality, the best gasifier is the plasma reactor; entrained flow gasifiers also ensure a very low tar content with a better and high capital and maintenance costs; rotary kiln gasifiers are characterized by good efficiency, low capital costs and high maintenance costs; plasma gasifiers show low efficiency versus high capital and maintenance costs.

References

[1] Molino, Antonio, SimeoneChianese, and Dino Musmarra. "Biomass gasification technology: The state of the art overview." Journal of Energy Chemistry 25.1 (2016): 10-25.

[2] C. Mohanraj& J. Kesavan, Performance Evaluation and Simulation of Pressurized Gasification. ISSN : 2319 – 3182, Volume-1, Issue-2, 2012.

[3] Worley M, Yale J. Biomass gasification technology assessment: consolidated report[R]. National Renewable Energy Laboratory (NREL), Golden, CO., 2012.

[4] Kitzler H, Pfeifer C, Hofbauer H. Pressurized gasification of woody biomass—variation of parameter[J]. Fuel Processing Technology, 2011, 92(5): 908-914.

[5] Kumar A, Jones D D, Hanna M A. Thermochemical biomass gasification: a review of the current status of the technology[J]. Energies, 2009, 2(3): 556-581.

[6] K.Qian,A.Kumar,K.Patil,D.Bellmer,D.Wang,W.Yuan,R.L.Huhnke,Energies6(2013)3972–3986.

[7] Y.Wu,W.Yang,W.Blasiak,Energies7(2014)2107–2122.

[8] B.Liu,S.Ji,J.EnergyChem.22(2013)740–746.

[9]   www.eubia.org

[10] L.Devi,K.J.Ptasinski,F.J.J.G.Janssen,Ind.Eng.Chem.Res.44(2005)9096–9104.

[11] Yamazaki, T.; Kozu, H.; Yamagata, S.; Murao, N.; Ohta, S.; Shiya, S.; Ohba, T. Effect of superficial velocity on tar from downdraft gasification of biomass. Energy Fuels 2005, 19, 1186–1191.

Carbonation of fly ash with a high content of calcium oxide

Marta Kamienowska[1], Jakub Sobala[1], Paweł Baran[1], Piotr Zabierowski[1], Katarzyna Zarębska[1]

[1]*AGH University of Science and Technology in Cracow, Faculty of Energy and Fuels, kamienowskamarta@gmail.com*

Abstract

Nowadays, around 45.9% of global emissions of carbon dioxide come from the coal combustion. The utilisation of CO_2 in a carbonation process may be an interesting alternative to the others sequestration methods. Moreover, fly ash is one of the most hazardous substances generated by the coal-fired power plants. Currently, the total annual production of coal fly ash is around 500 million tones worldwide, therefore scientists around the world put a lot of effort into finding the new application of this material. In this work, either fly ash from the combustion of lignite as well as from combustion of biomass were carbonatized with CO_2 under laboratory conditions 298-343 K under 0.4-1.5 MPa.

Keywords: carbonation, fly ash, carbon dioxide

1. Introduction

Currently, it is estimated that about 50% world emission of carbon dioxide comes from coal burning in the power plants. CO_2 emission has been increasing every year[1]. Thus, new ways of utilisation of carbon dioxide must be implemented[2]. Moreover, one of the most hazardous substances which are produced by the energy sector is fly ash[3]. Annual production of fly ash is around 500 mlntonnes[4]. What is more, the average use of fly ash is only 16% in the world[5]. Fly ash is mostly used to production of cement, building materials and as the component in road construction [6]. If fly ash contents more than 10% of calcium oxide, then it is included to the group called - high-calcium fly ashes. In Europe, more than 50% of the total production of fly ash is HCFA [7]. The carbonation process not only can be used in order to reduce the emission of carbon dioxide but also it may allow to utilize the HCFA as the substrate in this reaction [8]. This process has two steps. The following reactions show the chemical process of carbonation:

$$CaO + H_2O \rightarrow Ca(OH)_2$$

$$Ca(OH)_2 + CO_2 \rightarrow CaCO_3 + H_2O$$
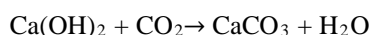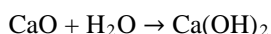
First, the hydration of CaO is taken place and next, it is followed by carbonation of calcium hydroxide. HCFA may be a low-cost and eco-friendly alternative, which can be used in this process.

2. Experimental part

2.1. Raw materials

Biomass fly ash and coal fly ash were examined in this research. The chemical analysis for the samples was conducted. Both samples are included as HCFA. The main components are silicon dioxide, calcium oxide and aluminium oxide. The mineral composition of the fly ash was determined by diffraction powder method (XRD) using a diffractometer (X'pert APD) from Philips with a goniometer PW 3020, a Cu lamp and a graphite monochromator. The analysis was carried out in the range of 15-70°2θ. XRD results for examined samples are presented in Tab. 1 and Tab. 2.

Tab. 1. Mineral composition of biomass fly ash

CHEMICAL COMPOUND	% CONTENT
SiO_2	51.3
CaO	12.0
Al_2O_3	10.4

MgO	3.18
Na_2O	0.37
P_2O_5	2.18
SO_3	5.66
K_2O	8.09
TiO_2	0.26
MnO	0.30
Fe_2O_3	1.30
NiO	0.06
ZnO	0.07
BaO	0.06
SrO	0.05

Tab. 2. Mineral composition of coal fly ash

CHEMICAL COMPOUND	% CONTENT
SiO_2	37.1
CaO	15.3
MgO	0.85
Al_2O_3	13.1
SO_3	2.93
K_2O	0.20
Na_2O	0.93
TiO2	1.59
V_2O_5	0.04
Cr_2O_3	0.02
MnO	0.02
Fe_2O_3	4.99
Co_3O_4	0.02
P_2O_5	0.45

2.2. Tests

The tests were carried out on the equipment for sorption and desorption of gases at elevated pressures (Fig. 1).

The principle of volumetric measurement was to expand a gas of known pressure and volume from a dosing ampoule into an ampoule containing a sorbent. The main part of the apparatus was the ampoule, which was a metal container with a capacity of 1 dm^3 placed in the thermostat. The compressed carbon dioxide, which was

in the bottle, was introduced into the dosing ampoule, and then, by opening the valves, it was dosed into the ampoule with a sorbent (fly ash). The thermostat provided a constant temperature with an accuracy of 1 K. In order to obtain correct results, the dead volume of the apparatus was calculated by subtracting the volume of ash grains from the total volume of the apparatus. The amount of absorbed carbon dioxide was calculated from gas laws, taking into account gas inertia. Before each experiment, the apparatus was degassed to the vacuum.

Fig. 1. Apparatus for the fly ash carbonation

The experiments were conducted at 3 different temperatures: 298, 323 and 343 K and a pressure range of CO_2 from 0.4 to 1.5 MPa. In each of the experiments, the pressure of carbon dioxide was increased by 3 points. The reaction time was from 48 to 72 h. The mass of the samples was selected so as to fill the measuring ampoule as much as possible. Tab. 3 and Tab. 4 present the individual data for samples.

Tab. 3. Experimental data for biomass fly ash

Sample mass [g]	Temperature [K]	Time [h]	Pressure [MPa]		
461.8	298	48	0.406	1.014	1.526
478.1	323	48	0.401	1.061	1.482
448.3	343	48	0.400	1.075	1.474

Tab. 4. Experimental data for coal fly ash

Sample mass [g]	Temperature [K]	Time [h]	Pressure [MPa]		
679.8	298	72	0.636	1.075	1.495
744.4	323	48	0.421	1.175	1.498
750.9	343	72	0.462	1.085	1.498

In Fig. 2, the results of the experiments at different temperatures and pressures are presented. The maximum sequestration capacity was achieved for biomass fly ash at 343 K and 0.7 MPa, and it was around 30 dm^3 CO_2/kg of fly ash. It has been noticed that the biggest values were obtained at the highest experimental parameters. Nevertheless, the slight change in sequestration capacity at the highest pressure and the different temperatures is observed. In order to fully explain this phenomenon additional studies are required.
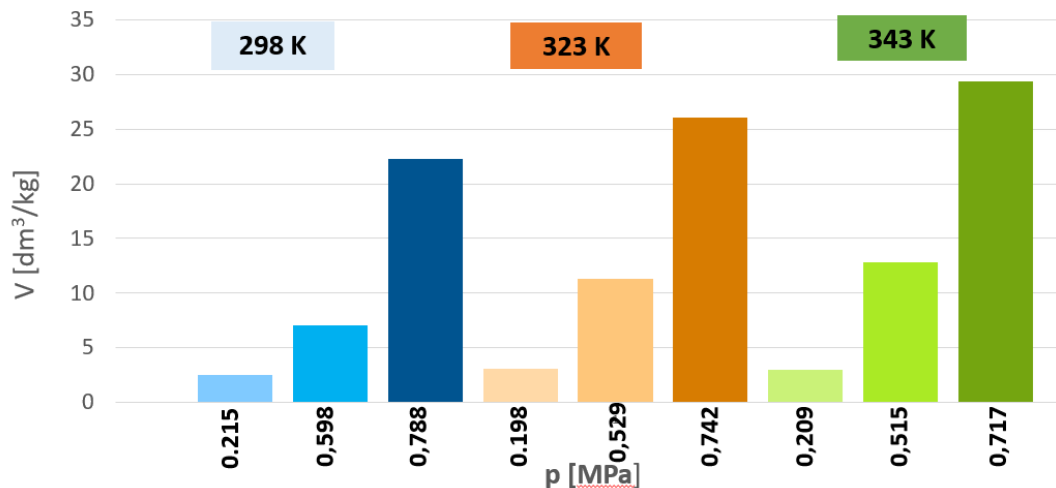
Fig. 2. Results of carbonation process for biomass fly ash

In Fig. 3, the results of experiments for fly ash fromthe power plant are shown. The maximum sequestration capacity was achieved at 298 K and 0,5 MPa, and it was around 26 dm^3 CO_2/kg fly ash. In opposite to biomass fly ash, the biggest value was obtained at the lowest temperature, however at the highest pressure. One of the possible reasons of this behaviour may be the occurrence of a physical CO_2 adsorption process.According to the literature, physical and chemical adsorption processes could take place simultaneously[9], [10]. First, the physical adsorption of carbon dioxide molecules appearedon the surface of the sorbent, and next the chemical reaction between CO_2 and calcium compounds occurred.
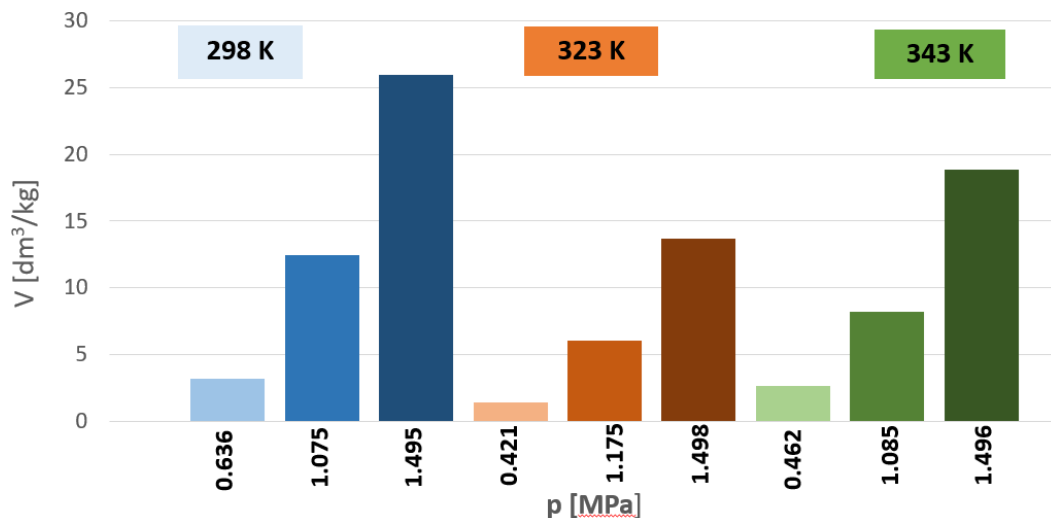
Fig. 3. Results of carbonation process for coal fly ash

3. Conclusions

The research has shown that increasing the pressure and temperature enhances the process of carbonation in case of biomass fly ash. However, it has been concluded that for fly ash from power plant increasing the temperature doesn't influence the effectiveness of carbonation process. Moreover, it has been proven that HCFA has a big potential in the carbonation process. Due to carbonation process, the reduction of carbon dioxide emission is possible as well asa new and promising way of fly ash utilisation is probable.

Acknowledgement

References

[1] M. Peters, B. Köhler, W. Kuckshinrichs, W. Leitner, P. Markewitz, and T. E. Müller, 'Chemicaltechnologies for exploiting and recycling carbondioxideinto the valuechain', ChemSusChem, vol. 4, no. 9, pp. 1216–1240, Sep. 2011.

[2] R. M. Cuéllar-Franca and A. Azapagic, 'Carbon capture, storage and utilisationtechnologies: A criticalanalysis and comparison of their life cycleenvironmentalimpacts', J. CO2 Util., vol. 9, pp. 82–102, Mar. 2015.

[3] K. Dombrowski, A. Buchwald, and M. Weil, 'The influence of calciumcontent on the structure and thermal performance of flyashbasedgeopolymers', J. Mater. Sci., vol. 42, no. 9, pp. 3033–3043, 2007.

[4] Z. T. Yao et al., 'A comprehensivereview on the applications of coalflyash', Earth-Sci. Rev., vol. 141, pp. 105–121, Feb. 2015.

[5] C. Modena, F. da Porto, and M. R. Valluzzi, Brick and Block Masonry: Proceedings of the 16th International Brick and Block Masonry Conference, Padova, Italy, 26-30 June 2016. CRC Press, 2016.

[6] M. Ahmaruzzaman, 'A review on the utilization of flyash', Prog. EnergyCombust. Sci., vol. 36, no. 3, pp. 327–363, Jun. 2010.

[7] A. Fauzi, M. F. Nuruddin, A. B. Malkawi, and M. M. A. B. Abdullah, 'Study of Fly Ash Characterization as a CementitiousMaterial', ProcediaEng., vol. 148, pp. 487–493, Jan. 2016.

[8] K.-H. Yang, E.-A. Seo, and S.-H. Tae, 'Carbonation and CO2 uptake of concrete', Environ. ImpactAssess. Rev., vol. 46, pp. 43–52, Apr. 2014.

[9] C. Siriruang, P. Toochinda, P. Julnipitawong, and S. Tangtermsirikul, 'CO2 captureusingflyash from coalfiredpower plant and applications of CO2-captured flyash as a mineraladmixture for concrete', J. Environ. Manage., vol. 170, pp. 70–78, Apr. 2016.

[10] A. Ćwik, K. Zarębska, P. Baran, and J. Szczurowski, 'Mineralna karbonatyzacja wysokowapniowego popiołu lotnego w warunkach podwyższonej temperatury i ciśnienia', Przem. Chem., vol. T. 96, nr 9, 2017.

Solution combustion synthesis as an efficient method for a catalyst preparation

Paulina Summa[1], Monika Motak, Bogdan Samojeden

[1]Faculty of Energy and Fuels, AGH University of Science and Technology, summa@agh.edu.pl

Abstract

Solution combustion synthesis(SCS) is a fast and precise method which provides uniform formation of nano-oxides. Such materials can be used directly as a support for a powder catalyst, or be deposited on structured catalysts, leading to a product with strong bond between active material and surface. Monoliths playan importantrole in environmental protection, among others in selective catalytic reduction currently used in power stations, or the future process of CO_2methanation. It was reported, that hydrotalcites can be produced throughout the SCS method. In order to handle the experimental part, the calculation path must be completed. The adiabatic temperature and reaction enthalpy had been calculated with accordance to a different ratio of fuels used, both for urea and glycine. Differences in a calculated flame temperature are not very significant, however glycine allows for a higher adiabatic temperature at the small percentage content of fuel.

Keywords: catalysis, hydrotalcites, solution combustion synthesis

1. Introduction

Dynamic development of industry and technology in last decades led to increasedenvironmental degradation, especially air pollution andgreenhouse effect, because of theconsiderableemissionsof flue gases from energy production, industry and transportation. Since the relation between industrial development and decline in conditions of the environment were settled, proper regulations were made to reduce the emissions of certain compounds to atmosphere. Usually the most efficient pollution control technologies are based on catalysis, such as e.g. selective catalytic reduction (SCR) used for reducing nitrogen oxides content in flue gases from power plants or diesel engines, or three way catalysts (TWC) purifying the outgases from mobile sources [1][2]. Also, some new proposed processes of chemical CO_2 utilization, such as e.g.methanationor dryreforming, require a catalyst.The latter processesresult not only in CO_2 mitigationbut also in the valuable gas products. Each of these technologies has its own specifics, however requirements for a good catalyst are similar despite the final application. A good catalyst should be selective, promoting the desired reaction, and reducing the amount of side products. Important is also catalytic activity, measured as the conversion of substrates to main product.Moreover, lifetime of a catalyst and itsdurability under the specific process conditions are significant. A catalyst can be deactivated by both temperature, pressure in bed or impurities in the inlet stream. Economy and feasibility of the catalyst preparation technologyare especially important from the industrial point of view[3]. Also, the catalyst preparation process should have as little steps as possible, in order to ensure satisfactory repeatability of the product, since the catalysts' performance isvery sensitiveto preparation process conditions. Solution combustion synthesis is gaining popularity, as illustrated by Figure 1, because thismethod allows fast preparation of a high-quality product. In 2018 SCS method was ca. six times more popular than 15 years ago, in 2003. In both SCR process used currently to reduce NOx emissions from power stations and future CO_2methanation applicationsthe applied catalyst must fulfill an additional requirement – it has to be prepared in a form suiTab. for the operation with high-volume gas streams. This explains the research directed towards monoliths and open-cell foams.

Hydrotalcites are layered hydroxides with brucite structure. The general formula is $[M^{II}_{1-x} M^{III}_x (OH)_2]_{x}+ A^{z-}_{x/z} \cdot nH_2O$, where: M^{II} and M^{III} are cations of di- and trivalent metals subsequently, A is type of interlayer anions, x is molar ratio[4].

In order to prepare the simple hydrotalcite-like material with a Ni^{2+}, Mg^{2+} and Al^{3+} in molar ratio 1:2:1, aluminum and magnesium nitrates have to be thermally transformed. During the preparation via combustion method, it is expected to obtain nano-oxides ofofNi, Mg and Al[5].

Such kind of nickel containing ex-hydrotalcitecatalyst can find application in the environmental protection processes. Nickel-hydrotalcite doped with lanthanum was tested as a catalyst in dry reforming of methane[6] and in carbon dioxidemethanation [7], confirming its applicability in this kind of reactions.

Goal of this paper was to compare preparation conditions of Ni-hydrotalcites specifically the adiabatic temperature in solution combustion synthesis, basing on the thermodynamic model, depending on the type of oxidizer used. This could then be used for the preparation of monolith-based hydrotalcite which would find application in CO_2 methanation process.
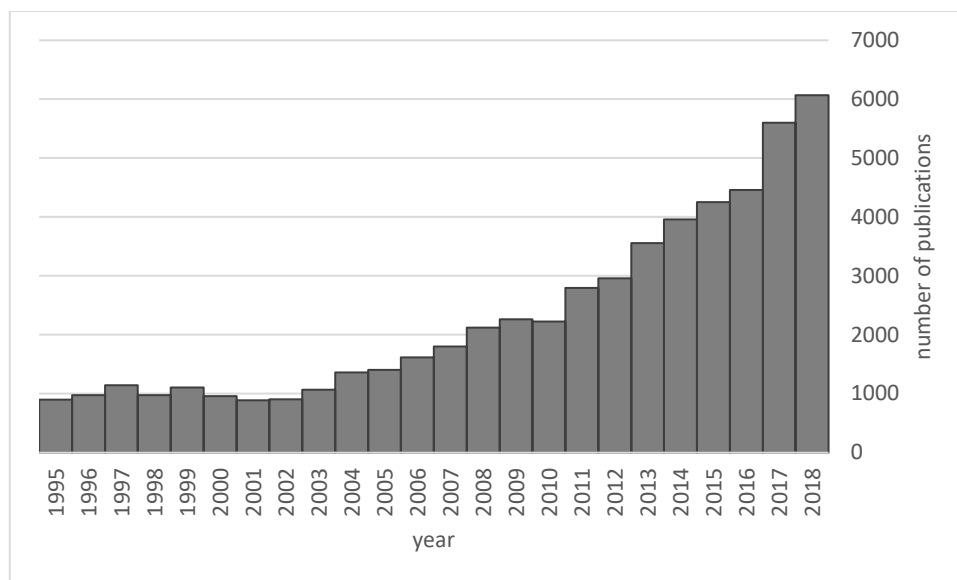

Fig. 1. Number of publications related to solution combustion synthesis method according to sciencedirect.com at 15th November 2018.

2.   Solution combustion synthesis

Solution combustion synthesis (SCS) is a methodbased on a redox reaction between proper precursors and a fuel. Precursors, usually in the form of highly reactive nitrates are mixed with thecombustible substance, forming an initial solution, that is later burned in a furnace. Stoichiometric parameters of the reaction are complex, depending strongly on theused ratio of fueltonitrates used[8]. The products of reaction are nano-oxides containing a metallic cation present in the initial mixture and high amounts of gases, such as carbon dioxide, nitrogen and water from the combusting compound [9]. Depending on the fuel content, oxygen may be a product (lean mixture, <100% of stoichiometric amount of fuel) or a substrate of the reaction (rich mixture, >100% of stoichiometric amount of fuel)[10]. Variety of reagents can be used as the combusting compound – the most popular is urea being a simple molecule, with low price and high availability. Likewise, glycine, saccharose, citric acid, sucrose, hydrazine-based fuels or acetylacetonewere proposed [11].

3.   Deposition of oxides over the structured catalyst

The deposition of a material on the surface of a structured catalyst is usually a challenge, due to the specific shape and properties of such structure. This is especially important for monoliths, which are currently used for applications where high flows and low-pressure drops are important, as in the case for SCR processes in power plants. The same will be important also for future chemical CO_2 mitigation processes, such as e.g. CO_2methanation which has already been introduced on a small industrial scale. The technique chosen in such cases should provide homogenous coverage of the surface, with uniform size of the crystallites, which will guaranteethe absence of the local limitations in mass transfer and pressure drop. Moreover, a deposited material is responsible for the porosity of the surface, so the deposition technique strongly influences the textural properties, among themspecificsurface area of formed nano-oxides, which should be possibly high. An additional problem when preparing monolith-supported materials is the strength of bonding between the monolith structure and the deposited material. Methods, such as impregnation or adsorption, do not always lead

to a very strong bond between the surface andthe material, in contrast tosolution combustion synthesis. Strong adhesion for so-prepared structures was confirmed by tests[12].

In case of solution combustion synthesis,it is important to precede the preparation procedure withproper thermodynamic calculations.

General reaction for all the SCS processes ispresented by Eq. 1:

$$Me^V(NO_3)_V + \frac{5}{9}v\varphi NH_2CH_2COOH + \frac{5}{4}v(\varphi-1)O_2 \rightarrow MeO_{\frac{V}{2}} + \frac{10}{9}v\varphi CO_2 + \frac{25}{18}v\varphi H_2O + \frac{5\varphi+9}{18}vN_2 \qquad [Eq.1][13]$$

Where:φ is ratio of fuel-to-nitrates used, $\varphi>0$,V is oxidation state of a cation.

In order to obtain magnesium oxide with urea as a fuel, the following reaction as in Eq.2 shouldoccur:

$$3Mg(NO_3)_2 + 5NH_2CONH_2 \rightarrow 3MgO + 8N_2 + 5CO_2 + 10H_2O \qquad [Eq.2]$$
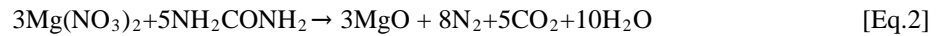
Depending on this equation, 2M solution of magnesium nitrate with stoichiometric amount of ureamust be prepared. The solution should be heated then for1 hour to 50 °C in order to dissolve the substrates, provide the homogenous mixing and to ensure the formation of complexes between the fuel and nitrates. The proper fuel is not only the energy supplier during the combustion process, but also the complexing agent, forming bonds with nitrates to provide stability during the combustion process, especially at the beginning when water evaporation occurs [14]. After one hour, the solution is ready to soak a monolith or a foam in it, for a 2-3 minutes. Afterwards, the structure is ready to be combusted in a furnace for 10 minutes, at a suiTab. temperature, which in case of MgO is 800 °C[15]. After the process, it is necessary to determinethe mass of the sample, to know the amount of species formed on the surface. The process should be repeated as many timesas necessary to obtain the desired amount of species on the structure.

4. Deposition of hydrotalcites

To estimate the temperature of a furnace and the amount of fuel used, the adiabatic temperature must be determined. It is calculated for different ratios of fuels and nitrates, usingEq. 3[16].

$$T_{ad} = T_O + \frac{\Delta H_r}{c_p} \qquad [Eq.3]$$

Where:T_0 is ambient temperature, ΔH_r is the enthalpy of the reaction and c_p is heat capacity of the products. These data for the discussed process are listed in Tab. 1.

Tab. 1 Enthalpies and heat capacities of the compounds [17]

	ΔH_0 [kJ/mol]	cp [J/molK]
$Al(NO_3)_3$	-3590.5	-
$Mg(NO_3)_2$	-3310.5	-
$Ni(NO_3)_2$	-2211.7	-
$C_2H_4N_2O$	-333.4	-
$C_2H_5NO_2$	-390.5	-
MgO	-601.6	47.27
Al_2O_3	-400.4	24.73
NiO	-239.7	44.00
N_2	0	27+0.004T
CO_2	-393.5	43+0.011T
O_2	0	25+0.015T

H_2O	-292.7	30+0.015T

5. Deposition with urea as a fuel

The reactions described by eq. 4, 5 and 6must occurin parallel in order to form a mixture of oxides, that will later be transformed into hydrotalcite.

$$2Al(NO_3)_3 \cdot 9H_2O + 5NH_2CONH_2 \rightarrow Al_2O_3 + 8N_2 + 5CO_2 + 20.5H_2O \qquad \text{[Eq.4]}$$

$$1Mg(NO_3)_2 \cdot 6H_2O + 1.667NH_2CONH_2 \rightarrow 1MgO + 2.667N_2 + 1.667CO_2 + 6.83H_2O \qquad \text{[Eq.5]}$$

$$1Ni(NO_3)_2 \cdot 6H_2O + 1.667NH_2CONH_2 \rightarrow 1NiO + 2.667N_2 + 1.667CO_2 + 9.33H_2O \qquad \text{[Eq.6]}$$
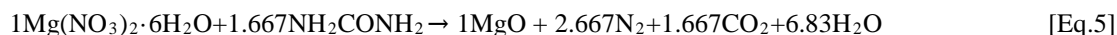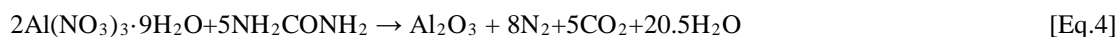
According to Davila et al. to produce Mg-Alhydrotalcites via solution combustion method, the process should occur attemperature range of 400-800°C for 10 minutesso the oxides will be formed.Then, after cooling, the obtained powder should be placed in a flask with 0.1M sodium carbonate and stirred for 5 minutes[5]. Subsequently, the sample should be dried and calcined to eliminate unsTab. phases.

With the change in the amount of supplied fuel, the stoichiometric coefficients change in a way presented in Tab.s2, 3 and 4, for the formation of magnesium oxide, alumina and nickel oxide. Since nickel and magnesium are both bivalent metals, the stoichiometric coefficients in redox reaction such as solution combustion synthesis are identical.

Tab.2 Stoichiometric coefficients for magnesium oxide formation through SCS with urea

$Mg(NO_3)_2$	$C_2H_4N_2O$	O_2	MgO	N_2	CO_2	H_2O	Fuelcontent
1	0,417	1,875	1	1,417	0,417	6,833	25%
1	0,83	1,25	1	1,83	0,83	7,667	50%
1	1,25	0,625	1	2,25	1,25	8,5	75%
1	1,667	0	1	2,667	1,667	9,33	100%
1	2,083	0,625	1	3,083	2,083	10,167	125%

Tab.3 Stoichiometric coefficients for aluminium oxide formation through SCS with urea

$Al(NO_3)_3$	$C_2H_4N_2O$	O_2	Al_2O_3	N_2	CO_2	H_2O	Fuelcontent
2	1,25	5,625	1	4,25	1,25	20,5	25%
2	2,5	3,75	1	5,5	2,5	23	50%
2	3,75	1,875	1	6,75	3,75	25,5	75%
2	5	0	1	8	5	28	100%
2	6,25	1,875	1	9,25	6,25	30,5	125%

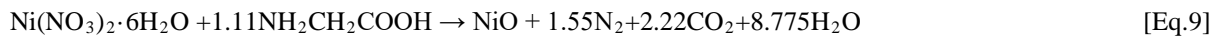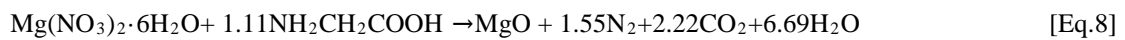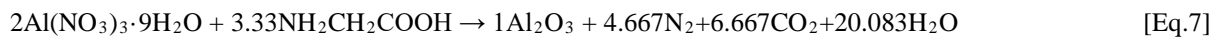Tab. 4 Stoichiometric coefficients for nickel oxide formation through SCS with urea

$Ni(NO_3)_2$	$C_2H_4N_2O$	O_2	NiO	N_2	CO_2	H_2O	Fuelcontent
1	0,417	1,875	1	1,417	0,417	6,833	25%

1	0,83	1,25	1	1,83	0,83	7,667	50%
1	1,25	0,625	1	2,25	1,25	8,5	75%
1	1,667	0	1	2,667	1,667	9,33	100%
1	2,083	0,625	1	3,083	2,083	10,167	125%

Asit may be seen,with the increase in fuel-to-nitrates ratio, the amount of gases produced during the reaction is growing. Therefore, in order to preserve the structure from dynamic formation of gases, which could decrease the formation of micropores and result in lowspecific surfacearea,the temperature should not be very high [14]. Additionally, the data indicate, that during the formation of alumina, almostthree times more gases are formed, than in case ofmagnesium oxide.

6.   Deposition with glycine as the fuel

The calculation procedure with glycine as the fuel was similar as in case of urea. The equations were balanced for the different amounts of the fuel supplied. Glycine decomposition leads to molar composition of the formed gasesdifferent from that for urea.Especially nitrogen and carbon dioxideamounts vary in comparison to those originating from urea decomposition. Equations 7,8 and 9 illustrate the basic reactions inside the furnace[18]:

$$2Al(NO_3)_3 \cdot 9H_2O + 3.33NH_2CH_2COOH \rightarrow 1Al_2O_3 + 4.667N_2 + 6.667CO_2 + 20.083H_2O \qquad [Eq.7]$$

$$Mg(NO_3)_2 \cdot 6H_2O + 1.11NH_2CH_2COOH \rightarrow MgO + 1.55N_2 + 2.22CO_2 + 6.69H_2O \qquad [Eq.8]$$

$$Ni(NO_3)_2 \cdot 6H_2O + 1.11NH_2CH_2COOH \rightarrow NiO + 1.55N_2 + 2.22CO_2 + 8.775H_2O \qquad [Eq.9]$$

The obtained stoichiometric coefficients are compared, depending on a percent offuel used,where 100% corresponds to stoichiometric amount in Tab.s 5, 6 and 7.

Tab.5 Stoichiometric coefficients for magnesium oxide formation through SCS with glycine

$Mg(NO_3)_2$	$C_2H_5NO_2$	O_2	MgO	N_2	CO_2	H_2O	Fuelcontent
1	0,277	1,876	1	0,82	0,555	6,692	25%
1	0,555	1,251	1	1,278	1,11	7,388	50%
1	0,833	0,624	1	1,426	1,667	8,083	75%
1	1,11	0	1	1,55	2,22	8,78	100%
1	1,39	0,625	1	1,695	2,78	9,47	125%

Tab.6 Stoichiometric coefficients for aluminium oxide formation through SCS with glycine

$Al(NO_3)_3$	$C_2H_5NO_2$	O_2	Al_2O_3	N_2	CO_2	H_2O	Fuel content
2	0,833	5,624	1	3,416	1,667	20,083	25%
2	1,667	3,753	1	3,834	3,33	22,167	50%
2	2,5	1,875	1	4,25	5	24,25	75%

| 2 | 3,33 | 0 | 1 | 4,667 | 6,667 | 26,33 | 100% |
| 2 | 4,167 | 1,875 | 1 | 5,083 | 8,33 | 28,417 | 125% |

Tab. 7 Stoichiometric coefficients for nickel oxide formation through SCS with glycine

$Ni(NO_3)_2$	$C_2H_5NO_2$	O_2	NiO	N_2	CO_2	H_2O	Fuelcontent
1	0,277	1,876	1	1,138	0,555	6,692	25%
1	0,555	1,251	1	1,278	1,11	7,388	50%
1	0,833	0,624	1	1,426	1,667	8,075	75%
1	1,11	0	1	1,55	2,22	8,78	100%
1	1,39	0,625	1	1,695	2,78	9,475	125%

7. Results

Considering the stoichiometry of the reactions, depending on the ratio of fuel used, adiabatic temperature was calculated according to the eq. 3. The enthalpy of the compounds and heat capacities usedwere taken fromTab.1. Figures 1, 2 and 3 show changes of adiabatic temperature as a function of fuel content.
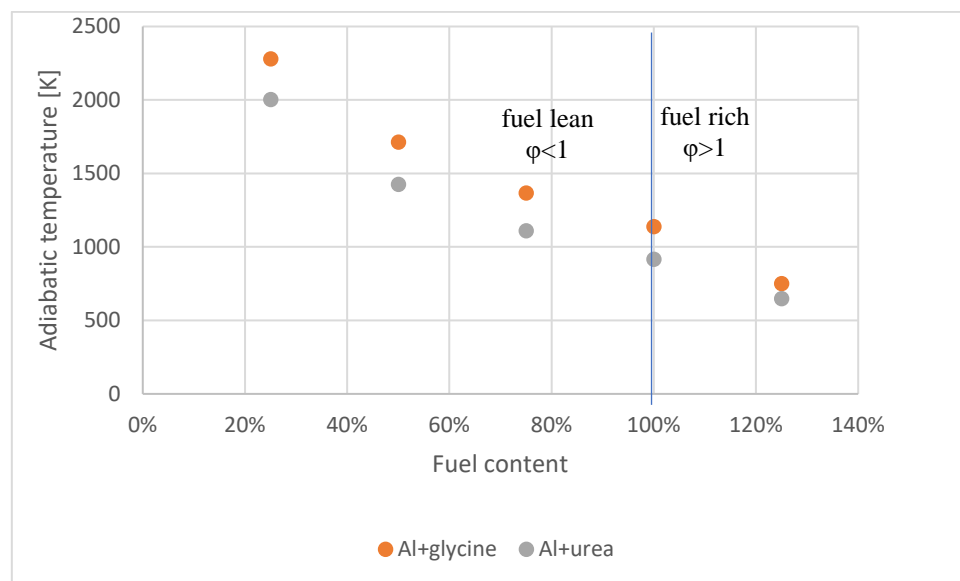

Fig. 2. Changes in a adiabatic temperature of Al_2O_3 formation, depending on a type of the fuel used as a function of the amount of the fuel
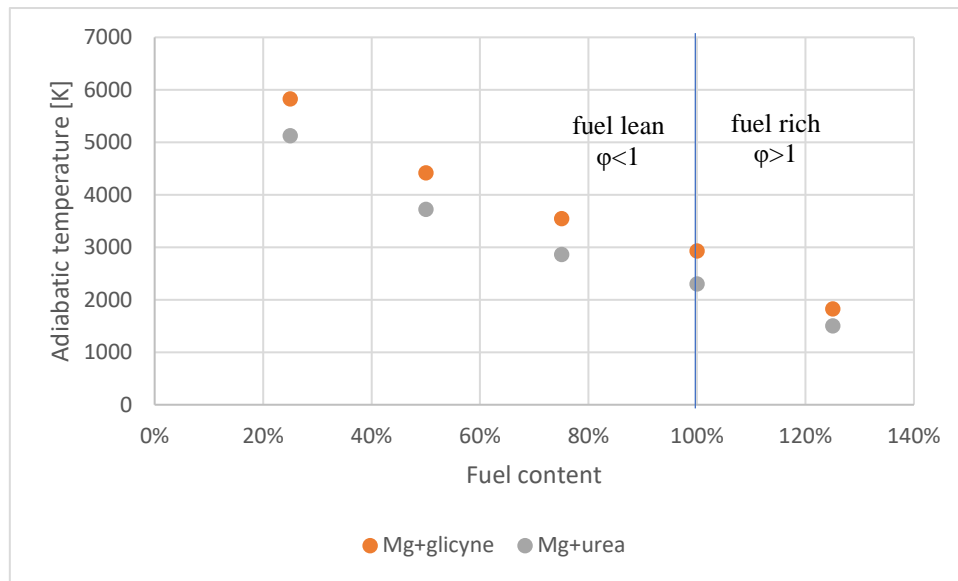
Fig. 3. Changes in a adiabatic temperature of MgO formation, depending on a type of the fuel used as a function of the amount of the fuel
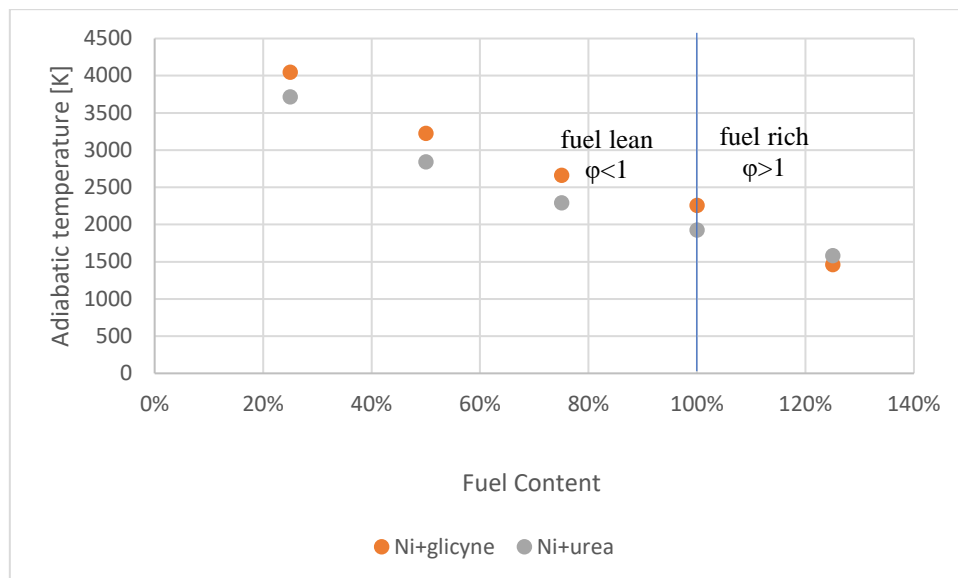

Fig. 4. Changes in a adiabatic temperature of NiO formation, depending on a type of the fuel usedas a function of the amount of the fuel

Inall Figures, higher possible adiabatic temperature is obtained with a glycine used as fuel. Temperature decreasesalmost linearly with the increased amount of fuel both for urea and glycine. For the fuel-rich mixturesthe appropriate temperatures are almost the same for both oxidizers. On the other hand, in fuel-lean mixtures therelevant temperaturediffers by 600 - 200°C. Only forabove-stoichiometric nickel oxide formation, urea gives higher adiabatic temperatures than glycine when mixture is rich in fuel. The difference between the temperature generated with urea and with glycine decreases with the increase of fuel-to-nitrates ratio.

8.   Conclusions

A mixture of oxides suiTab. for the preparation of hydrotalcites can be prepared via the solution combustion synthesis. Basing on the thermodynamics appropriate temperatures for the formation of hydrotalcite on a monolith were determined at different fuel-rich or fuel-lean mixtures. When using the stoichiometric ratios of fuel-to-nitrate precursors, the difference in adiabatic temperature of the reaction is negligiblefor urea and glycine applied as fuels. However, in the below-stoichiometric mixtures, glycine is a better choice, allowing to obtain higher temperature during the combustion and the shorter time of the reaction.

References

[1] J. Hagen, Industrial catalysis: A practical approach. 2015.

[2] N. Takahashi et al., "The new concept 3-way catalyst for automotive lean-burn engine: NOx storage and reduction catalyst," Catal. Today, 1996.

[3] G. Öhlmann, "Handbook of Heterogeneous Catalysis," Zeitschrift für Phys. Chemie, 1999.

[4] E. S. Publishers, "Hydrotalcite-type anionic clays: preparation, properties and applications, I I (I99 I) 173-301 Elsevier Science Publishers," Catal. Today, vol. 11, pp. 173–301, 1991.

[5] V. Dávila, E. Lima, S. Bulbulian, and P. Bosch, "Mixed Mg(Al)O oxides synthesized by the combustion method and their recrystallization to hydrotalcites," Microporous Mesoporous Mater., vol. 107, no. 3, pp. 240–246, 2008.

[6] H. Liu et al., "La-promoted Ni-hydrotalcite-derived catalysts for dry reforming of methane at low temperatures," Fuel, 2016.

[7] D. Wierzbicki, R. Debek, M. Motak, T. Grzybek, M. E. Gálvez, and P. Da Costa, "Novel Ni-La-hydrotalcite derived catalysts for CO2methanation," Catal. Commun., vol. 83, pp. 5–8, 2016.

[8] A. S. Mukasyan, P. Epstein, and P. Dinka, "Solution combustion synthesis of nanomaterials," Proc. Combust. Inst., vol. 31, no. 2, pp. 1789–1795, 2007.

[9] J. C. Toniolo, A. S. Takimi, and C. P. Bergmann, "Nanostructured cobalt oxides (Co3O4 and CoO) and metallic Co powders synthesized by the solution combustion method," Mater. Res. Bull., vol. 45, no. 6, pp. 672–676, 2010.

[10] S. T. Aruna and A. S. Mukasyan, "Combustion synthesis and nanomaterials," Curr. Opin. Solid State Mater. Sci., vol. 12, no. 3–4, pp. 44–50, 2008.

[11] S. T. Aruna, Solution Combustion Synthesis. Elsevier Inc., 2017.

[12] S. Specchia, G. Ercolino, S. Karimi, C. Italiano, and A. Vita, "Solution combustion synthesis for preparation of structured catalysts: A mini-review on process intensification for energy applications and pollution control," Int. J. Self-Propagating High-Temperature Synth., 2017.

[13] A. Kumar, E. E. Wolf, and A. S. Mukasyan, "Solution combustion synthesis of metal nanopowders: Nickel-Reaction pathways," AIChE J., 2011.

[14] W. Wen and J. M. Wu, "Nanomaterials via solution combustion synthesis: A step nearer to controllability," RSC Advances. 2014.

[15] F. Granados-Correa, J. Bonifacio-Martínez, V. H. Lara, P. Bosch, and S. Bulbulian, "Cobalt sorption properties of MgO prepared by solution combustion," Appl. Surf. Sci., 2008.

[16] S. K. Ghosh, S. Pal, S. K. Roy, S. K. Pal, and D. Basu, "Modelling of flame temperature of solution combustion synthesis of nanocrystalline calcium hydroxyapatite material and its parametric optimization," Bull. Mater. Sci., vol. 33, no. 4, pp. 339–350, 2010.

[17] A. Varma, A. S. Mukasyan, A. S. Rogachev, and K. V. Manukyan, "Solution Combustion Synthesis of Nanoscale Materials," Chem. Rev., vol. 116, no. 23, pp. 14493–14586, 2016.

[18] S. L. González-Cortés and F. E. Imbert, "Fundamentals, properties and applications of solid catalysts prepared by solution combustion synthesis (SCS)," Appl. Catal. A Gen., vol. 452, pp. 117–131, 2013.

Modified hydrotalcite-like derived materials as effective catalysts for DeNO$_x$ systems and N$_2$O decomposition

Agnieszka Szymaszek[1], Bogdan Samojeden[1], Monika Motak [1]

[1]*AGH University of Science and Technology, A. Mickiewicza 30, 30-059, Kraków, Poland, e-mail:agnszym@agh.edu.pl*

Abstract

In recent years, a serious problem of excessive emission of adverse nitrogen oxides is observed. The most efficient technology of NO$_x$ abatement is the selective catalytic reduction (SCR) and current, the majority of industrial DeNO$_x$ systems is based on this method. The SCR reaction involves reduction of harmful nitrogen oxides by the reducer (ammonia or hydrocarbons) into molecular nitrogen and water vapour. Although the commercial catalyst, alumina- or titania-supported V$_2$O$_5$-WO$_3$ or V$_2$O$_5$-MoO$_3$ gives relatively high conversion, its application is limited by relatively narrow temperature window and toxicity of vanadium oxide. Therefore, finding the novel, economic and eco-friendly catalyst is a big challenge.Layered double hydroxides have been investigated as potential catalysts and catalysts supports for NO$_x$ removal. The layer structure of these materials is closed to brucite in which a part of Mg^{2+}cations is replaced by Al^{3+}. Interlayer carbonate anions provide the electro-neutrality of the structure. LDHs are very attractive for catalytic applications, especially due to the direct synthesis and easy modulation of the chemical composition. The paper involves a mini-review of the application of modified LDHs in the SCR process.

Keywords: *Hydrotalcite, selective catalytic reduction, NO$_x$*

1. Introduction

Nitrogen oxides (NO$_x$) which are generated by combustion of fuels, have highly adverse impact on the environment, biological ecosystems and human health. NO$_x$ cause depletion of the ozone layer and acid rain. Moreover the combustion of fossil fuels is the major source of PM$_{2.5}$[1–4]. Another, very adverse nitrogen-containing compound emitted mainly due to anthropogenic activities is N$_2$O. It contributes to the global warming and stratospheric ozone depletion, therefore it strongly affects the world climate change[5]. According to that, the control of NO$_x$ and N$_2$O emissions from combustion and chemical processes is highly significant. Selective catalytic reduction (SCR) is nowadays considered to be the most efficient technology of nitrogen oxides

removal[6–11]. The process is based on the reaction of nitrogen oxides with the reducing agent (e.g. ammonia or hydrocarbons) and formation of harmless nitrogen and water vapour. Fig. 1.1. shows an idealized scheme of NH$_3$-SCR [2,12].
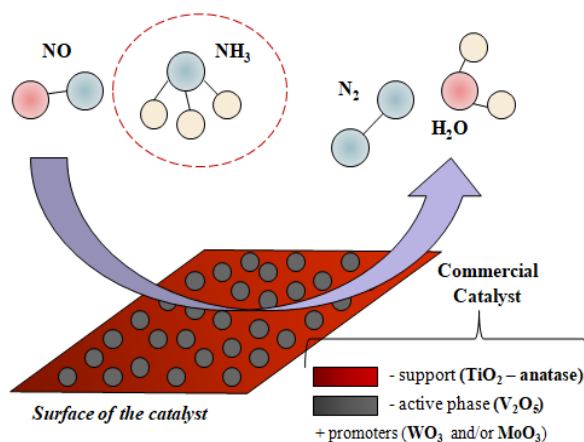

Fig. 1.1. The scheme of NH$_3$-SCR.

The catalyst used on industrial scale is V_2O_5-WO_3-TiO_2 on a ceramic monolith [13]. As the high efficiency of the catalyst is obtained at temperatures ranging from 300 to 400ºC, it is usually placed in the "high-dust" position, where it may undergodeactivation by SO_2 or fly ash. The application of the catalyst at the "tail-end position" or downstream of the electrostatic precipitator and upstream of desulphurization installation can be a reasonable solution. On the other hand, for the effective operation of the catalyst, the reheating of flue gas is indispensable [2,14]. In this context, many new catalysts for the NO_x reduction have been proposed, including modified clays, supported metal oxides, metal exchanged zeolites or activated carbon modified with nitrogen compounds or promoted by transition metals [3,15–21]. Recently, an increasing attention has been paid to mixed metal oxides derived from layered double hydroxides (LDHs) [1,14,22–25]. The paper summarizes the literature data on the possible applications of modified layer double hydroxides and their derivatives in the removal of NO_x and catalytic N_2O decomposition from outgases.

2. What are layered double hydroxides?

Layered double hydroxides (LDHs) are a group of ionic lamellar materials represented by the general formula $[M_{1-x}{}^{II}M_x{}^{III}(OH)_2]^{x+}(A^{n-})_{x/n} \cdot yH_2O$, where M^{2+} and M^{3+} are di- and trivalent cations, respectively and A^{n-} is a hydrated anion. The structure of LDHs derives from brucite, $Mg(OH)_2$ in which a fraction x of Mg^{2+} ions is substituted by a trivalent ion, e.g. Al^{3+}. Therefore, the generated positive charge is compensated by anions A^{n-} situated with the water molecules in the interlayer position. The molar ratio of $M^{2+}/(M^{2+} + M^{3+})$ is expressed by the value x and generally it is in the range of 0.2 - 0.33 [14,26,27]. The structure of LDHs is shown inFig. 2.1.[26,28].
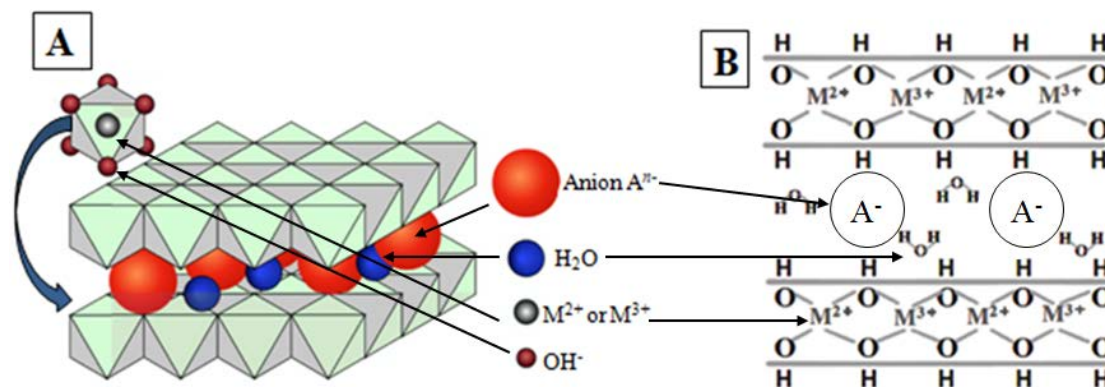

Fig. 2.1. The structure of hydrotalcite-like materials: layered structure (A), chemical bounds in interlayer (B) (based on [26,28]).

Some of the Mg^{2+} and Al^{3+}cations can be replaced by other divalent (e.g. Co, Cu, Ni, Zn) or trivalent (e.g. Cr, Ga, Mn, Fe, Co) ions, respectively [23,29,30]. Moreover, in contrast to layered clays, LDHs also called as "anionic clays" due to their anion-exchange properties. Therefore, incorporation of a large variety of interlayer anions is possible, e.g. oxovanadates[22], chromates [27], molybdates[31], NO_3^-, SO_4^{2-}[32].LDHs are thermally stable to about 400ºC. The low-temperature of LDHs decomposition (400-500ºC) results in the removal of interlayer water molecules, interlayer anions and hydroxyls. Consequently, the disordered phase which can be reconstructed by hydrothermal treatment is formed. Upon the calcination at a mild temperature (e.g. above 500ºC), the formation of mixed metal oxides or metal spinels with increased surface area and high dispersion of metal takes place [23,33]. In that case, rehydration of the lamellar structure leads to a drastic decrease in the specific surface area and changes in the morphology, related to the formation of compact aggregates of regenerated LDHs [34,35]. However, at certain temperatures of thermal treatment, hydrotalcite-like materials demonstrate so called "structural memory effect" [36]. Recently, a considerable interest has been focused on application of modified LDHs as the catalysts and catalysts supports for the $DeNO_x$ reaction, including reduction of NO with NH_3[14,24,37], hydrocarbons [38], CO [39] or catalytic decomposition of NO [40,41]. These materials were also found to have a considerable potential in the removal of N_2O via catalytic decomposition route [5,25,42–44].

3. Methods of preparation

The synthesis of layered double hydroxides is easy and inexpensive on both laboratory and industrial scale. Moreover, depending on the chosen method of preparation, materials with different physical and chemical properties can be tailored [29]. The most popular route of LDHs synthesis is "one-pot" co-precipitation at variable or constant pH. The method is based on adding a base solution to the solution that contains M^{II} and M^{III} salts. Chemical, structural and textural properties were reported to be determined by the pH of co-precipitation and the molar ratio of di- and trivalent cations[35]. Co-precipitation of hydrotalcites is the most frequently used method to synthesize materials for $DeNO_x$ application [14,24,38]. Another method of LDHs preparation is the sol-gel, described for the first time by Lopez et al. [45]. It was reported, that the materials obtained via sol-gel route show high thermal stability and enhanced specific surface area [46]. Wongkerd et al. [47] synthesized hydrotalcite-like materials intercalated with deoxycholate and Keggin-type polyoxometalates by hydrothermal treatment and anion-exchange. Subsequently the materials were impregnated with Fe and tested as NH_3-SCR catalysts and they appeared to yield high NO conversion and over 99% of N_2/N_2O, which is higher than for the commercial catalyst. Another synthesis route described by Dávila et al. [48] is based on the decomposition of organic fuels (e.g. urea, glycine, commercial sugar) and is much less time consuming than the common methods of LDHs synthesis. In order to obtain hydrotalcite-like materials, the precursors of Mg-Al-O mixed oxides are mixed with sodium carbonate and fuel and then the mixture is combusted for about 5 minutes at the temperature range 450-850°C. In order to recrystallize LDHs structure, obtained mixed metal oxides are subsequently put in contact with Na_2CO_3 solution. The combustion method is attractive due to the fact, that in comparison to the co-precipitation or sol-gel route, there is no necessity to spend high amounts of solvents or heat the precursors for a long time. However, LDHs synthesized by combustion has not yet been tested as nor $DeNO_x$ or N_2O decomposition catalysts.

4. Catalytic properties in NO_x removal

4.1. Application in NH_3-SCR

There is a considerable number of approaches that have been reported for the application of the hydrotalcite-derived materials in NH_3-SCR or N_2O decomposition. Chmielarz et al. investigated the catalytic properties of mixed metal oxides derived from hydrotalcites and doped with different amounts of transition metals (Co and Cu) in NH_3-SCR [23]. The catalysts were obtained by co-precipitation method from aqueous solutions of metal nitrates at constant pH of 10.0. The samples were calcined at 600°C for 16 h. XRD analysis indicated that as-prepared materials have a hexagonal structure. Reflections of(003), (006), (009), (015) and (018) planes characteristic forhydrotalcites were observed at the diffractogram. It was noticed that after the introduction of transition metal, the interlayer distance was reduced. Additionally, the specific surface area (SSA) determined by BET method for the calcined samples varied from 71 to 154 m^2/g. However, the increase of Cu and/or Co content resulted in the reduction of SSA.The study of the interactions between NO_x molecules and the catalyst surface was carried out by temperature-programmed experiment. An interesting observation was reported for the samples doped with copper. After introduction of Cu into Mg-Al, the amount of adsorbed NO significantly increased due to the formation of weakly adsorbed -NO surface species. The formation of NO sorption centres has a significant role in SCR process, which was proven by the catalytic tests. The highest NO conversion in range of 80-95% and selectivity towards N_2 at about 93-97%, depending on the transition metal content, was observed for Cu-Mg-Al. For Co-containing materials much lower conversion were observed, while for Cu-Co-Mg-Al catalytic performance strongly depended on the transition metal content.

The studies over hydrotalcite derived Cu-Mg-Al catalysts for selective reduction of NO with ammonia were continued by Basąget al.[24]. Cu-Mg-Al mixed metal oxide were doped with cerium (0.5 and 3.0 wt%) and tested in the NH_3-SCR. The samples were prepared by co-precipitation method, impregnated with cerium and calcined at 600°C for 12 h. XRD analysis performed after calcination indicated, that under thermal treatment the samples were decomposed to the mixed metal oxides. The appearance of characteristic reflections of CeO_2 at about 29°, 47° and 56° indicated its successful deposition on the catalysts surface. For the sample with 0.5 wt% of CeO_2 the reflections had very low intensity, while for 3 wt%, the formation of aggregated crystallites was proved by intense reflections. In case of the S_{BET}, both studied samples exhibited similar values of about 240 m^2/g. H_2-TPR analysis was performed in order to determine the reducibility of the hydrotalcite-based catalysts. The introduction of cerium resulted in the appearance of a peak at 110°C attributed to the reduction of Ce^{4+} to Ce^{3+} on

the surface by atomic hydrogen species, while peaks at 740 and 790°C for the samples with 0.5 wt% and 3.0 wt% related to Ce^{4+} to Ce^{3+} reduction in CeO_2. The major contribution into the reducibility of the sample had CeO_2 and only a small amount of surface cerium was reduced by hydrogen. Moreover, the reduction of Ce^{4+} to Ce^{3+} occurred at lower temperatures for smaller CeO_2 crystallites in comparison to the large crystallites of CeO_2. The most effective NO conversion was obtained at about 125 to 325°C for the non-modified sample. About 92% conversion was reached at 310°C. The selectivity to N_2 at the whole temperature range reached above 90%. For the both samples doped with cerium, considerable shift into the lower temperatures by about 30-50°C in comparison to the non-modified sample was reported. Independently on the cerium content, the samples exhibited the maximum NO conversion of 96% at 275°C. The extent of the decrease in NO conversion which is related to the side-reaction of ammonia oxidation, was less intensive for samples with higher loading of cerium.

Mradet al.[38] presented an attempt to apply mixed metal oxides derived from LDHs for simultaneous elimination of NO_x and volatile organic compounds (VOCs). The series of catalysts based on hydrotalcite-like materials containing copper and iron was synthesized by the co-precipitation method. The samples were prepared at the constant temperature of 60°C and pH of ca. 8, maintained by the addition of the solution of NaOH and Na_2CO_3. The obtained solids were calcined at 500°C. Four samples with various copper content and constant iron content were synthesised. The results of XRD analysis indicated the presence of characteristic hydrotalcite-like structures. After calcination, transformation into the mixed metal oxides and spinels of MgO, CuO, γ-Fe_2O_3 or Fe_3O_4, $MgFe_2O_4$ and $CuFe_2O_4$ took place. S_{BET} analysis indicated that the specific surface area of the samples significantly decreased after calcination (from 80 m^2/g to 49 m^2/g). Moreover, it was lower for the increased copper loading. It can be explained by higher crystallization and aggregation of copper species. Redox properties were determined by the H_2-TPR analysis. Two reduction regions were distinguished on the H_2-TPR profile: low-temperature range (T < 350°C) exhibited by CuO and $CuFe_2O_4$ and high-temperature range (T > 350°C) derived from the reduction of γ-Fe_2O_3 and Fe_3O_4. Additionally, the analysis indicated the presence of various forms of metals: highly dispersed copper species in a form of isolated ions and clusters and bulky CuO, as well as the reduction of Fe_2O_3 to Fe_3O_4 and Fe_3O_4 to 3·FeO. The results of the catalytic tests carried out with simultaneous elimination of NO and propene over the $Cu_xMg_{4-x}FeAl$ mixed metal oxides indicated that with the increasing Cu loading, T_{50} decreased and the maximum NO conversion increased. However, excessive copper content resulted in aggregation of metal species and blocking of the active sites for propene oxidation and NO reduction. With the intermediate value of Cu, the metal species were easily available for the reagents, therefore the conversion of NO_x and VOCs was enhanced.

4.2. N₂O decomposition

Recently, much attention has been also paid to the catalytic decomposition of nitrous oxide. The studies over catalysts for N_2O abatement indicated that especially noble metals[49–51], Fe-zeolites[52–56] and Cu-supported materials[54,57–60] exhibit high conversion. Additionally, mixed metal oxides prepared by the thermal treatment of layered double hydroxides were reported to be effective catalysts for N_2O removal. According to the literature, one of the most active catalysts for N_2O decomposition are LDHs-derived mixed metal oxides containing cobalt and manganese[5,25,43,61].

Obalová et al.[62] studied Co- and Mn-containing mixed oxides derived from LDHs for the catalytic decomposition of N_2O. The samples were prepared by the co-precipitation method with the various Co:Mg:Mn:Al molar ratio. XRD measurements indicated that only for the precursors of mixed metal oxides well-crystallized hydrotalcite phase was observed. After calcination, the samples exhibited relatively low crystallinty and diffraction lines observed were assigned to spinel-like Co-oxides. Therefore, thermal treatment of LDHs resulted in the formation of mixed oxides phase and hydrotalcite structure degradation. The analysis of S_{BET} showed that the specific surface area of the samples decreased with the increasing Co content and it reached from 44 to 106 m^2/g. Reducibility of the catalysts was determined by H_2-TPR studies. The results showed two temperature regions of the reduction of metal species: low-temperature peak (200-400°C) corresponding to Co and high-temperature peak from Mn. After substitution of Co for Mg or Mn for Al, the second temperature peak shifted to higher temperature, while the first peak stayed unchanged. Hence, the reducibility and consequently the catalytic activity was worse for materials with higher content of Al and/or Mg. Catalytic tests indicated that the highest activity was exhibited by the material with the highest Co content. The decomposition of N_2O started at 330°C and at 450°C it reached almost 100%. The result is in agreement with the

H_2-TPR analysis which showed that the highest reducibility of active metal species occurred between 350 and 450ºC. High catalytic activity of Co- and Mn- containing catalysts derived from LDHs in N_2O decomposition is a consequence of the favourable oxidation state of metal cations present on the surface. Due to the oxidation-reduction mechanism of N_2O confirmed by Jabłońska et al. [25], the amount of reducible components in the catalyst should be optimized in order to achieve high activity. Easily reducible active metal species incorporated into LDHs structure were reported to considerably enhance the catalytic activity in N_2O decomposition.

According to literature, noble metals [63,64] and alkali metals [65–67] were tested as promoters of the catalytic decomposition of nitrous oxide. Karásková et al. [5] studied the effect of promotion of Co-Mn-Al mixed oxide derived from hydrotalcite with noble metals (Pt, Pd) and alkali metals (Li, Na, K). The various amounts of the promoters were added into the Co-Mn-Al mixed oxide by two methods: impregnation or co-precipitation during the LDHs synthesis route. XRD analysis indicated that the well-crystallized hydrotalcite-like structure was formed and the addition of the promoters had no significant influence on the phase composition. H_2-TPR analysis was performed in order to determine the reducibility of the promoted mixed metal oxides. For the non-modified Co-Mn-Al, two temperature regions were distinguished. Low temperature peak at 200-400ºC corresponds to the reduction of Co^{3+} to Co^{2+} and Co^{2+} to Co^0 and reduction of Mn^{4+} species, while high temperature peak at 400-900ºC corresponds to the reduction of Co and Mn in a surrounding of spinel-like phase. The promotion of the samples with Pt and Pd resulted in the shift of high temperature peak to lower values for both impregnated and co-precipitated catalysts. However, in case of impregnation, bigger particles of noble metal were formed, while for co-precipitated materials the promoters species were well-dispersed, enhancing the reduction of Co and Mn. In case of alkali metals, the addition of Na and Li shifted the high temperature peak to lower temperature. No significant changes were observed in case of K-promoted catalysts. Catalytic tests indicated that a small amount of Pd or Pt enhanced the activity in N_2O decomposition, but a higher content of Pd leads to the decrease of the activity. For the catalysts promoted with alkali metals, the addition of K and Na increased the catalytic activity of Co-Mn-Al mixed oxides, while those doped with Li, the activity in N_2O conversion decreased with the rising Li content. Moreover, promoting with potassium had significantly higher impact on the catalytic activity, in comparison to Na. The discrepancy in the catalytic performance of Co-Mn-Al mixed oxides doped with alkali metals were explained by the modification of the surface of the catalyst that results in the changes of the metal-oxygen bond strength.

5. Conclusions

Layered double hydroxides (also known as anionic clays or hydrotalcite-derived materials) are an interesting class of materials, which may be synthesized via various routes. Their thermal treatment results in the formation of mixed metal nano-oxides with high specific surface area and enhanced catalytic performance. One of the biggest advantages is the possibility of simultaneous incorporation of several catalytically active species into one sample. There were a several approaches to apply modified LDHs as the catalysts for the DeNO$_x$ systems and N_2O decomposition. It was found that hydrotalcite-derived materials show catalytic activity comparable or even higher than that of the commercial SCR catalyst. According to literature, the most promising materials are mixed metal oxides containing copper and iron. Additionally, it was proven that Cu-Mg-Al exhibit better reducibility than the non-modified sample, hence, better catalytic performance in NO conversion was obtained. Mixed metal oxides derived from hydrotalcites can be also used for the simultaneous elimination of NO$_x$ and VOCs. Catalytic tests carried out over LDHs modified with Cu- and Fe- oxides indicated that with the increasing CuO content, the catalytic performance was enhanced, especially due to the high dispersion of active species on the catalysts surface. Moreover, hydrotalcite-derived mixed metal oxides, especially Co-Mn-Al, exhibit high activity in N_2O decomposition. Promoting with alkali metals, such as K and Na results in increased conversion of nitrous oxide, while for Li the opposite effect was observed. Additionally, promoting with noble metals, the incorporation ofPt and Pd also considerably contributes to the increased catalytic performance. In summary, LDHs-derived materials, due to their attractive properties and relatively simple and cheap synthesis route, are promising for the application in DeNO$_x$ systems and catalytic elimination of N_2O. However, the materials still need improvements and optimization of their properties in order to apply them on industrial scale.

Acknowledgment

References

[1] Wu, X. et al. Enhancing DeNOx performance of CoMnAl mixed metal oxides in low-temperature NH3-SCR by optimizing layered double hydroxides (LDHs) precursor template. Appl. Surf. Sci.467–468, 802–810 (2019).

[2] Motak, M., Kuterasiński, Ł., Da Costa, P. & Samojeden, B. Catalytic activity of layered aluminosilicates for VOC oxidation in the presence of NOx. Comptes Rendus Chim.18, 1106–1113 (2015).

[3] Samojeden, B., Motak, M. & Grzybek, T. The influence of the modification of carbonaceous materials on their catalytic properties in SCR-NH3. A short review. Comptes Rendus Chim.18, 1049–1073 (2015).

[4] Li, Z., Jiang, J., Ma, Z., Wang, S. & Duan, L. SC. Atmos. Environ. (2015). doi:10.1016/j.atmosenv.2015.08.046

[5] Karásková, K., Obalová, L., Jirátová, K. & Kovanda, F. Effect of promoters in Co – Mn – Al mixed oxide catalyst on N 2 O decomposition. 160, 480–487 (2010).

[6] Cheng, X. & Bi, X. T. A review of recent advances in selective catalytic NOx reduction reactor technologies. Particuology 1–18 (2014). doi:10.1016/j.partic.2014.01.006

[7] Guan, B., Zhan, R., Lin, H. & Huang, Z. Review of state of the art technologies of selective catalytic reduction of NO x from diesel engine exhaust. Appl. Therm. Eng.66, 395–414 (2014).

[8] Samojeden, B. & Grzybek, T. The influence of the promotion of N-modified activated carbon with iron on NO removal by NH3-SCR (Selective catalytic reduction). Energy116, 1484–1491 (2016).

[9] Samojeden, B., Klinik, J., Grzybek, T. & Papp, H. Charakterystyka modyfikowanych węgli aktywnych jako katalizatorów w reakcji DeNOx (The Characterization of Modified Active Carbons for DeNOx Reaction). Gospod. Surowcami Miner.24, 295–303 (2008).

[10]Samojeden, B. & Możdżeń, M. The influence of amount of copper of modified vermiculites on catalytic properties in SCR-NH 3. E3S Web Conf.2020, 1–10 (2017).

[11]Ziemiański, P., Kałahurska, K. & Samojeden, B. Selective catalytic reduction of NO with NH3on mixed alumina–iron (III) oxide pillared montmorillonite "Cheto" Arizona, modified with hexamminecobalt (III) chloride. Adsorpt. Sci. Technol.35, 825–833 (2017).

[12]Wachs, I. E. et al. Selective Catalytic Reduction of NO with NH3 over Supported Vanadia Catalysts. J. Catal.221, 211–221 (1996).

[13]Grzybek, T. Layered clays as SCR deNOx catalysts. Catal. Today119, 125–132 (2007).

[14]Wierzbicki, D. et al. Copper, cobalt and manganese: Modified hydrotalcite materials as catalysts for the selective catalytic reduction of NO with ammonia. the influence of manganese concentration. Comptes Rendus Chim.18, 1074–1083 (2015).

[15]Peng, Y. et al. Deactivation and regeneration of a commercial SCR catalyst: Comparison with alkali metals and arsenic. Appl. Catal. B Environ.168–169, 195–202 (2015).

[16]Baran, R., Grzybek, T., Onfroy, T. & Dzwigaj, S. Microporous and Mesoporous Materials High activity of mononuclear copper present in the framework of CuSiBEA zeolites in the selective catalytic reduction of NO with NH 3. Microporous Mesoporous Mater.226, 104–109 (2016).

[17]De La Torre, U., Pereda-Ayo, B. & González-Velasco, J. R. Cu-zeolite NH3-SCR catalysts for NOxremoval in the combined NSR-SCR technology. Chem. Eng. J.207–208, 10–17 (2012).

[18]Liu, K. et al. Manganese-based catalyst for NO removal at low temperatures : thermodynamics analysis and experimental validation. Pet. Sci. Technol.0, 1–9 (2018).

[19]Samojeden, B. & Grzybek, T. The influence of nitrogen groups introduced onto activated carbons by high- or low-temperature NH3treatment on SO2sorption capacity. Adsorpt. Sci. Technol.35, 572–581 (2017).

[20] Kim, Y. J. et al. Mn-Fe/ZSM5 as a low-temperature SCR catalyst to remove NOx from diesel engine exhaust. Appl. Catal. B Environ.126, 9–21 (2012).

[21] Casanova, M., Llorca, J., Sagar, A., Schermanz, K. & Trovarelli, A. Mixed iron-erbium vanadate NH3-SCR catalysts. Catal. Today241, 159–168 (2015).

[22] Carja, G. & Delahay, G. Mesoporous mixed oxides derived from pillared oxovanadates layered double hydroxides as new catalysts for the selective catalytic reduction of NO by NH3. Appl. Catal. B Environ.47, 59–66 (2004).

[23] Chmielarz, L., Ku, P., Majda, D. & Dziembaj, R. Catalytic activity of Co-Mg-Al , Cu-Mg-Al and Cu-Co-Mg-Al mixed oxides derived from hydrotalcites in SCR of NO with ammonia. 35, 195–210 (2002).

[24] Basąg, S. et al. Activating effect of cerium in hydrotalcite derived Cu–Mg–Al catalysts for selective ammonia oxidation and the selective reduction of NO with ammonia. React. Kinet. Mech. Catal.121, 225–240 (2017).

[25] Jabłońska, M. et al. Understanding the origins of N2O decomposition activity in Mn(Fe)CoAlOx hydrotalcite derived mixed metal oxides. Appl. Catal. B Environ.243, 66–75 (2019).

[26] Yang, R., Gao, Y., Wang, J. & Wang, Q. for simultaneous catalytic removal of soot and NO x. 10317–10327 (2014). doi:10.1039/c3dt52896k

[27] Prasanna, S. V., Kamath, P. V. & Shivakumara, C. Synthesis and characterization of layered double hydroxides (LDHs) with intercalated chromate ions. Mater. Res. Bull.42, 1028–1039 (2007).

[28] Hunter, B. M., Hieringer, W., Winkler, J. R., Gray, H. B. & Müller, A. M. Effect of interlayer anions on [NiFe]-LDH nanosheet water oxidation activity. Energy Environ. Sci.9, 1734–1743 (2016).

[29] Forano, C., Costantino, U., Prévot, V. & Gueho, C. T. Layered double hydroxides (LDH). Developments in Clay Science5, (2013).

[30] Jabłon, M. Thermal transformations of Cu – Mg (Zn)– Al (Fe) hydrotalcite-like materials into metal oxide systems and their catalytic activity in selective oxidation of ammonia to dinitrogen. 731–747 (2013). doi:10.1007/s10973-012-2935-9

[31] Ciocan, C. E., Dumitriu, E., Cacciaguerra, T., Fajula, F. & Hulea, V. New approach for synthesis of Mo-containing LDH based catalysts. Catal. Today198, 239–245 (2012).

[32] Ulibarri, M. A., Hernandez, M. J. & Cornejo, J. Hydrotalcite-like compounds obtained by anion exchange reactions. J. Mater. Sci.26, 1512–1516 (1991).

[33] Zhi, P. X. & Guo, Q. L. Hydrothermal synthesis of layered double hydroxides (LDHs) from mixed MgO and Al2O3: LDH formation mechanism. Chem. Mater.17, 1055–1062 (2005).

[34] Mascolo, G. & Mascolo, M. C. Microporous and Mesoporous Materials On the synthesis of layered double hydroxides (LDHs) by reconstruction method based on the " memory effect ". Microporous Mesoporous Mater. 34–36 (2015). doi:10.1016/j.micromeso.2015.03.024

[35] Ghosal, P. S., Gupta, A. K. & Ayoob, S. Effect of formation pH, molar ratio and calcination temperature on the synthesis of an anionic clay based adsorbent targeting defluoridation. Appl. Clay Sci.116–117, 120–128 (2015).

[36] Erickson, K. L., Bostrom, T. E. & Frost, R. L. A study of structural memory effects in synthetic hydrotalcites using environmental SEM. 59, 226–229 (2005).

[37] Jabłońska, M. & Palkovits, R. Nitrogen oxide removal over hydrotalcite-derived mixed metal oxides. Catal. Sci. Technol.6, 49–72 (2015).

[38] Mrad, R., Cousin, R., Saliba, N. A., Tidahy, L. & Siffert, S. Degradation of VOCs and NOxover Mg(Cu)-AlFe mixed oxides derived from hydrotalcite-like compounds. Comptes Rendus Chim.18, 351–357 (2015).

[39] Levi, C. et al. Cu-Al hydrotalcites-like compounds in the NO reduction by CO. Catal. Today 1–10 (2016).

doi:10.1016/j.cattod.2016.08.023

[40] Jie, J. et al. Journal of Colloid and Interface Science NO x decomposition , storage and reduction over novel mixed oxide catalysts derived from hydrotalcite-like compounds. J. Colloid Interface Sci.333, 423–430 (2009).

[41] La, F. J. Reactivity in the removal of SO 2 and NO x on Co / Mg / Al mixed oxides derived from hydrotalcites. 20, 257–266 (1999).

[42] Kannan, S. & Swamy, C. S. Catalytic decomposition of nitrous oxide over calcined cobalt aluminum hydrotalcites. 53, 725–737 (1999).

[43] Jira, K., Lacny, Z., Mikulova, Z. & Obalova, L. Catalytic decomposition of nitrous oxide over catalysts prepared from Co / Mg-Mn / Al hydrotalcite-like compounds. 60, 289–297 (2005).

[44] Jabłońska, M., Nothdurft, K., Nocuń, M., Girman, V. & Palkovits, R. Redox-performance correlations in Ag–Cu–Mg–Al, Ce–Cu–Mg–Al, and Ga–Cu–Mg–Al hydrotalcite derived mixed metal oxides. Appl. Catal. B Environ.207, 385–396 (2017).

[45] Lopez, T. et al. Synthesis and Characterization of Sol - Gel Hydrotalcites . Structure and Texture †. 189–192 (1996).

[46] Prinetto, F., Ghiotti, G., Graffin, P. & Tichit, D. Synthesis and characterization of sol-gel Mg/Al and Ni/Al layered double hydroxides and comparison with co-precipitated samples. Microporous Mesoporous Mater.39, 229–247 (2000).

[47] Wongkerd, T., Luengnaruemitchai, A. & Jitkarnka, S. Phase change of catalysts derived from a LDH-deoxycholate intercalated compound and its impacts on NO reduction from stationary source emissions. Appl. Catal. B Environ.78, 101–111 (2008).

[48] Da, V., Bulbulian, S. & Bosch, P. Mixed Mg (Al) O oxides synthesized by the combustion method and their recrystallization to hydrotalcites. 107, 240–246 (2008).

[49] Bebensee, R. H., De, L., Würz, H., De, E. & Stella, D. The two tonditu muuttuuntur. 1, (2018).

[50] Pachatouridou, E. et al. Journal of Environmental Chemical Engineering Nitrous oxide decomposition over Al 2 O 3 supported noble metals (Pt , Pd , Ir): Effect of metal loading and feed composition. Biochem. Pharmacol. 1–7 (2015). doi:10.1016/j.jece.2015.03.030

[51] Boissel, V., Tahir, S. & Koh, C. A. Catalytic decomposition of N 2 O over monolithic supported noble metal-transition metal oxides. 64, 234–242 (2006).

[52] Wood, B. R., Reimer, J. A., Bell, A. T., Janicke, M. T. & Ott, K. C. Nitrous oxide decomposition and surface oxygen formation on Fe-ZSM-5. 224, 148–155 (2004).

[53] Bulushev, D. A., Kiwi-minsker, L. & Renken, A. Dynamics of N 2 O decomposition over HZSM-5 with low Fe content. 222, 389–396 (2004).

[54] Abu-zied, B. M., Schwefer, M. & Turek, T. The e☐   ☐ect of NO x o
oxide over Fe-MFI zeolites. 2, 273–276 (2001).

[55] Pirngruber, G. D. The surface chemistry of N 2 O decomposition on iron containing zeolites (I). 219, 456–463 (2003).

[56] Zhou, T. et al. Fe-mordenite / cordierite monolith for the catalytic decomposition of nitrous oxide. 35, 3097–3101 (2009).

[57] Liu, Z., Amiridis, M. D. & Chen, Y. Characterization of CuO Supported on Tetragonal ZrO 2 Catalysts for N 2 O Decomposition. 1251–1255 (2005).

[58] Smeets, P. J. et al. The catalytic performance of Cu-containing zeolites in N 2 O decomposition and the influence of O 2 , NO and H 2 O on recombination of oxygen. 256, 183–191 (2008).

[59] Liu, Z., He, C., Chen, B. & Liu, H. CuO-CeO 2 mixed oxide catalyst for the catalytic decomposition of N 2

O in the presence of oxygen. Catal. Today 0–1 (2017). doi:10.1016/j.cattod.2017.05.074

[60] Zasada, F., Sojka, Z., Adamski, A. & Zaj, W. Copper ionic pairs as possible active sites in N 2 O decomposition on CuO x / CeO 2 catalysts. 191, 129–133 (2012).

[61] Matˇ, V. A comparative study of TiO 2 -supported and bulk Co – Mn – Al catalysts for N 2 O decomposition. 191, 112–115 (2012).

[62] Ludvíková, J. et al. Co-Mn-Al mixed oxides as catalysts for ammonia oxidation to N2O. Res. Chem. Intermed. 42, 2669–2690 (2016).

[63] Dacquin, J. P., Dujardin, C. & Granger, P. Surface reconstruction of supported Pd on LaCoO3: Consequences on the catalytic properties in the decomposition of N2O. J. Catal. 253, 37–49 (2008).

[64] Xu, X., Xu, X., Zhang, G. & Niu, X. Preparation of Co-Al mixed oxide-supported gold catalysts and their catalytic activity for N2O decomposition. J. Fuel Chem. Technol. 37, 595–600 (2009).

[65] Franken, T. & Palkovits, R. Investigation of potassium doped mixed spinels $Cu_xCo_{3-x}O_4$ as catalysts for an efficient N_2O decomposition in real reaction conditions. Appl. Catal. B Environ. 176–177, 298–305 (2015).

[66] Haber, J., Nattich, M. & Machej, T. Alkali-metal promoted rhodium-on-alumina catalysts for nitrous oxide decomposition. Appl. Catal. B Environ. 77, 278–283 (2008).

[67] Obalová, L. et al. Alkali metals as promoters in Co-Mn-Al mixed oxide for N2O decomposition. Appl. Catal. A Gen. 462–463, 227–235 (2013).

Soil application of municipal sewage sludge - possibilities and risks

Aneta Kowalska[1], Marta Jaskulak[1,2], Anna Grobelak[1]

[1]Institute of Environmental Engineering, Czestochowa University of Technology, anetamurtas@gmail.com

[2]University of Lille, Laboratory of civil engineering and environment (LGCgE), Envrionmental Axis, F-59650 Villeneuve d'Ascq, France;

Abstract

Application of sewage sludges into a soil become a leading approach of its management. The quantity and diversity in sewage sludge quality cause various effect on soil. Heavy metals, pharmaceutical or other contaminants such as PAH getting into a soil with sewage sludges can cause more problems than profits. Nevertheless, sewage sludge properly prepared may improve soil quality and increase yields. Due to the many cases of sewage sludge soil application, in this work it has been overall summarized both- benefits as well as risk of that approach.

Keywords: sewage sludge, soil application, assisted phytoremediation

1. Introduction

Sewage sludges consist a by-product and it is formed in a wastewater treatment conducted in wastewater treatment plants (WWTP). A quantity of produced sewage sludge (SS) requires suitable and ecologically accepted management [1]. It is estimated that up to 2020 in UE countries production of sewage sludge could exceed 13 million tons dry solids [2]. A structure of sewage sludge is formed by sludge and activated sludge. From a chemical point view sewage sludges consist mostly a mixture of micro- and macro nutrients as well as organic compounds, non-essential trace metals and microorganisms. In 2012 over 40% of produced sewage sludge has been applicated into a soil. Nevertheless, the differences in sewage sludge composition between seasons creates a necessity to monitor a composition of SS before its land application. SS can contain such chemicals as heavy metals, grease, phenolic compound as well as PAH that shows exceptional toxicity to plants, animals and getting into a groundwater also for humans [3]. In Kuman and Chopra work investigated increased electrical conductivity as well as soil pH value by addition of sewage sludge [22]. Due to the many cases of sewage sludge soil application in this work summarized both benefits and risks of that approach.

2. Fertilizing force of sewage sludge

Due to the high concentration of organic compound as well as micro- and macronutrients (N, P) in stabilized sewage sludges, its frequently used as a fertilizer in agriculture. Thus, sewage sludge soil introduction consist an alternative of recycling valuable components. Therefore, sewage sludges may contribute to minimalize the usage of commercial fertilizers in agriculture [4]. In the literature there are many studies focused on the positive aspect of SS land application. Addition of sewage sludge improves soil properties, for example: bulk density, porosity and water holding capacity [5]. Moreover, sewage sludge may interact with the soil pH value either via its lowering and increase [21]. At Fig. 1 contained overall influence of sewage sludge on physical and chemical soil quality.
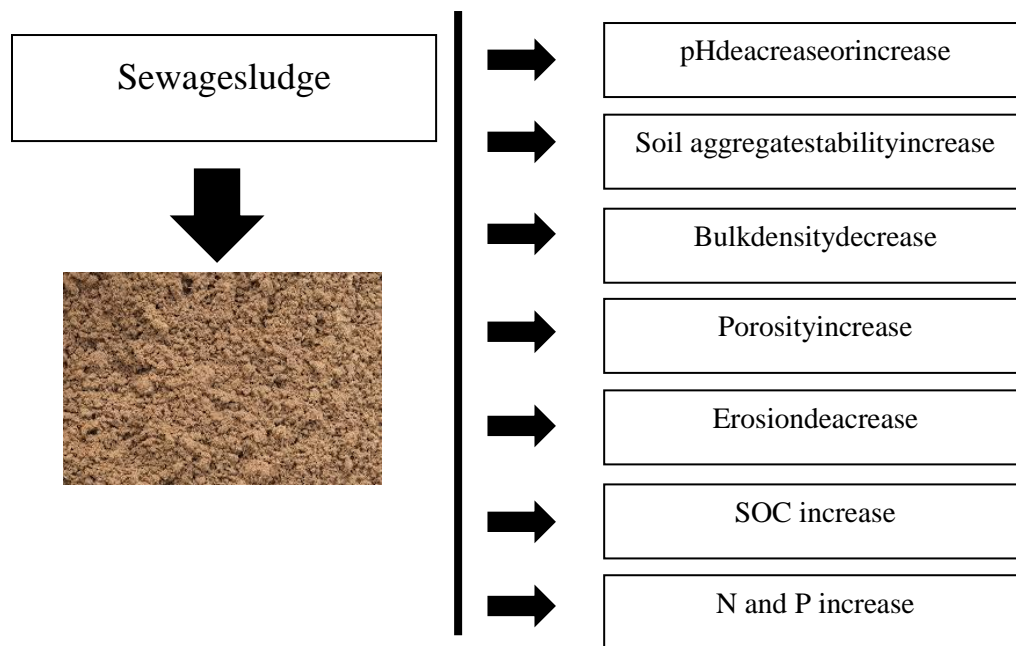
Fig. 1. Influence of SS on soil quality

The main aim of soil-making reclamation with sewage sludge application consist a shaping of vegetation that protect soil surface from destructive actions of water, wind as well as sun. A quantity of introduced sewage sludge is strictly regulated by law and it depend on the use of recultivated soil, heavy metal content in the sewage sludge, SS consistency as well as way of its application. The quantity of heavy metals present in sewage sludge is different and regulated by origin of sewage, treatment of sewage and treatment of sewage sludge [12].

2.1. Sewage sludge usability in agriculture and phytoremediation (reclamation)

Soil contamination with many substances causes problems for agriculture yield. Since, percentage of degraded soils increased in last few years, a surface of area possible for agriculture shrined. One of the soil recultivation method is phytoremediation using hyperaccumulators - plants that are capable to accumulate an abnormal, high concentrations of xenobiotic (including heavy metals, antibiotics and other contaminants) [6]. Phytoremediation may be conducted by two main ways: phytostabilisation and phytoextraction. Despite low environmental requirements of plants used in phytoremediation, they are not able to live in the environment bereft of organic compound and micro- and macronutrients. Therefore, such phytoremediation have to be assisted by addition of any fertilizer [8]. In assisted phytoremediation it is possible to use stabilized sewage sludges. It has been found that sewage sludge introduced in to with a law regulations may intensity phytoremediation process [10]. Placek A. et al. showed a positive influence of sewage sludge on proper growth and increased biomass. In that study also showed that accumulation of heavy metals with *Scot pine, Norway spruce* and *oak* in the soil enriched by sewage sludge has been intensified [10]. In turn, in Kubatova et al. study found that sewage sludge limited growth of *Salix* and *Populus*clones in first years of 6-year experiment. Nevertheless, in that study it has been showed that in samples amendment by sewage sludge the significantly decreased phytoextraction of heavy metals (in particular Zn). Sewage sludge land application has immobilized heavy metals in the soil [10]. Therefore, in study of Latare et al., showed an increased nutrient content (N, P, K) as well as heavy metals content (Cd, Cr, Ni and Pb) in straw and grain of rice and wheat in samples of soil with sewage sludge application. Moreover, in that study higher quantity of sewage sludge improved grain yield, even 2-times for 40tha^{-1} of SS [13]. Sewage sludge introduced into the depleted soil may allow plant growth and contribute to the restoration of the ecosystem homeostasis. Nevertheless, such reclamation process may take many years. The main advantages of this issue is the reduction of the usage of commercial fertilizers. Moreover, it consist a way of sewage sludge disposal. The overall positive effect of sewage sludge application in assisted phytoremediation has been showed in Fig. 2.
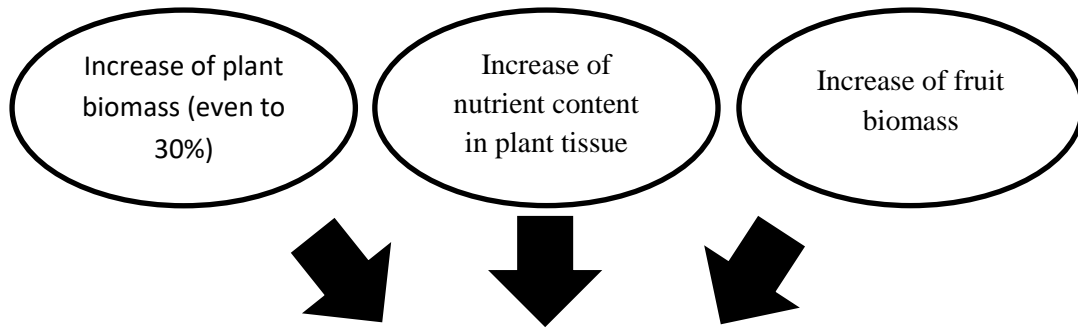
Fig. 2. The overall positive effects of sewage sludge on plants used in assisted phytoremediation.

Sewage sludge may be direct used as a soil fertilizer in agriculture improving soil quality. An addition of stable sewage sludge into a soil has a positive influence on the nutrient content and physical condition of the soil [14].

2.2. Sewage sludge and photosynthesis

Sewage sludge application into a soil may dually influence on plant growth and development. The desirable and positive affection of sewage sludge is closely connected with micro- and microelements as well as organic compounds in the used, stabile sewage sludge. The increased concentration of nitrogen, phosphorus and potassium in the soil caused by sewage sludge application escalate chlorophyll synthesis. In turn, carbon dioxide assimilation rate increased in photosynthesis which leads to growth and development support [21]. That relationship were showed at the Fig. 3.
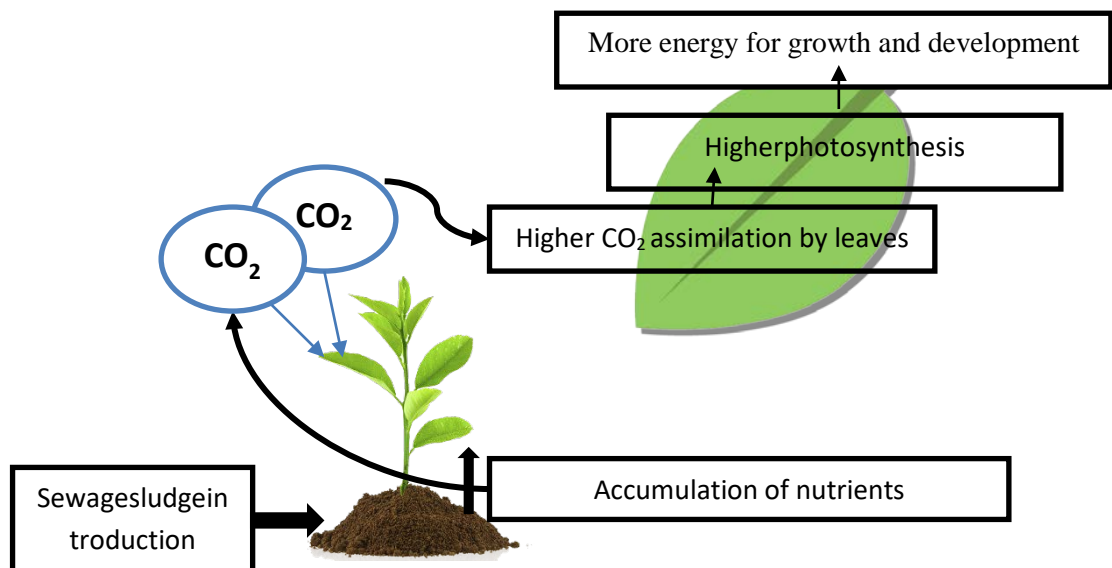

Fig. 3.The positive aspect of sewage sludge application into a soil on plant photosynthesis

3.   Risk of soil application of sewage sludge

In social consciousness problem of the soil degradation is primarily connected with a potential toxic effect in crops. Problem of soil contamination is identified only with decrease of yields and possible influence on food quality. Nevertheless, problem of soil degradation consists more and more complicated issue.

First of all, toxic substances present in the soil going through the ground may get to groundwater causing serious danger for human health. Therefore, contaminant from sewage sludge are accumulated by plants that consist one of the trophic chain link [23]. These contaminants accumulated in the plants and consumed by next trophic chain links circulate in the ecosystem [24]. Risks connected with application of sewage sludges in one point view may be compared with direct introduction of some contaminants.

3.1. Pathogenic organisms

In Kulling et al. research observed increase of the quantity of pathogenic organisms in the soil enriched by sewage sludge. Those organic matter introduced into a soil in that context may consist really serious danger. Patogenes present in the waste water may not be removed from the raw sewage sludge and in the soil conditions may alive for a long period of time. Moreover, some microorganisms creates spores and in its form may be activated in a favorable conditions. It has been noticed that *Salmonella* sp. may survive for 20-30 years. The biological contamination level can be decreased or excluded by stabilization of the sewage sludge before introducing into a soil. A huge danger consist helmints (e.g. tapeworms) that are not removed in a sufficient degree. Their eggs are founded in the sewage sludge even after few years of SS storage [26].

The second group of microorganisms with a potential danger consist a microorganisms from convalescent. Incomplete, insufficient or inaccurate sewage sludge stabilization process may not remove such potentially strong pathogenic factors. In that point view, sewage sludge may be consider as a ticking biological bomb introduced into a soil [27].

3.2. Accumulation of heavy metals in the soil

Sewage sludge contained heavy metals consist a serious problem due to high difficulties connected with metals assessment in soils [7].After the long-term research of Udom et al. (2004) it has been showed that sewage sludge land application increase accumulation of heavy metals in the soil (Zn, Pb, Cd, Cu). The concentrations of those toxic elements may consist a threat for human health and cause phytotoxic effects. Far-going effect of sewage sludge application into soil is entering of metal trace elements into a foodchain. The negative impact of heavy metals introduced into a soil with a sewage sludge can interact not only with plants but also with microbial biomass [28]. Metal trace elements emerging either into o depth levels of the ground either to a top layer may inhibit enzymatic processes. Those effect can have a state character. Nevertheless, as provided by many researchers- land application of sewage sludges with a high rate of organic matter may cause absorption of metal trace elements and decrease its toxicity level. In turn, those activity contribute to the accumulation and magazine of heavy metals into a soil that consist a long-term limiting agent [29].

3.3. Negative effect of sewage sludge onplant photosynthesis

Land application of sewage sludges may influence even on the basic processes at plant cell level. Photosynthesis consist the most important process in plant physiology. Different agents may cause some disorders in that process. Therefore, photosynthesis at certain stages may be useful for the determination of plants' physiology state [15]. It has been observed that many substances such as heavy metals may change photosynthesis efficiency and as effect, these substances has a huge contribution in plant development. For example cadmium and its compounds interact with key enzymes for phytoremediation causing its dysfunction. Inactivity of photosynthesis enzymes limits photosynthesis [16, 17]. The negative influence of heavy metal is not limited only for photosynthesis but also many other issues such as induction of oxidative damage in plant tissue [18]. Moreover, metal trace elements toxicity is strongly dependent on the amount of heavy metals in the sewage sludge as well as soil and plant characteristic and weather conditions [25].

Sewage sludge aimed for land application are controlled for heavy metal content. Nevertheless, the quantities of such pollutants as well many other compounds introduced into a soil with sewage sludges is huge. Among many sources of anthropogenic presence of HMs in the soil is mentioned the direct introduction of sewage sludges

[19]. It turns out therefore that usage of sewage sludge in order to improve soil quality many consists a serious danger for living plants by affection of contained contaminants on plant's photosynthesis [20].

4. Conclusion

Behind of sewage sludge usage in land application there are many advantages but also this usage brings some global risks, not only for environmental but also for human health. The long-lime effects of sewage sludge land application may be really dangerous for environmental homeostasis. Except many benefits connected with sewage sludge land application, far-reaching risk must be taken into account.

Acknowledgment

References

[1] Kelessidis A., Stasinakis A.S., Comparative study of the methods used for treatment and final disposal of sewage sludge in European countries, Waste Management, 32 (6), 2012, 1186-1195

[2] Leonard, A., 2011. Management of wastewater sludge's: a hot topic at the European level. Journal Residues Science Technology 8, 38.

[3] Cieślik B.M., Namieśnik J., Konieczka P., Review of sewage sludge management: Standards, regulations and analytical methods, Cleaner Production, 90, 2015, 1-15

[4] Singh R.P., Agrawal M., Potential benefits and risks of land application of sewage sludge, Waste Management, 28 (2008), 347-358

[5] Ramulu, U.S. Sree., 2002. Reuse of municipal sewage and sludge in agriculture. Scientific Publishers, Jodhpur, India

[6] Schiavon M., Pilon-Smits E.A.H., Selenium Biofortification and phytoremediation phytotechnologies: a review, Journal of Environmental Quality Abstract- Reviews & Analyses, 46, 2016, 10-19

[7] McGrath S.P., Chaudri A.M, Filler K.E., Long-term effects of metal in sewage sludge on soils, microorganisms and plants, Journal of Industrial Microbiology, 14, 1995, 94-104

[8] Nowak M., Kacprzak M., Grobelak A., Osady ściekowe jako substytut w procesach remediacji i rekultywacji gleb skażonych metalami ciężkimi, Inżynieria i Ochrona Środowiska, 13, 2, 2010, 121-131

[9] Pivetz, B.E., 2001. Phytoremediation of Contaminated Soil and Ground Water at Hazardous Sites. Ground Water Issue, EPA/540/S-01/500.

[10] Placek A., Grobelak A., Kacprzak M., Improving the phytoremediation of heavy metals contaminated soil by use of sewage sludge, International Journal of Phytoremediation 2016, 18, 605-618

[11] Kubatova P., Hejcman M., Szakova J., Vondrackova S., Tlustos P., Effects of Sewage Sludge Application on Biomass Production and Concentration of Cd, Pb and Zn in Shoots of Salic and Populus Clones; Improvement of Phytoremediation Efficiency in Contaminated Soils, Bioenerg. Res., 2016, 9, 809-819.

[12] Hue, N.V., Ranjith, S.A., 1994. Sewage sludges in Hawaii: chemical composition and reactions with soils and plants. WaterAirSoilPollut. 72, 265–283.

[13] Latare A.M., Kumar O., Singh S.K., Gupta A., Direct and residual effect of sewage sludge on yield, heavy metals content and soil dertility under rice-wheat system, Ecological Engineering, 2014, 69, 17-24.

[14] Phillips R., Fisher J.T., Mexal J.G., Fuelwood Production Utilizing Pinuseldarica and Sewage Sludge Fertilizer, Forest Ecology and Management, 1986, 16, 95-102.

[15] Bojko M., Lenrat K., Warkiewicz E., Kalicka B., Chyc M., Olchawa-Pajor M., Latowski D., Beneficial or toxic effects of soot on the plants-model Research, Archives of Waste Management and Environmental Protection, 2016, 18,2, 81-92

[16] Adrees M., Ali S., Rizwan M., Ibrahim M., Abbas F., Farid M., Zia-ur-Rehman M., Irshad M.K., Bharwana S.A., The effect of excess copper on growth and physiology of important food crops: a review,EnvrionSciPollut Res, 2015, 22, 8148-8162

[17] Wang Q., Zuo Y., Chen T., Zheng W., Yang Y., Effects of selenium on antioxidant enzymes and photosynthesis in the edible seaweed Grscilarialemaneiformis, Journal of Applied Phycology, 2018, 1-8

[18] Nagajyoti P.C., Lee K.D., Sreekanth T.V.M., Heavy metals, occurrence and toxicity for plants: a rewiew, Environmental Chemistry Letters, 2010, 8,3, 199-216

[19] Alloway Brian J., Sources of Heavy metals and Metalloids in Soil, in: Heavy metals in Soils. Trace Metals and Metalloids in Soils and their Bioavailability, Environmental Pollution 22, Springer 2010, ISBN 978-94-007-4469-1

[20] Sorrentino M.C., Capozzi F., Amitrano C., Giordano S., Arena C., Spagnuolo V., Performance of three cardoon cultivars in an industrial heavy metal-contaminated soil : Effects on morphology, cytology and photosynthesis, Journal of Hazardous Materials, 2018, 351, 131-137

[21] Mohamed B., Mounia K., Aziz A., Ahmed H., Rachid B., Lotfi A., Sewage sludge used as organic manure in Moroccan sunflower culture: Effects on certain soil properties, growth and yield components, Science of the Total Environment, 2018, 627, 681-688

[22] Kumar, V., Chopra, A.K., 2013. Accumulation and translocation ofmetals in soil and different parts of French Bean (Phaseolus vulgaris L.) amended with sewage sludge. Bull. Environ. Contam. Toxicol. 10, 128–142.

[23] Wang X., Chen T., Ge Y., Jia Y., Studies on land application of sewage sludge and its limiting factors, Journal of Hazardous Materials, 2008, 160, 554-558

[24] Muchuweti M., Birkett J.W., Chinyanga E., Zvauya R., Scrimshaw M.D., Lester J.N., Heavy metal content of vegetables irrigated with mixtures of wastewater and sewage sludge in Zimbabwe: Implications for human health, Agriculture, Ecosystems & Environment, 2006, 112, 41-48.

[25] Jin, Q., Zi-Jian, W., Xiao-quann, S., Qiang, T., Bei, W., Bin, C., 1996. Evaluation of plant availability of soil trace metals by chemical fractionation and multiple regression analysis. Environ. Pollut. 91, 309–315.

[26] Udom B.E., Mbagwu J.S.C., Adesodun J.K., Agbim N.N., Distributions of zinc, copper, cadmium and lead in a tropical ultisol after long-term disposal of sewage sludge, Environmental International, 2004, 30, 467-470

[27] Malej J., Właściowości osadów ściekowych oraz wybrane sposoby ich unieszkodliwania i utylizacji, Rocznik Ochrona Środowiska 2000, 2, 69-101.

[28] Udom B.E., Mbawgwu J.S.C., Adesodun J.K., Agbim N.N., Distributions of zinc, copper, cadmium and lead in a tropical ultisol after long-term disposal of sewage sludge, Environment International, 2004, 30, 467-470

[29] Bright D.A., Healey N., Contaminant risk from biosolids land application: Contemporary organic contaminant levels in digested sewage sludge from five treatment plants in Greater Vancouver, British Columbia, Environmental Pollution, 2003, 126, 39-49

The following publication consists of articles presented during the Environmental Protection and Energy Conference at Silesian University of Technology in Gliwice, 2018

This release as an activity of InnoEnergy Clean Fossil and Alternative Fuels Energy M. Sc. program students and Waste Mangment M. Sc. students